

AD-760 572

SEISMIC ARRAY DESIGN HANDBOOK

IBM Federal Systems Division

Prepared for:

Advanced Research Projects Agency

August 1972

DISTRIBUTED BY:

NTIS

National Technical Information Service
U. S. DEPARTMENT OF COMMERCE
5285 Port Royal Road, Springfield Va. 22151

DISCLAIMER NOTICE

THIS DOCUMENT IS THE BEST
QUALITY AVAILABLE.

COPY FURNISHED CONTAINED
A SIGNIFICANT NUMBER OF
PAGES WHICH DO NOT
REPRODUCE LEGIBLY.

**MISSING PAGE
NUMBERS ARE BLANK
AND WERE NOT
FILMED**

Seismic Array Design Handbook

AD-0572

D.D.C.
NOT REPRODUCED
EXCEPT BY
AUTHORITY
OF THE
D.D.C.

IBM

Approved for Public Release
Distribution Unlimited.

LEGAL NOTICE

When U.S. Government drawings, specifications or other data are used for any purpose other than a definitely related government procurement operation, the government thereby incurs no responsibility nor any obligation whatsoever; and the fact that the government may have formulated, furnished, or in any way supplied the said drawings, specifications, or other data is not to be regarded by implication or otherwise as in any manner licensing the holder or any other person or conveying any rights or permission to manufacture, use, or sell any patented invention that may in any way be related thereto.

OTHER NOTICES

Do not return this copy. Retain or destroy.

ACCESSION No.

WTS ☐ White Section

B/D ☐ Bulk Section

WMA ☐

TECHNICAL

BY

SUBSCRIPTION AVAILABILITY CODES

Area

4-101, 404, 405, 406, 407, 408, 409, 410, 411, 412, 413, 414, 415, 416, 417, 418, 419, 420, 421, 422, 423, 424, 425, 426, 427, 428, 429, 430, 431, 432, 433, 434, 435, 436, 437, 438, 439, 440, 441, 442, 443, 444, 445, 446, 447, 448, 449, 450, 451, 452, 453, 454, 455, 456, 457, 458, 459, 460, 461, 462, 463, 464, 465, 466, 467, 468, 469, 470, 471, 472, 473, 474, 475, 476, 477, 478, 479, 480, 481, 482, 483, 484, 485, 486, 487, 488, 489, 490, 491, 492, 493, 494, 495, 496, 497, 498, 499, 500

A

DOCUMENT CONTROL DATA: R & D

Security classification of title, table of contents, and abstracting information must be entered on the overall report to include:

1. ORIGINAL SOURCE ACTIVITY (Corporate activity)

International Business Machines Corporation
18100 Frederick Pike
Gaithersburg, Maryland 20760

20. PRESENT SOURCE OF CLASSIFICATION

UNCLASSIFIED

N/A

SEISMIC ARRAY DESIGN HANDBOOK

4. DESCRIPTIVE ABSTRACT

None

5. DATE OF ORIGIN

August 1972

6. CONTRACT OR GRANT NO.

F19628-68-C-0100

7. PROJECT NO.

10. INFORMATION AS TO:

Approved for public release; distribution unlimited

11. SPONSORING/PERFORMING AGENCY

Sponsored by ARPA

12. PERFORMING ORGANIZATION NAME(S)

Directorate of Planning and Technology
Hq Electronic Systems Division (AFSC)
L. C. Hanscom Field, Bedford, MA 01730

13. ABSTRACT

Key topics involved in designing and implementing large seismic arrays and their processing systems are discussed. Alternative approaches previously examined are reviewed, and some techniques deserving further consideration are identified.

SEISMIC ARRAY DESIGN HANDBOOK

Sponsored by

Advanced Research Projects Agency
Washington, D.C.

ARPA Order No. 800

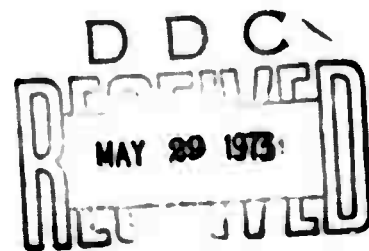
Prepared under USAF Electronic Systems Division
Contract No. F19628-68-C-0400

August 1972

Federal Systems Division
INTERNATIONAL BUSINESS MACHINES CORPORATION
18100 Frederick Pike
Gaithersburg, Maryland 20760

Approved for Public Release.
Distribution Unlimited.

100



FOREWORD

**This research is supported by the Advanced Research Projects Agency.
The Electronics Systems Division technical project officer for Contract
No. F19628-68-C-0400 is Mr. K. Handsaker (XRC).**

**K. Handsaker
Communications Development Division
Directorate of Planning and Technology**

CONTENTS

Section		Page
1	INTRODUCTION	1-1
2	ARRAY GEOMETRY	2-1
2.1	Array Design Fundamentals	2-2
2.2	NORSAR Design	2-26
2.3	Annotated Bibliography	2-52
3	SEISMIC SIGNAL AND NOISE CHARACTERISTICS	3-1
3.1	Seismic Wave Origins	3-1
3.2	Waveform Analysis Techniques	3-4
3.3	Background Noise Characteristics	3-16
3.4	Signal Characteristics	3-25
3.5	Waveform Filtering	3-44
3.6	Annotated Bibliography	3-55
4	DATA ACQUISITION	4-1
4.1	Field Instrumentation	4-14
4.2	Data Center Equipment	4-39
4.3	Array Monitoring and Control	4-45
4.4	Analog Channel Models	4-70
4.5	Annotated Bibliography	4-75
5	DETECTION PROCESSING	5-1
5.1	Detection Processor (DP) System Definition	5-2

Section		Page
5.2	Beam Deployment	5-21
5.3	Signal Processing Algorithms	5-35
5.4	Detection Reduction Algorithm	5-50
5.5	Detection Processor System Outputs and Offline Analysis Programs	5-58
5.6	Comparison of Alternative Detection Techniques	5-67
5.7	Annotated Bibliography	5-85
6	ARRAY BEAMSTEERING TECHNIQUES	6-1
6.1	Analog Matched-Filter Performance	6-8
6.2	Matched-Filter Performance: Digital Case	6-11
6.3	Application to the Correlation Process	6-14
6.4	Evaluation of ω_B^2	6-19
6.5	U-Space Estimation Errors	6-22
6.6	Example: Circularly Symmetric Array With Identical Errors	6-27
6.7	Posterior Probabilities for Multiple Peaks	6-29
6.8	Observation Probabilities for Multiple Peaks	6-33
6.9	Sequential Updating Procedure for the Slowness Vector Estimate	6-37
6.10	An Algorithm for the Sequential Estimation of the Slowness Vector	6-40
6.11	Annotated Bibliography	6-43
7	TIME ANOMALIES	7-1
7.1	Basic Theory	7-3
7.2	System Applications and Estimation Techniques	7-17
7.3	Storage and Retrieval of Time Anomaly Data	7-26
7.4	Annotated Bibliography	7-45

Section		Page
8	EVENT PROCESSING	8-1
8.1	System Structure	8-2
8.2	Event Process Controller (EPCON)	8-5
8.3	Short-Period Signal Processor	8-11
8.4	Large Event Processor (SAAC ONLY)	8-38
8.5	Output Processor	8-39
8.6	Editing Processor	8-50
8.7	SAAC Parameter Values	8-58
8.8	NDPC Parameter Values	8-58
8.9	Annotated Bibliography	8-69
9	IBM REPORT BIBLIOGRAPHY	9-1
9.1	IBM Quarterly and Final Reports	9-1
9.2	IBM Special Technical Reports	9-4
9.3	ISRSPS Reference (REF) Documentation, Annotated	9-7

ILLUSTRATIONS

Figure		Page
1-1	Seismic Array Systems Concept	1-2
2-1	Power Response Pattern Contours in Wave Number Space	2-9
2-2	Array Gain	2-14
2-3	Correlation Coefficient vs Distance Between Instruments at LASA	2-16
2-4	Principal Inverse Phase Velocity Region	2-20
2-5	Norway Inverse Velocity Space Map of the World	2-21
2-6	Hexagon Subarray Geometry Modified to Fit Site	2-29
2-7	Heptagon-Pentagon Array Geometry	2-30
2-8	Modified Hexagon Array Loss Contour	2-31
2-9	Filled Heptagon Array Loss Contour	2-32
2-10	Modified Hexagon Array LP Beam Pattern-Worst Case	2-33
2-11	Filled Heptagon LP Beam Pattern-Worst Case	2-31
2-12	Modified Hexagon Array SP Beam Pattern-Worst Case	2-35
2-13	Twenty-two Filled Heptagon with Pentagon Subarrays-Worst Case Beam Pattern	2-30
2-14	Cost Performance Tradeoff	2-40
2-15	NORSAR System Array Geometry	2-44
2-16	Optimized Array Beam Pattern Contours	2-45
2-17	Optimized Array LP Worst Case Beam Pattern	2-46
2-18	Optimized Array SP Worst Case Beam Pattern	2-47

Figure		Page
2-19	Optimized Array Antenna Pattern, 34.0° Steering	2-48
2-20	Worst Case Beam Patterns for 10 Randomly Perturbed Heptagon Arrays, $\sigma = 1$ km	2-49
2-21	NORSAR Beam Envelope Power Loss Pattern	2-51
3-1	Definition of Detectability and False Alarm Values	3-9
3-2	Noise Power Spectral Density Computed from Different Sample Lengths	3-14
3-3	Power Spectral Density Plot Showing Effects of Filtering and Correction	3-15
3-4	Power Spectral Density Function Determined Using Multiple Filters	3-17
3-5	Spectra of Seismic Noise Recorded at 16 Geographic Locations (Data Are Normalized to 1 Hz Bandwidth)	3-21
3-6	LASA and NORSAR Noise Power Spectral Density Functions	3-22
3-7	Beam and Sensor Background Noise Measured through a 0.75 to 4.0 Hz Filter with no Prewhitening	3-24
3-8	Average Long-Term Average (LTA) Noise Level for NORSAR (21 to 25 April 1971)	3-26
3-9	Correlation Coefficient vs Distance Between Instruments	3-27
3-10	Longshot Event	3-29
3-11	Seismic Signal Shapes	3-30
3-12	Subarray Waveform Variations	3-32
3-13	Relative Subarray Amplitude Anomalies--All Regions	3-33
3-14	Relative Subarray Amplitude Anomalies--Andreanof Island	3-33
3-15	Relative Subarray Amplitude Anomalies--Philippine Island	3-34
3-16	Relative Subarray Amplitude Anomalies--Kuril Island	3-34

Figure		Page
3-17	Relative Subarray Amplitude Anomalies- Eastern Kazakh	3-35
3-18	Relative Subarray Amplitude Anomalies-Mexico	3-35
3-19	Scaled Rayleigh and P-Wave Spectra from the NTS Event Pulse and Three Earthquakes	3-37
3-20	Normalized and Ideally Whitened Channel Signal Spectra and Median	3-38
3-21	Spectral Differences in P-Phase at Norway and Montana in the Form of a Histogram of Dominant Periods	3-39
3-22	Longshot S/N Spectrum	3-42
3-23	Discrimination Using LASA Short-Period Spectral Ratio	3-43
3-24	Wideband Filter Response Characteristics	3-47
3-25	Shaped Filter Response Characteristics	3-49
3-26	Effect of Selected Filters on the Spectral Density Functions of Average Beam Noise (with Arbitrary Scaling for Better Visibility)	3-52
3-27	Relative Detectability Comparison for Various Predetection Filters and Coherent Beamforming	3-54
4-1	Integrated Seismic Array Signal Processing System	4-2
4-2	SAAC Detection Processor	4-6
4-3	SAAC Event Processor System	4-7
4-4	SAAC Auxiliary Processor	4-8
4-5	NDPC Detector Processor	4-9
4-6	NDPC Event Processor	4-10
4-7	Data Acquisition System for One Subarray	4-13
4-8	Typical Short-Period Analog Channel	4-15
4-9	Synchronization of Data Sampling and Transmission	4-26

Figure		Page
4-10	SLEM ICW/ODW Formats for SEMC/L Mode	4-29
4-11	SLEM Block Diagram	4-31
4-12	Compression Technique for Short-Period Data	4-35
4-13	Blocking and Defloating of SP Data by the SPS	4-37
4-14	SPS Organization (NDPC)	4-41
4-15	AMCS Block Diagram	4-43
4-16	EOC Functional Organization	4-51
4-17	Physical Layout of Operations Console	4-54
4-18	Operations Console, Strip Chart Recorder, and 2250 Display Unit	4-55
4-19	Short-Period Analog Channel Model	4-71
4-20	Long-Period Analog Channel Model	4-73
5-1	Rectified vs Power Envelope	5-14
5-2	LASA Detection Processor Configuration	5-18
5-3	NORSAR Detection Processor Configuration	5-19
5-4	Number of Beams Required for Land and Seismic Area Coverage with LASA	5-28
5-5	Number of Beams Required for Teleseismic Zone Coverage with LASA	5-29
5-6	Number of Beams Required for Land and Seismic Zone Coverage with NORSAR	5-30
5-7	Number of Beams Required for Teleseismic Zone Coverage with NORSAR	5-31
5-8	System/360 Model 40 Processing Load Using Beamforming Microcode at 10 Samples per Second	5-36
5-9	System/360 Model 40 Processing Load Rectify- Integrate-Threshold Microcode, Input Data Rate 10 Samples per Second, Integration Interval 1.8 Seconds	5-37

Figure		Page
5-10	Sampling Loss	5-41
5-11	Phasing Loss	5-41
5-12	LASA Detection Processing Configuration	5-51
5-13	NORSAR Detection Processing Configuration	5-52
5-14	Spatial Grouping Algorithm Flow	5-56
5-15	NORSAR Beam Envelope Power Loss Contour	5-62
5-16	NORSAR Beam Envelope Power Loss Pattern	5-63
5-17	Selected NORSAR Beam Envelope History	5-64
5-18	NORSAR Detection Distribution Beam Set 306 (300 Beams)	5-66
5-19	Relative Detectability Comparison for Various Predetection Filters and Coherent Beamforming	5-73
5-20	Relative Detectability Comparison for Various Predetection Filters and Incoherent Beamforming (Envelope Processing)	5-75
5-21	Relative Detectability Comparison for Various Predetection Filters and 3 out of 8 Voting	5-76
5-22	Relative Detectability Comparison for Various Predetection Filters and 4 out of 8 Voting	5-77
5-23	Relative Detectability Comparison for Various Detection Techniques and Filter 09-35	5-78
5-24	Relative Detectability Comparison for Various Detection Techniques and Filter 12-32	5-79
5-25	Relative Detectability Comparison for Various Detection Techniques and Filter DDD	5-80
5-26	Relative Detectability Comparison for Selected Combination of Detection Processing Technique and Predetection Filter	5-82
5-27	Comparison of False-Alarm Indexes for Selected Combinations of Detection Processing Technique and Predetection Filter	5-84

Figure		Page
6-1	Time Delay Correlation Process	6-4
6-2	Linear Sequential Estimation Process	6-41
7-1	Earth Model Showing Variation in Sensor Depth and Propagation Velocity	7-10
7-2	Earth Model Showing Variation in Depth of Crust	7-13
7-3	Earth Model Showing Local Variation in Slope at Crust-Mantle Boundary	7-13
7-4	Example for Triangular Grid Node Search Algorithm	7-36
7-5	LASA U-Space Triangular Grid	7-42
7-6	Cumulative Distribution of Events Relative to Standard Deviation of Residual Time-Anomaly Error	7-43
7-7	Cumulative Distribution of Events Relative to Residual U-Space Calibration Error	7-43
8-1	EP System Configuration	8-3
8-2	Data Flow for the Short Period Signal Processor	8-12
8-3	Array Beamsteering	8-14
8-4	Correlation Process for Array Beamsteering	8-18
8-5	Beampacking Process for Array Beamsteering	8-22
8-6	Beampacking Grid	8-23
8-7	Waveform Parameter Extraction	8-25
8-8	Event Mode Determination	8-30
8-9	Event Characterization	8-35
8-10	Short-Period Summary Report	8-41
8-11	Event Tape Record Characteristics	8-44
8-12	Detection Report	8-45

Figure		Page
8-13	Seismic Bulletin	8-46
8-14	Detection/Bulletin Report-Partition 1	8-47
8-15	Output Processor General Flow	8-49
8-16	Partial Event Plot	8-51
8-17	SAAC SPSP Parameter Report	8-59
8-18	NDPC SPSP Parameter Report	8-64

TABLES

Tables		Page
4-1	Configuration Description	4-11
4-2	Data Acquisition Channel Tests	4-62
4-3	SLEM Test Signal Quality Checks	4-63
5-1	Microprogrammed Algorithm Performance	5-11
5-2	Detection State Table	5-48
5-3	Applicable Parameters	5-48
5-4	Digital Filter Coefficients	5-72
7-1	Typical Values for U, a, and b	7-8
7-2	Plane and Quadratic Deviation of Two Hakkaido Events	7-26
8-1	Filter Coefficients-NDPC and SAAC ISRSPS EP Systems	8-28

Section 1

INTRODUCTION

Under efforts for the Electronic Systems Division of the U. S. Air Force, sponsored by the Advanced Research Projects Agency, IBM has designed and developed large aperture seismic array processing systems, and analyzed other aspects of array technology, such as array geometry design. The progress of the studies and development work has been reported previously through periodic technical summaries and special publications, and the processing systems have been described in published manuals; a comprehensive list of these reports is given in Section 9 of this document. This Seismic Array Design Handbook supplements those publications by providing a consolidated discussion of key topics involved in designing and implementing seismic arrays and their processing systems. The topics are addressed from the viewpoint of the system designer or analyst, rather than the implementer. In several cases, various alternative approaches which were considered during development are mentioned and the basis for selection of the methods utilized are given. Also, some suggestions of techniques deserving of further analysis for potential improvement of the processing design are identified.

This handbook is based on the system concept as depicted in Figure 1-1; multiple array considerations are not included. This general system design is not restricted to any particular array, communications approach, or processing equipment or software, but provides the essential functions of array instrument calibration, field equipment condition monitoring, data acquisition, event detection and bulletin computation, interactive process interface with operators and seismic analysts (including array bulletin editing), storage of raw and processed data, and offline system parameter improvement based on previous data.

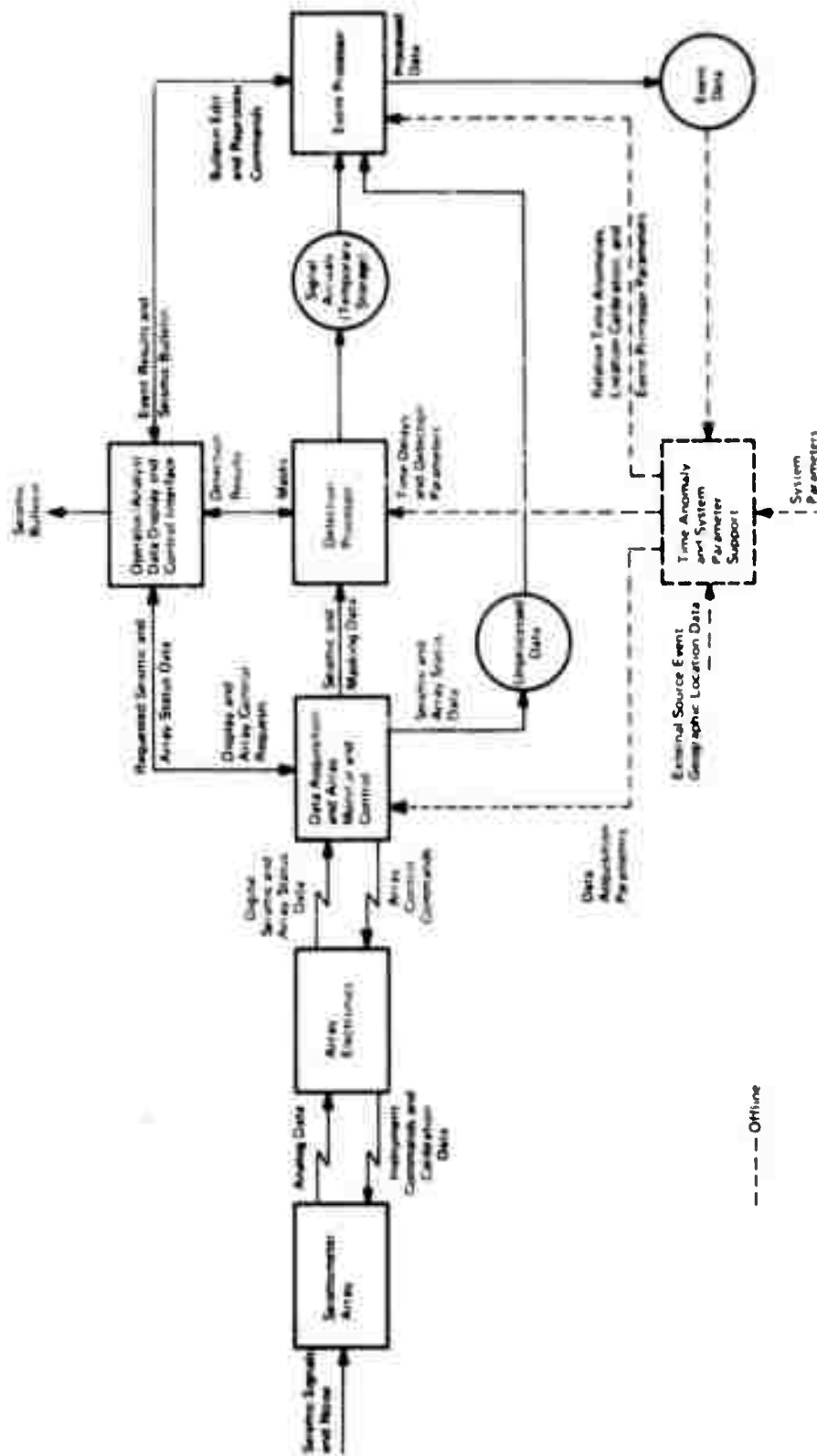


Figure 1-1. Seismic Array System Concept

Seismic signals and background noise are sensed by an array of seismometers which have been positioned in a configuration designed to achieve various signal processing objectives. The output of each sensor data channel is preconditioned and digitized at the array site, and the resulting digital data is formatted with additional array status and environmental data and transmitted via dedicated links to a data center. This data is simultaneously recorded and input in real time to a Detection Processor. Various array monitoring and control functions, including data channel calibration and synchronization of the data sampling, are automatically controlled from the data center.

The Detection Processor generates seismic event signal detections which are presented in real time to the operator and stored in temporary files. The Event Processor selects events from the signal detections in the temporary files for extended processing, and extracts the appropriate segments of sensor data from the previously recorded data. For each such event, an improved array beam is formed using an array beamsteering technique, and the resulting beam and associated parameters are further analyzed to produce detailed characterizations of the seismic event and the associated signal waveforms. Significant Event Processor results are presented to the analyst, and the complete set of processed event data is stored on a permanent file. The analyst may modify the results and request reprocessing until a satisfactory array bulletin is obtained.

A subset of the processed events is selected by the analyst with the assistance of various offline support programs, and the relative subarray arrival times for these events are edited and combined with externally provided event location information to produce improved beam-forming delays for the Detection Processor and both relative subarray time anomaly and location calibration data tables for the Event Processor. By this means, the processed data from past events is used to enhance the performance of the processing system on future events.

I

For practical reasons, the handbook does not treat the total array design problem exhaustively, but an attempt has been made to cover the principal issues and provide a guide to the key considerations in each. Seven general technical areas are covered, as delineated briefly below. Each section is intended to be self-contained with its own annotated bibliography, though some references between sections occur. Bibliography references are in the form [A-B] where A is the section and B is the item number. In certain instances, the Integrated Seismic Research Signal Processing System (ISRSPS) developed for the LASA and NORSAR arrays is specifically described, but the techniques may be extended to the general case.

Section 2, Array Design, deals with the concepts of array geometry and instrument spacing, including the constraints of communications costs.

Section 3 outlines and summarizes seismic signal and noise characteristics at the LASA and NORSAR arrays, including a preliminary analysis of the full NORSAR array data.

In Section 4, the significant aspects of the basic requirements, the design philosophy and the implementation of the data acquisition portions of a large seismic array processing system are presented. The data acquisition subsystem consists of the sensor instrumentation, the data acquisition control and recording equipment, the data communication network, and the field instrumentation monitoring and remote control facilities.

The LASA and NORSAR Detection Processors provide continuous online surveillance in real time of selected regions of the earth for possible natural or man-made seismic disturbances, in accordance with the Large Array Program objectives. The significant design decisions and tradeoff considerations involved in the Detection Processor system development are discussed in Section 5, and the resulting detection system configurations for LASA and NORSAR are presented and compared.

Array beamsteering may be defined as any process for estimating some or all of the pertinent array beamforming parameters from a set of array data that is assumed to include a signal of interest, in such a way that the beam which is formed from the data using the estimated parameters provides an improved representation of the signal. Section 6 presents a theoretical basis for the correlation process and an extension of this process which incorporates an adaptation of the recursive Bayes estimation technique to increase the cycle selection reliability. The presentation includes a detailed error analysis of the estimation techniques, and a demonstration that these techniques are near-optimum under certain reasonable assumptions.

Time anomalies are defined as the differences between the delays predicted by an appropriately chosen plane wavefront model and the perfect beamforming delays. Section 7 discusses elementary physical causes of time anomalies, methods of time anomaly estimation and use, and techniques for achieving practical computer storage and look-up procedures for the time anomaly data.

Section 8 describes the Event Processor (EP) as it was actually implemented for use at SAAC and NDPC. EP characterizes seismic events from the detections reported by the Detection Processor. System requirements for EP were formulated so that the process should satisfy dual system objectives: (1) the publication of a daily seismic bulletin, and (2) support of seismic research through provision of a tool for process experimentation and through the formation of a data base of seismic information stored on digital magnetic tape.

Section 2

ARRAY GEOMETRY

The design of a large seismic array should be based on careful consideration of the signal processing and data acquisition requirements imposed by the array system objectives, and on an evaluation of those economic factors which are variable functions of the array geometry. A combined long-period and short-period array presents unique design problems because of the interactions and tradeoffs which exist among the various design factors. Attempts to maximize the cost savings associated with combining the data acquisition systems of a long-period and a short-period array are not necessarily compatible with attempts to optimize the array beam pattern of each array separately. In this section, large seismic array geometries are discussed in terms of the significant design parameters and related considerations, and the design philosophy which guided the choice of the NORSAR array geometry is presented.

The potential capabilities and advantages of a large seismic array, upon which the array system objectives are based, include the following:

- a. Signal-to-Noise-Ratio Enhancement—Array beamforming suppresses the energy of incoherent seismic background noise relative to that of properly aligned coherent seismic signals.
- b. Interfering Signal Suppression—Array beam patterns in wavenumber space indicate the relative suppression of improperly aligned coherent signals.
- c. Spatial Resolution—Array beamsteering techniques may be used to locate a source of signal energy in wavenumber space with accuracy and resolution proportional to the diameter of the array beam pattern main lobe.

- d. Reduction of Waveform Distortion-The beamforming process reduces the effects of waveform distortions produced by reflection and refraction and by more complex geophysical phenomena if the array area is sufficiently large that the distortions are incoherent among sensors.
- e. Improved Signal Energy Estimation-Local geological variations within the earth's crust may produce focusing and/or defocusing of signal energy which results in significant variations in signal amplitude among the individual seismometer outputs. These amplitude variations are averaged in the beamforming process, and as a result more accurate estimates of signal energy and amplitude may be obtained.

The design of NORSAR which is described in Section 2.2 represents an attempt to optimize those aspects of array system performance which are most significant relative to Large Array Program objectives, with reasonable emphasis on engineering economics, and with some attention focused on all array performance factors. Preliminary considerations, including discussions of array design tools and techniques, are presented in Section 2.1.

2.1 ARRAY DESIGN FUNDAMENTALS

The observed signal and noise response characteristics of a typical array beam are generally a function of the seismic signal and noise characteristics at the array site, the number and configuration of the sensors (i.e., the array geometry), the frequency response characteristics of the data channels including the seismometers, the analog signal conditioning equipment and the digital filters, and the frequency and wavenumber response characteristics of the array beamforming operation. If different filters are to be applied to various data channels prior to

beamforming (referred to as filter-and-sum beamforming), or if there are significant differences in the signal and/or noise frequency spectra from sensor to sensor, then there is no clear-cut separation of frequency domain and wavenumber space characteristics to simplify the analysis of array beam response.

It will be assumed henceforth that the array geometry is to be specifically optimized for applications of simple delay-and-sum or weighted-delay-and-sum beamforming, and that signal and noise spectral characteristics among the various sensors are sufficiently similar that the differences can be ignored. The current experience with large seismic arrays generally supports this latter assumption. Under these assumptions, the total array beam response of the system may be regarded as a cascade of the following signal processing operations:

- a. Frequency domain filtering by the various data channel components, including the seismometers, amplifiers, analog filters and digital filters, with the same filter response characteristics being applicable to both seismic signal and seismic noise data. These response characteristics are discussed extensively in Section 4.4.
- b. Wavenumber space filtering by the array beamforming operation, as described in Section 2.1.1. Since wavenumber is the product of frequency and inverse velocity, this implies that an array beam has a different frequency response characteristic for each of two coherent signals having different inverse velocities. However, the frequency response characteristic for incoherent noise is flat, regardless of inverse velocity. Beamforming generally also causes a frequency domain filtering for coherent energy alone due to random errors in the delays, which results in greater attenuation at higher frequencies.

Furthermore, the overall system response at the array beam level is the same regardless of the assumed order of these operations.

The following subsections describe the significant array design parameters and their relationships with various array applications, the computation of array beam wavenumber space and inverse velocity space response characteristics, the considerations of array signal and noise characteristics that are related to array geometry design and array site selection, and a computational algorithm for the constrained optimization of array sensor locations to improve the wavenumber space response function.

2.1.1 Array Beam Patterns

A plane wave solution of the three-dimensional wave equation for simple harmonic motion of frequency f , may be expressed at the spatial location $\vec{r} = (x, y, z)$ as

$$\Omega(\vec{r}, t) = A \exp [i 2\pi (ft - \vec{k} \cdot \vec{r})] \quad (2-1)$$

where $\vec{k} = (k_x, k_y, k_z)$ is the wavenumber vector.

If this harmonic function is simultaneously sensed at a number of locations \vec{r}_n , $n = 1, 2, \dots, N$, and the sensor outputs are averaged, the resulting function will be

$$y(t) = A \exp [i\omega t] \left\{ \sum_{n=1}^N (1/N) \exp [-i2\pi \vec{k} \cdot \vec{r}_n] \right\}$$

The expression in braces will have magnitude less than unity unless all of the values $\vec{k} \cdot \vec{r}_n$ are equal or differ only by integer constants. However,

if the output of the nth sensor is delayed by $c - (1/f) \vec{k} \cdot \vec{r}_n$ seconds before averaging, where c is a constant selected to make all delays positive, then the resulting function will be

$$y(t) = A \exp [i\omega (t-c)],$$

and no reduction in signal amplitude occurs.

For an array of sensors located at the positions \vec{r}_n , the process of delaying and averaging the sensor outputs as described above is known as steering the array for frequency f and wavenumber \vec{k} and simple beamforming.

It is convenient to express \vec{k} in the form $f \vec{u}$, where \vec{u} is a vector which points in the direction of the wavefront propagation and has magnitude equal to the reciprocal of the propagation velocity. In three dimensions, the \vec{u} -vector may be written as

$$\vec{u} = v^{-1} \begin{bmatrix} \cos \theta \sin \phi \\ \sin \theta \sin \phi \\ \cos \phi \end{bmatrix} \quad (2-2)$$

where ϕ is the angle of the propagation vector relative to the vertical, θ is the projected angle of the propagation vector relative to the x -axis, and V is the speed of propagation at the array. However, if the array of sensors lies entirely in the x - y plane, then the z -component may be dropped and the two-dimensional \vec{u} -vector, hereafter referred to as the inverse velocity vector, expressed as

$$\vec{u} = \frac{\sin \phi}{v} \begin{bmatrix} \cos \theta \\ \sin \theta \end{bmatrix} \quad (2-3)$$

may be used for all computations. The apparent velocity of propagation in the x-y plane is $V/\sin \phi$ from (2-3).

Therefore, a planar array of sensors at locations $\vec{r}_n = (x_n, y_n)$, $n = 1, 2, \dots, N$, may be steered for the inverse velocity vector \vec{u} by delaying the nth sensor output by $c \cdot \vec{u} \cdot \vec{r}_n$ seconds. If the array is steered for the inverse velocity vector \vec{u}_1 , then the plane wave

$$p_2(\vec{r}, t) = B \exp [i\omega (t - \vec{u}_2 \cdot \vec{r})],$$

with inverse velocity vector \vec{u}_2 , will appear on the beamformed output as

$$y(t) = B \exp [i\omega (t - c)] \left\{ \sum_{n=1}^N (1/N) \exp [i\omega (\vec{u}_1 - \vec{u}_2) \cdot \vec{r}_n] \right\}$$

The function

$$G(\Delta \vec{u}, \omega) = \left| \sum_{n=1}^N (1/N) \exp [i\omega \Delta \vec{u} \cdot \vec{r}_n] \right| \quad (2-4)$$

is referred to as the beam pattern in inverse velocity space for simple delay-and-sum beamforming. The beam pattern represents the relative amplitude suppression of a signal having an inverse velocity vector which differs by $\Delta \vec{u}$ from the inverse velocity location for which the array beam is steered. A single beam pattern is sufficient for all inverse velocity steering points, since it depends only on the difference vector $\Delta \vec{u}$.

Weighted delay-and-sum beamforming is a somewhat generalized version of the above beamforming process in which a set of relative positive sensor weights W_n , normalized so that $\sum_{n=1}^N W_n = 1$, are employed in the averaging operation in place of the simple $(1/N)$ weighting factors. For weighted delay-and-sum beamforming, the pattern function becomes

$$G(\Delta \vec{u}, \omega) = \left| \sum_{n=1}^N W_n \exp [i \omega \Delta \vec{u} \cdot \vec{r}_n] \right| \quad (2-5)$$

It is usual practice to express the beam pattern values in decibels, as $20 \log_{10} G(\Delta \vec{u}, \omega)$. By algebraic manipulation and application of common trigonometric identities, the beam pattern (2-5) in dB may also be expressed in the form

$$20 \log_{10} G(\Delta \vec{u}, \omega) = 10 \log_{10} \left\{ \sum_{n=1}^N \sum_{m=1}^N W_n W_m \cos [\omega \Delta \vec{u} \cdot (\vec{r}_n - \vec{r}_m)] \right\} \quad (2-6)$$

The preceding equations have been developed for the case of simple harmonic motion. However, by application of the superposition theorem to the linear beamforming operation, the beam pattern power function for a signal having the one-sided power spectrum $S(\omega)$ may be evaluated as follows

$$G_S^2(\Delta \vec{u}) = \sum_{n=1}^N \sum_{m=1}^N W_n W_m \int_0^{\infty} S(\omega) \cos [\omega \Delta \vec{u} \cdot (\vec{r}_n - \vec{r}_m)] d\omega \quad (2-7)$$

For the simple case in which $S(\omega) = 1/(2B)$ over the frequency interval $[f_c - B, f_c + B]$, the beam power response function for center frequency f_c and bandwidth $2B$ becomes

$$20 \log_{10} G_{2B}(\Delta \vec{u}, f_c) = 10 \log_{10} \left\{ \sum_{n=1}^N \sum_{m=1}^N W_n W_m \frac{\sin [2\pi B T_{nm}(\Delta \vec{u})]}{[2\pi B T_{nm}(\Delta \vec{u})]} \cos [2\pi f_c T_{nm}(\Delta \vec{u})] \right\} \quad (2-8)$$

where $T_{nm}(\Delta \vec{u}) = (\vec{r}_n - \vec{r}_m) \cdot \Delta \vec{u}$. Both narrowband beam patterns of the type

(2-6) and broadband patterns of the type (2-8) have proved useful for seismic array beamforming analysis and synthesis.

If the array consists of identical or nearly identical clusters of sensors, called subarrays, then the location of the p th sensor of the k th subarray may be expressed as $\vec{r}_{p_k} + \vec{r}_k$, where \vec{r}_k is the position vector of the center of the k th subarray relative to the origin of the array coordinate system, and \vec{r}_{p_k} is the location vector of the p th sensor of subarray k relative to the center of subarray k .

If we assume that the relative weighting factors are applied only to the subarray sums, then the beam pattern function (2-5) may be written as

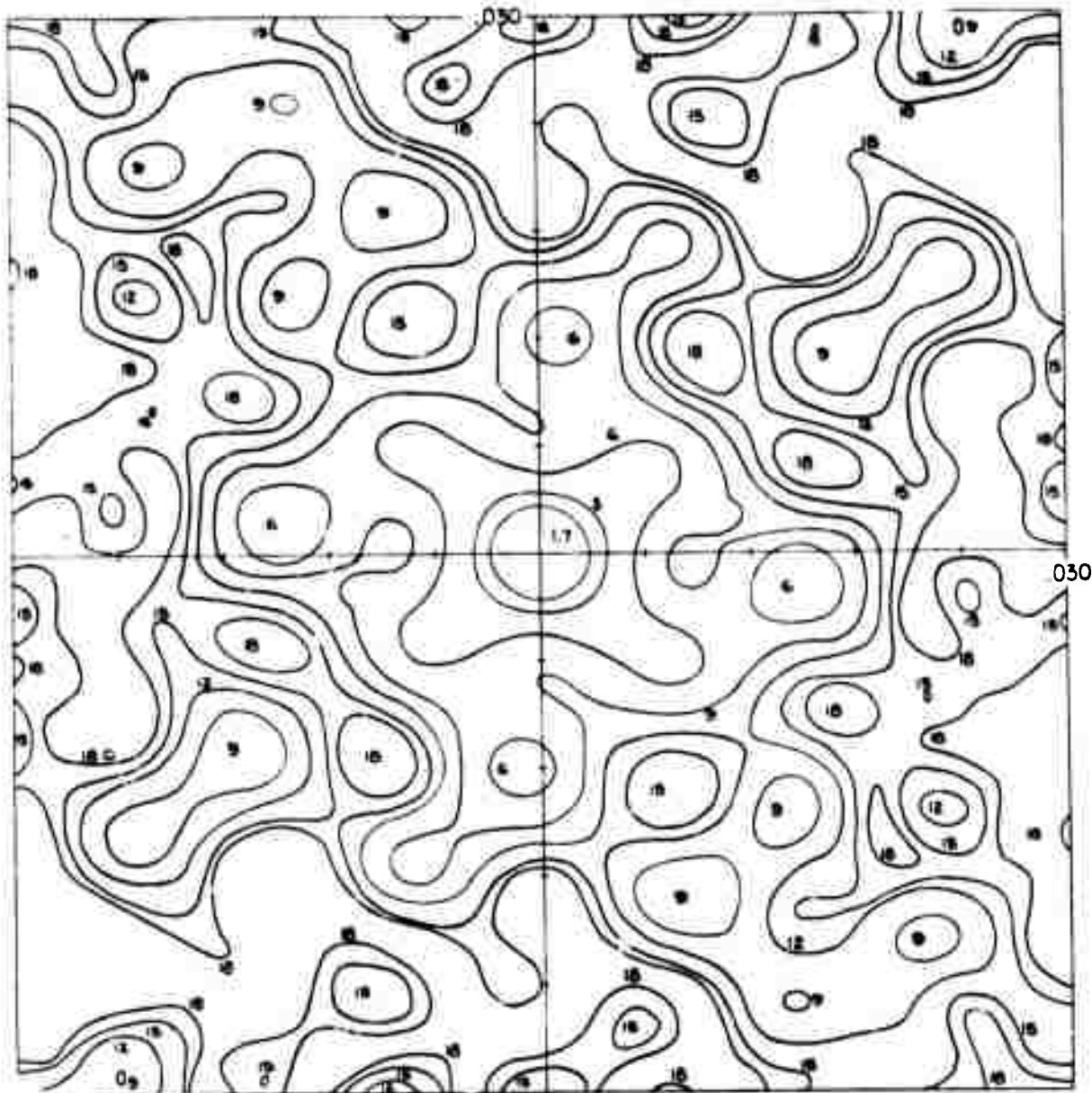
$$G(\Delta\vec{u}, \omega) = \left| \sum_{k=1}^K w_k \left\{ \sum_{p_k=1}^{P_k} \frac{1}{P_k} \exp [i\omega \Delta\vec{u} \cdot \vec{r}_{p_k}] \right\} \exp [i\omega \Delta\vec{u} \cdot \vec{r}_k] \right|, \quad (2-9)$$

where P_k is the number of sensors in the k th subarray and K is the number of subarrays. If all subarrays have P sensors and are configured identically, then the expression in braces is actually independent of k and may be factored out of the summation over k to yield

$$G(\Delta\vec{u}, \omega) = \left| \sum_{p=1}^P \frac{1}{P} \exp [i\omega \Delta\vec{u} \cdot \vec{r}_p] \right| \left| \sum_{k=1}^K w_k \exp [i\omega \Delta\vec{u} \cdot \vec{r}_k] \right|. \quad (2-10)$$

If an array consists of nearly identical subarrays, then the expression (2-10) serves as a convenient approximation for many applications.

Figure 2-1 shows a contour diagram of the beam pattern for LASA. The value at the origin in this figure is zero decibels, and the peak which occurs at the origin is the main lobe of the beam pattern. Other smaller peaks in the beam pattern correspond to side lobes. One of the goals of array



FULL LASA ARRAY, 21 SUBARRAYS
VALUES IN dB

Figure 2-1. Power Response Pattern Contours in Wave Number Space

design is to minimize the relative amplitude of the larger side lobes over some region of interest around the main lobe. It is common to refer to the area enclosed by the 3 dB contour surrounding the origin as the main lobe, and the average diameter of this area as the main lobe diameter.

If the array is steered for an inverse velocity vector \vec{u}_1 given by

$$\vec{u}_1 = \frac{\sin \phi}{V} \begin{bmatrix} \cos \theta_1 \\ \sin \theta_1 \end{bmatrix}$$

and if the relative beam response is evaluated for the inverse velocities $\vec{u}_2(\beta)$, where

$$\vec{u}_2(\beta) = \frac{\sin \phi}{V} \begin{bmatrix} \cos (\theta_1 + \beta) \\ \sin (\theta_1 + \beta) \end{bmatrix}$$

as β varies from $-\pi$ to π , then the resulting response function, considered as a function of β , is the azimuthal beam pattern for steering vector \vec{u}_1 and frequency ω . In Δu -space, these function values lie on a circle through the origin, with center at a distance $1/(\sin \phi)/V$ from the origin along the ray at an angle θ_1 relative to the u_x -axis.

For the azimuthal beam pattern, the angle subtended by the 3 dB contour of the main lobe is referred to as the beamwidth (BW) for frequency f , steering angle θ_1 and inverse velocity $1/(\sin \phi)/V$.

2.1.2 Array Design Parameters

In the most general sense, the array design parameters consist of the number and the specific geographic locations of each type of sensor used in the array. However, there are certain parameters which may be speci-

fied initially in order to control various overall aspects of array system performance. Within these constraints, the specific locations of the sensors may then be selected to optimize the array beam patterns, as described in Section 2.1.5. The effects of some significant array design parameters are described in the following paragraphs.

2.1.2.1 Effective Aperture

Lacoss has shown in [2-3, pp. 24-25] that a directional derivative of the beam pattern function (2-4) with respect to a displacement \vec{s}_n of the position vector \vec{r}_n is bounded above by

$$\left| \frac{\partial |G(\Delta\vec{u}, \omega)|}{\partial \vec{s}_n} \right| < \frac{\omega |\Delta\vec{u}|}{N} \quad (2-11)$$

For the weighted delay-and-sum beam pattern (2-5), this bound becomes

$$\left| \frac{\partial |G(\Delta\vec{u}, \omega)|}{\partial \vec{s}_n} \right| < W_n \omega |\Delta\vec{u}|. \quad (2-12)$$

These bounds represent the maximum sensitivity of a point on the beam pattern function due to the displacement of a single sensor; that is, if the n th sensor is displaced by a small amount ϵ_n , then the amplitude of the beam pattern for angular frequency ω and relative inverse velocity $\Delta\vec{u}$ will not change by more than $W_n \omega |\Delta\vec{u}| \epsilon_n$.

The sensitivity bounds indicate in particular that the region of $\Delta\vec{u}$ -space in the vicinity of the main lobe is relatively insensitive to the detailed location of the sensors. Also, the beam pattern functions (2-4) and (2-5) depend on the terms $\Delta\vec{u} \cdot \vec{r}_n$; hence, if the entire array is re-scaled with scaling factor S , so that $\vec{r}'_n = S \vec{r}_n$ for all sensors, then

the corresponding beam pattern in Δu -space will simply be rescaled by a factor $(1/S)$. In particular the size of the main lobe is inversely proportional to the array diameter, for a given array geometry.

Therefore, in the initial stages of array design, the approximate distribution of elements may be selected in the form of a spatial density function, and the diameter, or aperture, of the array may be adjusted to obtain a main lobe of the desired size.

The approximate relations between beamwidth (BW) and the ratio of wavelength ($\lambda = v/f$) to array diameter (D) are given below for a number of simple array configurations, where the propagation is in the plane of the array

- a. Line array of length L steered at an angle θ_0 relative to broadside:

$$BW \approx 0.89 \frac{\lambda}{L} \sec \theta_0.$$

- b. Circular array of diameter D with uniform element density within the circle:

$$BW \approx 1.02 \frac{\lambda}{D}.$$

- c. Circular ring of diameter D:

$$BW \approx 0.72 \frac{\lambda}{D}.$$

- d. Uniform square array with sides of length L, steered perpendicular to a pair of sides:

$$BW \approx 0.89 \frac{\lambda}{L}.$$

- e. Square array with density $(L-|x|)(L-|y|)/L^2$ for $|x| < L$, $|y| < L$, steered perpendicular to a pair of sides:

$$BW \approx 1.27 \frac{\lambda}{L}.$$

It is also frequently convenient to express the main lobe beamwidth in terms of the effective array aperture, which is the radius of gyration R_g of the array (that is, the second geometric moment about the array center of gravity). If this is done, then the resulting expressions for beamwidth are less dependent on the element distributions than in the above examples.

2.1.2.2 Number of Sensors

When simple delay-and-sum beamforming is employed, the signal-to-noise ratio gain of an array of N sensors is given by

$$\text{Gain} = 10 \log_{10} \frac{1+(N-1)\rho_s}{1+(N-1)\rho_n}, \quad (2-13)$$

where ρ_s and ρ_n are the average signal and noise correlations, respectively, between pairs of sensors. Equation (2-13) is based on the assumption that the same signal and noise power levels are received on all sensor data channels.

Figure 2-2 shows the array gain versus the number of sensors for various values of ρ_n , with $\rho_s = 1$. If the signals are approximately coherent across the entire array ($\rho_s = 1$), then the array gain relative to incoherent noise will be given by $10 \log_{10} N$. Results from the LASA array indicate a noticeable reduction in signal coherence between sensors at opposite extremes of the array, that is, spaced at approximately 200 kilometers. This observation imposes a practical limit on the size of arrays to be used for coherent array processing; the limitation may vary significantly with location.

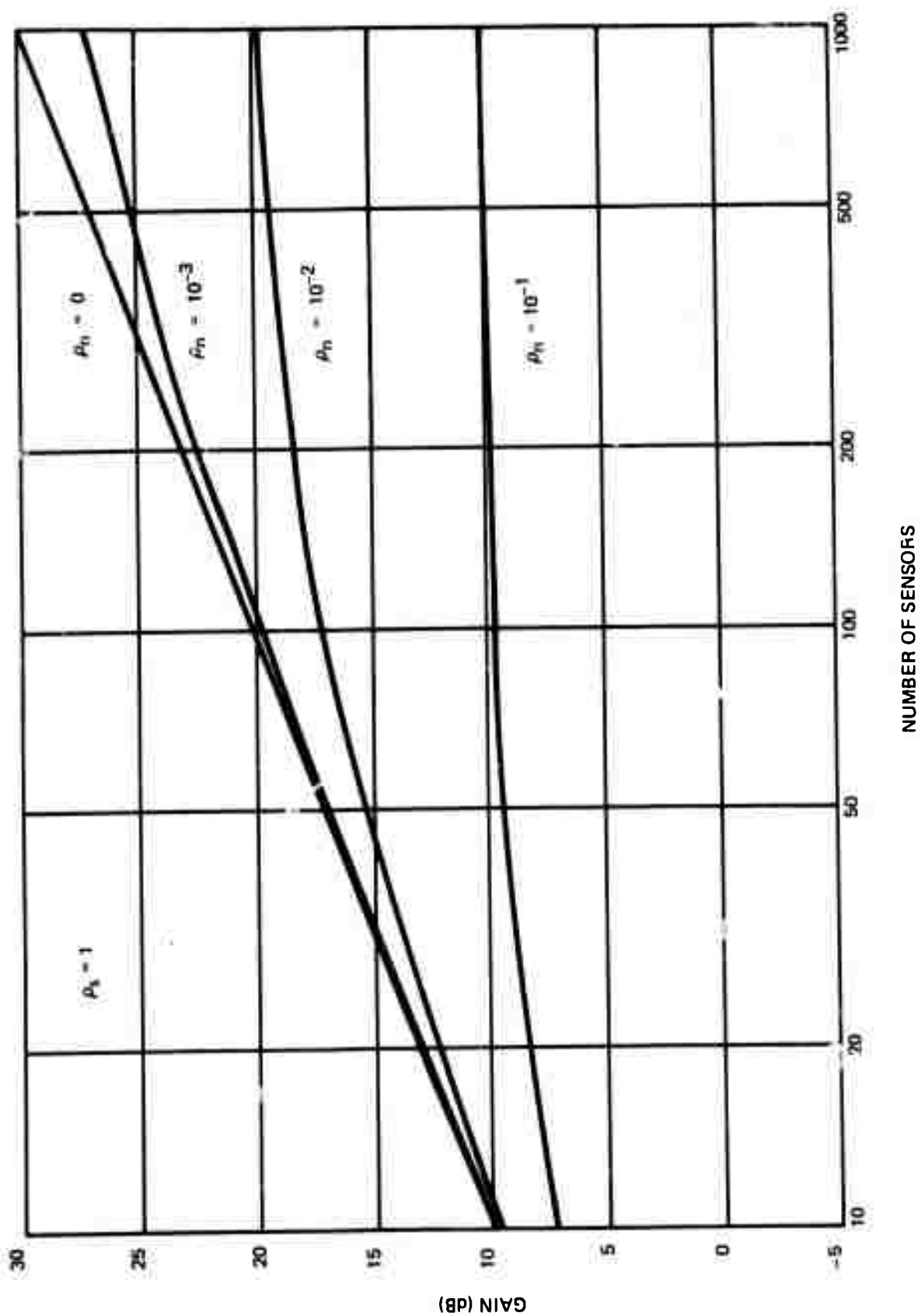


Figure 2-2. Array Gain

It has also been shown by Lo [2-4] that the achievable sidelobe reduction for a well-designed array depends directly on the number of sensors in the array, for a given λ/D .

2.1.2.3 Minimum Spacing Between Sensors

As shown in Figure 2-2, the achievable array gain for a fixed number of sensors depends on the average noise correlation between pairs of sensors. This dependence has been examined in some detail by Capon, et al. in [2-5]. Figure 2-3 shows the correlation coefficients between pairs for typical LASA noise data. This diagram, as well as various diagrams in [2-5], suggests that the pairwise noise correlation coefficients will not be excessive if the minimum sensor spacing is set at approximately 3 kilometers. However, it must be recognized that an increase in the minimum sensor spacing also increases the costs of the data acquisition system. This aspect of array design is examined further in Section 2.2.3.

2.1.2.4 Depth of Sensors

The signal-to-noise ratio on an individual seismometer at a particular geographic location will vary somewhat as a function of the depth at which the seismometer is placed within the earth, and will generally improve with increasing depth. However, the costs of drilling and encasing deep boreholes for the seismometers must also be considered. Therefore, a tradeoff study is advisable to weigh the relative improvement in array performance against the increased array costs. An analysis of this type was attempted for NORSAR by implanting both deep and shallow seismometers in the pilot arrays and comparing the resulting signal-to-

LONGSHOT-BAND PASS FILTER 0.9 - 1.4 Hz

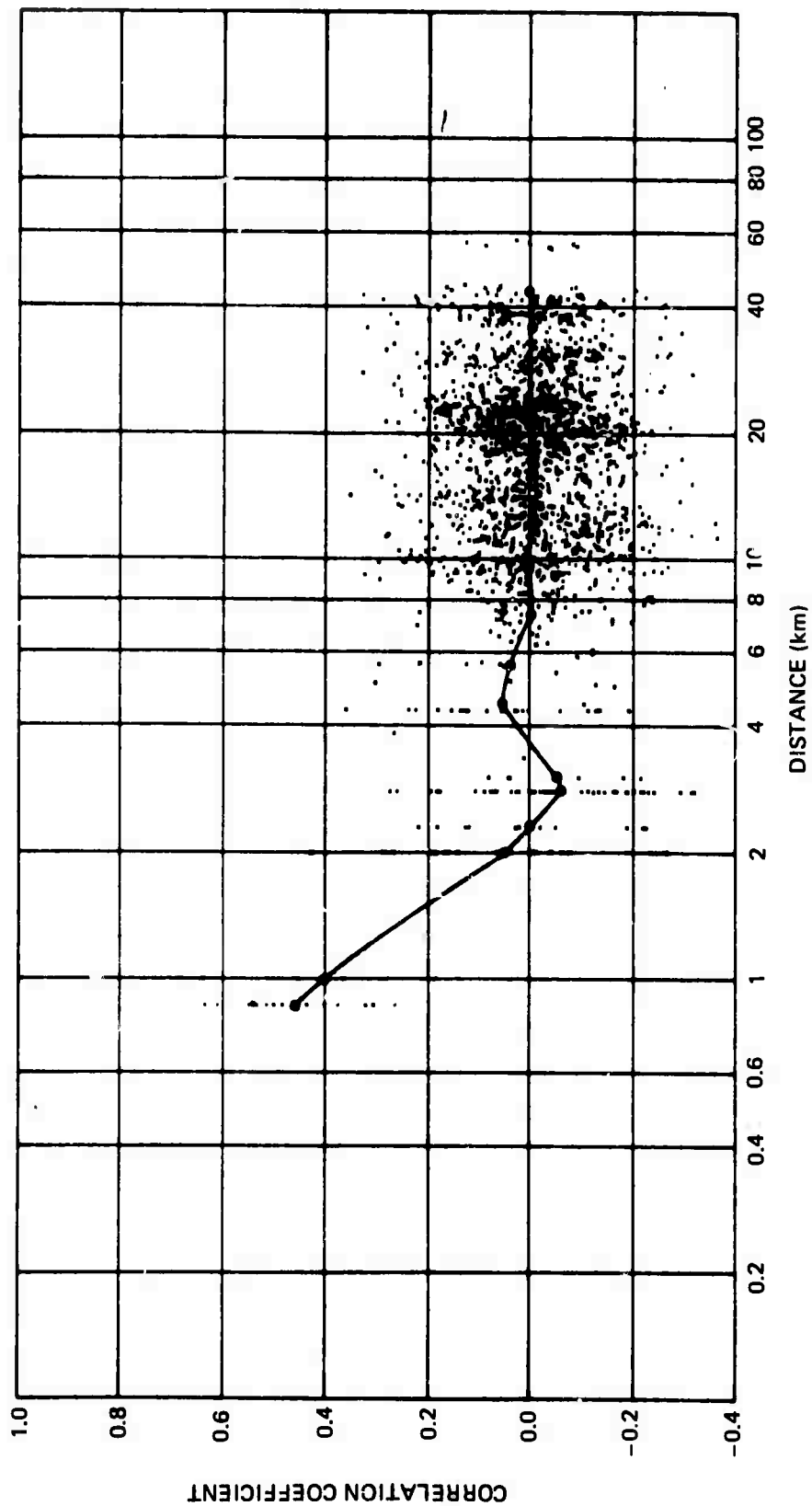


Figure 2-3. Correlation Coefficient vs Distance Between Instruments at LASA

noise ratios. The differences observed in the modest amount of data collected did not justify the significant expense of deep placement at that site.

2.1.2.5 Array Configuration

It was indicated in Section 2.1.2.1 that the general distribution of sensors within the array, together with the array aperture, approximately determines the shape of the array beam pattern near the vicinity of the main lobe in $\vec{\Delta u}$ -space. However, the relative size of side-lobes at greater distances from the origin in $\vec{\Delta u}$ -space depends to a correspondingly greater extent on the detailed locations of individual sensors. Therefore, it is typical in the design of arrays having a large number of elements to start with an aperture and distribution which yield the desired characteristics of main lobe and close-in side-lobes, and a number of elements which yield the desired array gain and the potential for the required side-lobe suppression, and to proceed from those initial parameters with a combination of cut-and-try techniques and computerized optimization programs. Both of these techniques are generally constrained to preserve the initially selected parameter values, and also to restrict the array design as required by various practical considerations, such as requiring that the instruments not be placed in water, roads, or in populated areas.

For an array of nearly identical subarrays, an approximate separation of the form given by equation (2-10) may be used to partition and simplify the detailed design problem. That is, the subarray and array beam patterns may first be designed separately, and the results combined by the use of (2-10); then the total array geometry may be modified somewhat to yield beam pattern improvements and to satisfy practical constraints. Section 2.1.4 describes an array optimization technique which is useful for fine tuning the array geometry design subject to various constraints.

2.1.2.6 Array Location

It should be noted that the signal-to-noise ratio at the individual sensors may vary considerably as a function of the general geographical location of the array. Therefore, if several array sites are available, an important consideration in the selection process should be the typical signal-to-noise ratios at the various sites, as determined by a series of pilot studies.

2.1.3 Array Signal and Noise Considerations

The characteristics and origins of seismic signals and of microseismic and general background noise are discussed in some detail in Section 3. Included in that section are discussions of signal and noise coherence versus sensor spacing, and of frequency bands of interest for seismic array processing. The purpose of this subsection is to develop array beam pattern requirements based on signal and noise considerations.

The propagation velocity (V) of a pressure wave (P-wave) in the crustal structure beneath an array is typically in the range 5.5 - 6.0 km/sec. If a value of 6.0 km/sec is used for planning purposes, then the maximum inverse velocity for P-waves is 167 ms/km, and occurs for a wave which propagates horizontally across the array. However, the signals for inverse velocities greater than about 80-100 ms/km have fairly long path lengths within the inhomogeneous crustal structure, and these signals are generally too distorted to be used for coherent array processing over even moderate apertures. Inverse velocities below 80 ms/km correspond approximately to P-waves from events at greater than 30 geocentric degrees from the array. P-waves having paths which just graze the core region in propagating from the source to the array have inverse velocities of approximately 40 ms/km, and correspond to events

at approximately 95 geocentric degrees. Inverse velocities of less than 40 ms/km correspond to waves which propagate through the core or reflect from the mantle-core interface. Generally the inverse velocity range 40-80 ms/km is regarded as the primary region of interest for P-waves, and is referred to as the teleseismic P-wave region. However, the so-called core phases (less than 40 ms/km) are also of considerable interest for geophysical research.

For shear waves (S-waves), and for the Rayleigh and Love waves which propagate through the crust, the velocity of propagation at the array is approximately 3.5 km/sec. Hence, the maximum inverse velocity is about 286 ms/km. Also, the teleseismic region for S-waves is approximately 69-137 ms/km.

The frequency range of interest for P-waves is generally less than 3 Hz, so that a wavenumber of 0.50 km^{-1} may be regarded as an upper bound in \vec{k} -space. Also, if the shortest periods of interest for Rayleigh and Love waves are assumed to be 17 seconds, then the upper boundary in \vec{k} -space is approximately 0.017 km^{-1} . These boundaries are illustrated in Figure 2-4.

Using a spherically-stratified earth model based primarily on the data of Jeffreys and Bullen [2-8], a one-to-one mapping may be established between points in the \vec{u} -space teleseismic P-wave region and the geographic source locations of the corresponding events. Hence, an inverse velocity map of the earth's teleseismic region relative to a particular array may be produced. Figure 2-5 shows such a map relative to the NORSAR array location, and also indicates the approximate size of the 3 dB and 9 dB NORSAR beam contours in \vec{u} -space.

As described in Section 5.2, the array surveillance problem consists essentially of forming a set of beams having aiming points which are

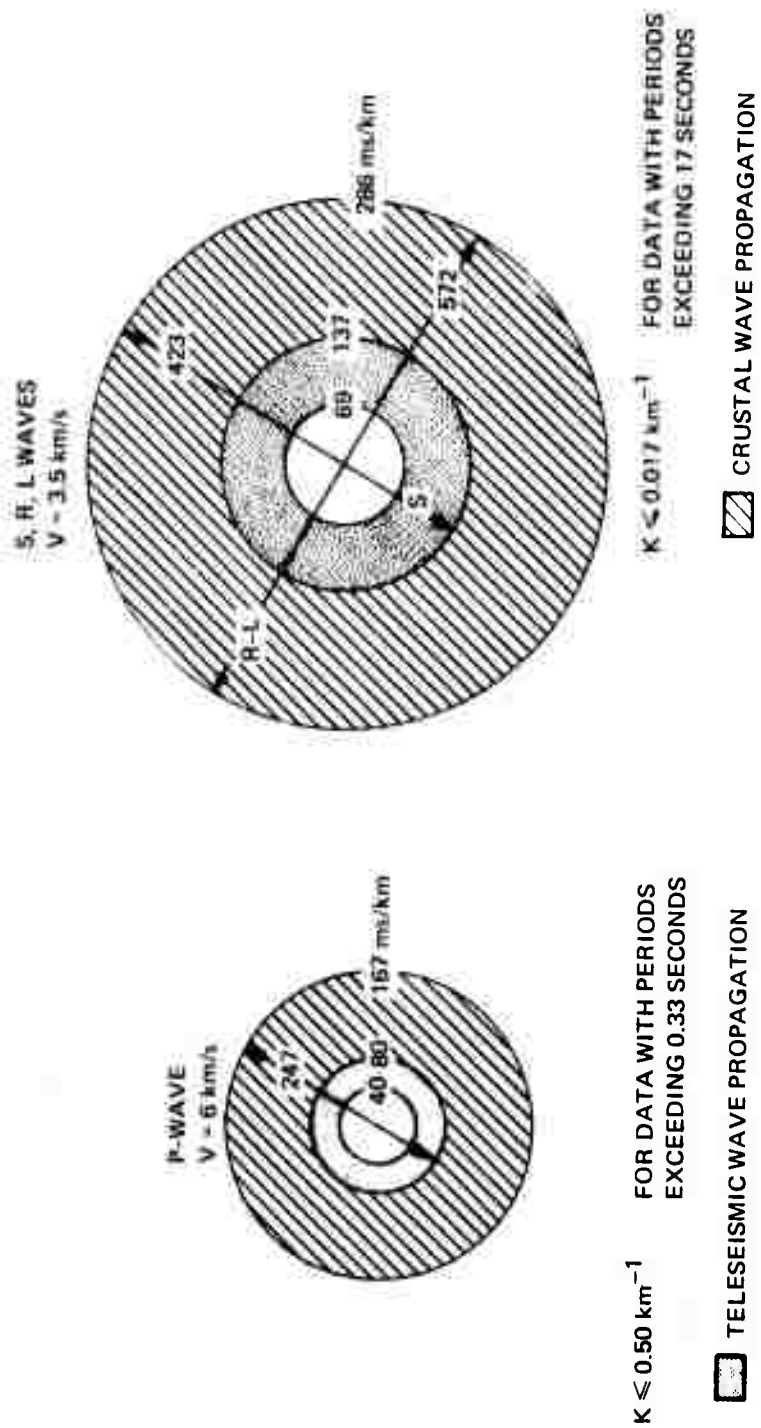


Figure 2-4. Principal Inverse Phase Velocity Region

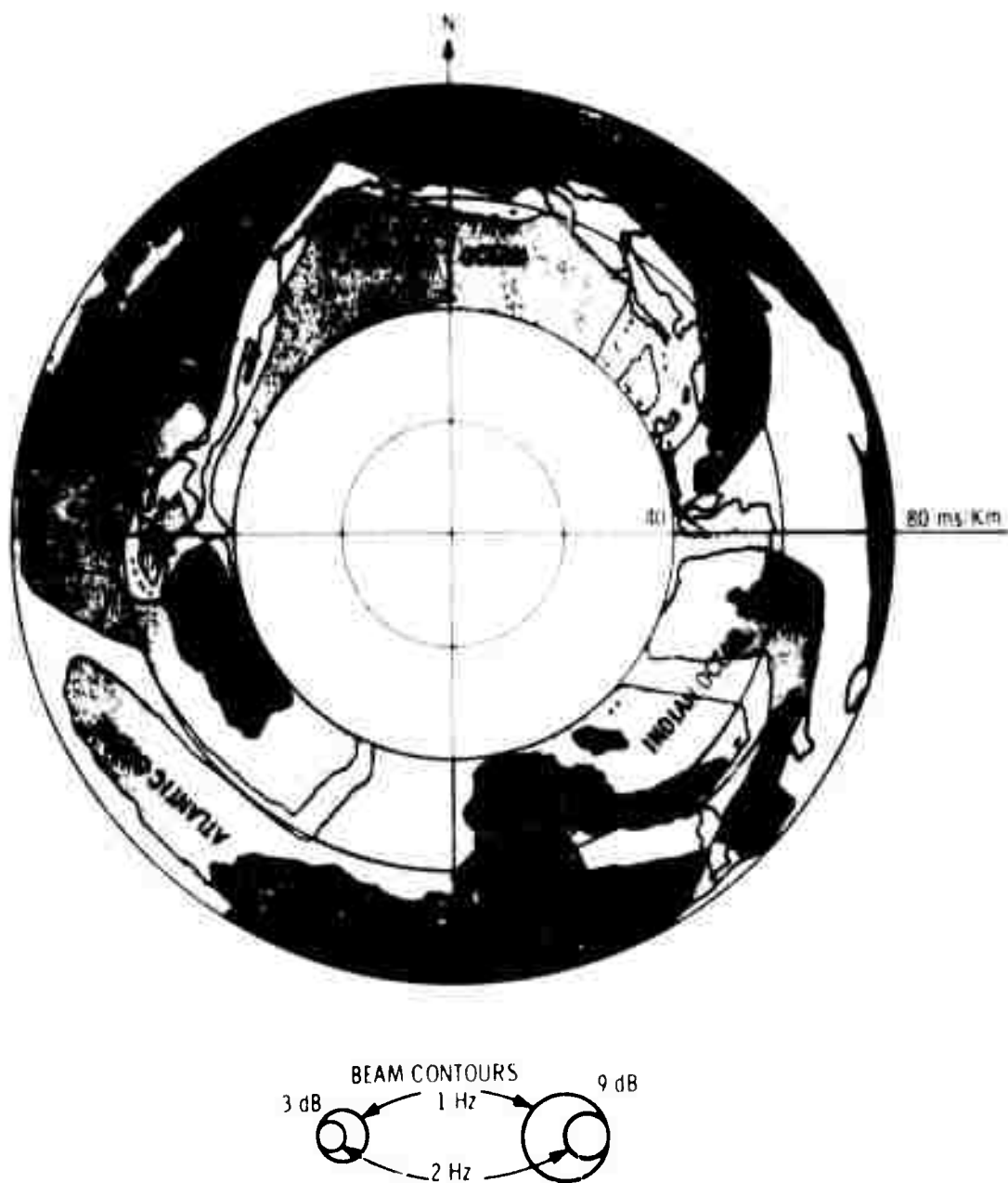


Figure 2-5. Norway Inverse Velocity Space Map of the World

situated in \vec{u} -space to provide adequate coverage of the regions of interest, and performing detection processing and other types of signal analysis on the resulting beam signals.

2.1.4 Array Beam Pattern Optimization

For a given array design there may be certain side lobes which enhance undesirable signals when the array is steered in a particular direction. By a slight adjustment of the seismometer locations, it should be possible to reduce these side lobes to acceptable levels. Mathematically the problem is stated as follows. We are given initial locations for N seismometers; \vec{r}_j (x_j and y_j) specify the position of the j th seismometer. The positions of M points, which are responsible for high side lobes, are given in \vec{u} -space by \vec{u}_p (u_{px} and u_{py}) related to the seismometer positions by

$$G_p = \left| \frac{1}{N} \sum_{j=1}^N \exp (i\omega \vec{u}_p \cdot \vec{r}_j) \right|^2$$

The objective is to calculate new values for \vec{r}_j so that the gain terms are reduced. The importance of the gain terms is relative, some being more important than others. A weighting term W_p is assigned to each G_p , expressing the relative importance. The greater W_p , the more G_p must be reduced.

The effectiveness of any minimization process must be judged by some performance index or criterion so that a figure of merit can be associated with each array placement. One of the most frequently used criterions is the weighted sum of the squares of the terms to be minimized. This approach also yields readily to mathematical techniques. Therefore, we define our performance criterion as:

$$C = W_1 G_1^2 + \dots + W_M G_M^2 = \sum_{P=1}^M W_P G_P^2$$

The performance criterion C is a function of the parameters \vec{r}_j , $j=1, 2, \dots, N$. These parameters are adjusted to make C small. This is accomplished by the gradient method; i.e., x_j and y_j are moved in the direction which decreases C . This direction is defined by the negative gradient of C :

$$-\text{GRAD}_x = \frac{-\partial C}{\partial x} = \frac{-\partial C}{\partial x_1}, \frac{-\partial C}{\partial x_2}, \dots, \frac{-\partial C}{\partial x_N}$$

$$-\text{GRAD}_y = \frac{-\partial C}{\partial y} = \frac{-\partial C}{\partial y_1}, \frac{-\partial C}{\partial y_2}, \dots, \frac{-\partial C}{\partial y_N}$$

The movement of the j th instrument in one iteration is proportional to the gradient

$$\Delta x_j = -L \frac{\partial C}{\partial x_j}$$

$$\Delta y_j = -L \frac{\partial C}{\partial y_j}$$

The coefficient L is chosen so that in one iteration the movement of the instruments is less than some maximum allowable step. The instrument which is the most sensitive, which has $[(\frac{\partial C}{\partial x_j})^2 + (\frac{\partial C}{\partial y_j})^2]^{1/2}$ the largest, is moved the maximum distance, Δ . The coefficient of motion is thus defined as:

$$L = \Delta / \max_j [(\frac{\partial C}{\partial x_j})^2 + (\frac{\partial C}{\partial y_j})^2]^{1/2}$$

So, in general, the j th instrument is moved a distance:

$$D_j = \frac{\Delta [(\frac{\partial C}{\partial x_j})^2 + (\frac{\partial C}{\partial y_j})^2]^{1/2}}{\max_j [(\frac{\partial C}{\partial x_j})^2 + (\frac{\partial C}{\partial y_j})^2]^{1/2}}$$

A mathematical expression for the gradient of the entire array is given as follows.

$$-\text{GRAD} = \begin{bmatrix} -\text{GRAD}_x \\ -\text{GRAD}_y \end{bmatrix} = \begin{bmatrix} -\partial C / \partial x \\ -\partial C / \partial y \end{bmatrix}$$

For an individual instrument the gradient is:

$$-\text{GRAD}_j = \begin{bmatrix} -\partial C / \partial x_j \\ -\partial C / \partial y_j \end{bmatrix} = \begin{bmatrix} -2 \sum_{P=1}^M W_P G_P \partial G_P / \partial x_j \\ -2 \sum_{P=1}^M W_P G_P \partial G_P / \partial y_j \end{bmatrix}$$

or

$$-\text{GRAD}_j = -2 \sum_{P=1}^M W_P G_P \begin{bmatrix} \partial G_P / \partial x_j \\ \partial G_P / \partial y_j \end{bmatrix}$$

The relationship of G_P to y_j and x_j is given by:

$$G_P = \vec{R}_P \cdot \vec{R}_P$$

where

$$\vec{R}_P = \frac{1}{N} \sum_{j=1}^N \exp (i \omega \vec{u}_P \cdot \vec{r}_j)$$

Then

$$\frac{\partial G_P}{\partial x_j} = 2 \vec{R}_P \cdot \frac{\partial \vec{R}_P}{\partial x_j}$$

$$\frac{\partial G_P}{\partial y_j} = 2 \vec{R}_P \cdot \frac{\partial \vec{R}_P}{\partial y_j}$$

The partial derivatives of R_p are:

$$\frac{\partial \vec{R}_p}{\partial x_j} = \frac{i\omega u_p}{N} \exp(i\omega \vec{u}_p \cdot \vec{r}_j)$$

$$\frac{\partial \vec{R}_p}{\partial y_j} = \frac{i\omega u_p}{N} \exp(i\omega \vec{u}_p \cdot \vec{r}_j)$$

Substituting for R_p and its partials, we obtain:

$$\frac{\partial G_p}{\partial x_j} = \frac{2\omega}{N^2} \left[\sum_{j=1}^N \exp(i\phi_{pj}) \right] \cdot \left[\exp(i\phi_{pj}) \right]_{x}; \text{ where: } \phi_{pj} = \omega (\vec{u}_p \cdot \vec{r}_j)$$

$$\frac{\partial G_p}{\partial y_j} = \frac{2\omega}{N^2} \left[\sum_{j=1}^N \exp(i\phi_{pj}) \right] \cdot \left[\exp(i\phi_{pj}) \right]_{y} u_{py}$$

The gradient finally becomes for the j th instrument:

$$-\text{GRAD}_j = \frac{-4\omega}{N^2} = \sum_{p=1}^M W_p G_p \left[\sum_{j=1}^N \exp(i\phi_{pj}) \cdot \exp(i\phi_{pj}) \right] \vec{u}_p$$

The j th seismometer is moved in the direction given by $-\text{GRAD}_j$. As previously stated,

$$D_j = \frac{-\Delta \text{GRAD}_j}{\max_j |\text{GRAD}_j|}$$

where now D_j is the displacement vector for the j th seismometer.

Repeated application of this algorithm will shift the location of the elements to reduce the array signal gain at the designated points in \vec{u} -space. The increment of motion need not be proportional to the magnitude of the gradient but may be specified so that all elements are moved an

equal distance. The distance should be reduced to zero as the gradient becomes very small to avoid hunting. Constraints may also be included in the program to prevent locating elements with less than a specified minimum spacing or at forbidden coordinates in geographic space.

When a point in the \vec{u} -space beam pattern contour is depressed, it is probable that other areas of the contour will rise; hence, it is desirable to furnish a grid of weighted points on the contour that are to be maintained below a specified level. When this is implemented, local minimums may exist and it is possible that no improvement is obtained.

This technique does not in general provide a unique solution to the element placement in a planar array; however, it does provide a method of improving an existing design.

2.2 NORSAR DESIGN*

The basic NORSAR design objective was to construct a combined long-period and short-period seismic array north of Oslo, Norway, for the purpose of gathering data for automatic detection and analysis of seismic events with reasonable resolution and accuracy. Based on considerations of the NORSAR inverse velocity map (Figure 2-5), and of the size and location of the significant regions of seismic activity, it was determined that a main beam radius of approximately 0.002 seconds/kilometer in inverse velocity space (which corresponds to a radius of 0.003 km^{-1} at 1.5 Hz. in wavenumber space) would provide adequate resolution. This choice led eventually to the selection of the 100 km NORSAR array diameter.

*The NORSAR design described in this section was developed jointly by J. H. Than and T. Johansen of A/S Tele-Plan, Lysaker, Norway, and by IBM personnel.

Additional NORSAR design objectives, assumptions and constraints included the following:

- a. The desired short period detection threshold should be consistent with LASA at 40° to 80° range distances. This objective may be tempered by economic considerations should the existing noise field require the use of an excessive number of sensors.
- b. The array should be adapted to fit the site and operate online to provide continuous surveillance.
- c. The horizontal wave number range of interest is equal to or less than 0.50 cycles/km for the short-period (SP) instruments and equal to or less than 0.017 cycles/km for the long period (LP) instruments.
- d. Frequency dispersion across the array is negligible.
- e. Meteorological disturbances in the North Atlantic Ocean produce strong, coherent signals with an energy peak corresponding to a wave number of about 0.017 cycles/km. This energy is primarily Rayleigh waves with a 17-second period propagating at a velocity of approximately 3.5 km/s. The long-period (LP) array should provide reasonable suppression of this noise for beam aiming points of considerable interest.
- f. Both the LP and SP arrays must be omnidirectional.
- g. The propagation velocity of signals is uniform over the array aperture and independent of azimuth.
- h. The array should utilize the existing subarray installed at Oyer.

Preliminary designs for the NORSAR long-period array developed by Lincoln Laboratories [2-7] and by AFTAC [2-6] were initially considered, and the best of these were selected as a starting point, as described in Section 2.2.1. The evolution of the final NORSAR design from these initial configurations is summarized in Section 2.2.4, and is described in detail in [2-1, Appendix I].

Section 2.2.2 presents a detailed analysis of the regular hexagonal array configuration, and serves to illustrate significant relationships between array geometry and beam pattern side-lobe structure. A brief example of a data acquisition cost versus array performance tradeoff comparison between two array configurations is given in Section 2.2.3. Finally, Section 2.2.5 presents some empirical evidence that short-period array beam pattern design objectives were met.

2.2.1 Initial Array Design Comparisons

One candidate LP array was a filled, regular hexagon with 19 instruments. The corresponding SP array was formed by locating the SP instruments in 19 hexagonal subarrays. The center element of each subarray was collocated with an LP instrument. This array geometry was modified to the proposed Norway site by making small deviations from the regular hexagonal geometry as shown in Figure 2-6. In this illustration each x represents a SP instrument. Another candidate geometry was a filled heptagon of 22 elements as the LP configuration with a filled pentagon of six instruments for the SP subarray as shown in Figure 2-7. The power response patterns for the modified hexagon and the heptagon-pentagon are shown respectively in Figures 2-8 and 2-9. The two dimensional contour plots shown in Figures 2-8 and 2-9 were collapsed to plots of a single variable in Figures 2-10 and 2-11. The abscissa of these plots represents the distance in wavenumber from the center of the main lobe, and the value of the curve is the maximum power response value found at that distance from the origin on the corresponding two-dimensional plots. Figures 2-12 and 2-13 show similar curves for the SP arrays. These figures show that a better SP response pattern, within the horizontal wavenumber region up to $240 \times 10^{-3}/\text{km}$, results from the heptagon-pentagon geometry, whereas Figures 2-10 and 2-11 indicate that the LP array performance for this geometry is also superior to that of the filled hexagon.

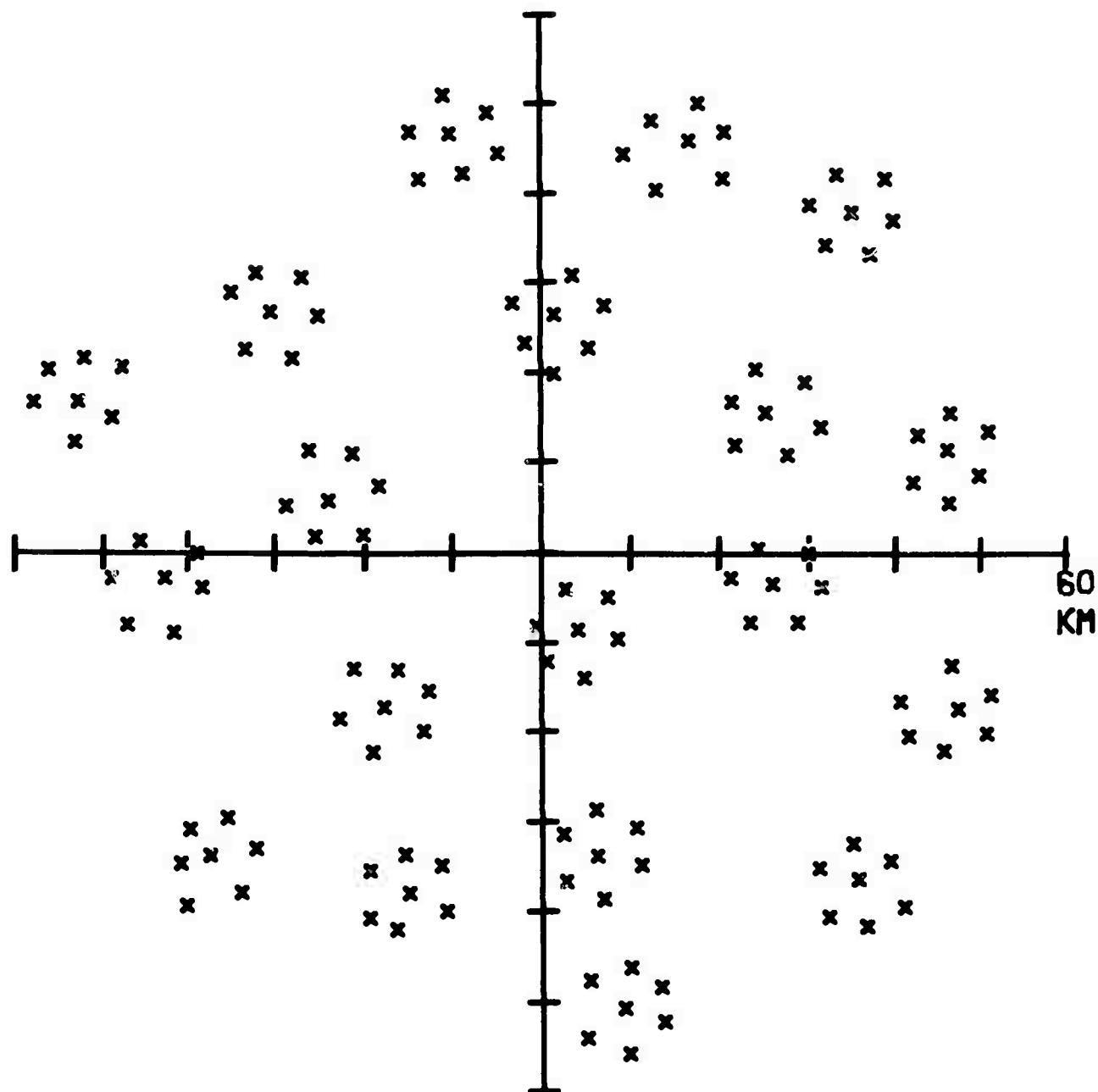


Figure 2-6. Hexagon Subarray Geometry Modified to Fit Site

RELATIVE ARRAY COORDINATES

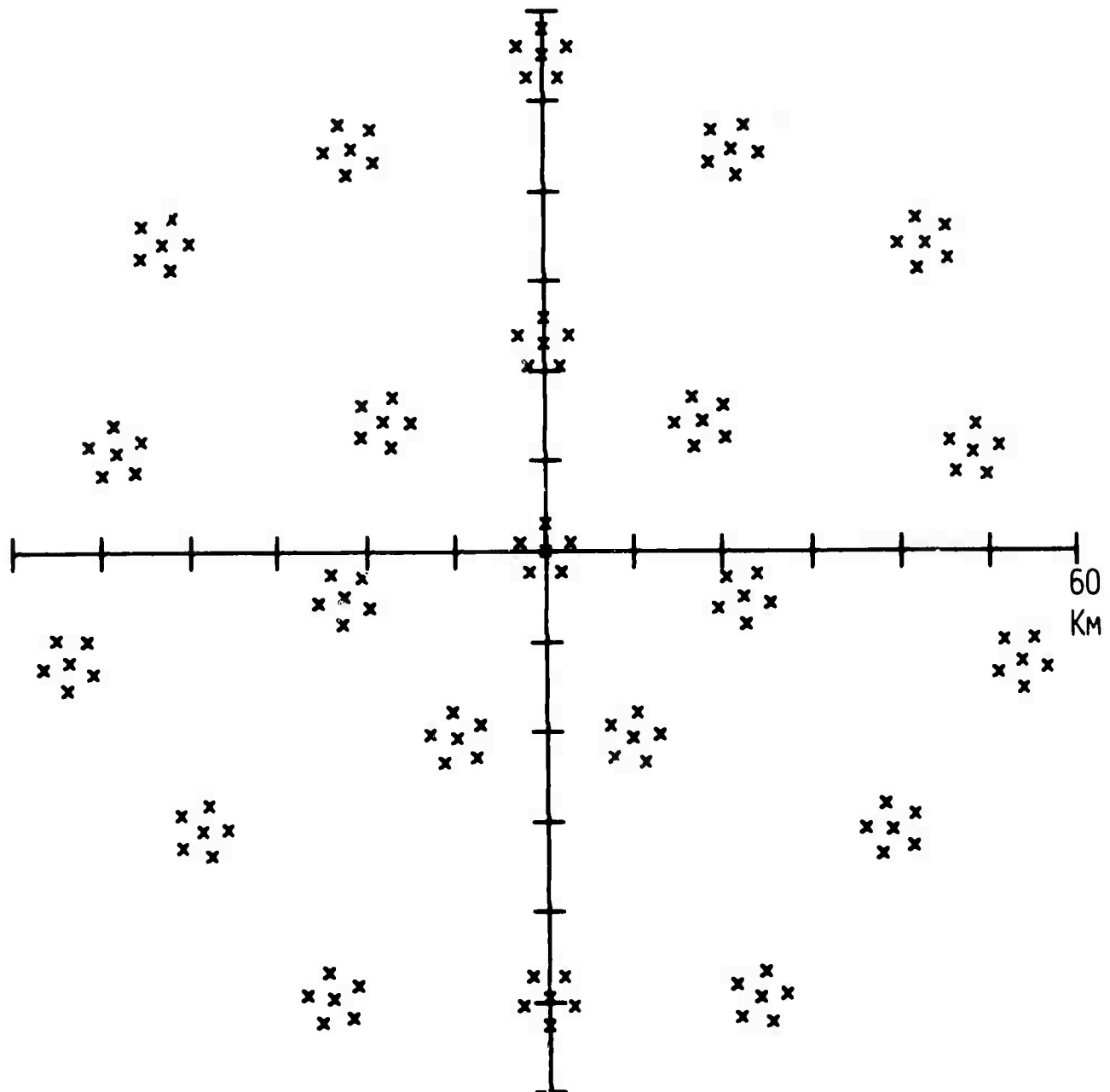
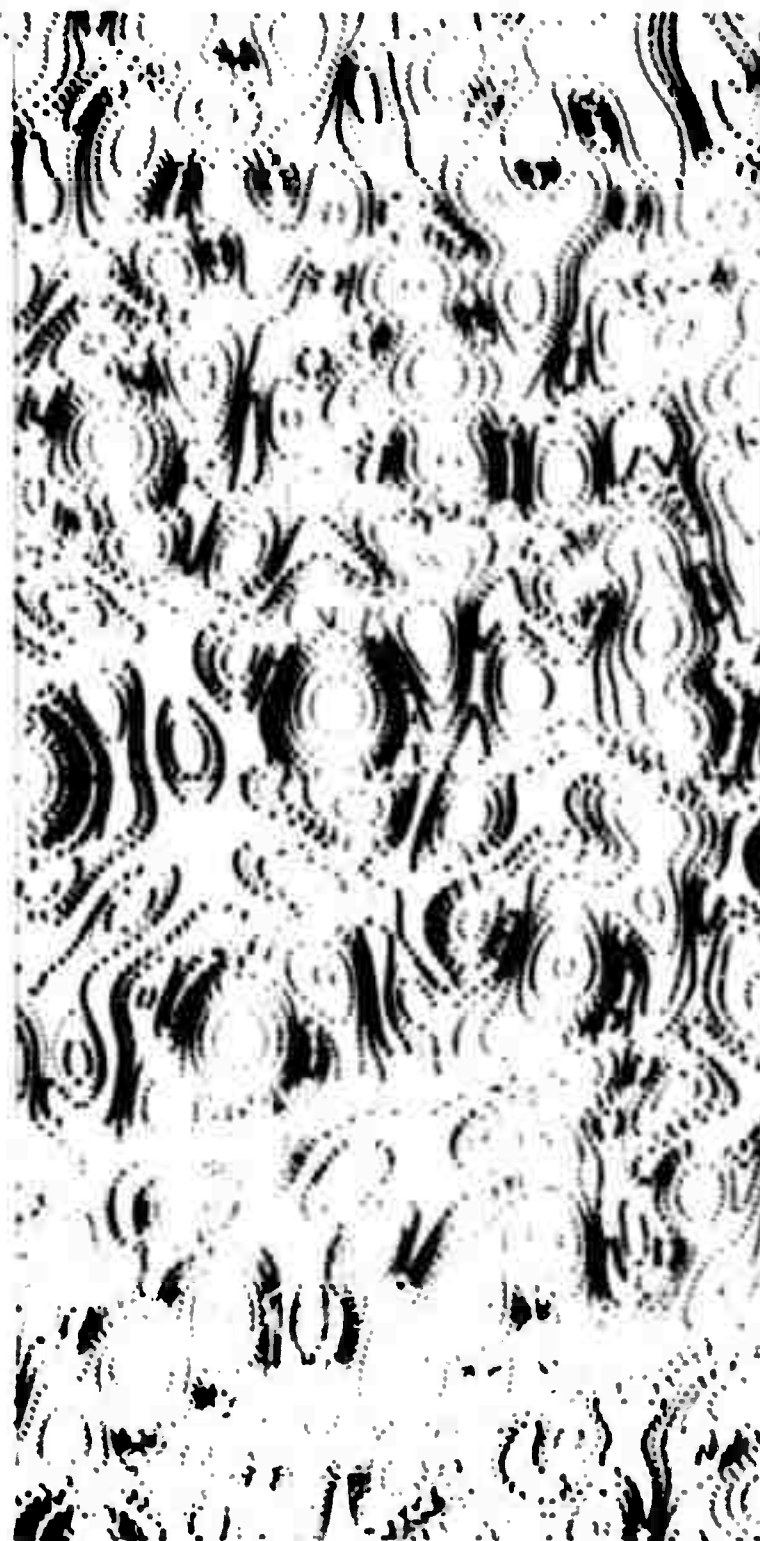


Figure 2-7. Hapteen-Pentagon Array Geometry



Loss	Contour
1	1.0
2	2.0
3	3.0
4	4.0
5	5.0
6	6.0
7	7.0
8	8.0

Figure 2-8. Modified Hexagon Array Loss Contour

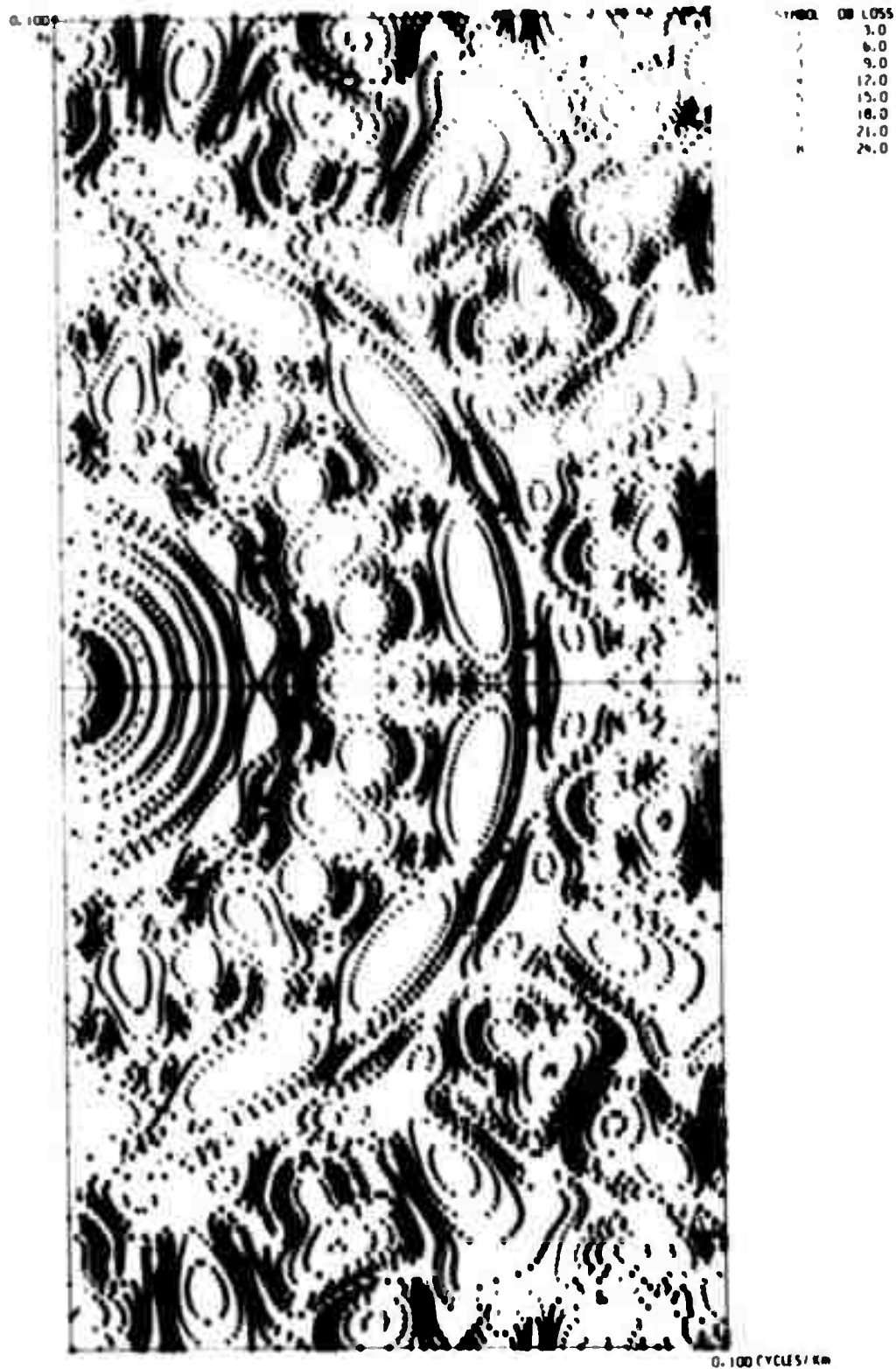


Figure 2-9. Filled Heptagon Array Loss Contour

MODIFIED NORWAY ARRAY PATTERN (L.P.) 19 ELEMENTS

RESOLUTION $10^{-3}/\text{km}$

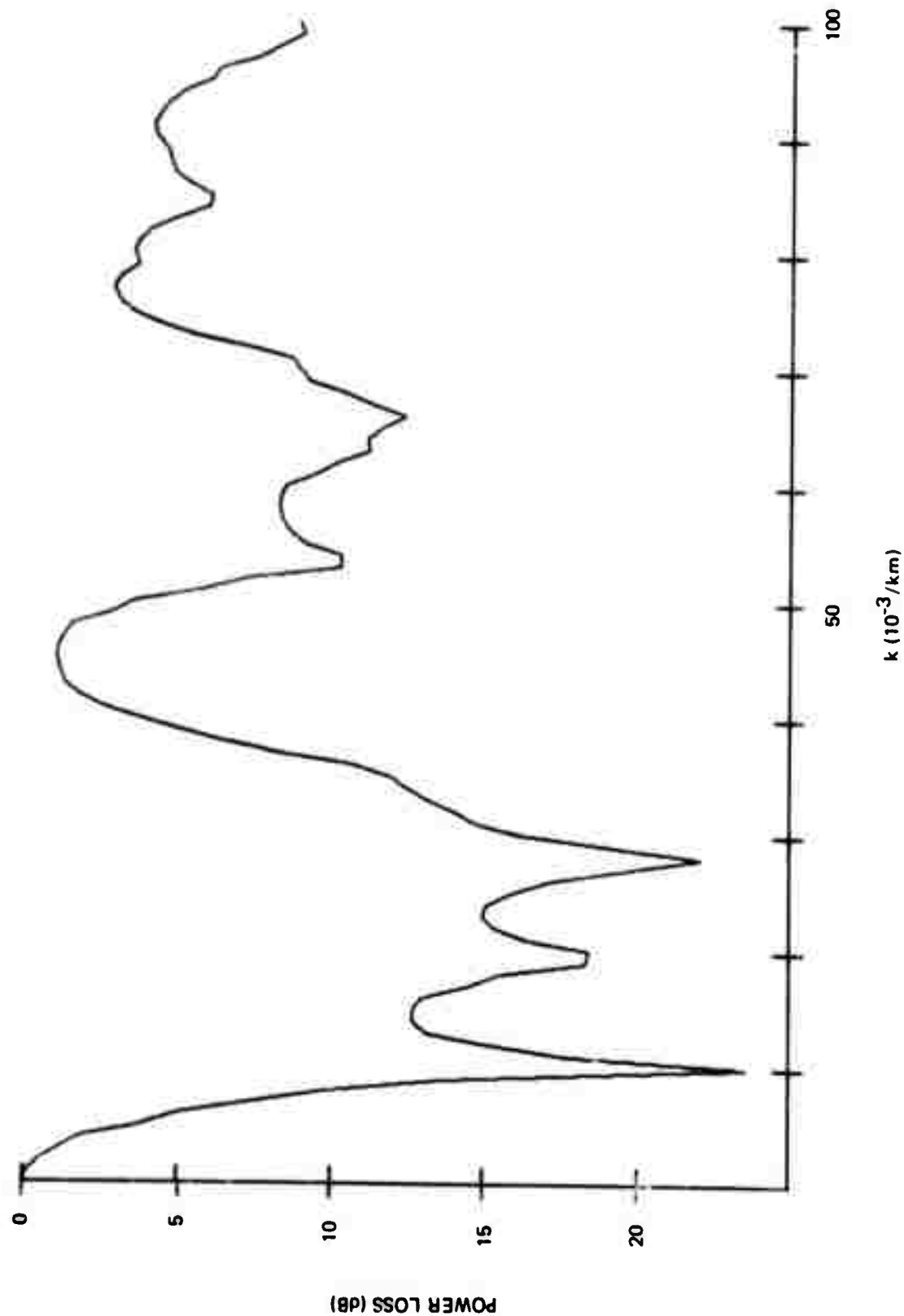


Figure 2-10. Modified Hexagon Array LP Beam Pattern-Worst Case

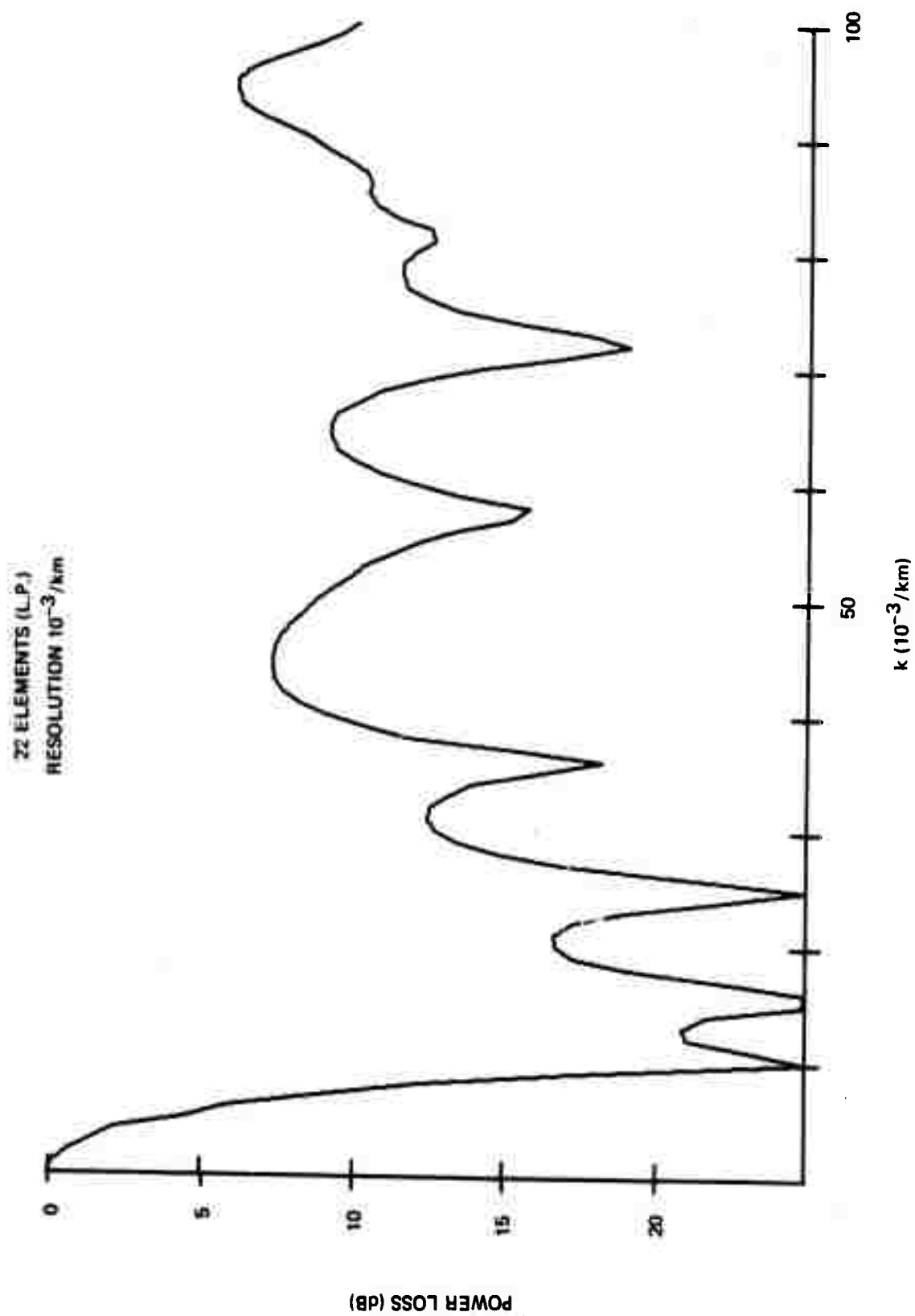


Figure 2-11. Filled Heptagon LP Beam Pattern—Worst Case

133 ELEMENTS RESOLUTION $4 \times 10^{-3}/\text{km}$

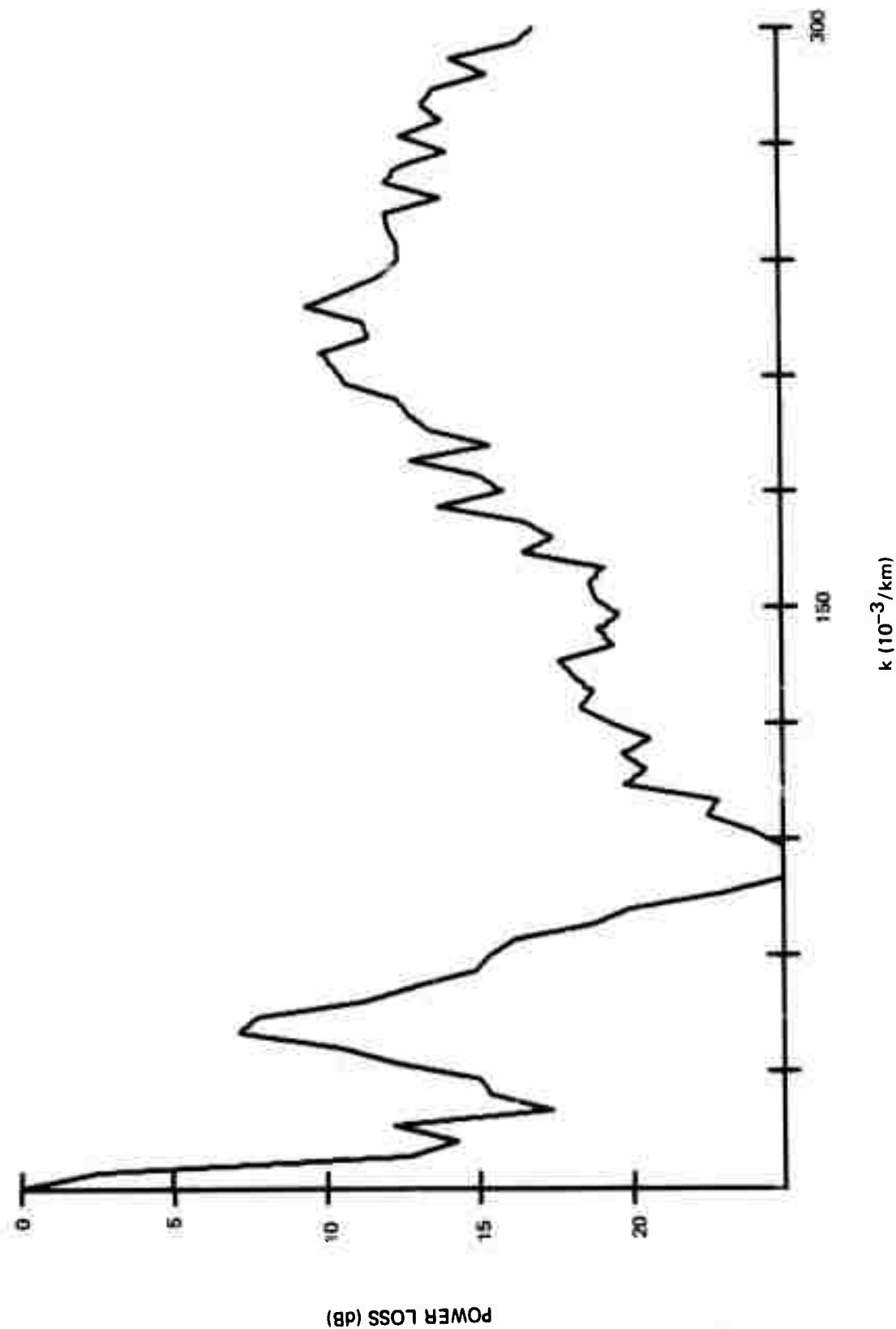


Figure 2-12. Modified Hexagon Array SP Beam Pattern-Worst Case

132 ELEMENTS RESOLUTION $4 \times 10^{-3}/\text{km}$

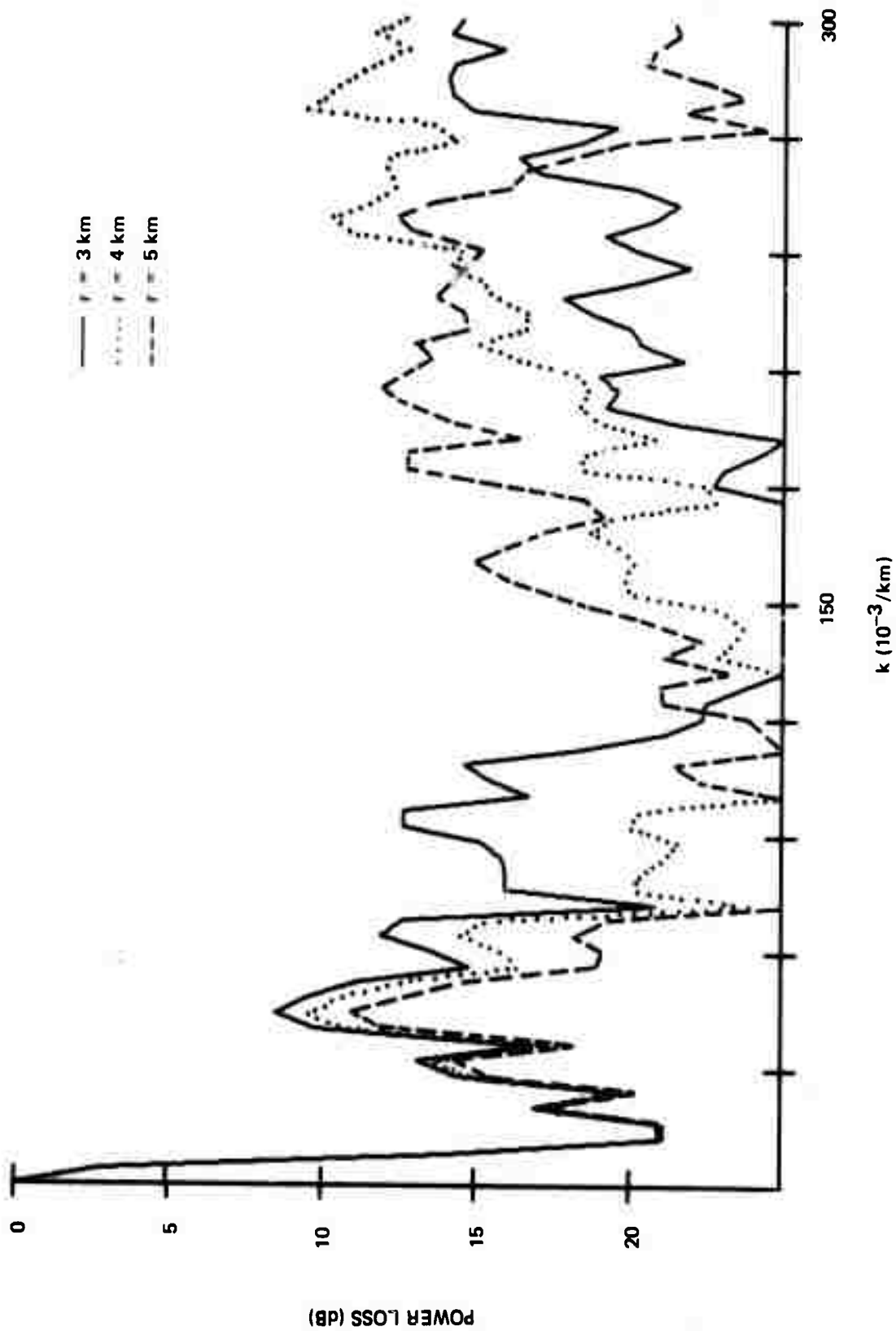


Figure 2-13. Twenty-two Filled Heptagon with Pentagon Subarrays—Worst Case Beam Pattern (for various values of minimum sensor spacing r)

2.2.2 Analysis of Regular Hexagon Configuration

In order to provide some insight into the side-lobe structure of a complex array beam pattern, this subsection presents an analysis of the beam pattern for a regular hexagonal array configuration. For the values of wave number being considered, of the various configurations investigated, the filled regular hexagon has a better LP side-lobe pattern than the other regular geometric figures having 20 or less instruments. For the regular hexagon the interelement spacing must be determined from the known range of wave number and the acceptable side-lobe level. Principal maxima will occur on the k-space loss contours of this configuration in a regular pattern; i.e., at discrete azimuths principal maxima will occur for

$$k = \left[(3)^{1/2} R \right]^{-1} \left[3a^2 + (2b-a)^2 \right]^{1/2}$$

where a and b are integers and R is the interelement spacing. The smallest non-zero value of k at the locus of a principal maximum is readily seen to be

$$k = \frac{1.155}{R}$$

If array beams are steered at $k \leq 0.577/R$, a side-lobe having zero dB loss will not occur within this deployment area. For a maximum frequency of 0.06 Hz and a minimum horizontal phase velocity of 3.5 km/s, the maximum value of k would be about 0.017 cycles/km, and therefore $R < 33.8$ km.

It is desirable to maintain the side-lobe level well below zero dB and a level of -13 dB, $(-10 \log_{10} N)$, is deemed acceptable. The beam loss contours for the regular hexagon are below -13 dB everywhere except in

the vicinity of the principal maxima. The smallest value of k at the locus of a -13 dB contour (other than the -13 dB contour about the origin) can be expressed as:

$$k = \frac{1.155}{R} - k' \text{ cycles/km}$$

where k' corresponds to the locus of the -13 dB contour about the origin. For values of kR less than 0.30, the loss contour is essentially independent of azimuth. The value of k' can be found by obtaining the smallest positive real root of the equation:

$$-13\text{dB} = 20 \log_{10} \frac{1}{19} |5 + 8\cos\sqrt{3}\pi k' R + 6\cos^2 \sqrt{3}\pi k' R|.$$

The smallest positive real root is $k' = \frac{0.21}{R}$. Hence, the worst case side-lobe will not exceed -13 dB if the array is steered for $k \leq (1.155 - 0.21)/2R$. Assuming the maximum value of k for which the array is to be steered is 0.017 cycles/km, the interelement spacing, R , must be equal to or less than 27.6 km for the worst case side-lobe pattern to be down at least 13 dB.

The SP instruments are to be dispersed throughout the array by constructing a subarray associated with each LP instrument. If the subarrays are identical, and each is situated with its geometric center at the locus of the corresponding LP instrument, the array pattern can be obtained by the technique of pattern multiplication. For a 7 element regular hexagon (subarray configuration), the power reduction achieved is

$$-20 \log_{10} \frac{1}{7} |3 + 4\cos \sqrt{3}\pi k r| \text{ (dB)}$$

where r is the interelement spacing in km, and k is the horizontal wave number. For small values of kr the subarray loss contour is essentially independent of azimuth ($kr < 0.30$). When $k = \frac{2}{\sqrt{3}R}$ (the smallest non-zero

value of k which is the locus of a principal maximum of the regular hexagon LP array) the array performance is equal to the SP array power rejection only:

$$\text{SP Array Power Rejection} = 20 \log_{10} \frac{1}{7} \left| 3 + 4 \cos \frac{2\pi r}{R} \right| \text{ (dB)}$$

From this it is evident that the regular hexagon subarray will require a relatively large aperture if this side-lobe is to be maintained at an acceptable level; i.e., for -10 dB side-lobe, $\frac{r}{R} = 0.283$.

2.2.3 Relative Costs of Array Configurations

Although the fixed costs per instrument in the LP and SP arrays are significant, they can be omitted from array cost comparison since they are independent of the array configuration. The principal variation in array cost with array configuration is due to subarray electrical cable and trenching costs. These costs are compared graphically in Figure 2-14, which shows the relative array cost of the hexagon array configuration and the heptagon array as a function of interelement spacing. The major side-lobe level of each array is also plotted as a function of interelement spacing. Although the cable and trenching costs for the regular heptagon are slightly higher than the hexagon, for a given element spacing, the same array performance can be achieved by the heptagon array with much smaller element spacing. For a major side-lobe level of -9 dB, the 4 km heptagon element spacing must increase to 8 km spacing in the hexagon. The corresponding relative costs are 121 for the heptagon versus 150 for the hexagon.

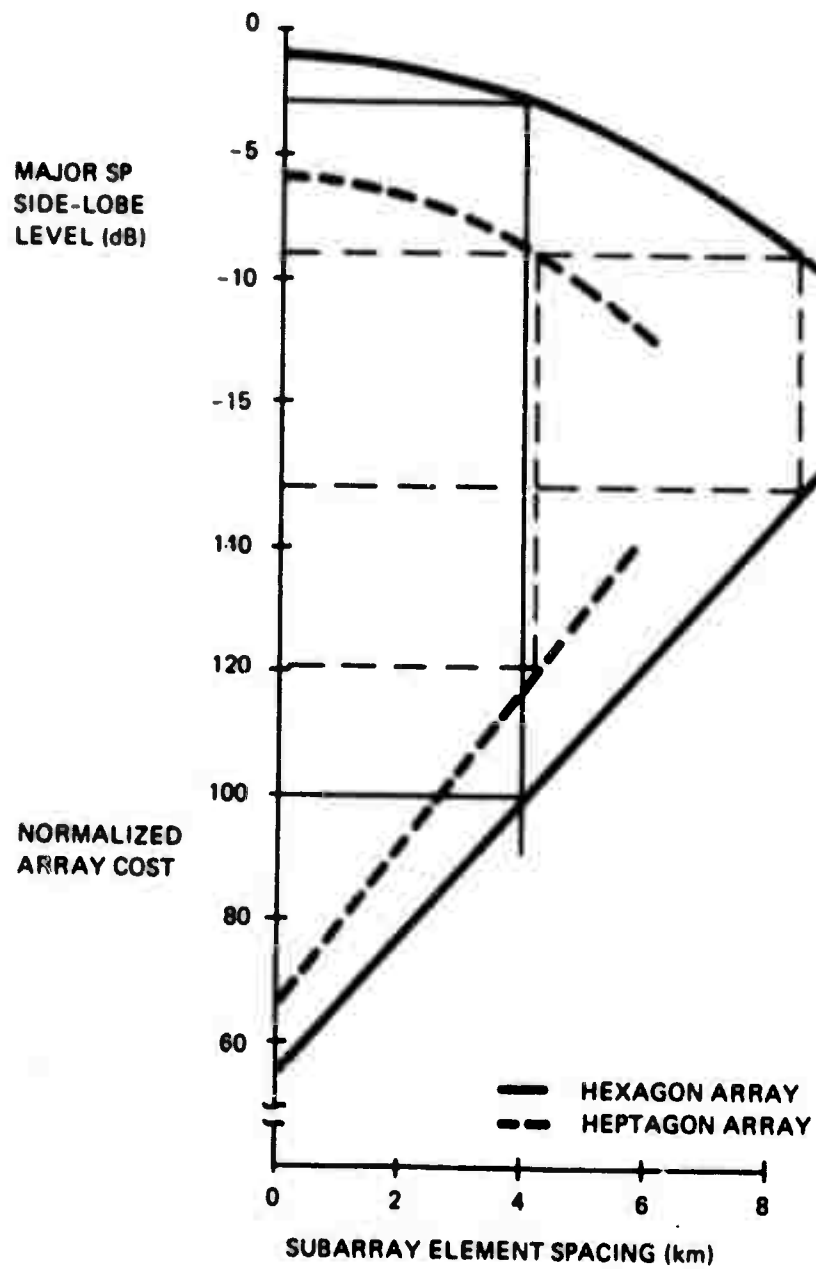


Figure 2-14. Cost Performance Tradeoff

2.2.4 NORSAR Design Evolution

When the heptagon-pentagon array was fitted to the Norwegian site, some initial deviations from the idealized positions were necessary. The resulting intermediate geometry also included the long-period instrument previously installed near Oyer.

As site survey data became available, additional subarray movement became necessary, modifying the geometry to accommodate the site geography and to improve the side-lobe pattern of both the LP and SP arrays. Certain instruments were maintained at the location previously specified to avoid relocating them in unsuitable areas. The initial step was to optimize the LP side-lobe pattern by reducing the array gain at a number of azimuths for values of horizontal wave number. The SP array was then optimized by reducing the SP array gain at a number of azimuths for values of horizontal wave number in the range of 30 to 55 mcycles/km. Each subarray consisted of five SP instruments, equally spaced on the circumference of a circle with a 4 km radius, and one SP instrument in the center. The subarray centers were allowed to shift either zero or 4 km so that one LP instrument associated with the subarray could be collocated with one of the SP instruments. The SP instrument locations for subarrays 01A, the B ring, 10C, and 14C were in areas of the site which afforded very little freedom to alter their locations due to local geographic restrictions. The subarray at 01C had been installed and was therefore not free to move. The LP instrument location within these subarrays, except for 01C, was collocated with the SP instrument which resulted in the lowest LP side-lobe level, as determined by the optimization program. The remaining 11 instruments were shifted in 0.2 km increments from their idealized locations in accordance with the direction of the sensitivity vectors computed by the computer program. The sensitivity vectors were computed for the set, S, of 112 points on the loss contour given by

$$S = \left\{ (k_x, k_y) : 0 \leq k_x, 4 \mid (k_x - 2), 4 \mid (k_y - 2), 12 \leq \sqrt{k_x^2 + k_y^2} \leq 36 \right\}$$

where k_x and k_y are the east and north components of the horizontal wave number in mcycles per km. After 50 program iterations, the 11 instruments were shifted an average of less than 2km each, providing an LP worst case side-lobe level down more than 15 dB everywhere in the region of k-space from 12 to 36 mcycles/km.

The eleven associated SP arrays were optimized using the same procedure. Two additional subarray locations, 3C and 8C, were fixed, to avoid neighboring water. The known subarray center locations of the 13 fixed subarrays were entered into the program along with the LP location of the remaining nine subarrays. The nine movable subarray centers were shifted from the location of the LP instrument in uniform steps of 0.2 km in the direction of the sensitivity vectors computed by the program. The sensitivity vectors were computed for the set, S' , of 150 points on the loss contour given by

$$S' = \left\{ (k, \theta) : 30 \leq k \leq 55, 5 \mid k, 0^\circ \leq \theta \leq 180^\circ, 10 \mid \theta \right\} \cup \left\{ (k, \theta) : k = 47.5 \text{ or } k = 52.5, 5^\circ \leq \theta \leq 175^\circ, 10 \mid \theta - 5 \right\}$$

where k is the horizontal wave number in mcycles per km and θ is the azimuth measured from North. After 22 program iterations the mean distance that the subarray centers were moved was approximately 4 km. This distance measured along the line joining the new location with the location of the corresponding LP instrument was rounded off to zero or 4 km. The new location was the center of the subarray. One SP instrument was located at this center point and five instruments equally spaced on the circumference of a circle with a 4 km radius. An LP instrument was collocated with the appropriate SP instrument either at the center or on the circumference of the subarray. The resulting SP worst case side-lobe pattern was down 8.5 dB everywhere in the k-space range of 30 to 55

mcycles/km. The actual NORSAR LP-SP array geometry after modifying the optimized geometry to avoid impossible locations is shown in Figure 2-15, and the corresponding beam response pattern in Δk -space is presented in Figure 2-16. The LP and SP worst-case beam patterns for the optimized array are given in Figures 2-17 and 2-18, respectively.

Figure 2-17 indicates a relative suppression of an interfering signal of at least 15 dB within a $0.009\text{-}0.036 \text{ km}^{-1}$ annulus concentric with the array beam aiming point. The worst side-lobe indicated by Figure 2-18 over the entire region of interest does not exceed approximately -8 dB.

When the LP array is steered to an azimuth of 34 degrees east of North, with an assumed propagation velocity of 3.5 km/sec, then the azimuthal beam patterns in Figure 2-19 are obtained at the frequencies indicated. These patterns indicate a low value of relative beam response for coherent energy propagating from the west, in the direction of the Atlantic Ocean and the Norwegian Sea.

Figure 2-20 indicates the relative insensitivity of the beam pattern to random displacements (instrument location errors) with a standard deviation of one km from the optimized array geometry.

2.2.5 NORSAR SP Beam Response Patterns

In order to analyze the actual beam response pattern of the NORSAR SP array, a computer program was developed to compute and plot the relative signal power on each detection beam during an event [2-2, Appendix I]. This program actually computes the maximum value of the waveform envelope for each beam over a specified time interval. These values are then plotted as a function of the \vec{u} -space distance from a specified point, which is generally either the aiming point of the beam having the

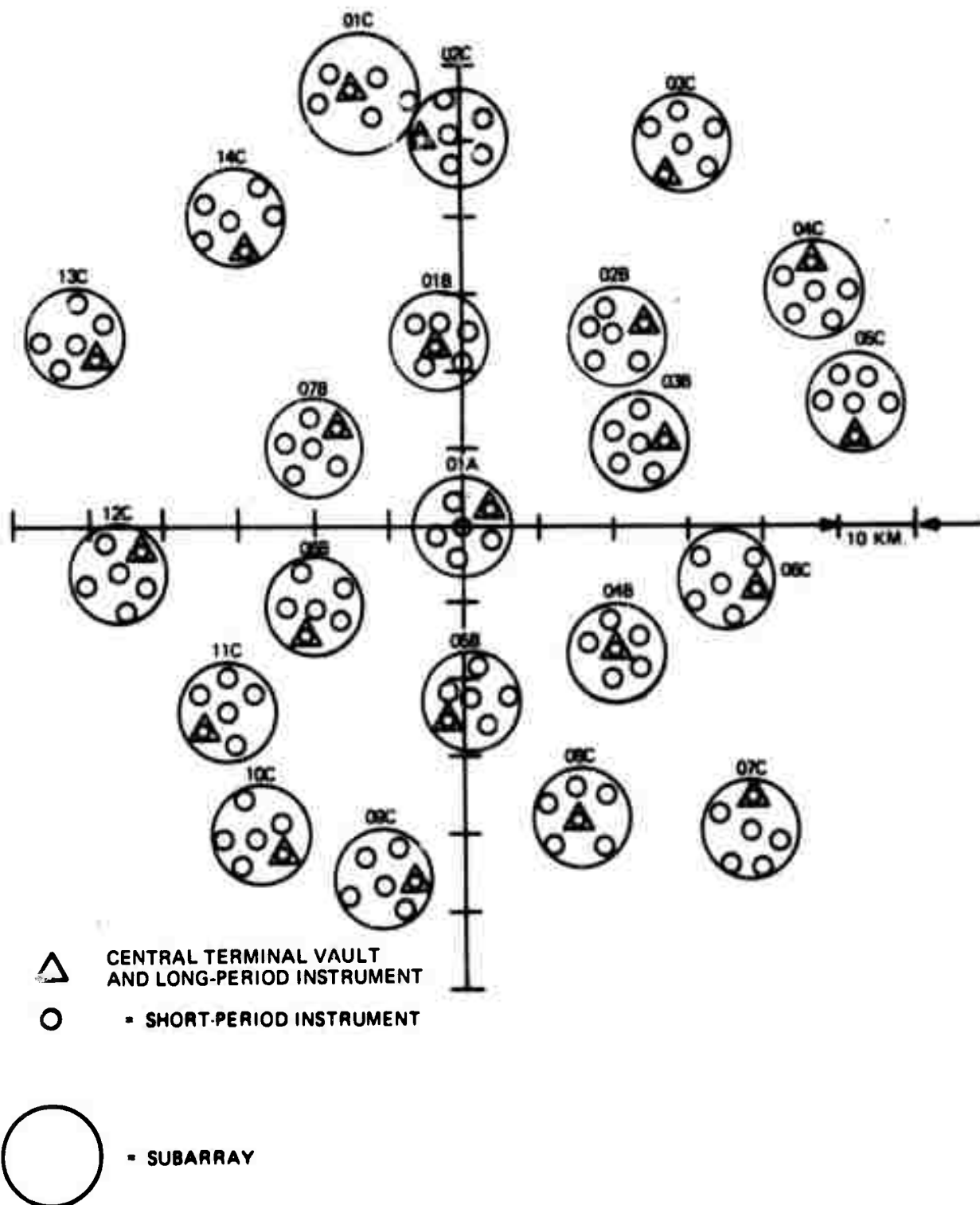


Figure 2-15. NORSAR System Array Geometry

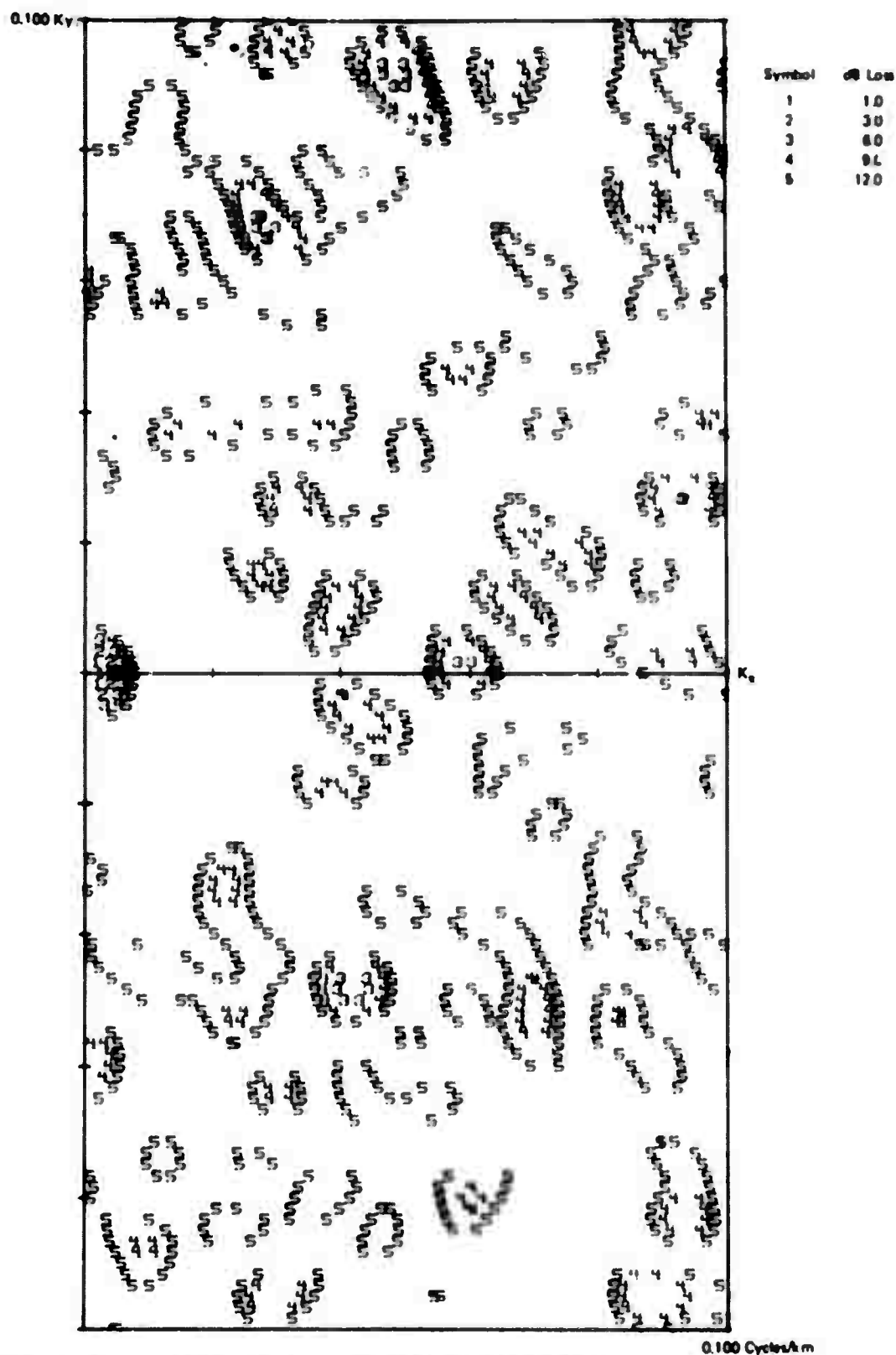


Figure 2-16. Optimized Array Beam Pattern Contours

NORWAY ARRAY 22 ELEMENTS RESOLUTION 1 mcycle/km

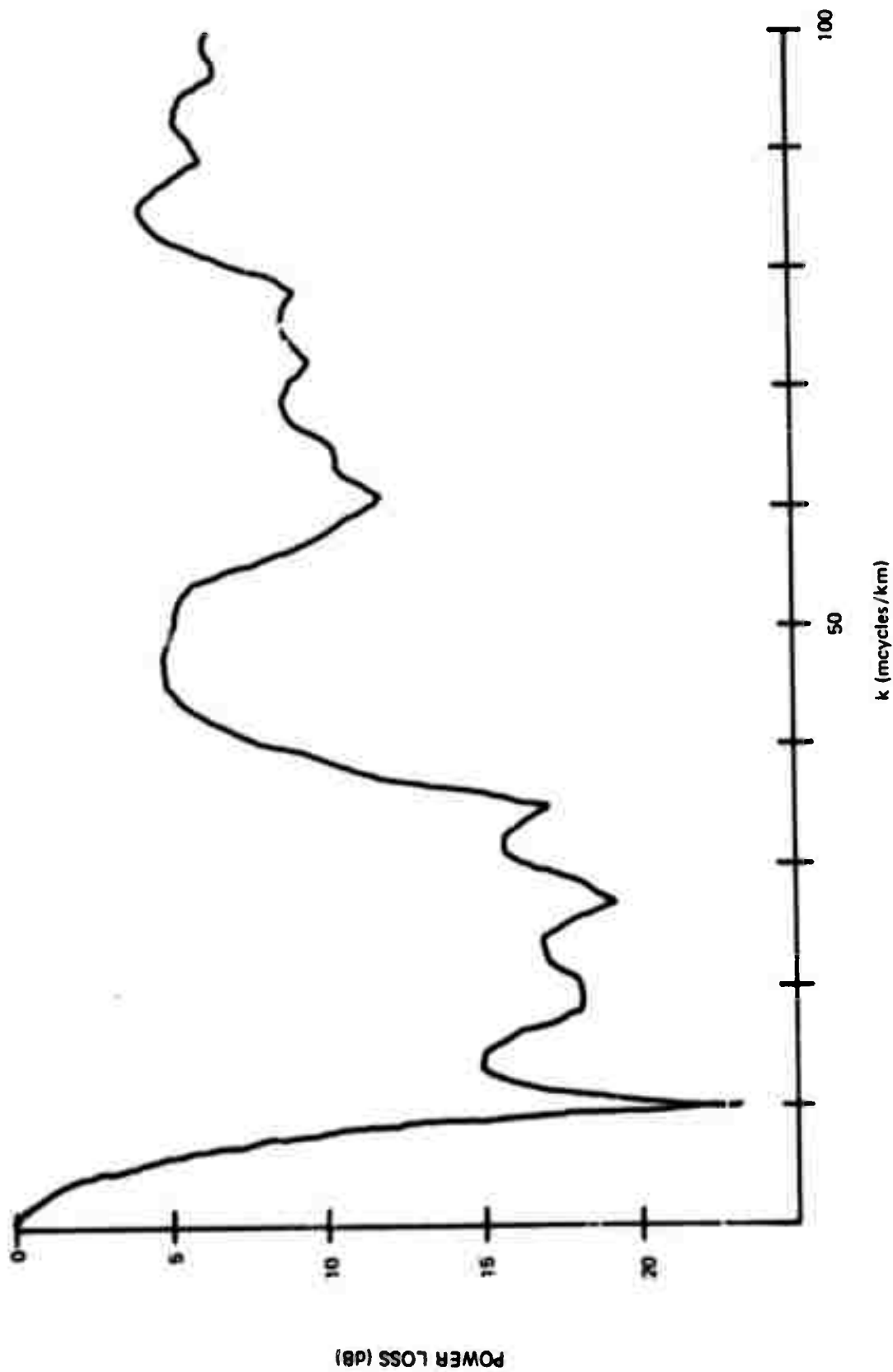


Figure 2-17. Optimized Array LP Worst Case Beam Pattern

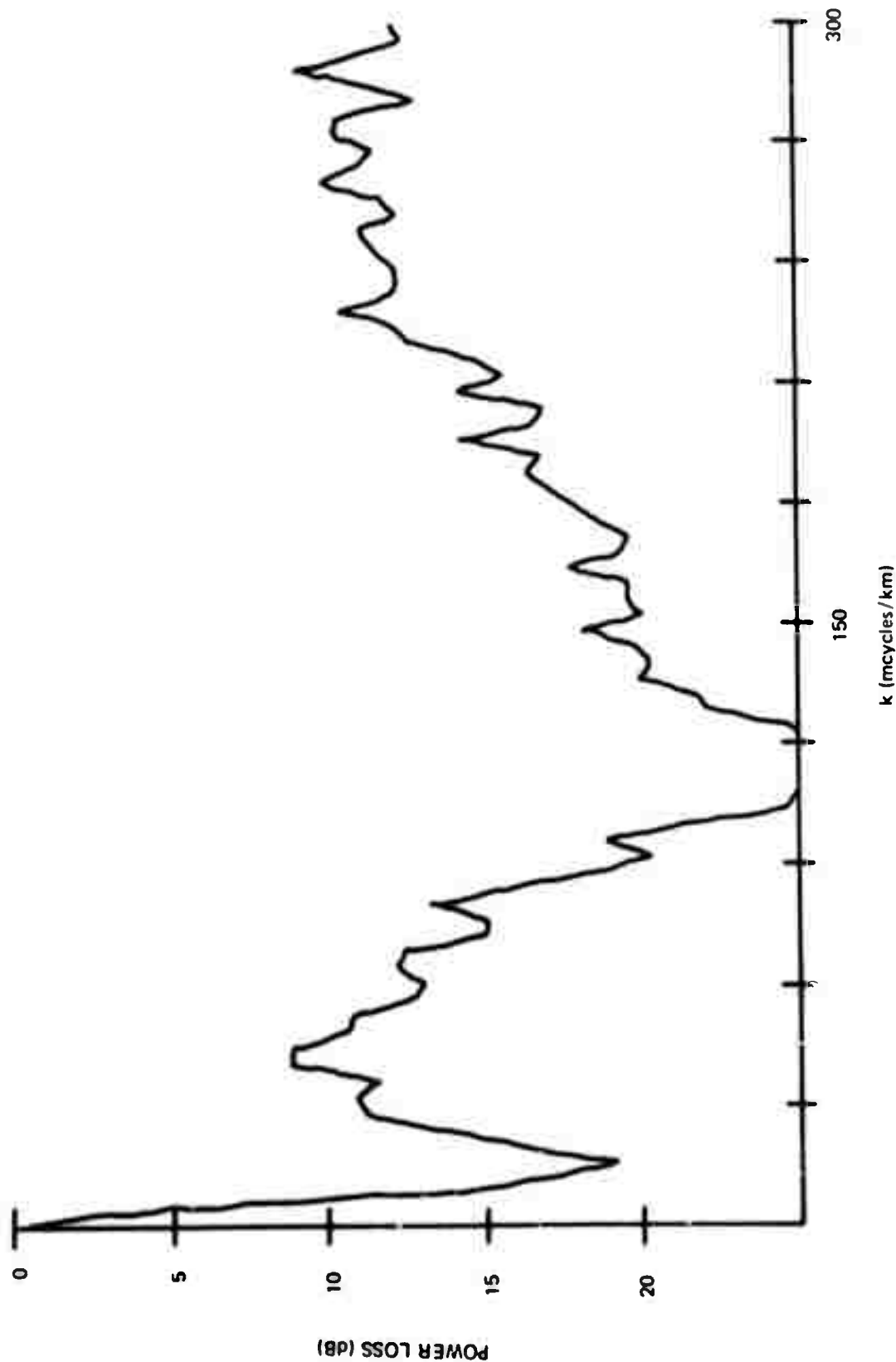


Figure 2-18. Optimized Array SP Worst Case Beam Pattern

$V = 3.5 \text{ km/S}$

— 0.04 Hz

- - - 0.08 Hz

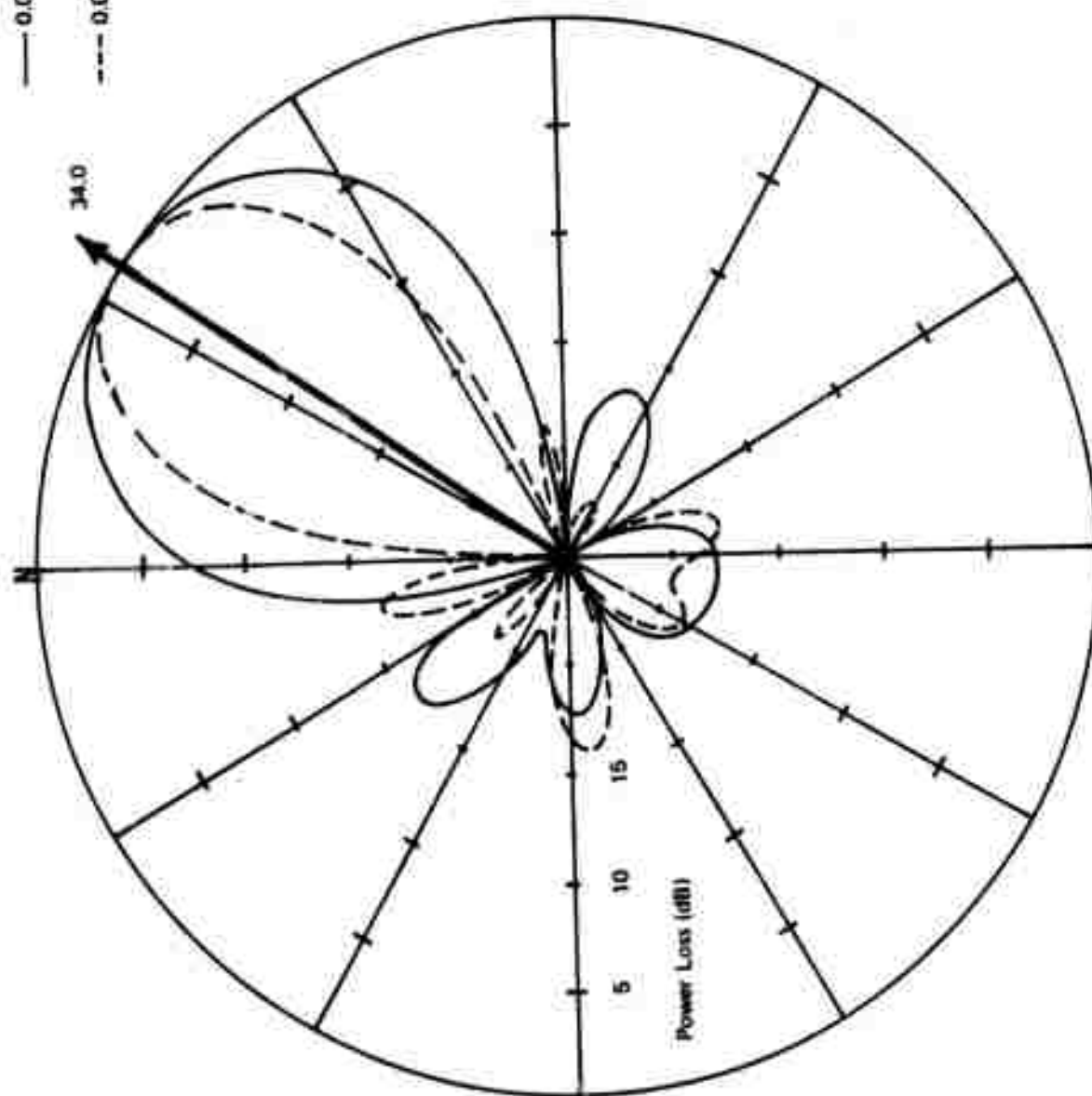


Figure 2-19. Optimized Array Antenna Pattern, 34.0° Steering

22 ELEMENTS RESOLUTION $10^{-3}/\text{km}$

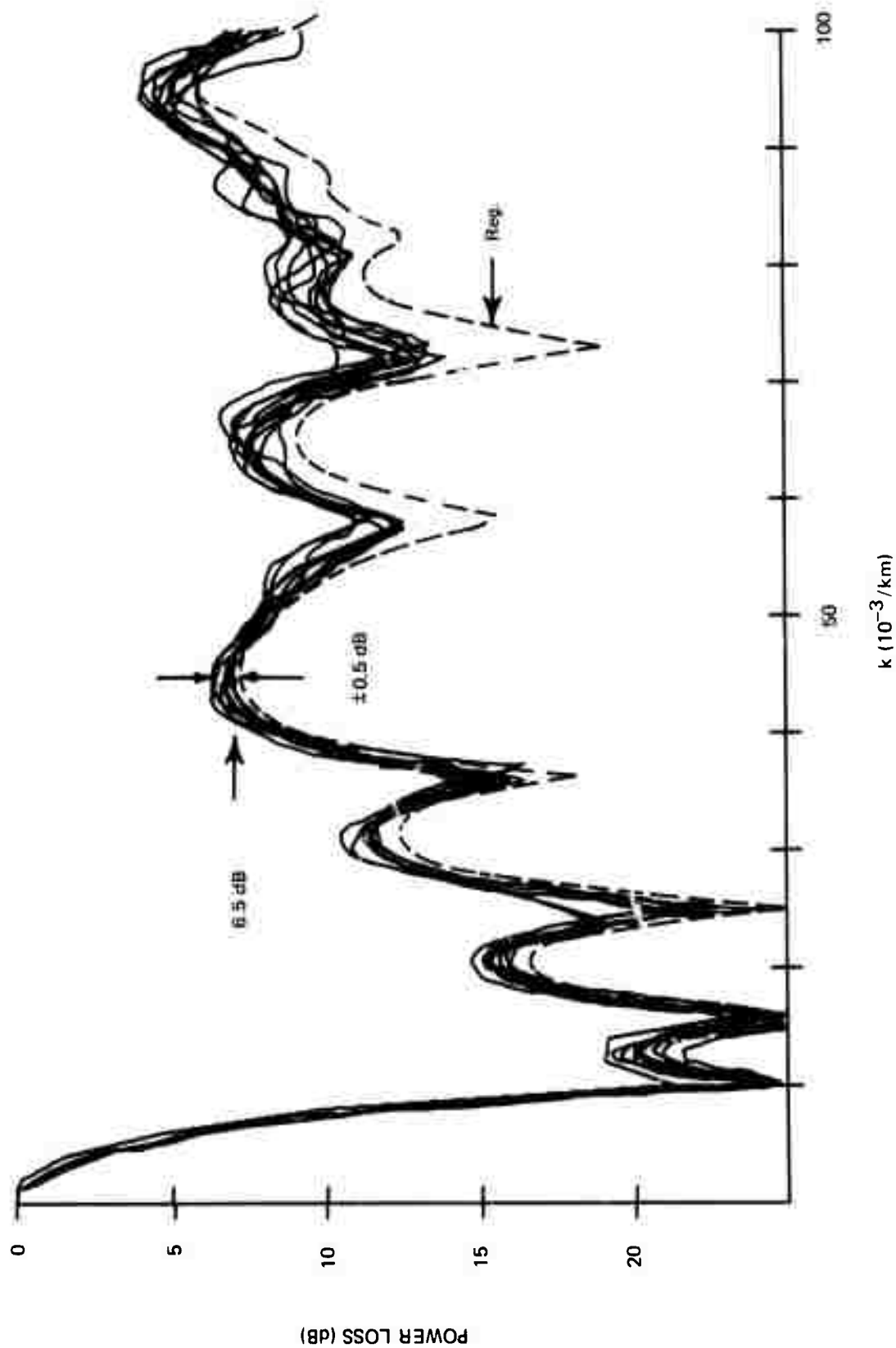


Figure 2-20. Worst Case Beam Patterns for 10 Randomly Perturbed Heptagon Arrays, $\sigma = 1 \text{ km}$

overall maximum signal envelope value during the time interval (MSTA) or some other assumed \vec{u} -space event location. The maximum envelope values for each beam are presented in dB relative to the known or interpolated MSTA value at the \vec{u} -space aiming point.

Figure 2-21 shows an example of this type of empirical beam response pattern for NOXSAR. There is a striking resemblance between the envelope of the data in this figure and the theoretical SP worst-case beam pattern in Figure 2-18. This resemblance may be somewhat anomalous. The empirical response pattern should not be the same as the theoretical pattern for various reasons, including the following:

- a. The complex nature of the actual signal envelope may differ considerably from the single steady state frequency usually assumed in the theoretical approach.
- b. The exact peak of the main lobe is not usually sampled by the detection beams.
- c. The effect of the background noise is not included in the theoretical pattern.
- d. The array beam power loss due to imperfect time anomaly data (see Section 7) cannot be included easily in the theoretical pattern.

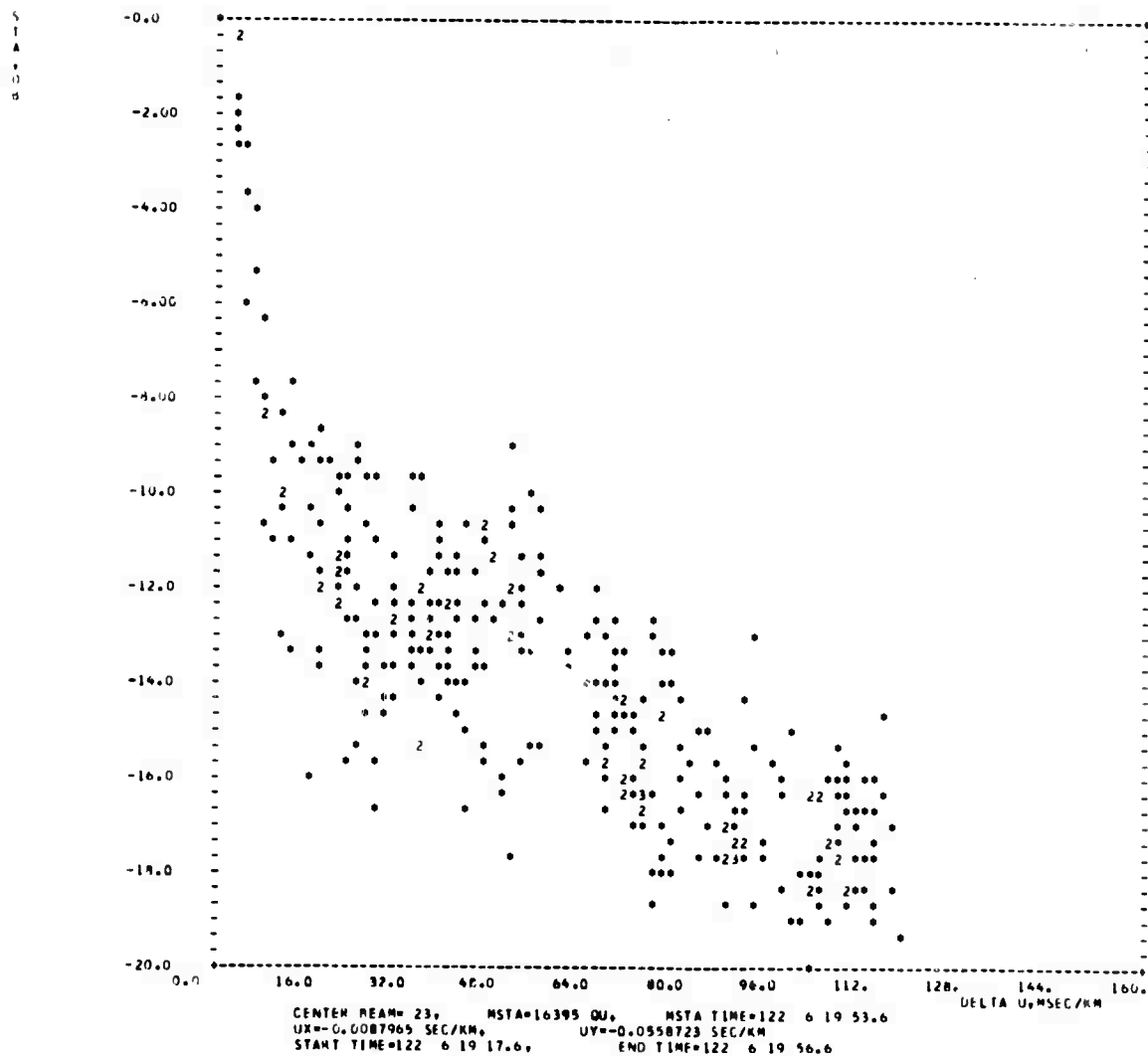


Figure 2-21. NORSAR Beam Envelope Power Loss Pattern

2.3 ANNOTATED BIBLIOGRAPHY

The references listed in this section are grouped in two categories. Subsection 2.3.1 consists of relevant IBM periodic reports. Subsection 2.3.2 contains other references.

2.3.1 IBM Quarterly and Final Reports

- 2-1. "LASA Experimental Signal Processing System," IBM Sixth Quarterly Technical Report, Contract F19628-67-C-0198, ESD-TR-68-451, May 1968.

Appendix I describes NORSAR design efforts and studies in greater detail than this section.

- 2-2. "Integrated Seismic Research Signal Processing System," IBM Tenth Quarterly Technical Report, Contract F19628-68-C-0400, ESD-TR-72-123, February 1972.

Appendix I contains discussion and analysis concerning various empirical array beam response programs.

2.3.2 Miscellaneous References

- 2-3. Lacoss, R.T., "Geometry and Patterns of Large Aperture Seismic Arrays," Lincoln Laboratory Technical Note 1965-64, 31 December 1965.

This report describes a study of possible large aperture seismic array configurations, and contains significant comments concerning u -space beam pattern contours.

- 2-4. Lo, Y. T., "A Mathematical Theory of Antenna Arrays with Randomly Spaced Elements," IEEE Transactions on Antennas and Propagation, May 1964.

A mathematical analysis of various statistical properties of large arrays is presented.

- 2-5. Capon, J., R. J. Greenfield and R. T. Lacoss, "Design of Seismic Arrays for Efficient On-line Beamforming" Lincoln Laboratory Technical Note 1967-26, 27 June 1967.

The signal-to-noise ratio improvement obtained with simple delay-and-sum processing is discussed for short period seismic data. It is shown that at least 3 km spacing should be maintained between seismometers at LASA or another site with similar noise environment, and that noise coherence measurements are of use in determining minimum sensor spacing at an array location.

- 2-6. "Relative Performance of Several Long Period Seismic Arrays," AFTAC/VELA Seismological Center, Technical Note VSC-24A, 24 October 1967, with Addendum, "An Alternate Long Period Seismic Array Configuration for Installation in Norway."

Various NORSAR LP array designs are developed and compared.

- 2-7. Lacoss, R. T., J. Capon and R. J. Greenfield, "Preliminary Design of a Long-Period Seismic Array for Norway," Lincoln Laboratory Technical Note 1968-4, 24 January 1968.

A set of array design parameters and constraints are assumed, and a number of array designs which satisfy these design requirements are analysed and evaluated.

- 2-8. Jeffreys, H. and K. E. Bullen, Seismological Tables, Brit. Ass., Gray-Milne Trust, 1940, 1958.

Section 3

SEISMIC SIGNAL AND NOISE CHARACTERISTICS

Knowledge of signal and noise characteristics is important for many facets of array system design. Measurements of the coherence of signals and noise as a function of distance help determine basic array configurations. Knowledge of noise sources and transmission mechanisms is essential to proper placement of seismometers. The design of amplifiers and filters depends on a knowledge of the frequency characteristics of both signals and noise to yield optimum signal enhancement with minimum distortion. This section is intended to outline and summarize what is known about seismic signal and noise characteristics at the LASA and NORSAR arrays, including a preliminary analysis of the full NORSAR array data.

Section 3.1 briefly describes the origins of seismic waves and Section 3.2 outlines the mathematical and computational techniques used to analyze the signals received by seismometers. Sections 3.3 and 3.4 summarize significant observations about signal and noise characteristics. The goals of the results from digital filtering of seismic signals are covered in Section 3.5. Finally, Section 3.6 is an annotated bibliography of pertinent publications, including all references used in this section.

3.1 SEISMIC WAVE ORIGINS

The vibrations recorded by any seismometer are a mixture of natural and man-made disturbances, both transient and continuous in nature. The transient disturbances (earthquakes and large underground explosions) are the signals sought by a seismic array system; the more-or-less continuous low-level disturbances (traffic, machinery, wind, water, etc.)

represent noise in the system which interferes with the detection of signals. Richter [3-29, page 151] outlines major types of earth disturbances and discusses each. In this section, the types of disturbances of most interest in large array design are described briefly.

3.1.1 Signal Source Mechanisms

Earthquakes usually result from relative slipping of large rock masses along a weak "fault" plane. Energy stored in the rocks as they deform slowly is released quickly when they slip. Some of the released energy is converted to heat at the point where slipping occurs, but much of it is radiated away as seismic waves. These waves vary in amplitude, of course, with the amount of energy released; they also vary in character as a function of fault size (a small fault can release all its energy almost impulsively; a large fault generally has a more complex pattern) and fault orientation (initial wave motion can be compressive, expansive or lateral in different directions).

Large underground explosions can produce seismic waves similar to those produced by earthquakes. Differences arise because the explosion is definitely impulsive and always initially produces a compressive wave with no directional properties. In addition, there is a small practical limit to the depth of an explosion, whereas earthquakes commonly originate tens of kilometers below the surface of the earth, and occasionally have depths of hundreds of kilometers.

3.1.2 Noise Source Mechanisms

In addition to the signal waveforms from earthquakes and explosions, a sensitive seismometer will show a continuous background of oscillations from various natural and artificial noise sources. Blasting, sonic booms,

heavy traffic, construction, machinery and other evidences of civilization add to a natural background of lake and ocean waves, surf, waterfalls, wind, thunder, volcanic tremor and other noises. Noises from identifiable localized sources can be minimized by locating seismometers as far as possible from such sources. The unavoidable background noise can be reduced to some extent by appropriate filtering, as discussed in Section 3.5.

3.1.3 Microseisms

Microseisms are discussed separately from general background noises because this term is reserved for a prevalent noise with a fundamental period around six seconds. The interference of microseisms divides seismic waves into two classes: long-period and short-period. Long-period waves have periods bounded below at approximately 10 seconds by microseismic interference and above anywhere from 40 seconds to 200 seconds. The periods of short-period waves range from about 2 seconds (above which microseismic interference is extreme) to about 0.1 second (below which there is very little energy to be detected).

Typically, microseisms appear to originate in large storm systems, and as such may be somewhat coherent across an array. This coherence can result in increased interference when an array beam is aimed in the direction of the microseism source. Microseisms are not a continuous source of noise, but may continue as long as the parent storm endures.

For a more thorough discussion of microseisms, see Richter [3-29, page 375 and following].

3.1.4 Wave Transmission Mechanisms

The long-period waves, potentially very important in discriminating between earthquakes and explosions, become dispersed in frequency as they propagate (higher frequencies travel more slowly than lower frequencies). The short-period waves, of primary interest in seismic event detection, can be severely distorted by inhomogeneities in the earth's crust. For this reason, reliable event detection is obtained only for events more than about 25 degrees from the detecting array, for which the crustal portion of the wave transmission path is nearly vertical and therefore comparatively short. Even for such distant events some crustal distortion may occur. If it occurs near the source, it will affect the signal seen by an entire array; if it occurs in the crust under the array, it will affect different seismometers in different ways and be only weakly dependent on source location. The latter case reduces signal coherence between subarrays and makes beamforming less effective, so arrays should be located, if possible, where the substructure is relatively uniform.

3.2 WAVEFORM ANALYSIS TECHNIQUES

The number of ways in which seismic waveforms can be manipulated for analysis is limited only by the imagination. In the time domain, it is possible to add appropriately delayed channels to form beams, smooth the waveforms in various ways, filter the waveform to change the relative emphasis of different frequencies, or manipulate the data in many other ways. The data also can be transformed into the frequency domain before similar manipulations are performed. Analysis techniques of these types are explored in some detail in this section.

A number of additional analysis techniques have been used by Lincoln Labs to present seismic waveform data in various useful ways. These techniques are simply mentioned here; all are discussed in [3-22]. The "vespagram" is a plot of contours of power on a graph of slowness versus time. This indicates details of power arrival in one way. The "sonogram" is an alternative indicator of power arrival; it shows power contours on a graph of frequency versus time. The "frequency-wavenumber" plots are yet a third way to display the details of power arrival. They indicate the two-dimensional pattern of power arrival for a single frequency, thus revealing the locations of sources of coherent noise.

3.2.1 Time-Domain Analysis

Seismometer output is simply a waveform in the time domain. Depending upon seismometer design, this waveform may more nearly represent either displacement of the earth's surface, or the velocity of that displacement. Modern seismometers convert the waveform to an electrical signal which may be sampled, digitized and stored in digital form. The digital record then can be plotted out for visual analysis or it can be used for computer processing.

3.2.1.1 Visual Analysis

An experienced seismologist can examine traces of time-domain waveforms and identify accurately the beginning of a seismic event signal of reasonable amplitude. He can also recognize the arrival of waves which have traveled different, longer paths, and calculate from the time differences between these arrivals the geocentric distance between source and seismometer (and sometimes the depth of the event). From estimates of the period and amplitude of the waves and the distance to the source, the analyst can calculate the magnitude of the event.

When waveforms from a number of seismometers distributed on a planar array are available, an analyst can determine the relative time displacement necessary to align the signals, and thereby define a two-dimensional vector for the arrival direction of the seismic wave.

In terms of signal and noise characteristics, the analyst can estimate amplitude quite well and fundamental frequency reasonably well, but spectral density hardly at all. He can give a qualitative statement on the ease of identifying a signal in the background noise, but has difficulty assigning events to more than a few broad categories on a scale of "detectability". He can rate pairs of waveforms on a crude scale of correlation with each other, but cannot visually add channels together to enhance a signal which is very weak, but coherent across channels.

3.2.1.2 Computer Analysis

Any well-defined measurement procedure which an analyst uses to characterize seismic waveforms can be programmed for a computer. Furthermore, some qualitative analysis functions (e.g., certain types of visual pattern recognition) can be made quantitative by appropriate programming, and many functions which are impractical or impossible for an analyst to do manually can be performed readily by a computer.

Important computer analysis functions performed on the basic time-domain waveforms include filtering, the formation of beams and envelopes, and the calculation of event 'detectability'. The former processes are steps in detecting the occurrence of events; the latter is a means of quantifying the ease of detecting events so that different detection techniques can be compared. The formation of beams, or beamforming, is simply the addition of many channels of data sample-by-sample after shifting each channel into the time alignment appropriate for a wave arriving from a particular beam direction.

Envelope formation is a "smoothing" process which replaces a rapidly oscillating waveform (positive and negative excursions) by a more slowly varying non-negative function indicating in some way the average amplitude or power of the original waveform. Two commonly used envelope functions are the rectify-and-sum envelope

$$x'(t) = \sum_{\tau = t-a}^{t+a} |x(\tau)| \quad (3-1)$$

and the square-and-sum envelope

$$x''(t) = \sum_{\tau = t-a}^{t+a} x^2(\tau). \quad (3-2)$$

The former definition is used in both the LASA and NORSAR systems because of its computational simplicity.

Whether the channels of an array are subjected to beamforming and envelope formation in that order or in the reverse order, the result is a non-negative function which oscillates constantly, but is generally higher when signal is present than when it is absent. An event is detected when the calculated waveform exceeds a threshold set at some level above the normal value existing when no signal is present. The lower the threshold, the more sensitive the detection algorithm, but also the more likely it is to be triggered by an instant of unusually high noise. Given an acceptable frequency of false alarms, the smaller the noise variance, the closer the detection level can be set to the mean noise level, and the more sensitive the test becomes. Therefore it is meaningful to define

"detectability" for any given waveform and to compare the detectability obtained with different processing techniques for the same event.

Detectability is defined as:

$$D = \frac{M' - \bar{N}}{\sigma_N} \quad (3-3)$$

where M' is the maximum value in the signal region of the processed envelope waveform, \bar{N} is the average value in the noise region, and σ_N is the standard deviation in the noise region. Figure 3-1 illustrates the meaning of this detectability measure. It is essentially a signal-to-noise ratio for the processed waveform.

3.2.2 Filtered Waveform Analysis

One way to learn more about signal and noise characteristics is to examine waveforms which have been passed through filters of various types. Any of the analysis procedures mentioned in Section 3.2.1 can be applied to the filtered version of the waveform, and differences from the results obtained with the unfiltered version will indicate certain properties of the waveforms. Unless there is prior knowledge of the spectrum of the signal and/or the noise, the most useful studies of this type are performed with a series of narrow bandpass filters. Then one can see roughly how noise and signal power vary with frequency, and can estimate the type of filtering likely to yield desired results. An example of this type of study is the NORSAR signal and noise analysis [3-20, Appendix III].

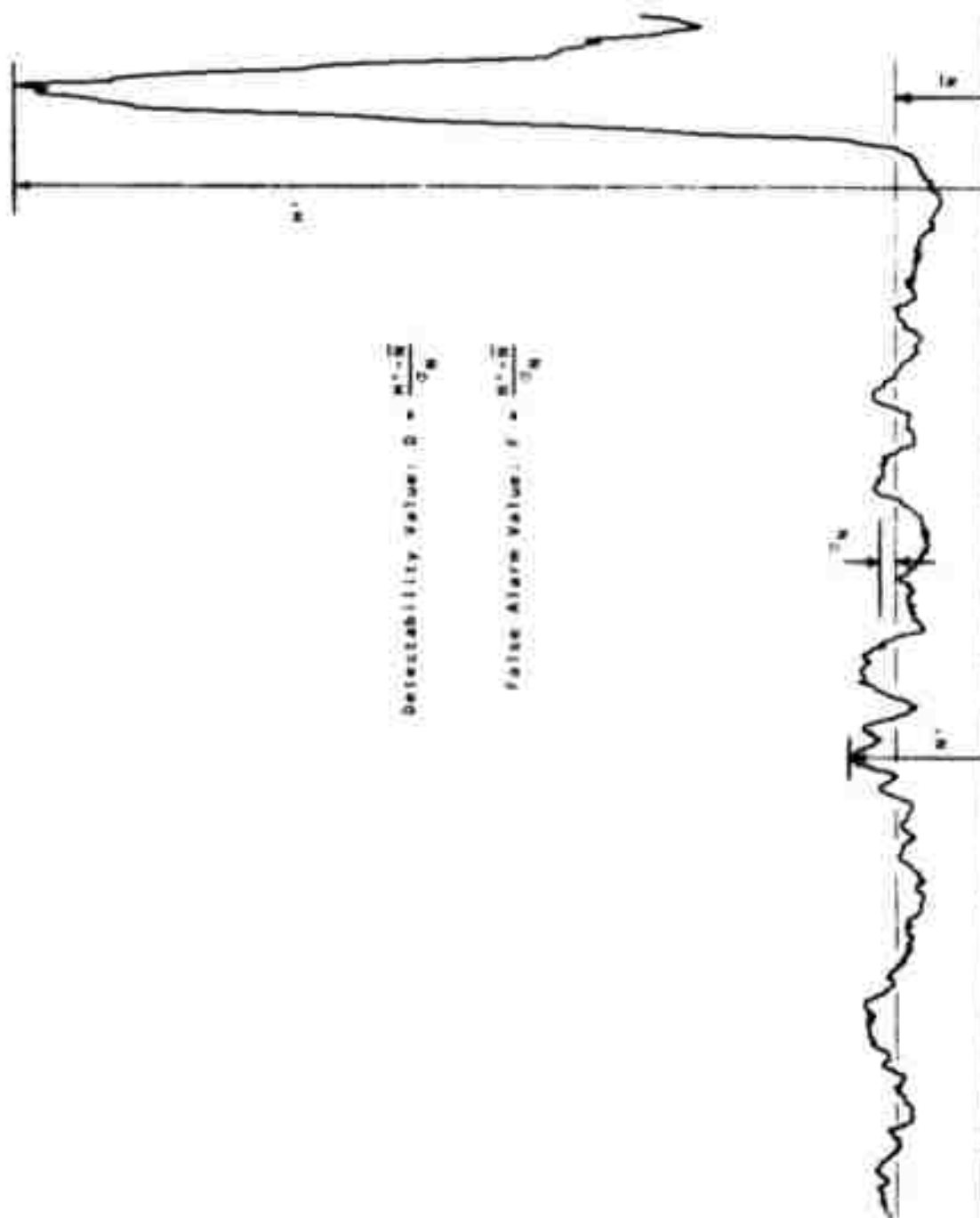


Figure 3-1. Definition of Detectability and False Alarm Values

3.2.3 Frequency-Domain Analysis

Frequency domain information can be extremely valuable to seismic data analysts in identifying the characteristics of signals and noise. The energy outputs of narrow-band filters may provide a crude indication of frequency content; however, discrete harmonic analysis techniques may yield spectral density estimates with a frequency resolution of $(N\Delta T)^{-1}$, where ΔT is the sampling interval and N is the number of data samples analyzed.

3.2.3.1 Fast Fourier Transformation

The best computational algorithm for transforming between the time domain and the frequency domain is the "fast Fourier transform." For each sequence of time samples used as input, a set of values of the power spectral density function is generated. The discrete Fourier transform of $a(t)$ ($t=0,1,\dots,N-1$) is defined as

$$F(n) = \frac{1}{N} \sum_{t=0}^{N-1} a(t) \exp(-2\pi i n t / N) \quad (3-4)$$

where $i = \sqrt{-1}$. When $a(t)$ is a set of real time samples, $F(n)$ has only $(N/2+1)$ independent complex values, corresponding to the $(N/2+1)$ equally-spaced frequencies including zero and half the sampling frequency. For example, if the time-domain data is sampled at 10 Hz, Fourier analysis of a sequence of 32 time samples will yield frequency-domain values at 0.0, 0.3125, 0.625, ..., 4.6875, and 5.0 Hz. (The end points, $F(0)$ and $F(16)$, are special cases because they have identically zero imaginary parts.)

From the above discussion it is apparent that higher resolution in the frequency domain is obtained by analyzing a longer string of time-domain samples. Unfortunately, this does not decrease the variability of the spectral estimates. For stationary Gaussian noise, with no window functions being applied, the standard deviation of each spectral power density estimate is identically equal to the mean value of the estimate. This means that a good estimate must be obtained by some form of smoothing, trading resolution for reduced variability. The smoothing can be a straightforward polynomial smoothing of the high resolution spectrum, but there are advantages in the alternative approach of simply averaging the spectra obtained from a number of shorter samples.

In the case of stationary background noise any desired resolution may be obtained through choice of sample length, and variability may be reduced as low as desired by the averaging of a large number of sample blocks. Analysis of a transient signal is an entirely different matter; in that case, extra time samples may merely introduce extraneous information which partially masks the signal of interest. Selection of a sample length for signal analysis consequently involves a tradeoff between an interval short enough to exclude extraneous data and one long enough to produce a reliable representation of the signal. Resolution, per se, can be increased artificially by adding zeroes to extend the chosen interval of data. The analyses performed on NORSAR data generally took 20 samples (2 seconds) of signal and extended it to 32 or 64 samples by adding zeroes. The fast Fourier transform algorithm generally uses a power-of-two number of samples. To obtain the advantages of a highly reliable estimate of the noise while maintaining compatibility with the resolution level of the signal, many different segments of noise (noise blocks) can be analyzed independently at the same resolution used for the signal, then the separate results can be averaged to yield much more reliable estimates of noise characteristics than could be obtained from any individual segment.

When B noise blocks from each of C channels or subarrays are subjected to Fourier analysis, the complex elements of the output may be presented as $F(n,b,c)$, where $0 \leq n \leq N/2$ indicates the frequency, $1 \leq b \leq B$ indicates the noise block, and $1 \leq c \leq C$ indicates the channel number. Assuming that the discrete Fourier transform is defined as in equation (3-4) and that the samples $a(t)$ represent Q nanometers per quantum unit at a sampling rate of R Hz, the Fourier transform output represents Q nanometers per quantum unit $\times (N \text{ samples}/R \text{ Hz})^{1/2}$. Then the following operations on elements are of interest.

- a. Power spectral density:

$$P(n,b,c) = |F(n,b,c)|^2 \quad (3-5)$$

- b. Cross-power spectral density:

$$X_{\alpha\beta}(n,b) = F(n,b,c_\alpha) \cdot F^*(n,b,c_\beta) \quad (3-6)$$

where $(*)$ designates the complex conjugate.

- c. Array-averaged power spectral density for one noise block:

$$P(n,b) = \frac{1}{C} \sum_{c=1}^C P(n,b,c). \quad (3-7)$$

This is useful for observing changes in the noise amplitude or spectrum from one time to another.

- d. Time-averaged power spectral density for one channel:

$$P(n,c) = \frac{1}{B} \sum_{b=1}^B P(n,b,c). \quad (3-8)$$

This can reveal differences in noise amplitude or spectrum from one channel (subarray) to another.

e. Time-averaged cross-power spectral density:

$$X_{\alpha\beta}(n) = \frac{1}{B} \sum_{b=1}^B X_{\alpha\beta}(n,b) \quad (3-9)$$

This is an intermediate product in determining coherency.

f. Coherency spectrum:

$$C_{\alpha\beta}(n) = \frac{X_{\alpha\beta}(n)}{\sqrt{P(n,c_{\alpha}) \cdot P(n,c_{\beta})}} \quad (3-10)$$

This indicates the degree of alignment or coherence between two channels as a function of frequency.

3.2.3.2 Leakage Effects and Their Removal

One problem with spectral estimates obtained using finite harmonic analysis, particularly at the coarse resolutions often necessary with seismic signals, is that energy tends to "leak" from higher energy parts of the spectrum to lower energy parts. In practical terms, this means that analysis of a waveform which actually rolls off as steeply as 18 dB/octave may yield a spectrum which apparently has a rolloff of only 12 or 14 dB/octave. Figure 3-2 shows this effect operating in a set of noise spectra generated using different sample lengths from the same noise segment. Figure 3-3 illustrates the extreme distortion possible when a waveform is first filtered (see [3-20, page 90] for the parameters of the SSDD filter), then subjected to harmonic (Fourier) analysis, and finally corrected for the original effects of the filtering. In this case the filter used was one with zero response at D.C. and at the Nyquist frequency (half the sampling frequency; 5 Hz in this case). Because of the extreme attenuation of high and low frequencies, the amount of energy leaked into these regions by the harmonic analysis simply overwhelms the amount

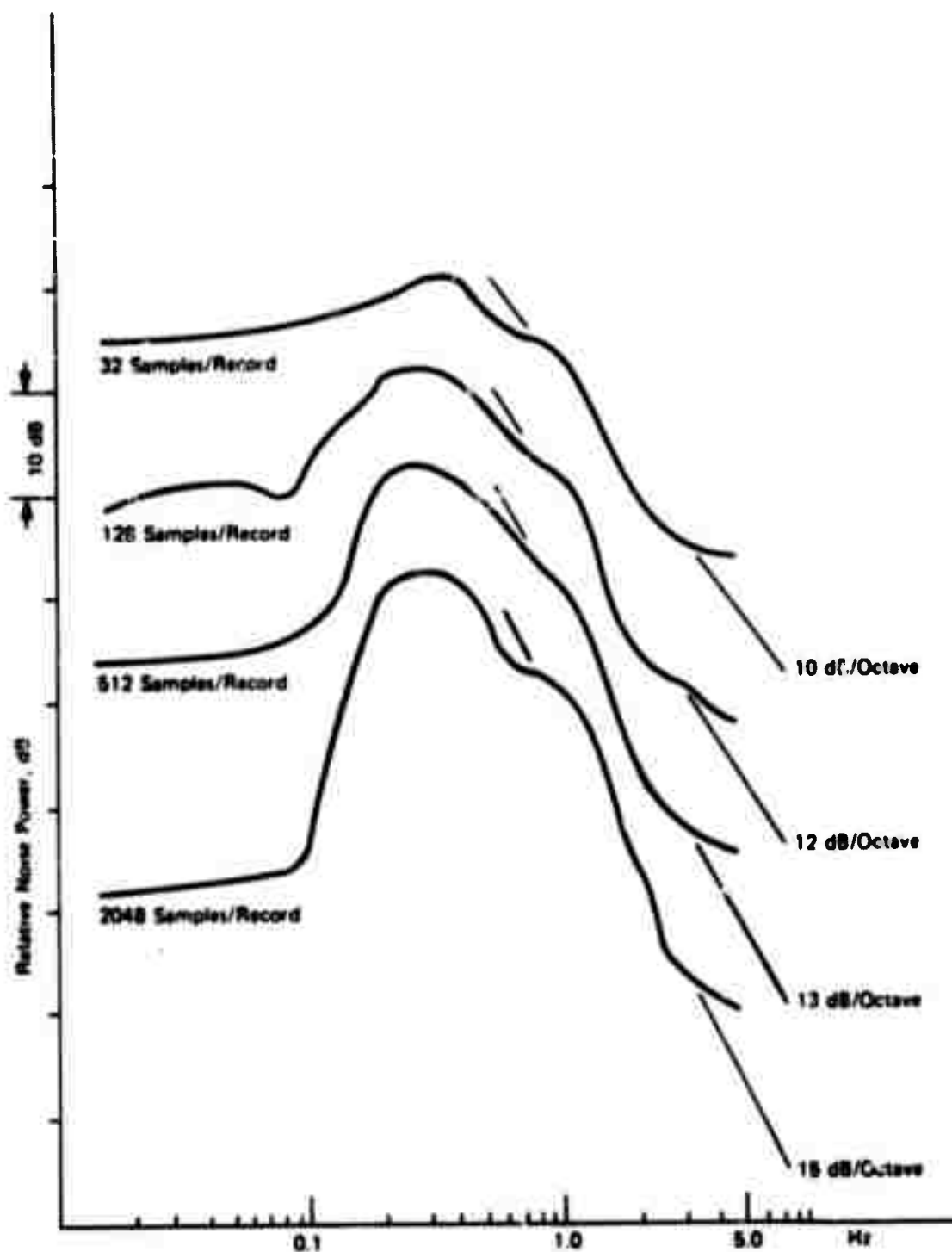


Figure 3-2. Noise Power Spectral Density Computed from Different Sample Logs

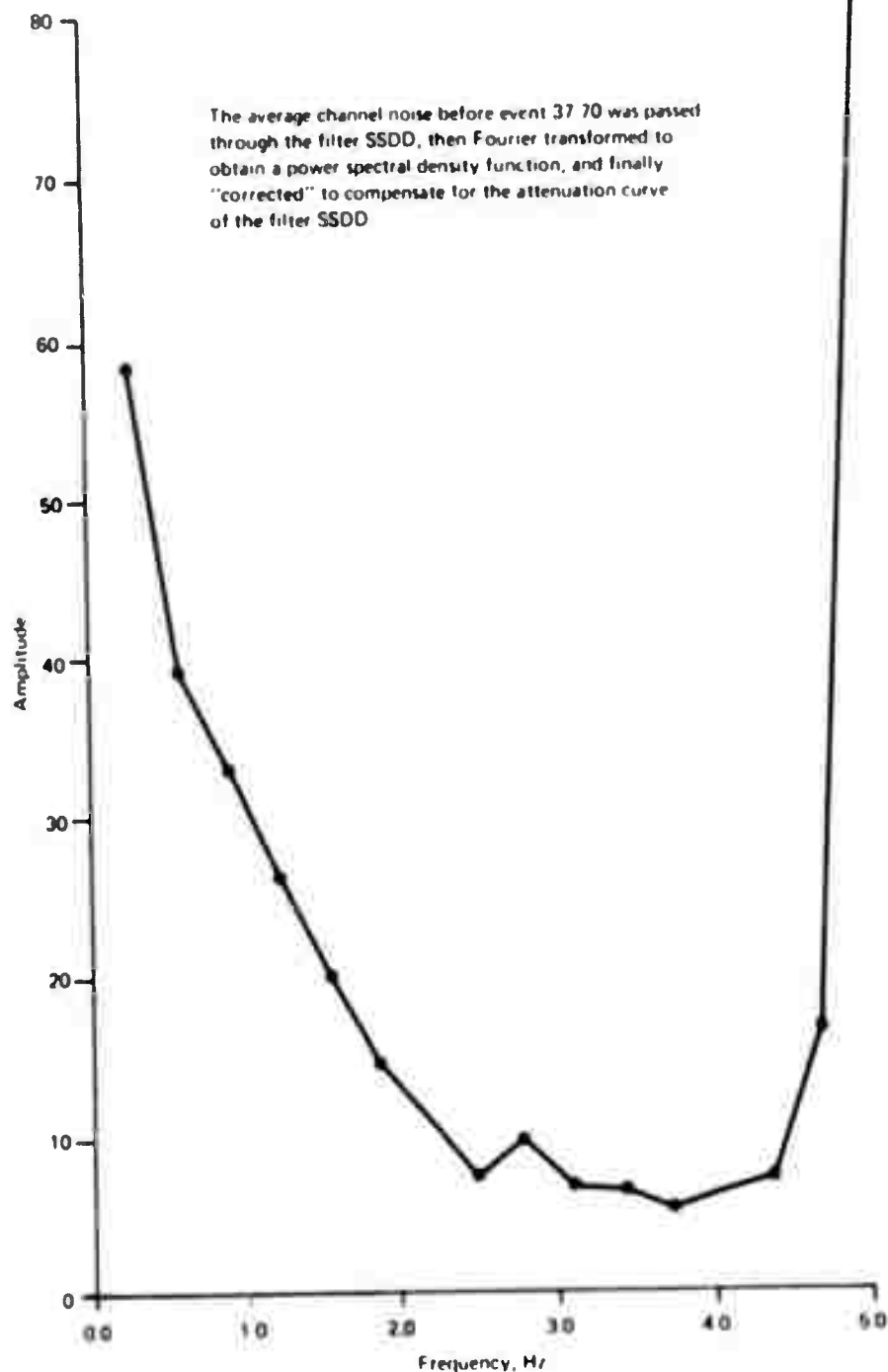


Figure 3-3. Power Spectral Density Plot Showing Effects of Filtering and Correction

actually there. Then removal of the effects of filtering applies extremely large recaling factors at the ends of the spectrum, resulting in excessive emphasis of the leakage.

Although filtering can cause extreme leakage distortion, it also can help eliminate the effects of leakage. The predominate effect of leakage is to make some spectral density values seem higher than they actually are. Thus, if spectra are generated using two different filters, the power spectral estimate obtained using the filter with larger relative gain at any one frequency should be smaller and more nearly correct. If several filters are used simultaneously, and those filters are selected to emphasize different regions of the spectrum, then the minimum envelope of the set of spectra can define a spectrum essentially free from leakage distortion. Figure 3-4 illustrates this process using just three filters.

3.3 BACKGROUND NOISE CHARACTERISTICS

The natural background noise spectrum tends to peak around 6 second period (where microseisms are most intense) and to decrease more or less steadily with increasing or decreasing frequency from that region. Other types of noise include ground noises associated with civilization, signal-generated noise (that portion of the signal energy which appears noise-like for the signal processing scheme being used), and the artificial noises of the data acquisition system itself, primarily quantization noise. In this section, the characteristics of the background noise in the short period region will be discussed in terms of amplitude, spectra and variations as a function of direction, season, location, etc.

Only a few general characteristics of long-period noise are mentioned here (see [3-36] for more details). The long-period noise spectrum peaks in the 0.06 - 0.08 Hz and 0.12 - 0.2 Hz regions, with a relative null

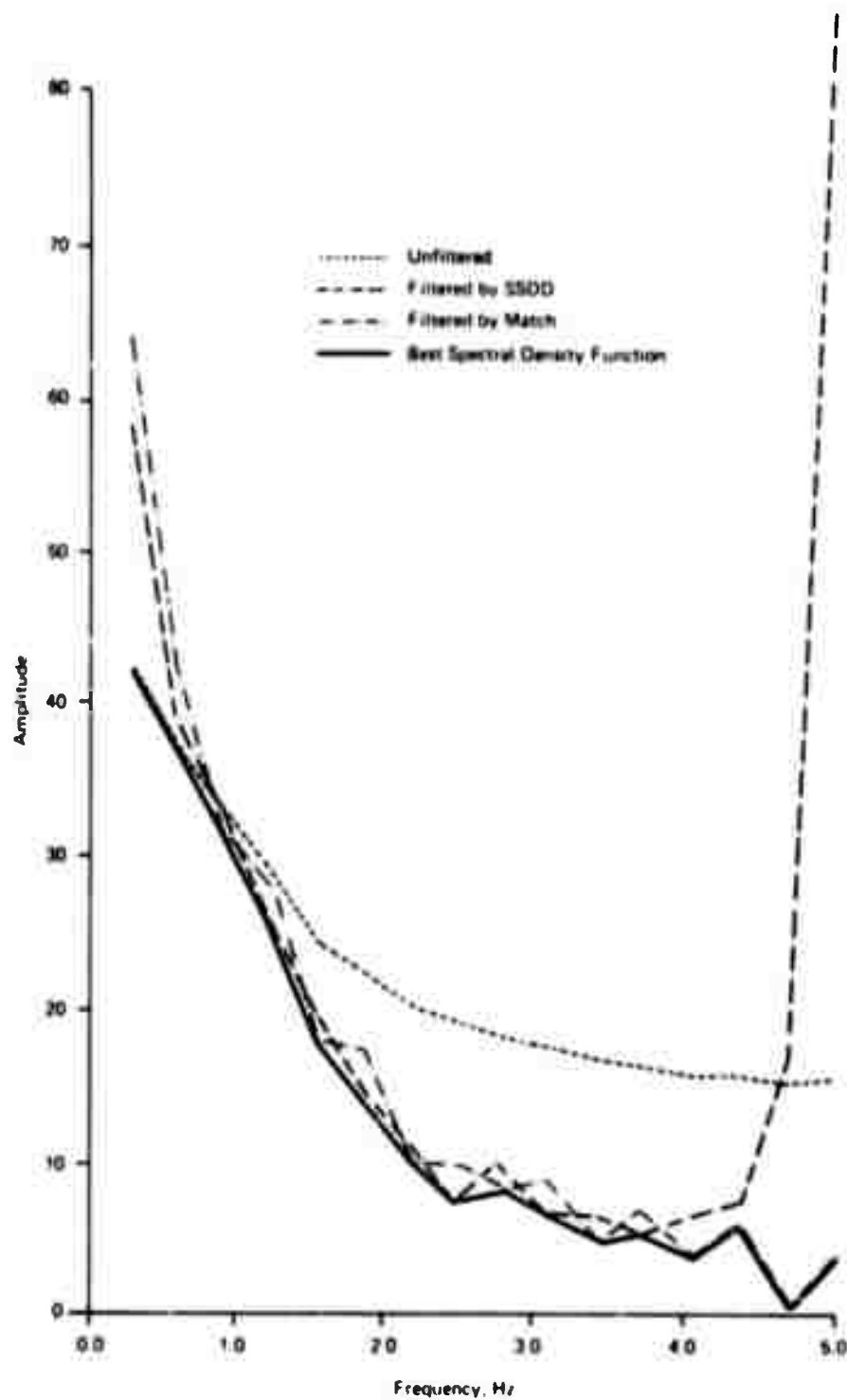


Figure 3-4. Power Spectral Density Function Determined Using Multiple Filters

near 0.09 - 0.1 Hz. The noise seems to be related to storms (particularly oceanic storms) and shows considerable stability over periods of a few hours but great variability over periods of several days or longer.

3.3.1 Noise Amplitude

Noise amplitude without qualification implies the amplitude of microseisms, by far the strongest natural seismic noise. The amplitude of such waves may range from about 30 to about 30,000 nanometers, averaging about 600 [3-30, page 20]. In practice, however, seismic wave detection and analysis is performed in some part of the short-period frequency band which does not include the microseisms. Therefore, it is appropriate to speak of the noise amplitude as seen by the detection system, and to quantify it in relation to the amplitude produced by an arbitrary reference (typically a 1-Hertz sine wave with a 1-nanometer zero-to-peak amplitude).

Assuming a system which responds only to noise with a frequency near 1 Hz, it is possible to make some simple but meaningful statements about noise amplitude. At the extremely quiet location of Tamanrasset (Africa) there are periods when the background noise amplitude is less than 0.2 nm but typical noise levels are 1-10 nm [3-30, page 17].

A more meaningful representation of noise in an actual detection system is the measure of noise power passing through the system filter. This view accommodates the necessity to use more than just a single frequency component for seismic wave detection. Noise data is available on this basis for both LASA [3-35] and NORSAR [3-12, Appendix IV]. LASA is a comparatively quiet site. The output of the 0.9 to 1.4 Hz surveillance filter has a noise level of only 0.56 nm. By contrast the NORSAR site has a noise amplitude of about 2.2 nm at the output of a 0.8 - 1.6 Hz filter. Noise analyses performed for the study in [3-20] indicate that the noise amplitude out of the 0.5 - 3.5 Hz filter at NORSAR varies with time in the range 0.9 - 1.6 nm.

The preceding discussion of noise amplitude has been concerned with natural background noise. Minimization of this noise component is accomplished by careful site selection, and by locating seismometers on bedrock away from trees, buildings, seacoasts and other noise sources. Cultural noise, such as that from traffic, heavy machinery, mining operations and the like also should be avoided. Cultural noises other than explosions usually cause negligible interference at distances greater than 5 or 6 kilometers. On the other hand, storms at sea can disturb a seismic array at least a few hundred kilometers inland [3-30, pages 86-87].

Other noises are generated in the system itself. Sensor design and installation must be planned to avoid noise from convection currents, barometric pressure changes, ground tilt and other extraneous disturbances. Amplifiers and transmission lines must be designed to avoid noise from internal instability or electromagnetic interference. The instrumentation should be stable over the expected range of temperature and humidity in the operational environment. Finally, assuming that the data is to be digitized, the quantization method should be designed so that quantization noise is not significant to the systems.

In the LASA and NORSAR systems, quantization is defined to be 0.0427 nm/quantum unit, but in order to obtain a wide dynamic range with a limited number of bits the least significant bit does not always represent a single quantum unit. There are two ways to look at quantization noise in this situation. For a quantization unit q , the error introduced by quantization is equivalent to a noise with rms amplitude $q/\sqrt{12}$. ($q = 0.0427$ nm implies rms noise = 0.0123 nm; this is only about 2% of the average filtered LASA noise amplitude). When the quantum units are scaled for increased dynamic range, then quantization noise is best expressed as a signal-to-noise ratio. If b is the number of bits used to represent the amplitude values during transmission (bits indicating scaling and sign not included) then the signal-to-noise ratio is $(10.8 + 6b)$ dB. In the

LASA and NORSAR systems $b=7$ so the signal-to-noise ratio is approximately 53 dB. At the maximum signal amplitude (2^{12} quantum units) this implies a noise amplitude near 0.4 nm. Such a noise level approximates the natural background noise, but that is unimportant when the signal is large enough to warrant such scaling. Further discussion of quantization noise appears in [3-8, Appendix I and 3-12, Appendix VII].

3.3.2 Noise Spectrum

It has been noted previously that the amplitude of background noise is meaningless without a frequency reference, and that in the short-period region (most often used for event detection) there is a relatively steady drop in noise level with increasing frequency. This is illustrated by Figure 3-5 (from [3-30, page 17], in which the short-period noise spectra from 16 locations are plotted). Amplitudes differ, but the shapes of these spectra are in general agreement and are virtually identical in the vicinity of 1 Hz. Near 1 Hz almost all of the 16 spectra evidence a slope of approximately 36 dB/octave (amplitude drops by a factor of 64 when frequency doubles). At slightly higher frequencies the slope becomes more erratic and less steep, but still averages 10 to 15 dB/octave.

The noise spectra observed at LASA and NORSAR (with no compensation for instrument and channel response) are not nearly as extreme as those in Figure 3-5, but still quite steep. Compensation for seismometer characteristics could produce a closer match. Figure 3-6 indicates both "typical" noise spectra and the limiting extremes observed in relatively few samples. The connected circles represent a typical LASA noise spectrum and the region between the two dot-shaded areas represents observed extremes. The connected crosses represent two distinct types of common NORSAR noise spectra and the region between the two line-shaded areas represents observed extremes.

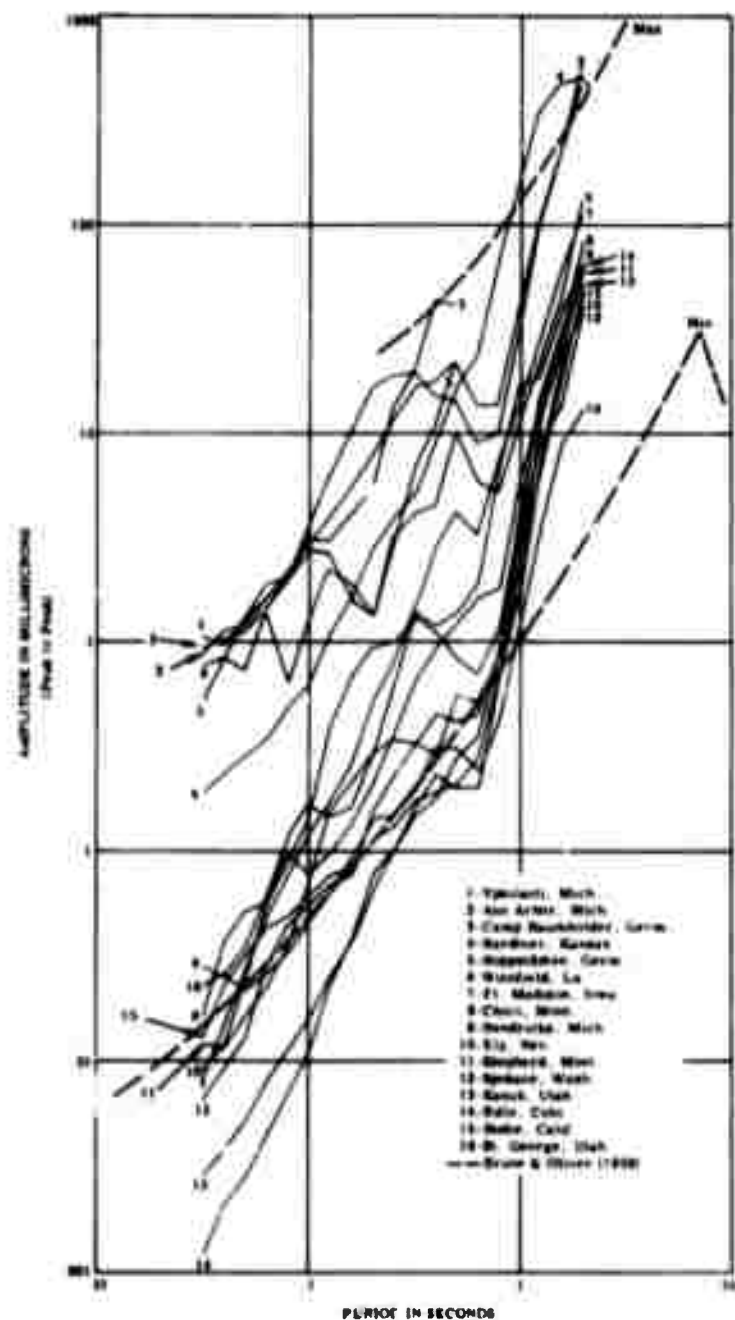


Figure 3-5. Spectra of Seismic Noise Recorded at 16 Geographic Locations (Data Are Normalized to 1 Hz Bandwidth) (from [3-30, page 17])

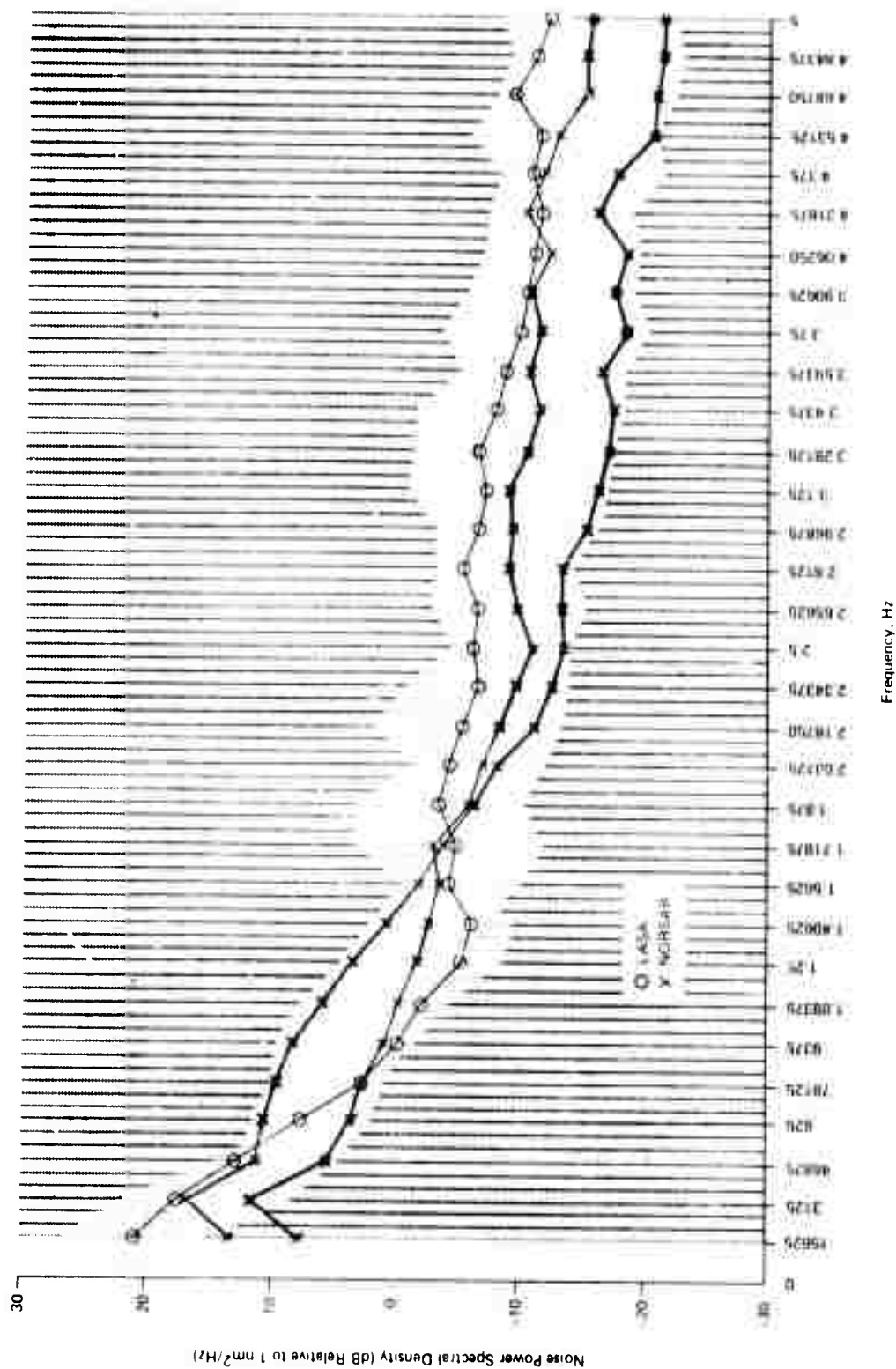


Figure 3-6. LASA and NORSAR Noise Power Spectral Density Functions

NORSAR data was notable for belonging largely to two classes with distinctly different slopes, as is suggested by the data in Figure 3-6. Signal processing techniques which were optimal when one type of noise was present could be appreciably less than optimal in the presence of the other type. LASA background noise is far more consistent, and has the additional advantage of a local minimum in the noise spectrum near or slightly above 1 Hz.

3.3.3 Noise Variations

Both the overall amplitude and the spectrum of seismic background noise have been observed to vary with such factors as array location, beam direction and time. Variations with time generally appear to be associated with meteorological changes, but tidal effects may also be a factor.

Figures 3-5 and 3-6 indicate the differences in background noise observed at different locations and different times. Figure 3-7 (extracted from [3-19]) illustrates that significant differences occur between sensors in the same array. For the 25 noise samples considered, the range of noise levels among the subarrays was never less than 2 dB, and once was nearly 10 dB. This figure also reveals a change of 8 dB in average noise level in less than one day (the time from event 'P' to event 'W').

An attempt to study the effect of sensor depth on background noise was reported in [3-12, page 71]. Some slight differences were observed, but it was not conclusive that these differences were in fact caused by the difference in sensor depth.

Directional intensity of background noise is revealed by frequency - wavenumber spectra. (See [3-32] and [3-33].) Studies utilizing this technique have shown not only that background noise often has directional

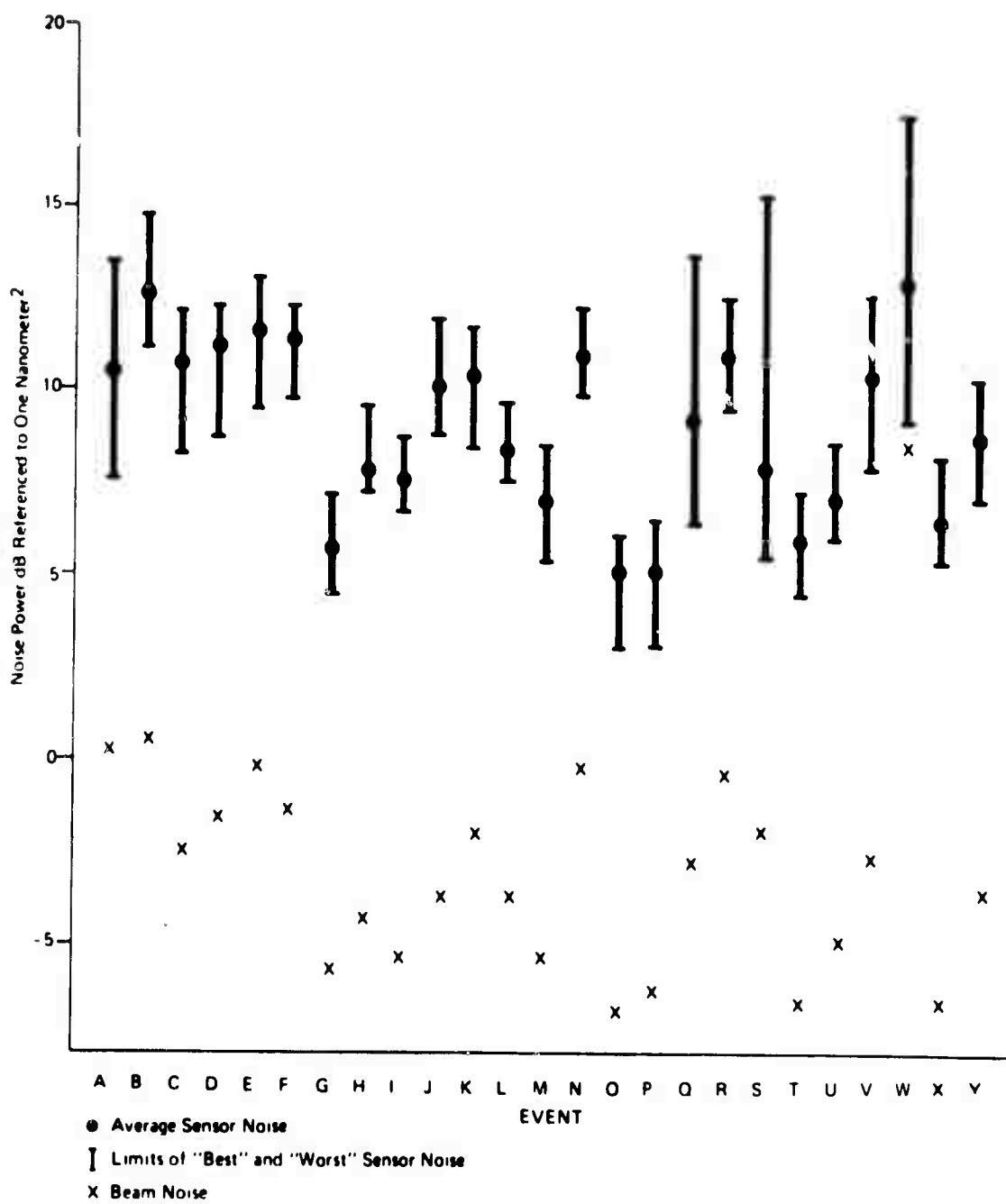


Figure 3-7. Beam and Sensor Background Noise Measured through a 0.75 to 4.0 Hz Filter With No Prewhitening

components, but also that the directional noise can be associated with low-pressure weather disturbances at sea [3-26, page 29]. The distinct difference in noise spectrum illustrated by the two NORSAR curves in Figure 3-6 seems to be associated with the weather in the North Sea and Northern Atlantic, although the cause-and-effect mechanism responsible for changing high and low frequencies in opposite directions is not clear. Figure 3-8 shows the near doubling of long-term-average noise amplitude in 48 hours.

There are many factors which cause noise characteristics to differ or change, but two seismometers sufficiently close together will exhibit correlation between their noise waveforms. The maximum distance at which such correlation exists is indicated by Figure 3-9 (from [3-6]). The erratic line of average correlation coefficients indicates a critical distance anywhere from 2.5 to 8 Km.

3.4 SIGNAL CHARACTERISTICS

Elementary approaches to seismic array and signal analysis are based on simplifying assumptions that the waveform detected at each seismometer is the sum of a signal component (identical, except for a relative time delay, at each instrument) and a random noise component (totally uncorrelated, but having the same constant noise statistics at each instrument). Unfortunately, the real situation departs significantly from these assumptions. As noted previously, background noise is essentially uncorrelated if seismometers are separated sufficiently, but noise amplitude and spectrum may vary appreciably from subarray to subarray and with time and beam direction. In this section, signal characteristics are discussed, with emphasis on deviations of actual signals from the simple model.

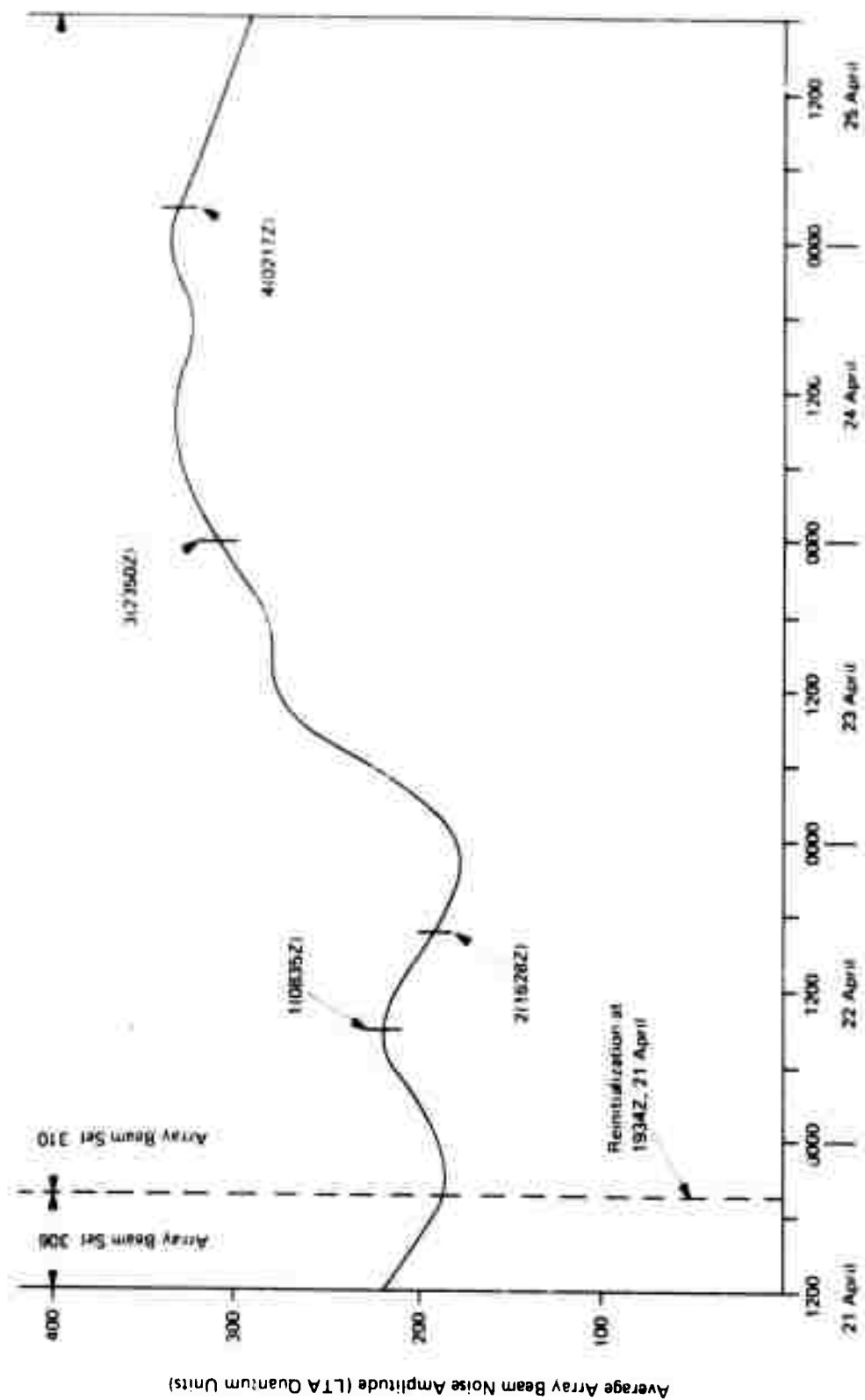


Figure 3-8. Average Long-Term Average (LTA) Noise Level for NORSAR (21 to 25 April 1971)

LONGSHOT-BAND PASS FILTER 0.9 - 1.4 Hz

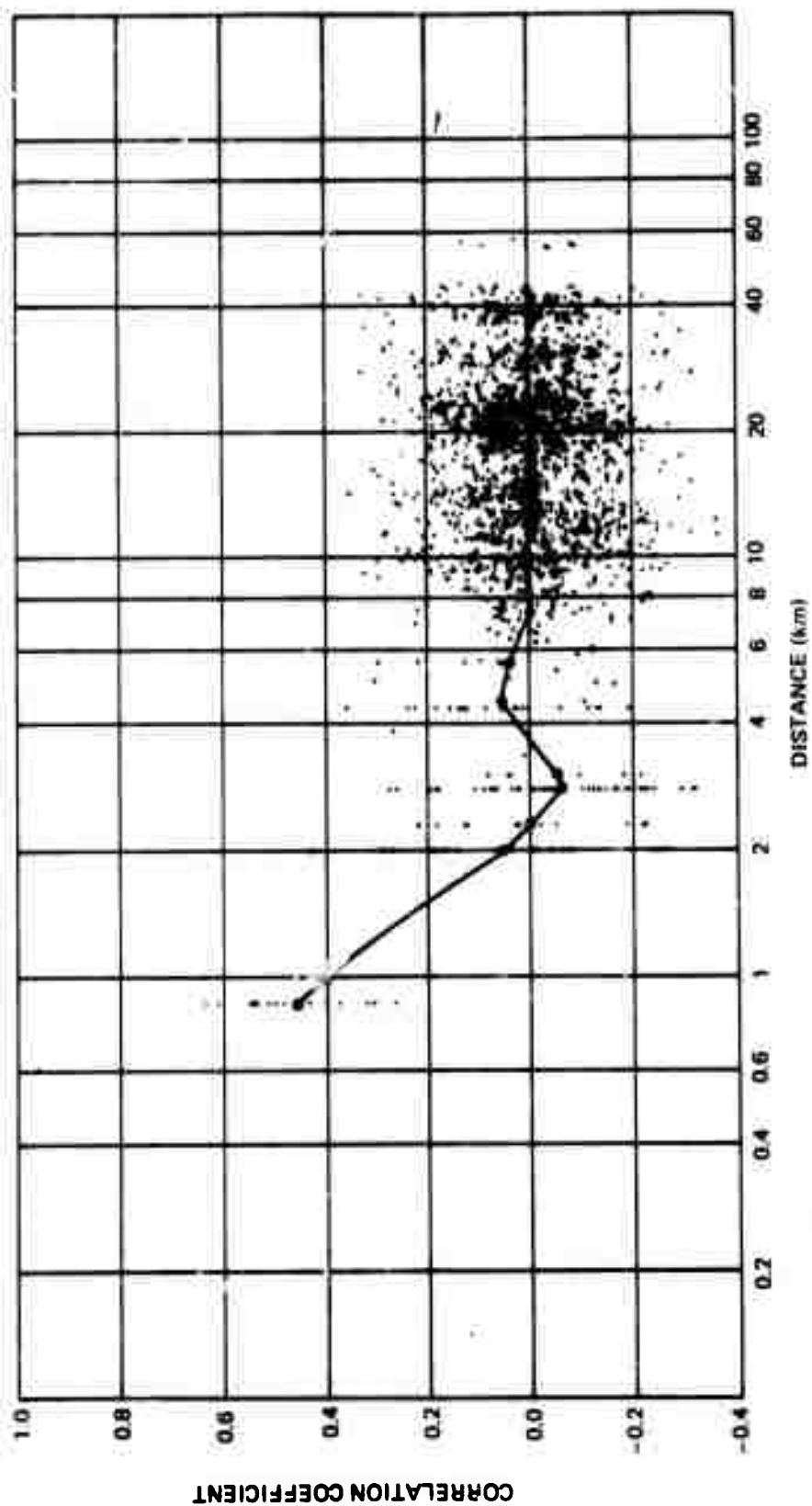


Figure 3-9. Correlation Coefficient vs Distance Between Instruments

3.4.1 Signal Amplitude

3.4.1.1 Envelope Shape

The idealized impulsive short-period signal is a sinusoid with an envelope which builds to peak amplitude within a cycle or two and then decays exponentially (reaching half-peak within one or two cycles). This ideal may be approached in seismic waves recorded near the source of a small, simple earthquake or explosion in a homogeneous medium. Larger events often consist of multiple shocks from points along a fault line which may extend more than 100 kilometers (although usually the first shock is much larger than any of the immediately succeeding ones). To complicate the picture further, variously reflected and refracted copies of the signal reach a distant seismometer at different times, and local crustal inhomogenieties (near the source or near the array) produce repeatable distortions in the signal. The overall result is a protracted period of activity with an energy maximum near the beginning and local maxima at later times. Figure 3-10 provides a typical example of a signal strong enough to evidence little interference from background noise.

The possible range of signal envelope shapes is indicated by the three waveforms in Figure 3-11. The first approximates the ideal signal, with all activity constrained to a few cycles. The second waveform, generated very near the source of the first, shows protracted oscillation after the initial impulse, and suggests a second phase arriving about 13 seconds after the initial one. The last of the three traces depicts an event which begins weakly and takes more than ten seconds to grow to full strength. A small event with this characteristic is extremely difficult to detect.

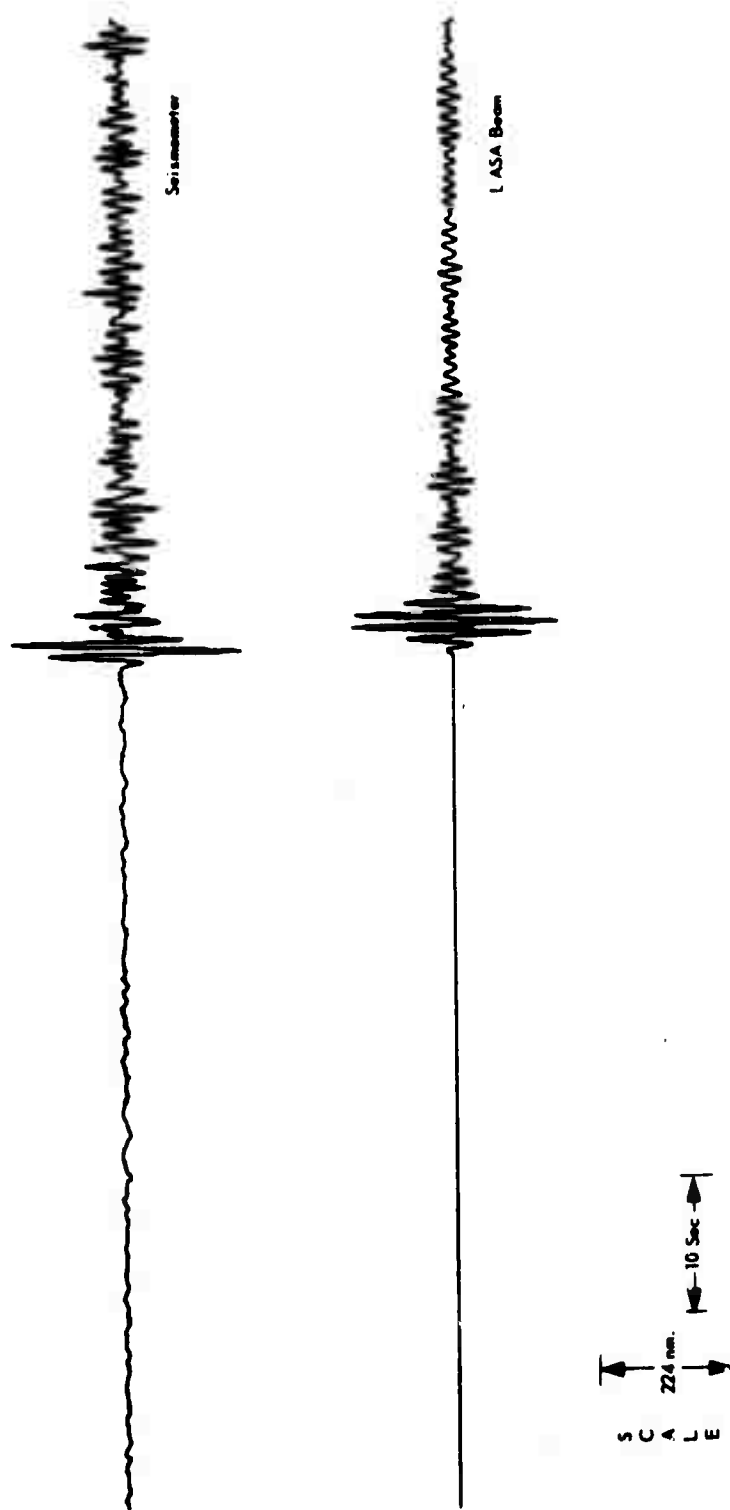
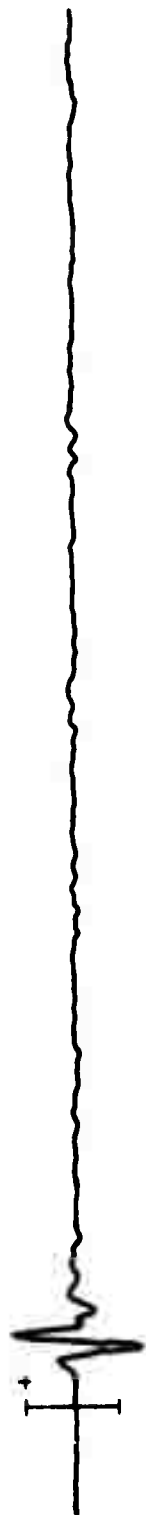
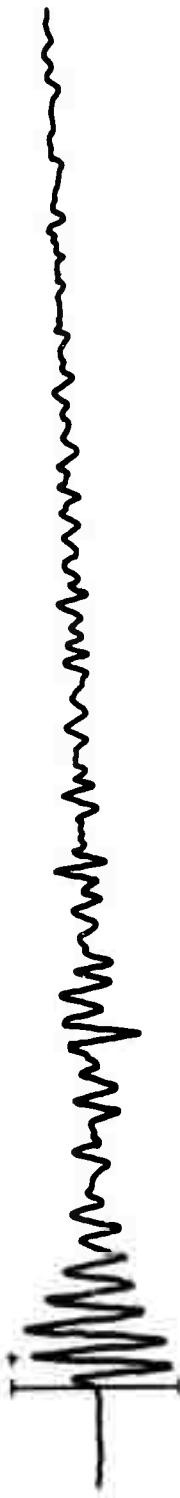


Figure 3-10. Longshot Event

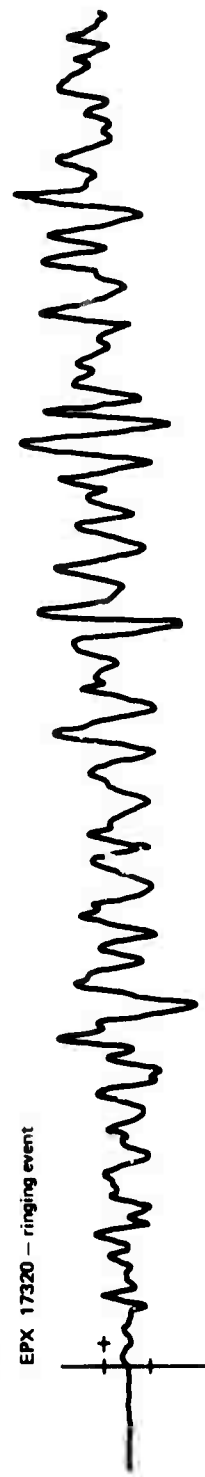
5 seconds



EPX 156080 — impulsive event



EPX 17320 — ringing event



EPX 152680 — emergent event

Figure 3-11. Seismic Signal Shapes

3.4.1.2 Amplitude Anomalies

The simple model of a seismic array has identical signal components received at each subarray. In actuality, the signals vary considerably in amplitude and somewhat in form from subarray to subarray, and this variation itself varies with the source of the signal. Figure 3-12 demonstrates the variation of signal waveform from subarray to subarray in LASA. NORSAR exhibits even greater differences because of the variability in the geologic structure. An impulsive disturbance can appear essentially as one positive and one negative peak on one subarray, but as two positive and three negative peaks on another.

The variations in signal strength from subarray to subarray are called amplitude anomalies. A set of 48 events (8 or 10 from each of 5 widely separated small regions, plus a few from miscellaneous locations), was analyzed for NORSAR signal amplitude anomalies. For each event, the signal envelope peak amplitude was computed for each subarray and expressed in dB relative to the median subarray amplitude for the event. The anomalies for the entire set, and for each of the five regions, are plotted in Figures 3-13 through 3-18. The plots reveal that some subarrays have a consistent bias (e.g., subarray 7 consistently exhibits a negative mean relative amplitude). The existence of such large biases within the array emphasizes the importance of applying bias corrections in the estimation of earthquake magnitude. At present, no compensation is made for the change in bias as a function of direction. For example, the mean relative amplitude recorded by subarray 17 changes by 14.5 dB from one region to another, and several other subarrays change by 9.5 dB. Since amplitude anomalies averaged over the six instruments in a subarray and over 8 or 10 events from a region have biases approximating half a magnitude, the application of a regionally-dependent bias correction should be provided.

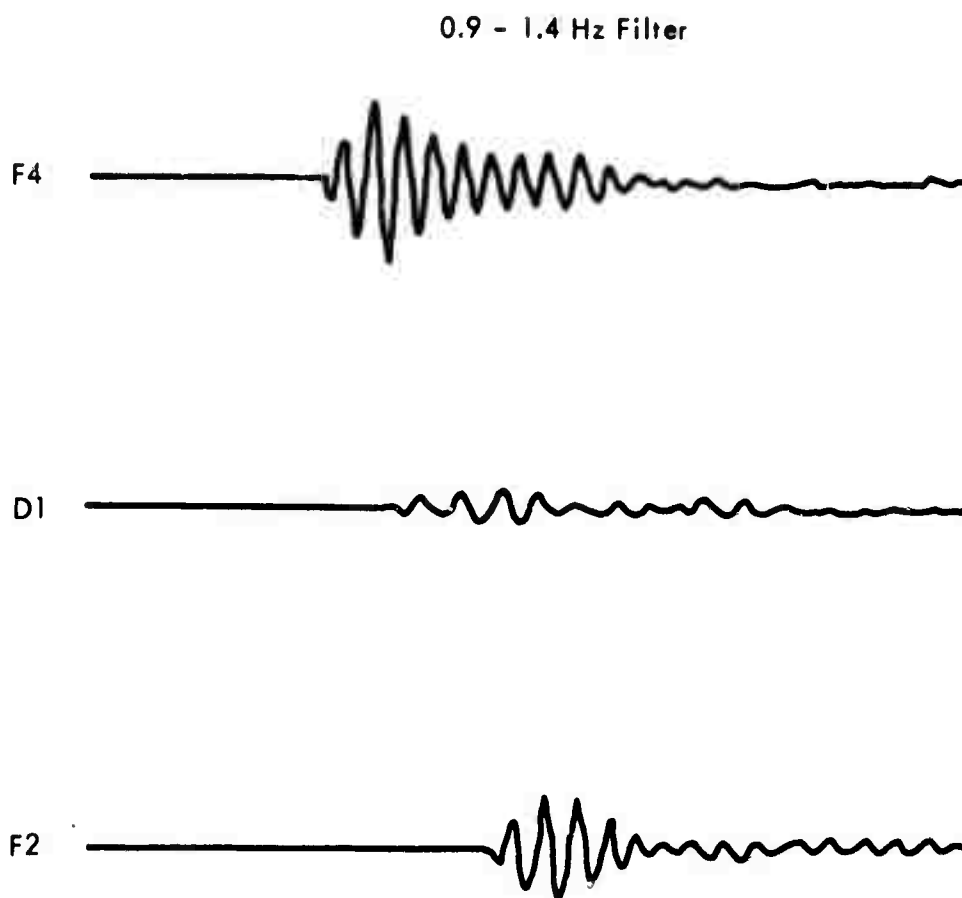


Figure 3-12. Subarray Waveform Variations

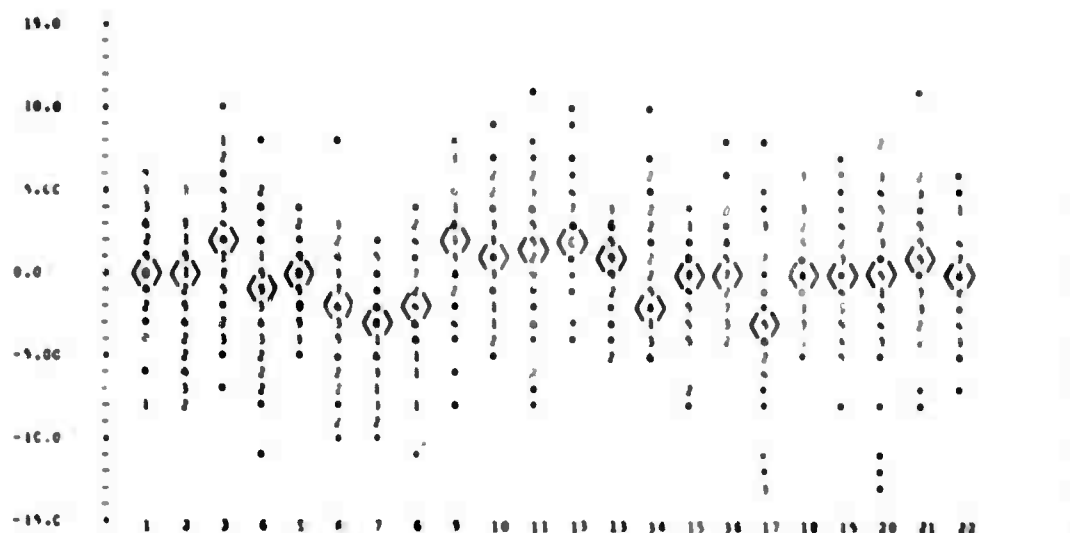


Figure 3-13. Relative Subarray Amplitude Anomalies-All Regions

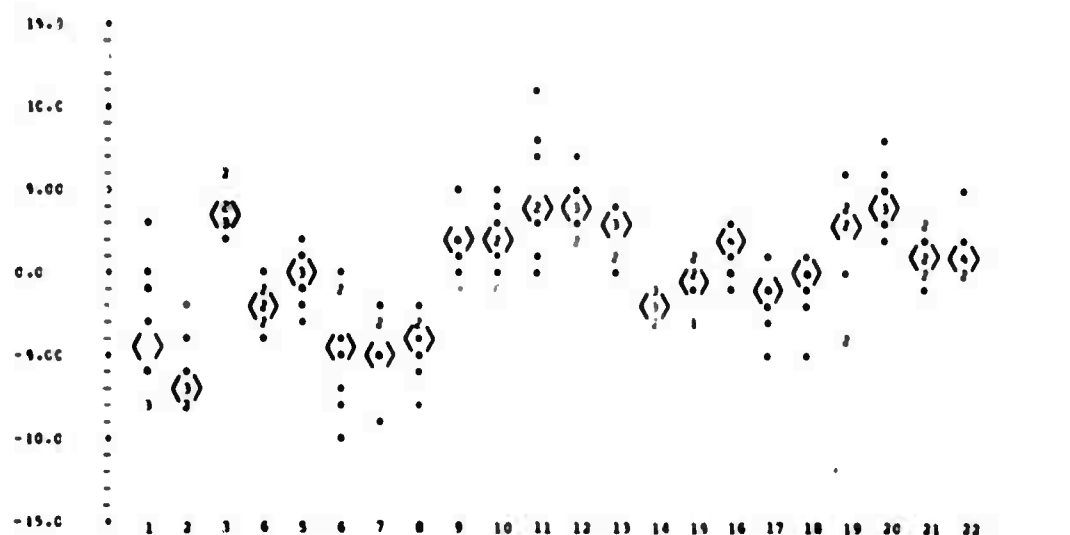


Figure 3-14. Relative Subarray Amplitude Anomalies-Andreanof Islands

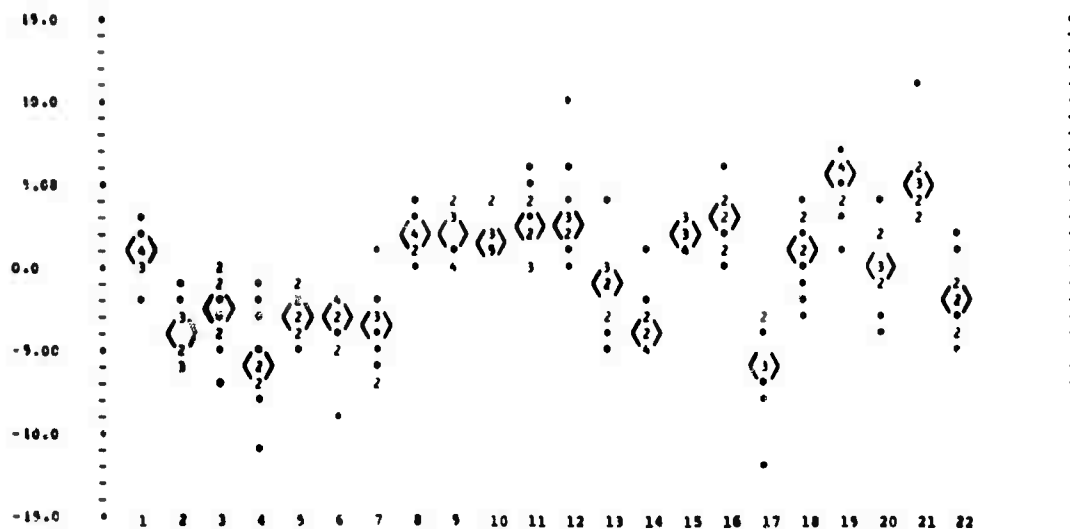


Figure 3-15. Relative Subarray Amplitude Anomalies-Philippine Island

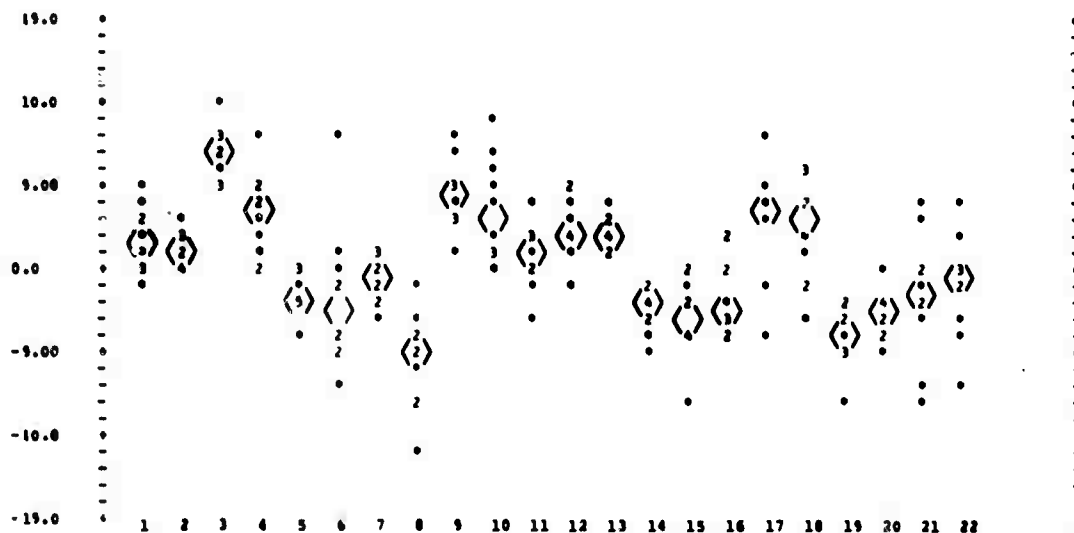


Figure 3-16. Relative Subarray Amplitude Anomalies-Kuril Island

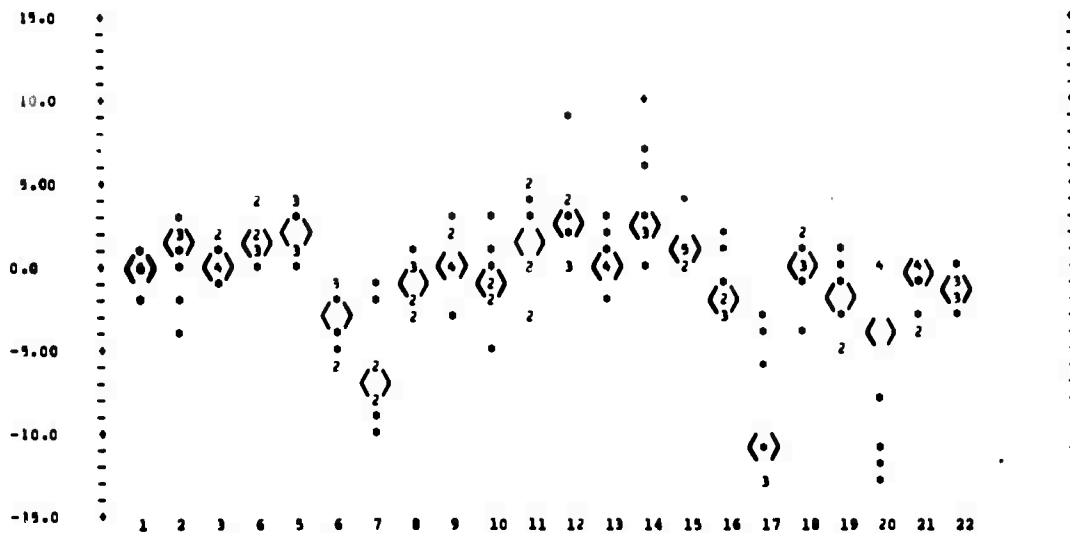


Figure 3-17. Relative Subarray Amplitude Anomalies-Eastern Kazakh

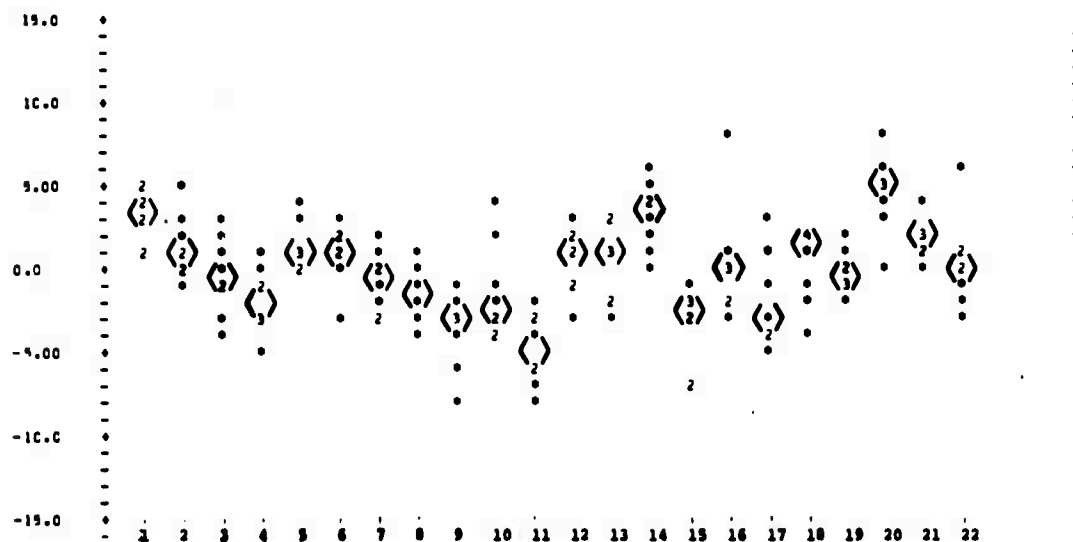


Figure 3-18. Relative Subarray Amplitude Anomalies-Mexico

3.4.2 Signal Spectrum

It has been observed [3-19, Section V.3.3] that individual signal spectra vary considerably, particularly for NORSAR data. More specifically, the signal spectra tend to peak somewhere between the regions designated long-period and short-period, and to drop off in each direction (see Figure 3-19). When signal-to-noise ratio is considered, however, the difference between signal and noise becomes apparent. Figure 3-20 illustrates the peak signal-to-noise ratio in the 1-3 Hz region for some NORSAR data. LASA data exhibits a similar peak, but it is more narrowly restricted to the region around 1 Hz. The differences in signal spectrum as a function of array location, beamforming level, and event type and location are discussed in the following sections.

3.4.2.1 Variations with Array Location

In a somewhat simplified model of seismic wave propagation, the signal waveforms from a single event would look very similar at any teleseismic array location. Under more realistic assumptions (considering the directional character of wave propagation from a fault) a large group of signals would nevertheless be expected to result in similar statistics at all array locations. Results from Montana and Norway strongly deny even this more general situation. As is illustrated in Figure 3-21, signals received at LASA show a strong tendency toward a dominant period in the 0.8-1.0 second range while signals recorded in Norway exhibited a much wider spread. Events with dominant periods of 0.5, 1.0 and 1.4 seconds were nearly equal in number. The tendency toward higher signal frequencies at NORSAR, coupled with a noise spectrum steeper than the one at LASA, makes the signal-to-noise ratio peak at frequencies up to, and occasionally beyond 3 Hz, whereas the LASA peak nearly always is near 1 Hz.

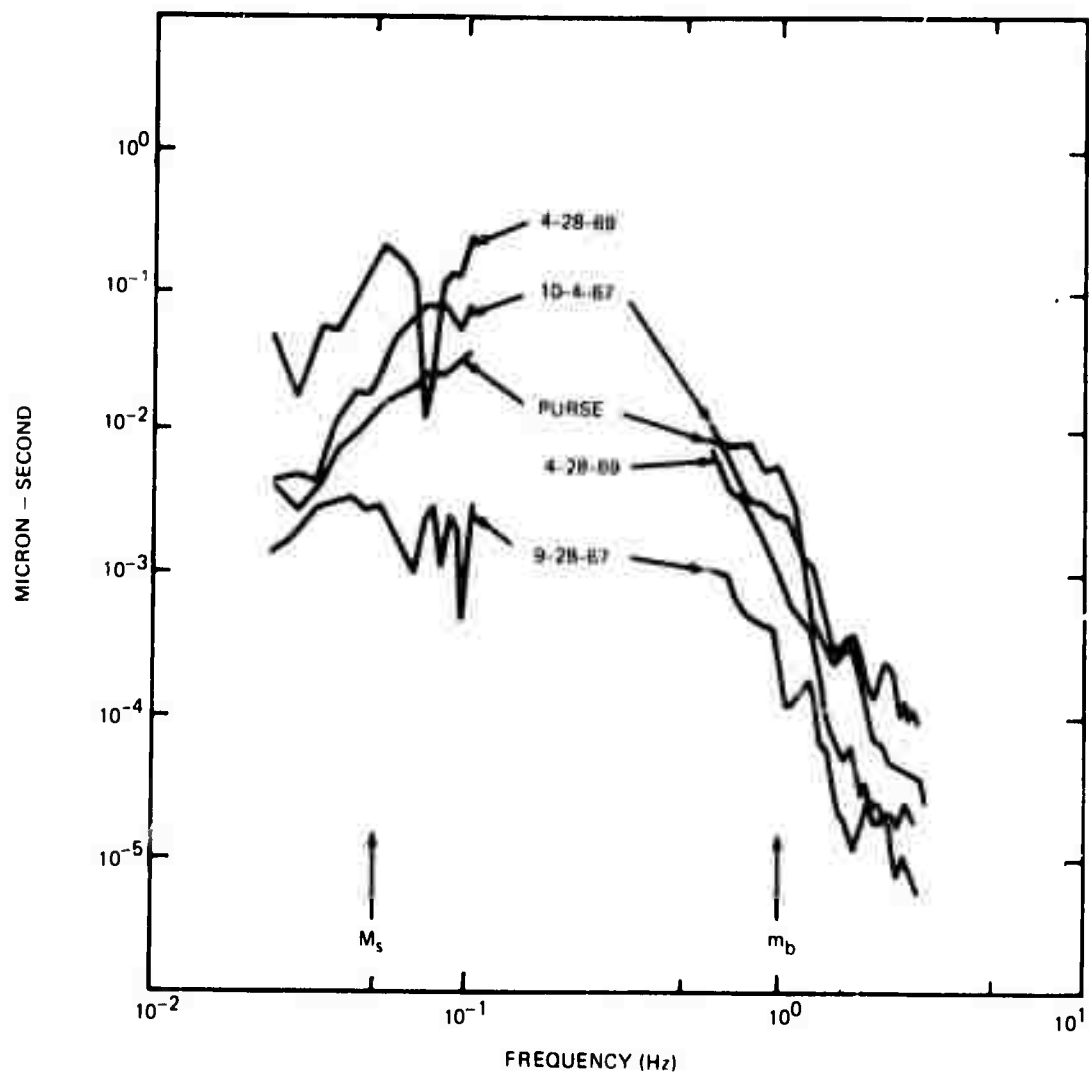


Figure 3-19. Scaled Rayleigh and P-Wave Spectra from the NTS Event Purse and Three Earthquakes (from [3-28, page 11])

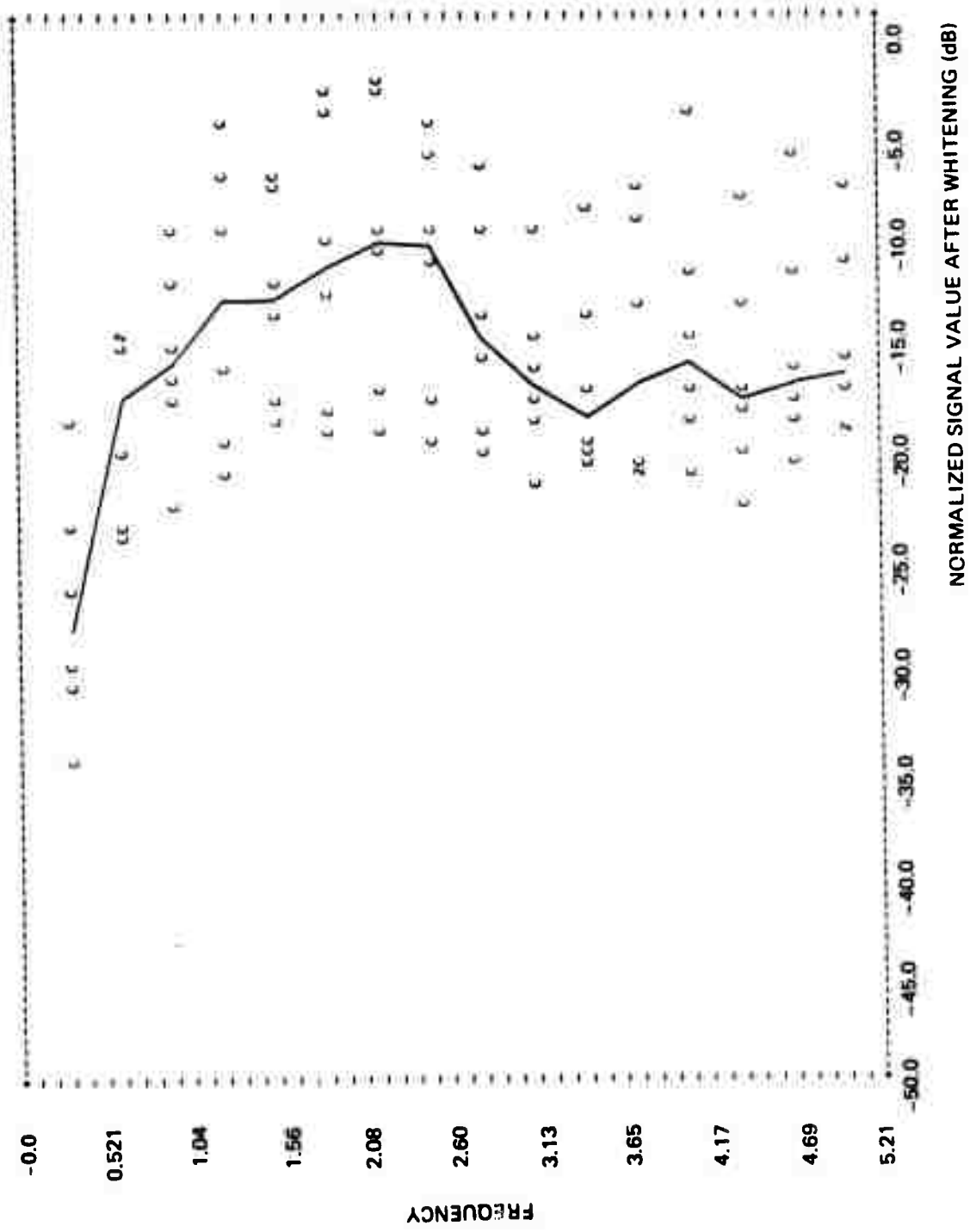


Figure 3-20. Normalized and Ideally Whitened Channel Signal Spectra and Median

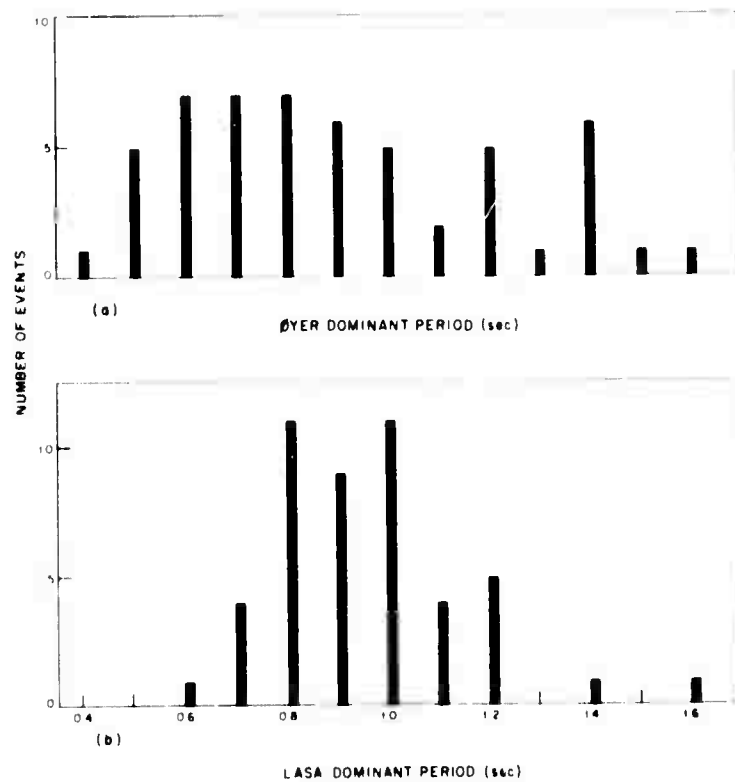


Figure 3-21. Spectral Differences in P-Phase at Norway and Montana in the Form of a Histogram of Dominant Periods (from [3-22, page 22])

3.4.2.2 Variations with Beamforming Level

In order to discuss a signal spectrum precisely, it is necessary to specify both the unavoidable and the deliberate signal processing which was applied to that signal. The instrument frequency response characteristic must either be compensated for or presented as additional information. Further distortion is introduced by analog amplifier and filter characteristics before seismometer data is digitized and recorded. The overall transfer function is very important in relating results to actual ground movement or in comparison with results obtained by different types of instruments. Transfer functions for NORSAR analog data channels are presented in Section 4.4. This section discusses only the effects of beamforming on signal spectra.

The process of delay-and-sum beamforming is simply the addition of appropriately delayed time samples from different instruments or subarray beams. Even if the signal were truly identical in all waveforms to be summed, the beamforming result would be distorted somewhat by digital quantization error in both amplitude and delay time. Amplitude quantization introduces white noise with rms amplitude $q/\sqrt{12}$ (where q is the quantization unit). This type of noise appears regardless of any beamforming. The error from quantization of delay time is strictly associated with beamforming, is frequency dependent, and is not really noise. The effect is a randomization of signal, reducing the signal components at the higher frequencies because the same time shift produces more phase shift in a shorter-period wave. Assume that sampling with period t produces in each waveform to be beamformed a random time shift (uniformly distributed in the range $\pm t/2$) from perfect alignment. Then the component with period T will be expected to have its beam amplitude reduced by a factor of $(T/\pi t) \sin(\pi t/T)$ from that which would have resulted with perfect alignment. It can be seen that for waves with periods long compared to the sampling rate ($T \gg t$), this factor is essentially unity, but

that it drops toward zero for waves with frequencies approaching the sampling frequency. At half the sampling frequency this amplitude reduction factor is $2/\pi$, or about 0.64.

Augmenting the effect of unavoidable time delay quantization is the occurrence of alignment errors which cause displacements beyond the range $\pm t/2$, and thus can result in more severe attenuation of high frequencies.

The above analysis indicates the minimum departure from idealized beamforming. In practice, the signals being summed are not identical, so real beamforming differs from ideal beamforming. Since signal coherency is to some extent a function of distance between instruments, array beamforming departs from the ideal much more than does subarray beamforming. Figure 3-22 indicates how subarray beamforming has little effect on the spectrum (signals are relatively coherent over subarray distances) but array beamforming causes a significant relative drop in the high frequency energy. This figure actually shows signal-to-noise ratio rather than signal alone, but the spectrum of the incoherent noise is essentially independent of beamforming level.

3.4.2.3 Variations with Event Type and Location

Signal spectra reaching a single array tend to vary characteristically as a function of type (earthquake or explosion, large or small, etc.) and location. The variation with type is used commonly in discrimination analysis. Figure 3-23 illustrates the distinct tendency for explosions to have higher frequency signals than do earthquakes, and the slight tendency for larger events to have relatively more energy at lower frequencies. Both trends can be partially explained in terms of the extent of the disturbance. When a signal is generated by an extended source it is less likely that high frequency energy would be in phase as it reached the detecting array.

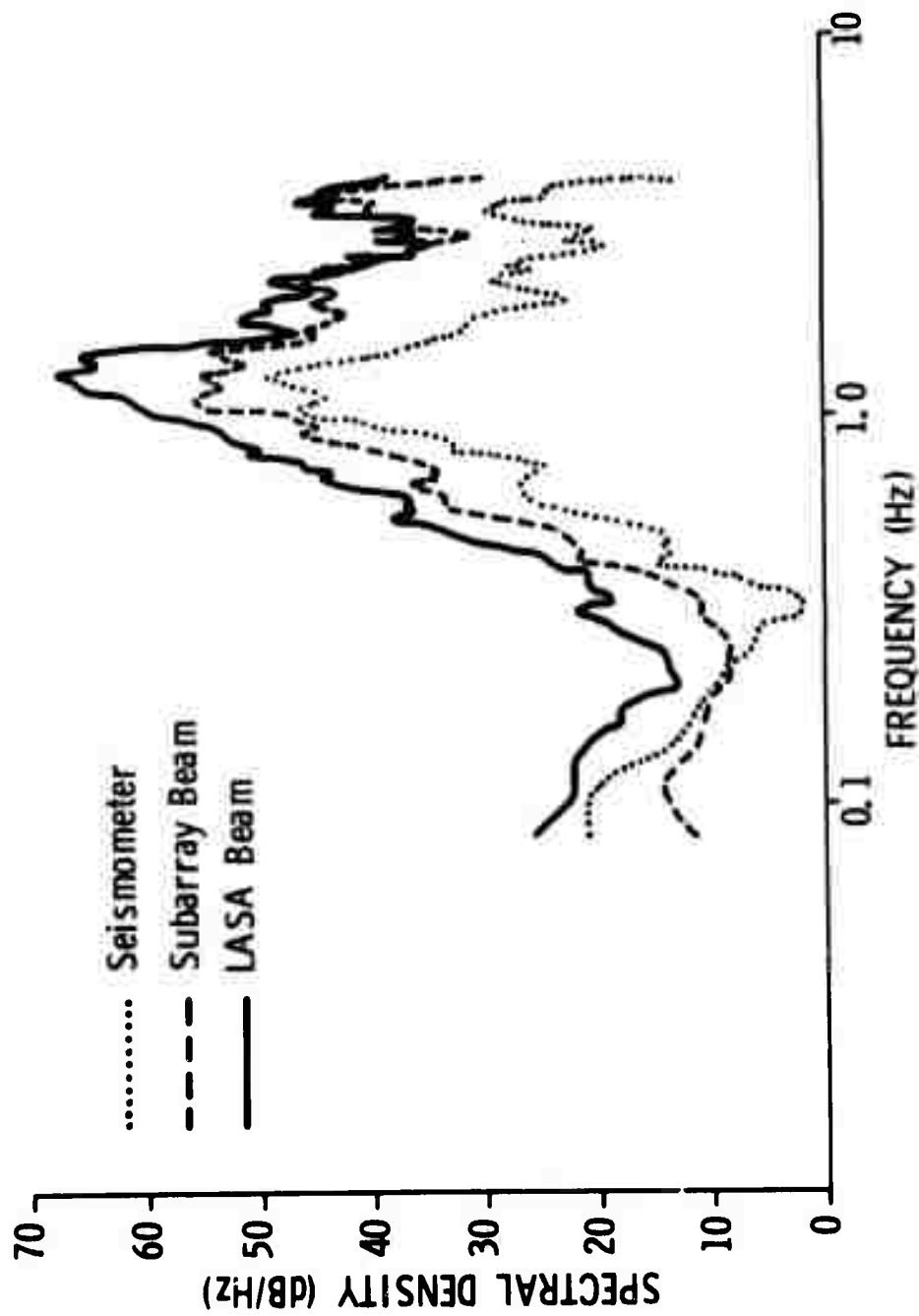


Figure 3-22. Longshot S/N Spectrum

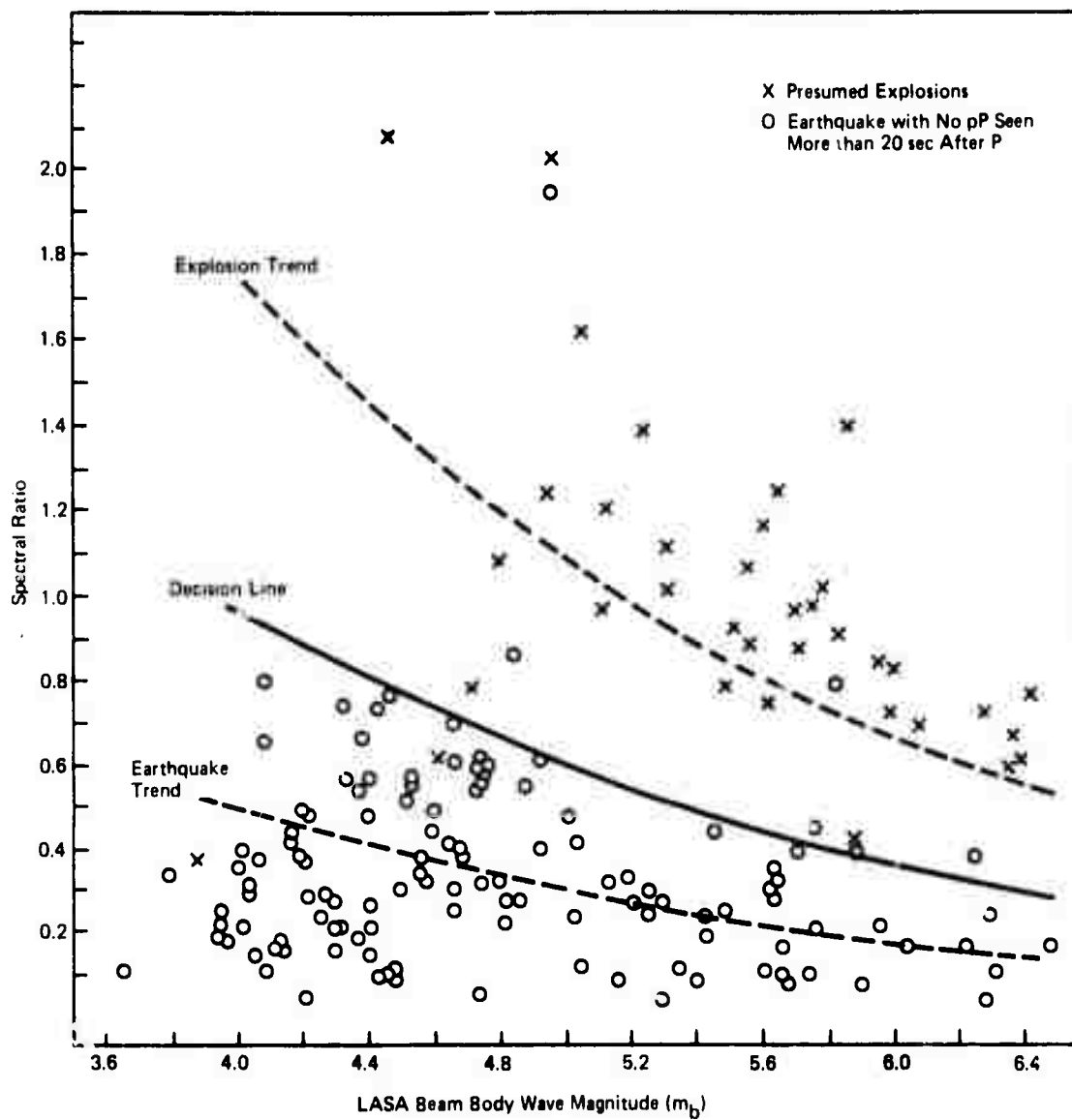


Figure 3-23. Discrimination Using LASA Short-Period Spectral Ratio
(from [3-23, page 3])

Variations with location can be explained in several ways, all relating to crustal structure. Different fault regions may differ in natural resonant frequency, thereby creating different seismic wave spectra right at the source. Even if two regions generate identical spectra, however, the differences in transmission path could produce different relative distortions. Fault orientation also can affect the spectrum. A fault perpendicular to the array beam can generate a relatively coherent signal along its entire length; one aligned with the beam is seen as an extended-duration, incoherent event because of the difference in travel time from one end of the fault to the other.

One indication of spectral variation with location may be seen in the differences between the fundamental dominant frequencies of events from different regions. For example, eleven events from the Kuril Islands area exhibited an average dominant frequency of 1.06 Hz (ranging from 0.82 to 1.37 Hz) while eight events from Central America had dominant frequencies which averaged only 0.88 Hz (ranging from 0.74 to 1.02 Hz). These events were among those selected for the study of NORSAR signal and noise characteristics reported in [3-20].

3.5 WAVEFORM FILTERING

3.5.1 Purpose and Theoretical Background

The analysis of seismic waves always involves filtering, even if that filtering is no more than the characteristic response of the seismometer itself. In practice, especially with seismic array systems, analog and digital filtering augment the natural filtering of the instrument. The purpose of filtering generally is to aid in detecting and analyzing seismic events by increasing the signal-to-noise ratio. This can be

accomplished simply by cutting off frequencies in which noise is relatively strong and signal relatively weak, or by much more sophisticated techniques.

If signal and noise had exactly the same spectral distribution of energy, or if both had completely unpredictable spectra, filtering would be fruitless. Because the two spectra are reasonably predictable and differ from each other, spectral filtering can be used to emphasize those parts of the spectrum in which signal-to-noise ratio (SNR) is relatively high, and attenuate those parts of the spectrum in which the ratio is low. It is well known (see [3-34, page 244] and [3-31, page 287]) that one particular filter maximizes SNR when the signal and noise spectra are known. That filter may be described as a noise-prewhitening filter in cascade with a signal-matching filter. The noise-prewhitening filter has a response which is the inverse of the noise spectrum; therefore, application of the prewhitening filter alone would make the background noise spectrum flat. The signal-matching part of this two-part filter then has a response identical to the "whitened" signal spectrum.

Unfortunately, the background noise spectrum is not really constant and the signal spectra may vary considerably from one event to another, as explained in Sections 3.3.3 and 3.4.2. Nevertheless, several types of filters approximating the matched filter to a greater or lesser degree can improve the SNR significantly. For example, the noise-prewhitening filter alone will perform within 1 dB of the optimum matched filter, provided its bandwidth is large enough to include all frequencies for which the output SNR is within 2.5 dB of its maximum value, but sufficiently narrow to exclude all frequencies for which the SNR is more than 12 dB below this maximum (see [3-1, page 2-16]).

3.5.2 Types of Digital Filters

The concepts of digital filtering are addressed in detail in [3-4]. The type of digital filters currently used in both the LASA and NORSAR DP systems is a recursive Butterworth bandpass filter. These filters have an essentially flat response over a particular range of frequencies, then cut off sharply (18 dB/octave) beyond that range. The bandpass region is selected to pass as much of the typical signal energy as possible while blocking frequencies in which seismic signals are weak compared to background noise. Figure 3-24 contains response characteristics of a number of bandpass filters (the designation 09-35 means the 3 dB points are 0.9 and 3.5 Hz) which have been used in various analysis programs. These filters sharply reduce the effect of strong low-frequency noise while preserving the essential part of short-period signals.

When the background noise has a known, relatively stable spectrum, a more refined type of filter is possible—the prewhitening filter. Making the background noise white assures that all parts of the signal spectrum with a good local SNR will contribute to the overall SNR. (With bandpass filtering, by contrast, a portion of the spectrum with high SNR but low amplitude would be dominated by another portion of the spectrum with comparatively low SNR but high amplitude.) Under certain circumstances, such as SNR essentially independent of frequency or signal spectrum completely unknown or unpredictable, this type of filtering is the best that can be done. No filter response characteristic is illustrated here; it is simply the inverse of the assumed noise spectrum.

With further knowledge of the signal spectrum, more sophisticated and more effective shaped filters (as opposed to flat bandpass filters) are possible. As indicated in Section 3.5.1, the matched filter is ideal when both signal and noise spectra are precisely known. It is unproductive to attempt to generate a matched filter for spectra which are variable or

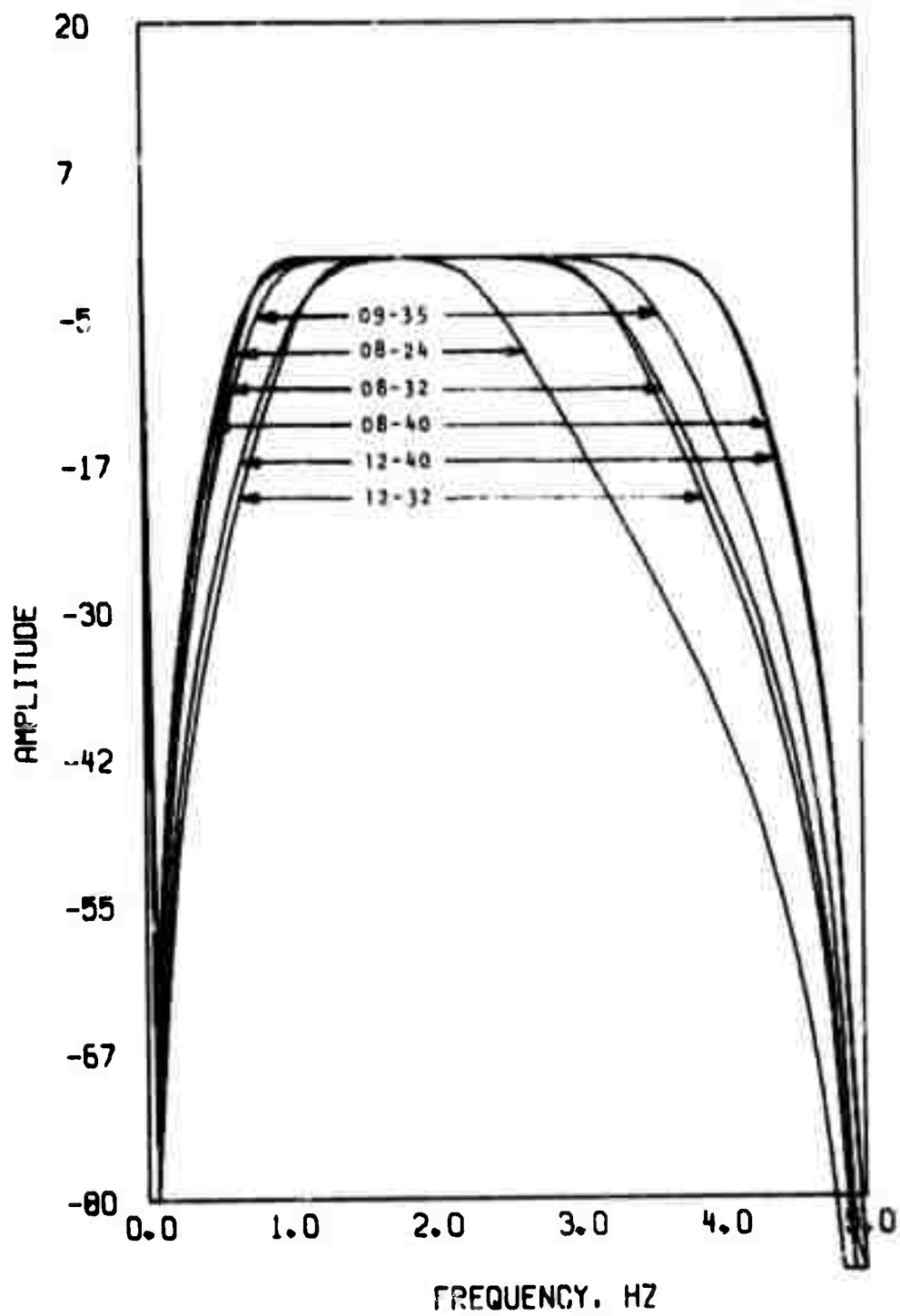


Figure 3-24. Wideband Filter Response Characteristics

imprecisely known, so the approach taken in NORSAR analysis was to test and compare a number of simple shaped filters approximating the range of matched filters optimal for different events. Some of the shaped filters considered are shown in Figure 3-25. The coefficients of these digital filters are given in [3-20]. All are nonrecursive filters, and none requires more than six coefficients.

The results of these analyses suggest that noise prewhitening filters may yield significant improvements compared to bandpass filters. However, because of the variability of the NORSAR signal spectra, matched filters are probably impractical.

3.5.3 Results of Filtering

A number of studies have been performed on the results of digital filtering applied to seismic wave analysis. Pertinent references include [3-10, 3-12, 3-18, 3-19, and 3-20].

There are a number of different possible goals of filtering which may be applied at different times or even at different stages in the analysis of the same event. It is generally desirable to maximize the SNR, but sometimes this goal must be subordinated to other considerations.

Determination of precise signal arrival time and relative time anomalies requires that the apparent start time of an event signal should not be shifted by the filtering process. Parameter extraction (determination of period, velocity, later phases, etc.) is best performed with an undistorted waveform, so only bandpass filtering is permitted before this stage. For initial detection of events, however, any distortion of the waveform is permissible so long as it does not cause serious errors in the initial determination of event location.

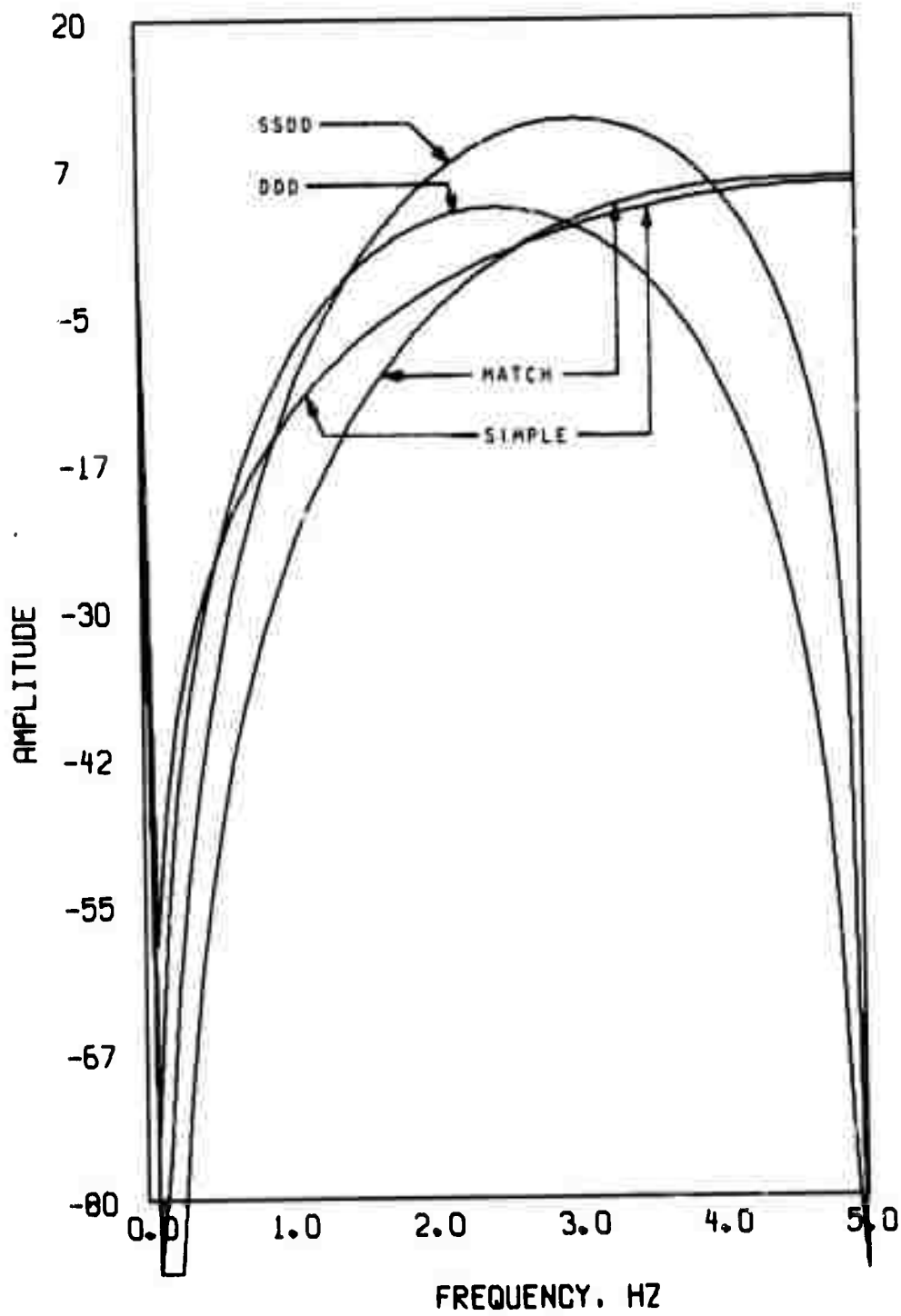


Figure 3-25. Shaped Filter Response Characteristics

Some of the results of digital filtering studies are summarized in the following sections.

3.5.3.1 Increasing the Signal-to-Noise Ratio

One possible objective of digital filtering is the maximization of filter gain, defined as the ratio of SNR after filtering to SNR before filtering (expressed in dB).

An early study of filtering gain is contained in [3-35]. LASA data for two different events is examined under a variety of array configurations, processing sequences and filters. Over all combinations, filtering gain ranged from 4.60 dB to 20.55 dB. The three filters used were all band-pass, and formed a nesting set. The widest filter (0.425-2.825 Hz) consistently gave the poorest performances, while the narrowest filter (0.9-1.4 Hz) always was best. It is interesting to note that the gain attributable to filtering after subarray beamforming is as much as 7 dB higher (20.55 dB vs 13.40 dB) than the gain of filtering performed before subarray beamforming, although overall gain is invariant to the order of these operations. The processing configuration must be well defined before a quantitative filtering gain is meaningful.

Appendix III of [3-18] contains the results of an analysis of 25 NORSAR events. In this study, effectively 33 different filters were applied to beams formed from 18 seismometers (the Interim NORSAR system). No one filter in this set proved best for more than four of the 25 events. Over the 25 events, maximum filtering gain ranged from 2.11 dB to 27.90 dB. These variable results indicated that no single filter was likely to be universally good (at least at NORSAR), but that shaped (as opposed to flat bandpass) filters were serious contenders for the rating of 'generally best'.

3.5.3.2 Prewhitening the Background Noise

As was mentioned in Sections 3.5.1 and 3.5.2, a prewhitening filter offers a near-optimal approach to maximizing SNR when the noise spectrum is known and stable, but the signal spectrum is completely unknown or widely variable. Unfortunately, there is no simple analytical procedure for generating the prewhitening filter corresponding to a given noise spectrum. In the NORSAR study cited in the previous section, it was shown that one or more stages of differentiation provided a crude prewhitening effect, but it was felt that a somewhat better approximation could be found. The four shaped filters in Figure 3-25 are the result of both trial-and-error and semisystematic attempts to produce a filter response characteristic matching the inverse of the NORSAR noise spectrum. (A different prewhitening filter probably would be required for any other site; LASA noise definitely differs from NORSAR noise.)

Plotted in Figure 3-26 are the results of applying each of the four candidate prewhitening filters to an average NORSAR noise spectrum. (The unfiltered noise spectrum and the output of the current NORSAR processing filter are shown, as well.) An ideal prewhitening filter would yield a horizontal line in this figure; none of these achieves that goal. Nevertheless, the filters designated MATCH and SIMPLE produce nearly white noise over most of the spectrum and the SSDD curve is relatively flat in the middle. These results indicate how closely a noise spectrum can be matched with relatively simple filters.

3.5.3.3 Maximizing Detectability

Maximizing the probability of detecting events is not necessarily accomplished by prewhitening the background noise, and is not the same as maximizing the SNR or filtering gain. Most event detection schemes,

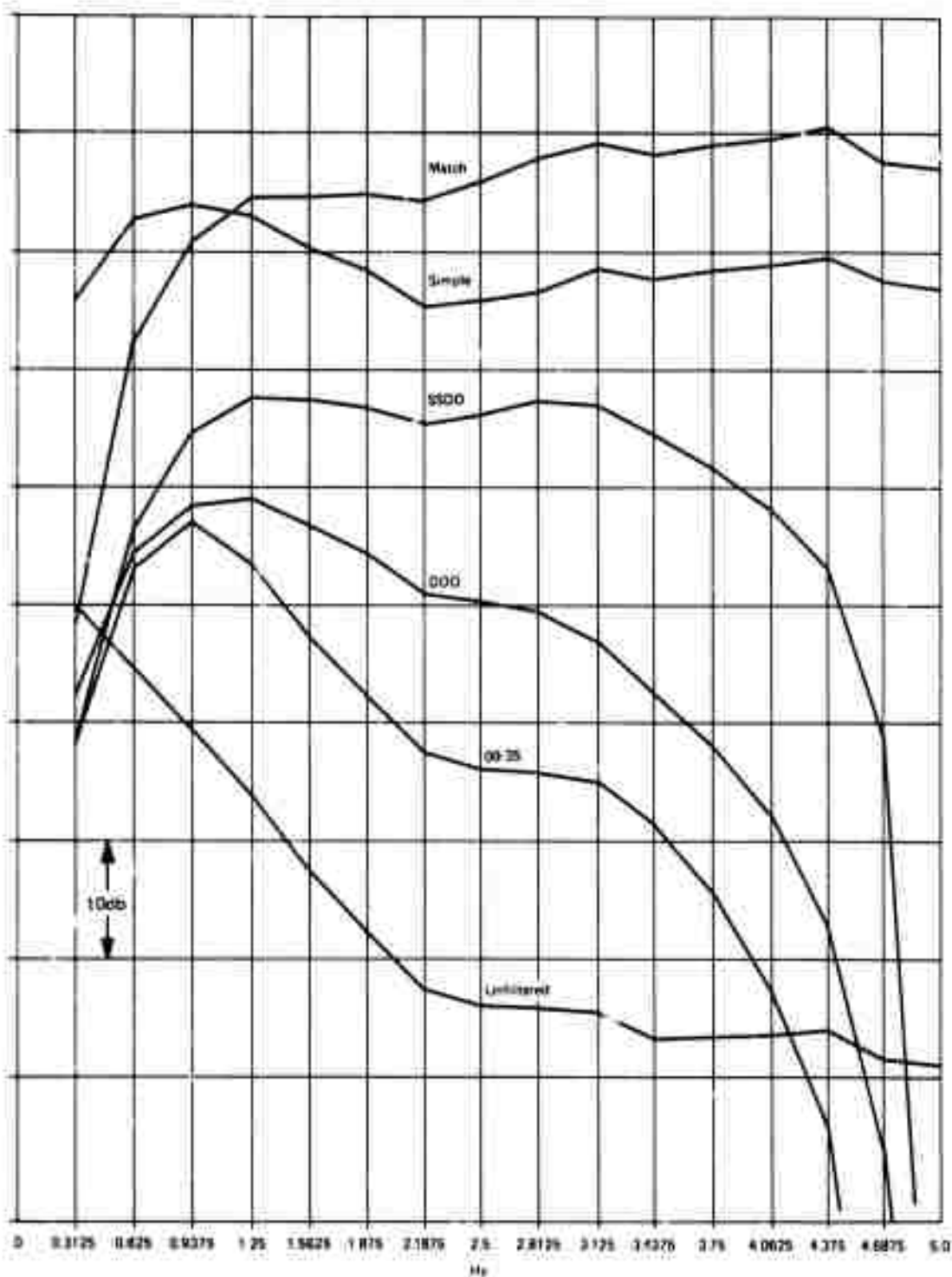


Figure 3-26. Effect of Selected Filters on the Spectral Density Functions of Average Beam Noise (with Arbitrary Scaling for Better Visibility)

in spite of their complex filtering, summing and other numerical manipulation, ultimately reduce to the observation of a single function of time, which is somehow related to seismic wave energy. When that function crosses a preset threshold it is assumed to indicate the arrival of an event. (See [3-19] for a more detailed explanation of this model.) The lower that detection threshold is set, the more likely it is that a small event will be detected; however, a low threshold also increases the probability of false alarms. The margin of safety between normal excursions of that detection function and the excursion created by an event is a measure of how good the detection processing (including filtering) is at enhancing detections. This measure is the detectability defined in equation (3-3) of Section 3.2.1. Calculation of this detectability value for large numbers of events processed in different ways has helped indicate the optimal processing techniques and filters for NORSAR events. Figure 3-27 (part of the complete results in [3-20]) is a plot showing how different filters compare in detectability. (A filter invariably better than the others would have all event points plotted at the right margin; the amount of dispersion to the left indicates the degree of departure from the ideal case. The filter which proves best in this type of analysis (here, apparently, either the 1.2-3.2 Hz bandpass or the DDD filter) is a good candidate for use in detection processing.

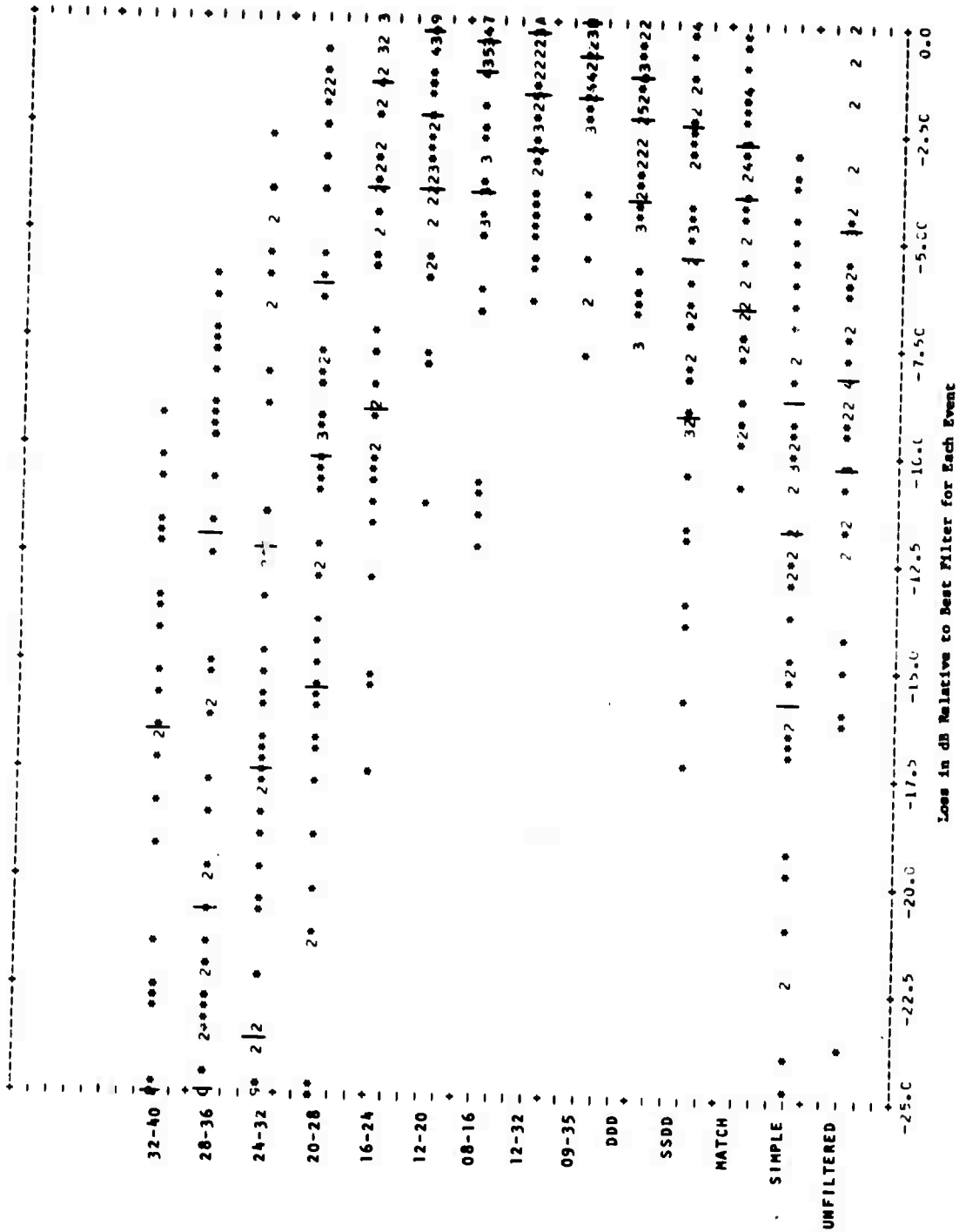


Figure 3-27. Relative Detectability Comparison for Various Predetection Filters and Coherent Beamforming

3.6 ANNOTATED BIBLIOGRAPHY

The following references pertaining to seismic signal and noise characteristics are divided into three groups. The first group (Section 3.6.1) consists of quarterly and final reports prepared by IBM under a series of contracts relating to seismic signal processing. The second group (3.6.2) consists of semiannual technical summaries of seismic discrimination studies performed at MIT Lincoln Laboratory. The third group (3.6.3) consists of pertinent miscellaneous references.

3.6.1 IBM Quarterly and Final Technical Reports

- 3-1. "Large Aperture Seismic Array Signal Processing Study," IBM
Final Report, Contract SD-296, 15 July 1965.

This early report contains general information on digital filtering and beamforming, including a brief discussion of various signal processing losses. Sections 1 and 2, and Appendices E and F are of particular interest in understanding the interactions between signal processing techniques and signal and noise characteristics.

- 3-2. "LASA Signal Processing, Simulation, and Communications Study,"
IBM First Quarterly Technical Report, Contract AF 19(628)-5948,
1 May 1966.

Early concepts of system data flow and filtering requirements are contained in Section 3 and Appendix E.

- 3-3. "LASA Signal Processing, Simulation, and Communications Study,"
IBM Second Quarterly Technical Report, Contract AF 19(628)5948,
September 1966.

Appendix B contains the results of an early study of signal and noise characteristics which revealed that performance of the LASA would be improved by eliminating some of the more tightly clustered seismometers. (At small separations noise was not independent, so beamforming gain enhanced noise as well as signals.) Appendix E describes a number of data analysis programs for generating recursive digital filter coefficients and calculating their frequency response, performing recursive digital filtering, calculating signal and noise power, calculating cross covariance factors, and calculating power spectra.

- 3-4. "LASA Signal Processing, Simulation, and Communication Study,"
IBM Final Report, Contract AF19(628)-5948, ESD-TR-66-635,
March 1967.

The basic LASA signal processing algorithms are defined in Figure 2-6. Digital filtering is addressed in detail in Section 3.7. Some spectral analysis was performed on signal-to-noise ratios and beamforming gain, and some effects of filtering were studied. These are reported in Section 3.8. Useful programs, including one for spectral analysis, are described in Section 4.

- 3-5. "LASA Experimental Signal Processing System," IBM First
Quarterly Technical Report, Contract F19628-67-C-0198,
ESD-TR-67-458, February 1967.

This report describes the data processing system configuration. It has only marginal interest relative to signal and noise characteristics, but is included for completeness.

- 3-6. "LASA Experimental Signal Processing System," IBM Second
Quarterly Technical Report, Contract F19628-67-C-0198,
ESD-TR-67-602, May 1967.

Noise correlation coefficient as a function of distance between subarrays is plotted in Figure F-7. Two examples of signal-to-noise spectra are presented in Figures F-8 and F-9. Appendix D contains the various equations employed in detection processing, with emphasis on the types of scaling which occur.

- 3-7. "LASA Experimental Signal Processing System," IBM Third Quarterly Technical Report, Contract F19628-67-C-0198, ESD-TR-68-149, August 1967.

This report contains an extensive discussion of the fast Fourier transform and some results of a study of noise correlation across the LASA array.

- 3-8. "LASA Experimental Signal Processing System," IBM Fifth Quarterly Technical Report, Contract F19528-67-C-0198, ESD-TR-68-450, February 1968.

Figure 1 shows a typical LASA seismometer noise spectrum. Appendix VIII deals with long-period signal processing, and includes plots of signal-to-noise spectra and filter characteristics. The use of spectral characteristics to distinguish between earthquakes and explosions is discussed briefly in Appendix IX.

- 3-9. "LASA Experimental Signal Processing System," IBM Sixth Quarterly Technical Report, Contract F19628-67-C-0198, ESD-TR-68-451, May 1968.

This report is concerned almost exclusively with the design of the NORSAR array under the assumption that Montana and Norway are similar as seismic array locations.

- 3-10. "LASA Experimental Signal Processing System," IBM Final Technical Report, Contract F19628-67-C-0198, ESD-TR-60, March 1969.

Appendix II contains plots of the noise spectrum at LASA. Figure 32 shows the spectral response of the seismometer itself, and Section VII.13 presents the use of filter compensating for seismometer response.

- 3-11. "Integrated Seismic Research Signal Processing System," IBM First Quarterly Technical Report, Contract F19628-68-C-0400, ESD-TR-69-299, November 1968.

Long-period signal characteristics are discussed in Appendix I. Appendix III presents the theory for high-resolution noise analysis (location and frequency content of noise in inverse phase velocity space).

- 3-12. "Integrated Seismic Research Signal Processing System," IBM Second Quarterly Technical Report, Contract F19628-68-C-0400, ESD-TR-69-357, February 1969.

Short-period signal and noise characteristics at NORSAR are covered extensively in Appendix IV. This study includes the effects of seismometer depth, beamforming and filtering on the signal-to-noise ratio.

- 3-13. "Integrated Seismic Research Signal Processing System," IBM Third Quarterly Technical Report, Contract F19628-68-C-0400, ESD-TR-70-25, May 1969.

Section IV.4 contains tables of noise correlation for different LASA configurations.

- 3-14. "Integrated Seismic Research Signal Processing System," IBM
Fourth Quarterly Technical Report, Contract F19628-68-C-0400,
ESD-TR-70-265, August 1969.

Appendix IV discusses Alaskan Array integration, including the long-period beamforming algorithms and an evaluation of beam signal loss and crosstalk.

- 3-15. "Integrated Seismic Research Signal Processing System," IBM
Fifth Quarterly Technical Report, Contract F19628-68-C-0400,
ESD-TR-70-306, November 1969.

Long period signal processing results are discussed in Appendix II. Appendix IV describes the Interim NORSAR system (one seismometer per subarray) which was used in early NORSAR signal and noise analysis studies.

- 3-16. "Integrated Seismic Research Signal Processing System," IBM
Sixth Quarterly Technical Report, Contract F19628-68-C-0400,
ED-TR-71-388, February 1970.

This report discusses weighted array beamforming (to maximize signal-to-noise power ratio) and NORSAR instrumentation characteristics in Appendices IV and VI, respectively.

- 3-17. "Integrated Seismic Research Signal Processing System," IBM
Seventh Quarterly Technical Report, Contract F19628-68-C-0400,
ESD-TR-72-128, May 1970.

Appendix VI discusses the problem of signal distortion as a result of multiple-path phenomena. It includes some analysis of the signal and noise spectra, and presents preliminary results of techniques for overcoming the losses caused by distortion.

- 3-18. "Integrated Seismic Research Processing System," IBM Eighth Quarterly Technical Report, Contract F19628-68-C-0400, ESD-TR-71-393, August 1970.

Short period signal and noise characteristics of the Interim NORSAR system are analyzed extensively in Appendix III. The possibility of filtering with other than flat-topped bandpass filters was investigated, and appeared very promising. It was discovered that some previous efforts to determine power spectra might have been misleading because "leakage" in the fast Fourier transform process tended to make steep slopes in the spectrum appear shallower.

- 3-19. "Integrated Seismic Research Signal Processing System," IBM Ninth Quarterly Technical Report, Contract F19628-68-C-0400, ESD-TR-72-122, November 1970.

Appendix V of this report is a sequel to Appendix III of Reference [3-19]. It presents more accurate signal and noise spectra (corrected for "leakage"), and suggests particular filters which might improve detectability in the NORSAR system.

- 3-20. "Integrated Seismic Research Signal Processing System," IBM Final Technical Report, Contract F19628-68-C-0400, ESD-TR-72-139, September 1971.

Appendix III of this report contains an extensive analysis of the signal and noise characteristics of the complete NORSAR array. It was learned in this study that the background noise spectrum can vary appreciably from time to time, so that no single filter can give the best results consistently, and painstaking filter design to match a particular curve may be wasted effort.

3.6.2 Lincoln Laboratory Semiannual Technical
Summaries in Seismic Discrimination

- 3-21. "Seismic Discrimination," Semiannual Technical Report to the
Advanced Research Projects Agency, Lincoln Laboratory, MIT,
31 December 1967.

Section IV briefly discusses signal and noise characteristics (especially noise coherency) in early Norway survey data. Section VI contains results pertaining to LASA noise, including typical short-period and long-period spectra.

- 3-22. "Seismic Discrimination," Semiannual Technical Report to the
Advanced Research Projects Agency, Lincoln Laboratory, MIT,
30 June 1968.

Figure 4 is a "sonogram" showing how the power in one particular event is distributed over frequency and time. Several parts of Section II are concerned with analysis of signals and noise. Of particular interest are Figures 12 and 13 which show, respectively, a typical Norway noise spectrum and histograms of dominant signal periods at Norway and at LASA.

- 3-23. "Seismic Discrimination," Semiannual Technical Report to the
Advanced Research Agency, Lincoln Laboratory, MIT,
31 December 1968.

Section I describes efforts to discriminate between earthquakes and explosions, largely on the basis of spectral differences. Section III-C describes the use of high-resolution frequency-wavenumber mapping to analyze short-period noise.

- 3-24. "Seismic Discrimination," Semiannual Technical Report to the Advanced Research Projects Agency, Lincoln Laboratory, MIT, 30 June 1969.

Section I includes the results of further studies on spectral discrimination. Subsection II-B briefly describes the use of computer-generated movies to depict seismic activity. The most striking revelation of the movies was a distinct and repeated migration of aftershock epicenters at approximately 100 km/hr.

- 3-25. "Seismic Discrimination," Semiannual Technical Report to the Advanced Research Projects Agency, Lincoln Laboratory, MIT, 31 December 1969.

Section I includes the results of a study of the short-period spectra of four presumed explosions seen at LASA.

- 3-26. "Seismic Discrimination," Semiannual Technical Report to the Advanced Research Projects Agency, Lincoln Laboratory, MIT, 30 June 1970.

Section III contains the results of frequency-wavenumber studies at NORSAR and signal coherence studies at LASA.

- 3-27. "Seismic Discrimination," Semiannual Technical Report to the Advanced Research Projects Agency, Lincoln Laboratory, MIT, 31 December 1970.

Long-period amplitude spectra and short-period transfer functions for explosions observed at LASA are presented in Section I. Section II-E describes an experiment to measure directly the earth's attenuation of short-period seismic waves. Several types of amplitude spectra appear in Section III.

- 3-28. "Seismic Discrimination," Semiannual Technical Report to the Advanced Research Projects Agency, Lincoln Laboratory, MIT, 30 June 1971.

Combined long and short-period spectra of several natural and nuclear events are presented in Section I.

3.6.3 Miscellaneous References

- 3-29. Charles F. Richter, Elementary Seismology, W. H. Freeman and Company, San Francisco, 1958.

A basic textbook, this includes sections on the sources and transmission mechanisms of seismic waves. Other chapters and appendices give a basic understanding of seismometers, earthquake location, earthquake statistics, etc.

- 3-30. "Problems in Seismic Background Noise", VESLAC Advisory Report, Acoustics and Seismic Laboratory, Institute of Science and Technology, The University of Michigan, Ann Arbor, Michigan, October 1962.

This report is a collection of sixteen independent papers on various aspects of the seismic noise problem. Included among these are several actual measures of background noise, and some discussions of the sources of such noise.

- 3-31. Mischa Schwartz, Information Transmission, Modulation and Noise, McGraw-Hill Book Company, Incorporated New York, 1957.

Page 327 and following pages define the concept of "quantization noise" and explain how to calculate it.

- 3-32. J. Capon, "High-Resolution Frequency-Wavenumber Spectrum Analysis", Proc. IEEE 57, pp 1408-1418, August 1969.

The titled technique is described here.

- 3-33. J. Capon, "Investigation of Long-Period Noise at LASA", Technical Note 1968-15, Lincoln Laboratory, M.I.T., 3 June 1968

Both conventional and high-resolution frequency-wavenumber techniques are described here.

- 3-34. Wilbur B. Davenport, Jr. and William L. Root, Random Signals and Noise, McGraw-Hill, New York 1963.

Section 11-7 contains a derivation of the "matched filter" which maximizes signal-to-noise ratio.

- 3-35. "Parametric Study of Seismic Array Gain", IBM Scientific Experiment Test Results, Contract F19628-67-C-0195, June 1968.

Both filtering and beamforming gains are determined for two selected LASA events, under a variety of array and processing configurations, using three different bandpass filters.

- 3-36. "Analysis of Long-Period Noise", Texas Instruments Incorporated Special Scientific Report No. 12, Contract AF 33(657)-16678, 18 October 1967.

Characteristics of LASA long-period noise are analyzed and discussed.

Section 4

DATA ACQUISITION

The data acquisition subsystem of a large seismic array signal processing system consists of the sensor instrumentation, the data acquisition control and recording equipment, the data communication network, and the field instrumentation monitoring and remote control facilities. In this section, the significant aspects of the basic requirements, the design philosophy and the implementation of the data acquisition portions of the Integrated Seismic Research Signal Processing System (ISRSPS) are presented and discussed.

Figure 4-1 shows the LASA, NORSAR and ALPA arrays and the principal features of the various data control and processing centers which comprise the ISRSPS, together with the interconnecting communication links. Since LASA and NORSAR are combined long-period and short-period arrays, the associated data acquisition subsystems are considerably more complex than that of ALPA, which is a long-period array only. The basic difference between the LASA and NORSAR systems is that the primary data acquisition and control functions for LASA are implemented at the LASA Data Center (LDC) in Billings, Montana, at a considerable distance from the Seismic Array Analysis Center (SAAC) near Washington, D.C. which contains the LASA data recording, processing and analysis functions, whereas for NORSAR all of these functions are implemented at the Norwegian Data Processing Center (NDPC) in Kjeller, Norway. This difference in system configurations has contributed significantly to the development of a more fully integrated and highly automated system for NORSAR.

Although various aspects of the ISRSPS are discussed, and significant differences between the LASA and NORSAR systems are described, the primary emphasis in this section is on the NORSAR system. For specific information on LASA field and special data collection equipment, see [4-26] and [4-27].

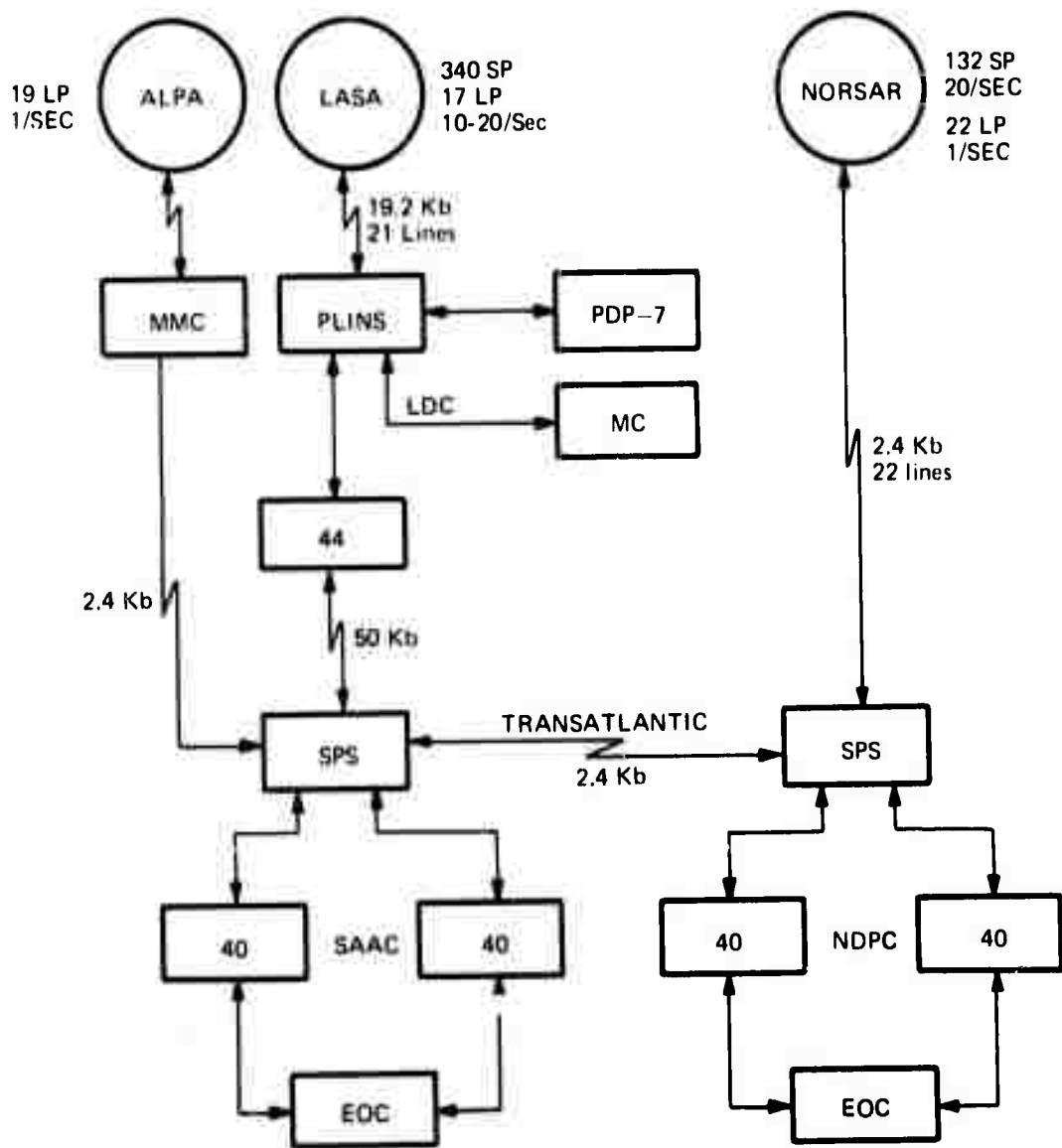


Figure 4-1. Integrated Seismic Array Signal Processing System

The basic functions of the data acquisition system are:

- a. Data collection in accordance with specific requirements of frequency range, dynamic range, accuracy, resolution, and sampling time
- b. Performance monitoring and special test and calibration of field instrumentation
- c. Data transmission with specified data rates, resolution, and error control capability.

Detailed engineering specifications for the NORSAR data acquisition system are presented in [4-16, Appendix IV]. Information on the installation, calibration and testing of NORSAR field instrumentation may be found in [4-28].

Two types of seismic sensors are used in the arrays. Long-period (LP) seismometers are three-axis orthogonal instruments where each of the three components is sampled once per second. LP instrument channel response is oriented toward signals with periods in the range of approximately 10-100 seconds. Short-period (SP) seismometers are single-axis instruments measuring vertical motion and are sampled at either twenty or ten times per second. SP instrument channel response is oriented toward signals with periods in the range of approximately 0.2-10 seconds. ALPA consists of isolated LP instruments while the other two arrays consist of multiple subarrays, each containing a cluster of SP instruments and most also containing a three-component LP instrument.

ALPA feeds a local Maintenance and Monitoring Center (MMC) where the data is multiplexed and transmitted to SAAC via a 2400 baud simplex data circuit. LASA feeds via the Phone Line Input System (PLINS) into a System/360 Model 44 at the LASA Data Center (LDC) where the data is edited and compacted to fit into the 50K baud line to SAAC. NORSAR data

is fed into a Special Processing System (SPS) at NDPC in which such functions as interfacing the modems, message error checking and encoding, word formatting, and communication control are performed; the NORSAR SPS also passes the formatted data to the twin System/360 Model 40s used for processing NORSAR data at NDPC as well as transmitting LP and other selected data over a 2400 baud transmission link to SAAC.

The transmission link between Norway and SAAC is via land line and cable from Norway to England, across the Atlantic via satellite to New York, and via land line to SAAC. It is specified as a four-wire, alternate voice/data circuit per CCITT, Recommendation M-89, with the U.S. carrier providing supplemental equalization, as required, to meet DCA S-1 conditioning. Milgo 2200/24 modems are in use at 2400 baud on this link.

The transatlantic link places restrictions on interactive operations. Because of this link length via satellite, there is a one-way transmission delay of approximately 0.4 seconds.

The equipment at both SAAC and NDPC includes an SPS (described in Section 4.2.1), twin System/360 Model 40s and an Experimental Operations Console (EOC) (described in Section 4.2.2), all of which are used principally for online seismic processing. In addition, a System/360 Model 44 is available at SAAC for offline processing and experimental development. All of the System/360 Model 40s contain a special feature which includes a sum-of-products unit and a set of special microcoded instructions that directly implement various seismic signal processing algorithms and provide a significant increase in processing speed relative to assembly language implementations. These algorithms and their performance are described in Section 5.1.

In order to maintain software compatibility, the four special instructions are also available in the emulator mode on the SAAC Model 44. Each SPS contains functions similar to three of these special instructions,

the exception being the rectify/integrate and threshold function. Figures 4-2 through 4-4 show the SAAC equipment configuration and Figures 4-5 and 4-6 show the NDPC equipment configuration. Table 4-1 contains definitions pertaining to the configuration charts.

There are significant differences between LASA and NORSAR in the communication network which links the subarrays to the data control center. First, error protection during data transmission (expected to be the largest contribution of data errors) has been increased by going from word parity at LASA to a 16-bit error-checking polycode at NORSAR. This significantly reduces undetected transmission errors, minimizes the number of bits required for error checking, and detects all message errors introduced by noise bursts of duration not greater than the protection polynomial period (16 bits), and approximately 99.997% of all longer bursts. The same polynomial error-checking is supplied to protect sampling and mode selection commands transmitted to the subarray.

Second, the LASA 13-bit plus sign and parity short-period seismometer word has been reduced at NORSAR to a 10-bit word in modified floating point. This word consists of a 2-bit base 4 characteristic, a 7-bit mantissa, and a sign bit, and allows approximately the same dynamic range as the 15-bit word. The resolution attainable is approximately 0.25 dB. In conjunction with a reduction in the number of SP seismometers per subarray at NORSAR, this shorter word length yields a reduction in the effective 9.6K baud data rate from the subarray at LASA to 2.4K baud at NORSAR, allowing use of common voice-grade lines.

Third, to accommodate maintenance and calibration activity concurrently with online operation of the single subarray, individual sensors at NORSAR may be addressed with mode commands.

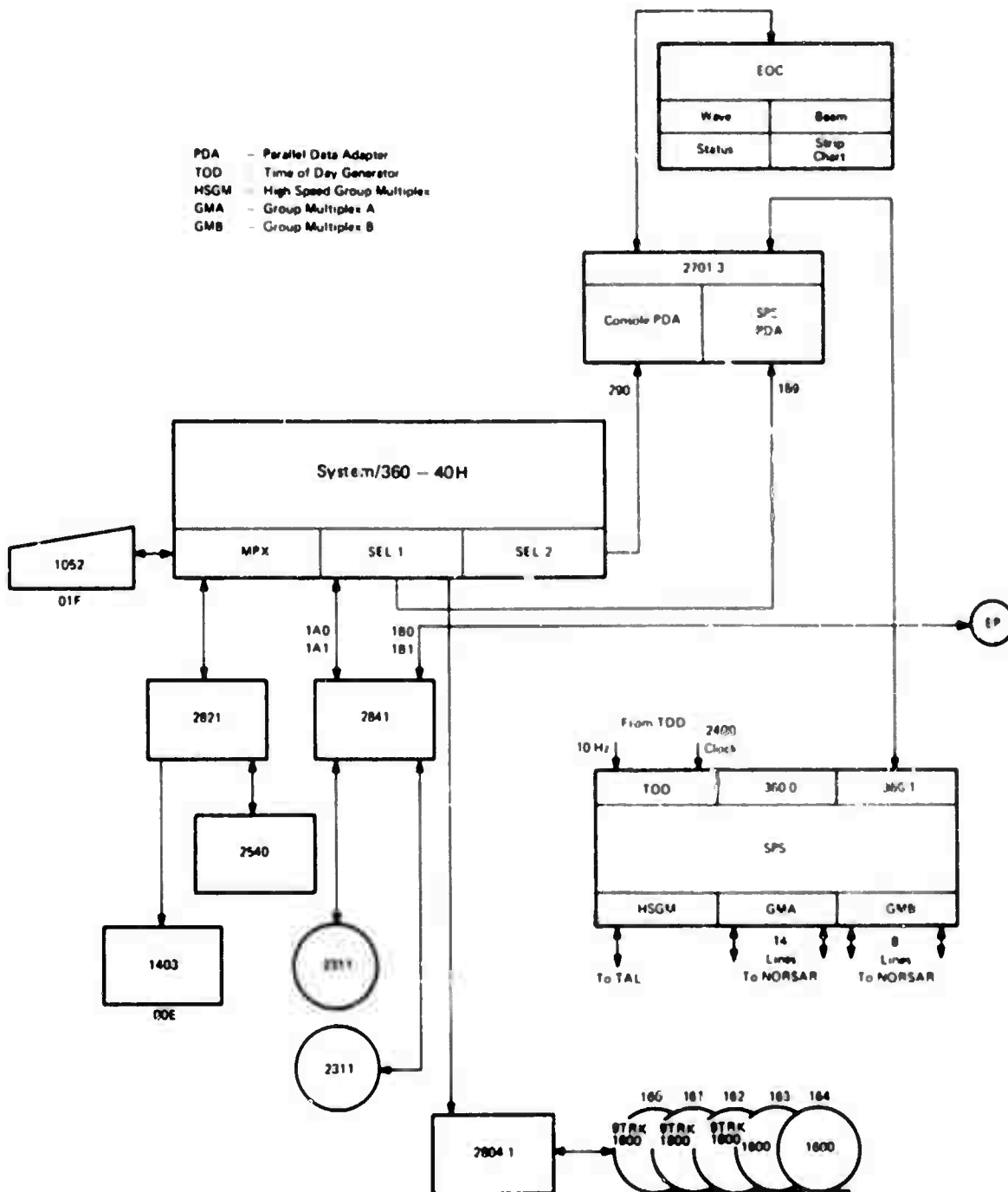


Figure 4-5. NDPC Detector Processor

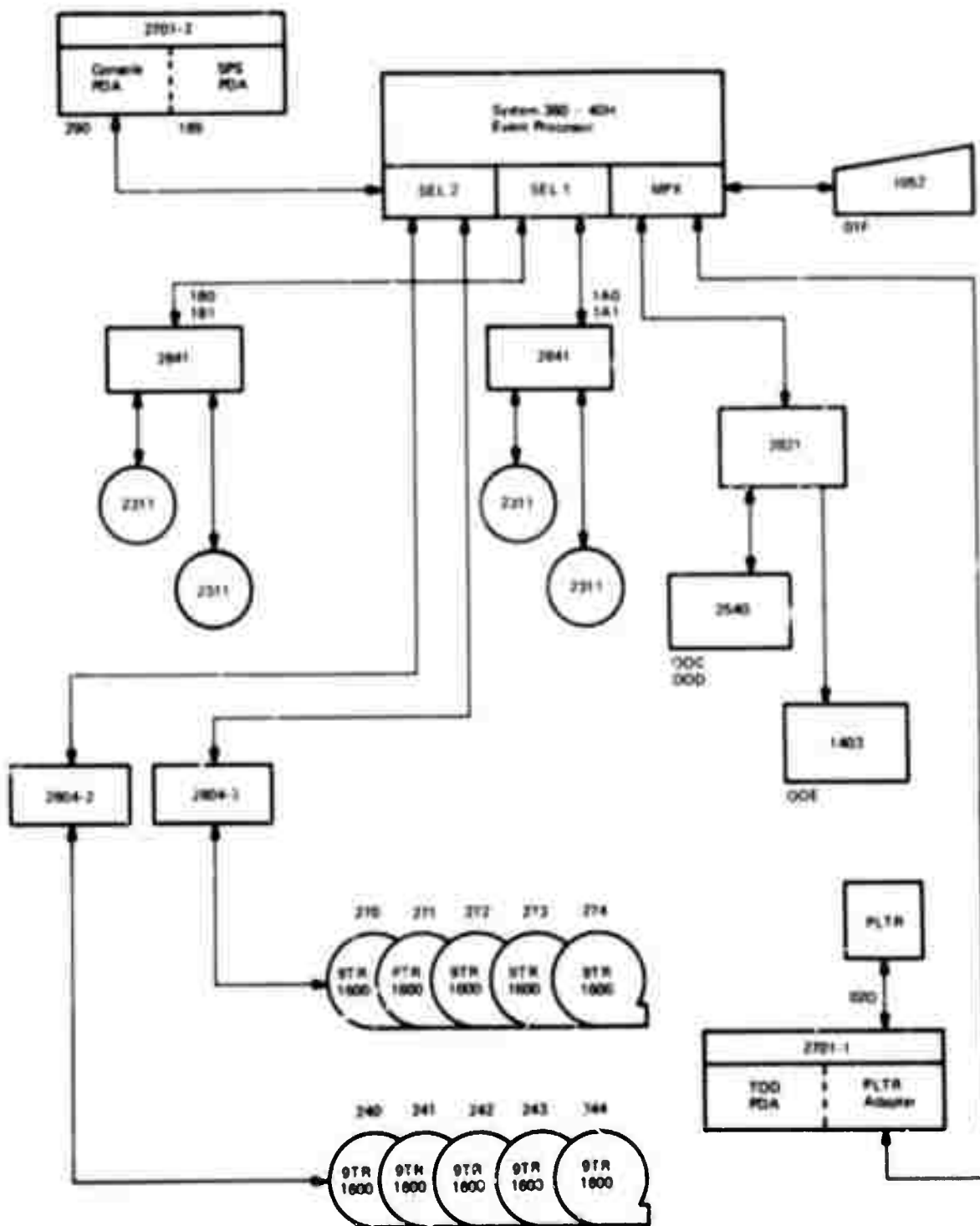


Figure 4-6. NDPC Event Processor

Table 4-1. Configuration Descriptions

Machine Type/Code	Description
2040	System/360 Model 40H Processing Unit
2044	System/360 Model 44H Processing Unit
1052	Printer/Keyboard
2540	Card Read Punch
1403	Printer
2841	Disk Storage Control
2311	Disk Storage Drive
2701	Transmission Control Unit
SDA/II	Synchronous Data Adapter
PDA	Parallel Data Adapter
2804	Tape Control Unit
2402	Tape Unit
2401	Tape Unit
SPS	Special Process System
Console (EOC)	Experimental Operations Console
TOD	Time-Of-Day Generator
2911/2914	Switching Unit
2848	Display Control
2260	Display Station
1053	Printer
TAL	Transatlantic Link
SEL	Selector Channel
MPX	Multiplexer Channel
2315	Disk Cartridge
HSGM	High-Speed Group Multiplexer
GMA/B	Group Multiplexer A/B
1627	Plotter
33KSR TWX	TWX Network Device

The hardware which was required for the implementation of the three modifications described above was incorporated into the design of the NORSAR SP LP electronics module (SLEM), which is located in each subarray central terminal vault (CTV). At LASA, the electronics unit which performs the analog-to-digital interface is called a subarray electronics module (SEM). The above capabilities, together with an increased flexibility in the choices of sampling rate, data transmission rate, and of modes of interconnecting the SLEMs to one another (for chained operation) and to the incoming analog lines, represent the primary functional differences between the SLEM and SEM units.

The SLEM functional capabilities and design features are described in Section 4.1.2.

For LASA, the incoming data rate at LDC is approximately 400K baud, consisting of 21 lines each having a capacity of 19.2K baud of digital data in the d1-bit mode. This data rate is reduced to 200K baud at the PLINS by discarding every other bit (complement bit) on each line. Data for transmission to SAAC is reformatted and blocked into 10 Hz messages in the System/360 Model 44 at LDC. The data rates to SAAC are reduced to 10 Hz for SP data and 1 Hz for LP data, although all data is received from the array at a 20 Hz sampling rate. Furthermore, the 15-bit fixed point data words are compressed to the 10-bit base 4 floating point format described above. The use of these techniques, together with an efficient blocking of the 10 Hz SAAC messages which takes advantage of the fact that the number of SP seismometers in 20 of the LASA subarrays has been reduced from 25 to 16, results in a 50K baud data transmission rate from LDC to SAAC. Error protection for this transmission is provided by a 16-bit cyclic-redundancy check (polycode).

A block diagram of the NORSAR data acquisition system for a typical subarray is shown in Figure 4-7. This system consists of the field instrumentation portion which is identically replicated for each subarray, and

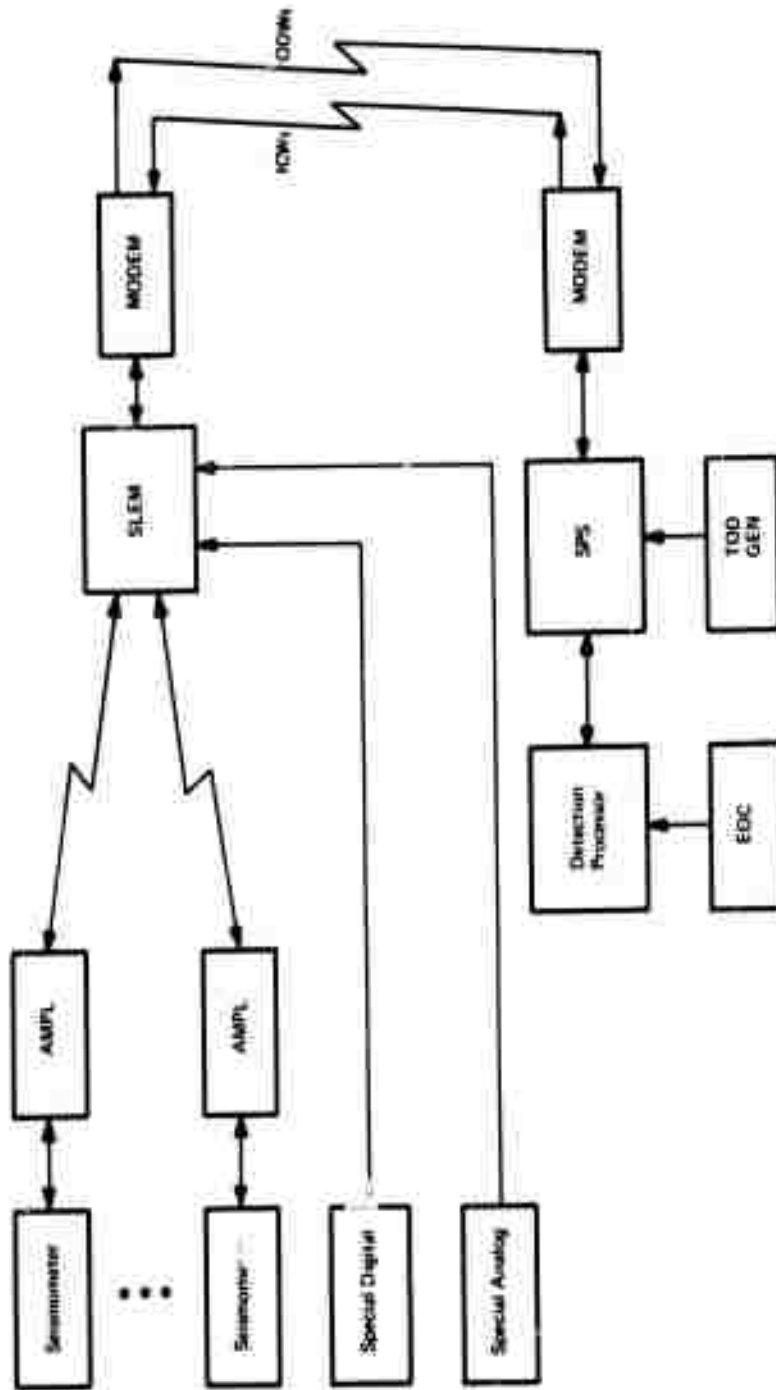


Figure 4-7. Data Acquisition System for One Subarray

the data center portion. The field instrumentation design philosophy and equipment, and particularly the SLEM, are discussed in Section 4.1. The data center portion of the data acquisition system is discussed in Section 4.2, with particular emphasis on the special-purpose units--the SPS and the EOC. Section 4.3 contains a discussion of the Array Monitor and Control subsystem, an integral part of the data acquisition system which provides for remote online calibration, monitoring and adjustment of the field instrumentation. Mathematical models for the SP and LP analog data channels are presented in Section 4.4.

4.1 FIELD INSTRUMENTATION

NORSAR field instrumentation consists of:

- a. Sensors and sensor electronics
- b. SLEMS
- c. Modems and communication lines
- d. Other central terminal vault (CTV) equipment.

The data path from the seismometer to the SPS is an analog channel for part of the distance and a digital channel for the remainder.

A typical SP analog channel is shown in Figure 4-8. All sections except the seismometer and the RA-5 amplifier are incorporated into the SLEM, which is discussed in Section 4.1.2.

Filtering in the data acquisition system is divided into two parts: analog filtering prior to digitizing at the SLEM, and digital filtering after receiving the data at the data center. Once the frequency range of interest is determined, and the data sampling rate is selected, analog filtering is provided to eliminate very low frequencies because they represent a confusion factor due to the slow modulation they impose on

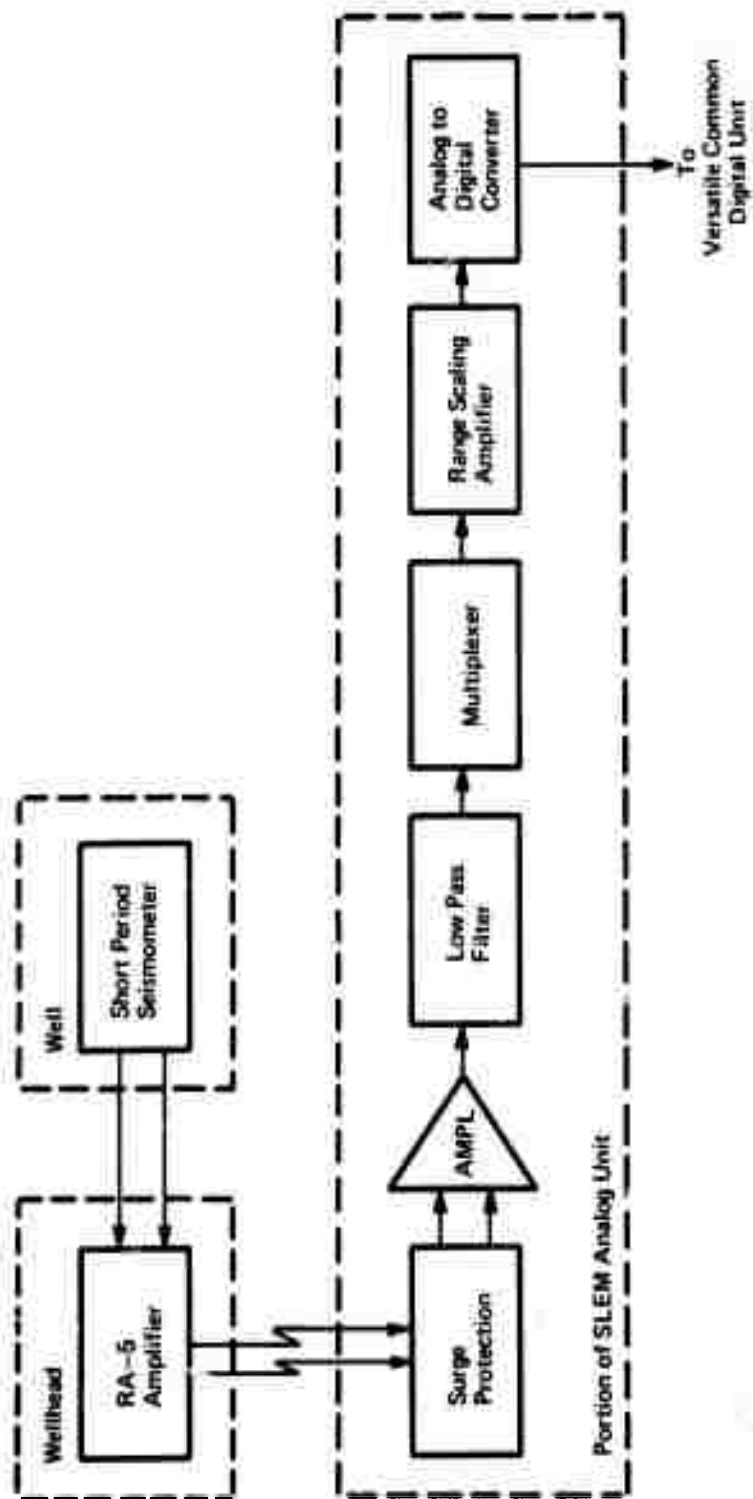


Figure 4-8. Typical Short Period Analog Channel

the data. In particular, DC bias should be effectively removed prior to sampling in order to avoid unnecessary loss of dynamic range and to permit meaningful application of data quality checking algorithms which utilize digital sums of rectified data values. It is desirable to eliminate frequencies above the band of interest prior to digitizing to avoid aliasing error.

Digital filtering is desirable in the final, preprocessing stage since it is stable and repeatable, and also easily modified; it is convenient since the samples are received at the data center in digital form. Easy modification of filter parameters is important since different filtering is desirable for different processes at the data center. This is illustrated by the fact that detection demands a high signal-to-noise ratio (SNR) but is not concerned with waveform fidelity. Thus, filtering for the real time detection function is adjusted to optimize SNR without regard for distortion of signal frequencies outside the band that provides optimum SNR. On the other hand, classification and waveform parameter estimation require analysis of detailed waveform characteristics and of the signal phase and amplitude spectrum, and the frequency band of interest is generally wider than that which optimizes SNR. Thus, separate filtering is required for this purpose. For example, NORSAR has used a 0.9 to 3.5 Hz filter for SP detection processing, but various filters ranging as low as 0.6 Hz and as high as 4 Hz have been used for SP waveform parameter analysis. See Section 3.5 for a detailed discussion of LASA and NORSAR digital filtering requirements.

Timing errors in the system are introduced by:

- a. Sampling rate, which introduces an unavoidable beamforming delay quantization error for all sensors
- b. Simultaneous receipt (by programmed intent) of all SLEM data words (ODWs) at the data center, which introduces timing errors between subarrays

- c. Sequential analog-to-digital conversion of the analog channels of a single subarray, which introduces timing errors between the samples of a single subarray
- d. Circuit jitter.

If individual seismometers are sampled at 10 times per second, then the sampling interval, ΔT , is 0.1 second. The necessary steering delays can be implemented to the nearest sampling instant. Hence, the delay errors are assumed to be uniformly distributed over the interval from $-0.5\Delta T$ to $+0.5\Delta T$. The resulting signal power loss is approximately

$$\frac{1}{12} (10 \log_{10} e) (2\pi f \Delta T)^2 \text{ dB},$$

where f is the frequency in Hz. Thus, even at $f = 3$ Hz, the loss is only 1.3 dB.

The ICWs sent out to the SLEMs by the SPS are intentionally staggered so that all ODWs are received by the Data Center simultaneously (i.e., normally within a 2.4 millisecond interval); the system has been programmed in this way for convenient handling of the received data. The result is that ODWs are actually formed at the array with a timing error between subarrays. This error, if actual simultaneous ODW receipt is assumed, is approximately equal to the one-way travel time of an electrical signal across the array. For NORSAR, which has a 75-mile diameter, that time is considered negligible.

Sequential analog-to-digital conversion (ADC) of seismometer outputs produces a difference of 50 bit-times between the first and last conversions when six 10-bit samples are being transmitted to the data center. At 2400 baud, this is a 20 millisecond difference between the actual time of the first and last sample. Compensation for this error is not considered necessary for the analysis at NORSAR although it could be provided in the computer if very fine-grained processing were performed.

Timing error due to circuit jitter is negligible.

Switching, under telephone company control, of the digital communication lines to the data center would introduce another source of timing error. This does not occur at NORSAR without prior warning because dedicated lines are used.

The sensitivity of the data acquisition system must be specified at a particular frequency. This is because seismometer output is approximately proportional to the derivative of ground motion, which is proportional to both the amplitude and frequency of displacement. Short period sensitivity is adjusted to 0.0427 nanometers per quantum unit ($\pm 10\%$) at 1 Hz. Long period sensitivity is 2.47 nanometers per quantum unit ($\pm 10\%$) at 0.04 Hz. Note that Richter magnitude, m_b , is the logarithm of an appropriately scaled version of A/T , where A is amplitude and T is period. (See Section 8.3.2.)

For purposes of specifying system parameters and tolerances, certain aspects of system performance could not be realistically analyzed for degradation of specific channel parameters (such as drift of seismometer natural frequency, variation in amplifier gain, or changes in filter response). It was decided to resolve corresponding requirements for NORSAR by specifying components and tolerances that were realizable at reasonable cost.

4.1.1 Sensors and Sensor Electronics

The principal array sensors are the short-period and the long-period seismometers. The principal sensor electronics are the seismometer amplifiers which provide the required signal conditioning prior to signal input to the SLEM Analog Unit. These sensors and amplifiers are described in separate subsections below.

4.1.1.1 Short-Period Seismometer

The short-period seismometer which is used for LASA and NORSAR is the Geo-Space Corporation type HS-10-1/A, which is a modified and repackaged version of a standard spring-mass type of refraction geophone (Sears-Hall type HS-10-1) used in oil exploration. The instrument is mounted in a pressure-tight case to minimize performance variations. Each short-period instrument rests on bedrock at the bottom of an individual borehole, inside a steel casing which is coupled to the ground by means of concrete. In Montana the average depth of the boreholes is 60 meters; in Norway most of the boreholes have an average depth of 15 meters, although a few instruments were installed in 60-meter holes for purposes of performance comparison.

The primary mechanism of this transducer is a moving coil and inertial mass assembly suspended by two helical springs, so that the coil moves vertically in the field of a fixed magnet attached to the instrument case. Vertical ground motion causes a corresponding motion of the case and magnet relative to the inertial mass and coil assembly, which induces an electrical signal proportional to relative velocity. The modified seismometer has also been equipped with a calibration coil and plunger so that the sensitivity can be measured from a remote location.

Selected specifications for NORSAR and LASA application of the HS-10-1/A seismometer are as follows:

- a. Alignment-Instrument response axis within four degrees of vertical
- b. Polarity Convention-Vertical ground motion upward gives a positive channel output signal
- c. Case Test Pressure-250 psi
- d. Case Size-4.75" O.D. x 11.25" long overall

- e. Moving Mass (total)-825 grams $\pm 1.5\%$
- f. Main Coil Resistance-50,000 ohms $\pm 5\%$ at 25° C.
- g. Main Coil Sensitivity-3.8 microvolts/nanometer at 1.0 Hz
- h. Main Coil Generator Constant-846 volt-seconds/meter (loaded)
- i. Calibration Coil Motor Constant-0.0326 newtons/ampere
- j. Calibration Coil Sensitivity-1 nanometer/microampere at 1.0 Hz
- k. Natural Frequency-1.0 Hz $\pm 10\%$
- l. Effective Damping Ratio-0.7 ± 0.05 .

4.1.1.2 Short-Period Amplifier

The short-period seismometer output is attenuated by a resistive network and fed into the preamplifier stage of a Texas Instruments type RA-5 solid-state reactance amplifier, which operates at low frequencies with little internal noise. The reactance amplifier is basically a double-sideband upconverter (or modulator) in which a band of low frequencies modulates an rf carrier. The nonlinear element which supports modulation is the junction capacitance of two matched silicon diodes reverse-biased by mercury cells. Operating power is supplied by an rf carrier (the pump) which modulates the transition capacitance of the parametric diodes.

Trimmer capacitors are used to compensate for diode mismatch and to provide a controlled unbalance in the bridge composed of the secondary windings of the pump transformer and the two diodes. This capacitive unbalance provides a constant amplitude signal which has the proper phase to serve as an am carrier for the sidebands resulting from application of an input signal. Output of the reactance section is fed into a conventional tuned amplifier and detector. The low frequency output of the detector is fed to line driver circuits that provide differential output signals.

Selected RA-5 specifications for the NORSAR and LASA applications are as follows:

- a. Input-Differential and floating with minimum input impedance of 15 megohms below 10 Hz
- b. Output-Differential with approximately 1200 ohms impedance and +8.5 volts nominal dc offset at each output with respect to ground
- c. Output Level-Minimum of 14 volts peak-to-peak differential
- d. Load Impedance-5000 ohms minimum
- e. Voltage Gain-Up to 10,000 for differential output (nominally 5410 to achieve desired quantization level)
- f. Gain Stability-Not more than 3 dB variation from nominal over the temperature range from -30°C to +50°C. Not more than 2 dB variation for supply voltage from 18 volts dc to 14 volts dc
- g. Dynamic Range-72 dB minimum
- h. Frequency Response--3 dB \pm 1 dB at 0.1 Hz, with -6 dB/octave roll-off below 0.1 Hz. High frequency cutoff beyond 90 Hz
- i. Distortion-5% maximum
- j. Noise-Equivalent input noise voltage no more than 0.05 microvolts rms over the band from 0.8 to 10 Hz
- k. Power Requirements-About 9 milliamperes at 18 volts
- l. Size-4-3/8" x 6" x 3".

4.1.1.3 Long-Period Seismometer

A three-axis long-period seismometer system is installed at most subarray sites in the LASA and NORSAR arrays, consisting of one Teledyne Geotech Model 7505B long-period vertical seismometer and two Teledyne Geotech Model 8700D long-period horizontal seismometers. The three instrument

response axes in each system are orthogonal, with the horizontal axes oriented in the north-south and east-west directions. Although the mechanical configurations of the vertical and horizontal seismometers are different, all of these sensors are mass-spring type moving-coil transducers. Each instrument is installed in a separate pressure-tight metal tank, and the three tanks are embedded in the floor of an underground concrete vault. Fiberglass insulation around each seismometer together with a blanket of earth over the concrete vault are used to reduce the effects of temperature variations. Underground cables are used to transmit the sensor signals from the Long-Period Vault (LPV) to the Central Terminal Vault (CTV), where the long-period amplifiers and the SLEM unit are located.

The mechanism of each long-period seismometer consists of a 10 Kg mass and coil assembly mounted at the end of a moveable suspension arm in such a way that the coil moves in the field of a fixed magnet attached to the frame. The suspension arm is mounted on flexure pivots, which operate by bending flexure ribbons of spring material, rather than by the movement of bearing surfaces. Gravity and the small net spring action of the flexures provide the restoring forces, and the relative motion between magnet and coil produces an electrical signal proportional to relative velocity. The motion of the inertial mass is constrained to occur only along the desired response axis of each instrument.

The period and mass position of each seismometer can be measured from a remote monitoring and control center, by the actuation of relays to remove seismometer damping and start the mass moving for a free period test, by applying power to the photoelectric mass position bridge built into each seismometer for a mass position measurement, and by reenergizing the circuits to their original configuration for normal operation. These parameters can also be adjusted from the remote location by activating motors which move weights on the suspension arm or tilt the seismometer base.

Furthermore, each seismometer is also equipped with a calibration coil to permit remote measurement of instrument sensitivity. Calibration is accomplished by passing a known current through the calibration coil, which is a single turn of wire wound about the damping coil, and measuring the channel output.

Selected NORSAR and LASA long-period system seismometer specifications are as follows:

- e. Alignment-Azimuth alignment ± 3 degrees
- b. Polarity Convention-Positive channel output signals for vertical ground motion upward, horizontal ground motion North, and horizontal ground motion East
- c. Dimensions-15.5" x 12" x 24", each instrument
- d. Inertial Mass-10 kilograms $\pm 1\%$
- e. Main Coil Resistance-50,000 ohms $\pm 10\%$ at 25°C
- f. Main Coil Sensitivity-0.111 microvolts/nanometer at 0.04 Hz
- g. Main Coil Generator Constant-750 volt-seconds/meter $\pm 2\%$
- h. Calibration Coil Sensitivity-50.6 nanometers/microampere at 0.04 Hz
- i. Calibration Coil Motor Constant-0.032 newtons/ampere
- j. Natural Period-20.0 \pm 0.5 seconds
- k. Effective Damping Ratio-0.64 \pm 4%.

4.1.1.4 Long-Period Amplifiers

The NORSAR long-period seismometer outputs are amplified by Ithaco model 6083-82 sub-audio frequency differential amplifiers, whereas the LASA system utilizes Texas Instruments Type II Multichannel Parametric Amplifiers. In this section, only the specifications and operating characteristics of the Ithaco amplifiers will be discussed; the Texas

Instruments Type II amplifier systems are presented in [4-26]. Each Ithaco amplifier-filter channel has a factory set gain of 80 dB and a passband which extends from 0.005 Hz to 0.033 Hz, with a low-frequency rolloff of -6 dB/octave and a high-frequency rolloff of -24 dB/octave.

In the first stage, the low-frequency signal is translated to 2 kHz and amplified by 46 dB in a fixed, balanced, low-noise circuit with 60 dB of common mode rejection. The signal is then demodulated and passed through a combination amplifier/low-pass filter stage with 20 dB gain and -12 dB/octave rolloff above 0.033 Hz. A plug-in Butterworth filter stage follows with unity gain and -12 dB/octave rolloff above 0.04 Hz. An R-C high-pass section follows which produces -6 dB/octave rolloff below 0.005 Hz and feeds into the first output stage. The gain of this stage may be adjusted (internally) by trimming the feedback resistor. The output of this stage is inverted in the second output stage, which is a unity gain dc amplifier.

Selected Ithaco amplifier specifications for the NORSAR long-period application are as follows:

- a. Input-Balanced differential, with minimum input impedance of 5 megohms
- b. Output-Balanced differential, with less than 100 ohms impedance and dc offset less than ± 1 volt
- c. Output Level-Minimum of 60 volts peak-to-peak into 100K ohm load
- d. Voltage Gain-Up to a minimum of 80 dB for differential output
- e. Gain Stability-Not more than ± 0.5 variation from nominal over the temperature range from -10°C to $+50^{\circ}\text{C}$
- f. Dynamic Range-80 dB minimum
- g. Amplifier Frequency Response-Low frequency cutoff -6 dB/octave, $-3 \text{ dB} \pm 0.3 \text{ dB}$ at 0.005 Hz
High frequency cutoff -12 dB/octave, $-3 \text{ dB} \pm 0.3 \text{ dB}$ at 0.033 Hz

- h. Filter Response-Low-pass -12 dB/octave Butterworth, -3 dB \pm 0.3 dB at 0.04 Hz
- i. Distortion-Less than 0.5%
- j. Noise-Equivalent input noise voltage no more than 0.1 micro-volt rms over the band from 0.005 Hz to 0.033 Hz, for source impedance of 50K ohm or less.
- k. Power Requirements-15 milliamperes maximum at 18 to 25 volts
- l. Size-6" x 8" x 10", each channel.

4.1.2 Short Period-Long Period Electronics Module

The SP-LP electronics module (SLEM) is used to interface all elements of a subarray to the data center. It receives continuous timing and control signals from the data center, and transmits continuous data signals to the data center. Signals from the data center are formatted in blocks designated as Input Control Words (ICWs) and signals to the data center in blocks designated as Output Data Words (ODWs).

4.1.2.1 Synchronization

The basic control flow for synchronizing data sampling and transmission under data center control is shown in Figure 4-9. The transmit clock from the SPS to the modem is under direct control of the time-of-day generator (TOD Gen). This is converted to the receive clock at the SLEM, which is used in the SLEM to synchronize its internal timing. This timing is used in the SLEM to control various internal functions and to provide the transmit clock to the modem, which becomes the receive clock at the SPS.

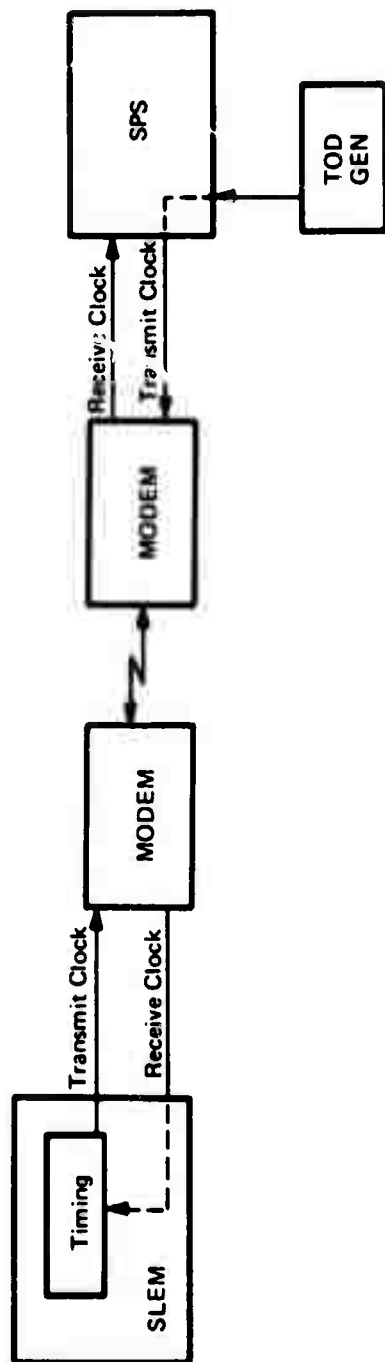


Figure 4-9. Synchronization of Data Sampling and Transmission

Timing of ICW operations in the SLEM is derived from a 2.4 MHz oscillator, which is divided down to feed 120 kHz signals to a divide-by-1000 counter. During 2400 baud or 1200 baud transmission, the positive-going transition of the modem serial clock receive signal from the modem to the SLEM (which indicates the beginning of a data bit period) resets the divide-by-1000 counter. This counter is decoded so that a clock pulse (designated IC) is generated during the middle of a data bit period. Thus, the IC clock is synchronized with the received clock and data, and its use in the SLEM provides bit synchronization relative to the incoming ICW.

Once bit synchronization has been achieved, it is necessary to acquire frame synchronization relative to the incoming ICW. This is done by scanning all incoming bits with a sliding window that examines all successive 16-bit patterns (updating a bit at a time) until a valid sync code is detected. The polycode is then checked at the appropriate time and if it is valid also, then frame sync is considered established.

ODW synchronization is derived in the SLEM directly from the timing signals that have been synchronized to the incoming ICW. However, the ODW bit timing is always delayed by 16-bit times with respect to ICW bit timing.

In the event that the SLEM does not receive ICWs, it continues to transmit ODWs. These ODWs are sent in free-wheeling (i.e., unsynchronized) mode. The reflected FS and FRS fields of the ODW indicate if this condition exists.

4.1.2.2 ICW and ODW Formats

The SLEM receives the following types of data from the subarray elements:

- a. SP seismometer data
- b. LP seismometer data
- c. Discrete inputs
- d. Analog inputs.

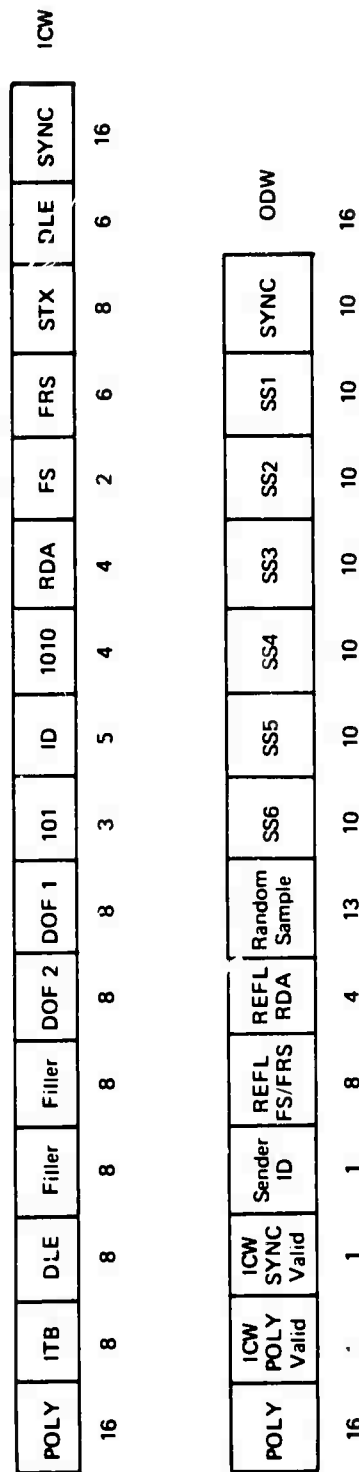
The SLEM provides to the subarray elements both calibration signals and discrete output signals for control purposes.

The SLEM is capable of operation in any one of five operational modes. One of these modes, SEMC/L, has three distinct variations, two of which along with one of the other modes (SEML) are supported by the data acquisition programs at NDPC. The supported configurations are:

- a. SEML-Eighteen short-period seismometers are sampled at a 10 Hz rate and data is transmitted at a 2400 baud rate.
- b. SEMC/L-10-Six short-period seismometers are sampled at a 10 Hz rate and data is transmitted at a 1200 baud rate.
- c. SEMC/L-20-Six short-period seismometers are sampled at a 20 Hz rate and data is transmitted at a 2400 baud rate.

The above variations all accommodate one 3-axis, LP seismometer in addition to the SP seismometers. The LP seismometer data is provided in the Random Sample field of the ODW, one axis at a time, in response to the appropriate random data address in the ICWs. Thus, three ODWs are used to transmit data for all three axes.

The formats of the ICW and ODW are different for different SLEM modes. Figure 4-10 shows ICW and ODW formats for the SEMC/L-20 mode. Regardless of mode, each ICW contains the information necessary to control one SLEM sample period; the results of this sample period are provided in a single ODW. In normal operation, the FS, FRS, and DOF fields of the ICW are zero, while the RDA field changes for successive ICWs according to a single specified sequence for all subarrays. During test and calibrate operations, the FS, FRS, DOF and RDA fields of the ICW for one subarray may be specified independently.



Key:

- | | | | | | |
|---------|---|---------------------------------------|-----------|---|---------------------------------------|
| POLY | — | Polynomial Residual Code | FRS | — | Function Route Select |
| ITB DLE | — | 2701 Compatibility Control Characters | DLE STX | — | 2701 Compatibility Control Characters |
| DOF n | — | Discrete Output Field n | SYNC | — | Synchronization Pattern |
| ID | — | SI.EM Identification | Sender ID | — | Part of SLEM Identification |
| RDA | — | Random Data Address | REFL | — | Reflected |
| FS | — | Function Select | SSn | — | Short Period Data Sample n |

Figure 4-10. SLEM Formats for SMC/L Mode ICW/ODW

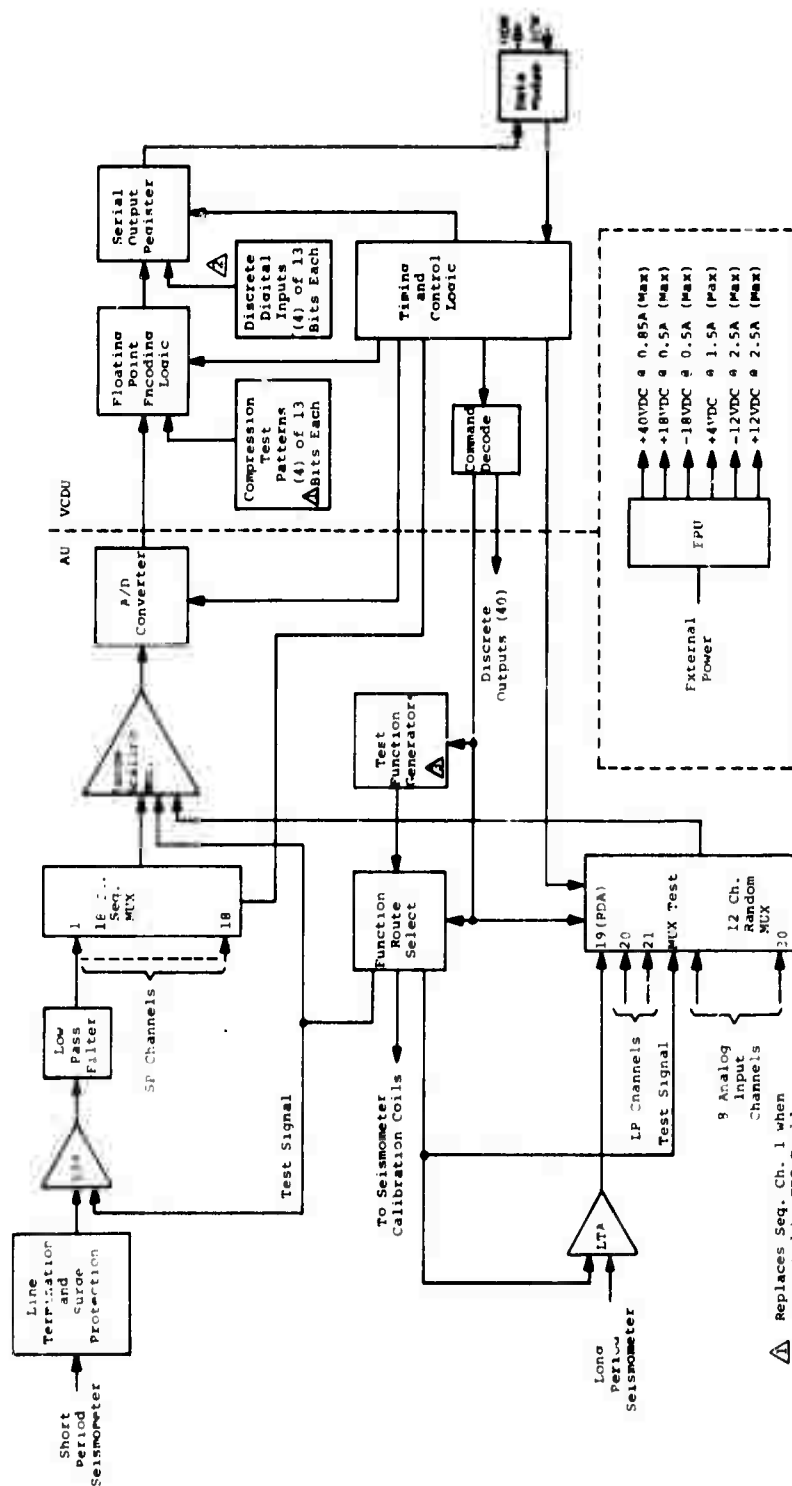
In Figure 4-10, the numbers under the various fields indicate the number of bits in that field. The DLE STX and DLE ITB fields of the ICW are control bytes in binary synchronous communications. However, they are disregarded by the SLEM. Their presence is related to the system evolution that is discussed in Section 4.2.1. The FS field specifies a desired test generation. The FRS field specifies desired routing of the selected test generator. The DOF fields specify the setting or resetting of discrete digital output points provided from a SLEM connector. The RDA field specifies the data that is to be inserted by the SLEM in the Random Sample field of the ODW. This data is one of 16 quantities that are designated as sub-multiplex channel data. They are:

- a. RDA 0-3-Vault discrete inputs
 - b. RDA 4-6-Three LP seismometer data channels
 - c. RDA 7-Test channels
 - d. RDA 8-10-Three LP seismometer mass position measurements
 - e. RDA 11-+28 volt battery
 - f. RDA 12-Battery current
 - g. RDA 13--18 volts
 - h. RDA 14-+18 volts
 - i. RDA 15-+40 volts
- } Not utilized at NORSAR

The ODW shown in Figure 4-10 has six sequential short period seismometer samples designated SS1 through SS6. This is followed by the Random Sample, reflected RDA and FS/FRS fields, and three one-bit fields used for validation purposes at the Data Center.

4.1.2.3 Hardware Organization

Figure 4-11 is a functional block diagram of the SLEM. It consists of an Analog Unit (AU), a Versatile Common Digital Unit (VCDU), and an External



- ▲ Replaces Seq. Ch. 1 when requested by FRS field
- ▲ PDA may select 1 of 4 words (when not selecting 1 of 16 random wux words)
- ▲ 1.0 Hz, 0.04 Hz, + 3c level, jr -dc level

Figure 4-11. SLEM Block Diagram

Power Unit (EPU). The VCDU provides the control functions necessary for gathering and formatting seismic data in any one of the five distinct operational modes. Mode selection is a function of the particular data sampling situation, and is implemented by switches on the VCDU. Depending on the mode selected, an appropriately configured AU samples, time-multiplexes, and digitizes the analog input signals under control of logic within the VCDU. In addition, various self-test procedures can be initiated by the AU under control of the VCDU. The EPU provides dc voltages to the AU, the VCDU, and other equipment. The AU, VCDU, and EPU are each separate rack-mounted units.

Figure 4-11 functional blocks do not necessarily correspond to discrete hardware sections. For example, the NORSAR SLEM uses a single random access type multiplexer controlled from the VCDU. Where sequential scanning is desired, it is achieved by generating the MUX addresses in the VCDU in a sequential manner.

The short-period Line Termination Amplifier (LTA) has a low pass filter but the long-period LTA does not. However, the long period channel is provided with a two-pole Butterworth low pass filter in the LPV amplifier. The filter in the short-period LTA is a four-pole Tchebyscheff type with ± 0.25 dB passband ripple. The overall response of the SP channel in the SLEM is $0.038 \text{ Hz} \pm 6\%$ to $4.75 \text{ Hz} \pm 5\%$. The overall response of the LP channel in the SLEM is 0.00372 Hz to $300 \text{ Hz} \pm 6\%$. Both channels have 84 dB dynamic range. For complete data on the SLEM, see [4-30]. Mathematical models of the overall SP and LP analog channels are presented in Section 4.4.

4.1.2.4 Range Scaling and Data Compression

The output of the multiplexer is provided to the Range Scaling Amplifier (RSA), which feeds the Analog-to-Digital Converter (ADC) that in turn furnishes inputs to the Floating Point Encoding Logic, as shown in Figure 4-11. The operation of these three blocks must be viewed together, as well as subsequent data defloating by the SPS at the Data Center, in order to appreciate the rationale for the techniques used.

The floating point encoding logic permits a reduction in the transmission rate required of the communication lines without a reduction in system performance since adequate amplitude precision and the field dynamic range are retained. Once the decision to use floating point encoding logic is made, an easy further enhancement is possible. A Range Scaling Amplifier can be provided to feed the ADC so that low level signals may be amplified prior to digital conversion to minimize the effect of ADC internal noise. A subsidiary benefit is that the ADC can have fewer bit positions than would otherwise be required.

In the NORSAR system a dynamic range of ± 78 dB was desired for seismometer data. Normally, this range is represented by 14 bits (a sign bit and 13 magnitude bits). However, it was decided to transmit both the sequential short period samples and the analog sub-multiplex channels (which are contained in the Random Sample field of the ODW and include the LP samples) in a base-4 floating point format.

The data compression technique used in the SLEM (VCDU section) converts the short period data into a 10-bit word consisting of sign, seven mantissa bits, and two modulo-4 characteristic bits. The two characteristic bits indicate the number of double-left shifts required to reconstruct the original data sample.

The technique also converts the analog sub-multiplex data into a 13-bit word consisting of sign bit, 11 mantissa bits, and one modulo-4 characteristic bit.

The SLEM has operating control switches that are set during initial system setup. Two of these impact range scaling and data compression. The first is the scaling switch which has auto, x1, and x4 positions. In auto, the SLEM provides automatic scaling and compression. In x1, the SLEM has an RSA gain of one and in x4 it has an RSA gain of four. The second switch is the data compress/data noncompress switch. It is overridden when the scaling switch is in auto, but otherwise it determines if data compression is available. The discussion here (of range scaling and data compression) assumes that the scaling switch is set to auto. For a description of SLEM operation corresponding to other switch settings see [4-30].

The RSA can provide a gain of either one or four. This gain is controlled by the VCDU, which switches it from one to four when the digital output from the ADC is below specified limits. The ADC performs a 12-bit conversion of the analog input data upon command from the VCDU, and provides 12 parallel bits of data to the VCDU.

However, increasing the gain of the RSA from one to four effectively increases the ADC conversion resolution from 12 to 14 bits.

The floating point encoding logic converts the sequential SP samples from a fixed point, 12-bit word to a floating point, 10-bit word. However, the dynamic range of the 10-bit word is equivalent to a 14-bit, fixed point dynamic range because the two bits of modulo -4 characteristic take into account the gain setting of the RSA. Figure 4-12 illustrates how this is accomplished from a functional point-of-view. The ADC output for either RSA gain =1 or RSA gain =4 is shown as sign

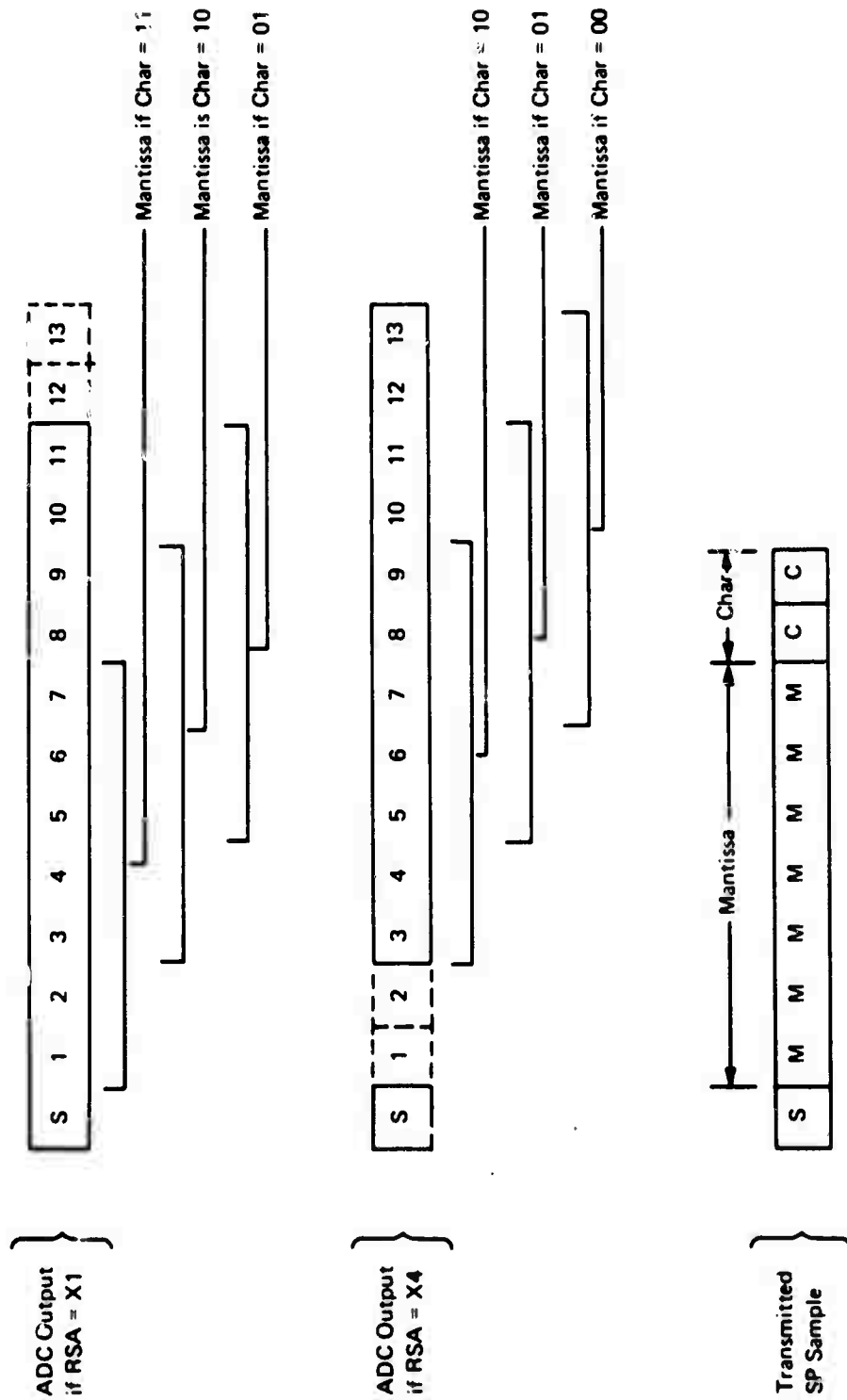


Figure 4-12. Compression Technique for Short-Period Data

bit and 13 magnitude bits. However, two magnitude bit positions are imaginary since only 11 bits of magnitude are presented by the ADC output. The mantissa and the characteristic bits (and the sign bit) are provided as the transmitted SP sample shown at the bottom of the figure. The correct mantissa is selected by the encoding logic by testing the data magnitude.

Figure 4-13 shows the raw input word as assembled by the blocking routine of the SPS. This routine separates each specified field of the ODW from the continuous bit stream. The figure also shows the defloated word as a function of the characteristic bits. Note that half-adjustment is provided for characteristics of 10 and 11.

The analog sub-multiplex data is converted to fixed point at the Data Center according to the formulas,

$$X = 4m + 2 \text{ if } c = 0$$

$$X = m \quad \text{if } c = 1$$

where X is the fixed point value, m consists of bits 0 through 11 of the received data sample, and c is the characteristic bit (i.e., bit 12) of the received data sample.

4.1.3 Modems and Communication Lines

The communication lines and modems provide data transmission between each SLEM and NDPC. The links provide full-duplex, 24 hours-per-day dedicated service with binary synchronous transmission at rates up to 2400 baud. GH2003 modems with modifications are used. The basic modem is described in [4-29]. The modifications to the modems provide for isolation of communication problems through use of a loop capability under control of the supervisory channel of the modem. The interface between the modems and the SLEMs consists of selected circuits from CCITT Recommendation V.24, February 1967 (equivalent to EIA SP-890 Standards plus EIA RS-232B).

Raw Input Word
As Presented By
Blocking Routine =

0 0 0 0 0 0 S M M M M M M M C C

Characteristic (CC)

Defloated Word

0 0	S S S S	S S S M	M M M M	M M 0 0
0 1	S S S S	S M M M	M M M M	0 0 0 0
1 0	S S S M	M M M M	M M 1 0	0 0 0 0
1 1	S M M M	M M M M	1 0 0 0	0 0 0 0

Figure 4-13. Blocking and Defloating of SP Data by the SPS

4.1.4 Vault Equipment

NORSAR uses both Long-Period Vaults (LPVs) and Central Terminal Vaults (CTVs). An LPV contains a 3-axis, long-period seismometer system. A CTV contains a SLEM, a modem, and supporting equipment. Each CTV services the data acquisition requirements for a single subarray. Thus, it receives signals from:

- a. Several SP seismometers via their RA-5 wellhead amplifiers
- b. One 3-axis LP seismometer system located in a LPV
- c. External analog sensors located in or near the CTV.

Power, control, and calibration signals are transmitted from the CTV to these external seismic and analog sensors. Balanced, shielded transmission cable, suitable for direct burial, is utilized for transmission of signals. Local telephone service is provided to the vaults to permit voice communication with the Data Center. Local commercial power is also supplied.

External analog sensors can be installed near each CTV to monitor environmental parameters such as wind speed and direction, temperature, and relative humidity. Provision is also made for analog sensors located inside the CTV to measure such parameters as barometric pressure and vault temperature.

All electrical interfaces to equipment outside the CTV are made through wall-mounted junction boxes, that also contain components for lightning protection.

4.2 DATA CENTER EQUIPMENT

The data center equipment that is directly concerned with data acquisition consists of the modems, the time-of-day generator (and its radio receiver), the SPS and the EOC. The online System/360 Model 40 handles the data recording task, but is not otherwise regarded as a part of the data acquisition system. All of these equipments are standard commercial units except for the SPS and the EOC. The NDPC online system hardware configuration and identification has been presented in Figure 4-5. The subsequent sections of this document will discuss briefly only the SPS and the EOC, which were developed especially for this system.

4.2.1 Special Processing System

The Special Processing System interfaces the Detection Processor to the communication lines and thus to the array. It performs two basic functions to accomplish this:

- a. It provides the proper electrical and logic interfaces for the modems that connect to the communication lines and also for the System/360 processors with which it exchanges data.
- b. It provides the proper data processing and formatting for the SLEMs and the System/360 processors.

A complete hardware description of the SPS is given in [9-54] and [9-58]; in addition, a generalized microcode specification based on the machine organization is presented in [9-54]. [9-56] describes the operational microcode for the SAAC SPS and [9-55] describes the operational microcode for the NDPC SPS.

In addition to its two basic data acquisition functions, the NDPC SPS also does digital filtering and subarray beamforming which are not discussed in this section.

A block diagram of the SPS is shown in Figure 4-14. The SPS consists of a special basic processor designated Adaptive Microprogrammed Control System (AMCS) and 2 groups of adapters. The first group of adapters are designated Base Adapters (BAs), and the second group of adapters are designated Transmission Adapter Unit (TAU). The BAs consist of: a time-of-day adapter (TODA); two adapters for the System/360s (360A), which are numbered 0 and 1; an EOC Adapter (EOCA); and a Status Adapter (SA), which was intended to interconnect two SPSs operating in a dual thread configuration. At SAAC, the EOCA is used as an interface to Develocorder Units. At NDPC, the EOCA is not used.

The TAU consists of: 32 Line Adapters (LAs); up to 8 Binary Synchronous Communication Adapters (BSCAs), although there is only one installed for the NDPC SPS; 2 Group Multiplex Adapters (GMAs) designated GMA A and GMA B; and one High Speed Group Adapter (HSGA). The Line Adapters connect to the modems for the SLEM communications lines, with a separate Line Adapter for each modem. The Group Multiplex Adapters interface the Line Adapters to the AMCS; GMA A interfaces to Line Adapters 1 through 16 and GMA B interfaces to Line Adapters 17 through 32. The Binary Synchronous Communication Adapter is used at NDPC to interface to the modem for the transatlantic data link. The High Speed Group Adapter interfaces the Binary Synchronous Communication Adapter to the AMCS.

All interfaces to the AMCS are accommodated by the storage access channel and by the multiplex bus of AMCS. The storage access channel is an 8-port direct channel to main storage in the AMCS that operates on a cycle-stealing basis and accommodates data flow between the AMCS and its

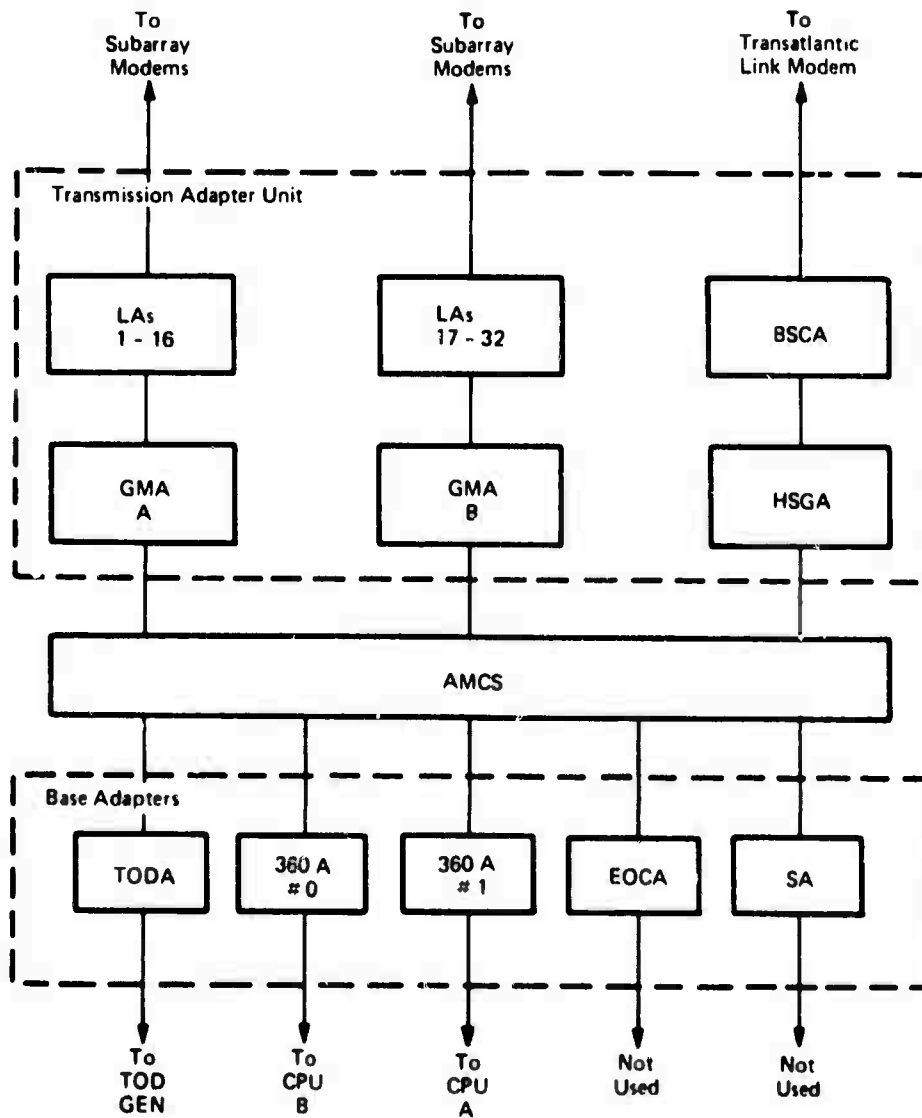


Figure 4-14. SPS Organization (NDPC)

adapters. The multiplex bus is a multiregister bus that provides all necessary control signals between the AMCS and its adapters. The AMCS section of the SPS is shown in Figure 4-15 which shows the following major components of AMCS:

- a. Core Memory (64K words of 18 bits each)
- b. Memory Control
- c. Data Flow
- d. Sequence Unit
- e. Transformer Read Only Storage (TROS)
- f. Storage Access Channel
- g. Multiplex Channel.

The Core Memory consists of four standard IBM M21 units each containing 16K 18-bit words randomly accessible with a one microsecond full cycle time. Memory Control consists of all logic needed to provide proper control signals to Core Memory, and also to select either the Data Flow or Storage Access Channel for Core Memory communication.

The Data Flow unit basically interconnects the major AMCS elements of Core Memory, Multiplex Channel, and Sequence Unit. The Data Flow unit consists of: Function Unit; High-Speed Data Stack; Condition Stack; and registers designated Q, X, Y, Z, D, MSAR, MSRR, and MSWR. The Function Unit is the Arithmetic/Logic Unit of the AMCS, and operates under micro-program control. The High-Speed Data Stack is a group of 64 auxiliary registers that is available for temporary storage within the Data Flow. The Condition Stack provides 32 groups of 4-bit indicators that contain status information. The Q, X, Y, Z, and D registers operate in conjunction with the Function Unit. The MSAR, MSRR, and MSWR registers interface the Data Flow to the Core Memory via Memory Control.

The Sequence Unit controls the addressing of the TROS, which is the Transformer Read Only Storage section of the AMCS. TROS contains 8,192 words of 56 bits each. The selected word during any particular cycle is provided to the appropriate sections of AMCS by the Sequence Unit.

The Storage Access Channel and the Multiplex Bus provide the data and the control interfaces, respectively, between the AMCS and its adapters, as described previously.

4.2.1.1 Interfaces

The interface between the SPS and the modems are selected lines of CCITT Recommendation V.24. The interface between the SPS and the TOD was specially designed to provide the desired signals. The interface between the SPS and the System/360s is the standard interface of an IBM 2701 equipped with a parallel data adapter; the SPS simulates the external device.

4.2.1.2 Functions and Interrupt Structure

The operation of the SPS is divided into two categories: normal mode and exception mode. Normal mode includes all functions except Test and Calibration and Resync, which are designated as exception mode (discussed in Section 4.2.1.5). The detailed discussion of the NDPC-SPS operations is given in [9-55] and is summarized in [9-52, Section 2-1]. The discussion here will review some key points.

The process functions of the SPS include:

- a. Executive/Interrupt Structure
- b. ODW Processing
- c. ICW Processing
- d. SPS Detection Processing
- e. Initialization
- f. System/360 Service
- g. NDPC/SAAC Communications
- h. Resynchronization
- j. Test and Calibrate.

The main process functions of the SPS are periodic. A relatively fixed amount of processing must be performed at a fixed rate to provide a continuous flow of information from the SPS to the SLEM, from the SLEM to the SPS, and from the SPS to the System/360. Information from the SPS to the SLEMs are transmitted in Input Control Words (ICWs). These are generated at a fixed rate. The information from the SLEMs to the SPS is transmitted in Output Data Words (ODWs). They are generated by the SLEM under timing control of the ICWs, and must be processed and transferred to the System/360 by the SPS.

The SPS processing priority is:

- a. TOD Interrupts
- b. Other Interrupts
- c. ODW Process, high rate (acceptance and processing)
- d. ICW Process, high rate
- e. SPS Detection Process Functions
- f. Resynchronization
- g. System/360 and Transatlantic Link Interface
- h. Test and Calibrate.

All tasks except the lowest three are generally referred to as synchronous. However, SPS processing should not be considered synchronous in the strict sense.

An interrupt service routine is used to determine interrupt level, to chain the interrupt being serviced by level, and to assign processing control to the routine required for the highest level interrupt pending.

Some functions, such as ODW processing, have multiple associated interrupts (one per communication line). The interrupts are stacked by level, and if multiple associated interrupts exist, they are chained within their level. Thus, processing is performed for all pending interrupts at one level before any processing is performed for interrupts at a lower level. During processing at a given level, occurrence of a higher level interrupt causes a change in processing to the higher level, with return to the interrupted process after all higher level interrupts have been serviced.

4.2.1.3 Sampling Control

The SPS generates ICWs to control SLEM operation. The ICWs have command fields to control operation of the SLEM, and an identification field to address a particular SLEM. A SLEM executes certain command functions only when it receives a valid ICW with its particular identification code. The RDA field of the ICW is used to select one of 16 submultiplexed channels. These contain data not required as often as the basic sampling rate. The polycode field is generated by the Line Adapter and transmitted with each ICW.

The present system is designed to handle a maximum of 32 SLEM communication lines. The functional requirements of the LA were established in the

development of the Interim System when an IBM 2701 Data Adapter Unit equipped with Synchronous Data Adapter II was modified for fixed-format operation with a SLEM-type unit.

The most significant modifications were to:

- a. Indicate an error condition if two SYN bytes do not follow two polycode bytes.
- b. Enter transparent mode after the second SYN byte.
- c. Ignore all control characters while in transparent mode.
- d. Leave transparent mode after accepting a preset count of data bytes and treat the next two bytes as polycode bytes.
- e. Transmit an error index byte to the computer containing the results of the polycode check.
- f. Modify the data transfer path within the 2701 to invert the byte format with respect to the order of bit significance within the byte. (The bit significance reversal was necessary for compatibility with the SLEM format.)

The two fundamental changes in the 2701 SDA II, that were retained for the SPS LAs, are:

- a. Utilization of a fixed-length frame after the sync bytes to begin counting for the polycode
- b. Compatibility with the SLEM bit format.

The LA permits continuous data stream operation without requiring ODW control characters other than two polycode bytes. The SPS program is responsible for verifying synchronization and requesting a search for new sync if necessary. The sync byte in Figure 4-11 is the 2701 SYN character used for synchronization. The data bytes are binary information. The polycode is the 2701 CRC-16 polynomial code.

The 10 Hz and 2400 Hz interrupts from the TOD are both used by the SPS in establishing transmission times for each ICW or for Resynchronization. Data establishing desired ICW transmission times are provided to the SPS as a part of the initialization routine. Transmission of ICWs is staggered to obtain all ODW responses from the SLEMs within a specific time window. The time of each ICW transmission is based on sampling-rate dependent parameters. Note that the SLEM performs its conversion in response to an ICW and that both ICWs and ODWs occur as a continuous, uninterrupted flow on the full-duplex lines. Unlike the ODW, the ICW contains control characters that represent a carry-over from the 2701 SDA II format. However, the SLEM regards these control characters only as filler bits.

4.2.1.4 ODW Processing

The SPS stores each incoming ODW in an ODW input buffer. The ODW process checks the polycode residual and sync bytes that are stored in the ODW input buffer with the ODW data bytes.

If there is no polynomial error, the ODW process deblocks the data fields from the ODW and defloats data from the seismometers and other analog sensors. The analog and discrete digital data for a half-second period are stored in the output buffer for transfer to the Detection Processor. The ODW process also scales (right shift n times, where $0 \leq n \leq 13$) the SP seismometer data samples in the output buffer. The ODW process also performs validity checks on each seismometer data channel by performing continuous checks on dc offset and rectified sums. Operational status is maintained by the ODW (and other) processes in the SPS and transferred to the Detection Processor for recording and for retransfer to the EOC for display.

When an ODW is received with a polynomial error indicated, the ODW is transferred to the appropriate locations in the output buffer for recording by the Detection Processor. However, the data samples for those instruments are each replaced by the last valid sample for that channel for use in the detection process.

4.2.1.5 Exception Mode

This mode exists when either Resynchronization or Test and Calibrate is being performed. These functions are implemented on an as required basis, and are referred to as asynchronous.

The ODW process maintains a count of sequential ODWs with both sync and polycode errors. When the count reaches four, the ODW process considers that synchronization has been lost (i.e., synchronization of ODWs relative to ICWs) and the resync process is initiated. This places the Line Adapter for that ODW line in the sync search mode. The Line Adapter then monitors all groups of 16 incoming bits with a sliding window. When it finds a bit pattern that matches the sync pattern, it places the pattern and the subsequent portions of the ODW data into the next input buffer area as a candidate ODW. The ODW process checks the contents of the polynomial residual field which is created by the Line Adapter as a polycode validation. If the field is zero, then the polycode was valid and the ODW process considers that synchronization has been achieved. If the field is not zero, then the polycode was not valid, and the ODW process reinitiates the sync search mode in the Line Adapter.

The Test and Calibrate function refers to all Array Monitor and Control (AM&C) (see Section 4.3) support provided by the SPS except for items continuously and automatically monitored by the SPS without request from the System/360. These are Synchronization and Polycode, and Seismic Data

Reasonableness (see Sections 4.3.1.3 and 4.3.1.4). This exclusion exists because the SPS by definition does not initiate any Test and Calibrate routines, but performs them only upon request from the System/360.

When a Test and Calibrate routine is being performed, it is the ODW process that extracts test data from the ODW for appropriate processing. Note that the Test and Calibrate, and other AM&C functions of the SPS are a subset of overall AM&C functions, and are not background processes that are automatically performed by the SPS whenever extra time is available.

4.2.2 Experimental Operations Console

The Experimental Operations Console, together with the 1052 CPU console typewriter and the 1403 printer, provides the operator's interface to the system. As such, it provides for three functions:

- a. Monitoring and controlling data center equipment status
- b. Monitoring and controlling field instrumentation
- c. Monitoring data acquired or computed by the system.

A complete description of the NDPC EOC is given in [9-59] and [9-61]. In particular, [9-61, Section 5] is a summary of the theory of operation.

A block diagram of the EOC is shown in Figure 4-16. Item a, data center equipment status control, is provided for by the System Control Panel. Item b, field instrumentation monitoring, is provided for by the Array Status Display. In the NDPC EOC this consists of a bank of discrete lamps, a few decimal readout displays, and appropriate switches for addressing and function identification. Item c, monitoring data acquired

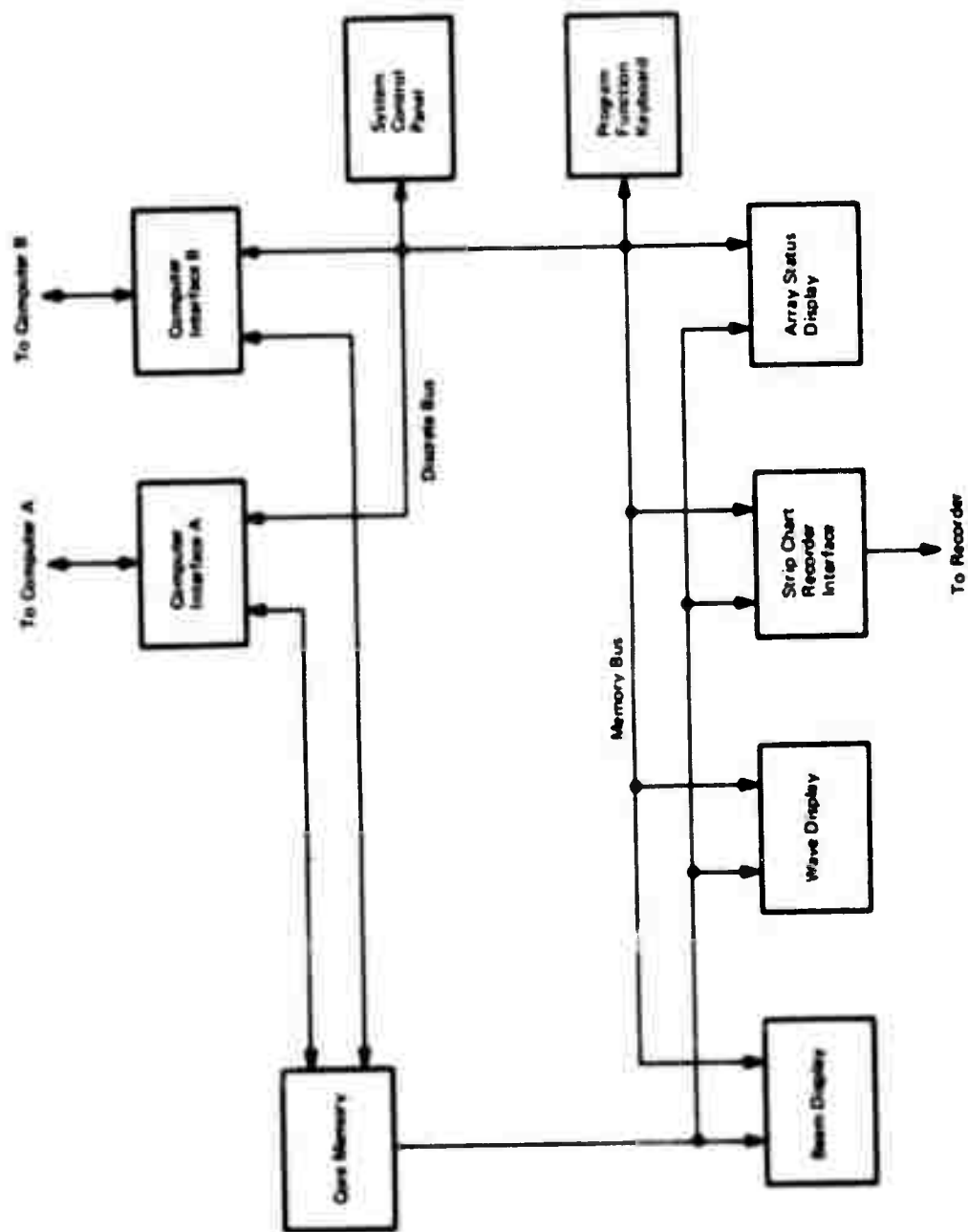


Figure 4-16. EOC Functional Organization

or computed by the system, is provided for by the Beam Display, the Wave Display, and the Strip Chart Recorder Interface. The online data monitoring capability is utilized primarily by the Detection Processor. However, the EOC also provides data presentation and operator interaction for seismic bulletin editing and waveform analysis (not in-line process monitoring) for Event Processor data. The program function keyboard is a general purpose keyboard that provides a convenient means for operator communication with the computers to which the EOC is attached. Its interpretation is entirely a function of the computer program that responds to it.

The EOC interfaces to two System/360 computers via the blocks designated Computer Interface A and Computer Interface B. These interfaces provide data to, or take data from, either Core Memory or the Discrete Bus (physically, this bus is separated into a read bus and a write bus, but that is not functionally significant). The Core Memory is a 16,000 word memory of 18 bits each. It accepts data from either computer and provides it to the four areas that it supports: Beam Display, Wave Display, Strip Chart Recorder Interface, and Array Status Display. The Discrete Bus services the discretes, which are merely those switches, latches or indicators that communicate directly with Computer Interface A or B (without Core Memory in the data path).

Normally, the computers only write to Core Memory. However, the ability exists for the computers to read from Core Memory, but this is usually reserved for diagnostic core dumps. The computers receive their control commands from the Discrete Bus. The basic operating mode of the EOC is to accept operator commands in the form of switch settings, communicate these to the computers, and accept data from the computers for display as requested.

The EOC supports its various functions without a priority scheme. This is accomplished by means of a master time cycle of 19.2 microseconds that is divided into 16 slots of 1.2 microseconds each. Each function of the EOC is allotted one or more of these time slots. For example, each computer interface is allotted two time slots, the wave display is allotted four time slots, and so forth. Thus, the wave display will accept the contents of the memory bus only during its four allotted time slots. In this way the time slot position becomes a sort of address to each function.

The physical layout of the NDPC console is shown in Figure 4-17. Frames 01, 02 and 03 contain status indication and control panels, and are primarily utilized for system monitoring and control functions. Frame 04 contains the Wave Display and Frame 05 contains the Beam Display. A photograph of the NDPC EOC is shown in Figure 4-18.

4.3 ARRAY MONITORING AND CONTROL

The techniques of AM&C are an essential and vital aspect of the data acquisition system. It is these techniques which verify the fidelity of data acquisition, upon which overall system performance is dependent. AM&C is handled differently for NORSAR and LASA. For example, most LASA array status information is displayed on the EOC at SAAC, but remote array control functions can only be initiated at LDC. However, all NORSAR array monitoring and control functions are integrated into the NDPC ISRSPS system. The NORSAR system is discussed here. At the time of this report, most of the items discussed below have been implemented, as described in [9-52, Chapter 8]. However, this section also discusses a few additional items that should be considered for future automation.

There are four categories of AM&C:

- a. Automatic Online
- b. Requested Online
- c. Requested Extended
- d. Requested Online Display.

Automatic Online AM&C refers to tests that are performed automatically under program control, either continuously or at regular intervals.

Requested Online AM&C refers to tests that are conducted only upon operator request, but during online operations. Requested Extended AM&C refers to tests that are conducted only upon operator request, and for which data is collected and recorded on the ISRSPS High Rate tape during online operations, but for which data is analyzed in an offline computer. Requested Online Display AM&C refers to output signal displays of selected channels in varying test modes on either the EOC Waveform Display or the Strip Chart Recorder.

The Automatic Online AM&C provides automatic recording on digital tape and display on the EOC of abnormal conditions or results. The requested AM&C categories provide automatic recording and display of the significant test results which are obtained.

It is important to note that two meanings apply to "control" in "array monitoring and control," and a third possible meaning does not apply. The first applicable meaning refers to the control required for various tests. An example of this is the disconnection of actual seismometer data and the connection in its place of a test generator internal to the SLEM. The second applicable meaning refers to remote adjustment of field instrumentation (under data center control) which modifies the channel characteristics for actual data acquisition. An example of this (and at present the only implementation of this type of control at

NORSAR) is adjustment of the long period seismometers. The meaning which is not applicable refers to actual time synchronization and control of the SLEM for normal data acquisition, which is a part of the SPS normal mode as opposed to the SPS exception mode under which AM&C occurs.

It is critically important that the line control computer be able to verify proper response to the remote command signals. For example, if the long-period motor is commanded ON and then OFF, it is vital that the OFF command be obeyed. Failure of the field instrumentation to comply could result in the LP seismometer being rendered inoperative until manual correction could be made at the instrument site. Thus, all commands should be reflected to the line control computer and verified.

4.3.1 Automatic Online AM&C

The tests conducted automatically under program control are:

- a. Vault Discrete Quantities
- b. Vault Continuous Quantities
- c. Synchronization and Polycode
- d. Seismic Data Reasonableness.

Array status monitoring is important to increase confidence in the validity of seismic data. A printout should be provided to permit reference to past status as the need arises.

The various tests are discussed in the following sections.

4.3.1.1 Vault Discrete Quantities

These are quantities that are provided to the SLEM as one bit digital signals. A group of these bits are transmitted in the Random Sample field of the ODW when requested by the RDA field of the ICW. Their purpose is to provide monitoring of various vault conditions such as: battery voltage high or low, AC power to CTV on or off, SLEM temperature high or low, CTV door open or closed, test panel switch in test or normalization. The various conditions require monitoring of transducers to make digital data available to the SLEM. A suggested list of conditions are presented in [4-16, Appendix IV]. The specific limit values listed for these conditions are based on the design and environment of the NORSAR field instrumentation.

The occurrence of an abnormal condition of any of the monitored quantities is displayed on the EOC. Each condition has available a separate discrete lamp to identify which condition has occurred. These are written automatically by the computer. However, only a single set of subarray CTV indicators are provided. A separate set of indicators can identify which subarray is responsible for an abnormal condition indication.

4.3.1.2 Vault Continuous Quantities

These are quantities that are provided to the SLEM in analog form. One of these quantities can be converted to digital form and inserted in the Random Sample field of the ODW when requested by the RDA field of the ICW. Their purpose is to provide monitoring of various vault conditions such as the CTV auxiliary battery voltage or charging current, the ± 18 vdc power supply (for the Ithaco amplifier for LP seismometer signals),

or the +40 vdc power supply (for the RA-5 amplifier for the SP seismometer signals). A suggested list of quantities to be monitored is presented in [4-16, Appendix IV]. The monitored quantities are evaluated at the Data Center with limit tests, and certain abnormal results are displayed as discretes on the EOC.

4.3.1.3 Synchronization and Polycode

The number of ODW transmission errors detected by the synchronization and polynomial error detection circuitry in the SPS as well as the number of ICW errors reported by the SLEM are recorded for the transmission links to each subarray. Whenever these numbers exceed preset limits (for example, 5 in a 30-minute period), appropriate indicators are activated on the EOC. Cumulative errors are printed out at the end of 16.5 minute intervals, and may be displayed at any time upon request from the EOC.

4.3.1.4 Seismic Data Reasonableness

The seismic data obtained from each SP and LP seismometer is monitored continuously to detect equipment malfunctions that are degrading the data. In particular, the bias and the envelope of the signal are monitored relative to preset acceptable ranges for the particular instrumentation. An out-of-tolerance condition is recorded and displayed on the EOC.

The total signal energy (i.e., envelope test) is determined by summing the absolute value of the SP samples over 13.2 second intervals, and the sums are compared to a preset acceptable range. The LP samples are similarly summed over a 26.4 second period and compared with an acceptable range.

The dc component of the samples (bias test) is determined by summing the arithmetic value of the SP samples over 13.2 second intervals and of LP samples over 26.4 second intervals. The absolute values of these sums are compared against preset maximum values for reasonableness.

The accumulation windows and tolerance limits for both bias and envelope monitoring are parameterized to allow for readjustment.

4.3.2 Requested Online AM&C

These tests will be discussed in two groups. The first group is similar to all other AM&C tests in that they are basically monitoring operations. However, the second group involves remote adjustment of field instrumentation.

4.3.2.1 Monitoring Tests

The tests to be discussed in this category are:

- a. DC offset
- b. Channel gains
- c. Common mode rejection
- d. Test generators
- e. Digital compression
- f. RSA/ADC.

These tests check the performance of various portions of the LP and SP data acquisition channels by application of known test signals at various points and examination of appropriate aspects of the received signals in the SPS. In addition, to the extent that it can be done remotely, the test signal generators within the SLEM are checked.

The techniques used in the online system to evaluate the results of the dc offset and channel gain tests are similar to those used for the bias and envelope tests, respectively, of Section 4.3.1.4, but the inputs consist of SLEM test generator signals applied at various signal insertion points rather than actual seismic data. The common mode rejection point test differs from the other SLEM LTA insertion point tests, in that the test signal is applied simultaneously to both differential inputs of the selected LTA as a common mode signal rather than across the inputs as a SLEM input signal.

The tests referred to in items a, b and c above are similar in that the test signal in each case is a sine wave (1.0 Hz for short-period channels and 0.04 Hz for long-period channels) from the test signal generators. In each of these tests, a delay time is allowed between the application of the test signal and the computation of the test parameter to allow the analog channel transient to decay. These tests are summarized in Table 4-2, which includes typical values of the test parameters.

Appropriate ICW codes from the SPS will also cause the internally generated SLEM test signals to be applied directly to the SLEM ADC input for remote testing. There are four different test signals to be checked: positive broadband (+BB), negative broadband (-BB), 1.0 Hz sine wave and 0.04 Hz sine wave. The tests which have been implemented are summarized in Table 4-3, which includes typical values of the test parameters.

The digital compression test is a self-test feature designed into the SLEM in order to test the fixed-point to floating-point conversion. Four individually-addressable test sequences are available, each of which lasts for 15 seconds and causes a specific bit pattern to be inserted by the SLEM in the ODW. This bit pattern is analyzed online by comparing the received data samples with the expected sample values.

Table 4-2. Data Acquisition Channel Tests

Short-Period Channel Tests

Test Name	Insertion Point(s)	Test Signal (Hz)	Delay Time (Seconds)	Test Parameter	Test Limits (q.u.)
DC Offset	SLEM LTA Input	1.0	57	Average Value-132 Samples	± 16
Common-Mode Rejection	Both LTA Inputs	1.0	57	Sine Wave Peak-to-Peak	4
Full Channel Gain	Seismometer Calibration Coil	1.0	20	Absolute Sum-101 Samples	281,689 - 324,109
Amplifier Insertion Gain	RA-5 Amplifier Input	1.0	20	Absolute Sum-101 Samples	260,000 - 300,000
LTA Insertion Gain	SLEM LTA Input	1.0	20	Absolute Sum-101 Samples	211,090 - 257,954

Long-Period Channel Tests

Test Name	Insertion Point(s)	Test Signal (Hz)	Delay Time (Seconds)	Test Parameter	Test Limits (q.u.)
DC Offset	SLEM LTA Input	.04	447	Average Value-26 or 27 Samples	± 16
Common-Mode Rejection	Both LTA Inputs	.04	447	Sine Wave Peak-to-Peak	4
Full Channel Gain	Seismometer Calibration Coil	.04	130	Absolute Sum-128 Samples	248,704 - 305,280
Amplifier Insertion Gain	Ithaco Amplifier Input	.04	130	Absolute Sum-128 Samples	310,000 - 380,000
LTA Insertion Gain	SLEM LTA Input	.04	130	Absolute Sum-128 Samples	267,520 - 326,912

Table 4-3. SLEM Test Signal Quality Checks

Test Name	Insertion Point(s)	Test Signal	Delay Time	Test Parameter	Test Limits
Short-Period Sine Wave Amplitude	ADC Input	1.0 Hz	---	Sine Wave Peak-to-Peak	4724 to 5436 q.u.
Short-Period Sine Wave Frequency	ADC Input	1.0 Hz	---	Dominant Frequency	0.96 to 1.04 Hz
Long-Period Sine Wave Amplitude	ADC Input	.04 Hz	---	Sine Wave Peak-to-Peak	4724 to 5436 q.u.
Long-Period Sine Wave Frequency	ADC Input	.04 Hz	---	Dominant Frequency	0.0384 to 0.0416 Hz
Positive Broadband	ADC Input	+BB	---	---	1842 to 1918 q.u.
Negative Broadband	ADC Input	-BB	---	---	1842 to 1918 q.u.

The RSA/ADC test causes a positive dc level to be applied to the range scaling amplifier input for 10 seconds followed by a negative dc level for 10 seconds. Analysis of the data requires that one short-period and one long-period sample of the positive and then the negative data be examined. If there is more than 16 quantum units difference between the short and long-period data samples, an out-of-tolerance condition exists.

The digital loop tests check the performance of various sections of the communication links between the SPS and each CTV. The available tests and the corresponding loopback points are as follows:

<u>Test Name</u>	<u>Loopback Point</u>
Local Loop	Line side of NDPC modem
Line Loop	Line side of CTV modem
Remote Loop	SLEM side of CTV modem

Each of these tests causes the transmission of a simulated ICW having normal message length, sync, control characters and polycode, but containing a seven-byte pseudo-random pattern (expressed as 15FB363D67CFB3 in hexadecimal notation) in lieu of other data.

This ICW is looped back to the data center by the transmission system. The point at which the loopback occurs is controlled by the supervisory control circuits of the transmitting modem. A bit-by-bit comparison of the received pattern indicates whether the communication equipment is operating properly. Adjusting the point at which the loopback occurs permits localization of the defective section of the communications equipment.

4.3.2.2 Adjustment Tests

With respect to NORSAR, the only tests in this category are the LP free period and mass position measurements and adjustments. The LP seismometers should have a free period (i.e., undamped natural period) of 20 ± 0.5 seconds and a mass position adjusted within ± 2.0 millimeters. These values must be maintained to ensure constant instrument sensitivity. Thus, the free period and mass position of the LP seismometers are adjusted whenever the test measurements indicate free period outside the range of 19.5 to 20.5 seconds, or mass position outside the range of +2 millimeters to -2 millimeters, which is represented by the instrumentation as the range of +2 volts to -2 volts.

Free period is adjusted to within the range of 19.8 to 20.2 seconds. Mass position is adjusted to within the range of +0.5 volts to -0.5 volts.

The adjustment of free period has a significant effect upon mass position, but the reverse is not usually true. Thus, free period should be adjusted first. However, after adjusting either of them the other should be rechecked.

The free period measurement requires use of the data coil output of the seismometer. Thus, it is subject to seismic background noise, and it is necessary to monitor this noise prior to making the measurement to avoid inaccurate readings. Seismic background noise peaks greater than 200 quantum units will impair accuracy. The discrete output field of the ICW is used to remove the damping resistors from the seismometers. Then a sequence of broadband picks (+BB or -BB) is transmitted to the calibration coils of the seismometer as follows: 5 seconds of -BB, 10 seconds of +BB, 10 seconds of -BB, 5 seconds of +BB. The data coil outputs of the seismometers are sampled and inserted into the ODWs under

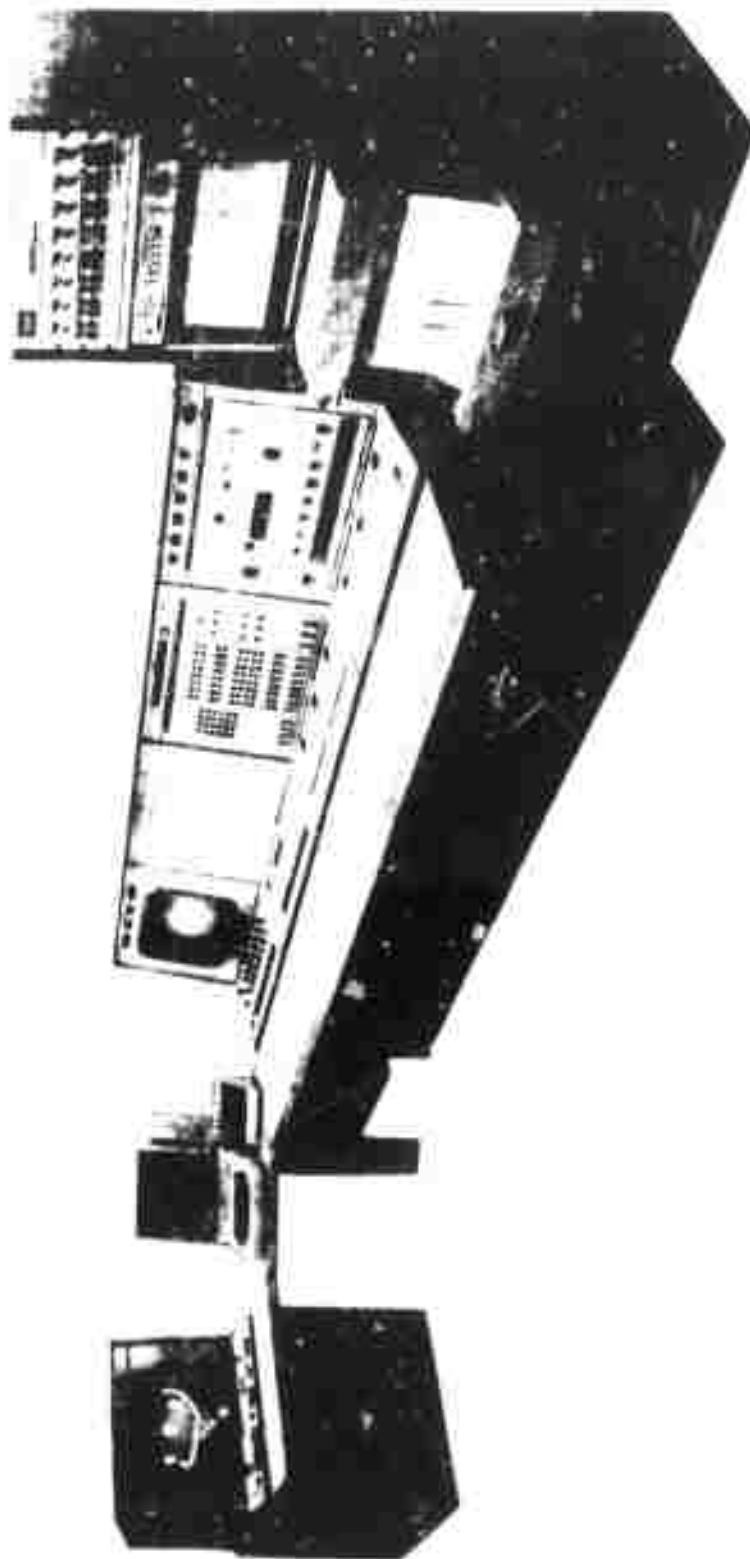


Figure 4-18. Operations Console, Strip Chart Recorder, and 2260 Display Unit

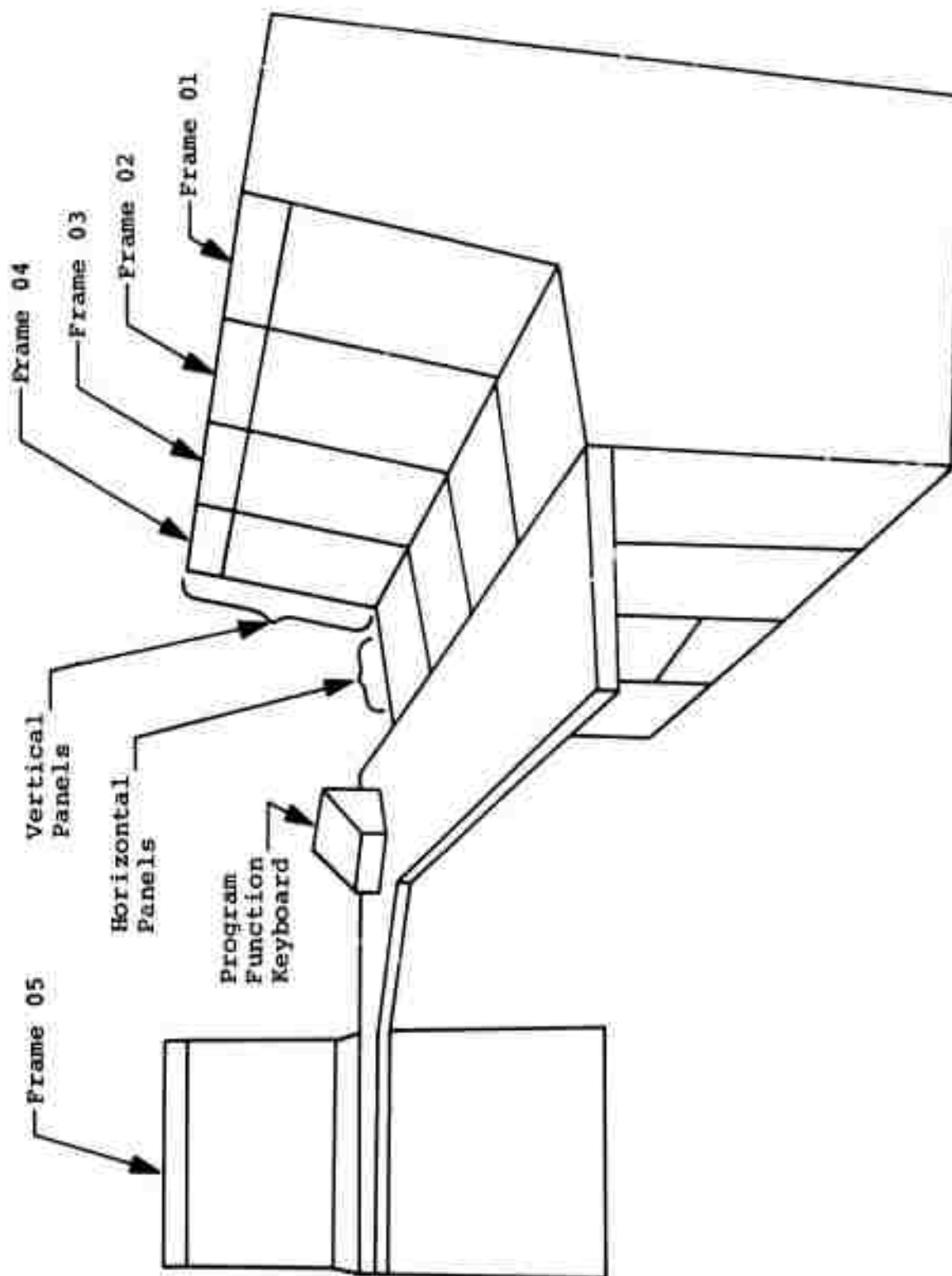


Figure 4-17. Physical Layout of Operations Console

command of the ICWs. The average period over several cycles (starting 20 seconds after the end of the broadband sequence) is computed as the free period. The discrete output field of the ICW is then used to command restoration of the damping resistors.

The mass position of each instrument is monitored by activating a photo-cell bridge circuit and reading the mass position in volts.

The discrete output field of the ICW is used to activate, and later deactivate, the mass position monitor circuits of the LP seismometers.

The adjustments are accomplished by a pair of ac motors which can be energized in the appropriate direction by means of code words in the discrete output field of the ICW. The amount of adjustment is determined by the length of time the motor is energized, but there is considerable variation in the sensitivity of the instrument to the adjusting motor. Individual code words are used to turn the vertical, East-West and North-South LP seismometer motors on and off, as well as for plus or minus corrections.

A 120-second delay must follow a free period or mass position correction before a free period measurement can be made, or before the instrument output can be accepted as a valid seismic signal.

The EOC contains switches to permit requests to be entered by the operator for mass position and free period measurements or combined measurements and adjustments. The subarray selector switches are set to indicate the subarray desired, and the channel selector switch is set to indicate the desired channel within that subarray. Measurements that are not within specified limits will cause indicators to be lit on the EOC.

The processor is programmed to accept commands from the EOC to initiate an automatic procedure of measuring and correcting the free period and mass position of LP seismometers.

4.3.3 Requested Extended AM&C

The AM&C tests that use an offline computer for evaluation of test data are of two types: quick mode testing and detailed analog channel analysis. These are discussed briefly in the following sections.

4.3.3.1 Quick Mode Testing

The quick mode testing uses an efficient computational method for estimating several parameters of the data acquisition system from the channel response to a psuedo-random input test signal. These parameters are seismometer damping ratio, seismometer natural frequency, and channel gain.

The input test signal consists of a standard voltage applied to the seismometer's calibration coil with a sequence formed by continuing or reversing the polarity of the voltage at 0.1 second intervals (for SP seismometers). The output is taken from the seismometer's data coil. One cycle of the psuedo-random sequence contains 64 bits. Typically, 21 cycles should be applied to the instrument. The first 5 cycles are not used for data results to allow the initial transient caused by initiation of the test signal to decay. The last cycle is not used for data results to avoid termination transients. Thus, only the intermediate 15 cycles are used. Since each cycle contains 64 bits, 960 bit times represent data results.

During the test, each ODW contains a reflected bit that indicates the polarity of the input test signal for that frame time, as well as the resulting output of the seismometers. In addition, it is necessary to monitor the reflected bit in frames preceding and following the test. These checks permit verification that the desired sequence has been correctly applied.

The collected data is transferred to and processed by the offline processor.

4.3.3.2 Detailed Analog Channel Analysis

These detailed tests require specified test signals to be routed through the channels in a particular fashion.

The sine wave tests provide the average peak value of the signal as well as an evaluation of the gain, phase shift and distortion of the RA-5 amplifier, Ithaco amplifier, and LTAs at a single frequency. The sine wave generator used for the sine wave tests is 1.0 Hz for the SP channels and 0.04 Hz for the LP channels.

The broadband analysis provides an evaluation of various channel parameters including channel sensitivity, filter ripple, upper and lower -3 dB frequencies, time constants, channel delay, instrument sensitivity, damping ratio, and natural frequency.

The broadband analysis uses a pseudo-random sequence designated BB1 for the SP channels, and a pseudo-random sequence designated BB2 for the LP channels. The BB1 function is a 64-bit sequence which defines the polarity of the broadband test signal (+BB or -BB) to be applied in each 0.1-second interval for 6.4 seconds. This function should be repeated about

25 times for each SP channel tested. The BB2 function is an 18-bit sequence with each bit representing the broadband test signal polarity for a 10-second interval. This function should be repeated about five times for each LP channel tested.

The basic concept of broadband testing is as follows:

- a. Postulate a mathematical model of the channel.
- b. Apply the broadband test and acquire output data samples.
- c. Compute the discrete Fourier transform of the output samples to obtain the transfer function of the channel.
- d. Modify the parameters of the mathematical model until its transfer function converges to the measured transfer function.
- e. Compare the adjusted parameters of the model to actual hardware specifications.

Note that the BB1 test signal should be considered as a single set of 64 input bits that produce 64 output samples. Since many cycles of the 64 bit test signal are applied, it is possible to average corresponding output data samples of many cycles as a noise reduction technique.

In addition to the general purpose sine wave and broadband tests, Requested Extended AM&C can include special purpose routines that are developed to solve specific operational problems. For example, NORSAR uses:

- a. A SACP program to evaluate sine wave test data
- b. A CHANEV program to evaluate SP BB1 test data
- c. A CHANLP program to evaluate LP BB2 test data
- d. A MISSING NUMBERS program to determine whether all expected digital numbers are producible at the SLEM output.

4.3.4 Requested Online Display AM&C

These tests require application of certain test signals at specified insertion points in the SP or LP data channels, just as is done in the Requested Online tests (Section 4.3.2). The primary difference is that the display tests require no automatic analysis, but rather provide signals for display on specified traces of the EOC waveform scope, or for recording on specified channels of the strip-chart recorder.

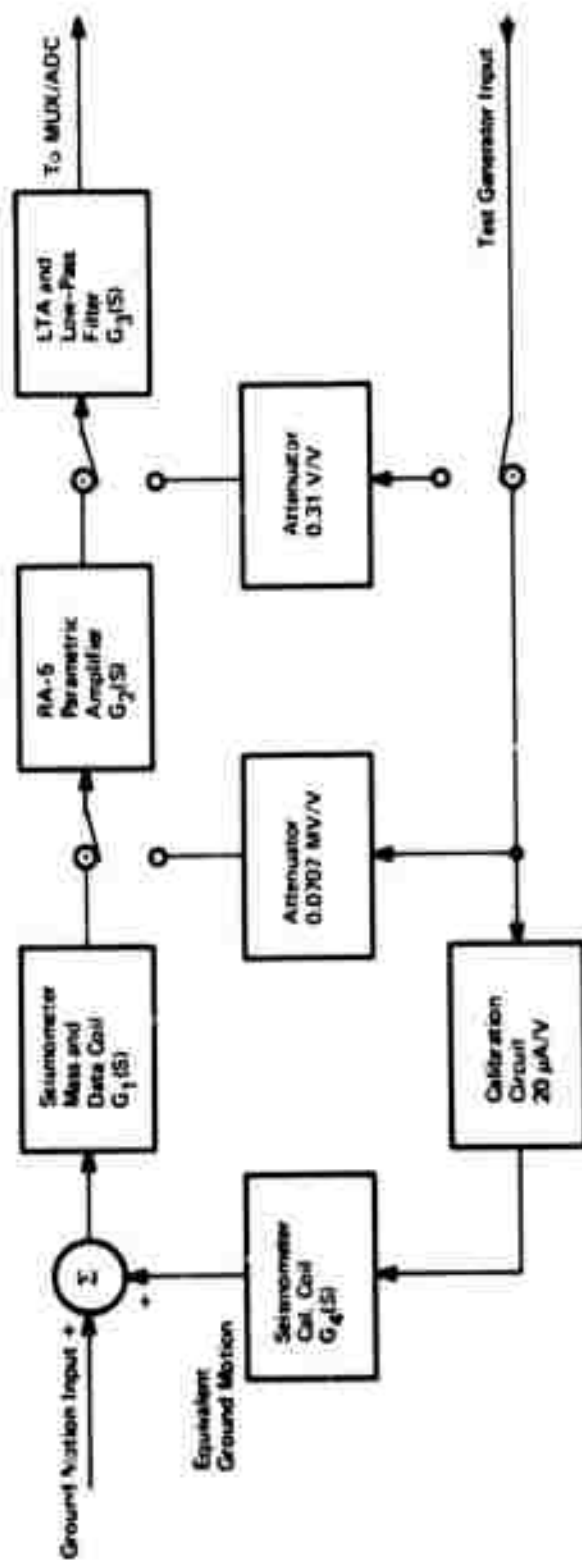
4.4 ANALOG CHANNEL MODELS

The SP and LP field instrumentation has been described in Section 4.2, with particular emphasis on the characteristics and specifications of the NORSAR system components. The short-period analog channel data flow was shown in Figure 4-8; the long-period analog channel is similar except that the low-pass filter stage is implemented as an integral part of the Ithaco amplifier.

Mathematical models of the SP and LP analog data channels and calibration circuits are presented in the following subsections.

4.4.1 Short-Period (SP) Analog Channel

The mathematical model for the short-period analog data channel and calibration circuits is presented in Figure 4-19. The individual component models are compatible with the specifications of the components in Section 4.2. Typical values of the model parameters given below, except for the amplifier gain settings, are equivalent to the nominal parameter values stated or implied by the manufacturer's specifications for the



$$G_1(S) = \frac{G_m S^3}{S^2 + 2\eta\omega_n S + \omega_n^2}$$

$$G_2(S) = \frac{K_2 S}{S + \alpha}$$

$$G_3(S) = \frac{K_3 S}{S + \beta} \cdot \frac{1}{(1 + f_1 S + f_2 S^2)(1 + f_3 S + f_4 S^2)}$$

$$G_4(S) = \frac{G_c}{MS^2}$$

Figure 4-19. Short-Period Analog Channel Model

various components. Current values of these parameters can be estimated directly for each NORSAR SP data channel by the use of the Array Monitor and Control SP broadband test capability and the CHANEV analysis program, as discussed in Section 4.3.3.2.

a. SP Seismometer Parameters

1. Inertial Mass (M)-0.825 kilograms
2. Data Coil Generator Constant (G_m)-846 volt-seconds/meter
3. Calibration Coil Motor Constant (G_c)-0.0326 newtons/ampere
4. Natural Frequency ($\omega_n = 2\pi f_n$)-1.0 Hz
5. Damping Ratio (h)-0.7

b. RA-5 Amplifier Parameters

1. Nominal Gain (K_2)-5410
2. 3 dB Low Frequency Cutoff (α)-0.1 Hz

c. Line Termination Amplifier Parameters

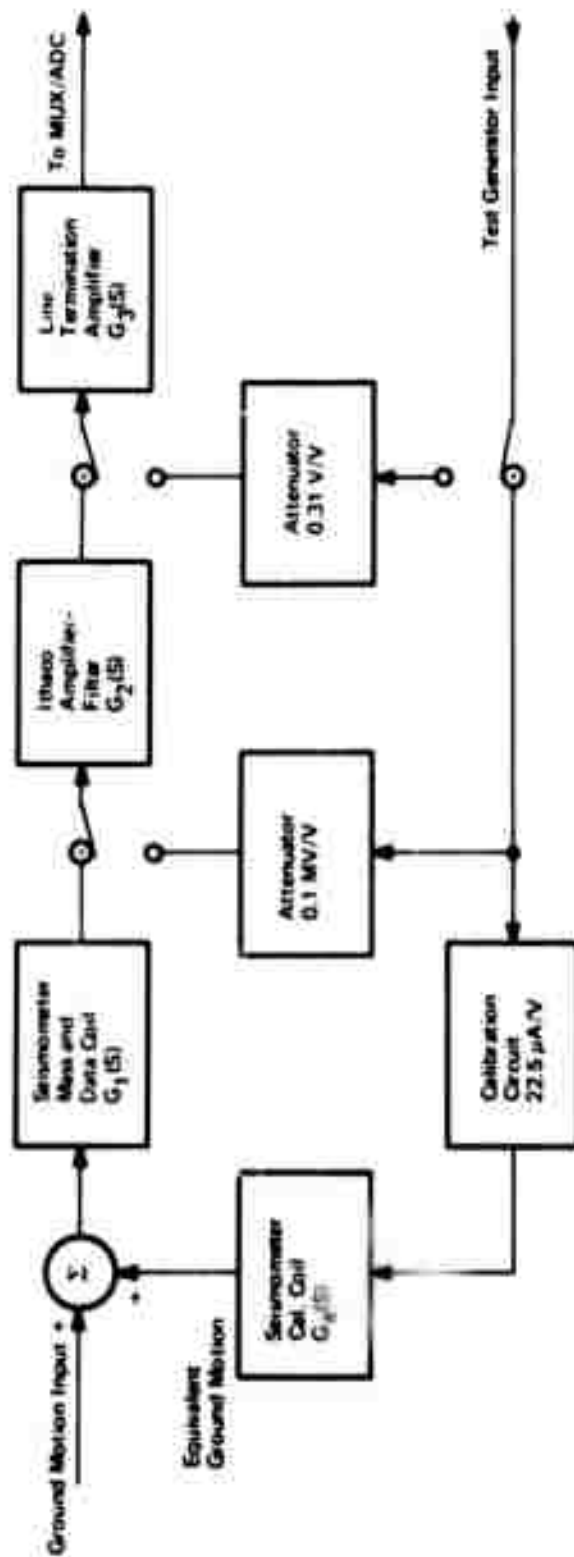
1. Nominal Gain (K_3)-0.714
2. 3 dB Low-Frequency Cutoff (β)-0.038 Hz

d. Tchebyscheff Low-Pass Filter Parameters

1. f_1 -0.0122 seconds
2. f_2 -0.001288 (seconds)²
3. f_3 -0.0872 seconds
4. f_4 -0.003844 (seconds)²

4.4.2 Long-Period (LP) Analog Channel

The mathematical model for the NORSAR long-period analog data channel and calibration circuits is presented in Figure 4-20. The component models are compatible with the specifications in Section 4.2. The typical values of model parameters presented below, except for amplifier gain settings, have been derived from the manufacturers specifications for the various components. Actual values of these parameters for each



$$G_1(s) = \frac{G_m s^3}{s^2 + 2\eta\omega_n s + \omega_n^2}$$

$$G_3(s) = \frac{\kappa_3 s}{s + \beta}$$

$$G_2(s) = \frac{\kappa_2 s}{(s + \gamma)(1 + \alpha s)^2 (1 + \tau_1 s + \tau_2 s)}$$

$$G_4(s) = \frac{G_c}{Ms^2}$$

Figure 4-20. Long-Period Analog Channel Model

NORSAR LP data channel can be estimated by the use of the Array Monitor and Control LP broadband test capability and the CHANLP analysis program, as discussed in Section 4.3.3.2.

a. LP Seismometer Parameters

1. Inertial Mass (M)-10 kilograms
2. Data Coil Generator Constant (G_m)-750 volt-seconds/meter
3. Calibration Coil Motor Constant (G_c)-0.032 newtons/ampere
4. Natural Frequency ($\omega_n = 2\pi f_n$)-0.05 Hz
5. Damping Ratio (h)-0.64

b. Ithaco Amplifier Parameters

1. Nominal Gain (K_2)-4000
2. 3 dB Low Frequency Cutoff (γ)-0.005 Hz
3. Two-Pole Low-Pass Filter Time Constant (α)-4.83 seconds
4. Butterworth Low-Pass Filter Parameters
 - (a) f_1 -5.627 seconds
 - (b) f_2 -15.83 (seconds)²

c. Line Termination Amplifier Parameter

1. Nominal Gain (K_3)-0.714
2. 3 dB Low Frequency Cutoff (β)-0.0037 Hz

4.5 ANNOTATED BIBLIOGRAPHY

The references listed here are divided into three groups. The first group (4.5.1) consists of quarterly and final reports prepared by IBM under a series of contracts relating to seismic signal processing. The second group (4.5.2) consists of IBM special technical reports prepared under the same series of contracts. Miscellaneous other references constitute the third group (4.5.3).

4.5.1 IBM Quarterly and Final Technical Reports

- 4-1. "Large Aperture Seismic Array Signal Processing Study,"
IBM Final Report, Contract SD-296, 15 July 1965.

Section 1 includes a discussion of signal levels and scaling, Section 2 discusses quantization and time sampling, and Section 4 documents the loss in performance due to quantum level, sampling interval, and seismometer sensitivity variations.

- 4-2. "LASA Signal Processing, Simulation, and Communications Study," IBM First Quarterly Technical Report, Contract AF 19 (628)-5948, 1 May 1966.

The general concept of calibration signals is discussed in Section 3, and that of the Experimental Operations Console in Section 4. In Appendix C, specifications for scaling, seismometer tolerances, sampling rate, quantization and word length are discussed.

- 4-3. "LASA Signal Processing, Simulation, and Communications Study," IBM Second Quarterly Technical Report, Contract AF 19 (628)-5948, September 1966.

Appendix C includes discussions of SAAC data communications concepts, array monitor and control, and a reliability analysis. Appendix D also incorporates a report on data communications possibilities between Montana and Washington, D.C.

- 4-4. "LASA Signal Processing, Simulation, and Communications Study," IBM Final Report, Contract AF 19 (628)-5948, ESD-TR-66-635, March 1967.

Section 2 includes documentation of LASA data communications, a discussion of a proposed SAAC communication interface equipment, and a conceptual description of the Experimental Operations Console that contains many features subsequently implemented in both units (at the operations and maintenance consoles).

- 4-5. "LASA Experimental Signal Processing System," IBM First Quarterly Technical Report, Contract F19628-C-67-0198, ESD-TR-67-458, February 1967.

Appendix B discusses sensor characteristics that should be tested and incorporates a useful diagram of LASA field instrumentation. Also documented is functional specification of SAAC-modem interface equipment.

- 4-6. "LASA Experiment Signal Processing System," IBM Second Quarterly Technical Report, Contract F19628-67-C-0198, ESD-TR-67-602, May 1967.

Appendix B describes the application of the proposed Experimental Operations Console for array monitor and control. Sampling rate, data encoding, and data reconstruction are discussed in Appendix C, quantization error in Appendix D, and dynamic range, array gain, sampling rate, and time delays in Appendix F.

- 4-7. "LASA Experimental Signal Processing System," IBM Fourth Quarterly Report, Contract F19628-67-C-0198, ESD-TR-68-309, November 1967.

Appendix II includes a discussion of the SAAC data acquisition system. Appendix III incorporates discussion of and specifications for SEM II and LEM (the units that evolved into the present SLEM); this report indicates the three principal differences between the SEM II concept and the LASA SEM.

- 4-8. "LASA Experimental Signal Processing System," IBM Fifth Quarterly Technical Report, Contract F19628-67-C-0198, ESD-TR-68-450, February 1968.

Appendix II discusses chaining concepts, Appendix IV includes a description of the SAAC Operations Console, and Appendix VII includes a reliability analysis of data acquisition performance.

- 4-9. "LASA Experimental Signal Processing System," IBM Sixth Quarterly Technical Report, Contract F19628-67-C-0198, ESD-TR-68-451, May 1968.

Section II comments on time-delay errors caused by a drift in seismometer resonant frequencies, and on the SAAC operations console and the NORSAR data acquisition equipment. Appendix II discusses the operational features of the Central Terminal Vault and its equipment. Appendix III discusses subarray power and equipment, and the communications network.

- 4-10. "LASA Experimental Signal Processing System," IBM Final Technical Report, Contract F19628-67-C-0198, ESD-TR-69-60, Volume I, March 1969.

Appendix I discusses NORSAR data communications requirements. Appendix III describes a method for controlling long-period seismometers from the data center through the discrete output field of the SEM. Appendix IV gives an operational description of the Signal Processing System.

- 4-11. "Integrated Seismic Research Signal Processing System," IBM First Quarterly Technical Report, Contract F19628-68-C-0400, ESD-TR-69-299, November 1969.

Appendix V describes the ISRSPS equipment configuration, with emphasis on the Signal Processing System and the Experimental Operations Console.

- 4-12. "Integrated Seismic Research Signal Processing System," IBM Second Quarterly Technical Report, Contract F19628-68-C-0400, ESD-TR-69-357, February 1969.

Appendix I describes the NORSAR Interim System. Appendix III describes SAAC data integrity control. Appendix V gives estimates of minimum sampling rates for microbarographs. Appendix VI discusses NORSAR data acquisition accuracy. Appendix III describes a proposed digital unit to replace the Montana SEM output unit.

- 4-13. "Integrated Seismic Research Signal Processing System," IBM Fourth Quarterly Technical Report, Contract F19628-68-C-0400, ESD-TR-70-265, August 1969.

Appendix V discusses planned system applications of the Experimental Operations Console, with emphasis on SAAC usage. Appendix III discusses the Interim NORSAR System configuration.

- 4-14. "Integrated Seismic Research Processing System," IBM
Fifth Quarterly Technical Report, Contract F19628-68-C-0400,
ESD-TR-70-306, November 1969.

Appendix IX describes techniques used to connect and calibrate a prototype SLEM at Subarray 01A, near Hamar, Norway, in 1969. Appendix X summarizes the microcoded functions of the SAAC-SPS.

- 4-15. "Integrated Seismic Research Signal Processing System,"
IBM Sixth Quarterly Technical Report, Contract
F19628-68-C-0400, ESD-TR-71-388, February 1970.

Appendix VI describes an interim system that used commercial FM data links at NORSAR.

- 4-16. "Integrated Seismic Research Signal Processing System,"
IBM Seventh Quarterly Technical Report, Contract
F19628-68-C-0400, ESD-TR-71-128, May 1970.

Appendix IV defines the specifications for the NORSAR field instrumentation including overall specifications for the data acquisition channel.

- 4-17. "Integrated Seismic Research Signal Processing System,"
IBM Eighth Quarterly Technical Report, Contract
F19628-68-C-0400, ESD-TR-71-393, August 1970.

Appendix IV contains the results of Category II tests performed on SLEMs manufactured by Philco-Ford. Appendix VI documents the SAAC-LDC 50 kilobaud line error tests.

- 4-13. "Integrated Seismic Research Signal Processing System,"
IBM Ninth Quarterly Technical Report, Contract
F19628-68-C-0400, ESD-TR-72-122, November 1970.

Appendix IV discusses link calibration and system maintenance, and describes the NORSAR Interim data acquisition system, including a detailed diagram. Appendix VI describes problems encountered and corrective actions taken during the course of integration testing of the SLEM units and related central terminal vault equipment.

- 4-19. "Integrated Seismic Research Signal Processing System,"
IBM Tenth Quarterly Technical Report, Contract
F19628-68-C-0400, ESD-TR-72-123, February 1971.

Appendix III documents the final SAAC ISRSPS configuration. Appendix IV reports the SAAC ISRSPS system and acceptance tests; the acquisition and recording of data from LASA and ALPA was part of the SAAC-ISRSPS system tests.

- 4-20. "Integrated Seismic Research Signal Processing System,"
IBM Eleventh Quarterly Technical Report, Contract
F19628-68-C-0400, ESD-TR-72-133, May 1971.

Appendix III describes the implementation and integration of the Array Monitor and Control Subsystem in the NDPC system. Appendix V discusses transatlantic data link utilization, in the NDPC-to-SAAC direction.

- 4-21. "Integrated Seismic Research Signal Processing System,"
IBM Final Technical Report, Contract F19628-68-C-0400,
ESD-TR-72-139, August 1971.

Appendix II documents a loading and timing study of the NDPC IERSPS online system.

4.5.2 IBM Special Technical Reports

- 4-22. "Signal Processing Studies for Large Array Research,"
Contract F19628-C-0198, March 1970.

This report compares two system configurations for large array seismic data acquisition, the difference lying in whether the array control and data analysis functions are integrated.

- 4-23. "Evaluation of the Transatlantic Data Link of the Integrated Seismic Research Signal Processing System," Contract
F19628-68-C-0400, September 1970.

This report presents error statistics for the data link between SAAC and NDPC.

- 4-24. "Computer Network Feasibility Considerations of SAAC,"
Contract F19628-68-C-0400, October 1970.

This report discusses the feasibility of interconnecting the SAAC facility with the Advanced Research Projects Agency computer network. Also, it examines the feasibility of operating the present 2400-baud transatlantic data link at a higher data rate to support interconnection of the ARPA computer network with the computer network of Britain's National Physics Laboratory.

4.5.3 Miscellaneous References

- 4-25. "Seismic Methods for Monitoring Underground Explosions,"
International Institute for Peace and Conflict Research,
Stockholm, 1968.

This report discusses site noise levels and general problems in seismic system data acquisition.

- 4-26. "Montana Large Aperture Seismic Array, General Description, MLM-1," prepared for Directorate of Planning and Technology, ESD, AFSC, USAF, Contract F19628-68-C-0401, Philco-Ford Corporation, April 1969.

This manual, one of a set of volumes which describe the Montana LASA, provides an overview of LASA, a brief description of available manuals, a description of the LASA physical facilities, a description of special test equipment, and system interconnection cabling information.

- 4-27. "Operation and Maintenance Manual for the Signal Acquisition System of the Montana Large Aperture Seismic Array," prepared for the AFTAC/VELA Seismological Center (Alexandria, Virginia), sponsored by Advanced Research Projects Agency, Contract AF 33 (657)-14104, Earth Sciences Division, Teledyne Industries, Inc., May 1966.

This manual was prepared for the use of field personnel in the operation and maintenance of the data acquisition system of the Montana LASA. The volume gives both general and detailed functional descriptions of the system and each of the system components, describes the maintenance program, gives cable specifications, and reports information furnished by equipment manufacturers.

- 4-28. "Norwegian Seismic System (NORSAR), Phase II," Norwegian Defense Research Establishment, 1968-1969.

These documents provide comprehensive technical documentation for Phase II of Project NORSAR. The set consists of six documents in ten volumes, as follows:

Preliminary Planning Report, Parts I and II, NORCONSULT A.S.
February 8, 1968.

Document I (1968-1969 Program) contains coordinate lists, access descriptions, subarray maps, sketches of LPV-CTV sites, and drilling reports.

Document II, Parts 1, 2, and 3 (1969 Program) contains air survey maps of subarrays.

Document III (1968-1969 Program) contains construction drawings for electrical installations.

Document IV (1968-1969 Program) contains test information for short and long period field instrumentation.

Document V (1968-1969 Program) contains construction drawings for vaults and boreholes.

4-29. "Handbook, Modem Equipment Type GH2003," Standard Radio and Telefon AB, Transmission and Data Systems Division, Solno, Sweden.

4-30. "Seismic Short and Long Period Electronics Modules (SLEM)," Volume I (Operations Manual), Volume II (Maintenance Manual), Volume III (Diagrams), Philco-Ford Corporation, December, 1970.

This set of volumes constitutes the technical manual for the SLEM equipment. Volume I describes the equipment, presents the electrical and mechanical characteristics, and includes the operating procedures and theory of operation. Volume II, in addition, includes installation,

adjustment, maintenance and testing procedures, and required diagrams. Volume III contains the foldout diagrams for the Functional Class circuits of the Digital Unit.

- 4-31. Consultive Committee on International Telephone and Telegraph (CCITT) Blue Book, Geneva, 1964.

The circuit interfaces for the 2400-bps telephone lines which connect the subarrays with the NORSAR data center are in accordance with the recommendations of CCITT.

Section 5

DETECTION PROCESSING

The LASA and NORSAR Detection Processors provide continuous online surveillance in real time of selected regions of the earth for possible natural or man-made seismic disturbances, in accordance with the Large Array Program objectives. The required online functions of acquisition, recording, signal processing and detection analysis of large quantities of seismic array data represent a significant computation load, and therefore demand efficient utilization of available computer resources. The significant design decisions and tradeoff considerations involved in the DP system development are discussed in this section, and the resulting DP system configurations for LASA and NORSAR are presented and compared.

The basic design philosophy of the LASA and NORSAR DP systems is discussed in Section 5.1, together with a summarization of the results of several early design tradeoff studies which led to the functional configurations of these systems. The following three sections discuss various phases of the DP system development. Section 5.2 is concerned with how beams should be deployed for surveillance purposes to provide adequate, selective coverage at a level of sensitivity which approaches the ultimate capability of the array, without exceeding computer storage and processing capabilities. The design, analysis and implementation of the principal signal processing algorithms are presented in Section 5.3, and the algorithm for combining detections on individual array beams at individual sample times into event detection groups is discussed in Section 5.4. The online DP system outputs are described in Section 5.5, and various techniques are discussed for the offline post-analysis of the available DP output data. Section 5.6 presents the results of a study of the comparative performances of various alternative detection processing techniques, for consideration and guidance in further DP system development.

5.1 DETECTION PROCESSOR (DP) SYSTEM DEFINITION

The purpose of the Detection Processor is to provide online, real time surveillance of selected regions of the earth, primarily at teleseismic distances from the associated seismic array. Occurrences of seismic events in the surveillance region are to be detected and recorded. The surveillance region is represented very conveniently in the horizontal inverse velocity plane, or U-space, as discussed in Sections 2.1 and 7.1. In terms of this representation, teleseismic events are observed approximately within the annulus between 0.04 and 0.08 seconds/kilometer.

5.1.1 System Concept

The primary techniques which are used to enhance the seismic signals relative to the background noise and to interfering signals are beamforming and filtering. As discussed in Section 3.5, filtering is effective because of the differences between the signal and noise spectral characteristics. Significant noise reduction is achieved merely by strong attenuation in frequency intervals containing a considerable amount of noise energy and very little signal energy. On the other hand, frequency intervals which generally contain high signal-to-noise-energy ratios are given relative emphasis in the filtering operation.

Linear array beamforming is the process of applying a relative time delay to the data from each seismometer data channel in order to approximately compensate for the unequal relative arrival times of a seismic signal at each sensor, and then summing the data values at each sample point. Since the signals are generally quite coherent from sensor to sensor across the array, and since the background noise is quite incoherent between sensors, linear array beamforming results in a signal-to-noise-ratio gain. Reference [5-25] contains the results of a study using LASA data to demonstrate the actual beamforming and filtering gains, and to compare the relative gains of various processing configurations.

Detection processing is accomplished primarily by computing a running estimate of the short-term-average (STA) energy on each detection beam, and testing this energy estimate to determine whether it exceeds a threshold set relative to the recent ambient noise level on that beam. This threshold must be set sufficiently above the ambient noise level to prevent the occurrence of an excessive number of false detections caused by short-term increases in the background noise level; conversely, the threshold must be set sufficiently close to the ambient noise level to achieve adequate sensitivity to small seismic signals.

The characteristics of seismic signals are discussed in Section 3.4, and it is indicated in particular that neither the time trace nor even the amplitude spectrum of a short-period seismic signal is generally known in advance with any reasonable degree of accuracy. Hence, the use of optimum coherent processing techniques such as matched-filtering does not appear to be feasible for short-period detection processing.

5.1.2 Design Considerations

There are two major areas for consideration in the design of the detection processing scheme outlined above: signal processing and beam deployment. Given the inputs from an array of seismometers, the DP signal processing requirement is to utilize the processes of beamforming, scaling, filtering, envelope (STA) computation, etc., so as to optimize event detectability for a given false alarm rate within the time constraints imposed by available core storage and processing time. Given a certain surveillance region in U-space, the beam deployment requirement is to specify the number and U-space location of beams which will cover the surveillance region with no excessive loss of sensitivity relative to the ultimate system capability, and within the available processing resources.

The beam deployment problem is treated separately in Section 5.2, and the signal processing algorithm development is described in Section 5.3. Some of the important considerations in the overall design of the Detection Processor are discussed below.

5.1.2.1 Alternate Beamforming Techniques

The simple delay-and-sum beamforming method can be described as follows. Let $f_k(t)$; $k = 1, 2, \dots, K$ denote the outputs of the K elements of the array. Each output $f_k(t)$ is the sum of a noise component $n_k(t)$ and (when present) a signal component $s_k(t)$. If the presence of a signal is to be detected, and if the signal wavefront shape and propagation speeds at the array are known, it is possible to generate the waveform:

$$B(t) = \sum_{k=1}^K f_k(t-t_k) \quad (5-1)$$

where the delay times t_k are chosen to compensate for the differences in arrival times of the signal wavefront in the various array seismometers. In this manner, signal reinforcement will be achieved as a consequence of the in-phase addition of the signal components $s_k(t)$. On the other hand, the noise components, having been generated by many sources at various locations, will not be added in phase and will, therefore, not be reinforced to the same extent as the signal components.

Since the various seismometer outputs should be weighted according to their respective signal-to-noise ratios for efficient signal-to-noise improvement, the unweighted sum (5-1) is often replaced by a weighted summation. In its simplest form the weighting may be frequency-independent; i.e., each output $f_k(t)$ is simply multiplied by some time-independent factor prior to addition. This method is called weighted-delay-and-sum

beamforming. Another common method consists of frequency-dependent weighting; i.e., of filtering of the seismometer outputs prior to their addition, and is referred to as filter-and-sum beamforming.

Although the beam (5-1) has been steered to receive and detect a specific signal wavefront (called the center of the beam), the beam can be used also to receive and detect other neighboring signal wavefronts. Of course, some loss in signal power will then be incurred. The number of beams required to monitor a given region is dependent on the maximum allowable signal power loss.

The weighting applied to delay-and-sum beam formation is usually the same for all beams, but different for different seismometers.

The delay-and-sum beamforming described above is satisfactory when the noise coherence across the array site is weak. However, for strong noise coherence (as, for example, in the case where the array dimensions are small compared to the dominant noise wavelength), delay-and-sum processing may not yield the maximum, or even near-maximum, output signal-to-noise ratio. In that situation, considerable signal-to-noise ratio enhancement can be achieved, in principle, by means of optimum filter-and-sum processing, which is specifically designed to maximize the output signal-to-noise ratio.

In optimum filter-and-sum beam formation each seismometer output $f_k(t)$ is passed through a filter, and the K resulting filter outputs are added to produce the optimum beam output. The amplitude and phase spectra of these filters can be calculated from the cross-spectral matrix of the signal and that of the noise.

At first sight, the filter-and-sum beam formation and the conventional weighted beam formation appear to be rather similar in their implementation. However, in practice there are substantial differences. First, the

optimum filters required are different for different beams, while the filters for delay-and-sum beamforming are the same for all beams. This obviously tends to make optimum processing relatively more expensive. Second, the filter design is not as critical as the optimum filter design. The signal-to-noise enhancement achieved by optimum processing is often very sensitive to small variations in seismometer performance and to slight changes in the noise distribution experienced by the array. This sensitivity is likely to occur when the signal-to-noise enhancement for optimum processing far exceeds that for delay-and-sum beamforming. The reason is that optimum processing relies on noise cancellation and often entails some signal cancellation. However, with the use of correctly designed optimum filters in certain correlated noise environments, the noise cancellation is sometimes so much more complete than the signal cancellation that a significant signal-to-noise enhancement is achieved. Unfortunately, even small deviations of the filters from optimum will undo much of the noise cancellation and will result in a beamforming performance which may not be materially superior to delay-and-sum beamforming. Thus, even assuming that accurate noise and signal coherence measurements have been used for the design of the optimum filters, the performance of the optimum processing can markedly deteriorate in time as a consequence of small changes in seismometer performance or slight changes in the noise field.

The potential gains which would be achieved by the implementation of filter-and-sum beamforming in the online system are rather limited, because it is not practical to continuously adapt the filter coefficients to the changing noise environment. Weighted-delay-and-sum beamforming has been implemented in the Event Processor systems, as described in Section 8.3.1.5. The experience which has been attained from the LASA EP system results has shown that the typical increase in gain which would result from the use of weighted delay-and-sum beams rather than simple delay-and-sum beams in the LASA DP system would be approximately 1 dB, which is not sufficient to justify the increased processing load and the corresponding reduction in the number of beams which can be formed.

Recent NORSAR studies, discussed in Section 3.4.1.2, have shown that the variations in signal strength from subarray to subarray are quite large (frequently greater than 10 dB) and generally repeatable as a function of U-space location. Therefore, although the current NORSAR DP system utilizes simple delay-and-sum beamforming, the relative advantages and disadvantages of weighted-delay-and-sum beamforming for NORSAR online processing merit further consideration.

5.1.2.2 Direct Beamforming vs Two-Stage Beamforming

Once the linear beamforming method is chosen, then the relative advantages of direct array beamforming and two-stage array beamforming may be examined. In direct beamforming, the seismometer signals are delayed and summed to form array beams directly. On the other hand, in two-stage beamforming the seismometer signals from a subarray are delayed and summed first to form an intermediate output of subarray beams; these beams from each subarray are subsequently delayed and summed to form array beams.

In the direct process, the array beam has lower beam signal loss because there is no subarray beam signal loss involved as in the two-stage process. However, there are certain desirable properties of two-stage beamforming as described below:

- a. Arithmetic Operations--In direct beamforming, the total number of arithmetic operations involved is the product of the total of number seismometers used in the beamforming operations and the total number of array beams. In the two-stage process, the total number of arithmetic operations involved is the sum of:

1. The number of seismometers used per subarray multiplied by both the number of subarrays and the number of subarray beams per subarray
2. The number of subarrays multiplied by the number of array beams.

The total number of operations required by two-stage beamforming is substantially lower than for direct beamforming. Consider the current LASA and NORSAR beam deployments, for example:

	<u>LASA</u>	<u>NORSAR</u>
Number of seismometers per subarray	16 (except 7 for E3)	6
Number of subarrays	17	22
Number of subarray beams per subarray	5	13
Number of array beams	300	331
Total processing requirements (additions) for direct beamforming	78900	43692
Total processing requirements (additions) for two-stage beamforming	6465	8998

Therefore, the two-stage processing requirement is only about one-twelfth at LASA and one-fifth at NORSAR of the corresponding direct processing requirement.

- b. **Data Values**—In direct beamforming, the digitized data values of all seismometers for the duration of the longest delays must be stored. However, in two-stage beamforming, only the data values of all the subarray beams for the same duration must be stored in addition to all the seismometer data values of the very short delays which are used for subarray beamforming. In some cases, the total number of subarray beams is less than the number of seismometers in the DP, so that two-stage processing requires less core storage. For example, in the case of LASA, the total number of seismometers is 263 and the total number of subarray beams is 85. However, this is a disadvantage at NORSAR.
- c. **Filtering**—Since beamforming and filtering are linear processes, the processing results are independent of the order of these two processes. In direct beamforming either the seismometer data or the array beam data can be filtered. In two-stage beamforming, in addition to the two possible filtering choices above, subarray beam data can also be filtered. Therefore, the number of filters required in two-stage beamforming is the smallest of the three. For example, at LASA, filtering at the seismometer level requires 263 filters; at the subarray beam level, 105; and at the array beam level, 300. Filtering at the subarray beam level requires the least number of filters and represents a considerable amount of saving in processing time and core storage. Again, this is not an advantage at NORSAR.

It should be noted at this juncture that the average signal loss in the two-stage process can be reduced if the subarray beams are dispersed radially in the teleseismic regions of U-space as shown in Section 5.2.

5.1.2.3 Microprogramming

For online processing, in order to achieve maximum speed advantage in the System/360 Model 40 computer, certain algorithms are implemented using the technique of microprogramming. The microprograms are stored in the form of read-only-storage in the computer to sequence the execution of hardwired instructions within the machine. In addition, there is a Sum of Products hardware unit which contains an 8x8 multiplier and adder matrix, several registers, partial result adders, and miscellaneous control logic. The purpose of this hardware is to realize a large performance improvement in the execution of filtering operations. The following signal processing algorithms are implemented using the technique of microprogramming: convolution filter, recursive filter, beam-form, and rectify and integrate.

In the Interim Integrated Signal Processing System, all the online signal processing in the SAAC DP was executed in the System/360 Model 40. A summary of the performance of these microprogrammed algorithms is shown in Table 5-1, in which the following items are compared for each process:

- a. The execution time of an efficient assembler language program
- b. The actual microprogram execution time.

For the Interim Integrated Signal Processing System, the use of the microprograms resulted in an estimated overall DP speed-up ratio of about 7 to 1.

In the Integrated Seismic Research Signal Processing System version for both the SAAC and NDPC DPs, all of the subarray beamforming and filtering operations are performed in the Special Processing System (SPS) in which all operations are microprogrammed. Array beamforming, and rectify and integrate algorithms are used for detection processing in the System/360

Table 5-1. Microprogrammed Algorithm Performance

Process	Assembler Language Program (msec)	Microprograms Actual (msec)	Speed-Up Ratio	Comments
Beamforming	4.5	0.69	6.5	One beam formed from 25 inputs.
Recursive filter	30.2	3.40	8.9	25 values were filtered with a filter of degree 6.
Convolution filter	16.2	1.90	8.5	Same as recursive filter.
Rectify/integrate	0.7	0.20	3.5	Five values are added to form the short time average. Every sample period 10 per- cent of the input beams experience the start or end of an arrival. An exponential is used for long-term averag- ing. The time shown is for one beam.

Model 40. The overall Model 40 processing speed-up ratio which is obtained by the use of special microcodes in the ISRSPS DP has been shown to be about 3.7 to 1 at NDPC by direct measurement (see [5-23, Appendix II]).

Furthermore, for efficient utilization of the internal data storage space in the DP machines, a fixed point half-word format is used for each data sample. Arithmetic operations are done in fixed full-word, and results are reduced to half-word length. Therefore, computation precision is preserved through the various signal processing stages.

5.1.2.4 Rectification vs Squaring

For detection processing purposes, the beam envelopes may be computed either by rectifying and summing the sample beam values:

$$R(t) = (2N+1)^{-1} \sum_{n=-N}^N |B(t+n\Delta t)|, \quad (5-2)$$

or by squaring and summing:

$$P(t) = (2N+1)^{-1} \sum_{n=-N}^N B^2(t+n\Delta t). \quad (5-3)$$

Obviously, the rectification requires less processing time, but there is generally a loss in output signal-to-noise ratio which is incurred by rectifying instead of squaring (note that squaring and summing is the optimum envelope computation for Gaussian signal and noise).

If the output signal-to-noise ratio for $R(t)$ is defined as the expected peak value of $R(t)$ when signal and noise are both present minus the expected value of $R(t)$ when noise alone is present, divided by the standard

deviation of $R(t)$ when noise alone is present, and similarly for $P(t)$, then the relative loss is found by dividing the signal-to-noise ratio of $P(t)$ by that of $R(t)$. If the signal and noise are both assumed to be Gaussian stationary processes (though unrealistic for these signals), then the resulting quotient Q is given by

$$Q = \frac{1 + \sqrt{1+(S/N)}}{2} A,$$

where S is total signal power, N is total noise power, and the parameter A depends on the correlation function of the Gaussian noise process.

It is shown in [5-1, Appendix E] that $1 \leq A \leq 1.07$, regardless of the shape of the noise spectrum. Therefore, the loss in performance may be approximated by the expression

$$\text{Loss} = 10 \log_{10} \left[\frac{1 + \sqrt{1+(S/N)}}{2} \cdot 1.035 \right] \text{ dB}, \quad (5-4)$$

where the error due to equating A to 1.035 is less than 0.2 dB. A graph of loss versus the signal-to-noise ratio (S/N) is given in Figure 5-1. On the basis of this result, the use of a rectification formula similar to (5-2) appears to be justified for envelope computation in order to attain a significant reduction in processing time.

5.1.2.5 Alternate Detection Techniques

There are several alternate detection processing techniques which are feasible and practical for seismic array processing, and each of these needs to be considered for a particular application in terms of its unique detectability, U-space coverage and resolution, and processing load and storage requirements. The techniques which are discussed below

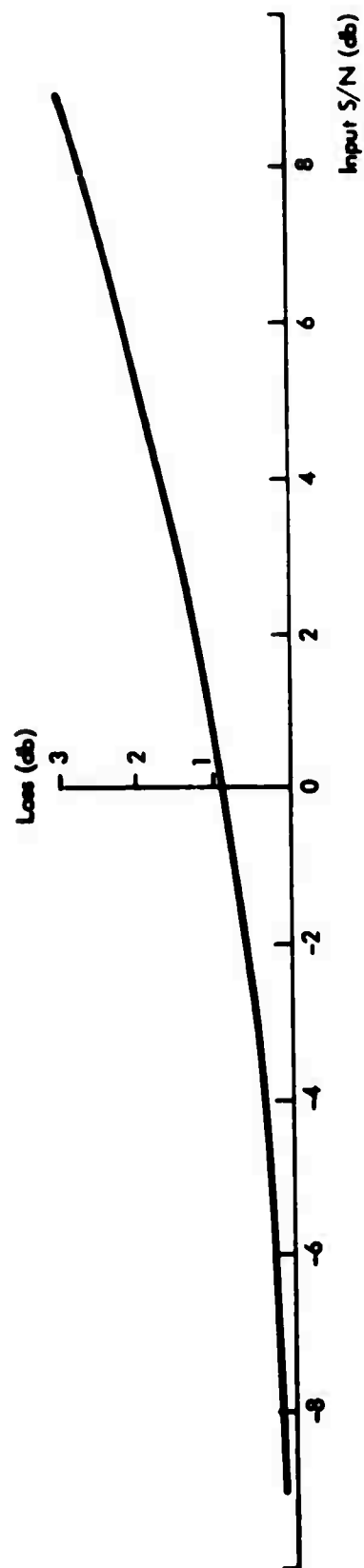


Figure 5-1. Rectified vs Power Envelope

include alternative coherent beamforming methods, the technique referred to as envelope processing or incoherent beamforming, and the method of detecting from subarray beam envelopes and voting on the resulting detections.

For surveillance purposes, each deployed beam is expected to provide signal detections for some region of U-space which includes the aiming point of the beam. For a circularly symmetric array, the beam loss contours for small losses in relative detectability (e.g., less than 2 dB) are approximately circles centered at the nominal U-space aiming point. For a fixed value of relative loss, the radius of the loss contour is inversely proportional to the signal frequency (e.g., the dominant frequency) and to the array aperture radius (e.g., the radius of gyration of the array geometry configuration). Furthermore, array beamforming gain in dB is proportional to the logarithm of the number of sensors used in the beamforming operation. Therefore, by excluding subarrays in the outer rings of the array, the U-space coverage of each beam is increased at the cost of a reduced array gain and a coarser U-space resolution. In addition, if the overall array diameter is reduced by the exclusion of outer ring subarrays, then the maximum transit time of a signal across the array will be reduced proportionally, yielding a reduction in the core storage size requirement for the array beamforming input buffers. This enables increasing the number of array beams to provide better coverage, in a fixed storage size. The above trade-offs have been used effectively for LASA detection processing, for which 9-subarray, 17-subarray and 21-subarray beam deployments have been designed for various purposes and applications (see Section 5.2).

Incoherent beamforming, or envelope processing, may be described as the detection process which results when the order of the array beamforming computation (equation (5-1)) and the envelope computation (equation (5-2)) are interchanged in a coherent processing configuration. That is, subarray beam envelopes are computed and used as input to the array beamforming

operation. No additional envelope computation is required at the array beam level, since the sum of properly aligned subarray beam envelopes is already a satisfactory envelope for detection analysis. The envelope computation is designed to effectively average out the dominant frequency of the signal waveform; typically, the dominant frequency of the envelope is less than that of the filtered signal by a factor of from four to eight. Hence, there is a corresponding increase in the radius of each beam loss contour, so that each beam provides greater U-space coverage with coarser resolution for the same relative loss. There is also a loss in absolute detection sensitivity relative to coherent beamforming for reasonably coherent signals, due to the fact that incoherent beamforming does not fully exploit the potential incoherent noise reduction. The results of an empirical study of various detection techniques are presented in Section 5.6; these results show the relative detectability (defined as envelope signal-to-noise ratio) for the techniques and pre-detection filters included in the study.

If the detection criteria (e.g., thresholding, the required number of samples which must exceed the threshold, etc.) are applied to the subarray beam envelopes, then a voting scheme may be used to identify event signal detections among the subarray beam detection results. Voting groups are defined as sets of subarray beams from different subarrays which are aimed at approximately the same U-space location. The voting group having the greatest number of subarray beam detections within a specified time interval is selected and, if the number of subarray beam detections exceeds a preset minimum, an event signal detection is declared. The radius of a subarray beam loss contour is considerably larger than that of an array beam, because this radius is inversely proportional to the aperture radius of the corresponding subarray or array geometry configuration. There is also a loss in detectability of subarray beam voting relative to coherent array beamforming for the same set of subarrays. For the three-out-of-eight voting scheme presently used in the NORSAR DP system, it has been estimated that this loss is approximately two to four dB if perfect signal coherence is assumed.

5.1.3 Detection Processor Functional Configurations

Once the problem of direct vs. two-stage beamforming was resolved, and the ordering of the signal processing operations was determined, then the Detection Processor system configurations for LASA and NORSAR were completed as shown in Figures 5-2 and 5-3, respectively. The differences in the design and implementation between the two systems are due primarily to the differences in array geometry and in the signal and noise characteristics observed at each array. There are two surveillance partitions in each DP: one partition is designed to have selected beam coverage primarily in the teleseismic regions; the other partition is designed to have general and uniform beam coverage in the teleseismic regions plus core phase regions.

5.1.3.1 LASA DP

At LASA, the system configuration for both partitions is the same. In the general surveillance partition, only the nine innermost subarrays are employed for beamforming. Therefore, the beam coverage is considerably broader, but detection capability is less than that of the selected surveillance partition which employs either 17 or 21 subarrays, depending on the choice of surveillance beam set. (See Section 5.2 for a detailed discussion of surveillance).

5.1.3.2 NORSAR DP

At NORSAR, the selected surveillance is similar to that at LASA; the general surveillance is performed by thresholding and voting on sets of subarray beams. This approach to general surveillance represents an effort to circumvent the problem of signal incoherence across subarrays and the fact that the dominant signal frequencies observed at NORSAR are

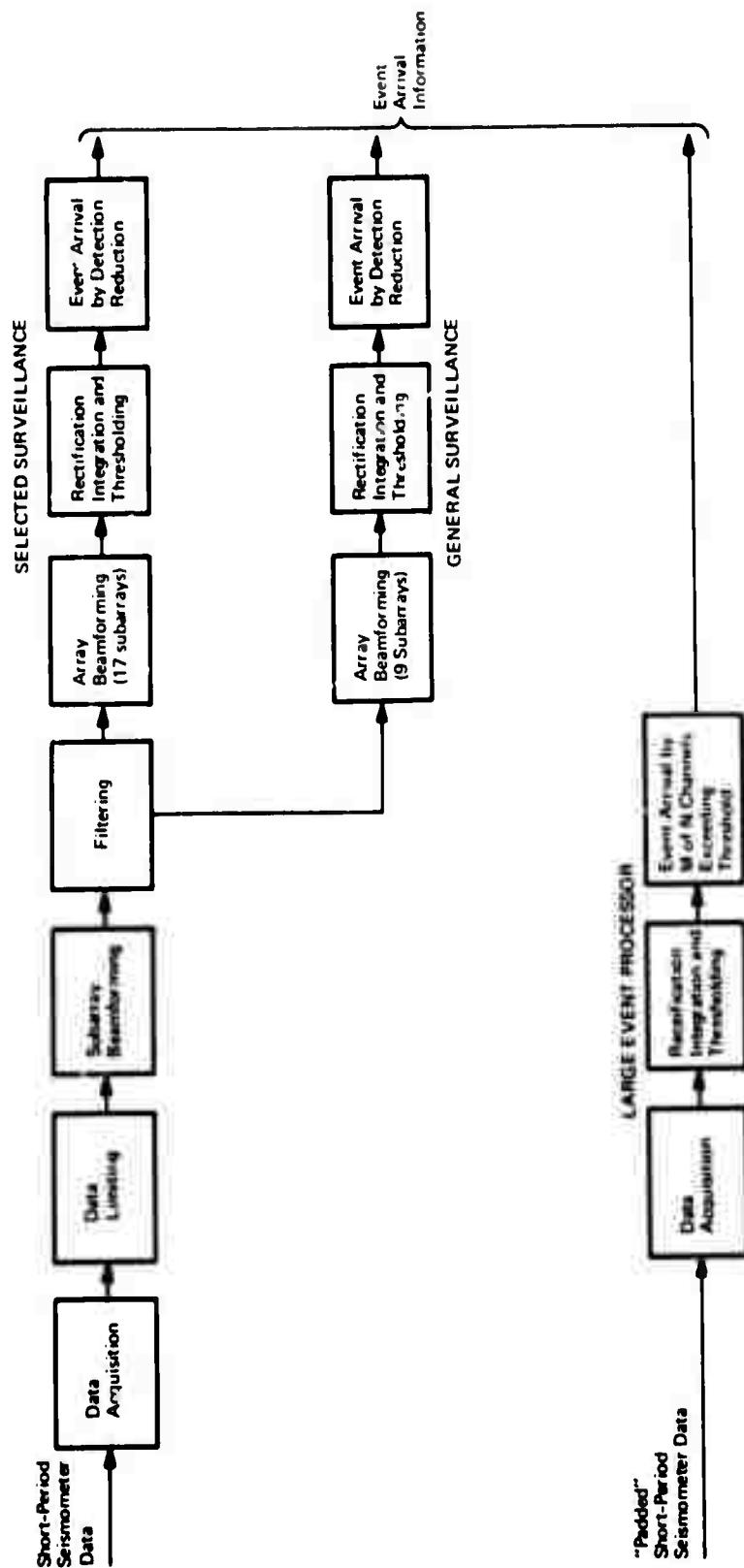


Figure 5-2. LASA Detection Processor Configuration

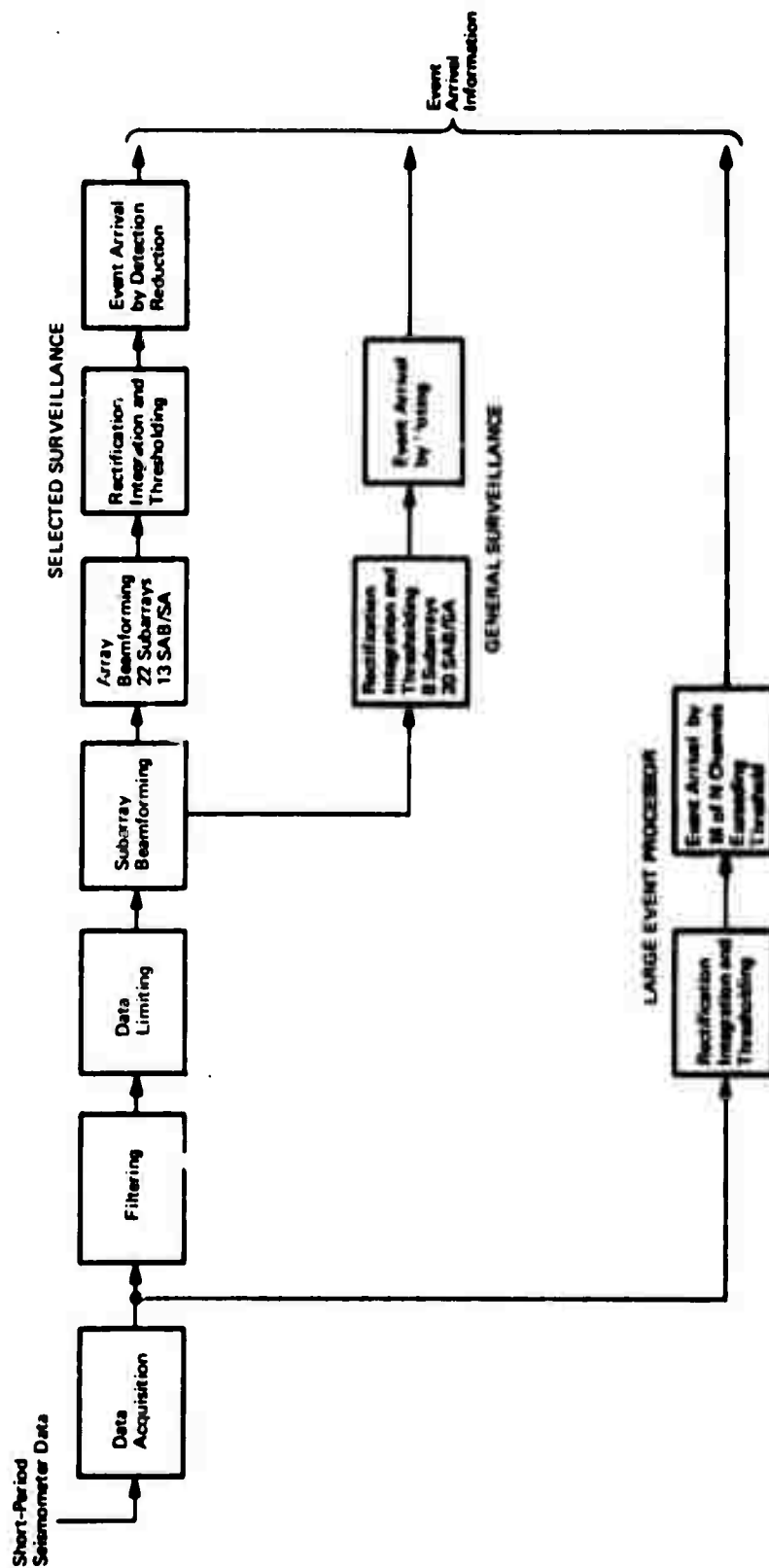


Figure 5-3. NORSAR Detection Processor Configuration

higher than those at LASA. To reduce the false alarm rate, multiple detections on subarrays within a time window are required for declaring an event arrival. This is done by counting the number of subarray beam envelopes aimed at a certain direction in the surveillance region that exceed the detection threshold within the specified time window. Event arrival is declared if the number exceeds a preset limit. For time-concurrent event arrivals, the direction with the largest average maximum subarray beam short term average is selected as the event arrival location (the average is taken over all subarray beams in the detection state for each direction).

5.1.3.3 Large Event Processing

In addition, there is a Large Event Processor in each DP for the prompt reporting and analysis of large event arrivals. The primary purpose of this special processing capability is to provide early warning for possible tsunamis and quick response to earthquake disasters. Inputs to the Large Event Processor at LASA are the data from the specially "padded" short-period seismometers which have 30 dB attenuation relative to the regular short-period sensors. There are 20 "padded" seismometers at LASA, located one at each subarray except subarray E3. Inputs to the Large Event Processor at NORSAR are the unclipped and unfiltered data from the center seismometer of each of the 22 subarrays.

Rectification, integration and thresholding are performed on the input data in the Large Event Processor. A large event arrival is declared if at least M out of N channels exceed the detection threshold within a T-second interval where M, N, T and the detection threshold are preset parameters. The detection window T is chosen so that it is sufficient to account for the transmit time of a near-regional event across the array. At the time that a large event arrival is detected at SAAC according to this algorithm, the detection times and associated STA

values of each detecting channel are passed to the Event Processor via the channel-to-channel communication for completion of the large event analysis and reporting. At NDPC, the average maximum signal amplitude (STA), the arrival time at the detecting seismometer closest to the center of the array, and an estimate of the U-space location of the event are computed in DP and reported via the console typewriter.

5.2 BEAM DEPLOYMENT

Selection of beam deployment parameters for detection processing requires trading off various system objectives while meeting certain system constraints. The objectives and constraints include: adequate subarray and array beam coverage of the teleseismic zone; maximization of aperture over all deployment azimuths; system operation at specified machine load level; maximization of array processing gain; and operation with a specified number of seismometers per subarray. Subject to these constraints, the selections of the following two parameters--the number of array beams formed, and the number of beams per subarray--are discussed. Generation of time-delay values for subarray and array beamforming, and processing load and core storage considerations for beam number selection are also discussed.

5.2.1 Subarray Beam Requirements

In order to provide uniform subarray and array beam coverage of the teleseismic zone, all of the subarray beams in a given region of U-space should not be aimed at a single subarray beam aiming point. Instead, the subarray beam centers should be aimed in a dispersed pattern about each nominal aiming point to minimize the worst case beam loss and to equalize steering loss among the beams. A set of subarray beam aiming points distributed uniformly over the desired regions of U-space constitutes a reference set, with respect to which operational sets of dispersed beams can be generated.

Dispersed beam deployment is accomplished by distributing the geometric orientation of each subarray beam set. Azimuthal phasing must be assigned to each subarray in a manner void of trends, to ensure homogeneous array beam characteristics.

5.2.1.1 Methods of Beam Dispersion

One dispersed set of subarray beams that has been considered is found by first constructing in U-space K circular subarray beam loss contours with centers uniformly distributed in azimuth at a common radius. The circular loss contours are overlapped so that the common chord of adjacent pairs forms a radial line between the teleseismic zone boundaries. These K centers are the aiming points for one subarray. The subarray beam aiming points for each successive subarray are obtained by rotating the preceding K points through $360^\circ/KJ$, where J is the number of subarrays. K is selected to be large enough to avoid excessive subarray beam loss at the contour radius which satisfies the above constraints.

The relaxation of the requirement that the common chord of adjacent circles equals the radial width of the teleseismic annulus leads to another dispersion method in which the contours have smaller radius (hence smaller loss) and are centered on a smaller common radius while complete coverage of the teleseismic zone is maintained.

Another dispersion method which has been considered is based on partitioning the teleseismic zone (that is, the annulus whose radii are $U_a = 0.04$ sec/km and $U_b = 0.08$ sec/km) into the two complementary annuli whose radii are, respectively, $U_a = 0.04$ sec/km, $U_b = 0.06$ sec/km and $U_a = 0.06$ sec/km, $U_b = 0.08$ sec/km. Subarray beams are dispersed separately to cover these two annuli.

In another method, the model for beam dispersion is based on minimizing that part of the LASA beam loss due to subarray beamforming.

Refer to [5-3, Appendix A.6] and [5-9, Appendix VII.3] for a detailed discussion of the methods.

5.2.1.2 Subarray Beam Steering Loss

The incremental gain per beam as a function of the incremental change in subarray beam radius may be computed starting with the approximate formula [5-1, Section 2]

$$\text{Gain} = -\text{Loss} = -A_{SA}(fr)^2 \text{ in dB}$$

where

$$A_{SA} = \text{constant dependent on subarray geometry} \\ = 20 \log_{10} e (\pi R_{SA})^2, \text{ where } R_{SA} \text{ is the} \\ \text{subarray radius of gyration in km}$$

$$f = \text{dominant frequency of a signal}$$

$$r = \text{subarray beam radius in sec/km.}$$

Differentiation of gain with respect to radius and replacement of derivatives by differentials results in the formula for incremental gain

$$\Delta G = -2A_{SA}f^2 \cdot r \cdot \Delta r$$

For any of the previously described dispersion methods, r may be reduced by increasing the number of subarray beams per subarray (K). The relationship between r and K is a function of the method.

5.2.1.3 Generation of Time Delays

The seismometer delays used in the subarray beamforming process are generated by the following formula:

$$t_{ijk} = U_{x_{kj}} X_{ij} + U_{y_{kj}} Y_{ij}$$

where

$$i = 1, \dots, I$$

$$j = 1, \dots, J$$

$$k = 1, \dots, K$$

t_{ijk} = time delays in seconds of the i th seismometer in j th subarray for the k th subarray beam

$U_{x_{kj}}, U_{y_{kj}}$ = k th subarray beam aiming point components in sec/km in U -space of j th subarray

X_{ij}, Y_{ij} = coordinate components in km of the i th seismometer of the j th subarray relative to the center instrument

- I = number of seismometers in a subarray
- J = number of subarrays in an array
- K = number of subarray beams in a subarray.

5.2.2 Array Beam Requirements

This subsection analyzes array beam requirements in terms of beam diameter, signal loss, number of subarrays, and areas of coverage. The number of beams required to cover several designated areas can be expressed as a function of the maximum loss component due to deployment quantization.

5.2.2.1 Beam Coverage vs Steering Loss

A formulation of the surveillance beam requirements is desired which readily portrays the loss encountered as the effective aperture is modified by deleting outer subarray rings.

The following list defines the nomenclature employed during this investigation.

- D = beam diameter (in sec/km)
- f = center signal frequency (in Hz)
- SA = number of subarrays used in forming the array beams
- H_{SA} = SA ensemble dependent aperture constant
- L = loss (in dB)
- A_b = beam area
- N_k = number of beams required to cover the k^{th} area
- T_k = k^{th} area of coverage. Three areas of coverage are considered. Thus let

- T_1 = coverage of land within teleseismic zone
- T_2 = coverage of land plus seismic areas not on land within teleseismic zone
- T_3 = coverage of the entire teleseismic zone.

Dense hexagonal beam packing is assumed, and thus the beam area is equivalent to that of a regular hexagon inscribed in a circle of diameter D . From elementary plane geometry it follows that $A_b = 0.65D^2$. If the area to be covered is sufficiently large so that edge effects may be neglected, the number of beams required to cover a specified area T_k is given by the formula

$$N_k = \frac{T_k}{0.65D^2}.$$

For the main lobe, the following quadratic approximation for U-space beam diameters is adequate:

$$D = \frac{H_{SA} \sqrt{L}}{f}$$

From the two equations above it follows that

$$N_k = \frac{f^2 T_k}{(0.65) (H_{SA}^2) (L)}.$$

5.2.2.2 Surveillance Requirements

Combining the above equation with the term $10 \log_{10}$ (total number of sub-arrays/SA) which reflects the fact that maximum performance is degraded whenever fewer than all subarrays are utilized, yields

$$L = \frac{f^2 T_k}{(0.65) (H_{SA}^2) (N_k)} + 10 \log_{10} (\text{total number of subarrays/SA) in dB}$$

Figures 5-4 and 5-5 show the array beam loss at LASA evaluated at 1.5 Hz when providing surveillance coverage of land plus seismic, and teleseismic areas with system configurations utilizing 13, 17, and 21 subarrays. Similarly, Figures 5-6 and 5-7 show the array beam loss at NORSAR evaluated at 1.5, 2.0 and 3.0 Hz when providing surveillance coverage of land plus seismic, and teleseismic areas with system configurations utilizing 7, 16, and 22 subarrays. It is apparent that the proper subarray utilization for surveillance processing is dependent upon the deployed beam density. The number of array beams deployed in the DP is substantially less than the total number of array beams required for total uniform coverage in the teleseismic areas of U-space. Thus, the processing load is correspondingly reduced. An extensive data base study portraying the relative seismicity of various regions on the earth has been conducted. See [5-20, Appendix I] for results of this study. Beams are deployed based on the relative seismicity of regions.

5.2.2.3 Generation of Delays

The delays used in the array beamforming process are generated by the following formula:

$$t_{jk} = U_{x_k} X_j + U_{y_k} Y_j + \text{relative time anomalies}$$

$$j = 1, \dots, J$$

$$k = 1, \dots, K$$

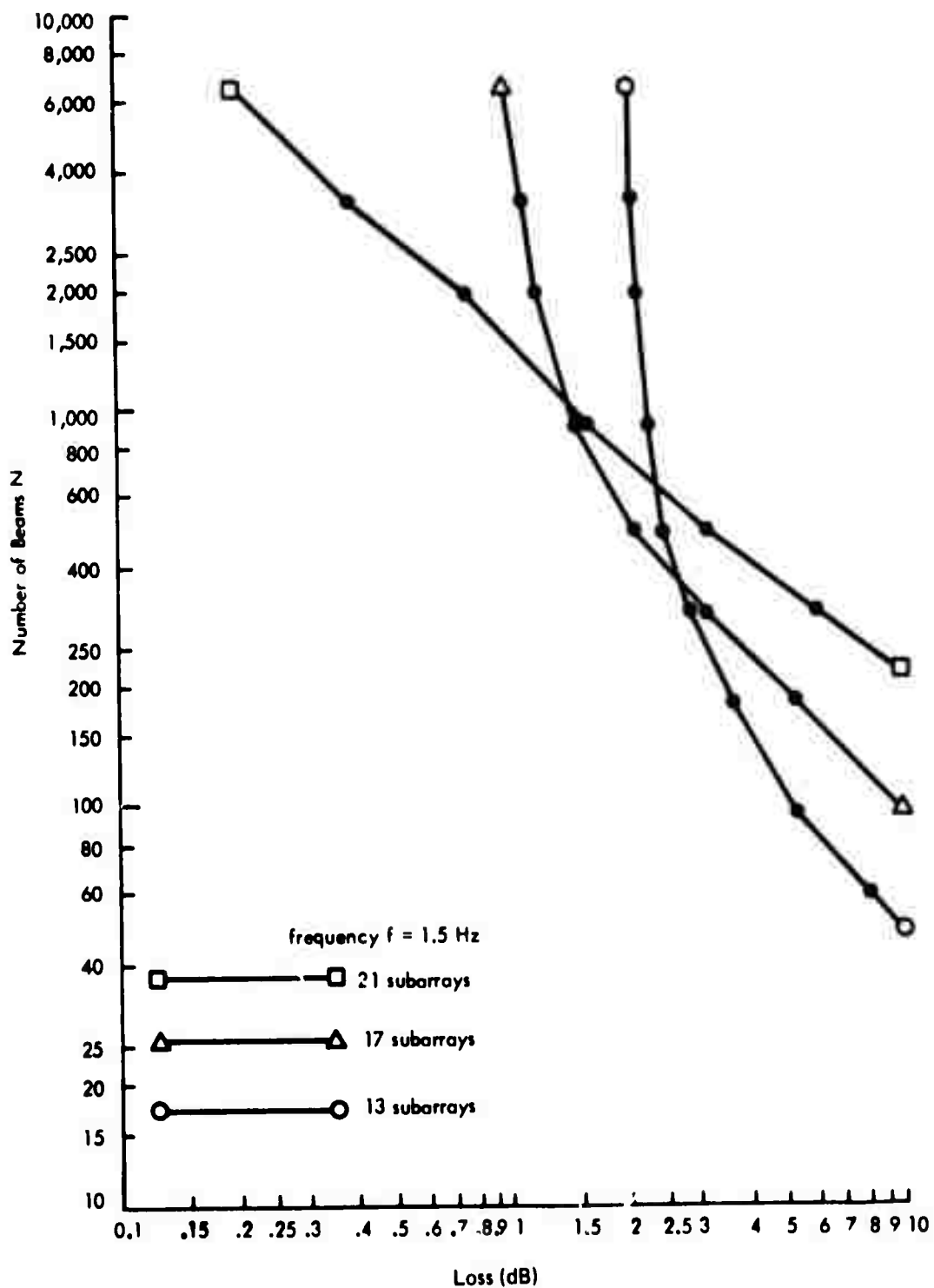


Figure 5-4. Number of Beams Required for Land and Seismic Area Coverage with LASA

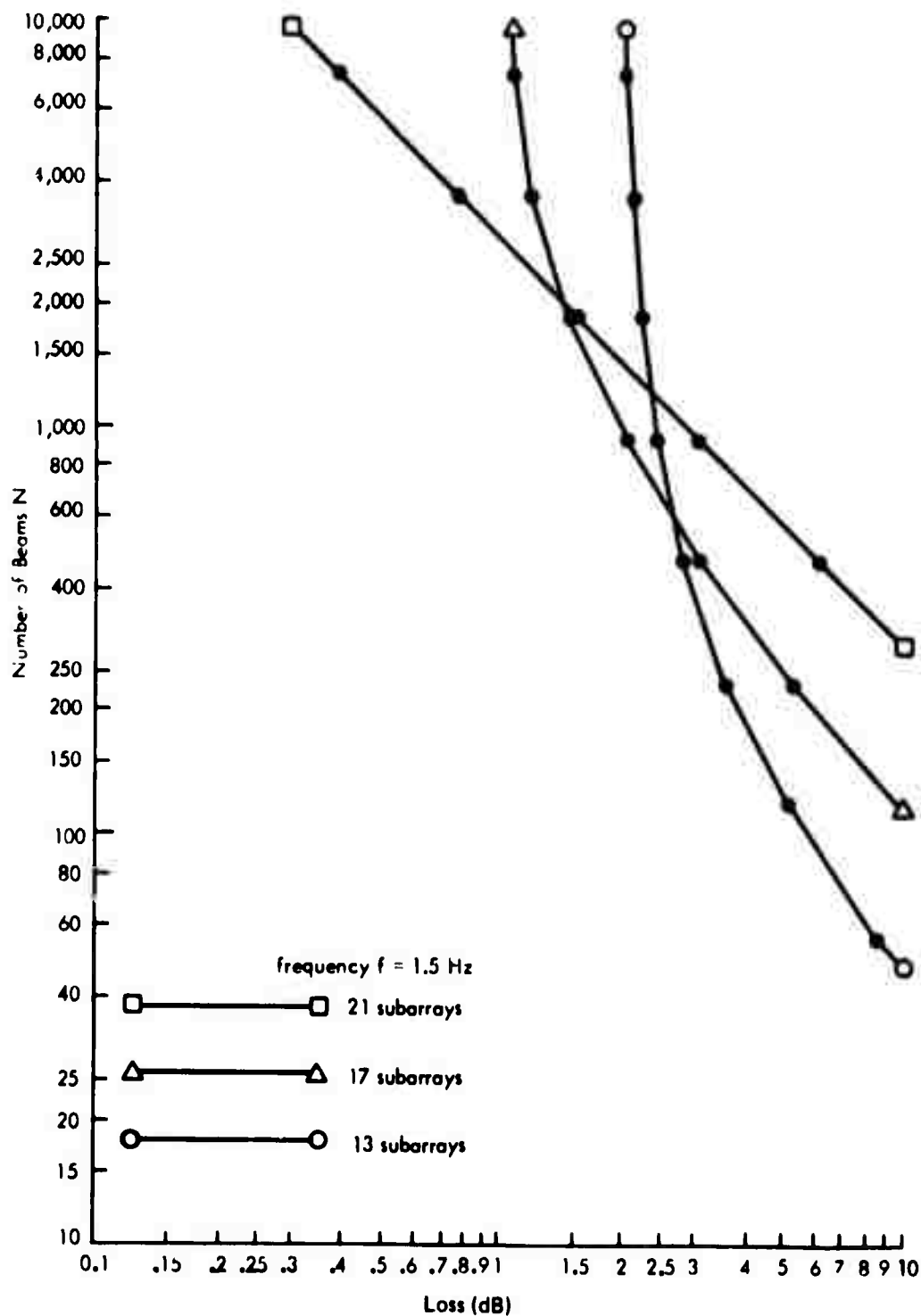


Figure 5-5. Number of Beams Required for Teleseismic Zone Coverage with LASA

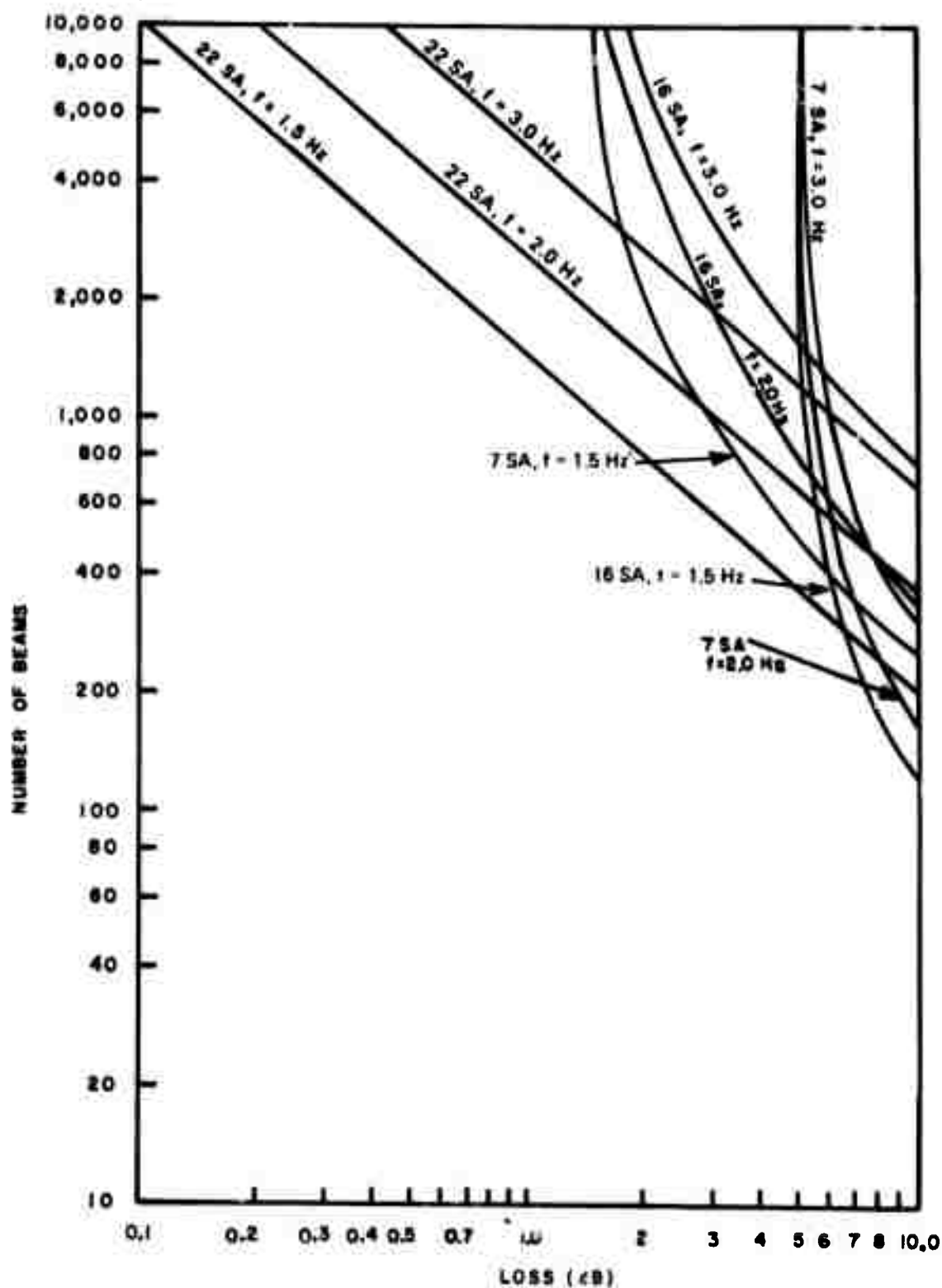


Figure 5-6. Number of Beams Required for Land and Seismic Zone Coverage with NORSAR

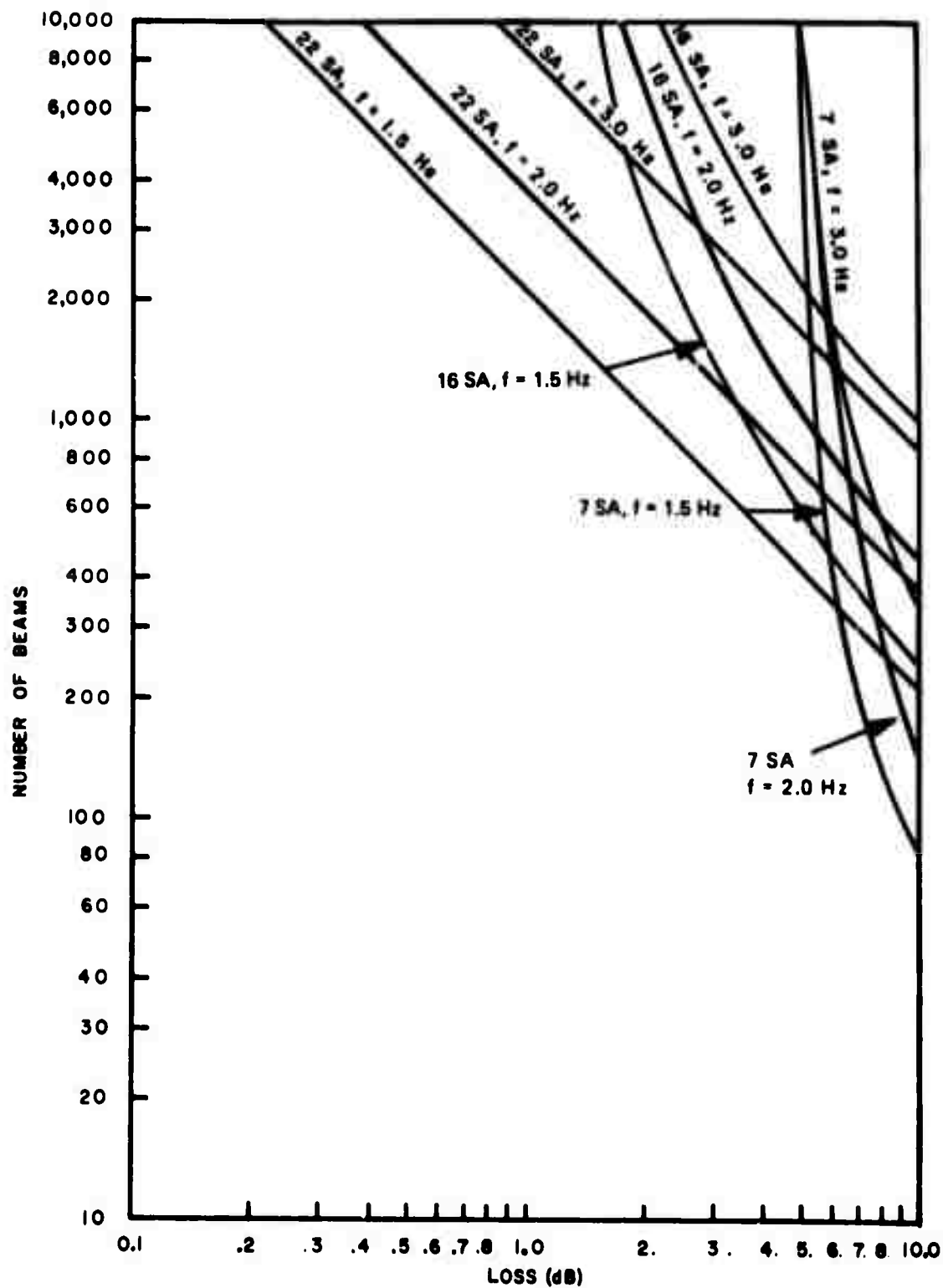


Figure 5-7. Number of Beams Required for Teleseismic Zone Coverage with NORSAR

where

t_{jk} = time delays in seconds of the j th subarray for the k th array beam

U_{x_k}, U_{y_k} = k th array beam aiming point components in sec/km in U-space

X_j, Y_j = coordinate components in km of the j th subarray relative to the center subarray

J = number of subarrays in an array

K = number of array beams deployed in the DP.

Relative time anomalies are steering correction factors added to the delays computed from plane wave fitting. See Section 7 for a detailed discussion of time anomalies.

5.2.3 Processing Load and Core Storage Considerations

The subarray beam deployment schemes, the subarray beam loss calculation, and the number of array beams required as a function of signal loss and coverage have been discussed in the previous sections. The overall beam coverage and beam loss budget are then selected based on consideration of the processing load and the available core storage. In other words, given certain desirable subarray and array beam loss levels, and certain desirable coverage, the number of subarray and array beams is determined by the methods and formulae in the previous sections; this number in turn determines the processing load and core storage requirements. If the

load is excessive or the core storage insufficient, then the beam loss budget and beam coverage have to be revised in order to stay within the constraints imposed by the available capacities. Either the number of subarray beams or the number of array beams, or the maximum time delay which controls the length of the buffer storage has to be reduced.

In the Integrated Seismic Research Signal Processing System version of the DP, data acquisition, subarray beamforming, and filtering are done by the Special Processing System (SPS). Signal processing following the formation of filtered subarray beams (i.e., array beamforming, rectification, integration, thresholding and detection reduction) is done by the System/360 Model 40H computer. This system structure is pertinent to the following discussion on the processing load and core storage at NDPC.

Some of the NDPC DP system design parameters selected are listed below.

<u>Special Processing System</u>	<u>Actual</u>	<u>Program Maximum Allowed</u>
Number of seismometers/subarray	6	6
Number of subarrays	22	22
Number of subarray beams/subarray (for 8 subarrays with 2 sets of filter coefficients)	20	30
Number of subarray beams/subarray (for 14 subarrays with 1 set of filter coefficients)	13	30
<u>System/360-40</u>		
Number of array beams	331	450

The core storage allocation in the SPS is as follows.

<u>Buffer Region</u>	<u>Number of Channels</u>	<u>Time Length Stored</u>	<u>Core Storage in (16-bit words)</u>
Filter input	132	1.0 sec	1320
Filter A output	132	0.9 sec	1197
Filter B output	48	0.9 sec	504
Subarray beam input	211	4.0 sec	8440
Subarray beam output	1074*	0.5	16384**
Beamforming delays			<u>6300</u>
			34145

*The maximum number of subarray beams per subarray allowed in the SPS is more than required in the current configuration. Therefore, core storage space in the SPS is adequate even if the requirement is increased.

**This number accounts for two SPS buffers, each with space for 0.5 seconds of data for 1074 subarray beam channels.

The SPS loading, by actual measurements, (see [5-23, Appendix II]) is 53.5 percent to 55.5 percent for filtering, 9.2 percent for subarray beamforming, while about 20 percent is idle time whenever the SPS is not performing any array monitoring and control tasks. This indicates that there is some reserve machine loading available in the SPS. Therefore based on these SPS loading measurements, a moderate increase in beamforming and filtering requirements is probably manageable within the SPS.

By contrast, the Model 40 is almost fully occupied with its processing tasks in the current configuration. The typical loading, by actual measurement, is approximately 85 percent for computation (consisting of 43.3 percent for beamforming, 13.2 percent for rectification and integration, and the remainder for operations other than the special microcodes),

7-9 percent for I/O wait only time, and about 6-8 percent idle time. Figure 5-8 shows the array beamforming microprogram processing load as a function of the number of subarrays and the number of array beams. Figure 5-9 shows the rectification and integration microprogram processing load as a function of the number of beam channels in both surveillance partitions. The current NDPC DP threshold rate is 1.67 times/sec.

A critical factor in the Model 40 core storage is the total size of the subarray storage buffers required for array beamforming. The storage required, in bytes, for subarray beams is a product of the following parameters, with actual NDPC DP values in parentheses at right:

- a. Number of subarrays (22)
- b. Number of subarray beams/subarray (13)
- c. Maximum time delay for array beamforming in seconds (11)
- d. Sampling rate of subarray beams in Hz (10)
- e. Length of each subarray beam sample in bytes (2)

The result for the NDPC DP is 62920 bytes, or about one quarter of the total core storage in the System/360 Model 40H computer.

5.3 SIGNAL PROCESSING ALGORITHMS

As shown in the system configurations in Section 5.1.3, the DP can be partitioned into data acquisition and limiting, beamforming, digital filtering, rectification and integration, thresholding, and detection reduction. Each functional component except detection reduction, which is discussed separately in Section 5.4, is described in detail in this section.

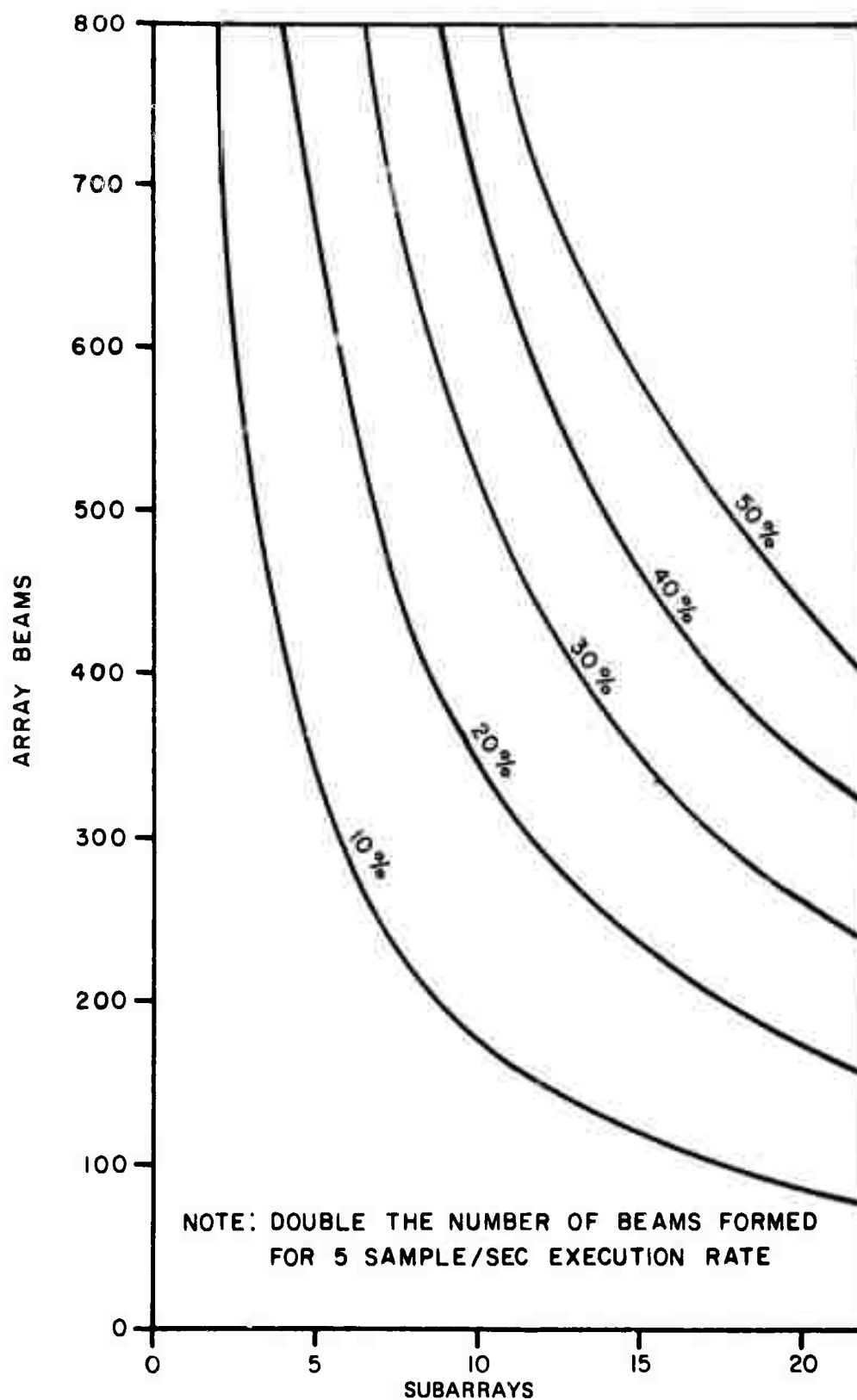


Figure 5-8. System/360 Model 40 Processing Load Using Beamforming Microcode at 10 Samples per Second

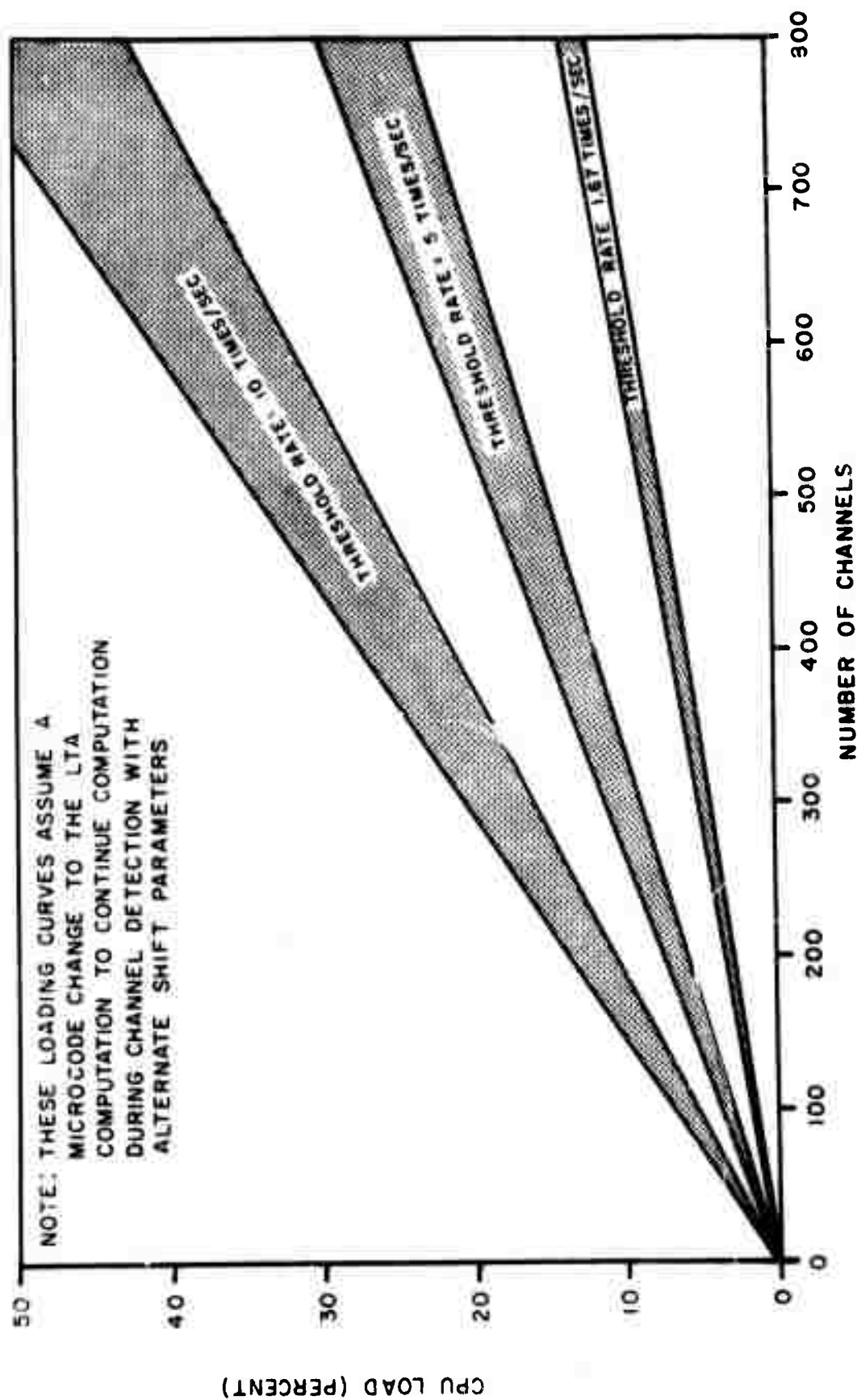


Figure 5-9. System/360 Model 40 Processing Load Rectify-Integrate-Threshold Microcode, Input Data Rate 10 Samples per Second, Integration Interval 1.8 Seconds

5.3.1 Data Limiting

To reduce the number of false detections, the amount of energy in a beam from a single short-period seismometer channel is constrained by limiting the dynamic range of the sensor data. Linear small signal operation is retained to achieve maximum beamforming gain. The spectral characteristics of the seismic noise show that the noise power is concentrated at the lower frequencies of the signal spectrum. Therefore, to prevent loss of small higher frequency signals superimposed upon the low frequency noise, the linear range of the signal must be extended above the expected noise amplitude. As implemented, the absolute data value of a seismometer channel, filtered or unfiltered, is limited by a judiciously chosen threshold. At LASA, the short-period seismometer channels which have a 30 dB attenuation (padded) do not require a limiting threshold.

5.3.2 Beamforming

The delay-and-sum linear beamforming operation has been described above in Section 5.1.2.1, equation (5-1). The linear beamforming process utilizes the time delays t_k as shown in equation (5-1) for all surveillance beams. The calculation of these delays based on a linear wavefront model is discussed in Section 5.2. However, actual wavefronts are, in general, nonplanar, and the differences between actual and planewave delays are referred to as time anomalies. A time anomalies data base is created using Event Processor (EP) results, as described in Section 7. The most recently updated version of this data base is used to compute time anomalies for the DP array beam delays each time the DP beam set is updated. Therefore, the beamforming delays will continue to improve with time as additional seismic data is processed by the system.

The beamforming gain which is achieved by the use of time anomaly data in DP is from 2 to 4 dB in the LASA system, and somewhat greater for

NORSAR. A significant reduction in processing load can be achieved by reducing the computation rate of array beams. If the resolutions of the input data and time delays are maintained at a high sample rate, then computing the output at a lower sample rate is equivalent to resampling a high sample rate array beam. In this way, the loss from the lower sample rate is avoided in the beamforming process. The only possible loss incurred is from undersampling the data used for estimating the signal and noise powers. Experimental results demonstrate that using 5 samples per second of array beam data at LASA results in insignificant loss, but this processing load reduction technique has not been used in the NORSAR system because of the higher signal frequencies which are encountered.

The beamforming gain, the signal loss due to time delay errors, the quantization bias compensation, and subarray masking are discussed separately below.

5.3.2.1 Beamforming Gain

Defining the beamforming gain as the ratio of the average signal power to the average noise power of the beam output divided by the ratio of the average signal power to the average noise power at a seismometer, it can be shown that

$$\text{Gain} = 10 \cdot \log_{10} \left[\frac{1 + (N-1) \rho_s}{1 + (N-1) \rho_n} \right] \quad (5-5)$$

where ρ_s and ρ_n are the average signal and noise correlation coefficients, respectively, and N is the number of seismometers in the array.

If it is assumed that the signal is correlated ($\rho_s = 1$) and the noise is uncorrelated ($\rho_n = 0$), then equation (5-5) reduces to the classical result:

$$G = 10 \cdot \log_{10} N \text{ dB.} \quad (5-6)$$

Analysis of actual noise power reduction with beamforming demonstrates the reasonableness of the assumption ($\rho_n \approx 0$) for the frequency bands of interest. However, experience with LASA indicates that for short intervals (≈ 2 seconds) at initial arrival, average signal correlation coefficients of 0.8 are a reasonable estimate. For larger or later windows, signal complexity is increased by the presence of signal echoes, which reduces the coherence among seismometers. A modified form of equation (5-5) is recommended:

$$\text{Gain} = 10 \cdot \log_{10}(\rho_s \cdot N) \text{ dB.} \quad (5-7)$$

5.3.2.2 Losses Due to Beamforming Delay Errors

The loss in beam signal power from sampling can be estimated by

$$\text{Sampling Loss} = \frac{5 \log_{10} e}{6} (2\pi f \cdot \Delta T)^2 \text{ dB.} \quad (5-8)$$

where f is the signal frequency and ΔT is the interval between samples. This expression assumes a uniform distribution of time delay errors over the sample interval. Figure 5-10 depicts the loss for selected frequencies as a function of sample interval. Other random errors in the time delays defocus the beam and result in a loss which is approximately given by

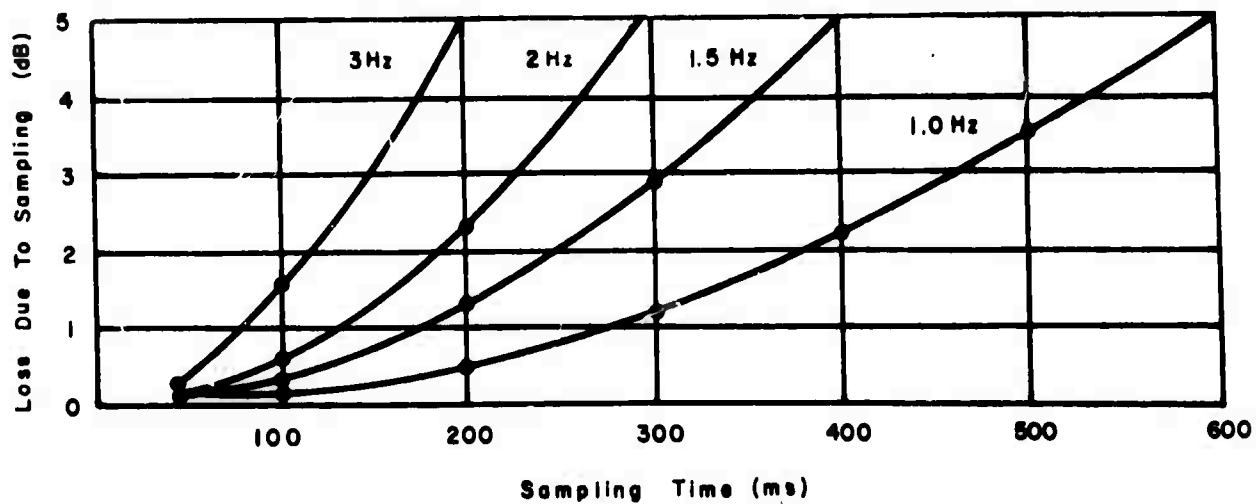


Figure 5-10. Sampling Loss

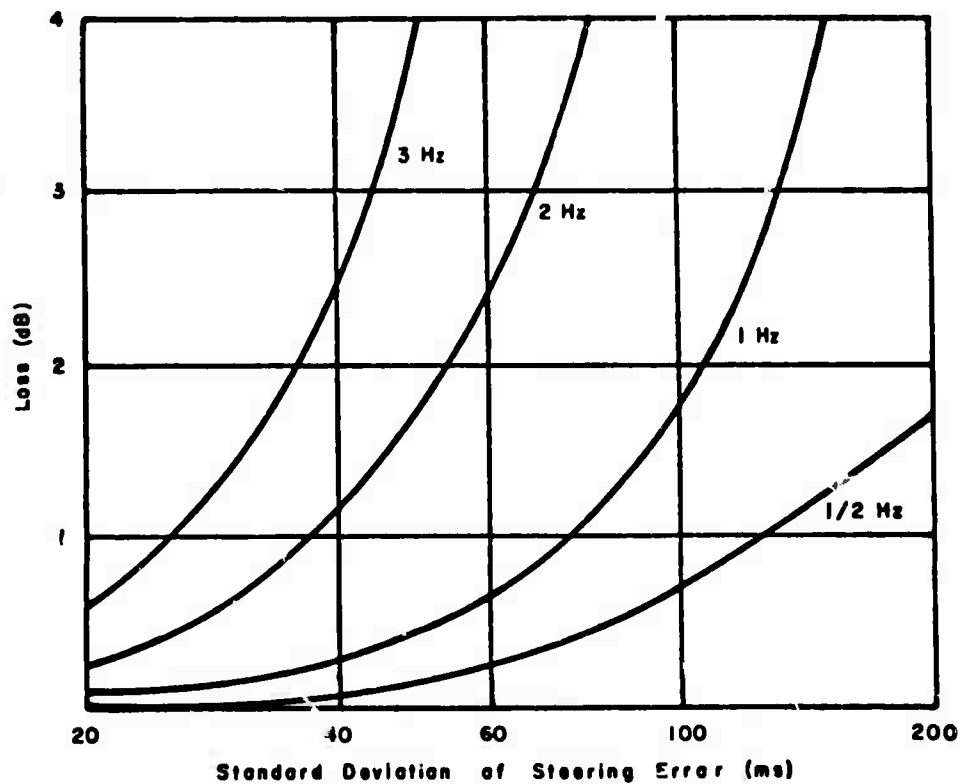


Figure 5-11. Phasing Loss

$$\text{Phase Loss} = (10 \log_{10} e)(2\pi f \sigma_T)^2 \text{ dB} \quad (5-9)$$

where f is the signal frequency in Hz and σ_T is the standard deviation of the steering error in seconds. Equation (5-9) is depicted in Figure 5-11.

5.3.2.3 Data Bias Compensation

Quantization of the seismometer data in 2's complement format introduces an error which is assumed to be a uniformly distributed random variable uncorrelated from sample to sample and having a nonzero bias. This bias has to be removed in order to minimize the post-detection noise. Therefore, a bias compensation constant is added to the subarray beams to null the quantization bias error prior to the rectification and integration operation. In addition, the filtering gain is permanently increased to minimize the residual bias error which exists when only a partial array is in operation.

5.3.2.4 Subarray Masking

A subarray is masked whenever array maintenance and control is being performed on it or when there is a subarray electronics or transmission failure. All beams from a masked subarray are forced to zero before being passed to the System/360. This substitution is applied to the final bias-compensated filtered output.

5.3.3 Digital Filtering

In the development of the DP system filters, there are three factors to be considered; namely, the implementation of the digital filters,

the analysis of the signal and noise spectral characteristics, and the filter bandwidth, center frequency and other response characteristics which achieve a desirable signal-to-noise improvement through filtering.

The recursive form of the digital filter is given as

$$y_n = \sum_{m=0}^M a_m x_{n-m} - \sum_{m=1}^M b_m y_{n-m}$$

where x_n and y_n are the input and output quantities, respectively, at the sampling instant n ; M is the filter degree; a_m and b_m are filter coefficients.

The equation above may be written in the one-sided z -transform notation

$$\frac{Y(z)}{X(z)} = H(z) = \frac{A(z)}{1+B(z)}$$

where

$$A(z) = \sum_{m=0}^M a_m z^{-m}$$

and

$$B(z) = \sum_{m=1}^M b_m z^{-m}.$$

Here $z = \exp(sT)$ where s is the Laplace transform complex frequency variable and T is the sample period in seconds. A convolution filter is a special case in which all b coefficients are set to zero. The filters which are utilized in the ISRSPS system have been synthesized in a continuous nonlinear frequency plane and then transformed to the discrete

process z-plane. Reference is made to [5-4, Section 3.7] where the z-transform treatment of the recursive form of digital filtering, the filter formulation, and the method for specifying the low-pass, high-pass, band-pass, and band-reject filter types are presented.

Experimental results on the spectral characteristics of the signal and the noise are presented in Section 3. The results of recent NORSAR DP filtering studies are discussed in Section 3.5. However, the initial system implementation was guided by the results of earlier studies. See [5-4, Section 3.8] for a discussion of LASA results, and [5-13, Appendix IV] for a discussion of NORSAR results.

The recent results indicate that a modification of the NORSAR filter might improve the DP's detection capability. See Section 3.5 for details.

An additional consideration is that using a higher degree filter improves the noise rejection but also increases the computation burden and core storage relative to a lower degree filter.

The effect of round-off can be most serious for the recursive filtering operation because this operation can enormously amplify the round-off errors generated in the filtering process. For this reason, in each sampling period, all products of numbers for filtering are summed using full double precision word length and only the final result is truncated to single precision. As a consequence, at each sampling instant, only one round-off error is generated by the filtering process.

5.3.4 Rectification and Integration

The array beam data is rectified and then integrated (summed). The proper choice of integration interval for estimating the signal energy is dependent upon signal characteristics.

As described in Section 5.6, the ratio of maximum average signal power to the standard deviation of the noise power is a useful figure of merit. The standard deviation of the noise is reduced as the integration interval T is lengthened, thus permitting a lower detection threshold for the same false alarm rate. If the noise is a stationary Gaussian process with a small correlation time compared with the integration time, the standard deviation of the noise power can be approximated by K/\sqrt{T} , where K is a constant proportional to the correlation function for the noise. However, the peak average signal power is also reduced as T increases. In the detection process, the signal power is estimated by rectification and integration of beam data; the result is defined as the short-term average (STA):

$$STA(n\Delta T) = \frac{1}{P} \sum_{p=0}^{P-1} |B[(n-p)\Delta T]|$$

where $B[n\Delta T]$ is the beam at the time $n\Delta T$ where n is an integer and ΔT is the sample interval, and the product of P times ΔT is the integration interval.

5.3.5 Thresholding

The ratio of the signal estimate (STA) to the noise estimate (LTA) is compared with a threshold. If the ratio exceeds the threshold, a detection is declared and continues until the signal-to-noise ratio drops below a second lower threshold. An additional detection constraint requiring that the threshold be exceeded for Q out of Q' successive comparisons is also imposed.

5.3.5.1 Signal and Noise Estimates

The signal estimate is the short term average (STA) obtained by rectification and integration of the array beam.

The noise estimate, i.e., long term average (LTA), is calculated using the STA as input to a recursive exponential filter where the time constant is controlled by the shift in the feedback path. The LTA formulation is as follows:

$$LTA_n = 2^{-\eta} STA_n + (1-2^{-\sigma}) LTA_{n-1}$$

where LTA_n and STA_n are the STA and LTA at nth LTA sampling time, and LTA_{n-1} is the LTA at the (n-1)th LTA sampling time. Input and feedback shifts are η_1 and σ_1 , respectively, when a beam is not in the detection state. The LTA computation continues while a beam is in the detection state but a new filter time constant is used. This procedure requires changing both the input and feedback shifts to η_2 and σ_2 , respectively, in order to keep the filter scaling constant. Permitting the LTA computation to continue uninterrupted enables the signal coda energy to raise the LTA, which then terminates the detection. For a short time thereafter, only later arrivals having sufficient signal-to-coda ratio will be detected. The filter time constant while a beam is in the detection state is increased to permit the LTA to reach an estimate of the coda more quickly. The LTA computation rate is a function of the STA integration interval.

5.3.5.2 Implementation of the Thresholding Process

Define \overline{STA} as the average value of the STA; it is related to the LTA by

$$\overline{\text{STA}} = 2^{(\eta-\sigma)} \text{LTA}$$

where η and σ are the input and feedback shifts of the LTA algorithm. The thresholding is then represented by

$$\frac{\text{STA}}{\overline{\text{STA}}} > k$$

where k is either the turnon or turnoff threshold. For implementation, the following test is made

$$\text{STA} > \begin{cases} v \cdot 2^{\omega} \cdot \text{LTA} & \text{if beam not in detection state} \\ u \cdot 2^{\omega} \cdot \text{LTA} & \text{if beam in detection state} \end{cases}$$

where v corresponds to the turnon parameter and u to the turnoff parameter and ω is a scaling parameter. If the STA of a beam satisfies the above condition for Q out of Q' consecutive samples, where Q and Q' are parameters, then the beam is in the detection state. Otherwise, the beam is not in the detection state.

The turnon and turnoff thresholds are as follows:

$$k_{\text{turnon}} = v \cdot 2^{(\omega+\sigma_1-\eta_1)}$$

$$k_{\text{turnoff}} = u \cdot 2^{(\omega+\sigma_2-\eta_2)}$$

The turnoff threshold is less than the turnon threshold. This "deadband" reduces the number of detections from small ripples on the STA.

The thresholding process is summarized in Tables 5-2 and 5-3.

Table 5-2. Detection State Table

Last Detection State	Q Out of Latest Q' Consecutive STAs Exceed Detection Threshold	Current Detection State
Off	No	Off
Off	Yes	On
On	Yes	On
On	No	Off

Table 5-3. Applicable Parameters

Detection State	Threshold Used	LTA Parameters
Off	k_{turnon}	η_1, σ_1
On	k_{turnoff}	η_2, σ_2

5.3.5.3 Additional Considerations

An extended data transmission failure may have a serious effect upon beam detections. In the absence of valid seismometer data samples during a transmission breakdown, the last good data sample is used to replace the lost or erroneous data. With such constant inputs, the filtered beam values decay to zero; so does the LTA. Once the cause of transmission error is corrected and good seismic data starts arriving again in the DP, there might be false beam detections due to the low LTA values and the initial filter transient. One measure to correct for this is to artificially increase the LTA after the end of an extended data transmission failure.

- a. To reduce the number of false detections at LASA, Q and Q' are each set at three. At NORSAR, Q and Q' are each set at one. For both systems the k_{turnon} is set at 10 dB and k_{turnoff} at 7 dB.
- b. At LASA a beam is declared on only if all three consecutive STA values are at least 10 dB greater than the scaled LTA values. Unless the three beam envelope values, i.e., STAs, are the same, then the maximum beam envelope value must be greater than 10 dB. Consequently, at LASA, the lowest possible beam detection must have a signal-to-noise ratio greater than 10 dB to be declared a detection. This loss in detection sensitivity is due to the fact that Q and Q' are set at three. The choices of Q , Q' and detection threshold result from a compromise between detection sensitivity and false detection rate.

5.3.6 Detection Processor Configurations

The details in each functional component of the DP signal processing system have been discussed in Sections 5.3.1 to 5.3.5. The selected surveillance configuration (or the general surveillance) of the SAAC ISRSPS DP system, containing the detailed features in each component and the necessary data scaling, is shown in Figure 5-12. Similarly the general and selected surveillance configuration of the NDPC ISRSPS DP system are shown in Figure 5-13.

5.4 Detection Reduction Algorithm

5.4.1 Description of the Algorithms

As discussed in Sections 5-2 and 5.3, several hundred array beams are formed in real time in the Detection Processor and their outputs are monitored for the detection of seismic events. The beam outputs are rectified and integrated, thus generating beam envelopes (or short term averages (STAs)). A beam is declared to be on whenever Q out of Q' consecutive times (where Q and Q' are DP parameters) its STAs exceed a certain threshold proportional to the long term average (LTA) on the same beam. Normally, a medium-to-large seismic event will cause many beams to be in the on state simultaneously. Therefore, the problem of reducing a large volume of beam detection information into signal arrival groups is an important part of the detection processing. The two detection reduction techniques which have been implemented and utilized are described below. One technique forms and maintains signal arrival groups as long as there is at least one beam in the on state. The other technique is used in ISRSPS and relies on the stability property of the maximum signal envelope in performing the detection reduction.

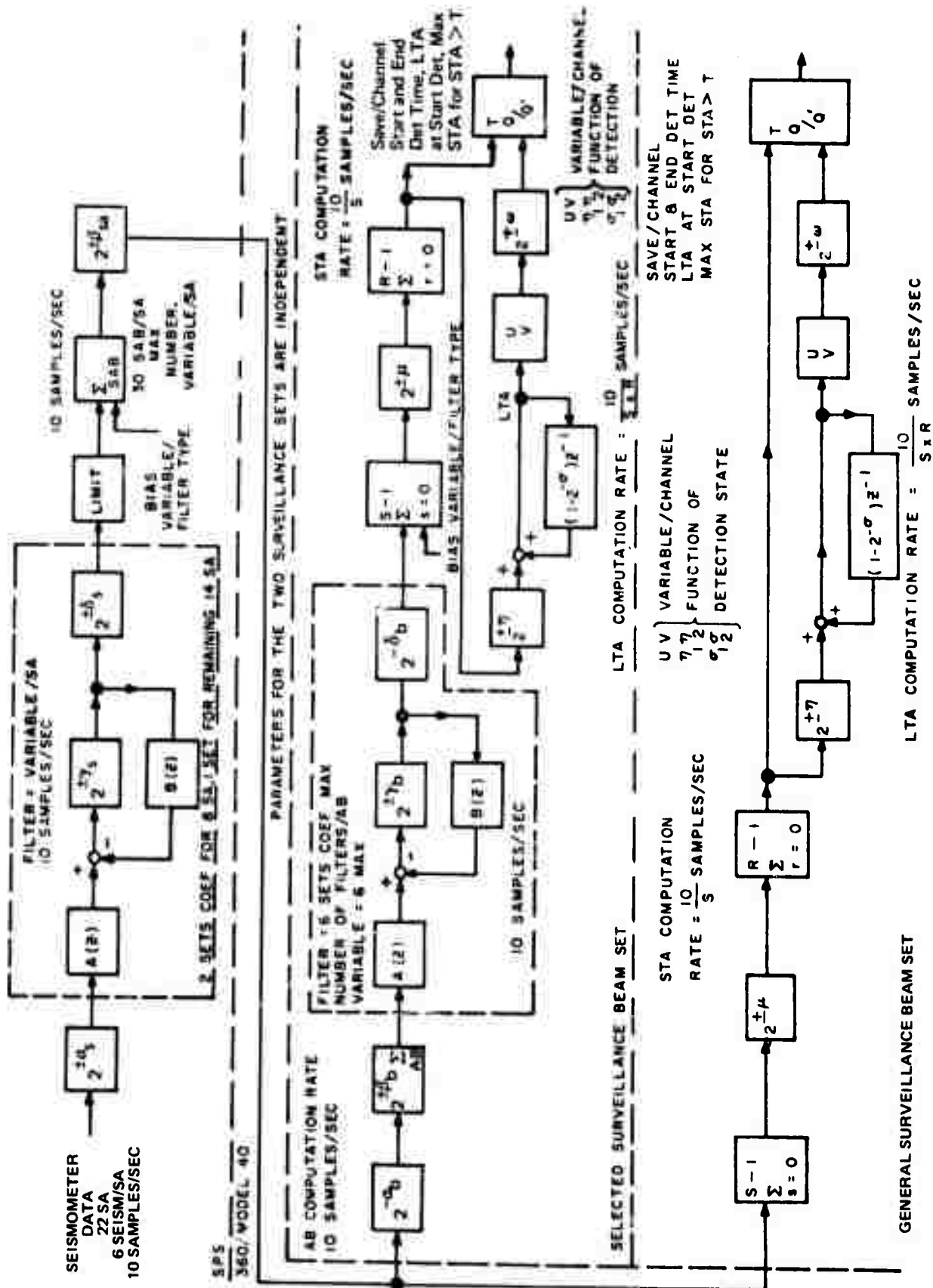


Figure 5-13. NORSAR Detection Processing Configuration

5.4.1.1 Temporal Grouping Technique

If an event occurs within the surveillance region, then the beam steered closest to the event arrival location indicates the maximum signal power; all other beams indicate less power. Consequently, one straightforward approach to the grouping of individual beam detections is to identify a continuous signal arrival time interval and to select the beam with the maximum short-term-average (from the subset of beams in the detection state) within that interval as the beam which appears to be aimed closest to the event location. The event interval begins when any beam satisfies the detection criterion, and extends until all beam detections have been terminated for a time interval corresponding to the maximum aperture transit time.

There are three parameters, p_1 , p_2 , and p_3 , used to control the formation of the event arrival group. An array beam must have p_1 or more STA samples out of p_2 consecutive samples that exceed the detection threshold for that beam to be included in the event arrival group. Successive beam detections are examined and included in the same event arrival group if the end of detection time of the first beam detection is within p_3 STA samples from the start of the second beam detection.

5.4.1.2 Spatial Grouping Technique

It has been observed that the envelopes of coherent signals have certain identifiable temporal and spatial characteristics as the signals move across the deployed beam field. For a signal of interest, the location of the beam having the maximum signal envelope stabilizes for a significant interval in the span between the time when the signal arrives at the first instrument and leaves the last instrument. For noncoherent signals, sidelobes of coherent signals, and signals outside the surveillance region, the location of the beam having the maximum envelope is typically spatially nonstationary in the deployed beam field. This observation suggests that a

constraint requiring the maximum signal envelope to be spatially stationary for a time interval would reject many noncoherent signal and sidelobe detections, and thus reduce false alarm detections.

On the basis of the above observations, the following spatial grouping algorithm has been designed for the Detection Processor. The maximum short time average (MSTA) over all the deployed beams at each STA sampling instant is found, and the associated beam is designated as the MSTA beam. In reducing beam detections to event arrival groups, the spatial grouping algorithm requires that the maximum beam envelopes satisfy certain spatial and temporal constraints. An event arrival group is started or continued as long as the constraints are satisfied.

There is a slight difference between the LASA and NORSAR constraints. The constraints as implemented in the LASA DP are as follows (P, R, and A are system parameters):

- a. The MSTA beams of the last P consecutive STA samples are within radius R of the center beam. The center beam, by definition, has either:
 1. The largest MSTA in the last A STA samples if no event arrival group is in progress
 2. The largest MSTA since the start of the group if a group is in progress.
- b. At least one of the MSTA beams in the last A STA samples is currently in the on state.

The constraints as implemented in the NORSAR DP are as follows:

- a. The MSTA beams of the last P consecutive STA samples are within radius R of the center beam. The center beam by definition has either:

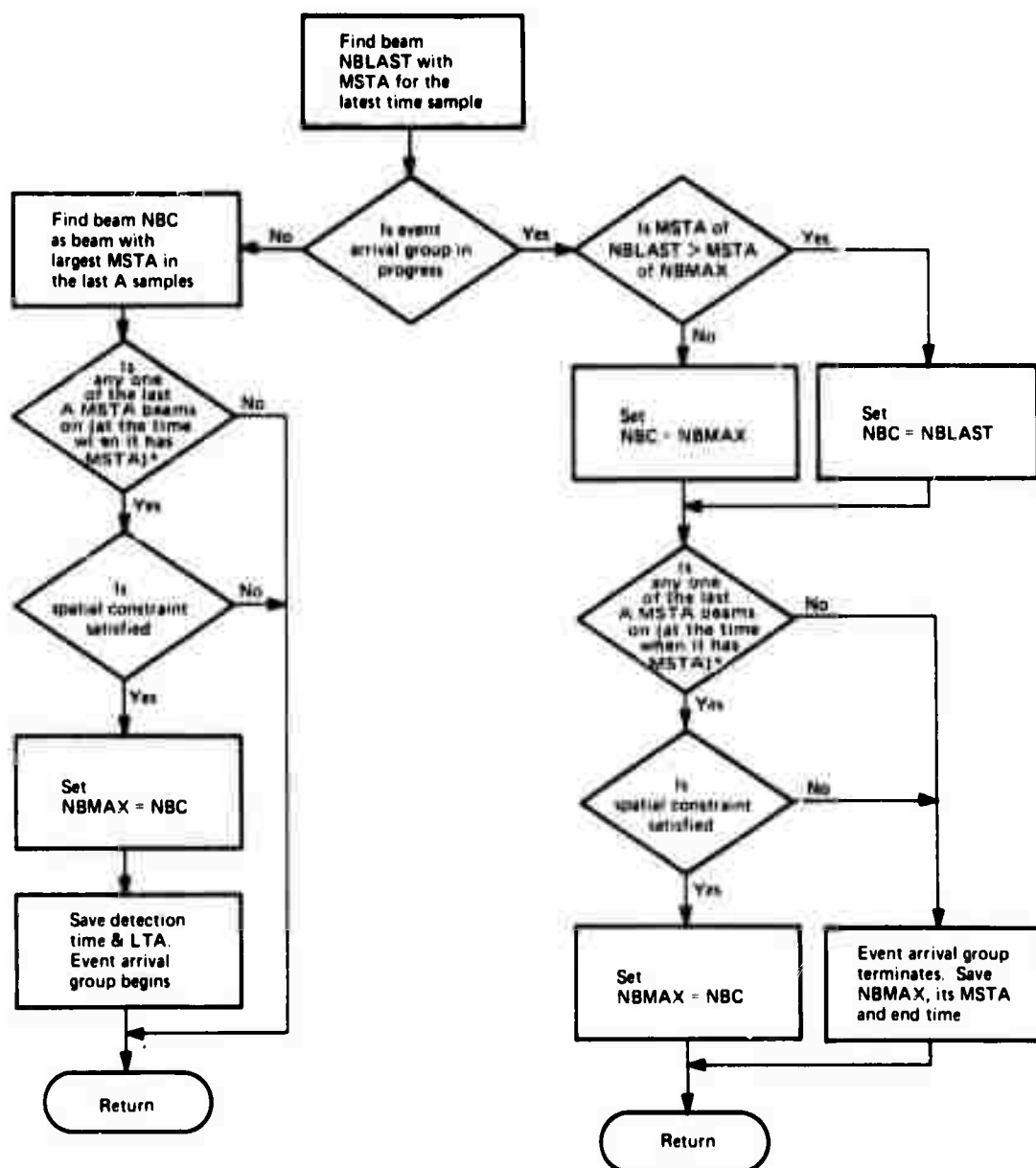
1. The largest MSTA in the last A STA samples if no event arrival group is in progress
 2. The largest MSTA since the start of the group if a group is in progress.
- b. At least one of the MSTA beams in the last A STA samples was on at the time when that beam had the MSTA.

The implementation at NDPC of the spatial grouping technique at each STA sampling instant is shown in Figure 5-14. The SAAC modification is indicated by the footnote in the figure.

If T_g is the time when the constraints are satisfied (either for the first time or following the end of the preceding group), then the group start time is $T_g - (P-1)\Delta T$ where ΔT is the STA sampling interval. The center beam and the largest MSTA associated with the center beam during the group time span are the beam and the MSTA reported for the group. Since only the two most recent LTA samples are available for the LASA detection reduction process at any time, the LTA of an event arrival group reported at LASA is the LTA of the center beam from the earlier of the two LTA samples available at time T_g . At NORSAR, when a beam enters the on state, the LTA value of that beam immediately before the state change is retained for the detection reduction processing (the retained LTA is zeroed when the beam goes into the off state). The LTA of an event arrival group reported at NORSAR is the retained LTA of the center beam at time T_g . The group end time is the time when the constraints are not satisfied for the first time following the start of the group.

5.4.2 Observations on the Spatial Detection Technique

- a. The temporal constraint P for spatial stability is set at three for both LASA and NORSAR DP (see [5-21, Appendix I]). This setting is based on the observation that the duration of the initial phase of a seismic event is typically two to three seconds.



Note: Q,Q': a beam is on when Q out of Q' consecutive STA samples of that beam exceeds the detection threshold
 P: temporal constraint for spatial stability
 A: max (Q', P)
 NBLAST: beam with the MSTA for current time sample
 NBMAX: beam with the largest MSTA during event arrival group span time
 NBC: center beam for spatial checking
 Spatial Constraint: last P MSTA beams are within radius R of NBC

*Delete parenthetical qualification for SAAC DP.

Figure 5-14. Spatial Grouping Algorithm Flow

- b. The radius R is specified such that the spatial constraint includes beams within two beam radii of the center beam. In the worst case, the event location is in the middle of a cluster of beams. The spatial constraint of one ring of beams seems adequate even for this case. However, it is observed that because of time anomalies, complexities of signal characteristics, immediate later phase arrivals and other effects, the location of the maximum beam envelope may move more than one beam-distance. Consequently, the spatial constraint is liberalized to include two rings of beams.
- c. An effort is made to retain the LTA values just prior to the start of an event arrival. This LTA, if uncontaminated by the signal, provides a good measure of the ambient noise and is used in the compilation of detection statistics. This same LTA is communicated to the Event Processor where the signal-to-noise ratios of each event from the DP are examined in order to control the number of events to be processed by the EP. Contaminated LTAs lower the estimate of signal-to-noise; this reduction affects detection statistics and may cause some events not to be processed by the EP which would otherwise be processed. Contaminated LTAs occur in about one of three detection groups at SAAC; at NDPC, contaminated LTAs are avoided by special coding.
- d. The number of event arrival groups per hour depends heavily upon the temporal constraints for spatial stability. The total number of groups at SAAC almost doubles when P is reduced from four to three. Thus, the number of event arrival groups whose actual duration is three STA samples is about the same as the number of those whose actual duration is four STA samples or longer.
- e. When P is reduced from four to three, some of the additional event arrival groups reported are undoubtedly false alarms. But approximately one out of every six

event arrival groups at SAAC with signal-to-noise ratio above the Event Processor threshold of 16 dB has signal duration of only three STA samples. These significant event arrivals would not be reported at all if P were set at four instead of three.

- f. The general surveillance partition at SAAC has more groups reported per hour than the selected surveillance partition, reflecting the fact that the general surveillance has wider inverse velocity space coverage in its beam deployment.

5.5 DETECTION PROCESSOR SYSTEM OUTPUTS AND OFFLINE ANALYSIS PROGRAMS

5.5.1 Online Outputs

During the online operation of the Detection Processor, short period sensor and beam waveforms may be presented on the Experimental Operations Console, and long-period sensor and beam waveforms are presented on the EOC or Develocorder. The signal arrival group information is stored on the shared disk to be used as input to the Event Processor. As noted in Section 4, all array sensor and status data is recorded on a data tape. The following other outputs are of particular interest to the data analyst.

5.5.1.1 On-Line Listing

The online listing contains the seismic event signal arrival information reported by the Detection Processor based on the data from the regular short-period seismometers. The information for each signal arrival group (detection group) is as follows:

- a. The start and stop times of the signal arrival group
- b. The number of the center beam (the beam being declared as closest to the event location by the detection reduction algorithm)
- c. The largest short term average (MSTA) of the center beam during the event arrival group span time
- d. The long term average (LTA) of the center beam at the time when the event arrival group is started.

In addition, the online listing contains the event signal arrivals, reported by the Large Event Processor in the Detection Processor, based on the seismic signals from padded seismometers from LASA, and from selected short-period seismometers from NORSAR. This information is as follows:

- a. The time for each seismometer when its short term average first exceeds the detection threshold (for seismometers whose STA is below the detection threshold, this time is zeroed)
- b. The maximum STA of each padded seismometer during the event arrival time interval
- c. Additional information either derived from the above values or obtained from the beam location table.

5.5.1.2 Detection Log Tape

The detection log tape contains the following detection information:

- a. The time, beam number, and LTA of each detecting beam at the time it enters the detection state
- b. The time, beam number, and the MSTA of each detecting beam at the time it leaves the detection state

- c. The STA values of all beams when the detection is in progress in any beam
- d. The same event arrival group information as in the online listing
- e. The LTA values of all beams at regularly spaced time intervals (NDPC only).

In addition, information such as the beam address table, arrival status, subarray and seismometer status, processing overflows and overruns, and sync and parity error counts are also on the tape.

5.5.2 Offline Analysis of Detection Log Tape

This subsection describes offline programs for presentation and analysis of DP outputs on the detection log tape. These programs and their functions are listed below.

5.5.2.1 Detection Log Tape Delog Program

This program prints out the data records on the detection log tape for a specified time interval. The user selects the types of data records desired.

5.5.2.2 Beam Envelope Pattern Program

In order to show the spatial relationship among the beam envelopes at selected STA sampling intervals, the beam envelope pattern is generated where the STA of each and every beam in quantum units appears at the beam's position in the two-dimensional inverse velocity space (i.e., U-space) for every STA sampling instant within the selected interval, if the STA record is available.

5.5.2.3 Beam Envelope Power Loss Contour Program

The largest STA of each and every beam during a specified signal time is found first. The beam envelope power loss, normalized with reference to the center beam, i.e., $20 \cdot \log(\text{largest STA}/\text{center beam's largest STA})$ in integer dB, appears at the beam's position in the two-dimensional U-space. See Figure 5-15 for a sample output.

5.5.2.4 Beam Envelope Power Loss Pattern Program

The envelope power loss of each beam in Section 5.5.2.3 is plotted against the beam's inverse velocity distance away from the center beam.

The beam envelope power loss pattern can also be generated for an event location which is within the coverage of the center beam but is not at its center. The power loss is normalized with reference to this event location. The largest STA of this location replaces the center beam's largest STA in the power loss computation. See Figure 5-16 for a sample output.

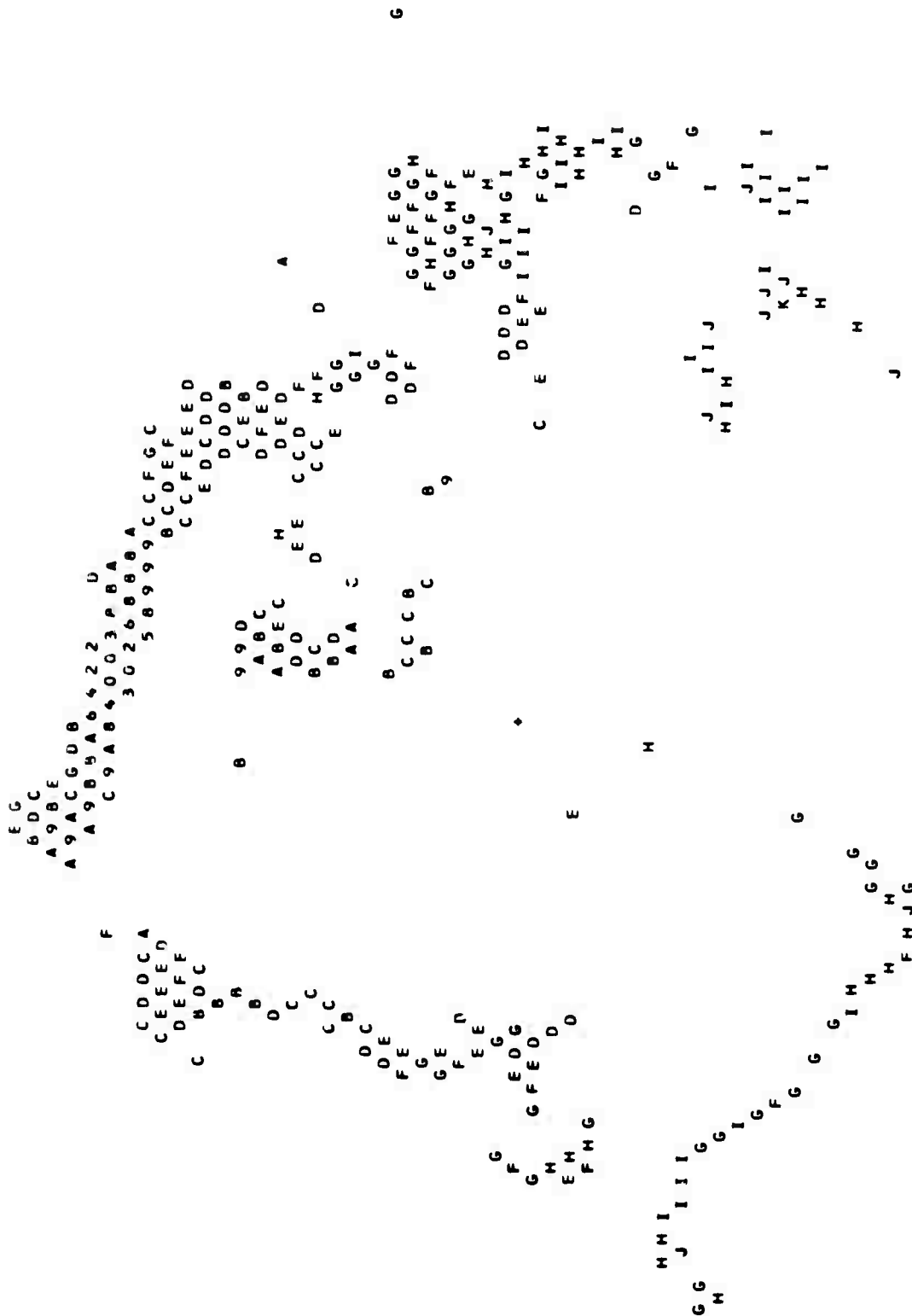
5.5.2.5 Selected Beam Envelope History Program

The beam envelope power in dB at each STA sampling instant, normalized with reference to the center beam, i.e., $20 \cdot \log(\text{STA}/\text{center beam's largest STA during signal interval})$, of a few selected beams for a specified time interval are plotted. See Figure 5-17 for a sample output.

5.5.2.6 LTA Beam Power Loss Pattern Program

The largest LTA of each and every beam during a specified time interval is found first. The LTA beam power in dB relative to the maximum STA of

880
AA



CENTER BEAM= 23, MSTA=16395 QU, MSTA TIME=122 6 19 53.6
 UX=-0.0087965 SEC/KM, UY=-3.0558723 SEC/KM
 START TIME=122 6 19 17.6, END TIME=122 6 19 56.6
 LOSS IN DB: A=10, B=11, C=12 TO 7=35

Figure 5-15. NORSTAR Beam Envelope Power Loss CCI Four

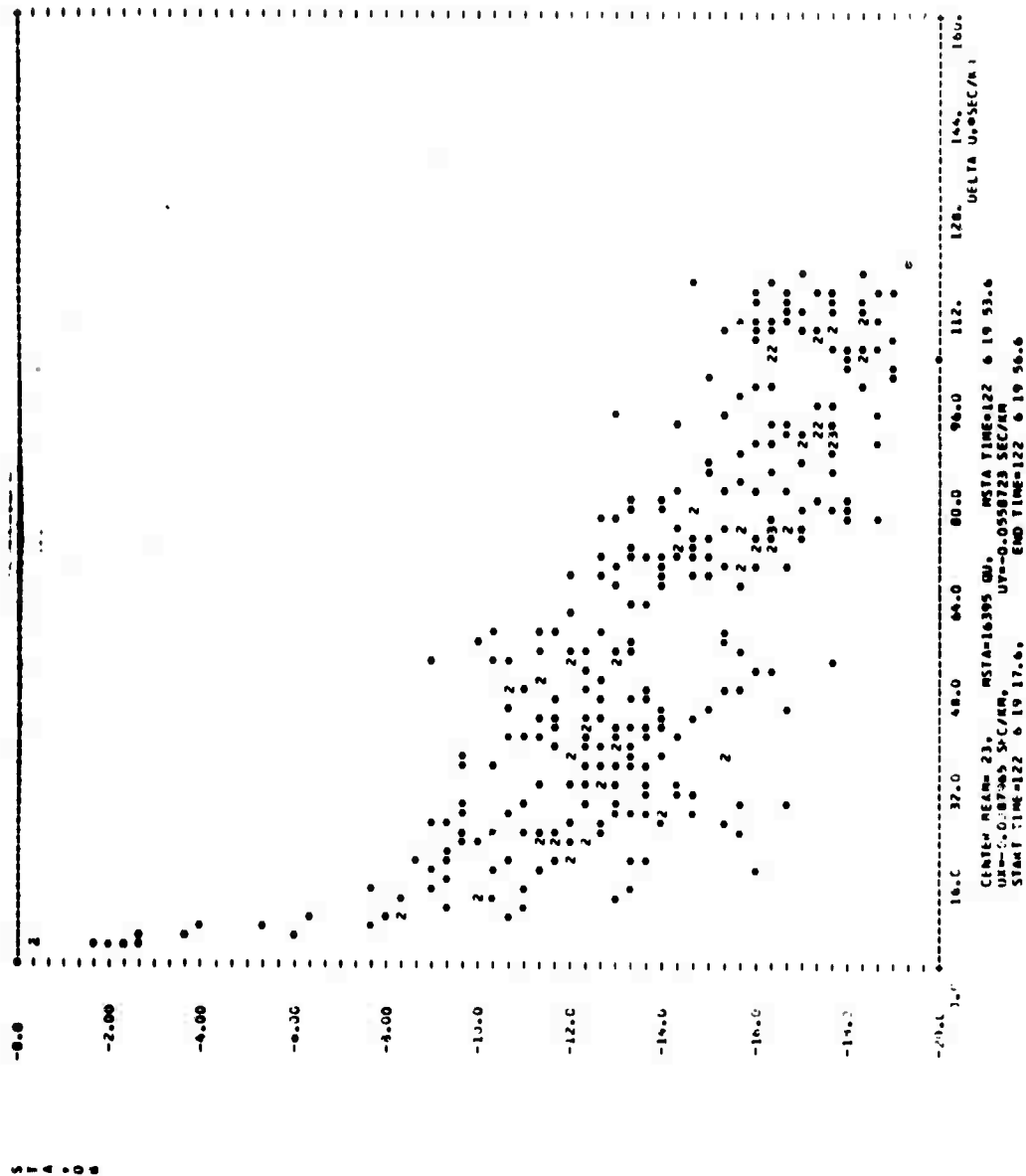


Figure 5-16. NORSAR Beam Envelope Power Loss Pattern

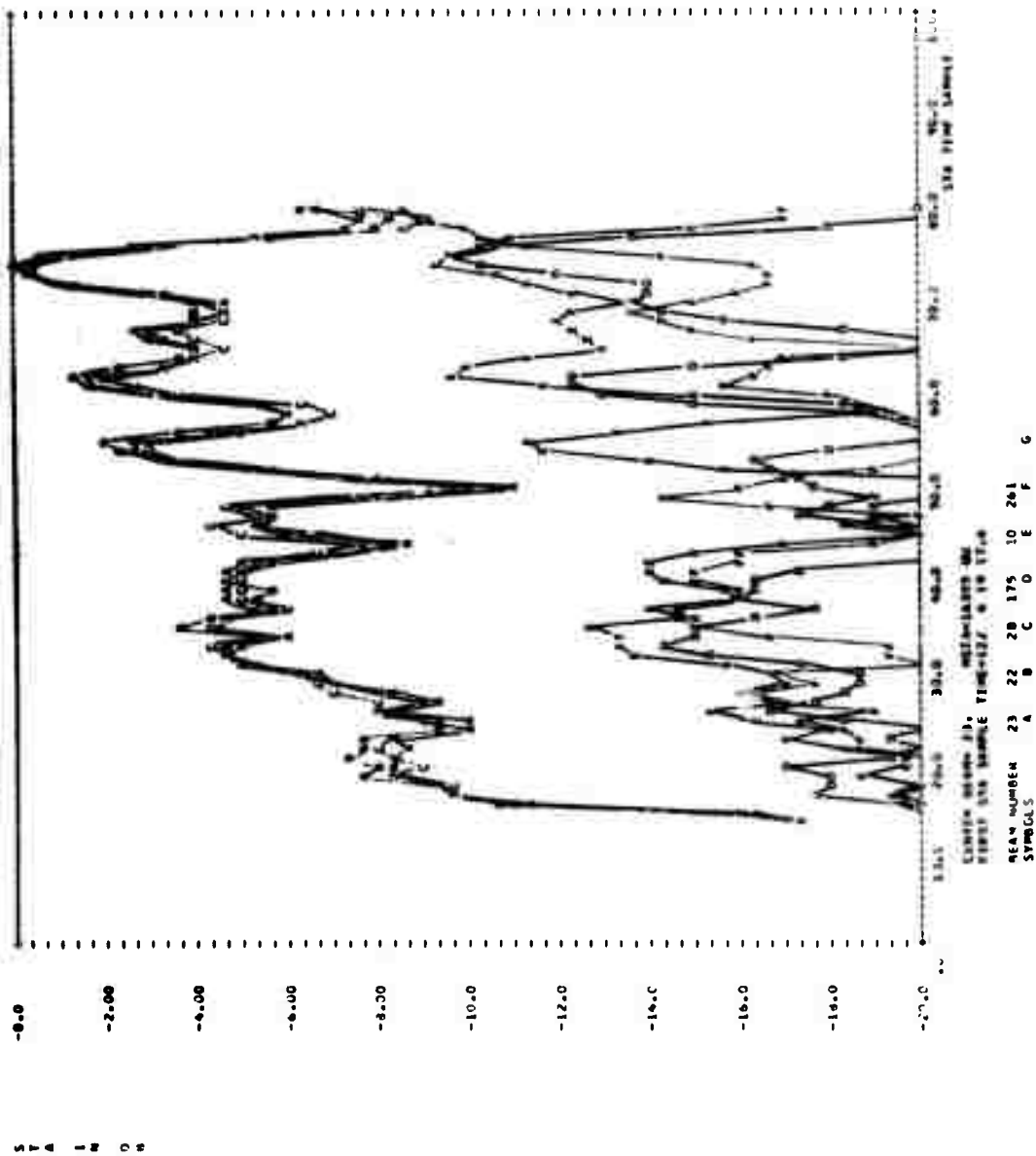


Figure 5-17. Selected NORSAR Beam Envelope History

the center beam, i.e., $20 \cdot \log[(\text{largest LTA})/(\text{center beam's largest STA during signal}) \cdot (\text{conversion factor})]$, is plotted against the beam's inverse velocity distance away from the center beam. The conversion factor scales LTA values to equivalent STA values.

5.5.2.7 Detection Statistics Distribution Programs

The detection statistics for an extended processing interval are compiled. The incremental and cumulative distribution of the event arrivals versus the MSTA of each event arrival group are plotted using a logarithmic scale on both axes. There are similar plots of the incremental and cumulative distribution versus signal-to-noise ratio (MSTA/LTA). LASA detection statistics are presented in [5-14] to [5-21]. An example of the plot of detection statistics versus MSTA is shown in Figure 5-18.

Two straight lines are drawn on the incremental distribution of event arrivals versus MSTA in Figure 5-18. One line approximates the distribution of events with high MSTA values and has a slope of about minus one. The other line approximates the distribution of events with low MSTA values and has a slope much more negative than minus one. The more negative slope reflects a disproportionately large increase in the number of event arrival detections with low MSTA values.

The point of intersection of these two straight lines conveniently separates the distribution into two parts. One part has mostly valid seismic events whose distribution coincides with empirically known results; the other part contains a large number of false event arrivals. Thus, the MSTA value (in nanometers) associated with the point of intersection provides a measure of the signal level at which the number of false detection groups reported by DP is approximately equal to the number of valid groups reported.

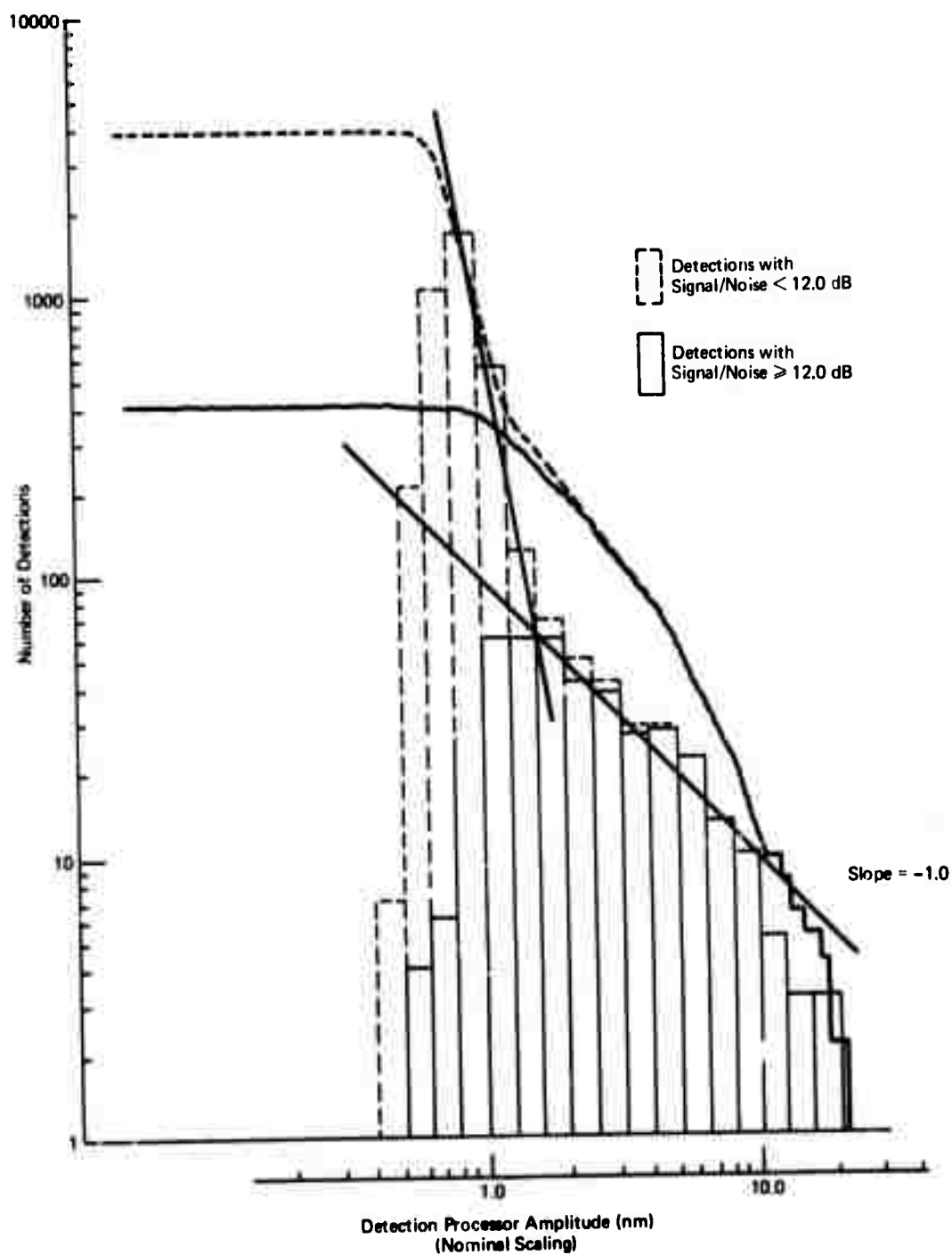


Figure 5-18. NORSAR Detection Distribution Beam Set 306 (300 Beams)

5.6 COMPARISON OF ALTERNATIVE DETECTION TECHNIQUES

The three detection techniques considered in this study are coherent beam-forming, envelope processing (sometimes referred to as incoherent beam-forming), and voting on subarray beam detections.

The coherent array beam is the average of the time-aligned subarray beam values $X_k(t)$, and the corresponding envelope M_c is a sum of rectified values of the array beam.

$$M_c(t) = \sum_{n=-N}^N \left| K^{-1} \sum_{k=1}^K X_k(t+n) \right|$$

where

- K = the number of subarray beams
- $2N+1$ = the number of rectified values used in the envelope computation.

The incoherent beam envelope $M_I(t)$ is computed as the sum of subarray beam envelopes, as follows:

$$M_I(t) = K^{-1} \sum_{k=1}^K \sum_{n=-N}^N |X_k(t+n)| .$$

Although the equations for the coherent and incoherent beam envelopes are quite similar, there are significant differences in the properties of the two. The primary difference is that the main lobe of an incoherent beam may cover approximately 50 times as much area in U-space as the main lobe of a coherent beam for a typical seismic event signal. Hence, the U-space

resolution provided by an incoherent beam is considerably less than that of a coherent beam, but considerably fewer incoherent beams are required to cover a given region of U-space for surveillance.

The subarray beam voting technique consists of selecting a subset of L subarray beams and computing the envelope for each of these subarray beams. As implemented in the NORSAR online detection processing system, a detection is declared whenever a preset number P of the L subarray beam envelopes exceed a threshold within a specified time interval. If the thresholds on all subarray beams were the same, this would be equivalent to declaring a detection whenever the P^{th} largest of the L subarray beams, which had first been time-aligned for the event in question, exceeded the common threshold. This latter version of the subarray beam voting algorithm is the one which has been used here.

Specifically, for the eight subarrays which are currently used in the NDPC ISRSPS Detection Processor voting algorithm, the subarray beams are time-aligned for each event, and the subarray beam envelopes are computed as follows:

$$M_k(t) = \sum_{n=-N}^N |x_k(t+n)|.$$

For each value of $P = 1, \dots, L$, an envelope is defined which is equal to the P^{th} largest of the L values $M_k(t)$ at each sample time point t_j ; this envelope will be denoted as $M_{P/L}(t)$. Clearly, $M_{P/L}(t)$ will exceed a particular threshold value at any sample time point at which P of the L subarray beam envelopes exceed the same common threshold value. Therefore, it is appropriate to use the values $M_{P/L}$, $\bar{N}_{P/L}$, and $\sigma_{P/L}$ for the peak of $M_{P/L}(t)$ in the signal region and the mean and (composite) standard deviation of $M_{P/L}(t)$ in the noise region, respectively, to compute a detectability measure as defined in 5.6.1 for a P of L voting algorithm with common threshold value for the subarray envelopes.

A possible variation of the above formulation, which has not been used here, is to normalize the subarray beam envelopes $M_k(t)$ so that they have a common average value in the noise region prior to ordering of the values at each time point and computation of the above-described statistics of $M_{P/L}(t)$. This version of the detectability index calculation could yield results which more accurately represent the NDPC voting algorithm.

5.6.1 Event Detectability Analysis

For each event detection technique it is possible to identify a signal envelope function so that the detection process consists essentially of the computation and thresholding of this envelope. The detectability index for each event is computed from a portion of the envelope function containing the event signal data and a significant interval of noise data preceding the event. This index of detectability (D) is the difference between the peak envelope value in the signal region (M') and the average envelope value in the noise interval (\bar{N}), divided by an estimate of the rms envelope value in the noise interval (σ_N).

$$D = \frac{M' - \bar{N}}{\sigma_N}.$$

Therefore, the detectability index is a measure of the signal-to-noise ratio of the detection envelope.

For the envelope noise interval, σ_N and \bar{N} should each be proportional to the rms value of the seismic noise data from which the envelope has been computed. Therefore, a relationship of the form $\sigma_N = k\bar{N}$ should hold, where the proportionality constant k depends on the noise amplitude distribution and the method used in computing the envelope.

For each type of envelope studied and for each digital filter which was used to prefilter the data prior to envelope computation, the estimates of \bar{N} and σ_N were obtained. All of the pairs of values (\bar{N}, σ_N) for a given envelope-filter combination were then used to compute a linear regression of the form

$$\sigma_N = a + b\bar{N} .$$

As expected, the value of a was generally quite small and could be ignored in subsequent calculations. Therefore, to reduce the dependence of the detectability index D on the variability of the estimate of σ_N , the composite value of σ_N was determined by regression for each envelope filter combination and was then used in the computation of D for each event for that particular envelope filter combination.

The detectability measures (D) for all of the signal envelope types discussed previously may be converted to decibels (dB) by the operation $20 \log_{10}(D)$, since each of these envelopes is proportional to waveform amplitude. For a given signal waveform, the relative performance of any two combinations of predetection filter and detection processing technique (envelope computation) may be determined simply by computing the difference between the two corresponding detectability measures expressed in dB.

However, in order to make meaningful comparisons of relative detectability among different event signal waveforms, some means of normalization is required to eliminate the dependence of the detectability measure on signal amplitude. Although several such normalizations are possible, the one which will be used in this report is as follows. The filter-technique combinations are sorted into various comparison groups of interest. For each such comparison group and for each event, the filter-technique combination is determined which has the largest value of detectability for that event. This detectability measure (in dB) is then subtracted from the detectability measures for all filter-technique combinations in the

comparison group for that event. Each resulting detectability measure can therefore be described as the detectability loss in dB relative to the best filter-technique combination for a particular event and a particular comparison group.

5.6.2 Comparison of Predetection Filters

The digital filters used in this study are indicated in the table of coefficients, Table 5-4. These filters are described in some detail in [5-20, Appendix V]. The filters have been used for two main purposes. First, all of the filters have been included in the detectability analysis to provide comparisons of the relative effectiveness of these filters for predetection filtering. Second, the six filters labeled 09-35, 12-32, DDD, SSDD, SIMPLE, and MATCH have been used to emphasize various frequency bands prior to power spectral density estimation.

Figure 5-19 shows the relative detectability measures for the coherent beamforming envelope and the 14 digital filters. For each filter, the relative detectability losses for the 48 events for NORSAR, as described in [5-23, Appendix III], are divided into quartiles. The choice of a best filter based on this data is subjective and depends on the specific objectives of the detection processing system. However, the filters labeled DDD, 09-35, and 12-32 clearly stand out as good choices.

It should be recognized that the detectability measure which has been used is somewhat dependent on the signal alignment prior to envelope computation, and that the alignment of the subarray beams for all events used in this study is based on the output of the EP correlation process. Since this process is specifically designed to produce a "best" coherent beam for data which has been filtered using a 0.9-3.5 Hz filter, the signal alignment which results is undoubtedly somewhat biased in favor of a coherent beam and filter 09-35.

Table 5-4. Digital Filter Coefficients

Filter	Coefficient		Filter	Coefficient		Filter	Coefficient		Coefficient	
	A	B		A	B		A	B	A	B
Match	0.0534939	1.0000000	09-35	0.1828182	1.0000000	12-20	0.0101826	1.0000000	28-36	0.0101826
	0.0261544	0.0		0.0	-0.7870601		0.0	-2.7681370		0.0
	-0.5796481	0.0		-0.5484547	0.1160316		-0.0305477	4.5912447		-0.0305477
	1.0000000	0.0		0.0	-1.1455385		0.0	-4.6328669		0.0
	-0.5796481	0.0		0.5484547	0.3760701		0.0305477	3.2781725		0.0305477
Simple	0.0261544	0.0	12-32	0.0	-0.0833045	16-24	0.0	-1.4009657	32-40	0.0
	0.0534939	0.0		-0.1828182	-0.0105028		-0.0101826	0.3617964		-0.0101826
	0.5000000	1.0000000		0.0985310	1.0000000		0.0101826	1.0000000		0.0101826
	-1.0000000	0.0		0.0	-0.8285509		0.0	-1.5964165		0.0
	0.5000000	0.0		-0.2955930	0.8227419		-0.0305477	2.8643723		-0.0305477
SSDD	0.0	0.0	09-14	0.0	-0.4883228	20-28	0.0	-2.3582144		0.0
	0.0	0.0		0.2955930	0.5070699		0.0305477	2.0560780		0.0305477
	0.0	0.0		0.0	-0.1368116		0.0	-0.8079538		0.0
	0.0	0.0		-0.0985310	0.0562974		-0.0101826	0.3617964		-0.0101826
	0.4000000	1.0000000		0.0029000	1.0000000		0.0101825	1.0000000		0.0101825
DDD	-0.8000000	0.0	08-16	0.0	-0.0814199	24-32	0.0	-0.3243866		0.0
	0.4000000	0.0		-0.0087000	7.9559193		-0.0305476	2.0393305		-0.0305476
	1.5999994	0.0		0.0	-9.0928192		0.0	-0.4487357		0.0
	-0.4000000	0.0		0.0087000	6.4449997		0.0305476	1.4722013		1.4722013
	-0.8000000	0.0		0.0	-2.6775398		0.0	-0.1641736		-0.1641736
	0.4000000	0.0		-0.0029000	0.5320800		-0.0101825	0.3617972		0.3617972
	0.2000000	1.0000000		0.1101825	1.0000000		0.0101826	1.0000000		1.0000000
	0.0	0.0		0.0	-3.7659302		0.0	0.9680246		0.9680246
	-0.6000000	0.0		-0.0305476	6.7927542		-0.0305477	2.3202200		2.3202200
	0.0	0.0		0.0	-7.2459717		0.0	1.3700333		1.3700333
	0.6000000	0.0		0.0305476	4.8361683		0.0305477	1.6709843		1.6709843
	0.0	0.0		0.0	-1.9059544		0.0	0.4899213		0.4899213
	0.0	0.0		-0.0101825	0.3617971		-0.0101826	0.3617964		0.3617964
	-0.2000000	0.0								

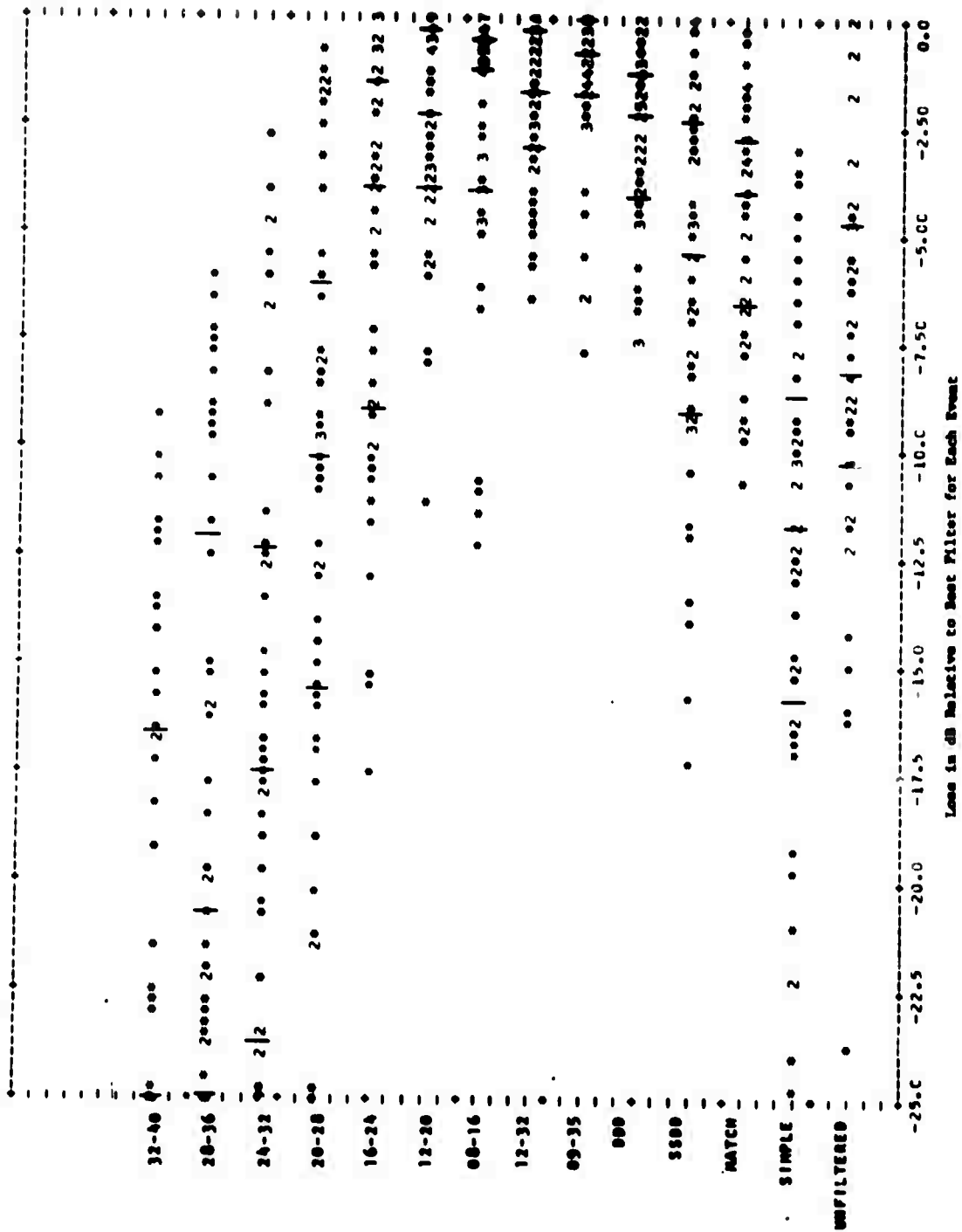


Figure 5-19. Relative Detectability Comparison for Various Prediction Filters and Coherent Beamforming

The narrowband filters having the lower values of center frequency, such as 08-16, 12-20, and 16-24, produce the best detectability values for several events which apparently have high signal-to-noise ratios in the corresponding frequency bands. However, there are also several events for which the performance of these filters is relatively poor.

Figures 5-20, 5-21, and 5-22 show the comparative performances of the 14 predetection filters for incoherent beamforming (envelope processing), and for three out of eight and four out of eight voting algorithms, respectively. In all cases, the performance of the filters DDD and 12-32 stands out, whereas the performance of filter 09-35 is occasionally inferior to that of a higher frequency narrowband filter.

5.6.3 Detection Processing Technique Comparisons

Figure 5-23 shows the comparative performance of 10 different detection processing schemes, including coherent beamforming (linear beamforming), incoherent beamforming (envelope processing), and eight different voting algorithms, for data processed by filter 09-35. This filter has been selected for special attention because it is currently the primary filter used in the NORSAR detection processing system. It is somewhat surprising that the incoherent (or envelope) beamforming process stands out so clearly as the process having the highest detectability values in this case, particularly since the signal alignment should be quite good for data processed by filter 09-35.

Figures 5-24 and 5-25 show the comparative performance of the various detection processing schemes for data processed by filters 12-32 and DDD, respectively. The incoherent beamforming process yields the highest detectability values for each of these filters as well, and the three out of eight and four out of eight voting algorithms stand out somewhat among the set of eight voting schemes.

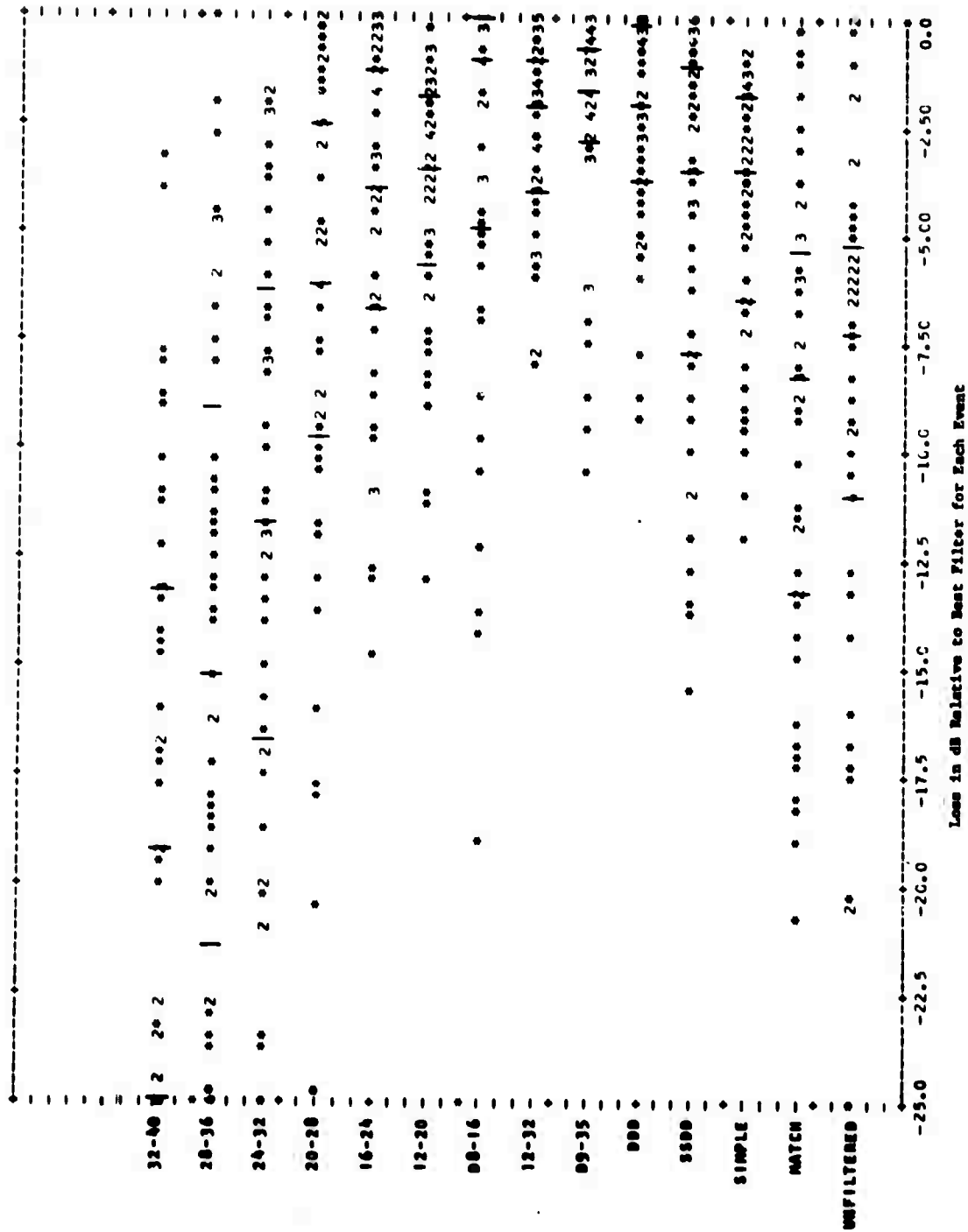


Figure 5-20. Relative Detectability Comparison for Various Predetection Filters and Incoherent Beamforming (Envelope Processing)

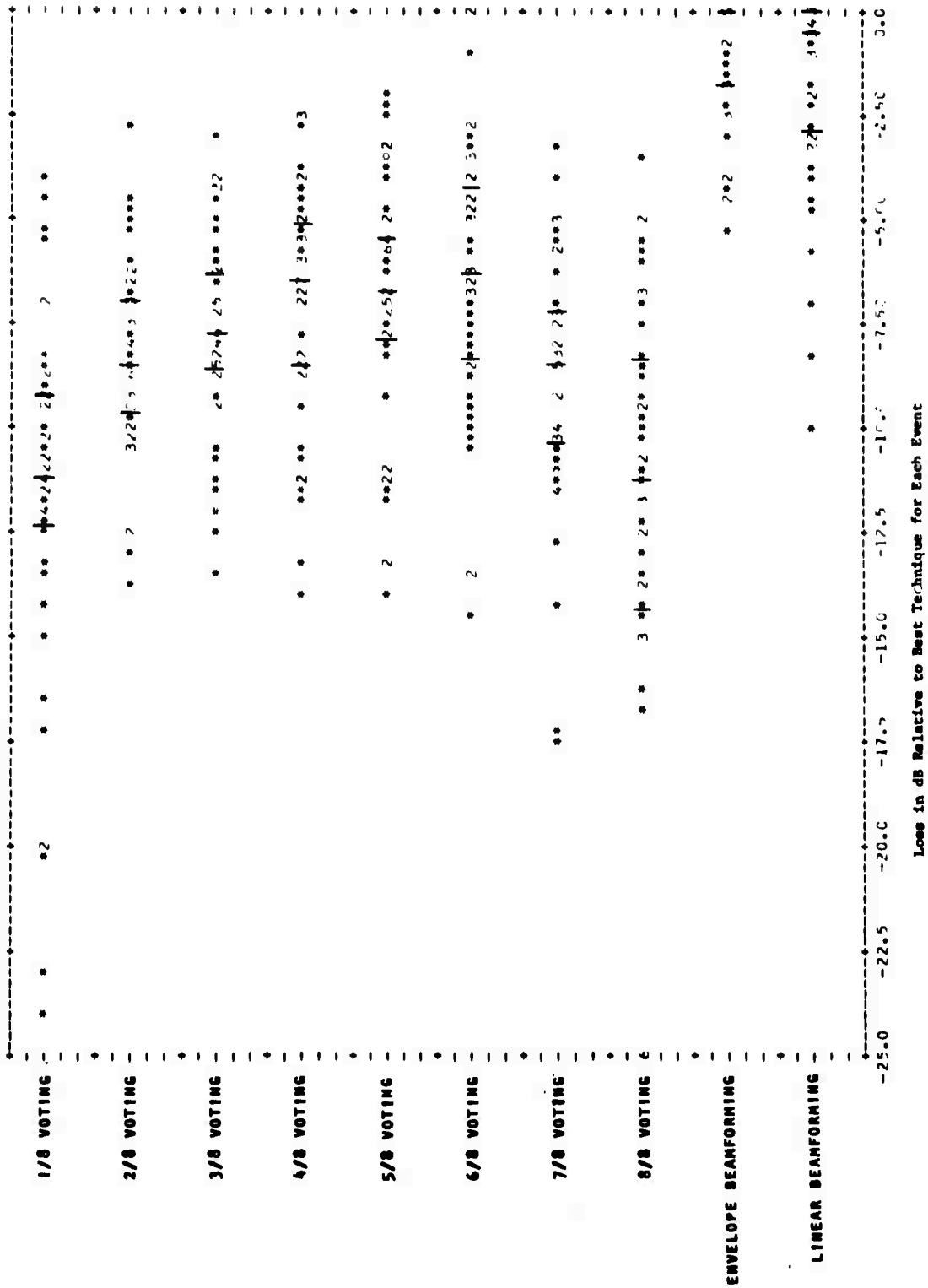


Figure 5-23. Relative Detectability Comparison for Various Detection Techniques and Filter 09-35

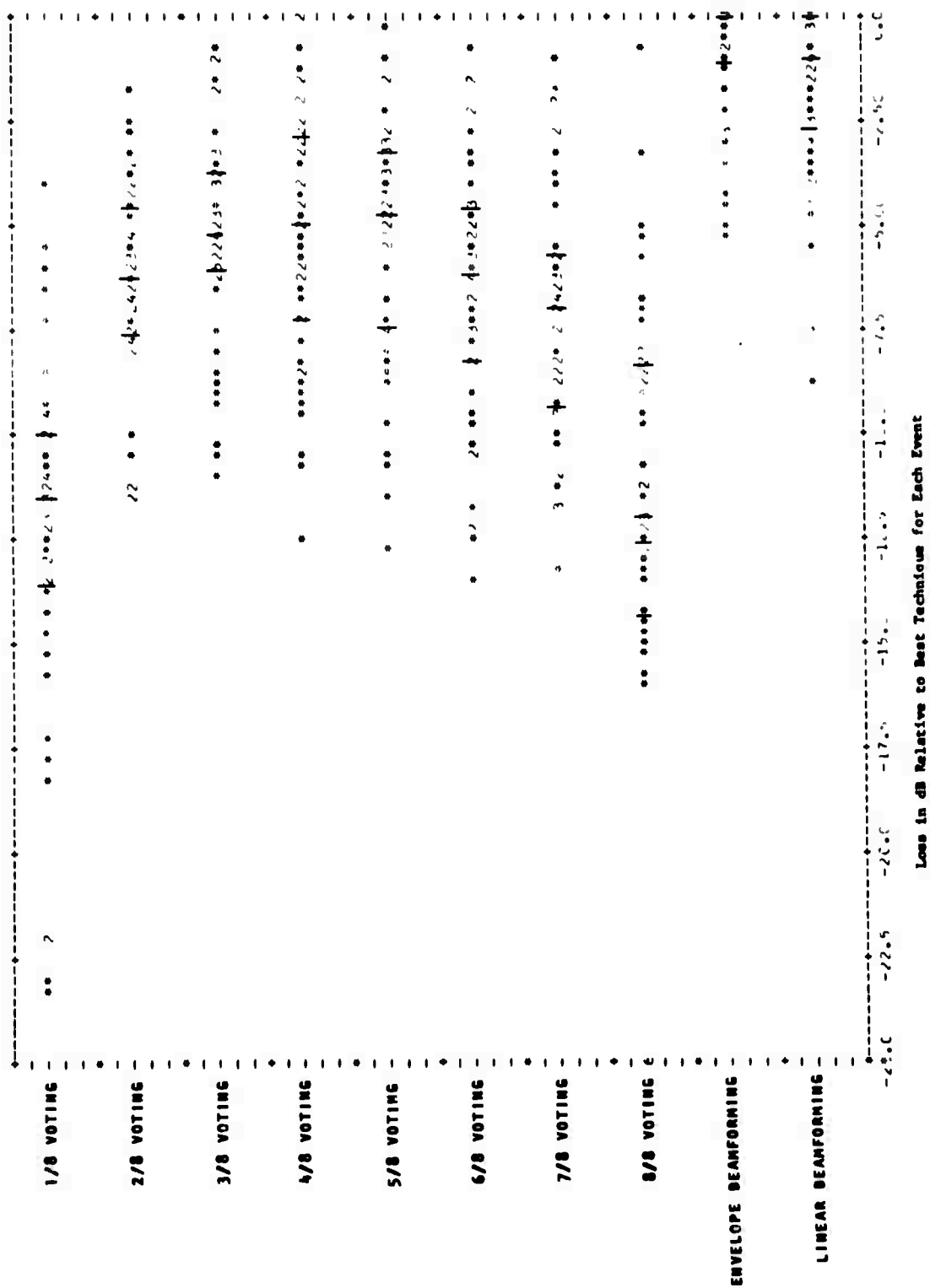
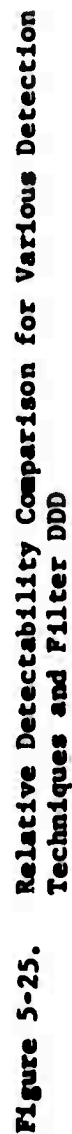


Figure 5-24. Relative Detectability Comparison for Various Detection Techniques and Filter 12-32



5.6.4 Comparison of Selected Filter-Technique Combinations

Figure 5-26 shows the relative detectability of a selected set of filter-technique combinations. If a single choice were to be made, it appears from this data that the incoherent beamforming process in combination with either filter DDD or filter 12-32 has a slight edge, but the choice is not a clear one. A different data set might well yield values which would lead to a different choice of the "best" combination.

There is also no clear choice between the three out of eight and four out of eight voting schemes which can be based on this data. Furthermore, it should be noted that the relative performance among different filters for a particular detection technique, or among different detection techniques for a particular filter, is in some cases distinctly different in Figure 5-26 from the relative performance indicated by the appropriate earlier figure. This is an effect of the normalization scheme that has been used, which causes interactions among the various filter-technique combinations in a comparison group.

The detectability measure is based on the assumption that the detection threshold for a given envelope will be set at some level $k\sigma_n$ above the average noise level \bar{N} . Furthermore, the preceding comparative detectability analysis contains an implicit assumption that the same value of "k" would be used for the various envelopes, so that the difference between two detectability measures in dB is independent of the factor "k." However, if the detection thresholds for two different envelopes are each based on the same factor "k" the false alarm rates of the two processes will not necessarily be equal.

If N' denotes the peak value of a noise envelope over some data interval, and if \bar{N} and σ_n still denote the mean and rms values of the noise envelope, respectively, then the parameter F , defined as follows:

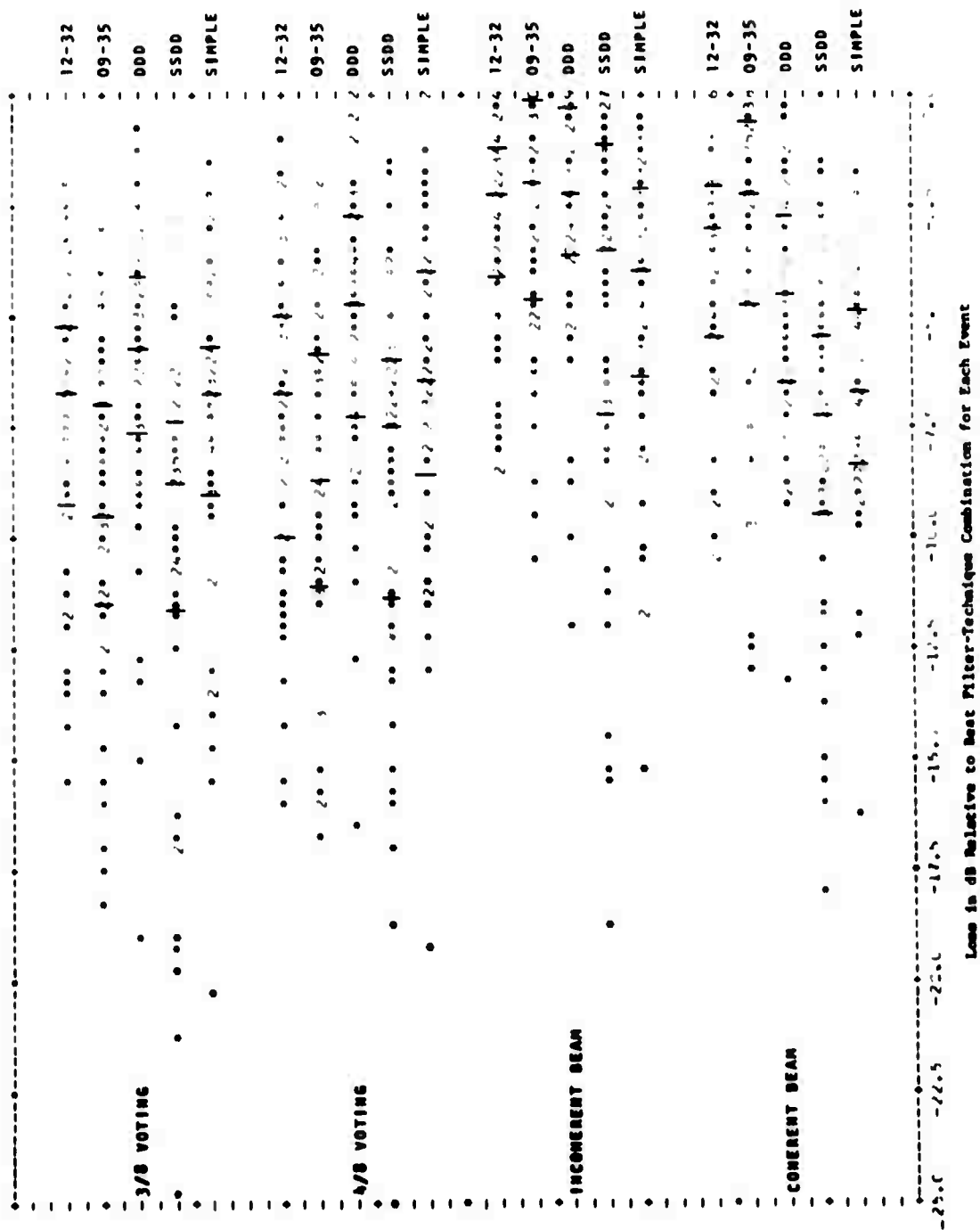


Figure 5-26. Relative Detectability Comparison for Selected Combination of Detection Processing Technique and Predetection Filter

$$F = \frac{N' - \bar{N}}{\sigma_n}$$

will provide at least a crude measure of the false alarm behavior of an envelope. The false alarm index F is essentially a measure of the tendency of the noise envelope peaks to be considerably larger than the rms values. Figure 5-27 shows the false alarm indices in dB for the same comparison group of filter-technique combinations presented in Figure 5-26. The main conclusion which can be drawn from Figure 5-27 is that the false alarm indices for coherent beamforming are 3-4 dB smaller than for the other detection processes. Hence, the threshold levels for the other processes may have to be set relatively higher (in terms of the threshold factor "k" discussed previously) in order to attain the same false alarm rate. However, no firm conclusions concerning false alarm rates should be drawn except as a result of applying the actual detection algorithms on an experimental basis to a large volume of real seismic data.

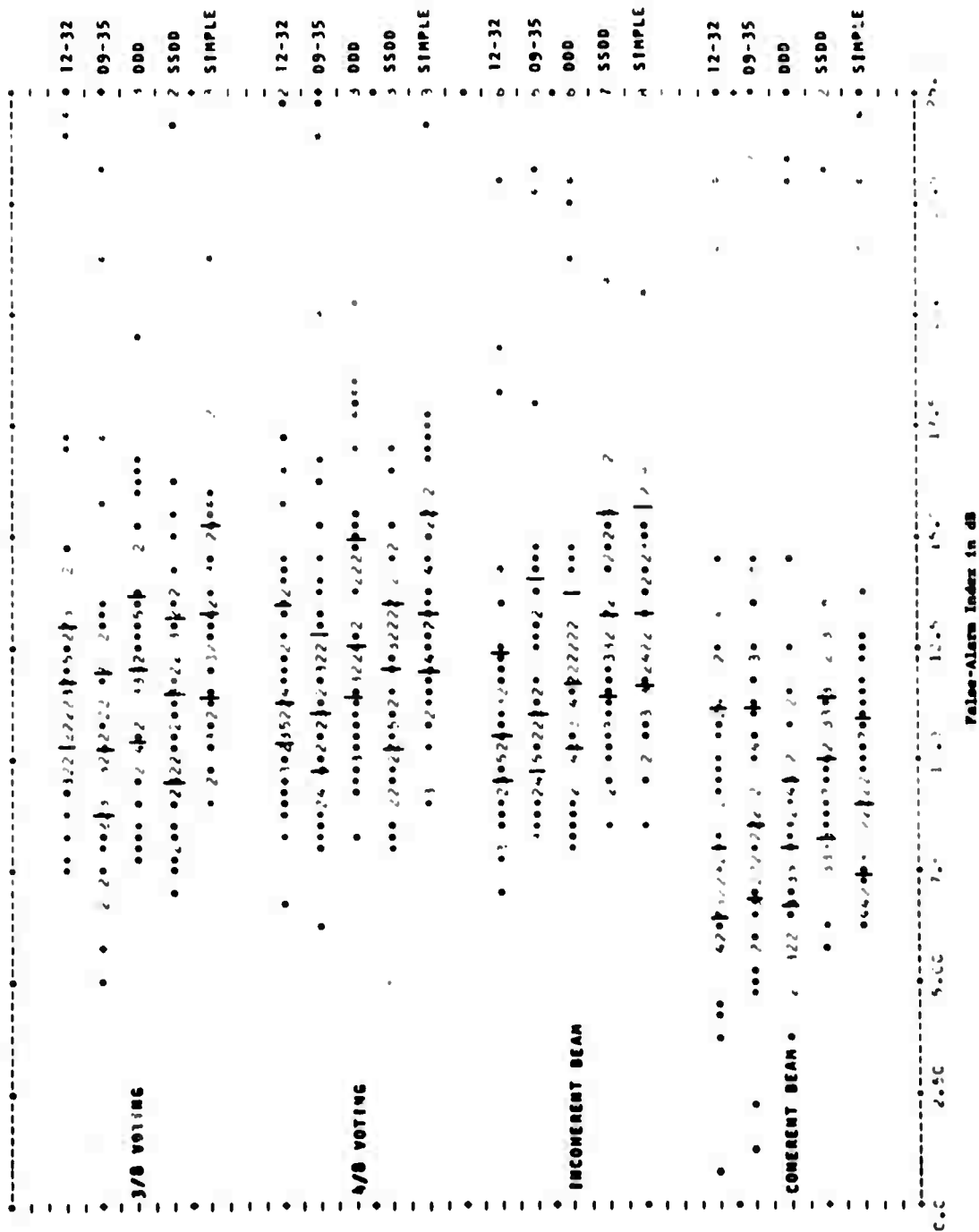


Figure 5-27. Comparison of False-Alarm Indexes for Selected Combinations of Detection Processing Technique and Predetection Filter

5.7 ANNOTATED BIBLIOGRAPHY

- 5-1. "Large Aperture Seismic Array Signal Processing Study,"
IBM Final Report, Contract SD-296, 15 July 1965.

This report defines the LASA signal processing requirements, specifies the characteristics of equipment needed to implement the processing requirements, and defines an experimental program to calibrate and evaluate the signal processing equipment.

- 5-2. "LASA Signal Processing, Simulation, and Communications Study," IBM First Quarterly Technical Report, Contract AF 19(628)-4948, 1 May 1966.

Section 1 presents the objectives of the LASA Signal Processing System and establishes surveillance requirements. Section 3 describes the system functional flow. Appendices A and B present the surveillance coverage considerations for detection processing. Appendix C documents specifications for scaling, seismometer sensitivity tolerance, sampling rate and quantization, and data word length. Appendix D discusses the generation of subarray beam delays. Appendix E describes the use of cross-spectral matrices of seismometer noise to compute the time-domain coefficients of optimum filters.

- 5-3. "LASA Signal Processing, Simulation, and Communications Study," IBM Second Quarterly Technical Report, Contract AF 19(628)-5948, September 1966.

Appendix A describes the program used for preparing inverse velocity space maps of the world, presents a method of estimating beam count requirements, and estimates the accuracy of event location on the earth's surface, in terms of the size of LASA beams in inverse velocity space. Appendix A also describes the generation of beam steering delays and

their significance with respect to array gain, and discusses event location estimate errors (1) due to finite beam width, (2) due to incorrect steering delays in beamforming, and (3) in relating measured phase speed to range. Appendix B presents the configuration and arithmetic characteristics of the LASA beamformer, reports experimental results based on an analysis of Longshot event data, defines two criteria for scaling in the beamforming process, and examines the scaling and sampling of two beamformer configurations. Appendix C.2 discusses the microcodes for recursive filter, convolution filter, beamformer, rectify and integrate, and threshold.

- 5-4. "LASA Signal Processing, Simulation, and Communications Study," IBM Final Report, Contract AF 19(628)-5948, ESD-TR-66-635, March 1967.

Section 2.3 defines the objectives and the two-stage beamforming and threshold detection system configuration of the Detection Processor. Section 3.1 discusses the number of detection beams required to cover the areas of interest lying within the P-telesismic zone as seen from the Montana LASA and from a second array location. Section 3.2 discusses the loss and phase patterns for the Montana LASA configuration. Section 3.3 estimates the event location capability of LASA. Section 3.4 describes methods of developing a set of steering delays. Section 3.7 discusses the Z-transform treatment of the recursive form of digital filtering and attendant stability considerations, contains formulation for lowpass, highpass, bandpass and band-reject Butterworth and Tschebyscheff filters, and indicates filtering error and precision requirements. Section 3.8 contains results of LASA data analysis of the Longshot and Kamchatka events. Included are subarray beam filter analysis, post-detection integration time analysis, system gain analysis, scaled signal/noise analysis, and power spectrum analysis.

- 5-5. "LASA Experimental Signal Processing System," IBM
First Quarterly Technical Report, Contract AF 19(628)-
67-C-0198, ESD-TR-67-458, February 1967.

Appendix A.2.1.1 contains results of an evaluation of the Detection Processor storage requirements.

- 5-6. "LASA Experimental Signal Processing System," IBM
Second Quarterly Technical Report, Contract F 19(628)-
67-C-0198, ESD-TR-67-602, May 1967.

Appendix C examines several data compression techniques to establish the feasibility of remote processing. Appendix D contains preliminary study results on quantization errors present in each stage of detection processing. Appendix F identifies an array-processing design synthesis procedure upon which an experimental data measuring plan can be based. Certain key system design parameters such as gain, noise correlation, and spectral density are measured to determine expected system performance.

- 5-7. "LASA Experimental Signal Processing System," IBM
Third Quarterly Technical Report, Contract F 19(628)-
67-C-0198, ESD-TR-68-149, August 1967.

Appendix II.2 uses an idealized model to examine the effect of seismic noise on the accuracy of the estimated event location, and describes location estimation errors due to imperfect "calibration." Appendix II.5 describes an array design based upon the principle of maximizing gain by choosing element placement in accordance with a model of the noise field. Appendix III describes the library organization of phase delays, and the generation of steering correction factors resulting from an examination of several hundred events. These sets of correction factors can be grouped to produce average sets of corrections which are

valid over selected regions. Appendix II also describes the method of covering an arbitrary location in inverse velocity space by a choice of preformed and presteered subarray beams.

- 5-8. "LASA Experimental Signal Processing System," IBM
Fourth Quarterly Technical Report, Contract F 19(628)-
67-C-0198, ESD-TR-68-309, November 1967.

Appendix IV discusses a study of the use of steering delays based on fitting a quadratic surface to observed event arrivals and describes the development of program specifications for the subarray assignment requirement.

- 5-9. "LASA Experimental Signal Processing System," IBM
Fifth Quarterly Technical Report, Contract F 19(628)-
67-C-0198, ESD-TR-68-450, February 1968.

Appendix I describes the channel distortion in the short-period seismometer's analog equipment, contains an analysis of the encoding noise introduced into the seismometer data as a result of data compression, and analyzes instrumentation rescaling. Appendix VII describes a mathematical model which generates, independently for each subarray, a uniformly dispersed set of beams covering the teleseismic zone, describes the azimuthal phasing which must be assigned to each subarray beam set, analyzes LASA beam requirements in terms of beam diameter, signal loss, number of subarrays, and areas of coverage, analyzes the instrument and beam parameters quantitatively and demonstrates tradeoff configurations which maximize gain while holding the processing load at a specified level, and formulates the relationship between the detection process parameters and the noise and saturation levels in the process. Appendix VII.4 contains results of a comparative study on the subarray deployment quantization losses associated with two subarray beam structures. Appendix VII.5 presents filter response results obtained by nulling the numerator coefficients for subarray masking. Appendix VII.6 describes detection reduction based on the spatial property of beam envelopes.

- 5-10. "LASA Experimental Signal Processing System," IBM
Sixth Quarterly Technical Report, Contract F 19(628)-
67-C-0198, ESD-TR-68-451, May 1968.

Appendix I presents the results of NORSAR design studies. Array design requirements and problems such as optimization techniques, sensitivity to element coordinate deviation and cost tradeoffs are described.

- 5-11. "LASA Experimental Signal Processing System," IBM
Final Technical Report, Contract F 19(628)-67-C-0198,
ESD-TR-69-60, Volume I, March 1969.

Appendix II presents the results of ESPS system evaluation. System gain, process generated noise, and detection processing capability for several process configurations are measured. Appendix VII.2 explains a detection reduction algorithm formulated by grouping beams in the detection state. Appendix IX describes three computer programs used for subarray and array beam deployment. Two additional LASA beam deployment grids are defined.

- 5-12. "Integrated Seismic Research Signal Processing System,"
IBM First Quarterly Technical Report, Contract F 19(628)-
68-C-0400, ESD-TR-69-299, November 1968.

Appendix III proposes a new method for generating subarray steering delay corrections. The teleseismic zone in inverse velocity space is partitioned into contiguous triangular regions. Appendix IV describes a detection reduction algorithm based on spatial and temporal characteristics of beam envelopes. Appendix V describes the IFRSPS equipment configuration for online seismic array control and diagnostics, data recording, detection and event processing, and data exchange with other seismic arrays.

- 5-13. "Integrated Seismic Research Signal Processing System,"
IBM Second Quarterly Technical Report, Contract F 19(628)-
68-C-0400, ESD-TR-69-357, February 1969.

Appendix II contains data and results associated with the generation of LASA beam set 133 and subarray beam set 104, which are used in the LASA ISRSPS Detection Processor's selected surveillance partition, and contains a list of parameter values used in the Detection Processor, Appendix III describes the reasons and algorithms for seismometer data limiting and deglitching. Appendix IV documents the results of processing certain NORSAR events in order to identify signal and noise characteristics. Appendix VI describes the detection processing using the short-period seismometers in NORSAR. Appendix VIII recommends that the seismometer channels be calibrated for 0.0427 nanometers per quantum unit.

- 5-14. "Integrated Seismic Research Signal Processing System,"
IBM Third Quarterly Technical Report, Contract F 19(628)-
68-C-0400, ESD-TR-70-25, May 1969.

Appendix sections II.2 and II.3 present cumulative detection statistics from April 14 to April 25, 1969. Appendix V.2 contains a list of parameters used in the detection reduction by beam grouping technique.

- 5-15. "Integrated Seismic Research Signal Processing System,"
IBM Fourth Quarterly Technical Report, Contract F 19(628)-
68-C-0400, ESD-TR-70-265, August 1969.

Appendix II.2 presents cumulative detection statistics from May 14 to July 31, 1969.

- 5-16. "Integrated Seismic Research Signal Processing System,"
IBM Fifth Quarterly Technical Report, Contract F 19(628)-
68-C-0400, ESD-TR-70-306, November 1969.

Appendix I describes the effect of filter scaling change in the Detection Processes to minimize the effect of quantization error bias. Appendix III.2 presents cumulative detection statistics from August 1, 1969 to October 31, 1969. Appendix IV describes the software for the expedited full aperture

NORSAR configuration to evaluate filtering and beamforming tradeoffs and to determine time delays for array beam deployment.

- 5-17. "Integrated Seismic Research Signal Processing System,"
IBM Sixth Quarterly Technical Report, Contract F 19(628)-
68-C-0400, ESD-TR-71-388, February 1970.

Appendix I.2 presents cumulative detection statistics from November 1, 1969 to January 31, 1970. Program changes which affect the statistics are indicated. Appendix VI.5 analyzes the detection statistics from 50 events at NORSAR and compares results for six different filters.

- 5-18. "Integrated Seismic Research Signal Processing System,"
IBM Seventh Quarterly Technical Report, Contract F 19(628)-
68-C-0400, ESD-TR-72-128, May 1970.

Appendix I.2 presents cumulative detection statistics from February 1, 1970 to April 30, 1970. Appendix II discusses the development of LASA beam set 140 for general surveillance.

- 5-19. "Integrated Seismic Research Signal Processing System,"
IBM Eighth Quarterly Technical Report, Contract F 19(628)-
68-C-0400, ESD-TR-71-393, August 1970.

Appendix I.2 presents cumulative detection statistics from May 1 to July 31, 1970. Appendix III describes the preliminary results of an analysis of seismic signals received by the Interim NORSAR system.

- 5-20. "Integrated Seismic Research Signal Processing System,"
IBM Ninth Quarterly Technical Report, Contract F 19(628)-
68-C-0400, ESD-TR-72-122, November 1970.

Appendix I.2 presents cumulative detection statistics from August 1 to October 31, 1970. Appendix I.5 contains results of quantitative estimates of the seismic activity on a world-wide basis from data published

in the ERL Preliminary Determination of Epicenter lists. Appendix I.5 presents seismicity data for a seven-year period for the 28 regions on the earth. Appendix III describes the programming process and the LASA data base for the nonuniform triangular grid for estimating region corrections and calibration parameters. Appendix V presents results of continuing investigations of the NORSAR signal and noise characteristics (including attempts to optimize the digital filtering) and some preliminary results comparing the effectiveness of different detection techniques.

- 5-21. "Integrated Seismic Research Signal Processing System,"
IBM Tenth Quarterly Technical Report, Contract F 19(628)-
68-C-0400, ESD-TR-72-123, February 1971.

Appendix I provides a detailed description of the spatial grouping technique as implemented in the LASA and NORSAR Detection Processors, examines the performance of the spatial grouping algorithms and highlights the significant behavior of selected beam envelopes. Appendix II.2 presents cumulative detection statistics from November 1 to December 31, 1970. Appendix IV describes the system and acceptance tests that were performed to verify and demonstrate the capabilities specified for the SAAC ISRSPS system.

- 5-22. "Integrated Seismic Research Signal Processing System,"
IBM Eleventh Quarterly Technical Report, Contract F 19(628)-
68-C-0400, ESD-TR-72-133, May 1971.

Appendix I reports the development of array and subarray beam sets for implementation in the NORSAR surveillance system; i.e., NORSAR array beam sets NBS 306, NBS 310, and NBS 310A, and NORSAR subarray beam sets NSBS 114-115 and NSBS 123-124. Appendix IV presents a chronology of scaling changes, beam deployment and changes in critical detection parameters in the NORSAR ISRSPS in 1971. Appendix VII presents the evaluation results on the performance of the ISRSPS signal processing algorithms and techniques

as a function of event size. The data set was obtained by scaling down the sample values of large seismic signals and embedding the scaled event data in unscaled seismic noise.

- 5-23. "Integrated Seismic Research Signal Processing System,"
IBM Final Technical Report, Contract F 19(628)-68-C-0400,
ESD-TR-72-139, August 1971.

Appendix I presents NORSAR cumulative detection statistics from February 15 to March 31 and May 1 to May 31, 1971. In addition, this study presents an estimation of the NORSAR processing system performance, and an evaluation of its false alarm rate. Appendix II presents some measurements of the utilization of different processing components while the system is performing in its normal operational mode. Appendix III presents results of a preliminary investigation of the full NORSAR array signal and noise characteristics and of the comparative performance of various predetection filters and event detection techniques for NORSAR data. Appendix IV presents a summary analysis of LASA detection performance by geographic region based on the data gathered during routine operation of the IISPS SAAC system, from May through December 1970.

- 5-24. "NORSAR Systems Evaluation," IBM Interim Technical Report,
Contract F 19(628)-68-C-0400, ESD-TR-72-145, January 1972.

Appendix I reports an analysis of the location determination performance of the NORSAR ISRSPS. Appendix III presents analysis results of the NORSAR ISRSPS short-period noise characteristics based on the study of the Detection Processor Long Term Averages.

- 5-25. "Parametric Study of Seismic Array Gain Test Results,"
Contract F 19(628)-67-C-0298, ESD-TR-68-425, June 1968.

This report presents results of a study of the LASA signal-to-noise gain, using filters of various bandwidths and selected system configurations based on the Longshot and Kamchatka data.

5-26. REF 112, ISRSPS System Test Specification

This document contains specifications for SAAC and NDPC system tests: purpose, concept, procedure, and results.

Section 6

ARRAY BEAMSTEERING TECHNIQUES

The parameters which are utilized in a simple delay-and-sum beamforming process include a set of channel delays and, generally, a set of zero-one weights or equivalent identifiers to indicate which channels are included in the beam. Weighted-delay-and-sum beamforming utilizes a similar set of parameters, except that the zero-one channel weights are replaced by relative weighting factors for various channels. Filter-and-sum beamforming may be regarded as a further generalization in which weighting factors are assigned to more than one data sample in each channel. Furthermore, as discussed in Section 7, the assumption of a plane wavefront model causes each channel delay to be represented as the sum of two components, a plane-wave portion and a relative time anomaly portion, in which the plane-wave portion for all channels is parameterized by the two components U_x and U_y of a point in U-space.

Array beamsteering may be defined as any process for estimating some or all of the pertinent array beamforming parameters, including at least the two components U_x and U_y of a plane-wave model, from a set of array data that is assumed to include a signal of interest, in such a way that the beam which is formed from the data using the estimated parameters provides a "best" (for example, most noise-free) representation of the signal.

In the case of delay-and-sum beamforming, the beampacking process which is described in Section 8.3.1.4 is an example of an array beamsteering process in which the relative time anomalies and weighting factors for the channels are preassigned, and only the parameters U_x and U_y are estimated. If the region of U-space over which the set of packed beams is deployed is too restricted, or if the grid of U-space aiming points is too coarse, then the beampacking process may converge to a U-space location which represents a side-lobe,

rather than the main-lobe, of the signal energy. Furthermore, this process is sometimes susceptible to local noise peaks in U-space.

The correlation and sequential estimation process which is described in Section 8.3.1.3 is an example of an array beamsteering process for delay-and-sum beamforming in which the relative time anomalies and the plane-wave parameters U_x and U_y are estimated from the seismic data. As noted in Section 7, the relative time anomalies have been found to be highly repeatable from one seismic event to another as a function of U-space location. Hence, the time anomaly parameters associated with a data base of previously recorded and edited seismic events have a number of useful array system applications, and the correlation and sequential estimation process provides an efficient, automatic means of extracting these time anomalies from the seismic data. Furthermore, the "best" beam which is formed using the correlation process parameter estimates is generally "sharper" (e.g., less distorted and less susceptible to the attenuation and spreading of sharp peaks caused by beamforming) than that which results using parameters derived from beampacking.

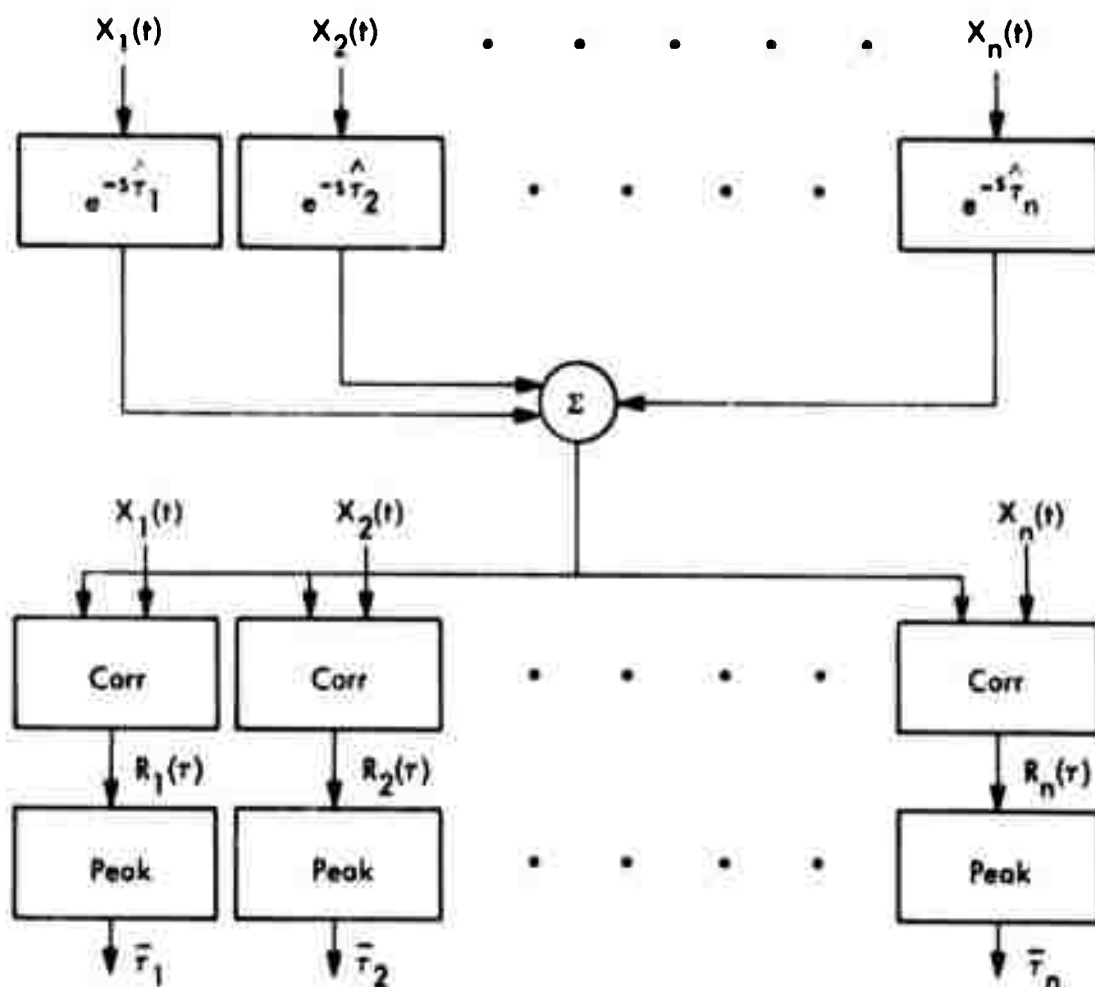
Under the assumptions that each channel contains a copy of a single representative signal waveform embedded in seismic noise which is uncorrelated from channel to channel, and that no interfering signal is present within the time interval of interest, there is no apparent restricting factor which would prevent the development of a successful array beamsteering process for the estimation of all beamforming parameters associated with a weighted delay-and-sum beam or even a filter-and-sum beam. However, for real seismic data there are differences among the signal waveforms on various channels which are sometimes quite significant, there are frequently echoes of the signal waveform on some channels, and there are occasionally superimposed signals from interfering events. Therefore, if the channel weights are not constrained in some predetermined manner, the notion of a reference signal waveform becomes imprecise. Furthermore, if the channel weights are allowed to vary at each stage of an iterative array beamsteering

process, then it is possible either that the process may not converge or that the signal waveform on the resulting "best" beam may be entirely unsatisfactory.

Figure 6-1 shows an early version of the correlation process which was originally presented in [6-2, Appendix II]. The actual computations which were implemented in the experimental computer programs were, of course, the digital equivalents of the equations shown in Figure 6-1. The process inputs included the digitized data from either n seismometer data channels or n subarray beams, filtered prior to the correlation process to approximately prewhiten the seismic background noise over the signal passband and to attenuate the noise outside this passband. Input parameters included initial estimates of the channel delays τ_n . Following each iteration of the correlation process, the delays were updated according to the last equation in Figure 6-1, using the parameter α to control the percentage of correction to be applied at that stage. The iterative process was terminated either when the correction terms for all n delays became insignificant or when the number of iterations exceeded some preset maximum value.

Analysis of the results obtained from application of this process to numerous LASA events led to several significant conclusions and modifications including the following:

- a. The process iterated to completion for almost all events for which the signals could be clearly identified on the subarray beams.
- b. Most of the estimated delays agreed with visual estimates determined by a seismic data analyst.
- c. Various modifications were found to improve the reliability and efficiency of the process, such as subtracting the channel data from the array beam prior to correlation and adding it back in afterwards using the corrected time delay, removing the constant dc bias from both channel and array beam data prior to



$$B(t) = (1/N) \sum_{n=1}^N X_n(t - \hat{\tau}_n).$$

$$R_n(\tau) = (1/T) \int_0^T B(t) X_n(t - \tau) dt$$

$$R_n(\bar{\tau}_n) = \text{Max } R_n(\tau)$$

$$\hat{\tau}_n(K+1) = \hat{\tau}_n(K) + \alpha \{ \bar{\tau}_n - \hat{\tau}_n(K) \}$$

Figure 6-1. Time Delay Correlation Process

- correlation, setting the process parameter α to one for all corrections, and carefully controlling the interval over which the correlation function was computed and searched for a maximum.
- d. To avoid process domination by extremely noisy subarray traces, the correlation function was normalized to a value between zero and one by dividing by the rms values of the channel and the reference array beam (see equation (24) below), and the peak correlation value was then compared with a minimum value to determine whether that channel contained a signal which correlated reasonably well with the reference array beam; if not, that channel was subsequently excluded from the array beam by setting the corresponding beamforming weight to zero.
 - e. Due to the narrow-band character of most seismic signals, and also to signal echoes, the correlation function for a single channel frequently contains several large peaks, and the simple criterion of selecting the maximum peak is frequently incorrect due to the presence of noise.
 - f. When the correlation process iterated to completion, most of the large residual delay errors were due to the selection of an incorrect cycle of the correlation function for the computation of the delay time estimate.

The remainder of this section is concerned primarily with the presentation of a theoretical basis for the correlation process and with the discussion of an extension of this process which incorporates an adaptation of the recursive Bayes estimation technique to increase the cycle selection reliability. The presentation includes a detailed error analysis of the estimation techniques, and a demonstration that these techniques are near-optimum under certain reasonable assumptions. The error analysis is extended to accommodate subarray correlation functions having multiple significant peaks which initially must be considered as candidates for the correct relative arrival-time indication.

In Sections 6.1 and 6.2, an error analysis is presented for the maximum likelihood estimate of the time of arrival of a known signal in additive Gaussian noise. Section 6.1 treats the ideal case of a continuous (analog) signal in white Gaussian noise, and Section 6.2 gives the practical extension of these results to the case of a sampled (discrete) signal in band-limited white noise, which is obtained from the general colored background noise situation by prewhitening over the frequency range of interest. These results are applied to the correlation process in Section 6.3 with the assumption that there is no difficulty in choosing the correct peak. The key result is the equation for the error variance of the arrival time estimate, given by (6-36). This variance is shown to depend on the mean square signal frequency, ω_B^2 , and the algorithm for computing this signal parameter from the available data is presented in Section 6.4.

In Section 6.5 consideration is given to the problem of estimating the U-vector using the individual subarray relative arrival-time estimates. The weighted least-squares procedure which uses the precisions (reciprocal variances) of the independent arrival-time estimates as weights is shown to be optimal according to several reasonable criteria. Furthermore, the covariance matrix associated with the estimation errors is shown to be a natural byproduct of this estimation procedure. An example of the results of the discussion in Section 6.5 is given in Section 6.6 for the case of a circularly symmetric array with equal subarray precisions. This example provides insight into the geometric nature of the estimation technique, and shows in particular that the estimation errors of the two components of the U-vector are independent and identically distributed under the assumptions of the example.

Sections 6.7 and 6.8 provide a probability-oriented treatment of peak selection from the multiple peaks of a correlation function. The information concerning the signal arrival time which is contained in a given correlation function independently of any prior knowledge obtained from other subarrays, is expressed in the form of a probability density function. This probability

modal expresses both the uncertainty in determining the exact location of each correlation peak and the probabilities, based only in the observed correlation function, that each of the significant peaks is the correct one. It is then shown how this observation probability function may be combined in the Bayes sense with the best available prior knowledge to obtain a set of posterior probabilities for the correlation peaks. Therefore, if the correct peak cannot be selected with sufficient confidence from the observation alone, it may be possible to make the selection on the basis of the posterior probabilities.

In Section 6.9, a sequential (Kalman) updating procedure is developed for assimilating the observation of an individual subarray signal arrival time into the U-vector estimate, and for updating the estimation error covariance matrix to account for the new observation. If a given set of relative arrival-time estimates and associated error variances are processed sequentially, beginning with an initial estimate whose error variances are so large that the final result is not significantly affected, then the result is the same as though the identical data had been processed by the concurrent estimation procedure of Section 6.7. Improved estimates of the U-vector should be possible to obtain by first processing those subarray channels for which correlation peaks are easily chosen. Then the prior information thus obtained is used in selecting the most probable of the remaining subarray multiple correlation peaks. Data from this subarray is then incorporated into the U-vector estimate process so as to refine the prior information before continuing the sequential peak selection process. The integrated sequential estimate updating and multiple peak selection process may be expected to operate reliably at low signal-to-noise levels which are beyond the capability of the present correlation program.

A detailed algorithm is described in Section 6.10 which combines the sequential updating and the multiple peak selection processes. This algorithm is parameterized by two probability levels Q_L and Q_U , which may be used to select the operating point on the trade-off between processing efficiency and the peak selection confidence levels.

6.1 ANALOG MATCHED-FILTER PERFORMANCE

To estimate the time of arrival t_0 of a known signal $s(t-t_0)$, which is imbedded in Gaussian white noise $w(t)$ having spectral height N , a filtering procedure based on the maximum likelihood estimate is generally used [6-6]. There are, however, at least two distinct implementations of the maximum likelihood filter. For purposes of illustration, let the received signal be

$$r(t) = A \cdot s(t-t_0) + w(t) \quad (6-1)$$

and assume that the integration interval T of the estimation filter is sufficiently large to contain the entire signal $s(t)$.

One version of the maximum likelihood filter requires the evaluation of the integral

$$\int_{t'_0}^{t'_0 + T} r(t) s(t-t'_0) dt \quad (6-2)$$

as a function of the parameter t'_0 . The value of t'_0 which maximizes the above integral is taken as the estimate of the arrival time.

Another interpretation of the maximum likelihood equations states that the integral

$$\int_{t'_0}^{t'_0 + T} r(t) \frac{\partial}{\partial t'_0} s(t-t'_0) dt \quad (6-3)$$

is to be evaluated as a function of t'_0 . In this case, the arrival time estimate is a value of t'_0 which causes the integral (6-3) to vanish.

Regardless of which implementation is used, the Cramer-Rao inequality shows that the mean square estimate satisfies

$$E(t_0 - \hat{t}_0)^2 > N \left\{ A^2 \int_{t'_0}^{t'_0 + T} \left[\frac{\partial}{\partial t'_0} s(t - t'_0) \right]^2 dt \right\}^{-1} \quad (6-4)$$

in which E denotes the expectation operator and t_0 is the estimated time of arrival. The right side of the inequality (6-4) is known to be a good estimate of the mean square error for sufficiently large signal-to-noise ratios.

Starting with the integral (6-3), a better understanding of the nature of the error estimate (6-4) is obtained by the following heuristic derivation. If (6-1) is substituted into (6-4), then the output of the estimation filter is seen to consist of a signal dependent term

$$A \int_{t'_0}^{t'_0 + T} s(t - t'_0) \frac{\partial}{\partial t'_0} s(t - t'_0) dt \quad (6-5)$$

and a noise dependent term

$$\int_{t'_0}^{t'_0 + T} w(t) \frac{\partial}{\partial t'_0} s(t - t'_0) dt \quad (6-6)$$

The slope of the signal dependent portion with respect to the arrival time t'_0 , at the point $t_0 = t'_0$, is

$$m = -A \int_{t'_0}^{t'_0 + T} \left[\frac{\partial}{\partial t'_0} s(t - t'_0) \right]^2 dt \quad (6-7)$$

Therefore, in the vicinity of this point, (6-5) may be approximated by the linear expression $m'(t_0 - t'_0)$.

The noise term (6-6), which will be denoted by $\eta_0(t'_0)$, has zero mean and the following variance:

$$\text{Var}\{\eta_0(t'_0)\} = N \int_{t'_0}^{t'_0 + T} \left[\frac{\partial}{\partial t'_0} s(t - t'_0) \right]^2 dt \quad (6-8)$$

Therefore, if the signal-to-noise ratio is sufficiently large so that the linear approximation to (6-5) remains valid over the error interval, then the estimated time of arrival t_0 is very nearly a solution of the equation

$$m(t_0 - t'_0) + \eta_0(t'_0) = 0$$

or

$$\hat{t}_0 = t_0 + \eta_0(t'_0)/m \quad (6-9)$$

Clearly (6-9) is an unbiased estimate of t_0 having variance equal to $\text{Var}\{\eta_0(t'_0)\}/m^2$. Using (6-7) through (6-9), it is seen that

$$\text{Var}\{\hat{t}_0\} = N \left\{ A^2 \int_{t'_0}^{t'_0 + T} \left[\frac{\partial}{\partial t'_0} s(t - t'_0) \right]^2 dt \right\}^{-1} \quad (6-10)$$

which is the same as the right side of (6-4).

The above derivation serves to clarify the nature of the assumptions on which the error estimate (6-10) is based. It also shows that an estimate of the form $\text{Var}\{\eta_0(t)\}/m^2$ may be valid even if true maximum likelihood filtering is not used as long as $\eta_0(t)$ is the noise at the filter output,

m is the slope of the signal output with respect to the arrival time, all bias terms are properly eliminated, and signal-to-noise ratio is sufficiently high.

If the additive noise is colored rather than white, then the maximum likelihood theory [6-6] shows that the signal plus noise should first be processed by a noise-whitening filter. The output of the prewhitening filter should then be processed by a filter which is matched either to the signal or to the signal derivative at that point, as described previously. In practical applications, the prewhitening filter need only whiten the noise over the portion of the frequency spectrum for which the signal possesses significant harmonic content and should sharply attenuate the input noise at all other frequencies.

Section 6.2 discusses the performance of a digital-matched filter which operates on a known signal plus band-limited white noise.

6.2 MATCHED-FILTER PERFORMANCE: DIGITAL CASE

Let the sampled values of the known signal, the additive noise and the received signal be denoted, respectively, as

$$\begin{aligned}s_k &= s(k\Delta) \\ w_k &= w(k\Delta) \\ r_k &= r(k\Delta)\end{aligned}$$

where Δ is the sampling interval. Then

$$r_k = A \cdot s_{k-k_0} + w_k \quad (6-11)$$

where k_0 is the sample point corresponding to the arrival time t_0 .

The digital equivalent of the integral (6-2) is the transversal digital filter having coefficients

$$a_n = s_n \text{ for } n = 0, 1, \dots, N-1 \quad (6-12)$$

Similarly, the digital equivalent of the integral (6-3) is the transversal digital filter with coefficients

$$h_n = s'_n \text{ for } n = 0, 1, \dots, N-1 \quad (6-13)$$

where s'_n is a sampled value of the derivative $s'(n\Delta)$ of the signal function.

Let the one-sided spectral density of the band-limited white noise $w(t)$ be defined as follows:

$$W(f) = \begin{cases} a & \text{for } |f - f_c| \leq B \\ 0 & \text{elsewhere.} \end{cases} \quad (6-14)$$

The autocorrelation function in this case is given by

$$R(\tau) = \int_{f_c - B}^{f_c + B} a \cos 2\pi f \tau \, df \quad (6-15)$$

and the noise variance, σ^2 , is equal to

$$R(0) = 2aB$$

Therefore, the substitution $a = \sigma^2/2B$ will be used in the following derivation.

The noise variance γ^2 at the output of the digital filter having coefficients b_n may be computed as follows:

$$\gamma^2 = \sum_{n=0}^{N-1} \sum_{k=0}^{N-1} b_n b_k R_{n-k}$$

where $R_{n-k} = R((n-k)\Delta)$.

Therefore,

$$\begin{aligned} \gamma^2 &= \frac{\sigma^2}{2B} \int_{f_c-B}^{f_c+B} \sum_{n=0}^{N-1} \sum_{k=0}^{N-1} \cos [2\pi f (n-k)\Delta] \cdot b_n b_k df \\ &= \frac{\sigma^2}{2B} \int_{f_c-B}^{f_c+B} |Y(f\Delta)|^2 df, \end{aligned} \quad (6-16)$$

where

$$Y(f\Delta) = \sum_{n=0}^{N-1} b_n \exp (-j2\pi n f \Delta) \quad (6-17)$$

If the integrand of the above integral is sampled at the points $f_k = k/N\Delta$, with associated sampling interval $\Delta f = 1/N\Delta$, then the following rectangular approximation is obtained:

$$\gamma^2 \approx \frac{\sigma^2}{2BT} \sum_{|f_c - f_k| \leq B} |Y(f_k \Delta)|^2 \quad (6-18)$$

where $T = N\Delta$. From (6-17) it follows that the set of complex numbers $\{Y(f_k \Delta) | k=0, 1, \dots, N-1\}$ is the discrete Fourier transform of the set $\{b_n | n=0, 1, \dots, N-1\}$. Hence, according to Parseval's identity for the discrete Fourier transform,

$$\sum_{k=0}^{N-1} |Y(f_k \Delta)|^2 = N \sum_{n=0}^{N-1} b_n^2 \quad (6-19)$$

Furthermore, if nearly all of the signal energy is contained in the frequency interval $|f - f_c| \leq B$, then (6-18) and (6-19) may be combined to produce the approximation

$$\gamma^2 \cong \frac{\sigma_N^2}{2BT} \sum_{n=0}^{N-1} b_n^2 \quad (6-20)$$

If the band-limited white noise $w(t)$ has been produced by processing the original received signal-plus-noise with a band-limited prewhitening filter, then the output signal energy is mainly contained within the frequency band of the filter. In this case, the assumptions which led to the approximation in (6-20) are well justified, and the resulting process will be near-optimal as long as there is an insignificant loss of signal energy through the prewhitening filter.

6.3 APPLICATION TO THE CORRELATION PROCESS

In the correlation process, the reference array beam for the k^{th} subarray, denoted by RAB_k , is defined as the array beam formed from all subarrays except the k^{th} . This reference beam may be regarded as a copy of the subarray beam on which most of the noise has been suppressed. Furthermore, because the k^{th} subarray was not used in forming the reference beam, the noise on the reference beam will generally be uncorrelated with that on the subarray beam.

As a result of the recursive filtering operation which is applied to the subarray beams prior to the start of the cross-correlation processing, it is also reasonable to assume that the noise spectrum is reasonably flat over those frequencies for which the seismic signals exhibit significant harmonic content. In calculating the noise power at the output of any filter whose spectral response is approximately matched to that of the signal, the input noise on the subarray beam may be regarded as band-limited white noise.

Once the subarray beam has been accurately aligned in time with its reference beam (as should be the case after several iterations through the correlation process), the mean square noise on the subarray beam may be expressed as

$$\sigma_k^2 = \min_{\alpha} \left\{ \frac{1}{NA} \sum_{m=1}^{NA} \left[SB_k(m + \lambda') - \alpha RAB_k(m) \right]^2 \right\} \quad (6-21)$$

where λ' is the number of samples of lead or lag which results in the best alignment, and NA is the correlation window length in samples. The purpose of the minimization with respect to the scale factor α is to provide the proper normalization of the reference beam in computing the mean square difference. Note that the above estimate actually accounts for the noise on the reference beam as well as that on the subarray beam.

The following notation will be convenient throughout the remainder of the derivation:

$$\overline{RAB_k^2} = (NA)^{-1} \sum_{m=1}^{NA} RAB_k^2(m) \quad (6-22)$$

$$\overline{SB_k^2} = (NA)^{-1} \sum_{m=\lambda'+1}^{\lambda'+NA} SB_k^2(m) \quad (6-23)$$

$$C_k(\lambda') = \left(\overline{RAB_k^2} \cdot \overline{SB_k^2} \right)^{-1/2} (NA)^{-1} \sum_{n=1}^{NA} RAB_k(n) SB_k(n+\lambda') \quad (6-24)$$

Thus, $\overline{RAB_k^2}$ and $\overline{SB_k^2}$ denote the mean square values of the reference array beam and the subarray beam, respectively, and $C_k(\lambda')$ is the peak value of the correlation coefficient for the k^{th} subarray beam.

If the minimization indicated in (6-21) is carried out, the minimizing value of α is found to be

$$\alpha' = \left[\frac{\overline{SB_k^2}}{\overline{RAB_k^2}} \right]^{1/2} C_k(\lambda') \quad (6-25)$$

Substituting (6-25) into (6-21) produces the result

$$\sigma_k^2 = \left[1 - C_k^2(\lambda') \right] \overline{SB_k^2} \quad (6-26)$$

The cross correlation process may be described as the operation of a linear matched filter having coefficients a_n given by

$$a_n = \frac{RAB_k(n)}{\left[(NA) \overline{RAB_k^2} \right]^{1/2}} \quad (6-27)$$

cascaded with the normalizing factor $\left[(NA) \overline{SB_k^2} \right]^{-0.5}$. This matched filter operation is the digital analog of that given by (6-2). Similarly, the digital version of (6-3) may be represented by a linear filter having coefficients b_n given by (6-3)

$$b_n = \frac{RAB'_k(n)}{\left[(NA) \overline{RAB_k^2} \right]^{1/2}} \quad (6-28)$$

in which $RAB'_k(n)$ is a sampled value of the time derivative $RAB'_k(t)$. To maintain the similarity, this filter should also be cascaded with the normalizing factor $\left[(NA) \overline{SB_k^2} \right]^{-0.5}$.

The estimated delay for the k^{th} subarray may be obtained either by searching for the peak of the output of the former process, or by finding the zero

crossing of the output of the filter. As above, it is more convenient to estimate the mean-squared error on the basis of the null detection formulation.

As discussed previously, the spectrum of the noise on the subarray beam after prefiltering will be assumed to be flat over a frequency band which contains the signal energy. The results of the previous section show that, after filtering and normalization, the variance of the noise at the output of the latter filter is given by

$$\gamma_k^2 = \frac{\sigma_k^2}{(2BT) S B_k^2} \sum_{n=1}^{NA} b_n^2 \quad (6-29)$$

Since the value of the quantity

$$\sum_{n=1}^{NA} b_n^2 = \sum_{n=1}^{NA} \left[RAB'_k(n) \right]^2 / \sum_{n=1}^{NA} \left[RAB_k(n) \right]^2$$

is approximately the same for each reference array beam, $\sum_{n=1}^{NA} b_n^2$ may be replaced by $\overline{\omega_B^2}$, which is defined below as a function in terms of the final array beam $B(n)$.

$$\overline{\omega_B^2} = \sum_{n=1}^{NA} \left[B'(n) \right]^2 / \sum_{n=1}^{NA} \left[B(n) \right]^2 \quad (6-30)$$

Using this definition, and substituting for σ_k^2 according to (6-26), (6-29) may be replaced by the expression

$$\gamma_k^2 = \left[1 - C_k^2(\lambda') \right] \overline{\omega_B^2} / 2BT \quad (6-31)$$

It will subsequently be shown in detail how the value of $\overline{\omega_B^2}$ may be computed by applying the discrete Fourier transform operation to NA samples of the array beam. Prior to this discussion, however, the problem of estimating the slope of the signal-dependent portion of the filter output will be addressed. This result, in conjunction with (6-31), will

enable computation of the error variance for the delay time estimate of the k^{th} subarray.

It follows from (6-21), (6-26), and (6-25) that

$$SB_k(n) = \alpha' RAB_k(n) + w_k(n) \quad (6-32)$$

where $w_k(n)$ is a noise term having variance σ_k^2 . Therefore, the signal-dependent portion of the output of the filter having coefficients b_n , as given by (6-28), is

$$\sum_{n=1}^{NA} \frac{\alpha' RAB_k(n-\Delta n) RAB'_k(n)}{\left[(NA) \overline{RAB_k^2} \right]^{1/2}} \quad (6-33)$$

in which Δn denotes the lead or lag of the subarray beam with respect to the reference beam.

The desired slope may be obtained by differentiating (6-33) with respect to Δn , setting $\Delta n = 0$, and dividing the result by the normalizing factor $\left[(NA) \overline{SB_k^2} \right]^{1/2}$. That is,

$$m_k = \frac{-\alpha'}{\left[(NA) \overline{RAB_k^2} \right]^{1/2}} \frac{\sum_{n=1}^{NA} \left[RAB'_k(n) \right]^2}{\left[(NA) \overline{SB_k^2} \right]^{1/2}}$$

or, equivalently, using (6-25) and (6-27),

$$m_k = -C_k(\lambda') \frac{\sum_{n=1}^{NA} b_n^2}{\overline{b_n^2}} \quad (6-34)$$

As above, $\sum_{n=1}^{NA} b_n^2$ may be replaced by $\overline{w_B^2}$ to obtain

$$\bar{m}_k = -C_k(\lambda') \overline{\omega_B^2} \quad (6-35)$$

Using (6-31) and (6-35), the following expression for the error variance η_k^2 of the delay time estimate for subarray k is obtained:

$$\begin{aligned} \eta_k^2 &= \frac{\gamma_k^2}{\bar{m}_k^2} \\ &= \frac{1}{(2BT) \overline{\omega_B^2}} \left[\frac{1 - C_k^2(\lambda')}{C_k^2(\lambda')} \right] \\ &= \left[(2BT) \overline{\omega_B^2} \text{SNR}_k \right]^{-1} \end{aligned} \quad (6-36)$$

where $\text{SNR}_k = C_k^2(\lambda') / [1 - C_k^2(\lambda')]$ is the estimated signal-to-noise ratio for subarray k at the correlation filter input.

6.4 EVALUATION OF $\overline{\omega_B^2}$

The array beam characteristic $\overline{\omega_B^2}$ was defined previously (6-30)

$$\overline{\omega_B^2} = \frac{NA}{\sum_{n=1} [B'(n)]^2} \bigg/ \frac{NA}{\sum_{n=1} [B(n)]^2}$$

where (NA) is the number of samples in the correlation window, and the B(n)'s are the sampled values of the final version of the array beam at the end of the iterated correlation process. The B'(n)s are the sampled

values of the time derivative of the array beam, and they are obtained as described in the following paragraphs.

Let $b(t)$ be the trigonometric polynomial of lowest order which interpolates the data $\{B(n)\}$. Assuming that (NA) is a power of 2 (zeros may be added to the data, if necessary), set $M = NA/2$ and let

$$b(t) = (2M)^{-1} \sum_{m=-M}^M c_m \exp(i\pi m R t / M) \quad (6-37)$$

where R = sampling rate (samples/second).

The coefficients c_m in (6-37) may be obtained as follows. For $m = 0, 1, \dots, 2M-1$

$$C(m) = \sum_{k=0}^{2M-1} B(k+1) \exp[-i\pi k m / M] \quad (6-38)$$

is computed, which is the discrete Fourier transform of the data set $\{B(k+1) \mid k = 0, 1, \dots, 2M-1\}$. The coefficients c_m are as follows:

$$c_m = \begin{cases} C(m) & m = 0, 1, \dots, M-1, \\ C(2M+m) & m = -1, \dots, -(M-1) \\ (1/2) C(M) & m = \pm M. \end{cases} \quad (6-39)$$

By using the inverse transform relation

$$B(k+1) = (2M)^{-1} \sum_{m=0}^{2M-1} C(m) \exp[i\pi k m / M] \quad (6-40)$$

it may be shown that $b(k/R) = B(k+1)$ for $k = 0, 1, \dots, 2M-1$.

Hence, the continuous array beam may be assumed to be the function $b(t)$ defined above. The time derivative of this function is

$$b'(t) = (i\pi R) (2M)^{-1} \sum_{m=-M}^M (m/M) c_m \exp(i\pi m R t / M) \quad (6-41)$$

from which can be obtained the sampled values

$$\begin{aligned} B'(k+1) &= b'(k/R) \\ &= (i\pi R) (2M)^{-1} \sum_{m=-M}^M (m/M) c_m \exp(i\pi k m / M) \end{aligned} \quad (6-42)$$

According to Parseval's identity for the discrete Fourier transform, it is seen that

$$\sum_{k=0}^{2M-1} [B(k+1)]^2 = (2M)^{-1} \sum_{m=0}^{2M-1} |C(m)|^2 \quad (6-43)$$

Similarly,

$$\sum_{k=0}^{2M-1} [B'(k+1)]^2 = (\pi R)^2 (2M)^{-1} \sum_{m=0}^{2M-1} |D(m)|^2 \quad (6-44)$$

where

$$D(m) = \begin{cases} 1(m/M) C(m) & (m = 0, 1, \dots, M-1) \\ -1(2 - m/M) C(m) & (m = M+1, \dots, 2M-1) \\ 0 & (m = M) \end{cases} \quad (6-45)$$

The data set $\{(\pi R) D(m) \mid m = 0, 1, \dots, 2M-1\}$ is the discrete Fourier transform of the set $\{b'(k+1) \mid k = 0, 1, \dots, 2M-1\}$.

Furthermore, since $C(2M-m)$ and $D(2M-m)$ are the complex conjugates of $C(m)$ and $D(m)$, respectively, for $m = 1, \dots, (M-1)$,

$$\sum_{m=0}^{2M-1} |C(m)|^2 = |C(0)|^2 + |C(M)|^2 + 2 \sum_{m=1}^{M-1} |C(m)|^2 \quad (6-46)$$

and

$$\sum_{m=0}^{2M-1} |D(m)|^2 = 2 \sum_{m=1}^{M-1} (m/M)^2 |C(m)|^2 \quad (6-47)$$

It follows from the above results that the number $\overline{\omega_B^2}$ defined by (6-19) may be computed as follows:

$$\overline{\omega_B^2} = (\pi R)^2 \frac{\sum_{m=1}^{M-1} (m/M)^2 |C(m)|^2}{(1/2) |C(0)|^2 + (1/2) |C(M)|^2 + \sum_{m=1}^{M-1} |C(m)|^2} \quad (6-48)$$

in which R is the sampling rate (samples/second), $M = NA/2$, and $C(m)$'s are the discrete Fourier coefficients specified by (6-33).

The right side of (6-42) may be interpreted as a weighted average of the squared angular frequencies ω_m^2 with respect to the discrete power spectrum of the array beam $B(t)$, when $\omega_m = \pi R m/M$, where πR is the Nyquist frequency in radians per second. This fact justifies the notation $\overline{\omega_B^2}$.

6.5 U-SPACE ESTIMATION ERRORS

In the following discussion of the estimation errors associated with the reciprocal phase speeds (U_x, U_y) , it will be assumed that the wavefront shape is accurately known. Hence, an accurate station correction may be applied to the estimated arrival time delay for each subarray and it may be assumed thereafter that the wavefront is planar.

If t_k denotes the corrected time delay estimate for the k^{th} subarray, and if (X_k, Y_k) is the pair of position coordinates of the subarray center, then

$$t_k = -X_k U_x - Y_k U_y + e_k + t' \quad (6-49)$$

where e_k is the estimation error associated with t_k , and t' is the time of arrival of the planar wavefront at the origin of the spatial coordinate system.

Let NS denote the number of subarrays, where $\{w_k | k = 1, 2, \dots, NS\}$ is a set of nonnegative numbers such that

$$\sum_{k=1}^{NS} w_k = 1.$$

Then (6-49) remains valid if X_k and Y_k are replaced by $X_k - \sum w_j X_j$ and $Y_k - \sum w_j Y_j$, respectively, and if at the same time t' is replaced by $t' - U_x \sum w_j X_j - U_y \sum w_j Y_j$. These substitutions are equivalent to a translation of the origin of the spatial coordinate system to the center of gravity relative to the set of weights $\{w_k\}$, together with a corresponding modification of the time of arrival of the wavefront at the origin. The set of equations of the form in (6-49), for $k = 1, 2, \dots, NS$, may be written as

$$\underline{t} = A\underline{p} + \underline{e} \quad (6-50)$$

where

$$\underline{t} = \begin{bmatrix} t_1 \\ t_2 \\ \vdots \\ t_{NS} \end{bmatrix} \quad \underline{e} = \begin{bmatrix} e_1 \\ e_2 \\ \vdots \\ e_{NS} \end{bmatrix}$$

$$A = \begin{bmatrix} -X_1 - Y_1 & 1 \\ -X_2 - Y_2 & 1 \\ \vdots & \vdots \\ -X_{NS} - Y_{NS} & 1 \end{bmatrix} \quad \underline{p} = \begin{bmatrix} U_x \\ U_y \\ t' \end{bmatrix}$$

The problem of estimating the reciprocal phase speeds (U_x, U_y) may therefore be imbedded in a linear estimation problem described by (6-50), in which \underline{t} is a vector of observations, \underline{e} is the observation error vector, \underline{p} is a vector of unknown parameters, and A is a system matrix which describes the array geometry. This linear estimation problem is further specified by assuming that the observations are unbiased (so that the mean of \underline{e} is the zero vector), and correspond to NS independent observations (so that the covariance matrix of \underline{e} is positive definite). The covariance matrix of \underline{e} will be denoted by Q .

There are a number of possible solutions to the above-described type of linear estimation problem, and the following material will briefly discuss three that are frequently applied.

6.5.1 Least-Squares Estimate

If detailed information concerning the error variances is not available, but it is reasonable to assume that the errors are essentially independent and of about the same order of magnitude, then the least-squares estimate is commonly used. The least-squares estimate of \underline{p} is given by

$$\hat{\underline{p}}_{LS} = (A^T A)^{-1} A^T \underline{t} \quad (6-51)$$

where A^T is the matrix transpose of A , and $(A^T A)^{-1}$ is the inverse of the product matrix $A^T A$. The covariance matrix K_{LS} of the estimation errors associated with $\hat{\underline{p}}_{LS}$ is

$$K_{LS} = (A^T A)^{-1} A^T Q A (A^T A)^{-1} \quad (6-52)$$

but this clearly cannot be computed if Q is unknown.

6.5.2 Maximum-Likelihood Estimate

If the observation errors \underline{e} are assumed to be Gaussian, with zero mean vector and covariance matrix Q , then the maximum-likelihood estimate $\hat{\underline{p}}_{ML}$ is the unique choice of the vector \underline{p} which maximizes the log likelihood function

$$(-1/2) [\underline{t} - A\underline{p}]^T Q^{-1} [\underline{t} - A\underline{p}]$$

If this maximization is carried out, the result is

$$\hat{\underline{p}}_{ML} = (A^T Q^{-1} A)^{-1} A^T Q^{-1} \underline{t} \quad (6-53)$$

and the estimation error covariance matrix is

$$K_{ML} = (A^T Q^{-1} A)^{-1} \quad (6-54)$$

In this case, it is not necessary to assume that the estimate be linear in \underline{t} ; this follows from the linearity of (6-50) and the Gaussian error distribution.

6.5.3 Minimum-Variance (Unbiased) Estimate

In the two previous examples, the expected value of either $\hat{\underline{p}}_{LS}$ or $\hat{\underline{p}}_{ML}$ is \underline{p} ; i.e., the estimates are unbiased. If this desirable property is retained, and if it is required that the estimate be linear in \underline{t} , then the Gauss-Merkov theorem [6-7] shows the existence of a unique estimator given by

$$\hat{\underline{p}}_{MV} = (A^T Q^{-1} A)^{-1} A^T Q^{-1} \underline{t} \quad (6-55)$$

which minimizes the trace of the covariance matrix of estimation errors, subject to these constraints. In this case, the result is known as the minimum-variance unbiased estimate of \underline{p} . It is clearly the same as $\hat{\underline{p}}_{ML}$; similarly, the error covariance matrix is

$$K_{MV} = (A^T Q^{-1} A)^{-1} \quad (6-56)$$

which is the same as K_{ML} .

6.5.4 Computation of Estimates and Error Variances

The estimate given by (6-53) and (6-55) also turns out to be optimal for a large number of other meaningful error criteria [6-6]. Hence, if the necessary information is available, and if the required computations are not overly time consuming, this is a generally acceptable estimation procedure.

The components of the error vector \underline{e} are here assumed uncorrelated, so that Q is a diagonal matrix having the element η_k^2 in the k^{th} diagonal position. If w_k is defined as

$$w_k = \eta_k^{-2} / \sum_{k=1}^{NS} \eta_k^{-2} \quad (6-57)$$

and if the origin of the spatial coordinate system is translated to the center of gravity with respect to the weights $\{w_k\}$, then

$$A^T Q^{-1} A = (\sum \eta_k^{-2}) \begin{bmatrix} \sum w_k x_k^2 & \sum w_k x_k y_k & 0 \\ \sum w_k x_k y_k & \sum w_k y_k^2 & 0 \\ 0 & 0 & 1 \end{bmatrix} \quad (6-58)$$

The 2 x 2 matrix M, defined as

$$M = \begin{bmatrix} \sum w_k x_k^2 & \sum w_k x_k y_k \\ \sum w_k x_k y_k & \sum w_k y_k^2 \end{bmatrix} \quad (6-59)$$

may be interpreted as the moment of inertia matrix of the array with respect to the normalized weights $\{w_k\}$.

$$A^T Q^{-1} \underline{t} = (\sum \eta_k^{-2}) \begin{bmatrix} \sum w_k x_k t_k \\ \sum w_k y_k t_k \\ \sum w_k t_k \end{bmatrix} \quad (6-60)$$

Hence, the estimate of the arrival time t' is $\sum w_k t_k$, with estimation error variance $(\sum \eta_k^{-2})^{-1}$.

The estimate of the reciprocal phase velocity vector is

$$\hat{\underline{u}} = \begin{bmatrix} u_x \\ u_y \end{bmatrix} = M^{-1} \begin{bmatrix} \sum w_k x_k t_k \\ \sum w_k y_k t_k \end{bmatrix} \quad (6-61)$$

and the covariance matrix of estimation errors is

$$\text{cov}(\hat{\underline{u}}) = (\sum \eta_k^{-2})^{-1} M^{-1} \quad (6-62)$$

6.6 EXAMPLE: CIRCULARLY SYMMETRIC ARRAY WITH IDENTICAL ERRORS

Suppose that the variances η_k^2 of the time delay errors e_k are each equal to a common value η^2 . Then the covariance matrix of estimation errors of the reciprocal phase velocity \underline{u} , given by (6-62), reduces to

$$\text{cov } (\hat{\underline{u}}) = n^2 \begin{bmatrix} \Sigma X_k^2 & \Sigma X_k Y_k \\ \Sigma X_k Y_k & \Sigma Y_k^2 \end{bmatrix}^{-1} \quad (6-63)$$

The array will be said to have circular symmetry (with respect to a particular set of weights) if the in-plane moment of inertia matrix is invariant with respect to a rotation about the center of gravity. This will be true if and only if the off-diagonal elements of this matrix (the so-called product of inertia) are zero ($\Sigma X_k Y_k = 0$), and if the diagonal elements (the principal moments) are equal. Hence, for the case of equal weights, the conditions of $\Sigma X_k Y_k = 0$, and $\Sigma X_k^2 = \Sigma Y_k^2$ must be met. But note that $\Sigma X_k^2 + \Sigma Y_k^2 = (NS) R_g^2$, where R_g is the radius of gyration of the array about an axis through the center of gravity. Therefore, $\Sigma X_k^2 = \Sigma Y_k^2 = (NS) R_g^2/2$, and (6-63) becomes

$$\text{cov } (\hat{\underline{u}}) = \frac{2n^2}{(NS) R_g^2} \begin{bmatrix} 1 & 0 \\ 0 & 1 \end{bmatrix} \quad (6-64)$$

Hence, the estimation errors associated with the components U_x and U_y of \underline{U} are uncorrelated and identically distributed. Utilizing the result given by (6-36),

$$\text{Var } (\hat{U}_x) = \text{Var } (\hat{U}_y) = \frac{2}{\omega_B^2 R_g^2} \left[\frac{1}{(2BT) (NS) (SNR)} \right] \quad (6-65)$$

where (SNR) is the signal-to-noise power ratio of the subarray beam samples prior to correlation processing. The reciprocal of the expression in square brackets in (65) may be interpreted as the signal-to-noise ratio after integrating over the array beam and also over the correlation window.

The mean square distance (in \underline{U} -space) between \underline{u} and $\hat{\underline{u}}$ is

$$\overline{\delta U^2} = \frac{4}{\omega_B^2 R_g^2} \left[\frac{1}{(2BT) (NS) (SNR)} \right] \quad (6-66)$$

6.7 POSTERIOR PROBABILITIES FOR MULTIPLE PEAKS

If, at the conclusion of the correlation process, there is one and only one dominant peak in the correlation function for each subarray, then the results of the preceding sections show clearly how to obtain an optimal estimate of the U-vector: A precision $P_k = 1/\eta_k^2$ is computed for each subarray according to (6-36). If an error variance V_R is specified to account for the error in the region correction which modifies the arrival time estimate for each subarray, then the precision is modified according to the equation

$$P'_k = P_k / (1 + V_R P_k) \quad (6-67)$$

In the latter case, the weights w_k which are used in the estimate (6-61) are computed as

$$w_k = P'_k / \sum_{k=1}^{NS} P'_k \quad (6-68)$$

rather than the form given by (6-57). After translating the origin of the spatial coordinate system to the center of gravity of the array relative to the weights w_k , the U-vector estimate is computed according to (6-61), where the t'_k 's are the locations of the correlation peaks on the time axis, modified by the region corrections to account for wavefront curvature and local anomalies. Finally, the covariance matrix of estimation errors is also easily obtained according to (6-62).

However, because of the narrow-band character of most seismic signals and because of multipath effects and the effects of background noise in low magnitude events, there will frequently be a number of the correlation functions having more than one peak which must be considered as candidates for the arrival time estimate.

Suppose that, for a particular subarray, the correlation program produces M peaks, and let p_i be the probability (based only on information deducible from the correlation function) that the i^{th} peak is the correct one, so that

$$\sum_{i=1}^M p_i = 1.$$

Let t_i denote the estimated center of the i^{th} peak (modified by the region correction) and let η^2 be the error variance associated with this estimate.

It will be assumed that the information contained in the correlation function for this subarray is described by the probability density function

$$P_{\text{obs}}|t = \sum_{i=1}^M p_i \phi(t - t_i, \eta^2) \quad (6-69)$$

where

$$\phi(x, \sigma^2) = (2\pi\sigma^2)^{-1/2} \exp(-x^2/2\sigma^2)$$

is the Gaussian density function. The use of the Gaussian density function to describe the distribution of error in locating the center of a peak is justified by (6-9), if the noise amplitude has a near-Gaussian distribution. The determination of the prior probabilities p_i will be postponed until the following section.

The mean of the distribution of (6-69) is

$$\bar{t} = \sum_{i=1}^M p_i t_i \quad (6-70)$$

and the mean square is

$$\overline{t^2} = \sum_{i=1}^M p_i (t_i^2 + n^2) \quad (6-71)$$

Using these values, we may compute the variance as

$$\text{Var}(t) = \overline{t^2} - (\overline{t})^2 \quad (6-72)$$

Once the prior probabilities p_i have been determined, the means and variances of the distributions of the form of (6-69) for all the subarrays may be used as a basis for an estimate of the U-vector according to (6-61). Such an estimate is, in fact, useful for intermediate purposes, but it is generally unacceptable as a final estimate. This is true because the weights of those subarrays having multiple correlation peaks will be so small compared to those having only one dominant peak that the information contained in the former will be almost totally ignored in the U-vector estimate.

If an initial estimate is obtained using only those subarrays having a single, dominant correlation peak, and if this estimate is then used to aid in the selection of the correct peaks for the remaining subarrays, the information associated with the multiple-peaked subarrays might be incorporated in a much more efficient manner. The problem of sequentially updating the U-vector estimate after the selection of the correct peak will be discussed in a later section. At this point, a theoretical basis for the selection process will be established which is based on the computation and evaluation of a set of posterior probabilities.

Let the prior information (which exists at the time that a particular multip peaked correlation function with distribution in (6-69) is considered for processing) be described by

$$P_t = \phi(t - \tau, \sigma^2) \quad (6-73)$$

This prior information is assumed to be independent of that given by the distribution in (6-69) which has been generated by observation of the correlation function only.

Bayes' rule states that the conditional probability of t , based on the observed and the prior information, may be computed in the form

$$P_{t|obs} = \frac{P_{obs|t} \cdot P_t}{P_{obs}} \quad (6-74)$$

where P_{obs} is a normalizing constant, making $P_{t|obs}$ a valid probability density function.

Substituting (6-69) and (6-73) into (6-74) and combining the resulting products of Gaussian functions in order to isolate the unknown ' t ' yields.

$$P_{t|obs} = \frac{1}{P_{obs}} \sum_{i=1}^M p_i \phi(t_1 - \tau, \eta^2 + \sigma^2) \phi\left(t - \frac{\eta^2 \tau + \sigma^2 t_1}{\eta^2 + \sigma^2}, \frac{\eta^2 \sigma^2}{\eta^2 + \sigma^2}\right) \quad (6-75)$$

Assigning $c_1 = p_i \phi(t_1 - \tau, \eta^2 + \sigma^2)$, the relations may be expressed as

$$P_{obs} = \sum_{i=1}^M c_1,$$

and

$$P_{t|obs} = \frac{1}{P_{obs}} \sum_{i=1}^M q_i \phi\left(t - \frac{\eta^2 \tau + \sigma^2 t_1}{\eta^2 + \sigma^2}, \frac{\eta^2 \sigma^2}{\eta^2 + \sigma^2}\right) \quad (6-76)$$

where $q_i = c_i / P_{obs}$.

The various terms on the right side of (6-76) may be interpreted as follows:

$$a. \quad \phi \left(t - \frac{\eta^2 \tau + \sigma^2 t_1}{\eta^2 + \sigma^2}, \frac{\eta^2 \sigma^2}{\eta^2 + \sigma^2} \right)$$

is the probability distribution of t , given the information that the i^{th} peak is the correct one, and

b. q_i is the posterior probability that the i^{th} peak is the correct one.

The selection criterion might, for example, be based on the computation and determination of the maximum posterior probability q_i , and the comparison with a minimum threshold value.

6.8 OBSERVATION PROBABILITIES FOR MULTIPLE PEAKS

In the previous subsection, it was assumed that the signal arrival time information which is contained in a particular subarray correlation function having m significant peaks could be described by the probability density function in (6-69).

$$P_{\text{obs}}|t = \sum_{i=1}^M p_i \phi(t - t_i, \eta^2)$$

where t_i = location of the i^{th} correlation peak

η^2 = error variance associated with the location of the correlation peaks in the presence of noise

p_i = observed probability that the i^{th} correlation peak is the one which represents the actual signal arrival.

The following discussion is to establish a reasonable basis for computing the observation probabilities p_i , using only the information contained in the given multi-peaked correlation function.

The value of the i^{th} correlation peak is made up of a signal portion s_i and a noise portion n_i . Hence, the difference in heights, δ_{ij} , between the i^{th} and the j^{th} peak may be represented as

$$\delta_{ij} = (s_i - s_j) + (n_i - n_j)$$

Let the index i represent the largest of the m correlation peaks, and let j represent any arbitrary peak. Then δ_{ij} is nonnegative for all j , and the difference term $(s_i - s_j)$ will be nonnegative for all j if the i^{th} peak corresponds to the correct alignment between the filter characteristic and the incoming signal.

If the i^{th} peak is the correct one and if $R_s(\tau)$ is the auto-correlation function of the incoming signal, then

$$s_i - s_j = C[1 - R_s(t_i - t_j)]$$

where C is the true value of the correlation peak.

However, if the j^{th} peak represents the correct alignment between incoming signal and filter characteristic, then

$$s_i - s_j = -C[1 - R_s(t_i - t_j)]$$

since $R_s(t_i - t_j) = R_s(t_j - t_i)$. Henceforth, the hypothesis that the j^{th} peak is the correct one will be designated as H_j .

The noise term $(n_i - n_j)$ has zero mean and variance

$$\text{Var } (n_i - n_j) = 2\gamma^2 [1 - R_n(t_i - t_j)] \quad (6-77)$$

where γ^2 is the variance of either n_i or n_j separately, and $R_n(\tau)$ is the autocorrelation function of the output noise process.

According to the hypothesis H_1 , it follows that

$$n_i - n_j = \delta_{ij} - C[1 - R_s(t_i - t_j)] \quad (6-78)$$

Similarly, hypothesis H_j gives

$$n_i - n_j = \delta_{ij} + C[1 - R_s(t_i - t_j)] \quad (6-79)$$

If the noise term $(n_i - n_j)$ is assumed to be Gaussian, then the likelihood ratio of H_j relative to H_1 is:

$$\begin{aligned} L_{j1} &= \frac{\text{Prob } (H_j)}{\text{Prob } (H_1)} \\ &= \exp \left\{ \frac{\{\delta_{ij} - C[1 - R_s(t_i - t_j)]\}^2 - \{\delta_{ij} + C[1 - R_s(t_i - t_j)]\}^2}{2 \text{Var } (n_i - n_j)} \right\} \\ &= \exp \left\{ - \frac{C\delta_{ij}[1 - R_s(t_i - t_j)]}{\gamma^2 [1 - R_n(t_i - t_j)]} \right\} \end{aligned}$$

Furthermore, since the correlation filter is matched to the incoming signal, and since the noise at the filter input is white over the signal spectrum, it follows that the autocorrelation function $R_n(\tau)$ of the output noise process is equal to the autocorrelation function $R_s(\tau)$ of the input signal process. Hence, the likelihood ratio reduces to the simple expression

$$\begin{aligned} L_{j1} &= \exp \left\{ - \frac{C \delta_{1j}}{\gamma^2} \right\} \\ &= \exp \left\{ - (2BT) \frac{C^2}{(1 - C^2)} \frac{\delta_{1j}}{C} \right\} \\ &= \exp \left\{ - (2BT) (SNR) (\delta_{1j}/C) \right\}, \end{aligned} \quad (6-80)$$

where the latter expressions are obtained by substituting $\gamma^2 = (1 - C^2)/(2BT)$, and noting that $C^2/(1 - C^2)$ is the input signal-to-noise ratio (SNR) for the given subarray. The product $(2BT) (SNR)$ is the estimated signal-to-noise ratio at the filter output. The above expression for γ^2 is obtained by a derivation similar to that which produced (6-31), except that the coefficients a_n given by (6-27) are used in place of the coefficients b_n given by (6-28).

The observation probabilities p_j may be obtained from the formula

$$p_j = L_{j1} / \sum_{j=1}^M L_{j1} \quad (j = 1, 2, \dots, m,) \quad (6-81)$$

having the properties that

$$\sum_{j=1}^M p_j = 1,$$

and also $p_j/p_1 = L_{j1}$. This formula is not only intuitively reasonable, but it is also convenient for computational purposes since it depends entirely on quantities that are readily observed or estimated from the available data.

6.9 SEQUENTIAL UPDATING PROCEDURE FOR THE SLOWNESS VECTOR ESTIMATE

In this subsection we will describe the procedure for sequentially updating the U-vector estimate one subarray at a time, starting from some initial estimate and an associated error covariance matrix. Unless this initial estimate has been computed from some totally independent source, the diagonal terms of its error covariance matrix should be set quite large so that it has a negligible effect on the final estimate. On the other hand, if this is done, then any reasonable initial estimate will suffice to start the process.

The procedure which is described below is simply the sequential (Kalman) estimation [6-7] of (U_x, U_y) based on the linear model (6-49), and assumed independent errors e_k . Let

$$\underline{p} = \begin{bmatrix} U_x \\ U_y \\ t' \end{bmatrix} \quad \text{and} \quad \underline{a}_k = \begin{bmatrix} -X_k \\ -Y_k \\ 1 \end{bmatrix}, \quad k=1, 2, \dots, K,$$

where U_x and U_y are the rectangular components of the slowness vector; t' is the relative time of arrival of the wavefront at the center of gravity of the array, and X_k and Y_k are the rectangular coordinates of the k^{th} subarray center relative to the center of gravity of the array.

The relative time of arrival of the plane wavefront at (X_k, Y_k) is given by

$$t_k \text{ (plane)} = \underline{a}_k^T \underline{p} \quad (6-82)$$

where \underline{a}_k^T denotes the transpose of the vector \underline{a}_k .

The observed relative arrival time, based on an interpretation of the correlation function and a subsequent modification by a region correction term, is given by

$$y_k = t_k \text{ (plane)} + e_k \quad (6-83)$$

It will be assumed that e_k has zero mean (no observation or region correction bias) and known variance η_k^2 , and that the observation errors associated with any two distinct subarrays are uncorrelated. This latter assumption may be questionable, since the errors in the region corrections are undoubtedly slightly correlated.

If the arrival time observations are being processed sequentially, then it may be assumed at any stage that there exists a prior estimate $\hat{\underline{p}}$ of the state vector \underline{p} , and an error covariance matrix K associated with the estimate $\hat{\underline{p}}$. Each pass through the updating process will comprise the assimilation of a single observation y_k which has not previously been processed, along with a revision of the error covariance matrix using the variance η_k^2 of the observation error e_k .

Assuming that $(k-1)$ observations have been processed, let $\hat{\underline{p}}(k-1)$ and $K(k-1)$ denote the current estimate of \underline{p} and the associated covariance matrix, respectively. Ignoring for the moment both the rationale for choosing the next subarray to be processed and the detailed interpretation of the correlation function generated by this subarray, the text will describe the updating process for the observation y_k with error variance η_k^2 and for the subarray whose location is specified by the vector \underline{a}_k .

The optimal linear updating process in the minimum variance sense is described as follows:

- a. Compute the residual

$$\delta y_k = y_k - \underline{a}_k^T \hat{\underline{p}}(k-1) \quad (6-84)$$

which is the difference between the observed and predicted arrival times for a plane wavefront.

- b. Compute the optimal gain vector

$$\underline{b}(k) = K(k-1) \underline{a}_k \left(\underline{a}_k^T K(k-1) \underline{a}_k + \eta_k^2 \right)^{-1} \quad (6-85)$$

where the quantity within parentheses may be recognized as the total variance of the observation or, equivalently, the variance of the residual.

- c. Compute and save the updated estimate of the state vector

$$\hat{\underline{p}}(k) = \hat{\underline{p}}(k-1) + \underline{b}(k) \delta y_k \quad (6-86)$$

- d. Compute and save the updated covariance matrix

$$K(k) = \left[I - \underline{b}(k) \underline{a}_k^T \right] K(k-1) \quad (6-87)$$

where I is the identity matrix.

Furthermore, if all of the observation errors and the errors of the prior estimate which is used to start the process are Gaussian and independent, then the estimation errors throughout the process remain Gaussian. In this case, the optimal linear estimate is, in fact, optimal in the minimum variance sense.

6.10 AN ALGORITHM FOR THE SEQUENTIAL ESTIMATION OF THE SLOWNESS VECTOR

In this subsection, an algorithm for the sequential estimation of the U-vector is described including the decision-making processes which apply whenever a subarray having a multipeaked correlation function is encountered. It is assumed that, prior to the initiation of this algorithm, the correlation process has been completed and the results have been analyzed and reduced to parametric form.

Specifically, the following information must be available for each subarray:

- a. The number of peaks of the correlation function which are likely candidates for the one which indicates the true wavefront arrival
- b. The magnitude (peak value) of each of these peaks
- c. The estimated location, relative to an arbitrary but fixed reference, of each of these peaks
- d. The a priori probability p_{ik} associated with each of these peaks
- e. The precision (reciprocal variance) of the estimation error associated with the location of each peak.

The details of the algorithm are given by the functional flow diagram shown in Figure 6-2.

Whenever a subarray is encountered which has multiple peaks, the posterior probabilities q_{ik} are computed using the best prior information which is available. There are two prior estimates of the wavefront arrival time which must be considered; namely, the one based on the current U-vector estimate and the one based on the final U-vector estimate from the previous pass used to initialize the current process.

The error variances of both arrival time estimates for the subarray in question are computed and compared, and the estimate having the smallest error variance is adopted as the prior information in the computation of the q_{ik} 's. The maximum posterior probability for the subarray k in question is determined and designated as Q_k , and the associated peak becomes the prime candidate for the true wavefront arrival.

The decision-making process is controlled by two system parameters, Q_L and Q_U , where $0 \leq Q_L < Q_U \leq 1$. The functions of these parameters may be described as follows:

- a. No subarray having maximum posterior probability less than Q_U will be processed until it has been determined that there are currently no remaining subarrays with $Q_k > Q_U$.
- b. No subarray will be processed for which the maximum posterior probability Q_k is less than Q_L .
- c. If all remaining subarrays have multiple peaks, with maximum posterior probability $Q_k < Q_U$, and if at least one subarray remains having $Q_k > Q_L$, then the subarray for which Q_k is maximum will be processed.

The sequential estimation process terminates when either all subarrays have been processed or there is no subarray remaining with $Q_k > Q_L$. At this point, the parameter NP is equal to the total number of subarrays which have been processed.

The initial estimate which is used to start the sequential process is the final estimate from the previous pass. The initial covariance matrix is obtained by multiplying the covariance matrix from the previous pass by a large, positive scalar. On the first pass, the estimate and covariance matrix given by (61) and (62), respectively, may be applied as described in Section 6.8 to obtain a set of initializing values.

6.11 ANNOTATED BIBLIOGRAPHY

The references listed here are divided into two groups. Subsection 6.11.1 consists of periodic reports prepared by IBM. Miscellaneous other references constitute subsection 6.11.2.

6.11.1 IBM Quarterly and Final Reports

- 6-1. "Large Aperture Seismic Array Signal Processing Study,"
IBM Final Report, Contract SD-296, 15 July 1965.

Section 1 discusses LASA beamforming and compares conventional delay-and-sum, weighted delay-and-sum, and filter-and-sum beamforming techniques. Sections 2 and 4 discuss LASA beam patterns and Appendix A presents the beam pattern programs. Appendix B describes a seismic ray-tracing program. The seismic wavefront shape and parameterized models are discussed in Appendices C, D, and G.

- 6-2. "LASA Experimental Signal Processing System," IBM
Third Quarterly Technical Report, Contract F19628-
67-C-0198, ESD-TR-68-149, August 1967.

The initial version of the time delay correlation process, together with experimental results based on scaled Longshot data, is derived in Appendix II.1. Appendix II.3 describes a version of the adaptive beam-forming process known as fidelity optimum processing.

- 6-3. "LASA Experimental Signal Processing System," IBM
Final Technical Report, Contract F19628-67-C-0198,
ESD-TR-69-60, Volume I, March 1969.

Appendix VII specifies and describes an Event Processor which was considered for implementation in the ESPS; subsection VII.5 describes a correlation beamsteering process and subsection VII.6 presents system specifications for a beampacking process.

- 6-4. "Integrated Seismic Research Signal Processing System,"
IBM Fifth Quarterly Technical Report, Contract F19628-
68-C-0400, ESD-TR-70-306, November 1969.

Appendix V reports a "channel-recursive Bayes' processing" technique for array beamsteering, which incorporated a parameterized model for a seismic signal, and estimates both the signal parameters and the array beamsteering parameters. Appendix VI provides the theoretical basis for the correlation beamsteering process and describes an extension of this process which utilizes sequential estimation and Bayesian decision techniques to avoid the cycle-skipping problem which frequently arises in the correlation beamsteering process.

- 6-5. "Integrated Seismic Research Signal Processing System,"
IBM Eleventh Quarterly Technical Report, Contract
F19628-68-C-0400, ESD-TR-72-133, May 1971.

Appendix VI describes the ISRSPS Event Processors, which were implemented at SAAC and NDPC, respectively; Subsection VI.4.1 describes the array beamsteering processes. Appendix VII reports the results of applying the SAAC ISRSPS processor to scaled seismic event data; the EP results, which provide some insight into the performance of the correlation and the beampacking processes, are presented in Subsection VII.5.2.

6.11.2 Miscellaneous References

- 6-6. H. L. Van Trees, Detection, Estimation, and Modulation Theory, Part I, John Wiley and Sons, Inc., New York, 1968.

This book includes an extensive discussion of maximum likelihood estimation techniques. The conditions are described for which maximum likelihood estimation and minimum variance estimation yield the same results. Also it is shown that these estimates are optimal for many other error criteria.

- 6-7. David G. Luenberger, Optimization by Vector Space Methods, John Wiley and Sons, Inc., New York, 1969.

The Gauss-Markov Theorem and its applications are discussed in a vector-space context.

Section 7

TIME ANOMALIES

A seismic disturbance impinging on a planar array of seismometers can be approximately modeled by a wavefront of some simple shape traveling across the array with a fixed velocity. According to this model, the relative arrival times are exact functions of only the sensor locations together with the wavefront shape and velocity. Furthermore, within the context of this simple model, the same signal is received at each instrument at the appropriate relative arrival time. Beamforming, the process of delaying each of the sensor outputs by the appropriate time delay (the negative of the relative arrival time) and summing the resulting signal waveforms, is generally done in order to achieve a gain in the signal-to-noise power ratio. Under certain ideal conditions, this gain equals the number of sensors. Failure to achieve this ideal gain may be attributed to the following factors: (a) signal incoherence, (b) noise coherence, (c) signal amplitude variations, and (d) beamforming delay errors. The purpose of this section is to discuss refinements in the computation of beamforming delays in order to reduce the last source of error.

The plane wavefront model provides a reasonably accurate approximation to the actual beamforming delays, particularly for events occurring at teleseismic distances from the array. Deviations from this model may be regarded as measurable and repeatable corrections. The plane wavefront model results in the mathematically simple computation of the sensor delays as $t_1 = \vec{u} \cdot \vec{r}_1$, where \vec{u} is the two-dimensional vector describing the wavefront direction and slowness, and \vec{r}_1 is the relative location vector of the i^{th} sensor with respect to the origin of the array coordinate system. Time anomalies are defined as the differences between the delays predicted by an appropriately chosen plane wavefront model and the perfect beamforming delays.

Experience with LASA data has shown that beamforming with plane-wave delays alone results in power losses of two to four dB [7-4, page 69] as compared to beamforming with perfect delays. Somewhat higher power losses will occur at NORSAR because of the higher frequencies sometimes observed at the Norway array. Thus, beamforming without the use of time anomalies results in a decrease in the detection capability of 0.1 to 0.2 magnitude units at LASA and in a somewhat greater decrease at NORSAR. From these numbers it is clear that a significant increase in the performance of the array may be realized if the time anomalies are accurately determined and applied to the beamforming delays.

The primary application of time anomaly data is for computing accurate delays for detection beams in order to maximize the beamforming gains. Since delays for the detection beams must be known before the event occurs, any time anomaly data for detection beam delays must be derived from previous events.

Due to the curvature of the actual wavefront, a significant error in estimating the mean plane-wave vector can occur as a result of the loss of outer array sensors. This error leads to a corresponding error in the estimation of the event geographic location. A secondary use for time anomaly data is to flatten (effectively) the wavefront and thus minimize these location errors [7-10, pp. 31-32].

Data gathered from NORSAR and LASA confirms the fact that time anomalies are essentially independent of time. The time anomalies seem to be a function only of sensor location and wavefront direction (inverse velocity) [7-11]. There is no apparent correlation between subarray relative time anomalies and the short-period propagation phase [7-12]. From a data processing viewpoint, the objective in utilizing time anomaly data is to develop practical means for estimating, storing, and retrieving time anomaly values.

It is not necessary to understand the specific physical causes of time anomalies in order to measure and use them properly in a signal processing system. However, for those interested in the earth structure under the array, time anomalies may provide useful information.

The following sections discuss elementary physical causes of time anomalies, methods of estimation, applications, and techniques for achieving practical computer storage and lookup procedures for the time anomaly data.

7.1 BASIC THEORY

For array signal processing purposes, the signal wavefront must be expressed as a set of relative arrival times of the wavefront at the array sensors. The negatives of the relative arrival times, shifted by a constant bias factor to ensure that all values are non-negative and quantized to the data sampling interval, are the time delays used in the beamforming operation. The plane wavefront model provides a convenient computational algorithm for approximating the beamforming delays as functions of the wavefront velocity and the known sensor locations.

Unfortunately, this simple model is not sufficiently accurate for state-of-the-art array signal processing tasks, when the full potential capability of the array processing system must be utilized for the detection and characterization of small seismic signals. It will be shown below that losses as great as 5 dB would occur in some instances if no provision was made for a more accurate representation of the beamforming delays.

The improved accuracy is obtained by the application of correction terms to the initial plane-wave delay estimates. No simple mathematical model

exists for the computation of these correction terms, but a technique has been devised and implemented for the table lookup and interpolation of the delay corrections, or time anomalies, from a precompiled data base. The remainder of this section contains basic theoretical considerations and empirical results which have guided the development of the implemented technique.

7.1.1 Inverse Velocity Space

The plane wavefront model is most conveniently represented in terms of the components of the inverse velocity (slowness) vector, because the relative arrival times are linearly related to these components. Hence, the estimation of inverse velocity from a set of relative arrival time data is achieved using standard linear estimation techniques, and the computation of a given slowness vector is quite efficient. Furthermore, as discussed in Section 2, the relative beam loss contours due to missteering are invariant when represented in U-space, which is the projection of the three-dimensional inverse velocity space onto the plane of the array. Another related invariance property of the inverse velocity will be described below.

The propagation group velocity for seismic waves depends in general on the wavelength, the density and elasticity of the propagation medium, and the mode of propagation (transverse (S) waves or longitudinal (P) waves). The dependency of velocity on wavelength constitutes dispersion, and is almost entirely negligible for seismic body waves. Therefore, the propagation velocity for either P or S waves will be essentially constant in any region which is homogeneous with respect to density and elasticity. Within the continental crust, P-wave velocities typically range from 5 to 7 kilometers/second, and S-wave velocities from 3 to 4 kilometers/second. Within the earth's mantle region, P-waves typically propagate at

velocities between 8 and 13.5 kilometers/second, and S-waves at velocities between 4.5 and 8 kilometers/second. Furthermore, propagation velocity typically increases with depth, so that the lower values of the above ranges are typical for the outer portions of the corresponding regions.

If \vec{v}_c denotes the three-dimensional propagation velocity vector of an arbitrary wavefront at some point, then the inverse velocity vector \vec{u}_c is defined as

$$\vec{u}_c = \frac{\vec{v}_c}{|\vec{v}_c|^2} \quad (7-1)$$

Note that the magnitudes of both the velocity and inverse velocity vectors are bounded away from both zero and infinity for actual seismic waves. The time required for a plane wavefront with inverse velocity \vec{u}_c to travel from the origin of the array coordinate system to the k^{th} sensor is

$$t_k = \vec{u}_c \cdot \vec{p}_k \quad (7-2)$$

where $\vec{p}_k = [x_k, y_k, z_k]^T$ is the position vector of the k^{th} sensor. It will be assumed in the following that the x, y and z axes of the array coordinate system are aligned with the east, north and vertical directions, respectively.

The inverse velocity vector $\vec{u}_c = [u_x, u_y, u_z]$ may be decomposed into a horizontal component $\vec{u} = [u_x, u_y]$ and a vertical component with magnitude u_z . Since the array is approximately in the horizontal plane, the $u_z z_k$ terms in equation (7-2) for $k = 1, 2, \dots, K$ deviate only slightly from their average value, and therefore may be regarded as a second-order effect in the computation of relative time delays. Equivalently, if a set of relative arrival time data is measured

for a given signal arrival, the components of the horizontal vector \vec{u} are observable in the sense that they can be estimated from the data with reasonable accuracy whereas the component u_z of the vertical vector is essentially unobservable because it cannot be estimated from the data without incurring a large estimation error.

Therefore, the observation space of interest for a large, horizontal planar array is the projection of the three-dimensional inverse velocity space onto the horizontal plane. Henceforth, this observation space will be referred to simply as U-space, and the horizontal projection of \vec{U}_c will be called the u-vector. If the propagation velocity vector \vec{V} has magnitude V and is inclined at an angle ϕ from the vertical, then the magnitude u of the u-vector is

$$u = \frac{\sin \phi}{V}. \quad (7-3)$$

By Snell's Law, u is invariant across any horizontal refraction boundary. Clearly, since V is bounded, U-space has finite extent, and the value $u = 0$ is possible for waves propagating vertically from the core.

7.1.2 Physical Causes of Time Anomalies

If $\vec{r}_k = [x_k, y_k]$ denotes the horizontal projection of the position vector \vec{P}_k , then the plane-wave having inverse velocity \vec{u} travels from the origin of the two-dimensional array coordinate system to the point represented by \vec{r}_k in $\vec{u} \cdot \vec{r}_k$ seconds. Let t_k denote the travel time of an actual wavefront from the origin to the position \vec{P}_k (which is not necessarily located on the array coordinate plane), and define the time anomaly δt_k associated with \vec{P}_k as the difference

$$\delta t_k = \vec{u} \cdot \vec{r}_k - t_k. \quad (7-4)$$

The precise relationship between the u -vector and the set of arrival time data $\{t_k; k=1,2,\dots,K\}$ will be discussed in Section 5.2. For the time being, it will simply be assumed that the plane wavefront associated with \vec{u} represents a reasonable approximation to the actual wavefront.

The physical causes of time anomalies which are discussed below include the following:

- a. Wavefront curvature due to propagation from a small source region through a spherically stratified earth.
- b. The effects of variations in instrument depth due to the neglect of the $u_z z_k$ term in the plane-wave model.
- c. Variations in the propagation velocity under different parts of the array.
- d. Variations in the propagation path due to reflection and refraction of the wavefront beneath the array and near the source.

Although the models to be presented are somewhat oversimplified, they nevertheless provide a means to estimate quantitatively the effects of the most significant physical causes.

Time anomalies are first examined for a spherical earth which is layered in a spherically symmetric fashion, i.e., for which the propagation speed is a function only of the radial distance to the earth's center. In addition, the array is assumed to be at the earth's surface; i.e., all of its seismometers are assumed to be at the same radial distance from the earth's center. The source is taken to be in the earth's crust.

For a wavefront whose reciprocal phase speeds at the array center are (u_x, u_y) , the time anomalies δt_k are given by the following expression,

where higher order terms have been neglected:

$$\delta t_k(u_x, u_y) = \frac{1}{2} a(x_k \cos \beta + y_k \sin \beta)^2 + \frac{1}{2} b(-x_k \sin \beta + y_k \cos \beta)^2 \quad (7-5)$$

$$k = 1, 2, \dots, K$$

Here β is the bearing of the wavefront at the array center, i.e., $\beta = \arctan(u_y/u_x)$. The coefficients a and b are

$$a = \frac{1}{R_E} \frac{du}{d\Delta}; \quad b = \frac{u}{R_E} \cot \Delta$$

where $u = \left(u_x^2 + u_y^2\right)^{\frac{1}{2}}$ is the reciprocal horizontal phase speed of the wavefront at the array center, Δ is the angular great circle distance from the source to the array center, and R_E is the earth's radius. The quantities a and b are measured in sec/km^2 . They can be calculated by means of ray-tracing. The error in (5-5) associated with neglecting the higher order terms is less than 0.015 seconds within LASA (i.e., for the point (x_k, y_k, z_k) on the earth's surface within 100 km from the LASA center), and the error within NORSAR is less than 0.004 seconds. Table 7-1 lists some typical values for u , a , and b as functions Δ .

Table 7-1. Typical Values for u , a , and b

$\Delta(^{\circ})$	$u \left(\frac{\text{sec}}{\text{km}} \right)$	$a \left(\frac{\text{sec}}{\text{km}^2} \right)$	$b \left(\frac{\text{sec}}{\text{km}^2} \right)$
30.75	0.08006	-0.244×10^{-5}	2.11×10^{-5}
40.11	0.07535	-0.586×10^{-5}	1.40×10^{-5}
93.41	0.04160	-0.565×10^{-5}	-0.045×10^{-5}

Note that a and b are of opposite signs when the range Δ is less than 90° , indicating a saddle-shaped apparent wavefront received by the array. For Δ larger than 90° , the apparent wavefront is convergent.

The anomalies δt_k are largest for Δ about 30° . Assuming a maximum distance of 100 km from the array center, it is seen that δt_k typically will not be in excess of about 0.2 sec when $\Delta = 30.75^\circ$. These large values are primarily due to spherical spreading of the disturbance. For ranges on the order of 90° , δt_k is much smaller and normally will not exceed about 0.05 sec. The spherical spreading is nearly zero at these ranges.

Although the values of δt_k for angular distances Δ of about 90° are small enough to be ignored, the values of δt_k of about 0.2 sec for Δ about 30° must be compensated when computing array beam delays.

The above considerations assumed a perfectly spherically stratified earth and did not allow for geological differences between subarray sites. Yet, with distances of up to 200 km between subarrays, such geological variations from one subarray site to another may effect substantially the steering delay anomalies δt_k . The effects of variable instrument depth and variable propagation velocity are examined next.

The mathematical model to be used is depicted in Figure 7-1. It assumes that the earth is homogeneous below a flat horizontal boundary H , and that the teleseismic wavefronts in this region are indeed planar. This horizontal boundary is assumed to be located at a mean depth L below the array site.

The model does not require all subarrays to be at the same horizontal level. Thus, if L_k denotes the depth of the boundary plane H below the k^{th} subarray, these depths L_k ; $k = 1, \dots, K$ need not be the same, but are allowed to vary from one subarray to another. L is defined to be the arithmetic average of all L_k 's.

A teleseismic disturbance, after crossing the boundary plane H on its way to the k^{th} subarray, is assumed to travel at an average speed v_k , which is independent of the direction of travel. However, in order to account for geological differences between subarray sites, v_k is permitted to vary from one subarray site to another.

In spite of its simplicity, the assumption that the average propagation speed, v_k , from the boundary H to the k^{th} subarray is independent of the direction of travel appears to be quite accurate, owing to the large horizontal teleseismic phase speeds (>12.5 km/sec) compared with the low average crustal speed (about 6 km/sec) below the array site. The validity of the assumption for various horizontally stratified, crustal velocity profiles can be readily checked.

The depth L at which the boundary H in the model is placed below the array should be so chosen that the major portion of the geological variations across the actual array site indeed takes place within this depth region. Hence, it is reasonable to choose L to be the average crust thickness at the array site (about 45 km for LASA). Little is known about the variations of the mean propagation speed, v_k , under the arrays. Inspection of various crustal models with their possible velocity ranges indicates that a maximum variation of 2 km/sec among the v_k 's appears to be excessive. Thus, it is assumed that $L = 45$ km and that the v_k 's ($k=1, 2, \dots, K$) are uniformly distributed over an interval with a width of 1 km/sec. The midpoint of this interval will be denoted by v .

In order to present a formula for the time anomalies δt_k , a reference planar wavefront is needed for comparison. Let it be defined as the (fictitious) planar wavefront which would have arrived at the array if (a) the region above the boundary H would also have been homogeneous with the propagation velocity v (defined above as an average of the v_k 's), and (b) all subarrays would have been in the same horizontal plane such that the boundary H would have been at the depth L below the array

(L being the average of the L_k 's). The situation is depicted in Figure 7-1, where AF is the actual path of the teleseismic disturbance from H to the k^{th} subarray, while EBD is the path of the fictitious disturbance to the fictitious location D of the k^{th} subarray. According to the definition given in equation (4), $\delta t_k(u)$ is the time difference between the paths EBD and AF. Thus, the following relationship is established:

$$\delta t_k(u) = L \left(\frac{1}{v^2} - u^2 \right)^{\frac{1}{2}} - L_k \left(\frac{1}{v_k^2} - u^2 \right)^{\frac{1}{2}} \quad (7-6)$$

To estimate the magnitude of $\delta t_k(u)$, note that u lies between 0.04 sec/km and 0.08 sec/km for teleseismic P-waves, and that the crustal mean speeds v and v_k are on the order of 6 km/sec. It is already assumed that $|v - v_k| \leq 0.5$ km/sec. Taking $L = L_k = 45$ km, one finds that $|\delta t_k| \leq 0.8$ sec. Also, for $v = v_k = 6$ km/sec, $|\delta t_k| \leq 0.16 |L_k - L|$ sec.

The model in Figure 7-2 shows the effect of a local variation in the depth of the crust under a subarray relative to the average or nominal crust depth under the entire array. In this case, the anomaly is the difference in travel time between path CB and path AB. This difference is given by

$$\delta t_k(u) = h_k \left(\frac{1}{w^2} - u^2 \right)^{\frac{1}{2}} - h_k \left(\frac{1}{v_k^2} - u^2 \right)^{\frac{1}{2}} \quad (7-7)$$

For $w = 8$ km/sec and $v_k = 6$ km/sec, equation (7-7) yields $|\delta t_k| \leq 0.05 |h_k|$ sec.

The model in Figure 7-3 shows the effect of a local variation in the slope of the crust-mantle boundary under a subarray. Ignoring the effects of the associated changes in crust depth, which are given by equation (7-7),

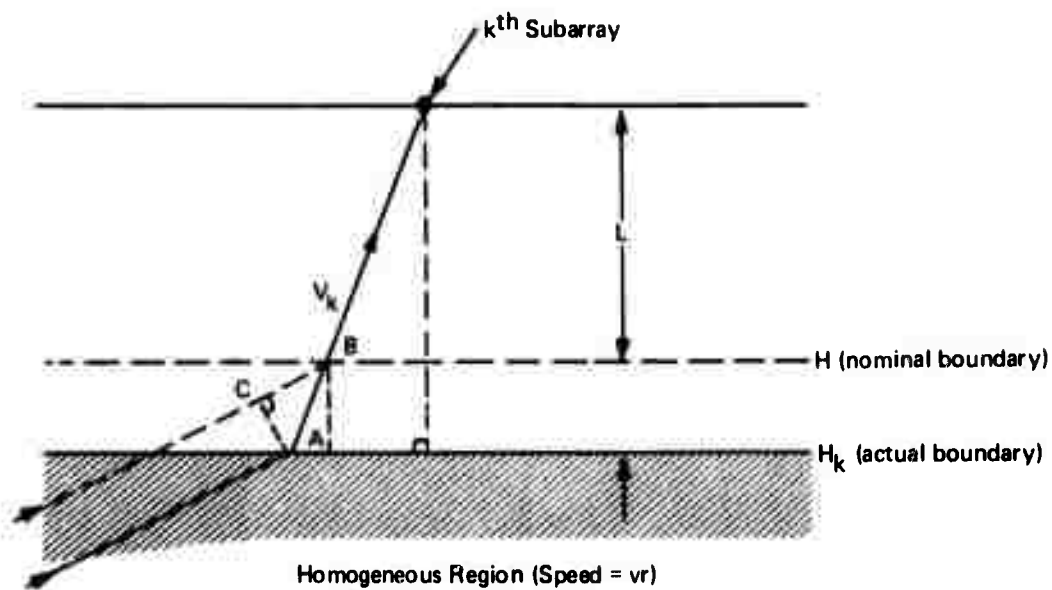


Figure 7-2. Earth Model Showing Variation in Depth of Crust

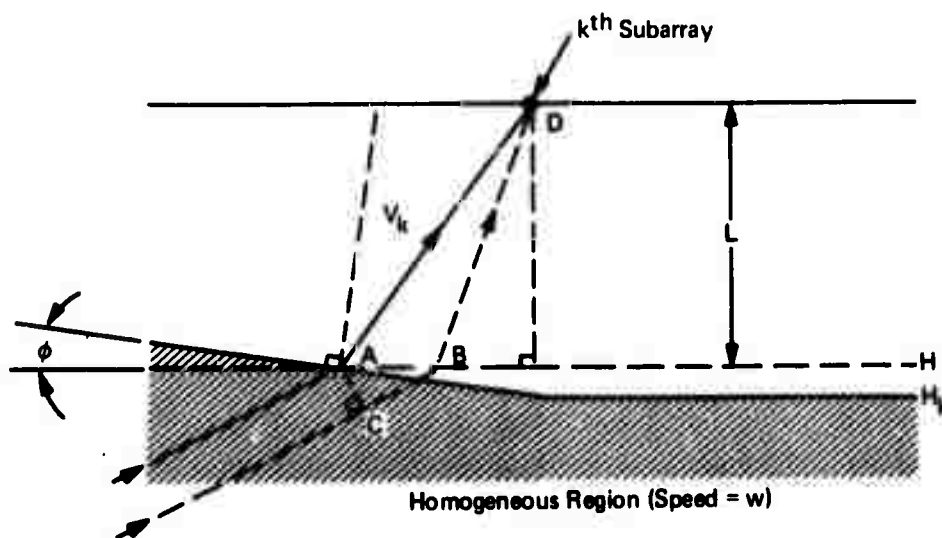


Figure 7-3. Earth Model Showing Local Variation in Slope at Crust-Mantle Boundary

the time anomaly due to the slope only is given by the travel time difference between path CBD and path AD in Figure 7-3. This difference is negligible in the sense that it is of second order with respect to the angle ϕ .

The diagram in Figure 7-3 may also be used as a model for the effects of an average tilt in the crust-mantle boundary underneath the entire array. Assume that the average boundary plane is tilted at an angle ϕ , and consider an incoming plane wave with propagation vector which is coplanar with normal vectors to the boundary plane, and the horizontal speeds in the mantle and the crust are given by w and v , respectively. If θ denotes the angle of inclination of the propagation vector in the mantle relative to the vertical, then $u = (\sin \theta)/w$ is the magnitude of the projection of the associated inverse velocity vector onto the horizontal array plane. If the tilt angle ϕ is zero, then u remains unchanged as the wavefront crosses the boundary, according to Snell's Law. Therefore, assuming constant average velocity in the crust, u is the magnitude of the observed slowness vector at the array.

If the tilt angle ϕ is non-zero, then the projection of the inverse velocity vector in the mantle region onto the boundary plane has magnitude u' given by

$$u' = u \cos \phi - \left(\frac{1}{v^2} - u^2 \right)^{\frac{1}{2}} \sin \phi \quad (7-8)$$

In this case, Snell's Law states that u' remains unchanged across the boundary plane. If the resulting inverse velocity vector in the crust is projected onto the horizontal array plane, the magnitude u'' of the projection is given by

$$u'' = u' \cos \phi + \left(\frac{1}{v^2} - (u')^2 \right)^{\frac{1}{2}} \sin \phi \quad (7-9)$$

Therefore, according to this simplified model, the wavefront observed at the array is a plane wavefront (i.e., it has no relative time anomalies), and the observable component of the associated inverse velocity vector has magnitude u . This result is distinguished from the previously considered effects in that they yielded only relative time anomalies.

It should be noted that a similar refraction phenomenon may occur near the source of the energy, and also that the equations become somewhat more complex when the vectors discussed above are not all coplanar. However, the essential aspect of refraction effects due to non-horizontal boundary planes is that the presence of these effects cannot be determined from array observations alone. The difference between the u -vector that is actually observed and the u -vector which would correspond to the relative travel times from the energy source to the various array sensors according to a simple spherically stratified earth model must be determined on the basis of an external reference for the energy source location.

In the ISRSPS systems, the corrections which are applied to observed u -vectors in order to force them into correspondence with a spherically stratified earth model are called U-space location calibration vectors. Furthermore, a distinction must be made in all references to U-space, either explicitly or implicitly, between calibrated and observed U-space.

For array processing system design purposes, the above discussion and extension of it to related models may be summarized as follows:

- a. The relative time anomaly factors associated with spherical earth effects (equation (7-5)), as well as those associated with the variable depths of sensors (equation (7-6)), are generally predictable on the basis of relatively simple models having known or easily measured parameters. However, the

relative time anomaly factors associated with variable propagation speeds (equation (7-6)) and with variable crust depth (equation (7-7)) can only be predicted on the basis of a detailed model of the earth's structure under the entire array. Furthermore, it must be assumed that the actual refractions which occur underneath the array are considerably more complex than those described in the simplified models above.

- b. The relative time anomaly contributions which can be predicted from simple models are of approximately the same magnitude as the contributions which are produced by complex mechanisms.
- c. The physical causes of relative time anomalies may be regarded as separate from those of u-vector observation errors.
- d. The relative time anomalies are observable from the array output data whenever individual signal arrival times can be measured.
- e. The relative time anomalies apparently depend almost entirely on the earth's structure beneath the array, and therefore should be repeatable for arrivals having the same observed u-vector.
- f. The errors in the u-vector are unobservable using only array output data; an external reference location of the energy source must also be used in conjunction with a spherical earth model.
- g. The U-space calibration vectors should be repeatable as a function of the observed u-vector and the seismic phase. Knowledge of the seismic phase is important because of the reflections and refractions which occur at boundaries not local to the array.
- h. The physical models shown in Figures 7-1 and 7-2 may be used to demonstrate that relative time anomalies between sensors within a subarray may generally be regarded as negligible, unless the sensor depths vary considerably within the subarray.

1. The model shown in Figure 7-3 serves to demonstrate the fact that two or more distinct propagation paths may exist for some subarrays for a given wavefront. For example, if the shape of the actual boundary in Figure 7-3 were somewhat modified, then the two paths AD and CBD might exist simultaneously. If the travel times along simultaneous paths are approximately equal, then signal reinforcement results; this is undoubtedly one of the causes for the subarray relative amplitude anomalies discussed in Section 3.4. However, if these travel times are significantly different, then distinct multiple arrivals will be present in the signal waveform as discussed in [7-13]. These multiple arrivals have been considered in the development of the correlation beamsteering process (see Section 6).

7.2 SYSTEM APPLICATIONS AND ESTIMATION TECHNIQUES

The significant property of relative time anomalies for array signal processing purposes is their repeatability as a function of U-space location only. This repeatability makes it possible to estimate the relative time anomalies from signal waveforms having large signal-to-noise ratios and distinct signal characteristics, and to utilize these relative time anomalies in the ISRSPS DP and EP systems for processing future signals having (approximately) the same U-space locations. Furthermore, if the variation of the relative time anomaly values as a function of U-space is reasonably smooth, the interpolation over U-space among previously estimated values becomes feasible.

Clearly, the techniques which are used to estimate relative time anomaly values must be compatible with the intended uses of these values in the DP and EP systems. For example, if any residual u-vector component remains in a set of estimated relative time anomaly data, then any set

of planewave delays to which this time anomaly data is applied will be resteeered by the amount of this residual u-vector. Furthermore, if multiple arrivals exist in a signal waveform which is being used for the estimation of relative time anomalies, then it must be determined whether the initial arrival time is the appropriate one to use for all system applications. There are also compatibility considerations which must be resolved relative to the estimation and application of U-space location calibration data.

The array signal processing applications of time anomaly data are discussed in Section 7.2.1, and the possible estimation techniques to be used in generating a time anomaly data base are compared in Section 7.2.2.

7.2.1 Applications of Time Anomaly and Calibration Data

The primary application of time anomaly data in the ISRSPS is for computing accurate delays for detection beams so as to maximize the system detection capability. Since delays for the detection beams must be known before the event occurs for online detection processing, the time anomaly data for these beam delays must be derived from previous events. The method of computing DP beamforming delays using time anomalies interpolated from a prestored data base is given in Section 5.2.2.3.

It was noted in Section 5.3.2.2 that the relative beamforming loss associated with a set of residual delay errors having variance σ_T^2 is given by equation (5-9), repeated here for convenience.

$$\text{Beamforming Loss} = (10 \log_{10} e) (2\pi f \sigma_T)^2 \text{ dB}$$

If planewave delays alone are used for beamforming, with no application of time anomaly data, then the loss given by the above formula for LASA

is typically from 2 to 4 dB. The corresponding losses for NORSAR are sometimes greater than 5 dB, because of the higher signal frequencies observed at NORSAR for many event locations (see Section 3.4). Therefore, the application of relative time anomaly corrections potentially increases the detection capability by 0.1 to 0.2 magnitude units at LASA, and the potential improvement is somewhat greater at NORSAR.

The initial set of beamforming delays in the ISRSPS EP system are computed using relative time anomaly correction factors interpolated from the prestored data base (Section 8.3.1.2). When the EP correlation process fails, or is bypassed (Section 8.3.1.3), then the final EP beam which is used for waveform parameter estimation purposes (Section 8.3.2) will also be formed using prestored estimates of relative time anomaly correction factors. Furthermore, although the correlation process eventually converges to a set of internally derived beamforming delays which are independent of the time anomaly data base, this convergence will be enhanced by the improved initial beam, which is used as a signal waveform reference by the correlation process.

The correlation process produces as output, among other things, a set of relative signal arrival times for the subarrays. These relative arrival times are then modified by the prestored time anomaly correction factors to produce a set of approximate planewave arrival times $\{T_k | k = 1, 2, \dots, K\}$. As shown in Section 6.5, these time estimates are then used to obtain an estimate of the u -vector for the planewave according to the formula

$$\vec{u} = \begin{bmatrix} \sum w_k X_k^2 & \sum w_k X_k Y_k \\ \sum w_k X_k Y_k & \sum w_k Y_k^2 \end{bmatrix}^{-1} \begin{bmatrix} \sum w_k X_k T_k \\ \sum w_k Y_k T_k \end{bmatrix}$$

where (X_k, Y_k) are the coordinate locations of the subarray centers relative to the weighted center of gravity of the array coordinate system, and the w_k 's are subarray weighting factors.

Suppose that the weighting factors w_k are all equal, and that the array has circular symmetry in the sense described in Section 6.6. Then, if the time estimate T_j contains an error δT_j , the corresponding error in the u-vector estimate is

$$|\delta \vec{u}| = \frac{2R_j}{\sum R_k^2} \delta T_j \quad (7-10)$$

where $R_k = \left[x_k^2 + y_k^2 \right]^{\frac{1}{2}}$. For an outer subarray at LASA with a time error of δT_j seconds, the u-vector error is approximately $3.3 \delta T_j$ ms/km, and the error for an outer NORSAR subarray is approximately $2.7 \delta T_j$ ms/km.

This error estimate indicates the importance of minimizing the errors in both the subarray arrival time estimates and the relative time anomaly values. However, it also shows the importance of using the time anomaly data to correct the subarray arrival time estimates and effectively flatten the wavefront prior to computing the u-vector estimate. For example, if one of the data values is missing, due to the fact that the corresponding subarray has been masked out ($w_j = 0$), then the data error δT_j may be quite large when no time anomaly corrections have been used.

Furthermore, as described in Section 8.3.1.3, the residual planewave deviations in the above u-vector estimation are used to form a chi-square sum in the EP system; this chi-square statistic then provides a sensitive test to determine whether or not the automatic correlation process has converged successfully. If the time anomaly biases were not removed prior to u-vector estimation, the sensitivity of this test would be greatly reduced.

Finally, it is apparent that the stored relative time anomaly data must be completely compatible with the correlation process estimation procedures, so that the above EP applications of this data will be meaningful.

The U-space location calibration vectors are applied in ISRSPS whenever it is necessary to convert from an observed U-space location to the corresponding geographic space location, or vice versa. The computations and table lookup operations associated with this mapping procedure are described in Section 8.3.3. The DP system applications include the mapping of detection beam aiming points from U-space into geographic space and the inverse mapping of seismicity information into observed U-space, both of which are offline DP support processes. The primary EP application of location calibration data is the mapping of the observed U-space location into the corresponding geographic space location, for event reporting purposes. The inverse mapping operation is also required when an EP rerun is initiated with a geographic location.

7.2.2 Estimation of Relative Time Anomalies and Calibration Vectors

When a new array is installed, time-anomaly corrections are not initially available for the beamforming process. Some form of data processing capability must exist before the time anomalies may be determined. One straightforward approach is to produce a time plot of the data from each channel. This permits the manual determination of the delays for large events. In this manual approach the simplest procedure may be to reference the delays to the center-most seismometer or subarray. This convention, of course, assumes that the center-most seismometer or subarray is in operation. Given a set of delays, the wavefront direction may be determined by solving for u_x and u_y by a least-squares fit to the measured delays. Best steering will result if the array is symmetric, since in this case symmetric effects such as wavefront curvature will be minimized. The time anomalies Δ_k are the deviations of the measured arrival times T_k from the planewave arrival times given by the equation

$$\Delta_k = u_x X_k + u_y Y_k - T_k$$

The manual work required in the above process is disadvantageous; on the other hand, the process is independent of any outside data or reference and requires very little data processing capability. This technique was used to produce the initial set of LASA time-anomaly data [7-11].

The array data processing system may include a capability to measure relative arrival times automatically by means of thresholding, correlation, or deconvolution filtering [7-10]. This ability allows the data processing system to do dynamic beamsteering (Section 6) and to automatically and routinely generate a time-anomaly data base. Beamsteering is the process of estimating a set of beamforming parameters, such as relative time delays.

The relative time anomalies for LASA and NORSAR were measured by the following process:

1. A data base was formed of events that had strong correlation between the array beam waveform and the individual subarray waveforms. The events were selected so as to sample as much of U-space as possible. Fortunately a sufficient number of such events with all subarrays operational was available.
2. An initial array beam was formed using planewave delays.
3. The revised subarray delays were determined from the time of maximum correlation between the subarray and the array beam.
4. The array beam was improved by the subarray delays generated in step 3. The process of alternately forming improved array beams and determining subarray delays was repeated until a stable condition was reached.
5. A reference plane wave (u_x, u_y) was determined by a least squares fit to the final set of measured delays.
6. The relative time anomalies for this data base event were the set of deviations of the measured subarray delays from the reference plane wave.

The automatic correlation process outlined in steps 2-6 has been described in detail in Section 6. Time anomaly corrections were then available for any point in U-space by interpolating between the data base values, as described in Section 7.3.

Time anomaly values generated by steps 1-6 have the following characteristics:

- a. They are independent of external references.
- b. The procedure is automated, thus minimizing manual measurement and transcription errors.
- c. The procedure aligns initial arrivals; thus the time anomaly corrections are appropriate for both detection beamforming and dynamic beamsteering.
- d. The same delay-measuring technique is used for online processing and time anomaly determination. This technique results in a processed wavefront direction (u_x, u_y) that is largely independent of the set of subarrays used in the estimation.
- e. The relative time anomaly corrections do not affect beamsteering; that is, their addition to a set of plane-wave delays does not cause a change in the wavefront direction.

An important variation to the above approach (Steps 1-6) should be mentioned here. In Step 5, the reference plane-wave (u_x, u_y) may be generated in the following way. An accurate determination of the event location is obtained from an external source, such as ERL. The correct arrival azimuth and range are computed using the known locations of the event and the array. The magnitude of the u-vector ($|\vec{u}|$) is determined by differentiating the travel-time tables at the given range. The polar coordinates ($|\vec{u}|$ and azimuth) are then converted to Cartesian coordinates (u_x and u_y). Some of the properties of this alternate approach are the following:

- a. The method is dependent upon an outside reference for event location; however, only three data values are required: event latitude, longitude, and depth.
- b. The reference planewave is independent of the measured data. This independence eliminates some of the concern about the introduction of array asymmetry due to missing data channels. It also reduces slightly the need for events with large signal-to-noise ratios.
- c. The time anomalies are dependent on the travel-time tables; thus the same version of the travel-time tables should be used for event location and for time-anomaly determination.
- d. These time-anomaly corrections affect beamsteering, but this is beamsteering correction with a purpose. The application of these time anomaly corrections results in a u-vector pointed at the event location, thus eliminating the processes of calibration and decalibration.

The approach which is used in the ISRSPS systems is to reference the relative time anomaly data to the least squares wavefront, as in the former method, and to compute and maintain separately the difference between the u-vector derived from ERL data and the least squares plane-wave u-vector. This approach requires only a slight increase in the data storage requirements which may be offset by the following advantages:

- a. In Section 7.1.2 it was indicated that the physical causes of relative time anomalies and location calibration vectors may be regarded as separate. The separation should facilitate the use of time anomaly data for modeling the earth's structure under the array and possibly near the source.
- b. The estimation errors associated with the calibration vectors are independent of those associated with the relative time anomalies, and are of a different nature entirely. This is desirable for purposes of statistical error analysis of the time anomaly data base.

- c. There is no guarantee that calibrated U-space is either single-valued or simple. This may cause discontinuities and ambiguities which would prevent the correlation process from converging.
- d. The ISRSPS system applications of relative time anomaly data are generally separate from the applications of the location calibration data. Hence it is unnecessary to incur the errors and ambiguities of the location calibration data in a signal processing component of the system in which this data is not required, and vice versa. The errors incurred in determining time anomaly data by table lookup and interpolation for an arbitrary U-space location may result from three independent sources:
 - 1. Lack of repeatability
 - 2. Data base errors
 - 3. Data interpolation errors.

Hence, there is a natural basis for the separation from both a physical and a statistical viewpoint.

If for any reason the time anomaly values are a function of any parameter other than the U-space location, then time anomalies for events from the same location may not repeat from one event to another. Errors in generating the time anomaly data can result from errors in measuring the relative signal arrival times, and errors in estimating the U-space location (u_x, u_y) associated with the reference event. Interpolation of time anomaly values from data base U-space locations result whenever the desired U-space location does not coincide with the location of a data base event.

Data from large events having nearly the same location (Table 7-2) indicate that time anomalies are highly repeatable and are accurately estimated when generated by the correlation beamsteering procedure used in

Table 7-2. Plane and Quadratic Deviation Differences of Two Hokkaido Events

Event Parameter	Quadratic Wavefront Fit			Plane Wavefront Fit		
	Event A	Event B	Difference	Event A	Event B	Difference
u_x (s/km)	0.040792	0.040925	0.000133	0.040843	-0.040987	-0.000144
u_y (s/km)	-0.037245	-0.037183	-0.000062	-0.036881	-0.036820	-0.000061

Subarray Identifi- cation	Deviation from a Quadratic Fit (seconds)			Deviation from a Plane Wave Fit (seconds)		
	Event A	Event B	Difference	Event A	Event B	Difference
B1	0.0862	0.0807	0.0055	0.0288	0.0261	0.0027
F3	0.0418	0. 418	0.0000	0.1588	0.1448	0.0140
F4	0.0474	0.0503	-0.0029	0.3111	0.3123	-0.0012
A0	-0.0698	-0.0695	-0.0003	-0.1320	-0.1288	-0.0032
B3	-0.0631	-0.0686	0.0055	-0.1289	-0.1319	0.0030
C4	-0.0140	-0.0218	0.0078	-0.0787	-0.0840	0.0053

Table 7-2. Plane and Quadratic Deviation Differences of Two Hokkaido Events (cont.)

Subarray Identifi- cation	Deviation from a Quadratic Fit (seconds)			Deviation from a Planewave (seconds)		
	Event A	Event B	Difference	Event A	Event B	Difference
B4	-0.0209	-0.0136	-0.0073	-0.0754	-0.0652	-0.0102
C1	0.0489	0.0435	0.0054	0.0095	0.0069	0.0026
C2	0.0342	0.0445	-0.0103	-0.0327	-0.0195	-0.0132
B2	-0.0903	-0.0905	0.0002	-0.1523	-0.1495	-0.0028
C3	-0.0673	-0.0715	0.0058	-0.1261	-0.1270	0.0009
D3	0.0860	0.0830	-0.0030	0.0154	0.0138	0.0016
D4	-0.1520	-0.1544	0.0024	-0.1626	-0.1625	-0.0001
D1	0.1069	0.1108	-0.0039	0.0533	0.0589	-0.0058
D2	0.1085	0.1071	0.0014	0.0597	0.0612	-0.0015
E3	-0.0259	-0.0159	-0.0100	0.0936	0.1042	-0.0106
E4	-0.0429	-0.0430	0.0001	-0.1899	-0.1929	0.0030
E1	0.0518	0.0550	-0.0032	0.1695	0.1740	-0.0045
F1	-0.0527	-0.0556	0.0029	0.0785	0.0614	0.0171
E2	0.0278	0.0340	-0.0062	-0.1300	-0.1264	-0.0036
F2	-0.0400	-0.0461	0.0061	0.2302	0.2241	0.0061
Mean	0.0000	0.0000	0.0001	0.0000	0.0000	-0.0004
Standard Deviation	0.06947	0.07042	0.0052	0.1367	0.1366	0.0071

the ISRSPS EP system. The size of the interpolation error depends on the fluctuation of the time anomaly values over U-space in combination with the spacing of the data base events. This condition leads to small known interpolation errors in U-space areas of high seismicity and unknown but possibly large interpolation errors in low seismicity areas.

Table 7-2 demonstrates the accuracy to which the LASA ISRSPS correlation process can determine the relative time anomalies. The time anomalies for two earthquakes from Hokkaido are compared, using first a quadratic wavefront model as a reference and second, a plane wavefront model. The differences between the wavefront deviations of these two events for individual subarrays are an indication of the accuracy with which the time anomalies can be determined. The overall accuracy in the planewave case (standard deviation of 0.007 seconds) is about an order of magnitude better than that required for beamforming delays. The unexpectedly high repeatability of the time anomalies was found to occur with explosions, as well as with earthquakes. Consideration of Table 7-2 suggests the possibility that the need for time-anomaly data might be eliminated if a quadratic wavefront model were employed. The quadratic model was found not to be effective for detection beams at LASA. The problem with this model was that estimates of the quadratic coefficients were statistically unstable over the two-dimensional U-space, so that the coefficients could not be accurately predicted.

7.3 STORAGE AND RETRIEVAL OF TIME ANOMALY DATA

Since a considerable amount of relative time anomaly and location calibration data may be required for adequate definition of the variation of these parameters over all of U-space, the data storage and retrieval algorithms must be designed for efficient operation and storage utilization.

The relative advantages and disadvantages of some of the possible methods for storing and retrieving this data are discussed in Section 7.3.1, and the development and initial performance of the technique which was selected for implementation in ISRSPS is described in Section 7.3.2.

7.3.1 Alternative Techniques

For each processed event which is included in the time anomaly data base, it will be assumed that the data of interest consists of the event location in observed U-space (u_x, u_y), a set of relative subarray time anomalies $\{\delta t_k \mid k=1,2,\dots,K\}$, and the U-space location calibration values ($\Delta u_x, \Delta u_y$). If the conventions are adopted that the relative time anomalies are referenced to the planewave arrival time at a particular point in the array, and that they contain no residual u-vector component which would steer the reference planewave away from the (u_x, u_y) aiming point, then the above data set is redundant by three values. However, this is a practical choice for computational convenience in the applications of this data.

Clearly, the system performance might be somewhat enhanced by the availability of relative time anomalies for every sensor in the array, but the potential performance improvements are far too small to justify the increased computer storage and processing load requirements. On the other hand, some reduction in the data requirements might be realized by demonstrating that the relative time anomalies for certain subarrays are sufficiently small over all of U-space that they can be ignored without incurring significant processing losses. For example, the nine subarrays near the center of LASA and the eight near the center of NORSTAR may possibly be in this category. However, it is doubtful that the potential savings in computer resources are sufficient to justify the special handling and analysis of the data, as well as the resulting performance losses.

The relative time anomaly values for each subarray, as well as each component of the location calibration vector, can be thought of as defining a surface over observed U-space, which is a single-valued function of the coordinates u_x and u_y . The relative time anomaly and calibration data for a single processed event represent point estimates of each of these functions, or surfaces, at a single U-space coordinate location. A data base of processed events must therefore be compiled having sufficient accuracy and resolution to adequately define each of these surfaces over U-space. Furthermore, a computational algorithm is required which utilizes the relative time anomaly and calibration data associated with the data base events to produce an estimate of each function, or surface, at an arbitrary U-space location.

One possible approximation to each of the surfaces is a polynomial in the two variables u_x and u_y . Polynomials provide a very efficient method of storing data, and the data retrieval process is straightforward. The polynomial coefficients are generated offline using existing polynomial fitting programs. However, there are certain characteristics of polynomial fits that are not well suited to this application. For example, polynomials tend to take on unreasonable values in areas where they are not constrained due to the lack of data. Furthermore, although a continuous surface can theoretically be approximated arbitrarily closely by a polynomial, a relatively high order polynomial is required in practice to fit a surface having abrupt slope changes. Another characteristic of polynomial fits is that each input data value affects the entire surface. A bad data point may have a detrimental effect on the surface for a large area of U-space.

The results in [7-12] indicate that the subarray relative time anomalies describe a continuous but sometimes rapidly changing surface over U-space, with occasional abrupt changes of slope. Furthermore, available seismic data is very sparse over large regions of U-space which are associated with aseismic regions of the earth. For these reasons, a polynomial fit is probably not appropriate for this application.

The interim version of the LASA data processing system employed polynomials to store calibration data [7-5, p. 119] and [7-6, pp. 116-119]. It was necessary

to add several artificial data points to the data base in order to maintain the polynomial surface within reasonable bounds, and the resulting fit was still unsatisfactory for significant portions of U-space.

A different procedure for storing and retrieving relative time anomaly data was implemented in earlier versions of the LASA processing systems [7-3, p. 126]. At that time 35 high seismicity regions of U-space were selected. One set of constant relative time anomaly data was estimated for each region, and these time anomalies were applied to all beams having their aiming points within that region. These sets of data were appropriately called region corrections. Within certain sectors of U-space containing at least two of the smaller regions, values outside the regions were computed by linear interpolation. The time anomalies were taken as zero for all other parts of U-space.

A study of selected events within these regions showed an average beam-forming loss due to time delay errors of only 0.4 dB. However, sharp reductions in beam power were observed to occur at the boundaries where time anomaly values changed suddenly to zero. This effect frequently caused the selection of an incorrect detection beam in DP, and occasionally resulted in a side-lobe detection even though a beam was deployed in the U-space vicinity of the event. It was also noted on some occasions that the correlation beamsteering process would fail because of this region correction process. The successive iterations of the correlation process resulted in a sequence of estimated u-vectors that would not converge because of the discontinuities at the boundaries and occasional poor data values in some regions.

It was then decided to cover all of U-space with a triangular grid, and to assign a complete set of relative time anomaly and calibration data to each node of the grid. This grid can be subdivided as finely as desired in any given region of U-space simply by adding interior nodes and defining connections between these and existing nodes. The relative time anomaly and calibration data values at an arbitrary U-space location are defined by linear interpolation among the corresponding values at the nodes of the unique enclosing triangle. Thus, the surface defined over U-space to approximate the data values for each subarray time anomaly and each calibration vector coordinate is continuous and consists of connected triangular plane sections.

Initially there was no efficient solution to the problem of finding the nodes of the unique enclosing triangle for an arbitrary U-space location except for the case in which the node points are constrained to coincide with a subset of points from a uniform grid. For the uniform triangular grid there are various indexing schemes that can be used to identify the nodes of the unique enclosing triangle, even though some regions of the space are subdivided much more finely than others.

Therefore, an experimental version of a uniform triangular grid technique was developed for the storage and retrieval of time anomaly and calibration data [7-7, Appendix III]. Data values at the node points are computed on the basis of a global least squares fit of the segmented-triangular surface to the data base values. Slope constraints are used to prevent the surface from varying erratically, particularly over regions for which there are few or no data base events. Additional subdivisions are defined where necessary to enhance the fit.

The uniform triangular grid approach generally works well in areas of high seismicity. However, unreasonably large values sometimes occur in low seismicity regions, unless considerable care is taken to constrain the surfaces. This method also suffers from the usual problems associated with any global fitting technique; namely, the influence of a bad data value may extend over a large area of U-space, and it is not generally possible to modify the surface locally or to account for the data base without reestimating the entire surface. Furthermore, the requirement to constrain the node points to a uniform grid results in a loss of flexibility in the fit, and it is sometimes necessary to subdivide rather finely in order to obtain an adequate fit in the vicinity of a sharp ridge or valley in the data surface.

Least squares fits (including polynomial fits) are frequently used to smooth out data errors in addition to approximating the actual data values.

Large amounts of data are generally desirable in order to obtain maximum benefit from the smoothing effect. It was initially felt that the effects of data smoothing were desirable, if not necessary, for the time anomaly and calibration data. However, a considerable amount of evidence of the type shown in Table 7-2 has served to demonstrate that data smoothing is unnecessary, and large amounts of data need not be used, as long as the data which is included in the data base is carefully estimated and edited.

On the basis of the above considerations, it was concluded that a triangular grid in which the node points correspond to U-space locations of actual data base events would represent a satisfactory solution to the problem of fitting the data surfaces. Since actual data values for a selected event are used at each node, the replacement of a node which is found to have erroneous data values is quite straightforward. Additional events can be added to the data base to improve the fits for some of the data surfaces simply by attaching the new node to the vertices of the enclosing triangle, thereby subdividing that triangle into three smaller ones. Other advantages of this nonuniform triangular grid technique are as follows:

- a. The flexibility of the nonuniform triangular grid allows a variety of irregular surfaces, which may be quite smooth and slowly varying in some regions and rapidly changing and uneven in others, to be approximated as accurately as desired with effective utilization of the data.
- b. The resulting surface will be continuous and single-valued over all of U-space.
- c. The interpolated time anomaly and calibration values are never larger than the maximum of the corresponding values at the three nodes.
- d. The actual data base values are used when the input U-space location corresponds to a node.

- e. The domain of influence of the data associated with a node is limited to the set of triangles in U-space having that node as a vertex.

The primary problem that had to be solved in order to implement the non-uniform triangular grid technique was to develop an efficient algorithm which would, in all situations, find the three nodes of the unique minimum triangle enclosing an arbitrary point in U-space, without imposing restrictive constraints on the triangular grid. The significant aspects of the implemented data retrieval process, including the node search algorithm, are described in the following section.

7.3.2 Grid Search and Interpolation Algorithms

The U-space data retrieval scheme that was implemented in ISRSPS consists of three parts, which perform the following functions:

1. Find a node of the triangular grid which is in the general vicinity of the specified U-space location.
2. Find the three nodes of the unique minimum triangle enclosing the specified location.
3. Compute the data values at the specified location by planar interpolation of the data values at the nodes.

In preparation for the first of these operations, once a triangular grid had been developed, U-space was divided into sectors, and each of these sectors was subdivided into annular segments in such a way that each segment contained a small but nonzero number of nodes of the grid. After converting a specified U-space location to polar coordinates, an orderly search is employed to find first the sector which contains the magnitude of the specified point. An arbitrary node within the annular segment may be selected to satisfy the requirements of the first function.

The algorithm which performs the second function may be described by means of an example. Figure 7-4 shows a portion of a hypothetical triangular grid. Let the specified location be represented by point "p", and assume that the node "a" has been selected in the first part of the process. Suppose that there is a list associated with node "a", and in fact with each node of the grid, which contains the U-space locations of each node that is directly connected to the subject node by a line (or branch), in counterclockwise order. For example, suppose that the list associated with node "a" contains the locations of nodes "b", "c", "d", "e" and "f", in that order. Let \vec{Y}_{ab} denote the vector from "a" to "b", \vec{Y}_{ap} the vector from "a" to "p", and so forth. The algorithm makes use of the fact that a vector cross-product $\vec{Y}_1 \times \vec{Y}_2$ is directed positively if the angle from \vec{Y}_1 to \vec{Y}_2 in the counterclockwise direction is less than 180° , and negatively otherwise. (A vector cross-product, in this context, is defined to be positive/negative if $\sin \theta$ is positive/negative, where θ is the counterclockwise directed angle from \vec{Y}_1 to \vec{Y}_2 .)

The vector cross-product $\vec{Y}_{ab} \times \vec{Y}_{ap}$ is computed and found to be positive, which indicates that "p" is counterclockwise of "b" relative to the center "a". Similarly, $\vec{Y}_{ac} \times \vec{Y}_{ap} > 0$ indicates that "p" is counterclockwise of "c", but $\vec{Y}_{ad} \times \vec{Y}_{ap} < 0$ shows that "p" is clockwise of "d". Therefore "p" is contained in the sector described by angle d-a-c.

Taking "d" (the first node for which the associated vector cross-product produced a sign change) as the new central node, the list for node "d" is searched to determine the node which is counterclockwise of the previous central node "a", in this case node "c". The test $\vec{Y}_{dc} \times \vec{Y}_{dp} > 0$ shows that "p" is counterclockwise of "c" relative to the center "d". Since $\vec{Y}_{da} \times \vec{Y}_{dp}$ is known to be positive from a previous test, this means that "p" is not contained in the triangle d-a-c. The process

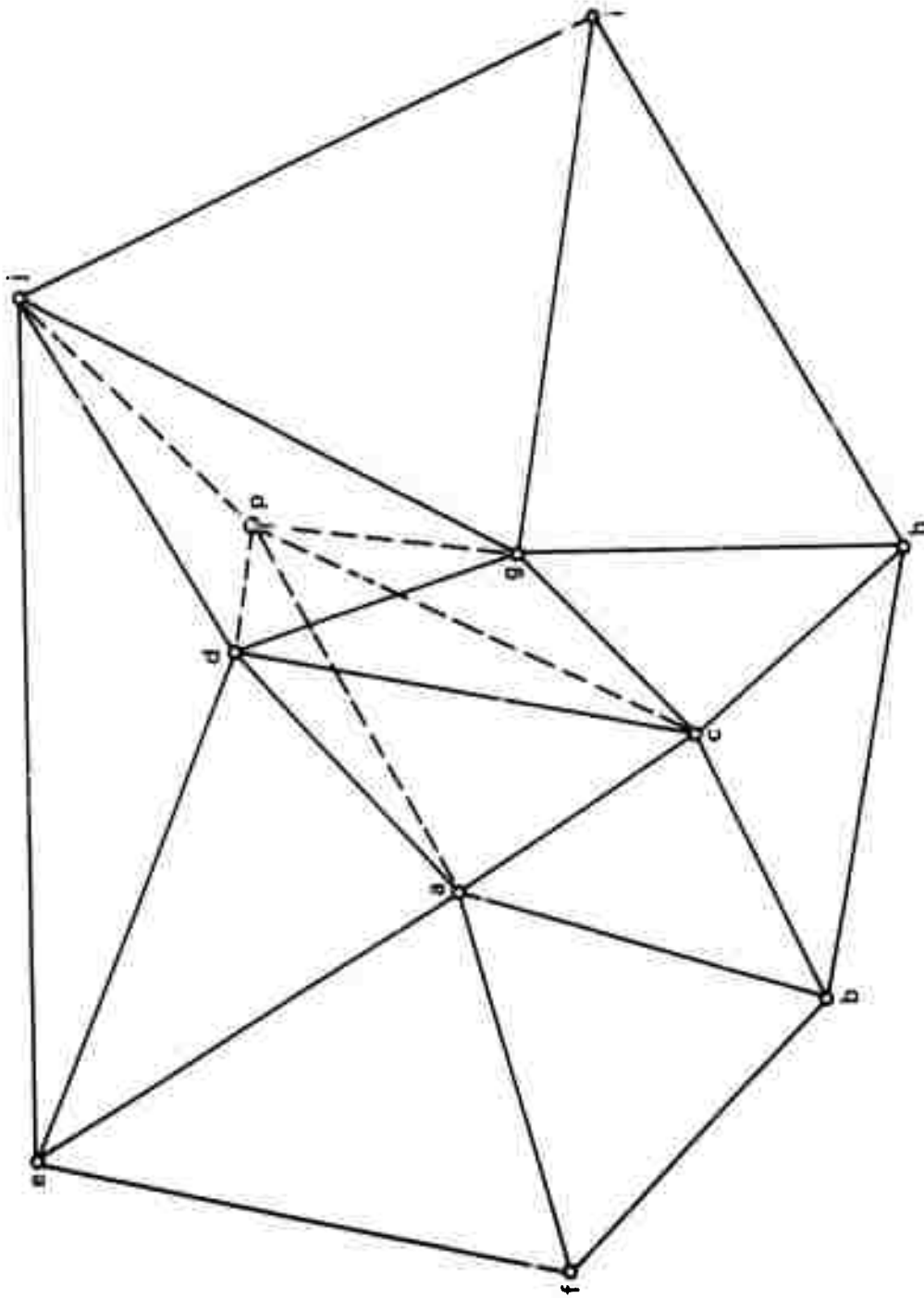


Figure 7-4. Example for Triangular Grid Node Search Algorithm

therefore continues and it is found that $\vec{y}_{dg} \times \vec{y}_{dp} > 0$, but $\vec{y}_{dj} \times \vec{y}_{dp} < 0$, so that "p" is also contained in the sector described by angle j-d-g. Taking "j" as the new central node, it is then found that $\vec{y}_{jg} \times \vec{y}_{jp} < 0$, so that "p" is also contained in the sector described by angle d-j-g. Hence, "p" is contained in the triangle d-j-g, which is the desired result.

Note that, once the process begins in a counterclockwise sense, a positive cross-product always implies that the next node in counterclockwise order relative to the current central node is tested next. A negative cross-product generally implies that the central node is to be replaced. However, if the central node has just been replaced on the previous step, then a negative cross-product is the criterion for stopping.

If the first vector cross-product happens to be negative, then the corresponding process description may be obtained by replacing the word "counterclockwise" in the preceding paragraph with the word "clockwise", and interchanging the words "positive" and "negative". The information on node locations and on the order of nodes about each central node is stored in the ISRSPS system in the form of tables which have been organized to facilitate the execution of this algorithm. Each of these so-called region tables is associated uniquely with one of the annular segments, or regions, discussed above. The formats and contents of the various grid description and data tables are presented in [7-8, Appendix II], and flowchart descriptions of the node search and interpolation routines are also given in that report.

Let the U-space coordinates of the three nodes of the enclosing triangle be designated as (u_{x1}, u_{y1}) , (u_{x2}, u_{y2}) and (u_{x3}, u_{y3}) , and let (u_{xp}, u_{yp}) designate the U-space location of the specified point. Then a set of interpolation coefficients C_1 , C_2 and C_3 , associated with the three nodes and the specified point, are computed as follows:

$$C_1 = N_1/D \quad \text{for } i = 1, 2, 3$$

where

$$D = \begin{vmatrix} u_{x1} & u_{x2} & u_{x3} \\ u_{y1} & u_{y2} & u_{y3} \\ 1 & 1 & 1 \end{vmatrix} \quad N_1 = \begin{vmatrix} u_{xp} & u_{x2} & u_{x3} \\ u_{yp} & u_{y2} & u_{y3} \\ 1 & 1 & 1 \end{vmatrix}$$

$$N_2 = \begin{vmatrix} u_{x1} & u_{xp} & u_{x3} \\ u_{y1} & u_{yp} & u_{y3} \\ 1 & 1 & 1 \end{vmatrix} \quad N_3 = \begin{vmatrix} u_{x1} & u_{x2} & u_{xp} \\ u_{y1} & u_{y2} & u_{yp} \\ 1 & 1 & 1 \end{vmatrix}$$

The relative time anomaly δt_{kp} for each subarray k is found as

$$\delta t_{kp} = C_1 \cdot \delta t_{k1} + C_2 \cdot \delta t_{k2} + C_3 \cdot \delta t_{k3}$$

where δt_{k1} , δt_{k2} and δt_{k3} are the time anomalies for subarray k at nodes 1, 2 and 3 respectively. The interpolated calibration vector coordinates are obtained similarly.

7.3.3 LASA Data Base Selection

A data base of some 700 events was carefully selected and specially processed to provide quality reference events for time anomaly and calibration values for LASA. Only a portion of these were used for the triangular grid nodes. Planewave deviation contours for the complete data

base were plotted as a function of the corresponding events, and these were examined to determine the general behavior of LASA time anomalies.

Based on these plots, 51 well-placed events were selected as a starting network for the U-space triangular grid. A network analysis program was developed which used an existing triangular grid network to estimate time anomaly and calibration values for data base events not included in the grid. Whenever these estimated data values did not compare well with the actual data values for a test event, then this event was itself added to the network. This procedure of adding nodes only where required to improve the fit keeps the number of nodes relatively small while maintaining the desired accuracy.

For reasons of data storage efficiency, the data base events are generally required to have a complete set of subarray relative time anomaly and location calibration data. However, in certain cases, it may be desirable to insert artificial calibration values in order to preserve a node in an area of low seismicity. In a situation where a reference event is needed to provide a node in the interpolation network, but where a subarray had been inoperative during the event, the missing time-anomaly value may be estimated by interpolation of near-by events.

One of the objectives in developing the non-uniform node network was to avoid extrapolation. The highest possible U-value for a phase arrival is 0.12 ssc/km but the seismicity at this value is very low. Eight artificial nodes were placed around this outer edge of U-space to ensure complete coverage and to guarantee that extrapolation would not be employed. The time anomaly and calibration values at each of these eight outer nodes were set equal to the values at the nearest node.

The nodes on the interpolation grid were selected to satisfy the requirements of both time anomaly and calibration purposes. The problems in

selecting nodes are: (1) assuring the quality of the node data, (2) determining the density of the nodes in U-space, and (3) selecting the way in which the nodes are linked together.

To assure the data quality of each node, the event parameters from the automatic LASA Data Processing System were examined. The signal trace for each subarray was examined for the proper delay and signal content. If the automatic processing had not included a useable subarray, the analyst reinstated the subarray and the U-space location and planewave deviations were recomputed. Sometimes the analyst changed the delay of the unused (masked) subarray before it was reinstated. Manual delays were multiples of 0.1 second. A special version of the correlation beam-steering process was developed to apply the correlation process to manual delays. This program had a 1.5-second correlation interval and was limited in delay movement so that cycle skipping was not possible. The short correlation interval was practical because of the good initial alignment of the subarrays. A quality factor (Q) which represents the weight or quality of the beam was computed and displayed for each node candidate. The quality value (Q) was computed for each node by the formula

$$Q = \sum_1 \min \left(\left[\frac{c_1^2}{1-c_1^2} \right], 25 \right)$$

where c_1 is the correlation coefficient for the 1th subarray beam relative to the array beam.

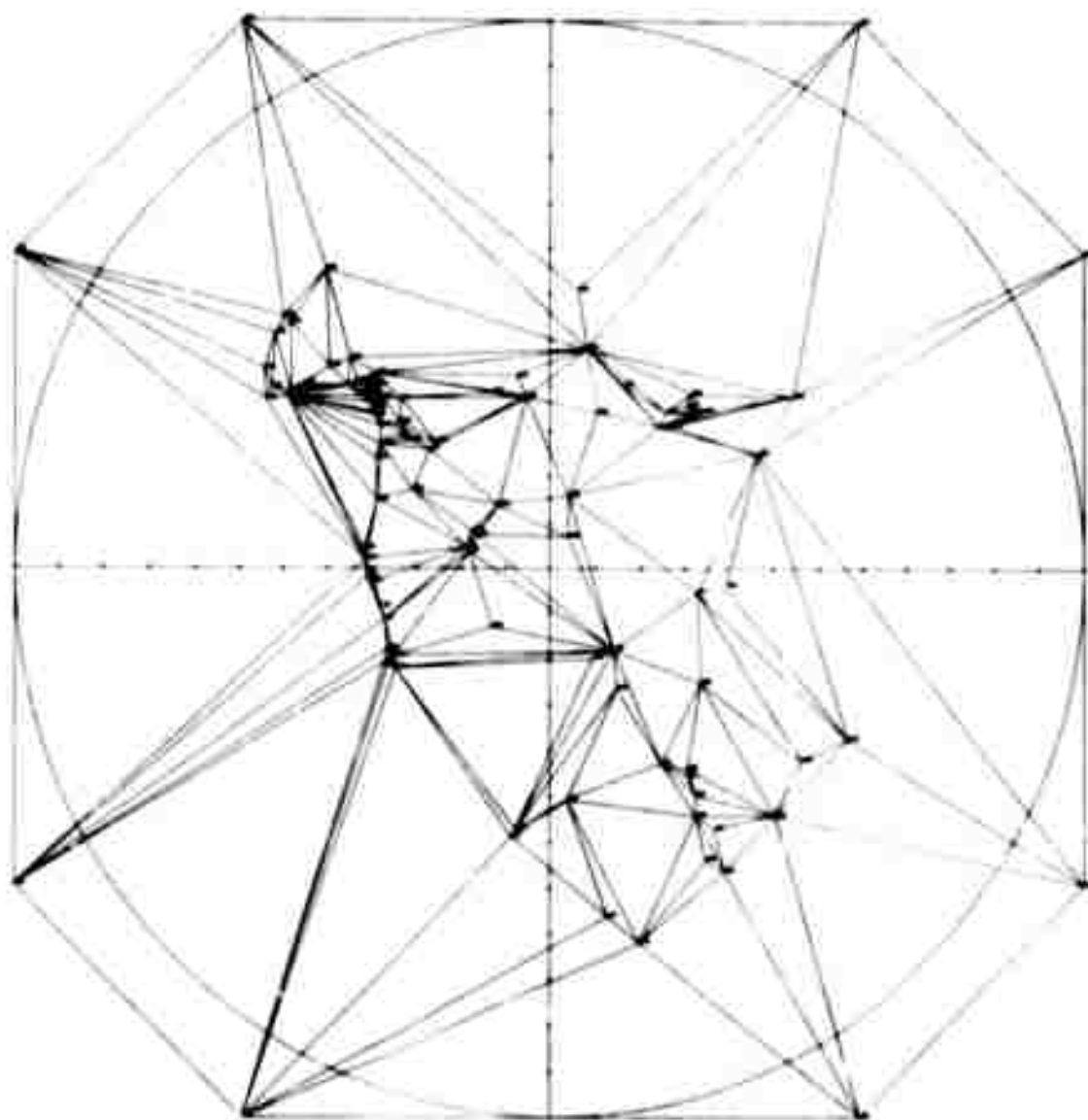
Errors in event location and depth directly affect the size and direction of the calibration vector. To aid in identifying calibration error, due to depth errors, the component of calibration parallel to the U-vector was contour-plotted. Where possible, events with positive depth determination were selected to obtain maximum depth accuracy (i.e., the nominal depth of 33 km was avoided).

A contour plot of each subarray time anomaly was useful in selecting the nodes. These contour plots utilized all of the events from the data base. This procedure provided the most detailed description of the time anomaly and calibration surfaces available. Areas having nearly straight and parallel contour lines are areas where few nodes were required. For LASA, calibration values vary more than time anomalies, and thus set the requirements for node spacing. Two parameters constitute the calibration vector; thus two surfaces (Δu_x over u_x and u_y , and Δu_y over u_x and u_y) are described by the interpolation grids for calibration.

A nonuniform triangular grid for LASA, consisting of 105 nodes, is shown in Figure 7-5. This LASA data base has been evaluated, and preliminary results are presented in the following section.

7.3.4 Data Base Evaluation

To test a particular triangular grid network, the locations of previously processed events were input to the interpolation process. The time anomaly values and calibrations had been previously established for these test events. The results of the U-space interpolations were compared to the known values. With the network of 105 nodes (shown in Figure 7-5) in the U-space interpolation grid, time anomaly and calibration values were interpolated for 182 test events. A standard deviation was computed for each event based on the disagreement between the computed and known time anomaly values. The average standard deviation of these disagreements was 0.051 seconds with a maximum of 0.24 seconds. This accuracy in computing time anomaly corrections results in a very low power loss in the beamforming process; a standard deviation of 0.06 seconds equates to 1 dB power loss. The performance of the triangular grid used at LASA is summarized in Figures 7-6 and 7-7. Figure 7-6 shows a percentage curve similar to a cumulative probability curve. This curve shows the percentage of



PROBE/PROBUS (IN.)

120.0

10.920

JOB RSN

DATE 03/16/71

LTP115 F1MR P.C. SET

Figure 7-5. LASA U-space Triangular Grid

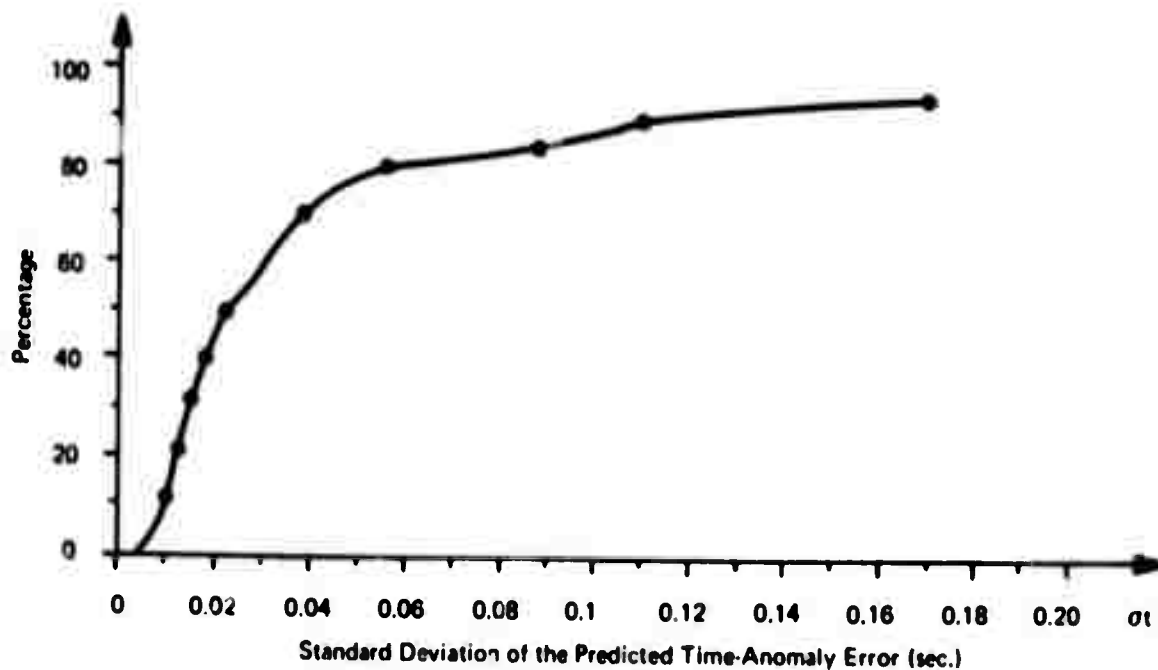


Figure 7-6. Cumulative Distribution of Events Relative to Standard Deviation of Residual Time-Anomaly Error

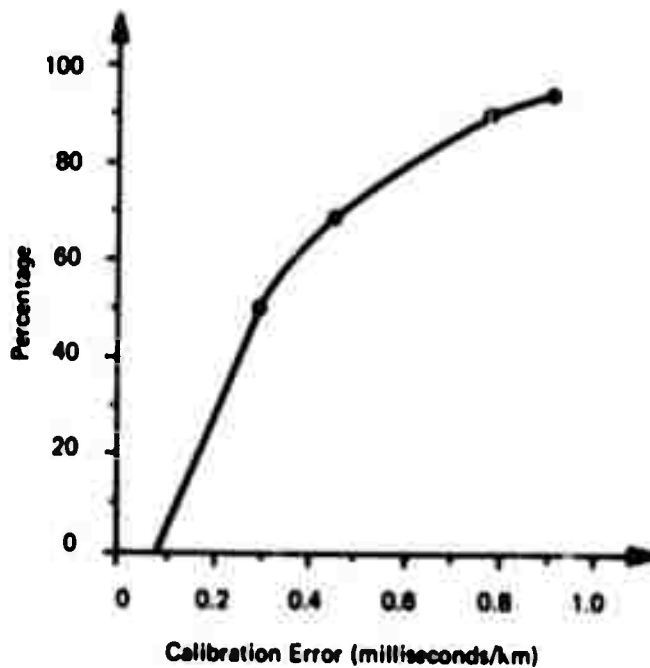


Figure 7-7. Cumulative Distribution of Events Relative to Residual U-space Calibration Error

the 182 test events with standard deviations less than the corresponding abscissa values. The curve in Figure 7-7 is similar to that of Figure 7-6 with the exceptions that the abscissa shows the calibration error and that the number of test events was reduced to 171 events. The disagreement in the calibration has an average rms value of 0.446 milliseconds per kilometer. At a range of 70 degrees, 0.775 milliseconds per kilometer error in u results in a one-degree error in range.

7.4 ANNOTATED BIBLIOGRAPHY

The references listed here are divided into three groups. Subsection 7.4.1 consists of quarterly and final reports prepared by IBM under a series of contracts relating to seismic signal processing. Subsection 7.4.2 contains an IBM special technical report prepared under the same series of contracts. Miscellaneous other references constitute subsection 7.4.3.

7.4.1 IBM Quarterly and Final Reports

- 7-1. "Large Aperture Seismic Array Signal Processing Study," IBM Final Report, Contract SD-296, 15 July 1965..

Section 4.2 is a theoretical study, in which the maximum possible time-delay residual (time anomaly) is estimated for the two possible causes of wavefront curvature and geological inhomogeneities.

- 7-2. "LASA Signal Processing, Simulation, and Communications Study," IBM Final Report, Contract AF 19(628)-5948, ESD-TR-66-635, March 1967.

Section 3.4 discusses the organization of the data collection, estimation, storage, and retrieval techniques, associated with the accumulation and use of a data base for LASA beamforming delays.

- 7-3. "LASA Experimental Signal Processing System," IBM Third Quarterly Technical Report, Contract F19628-67-C-0198, ESD-TR-68-149, August 1967.

In Appendix III a region correction procedure for storing and retrieving time anomaly data is described. Seismic areas are divided into 35 regions for which time anomalies are considered constant.

- 7-4. "LASA Experimental Signal Processing System," IBM Fourth Quarterly Technical Report, Contract F19628-67-C-0198, ESD-TR-68-309, November 1967.

The experimental study discussed in Appendix IV compares the relative sizes of time anomalies when referenced to a plane-wave fit and a quadratic fit to the measured delays.

- 7-5. "LASA Experimental Signal Processing System," IBM Final Technical Report, Contract F19628-67-C-0198, ESD-TR-69-60, Volume I, March 1969.

Appendix VIII discusses a location calibration procedure that was developed for the Phase Zero Event Processor.

- 7-6. "Integrated Seismic Research Signal Processing System," IBM Third Quarterly Technical Report, Contract F19628-68-C-0400, ESD-TR-70-25, May 1969.

Appendix V presents the Phase Zero Event Processor parameters; subsection V.5 describes the location calibration polynomials used in the mapping from inverse velocity space to geographic space.

- 7-7. "Integrated Seismic Research Signal Processing System," IBM Fourth Quarterly Technical Report, Contract F19628-68-C-0400, ESD-TR-70-265, August 1969.

Appendix III is a description of a procedure for storing and retrieving time anomaly data. This procedure utilizes a uniform triangular grid covering all of U-space. Time anomalies for the node points are obtained from a least-squares fit to a time anomaly data base. Time anomaly values for an arbitrary U-space location are determined by interpolating between the node values.

- 7-8. "Integrated Seismic Research Signal Processing System," IBM
Eighth Quarterly Technical Report, Contract F19628-68-C-0400,
ESD-TR-71-393, August 1970.

Appendix II includes a description of a procedure of storing and retrieving time anomaly data from a nonuniform triangular grid in which the nodes are past events. Time anomaly values for arbitrary U-space locations are obtained by interpolation between the node values.

- 7-9. "Integrated Seismic Research Signal Processing System," IBM
Ninth Quarterly Technical Report, Contract F19628-68-C-0400,
ESD-TR-72-122, November 1970.

Appendix III includes a description of the nonuniform triangular grid node set used in the LASA short-period data processing system. Also included is an evaluation of the above node set and a procedure for changing it.

7.4.2 IBM Special Technical Report

- 7-10. "Evaluation of LASA Beam Precision Test Results," Contract
F19628-67-C-0198, ESD-TR-79-187, June 1968.

This report describes an experiment which was conducted to evaluate the LASA epicenter location capability. The results illustrate the repeatability of the wavefronts from event to event, for a given epicenter, and indicate the importance of implementing and utilizing a carefully edited location calibration data base.

7.4.3 Miscellaneous References

- 7-11. E.F. Chiburis, LASA Travel-Time Anomalies for Various Epicentral Regions, ARPA Order No. 624, SDL Report No. 159, September 1966.

The LASA travel-time anomalies tabulated in this report were used in the development of the time anomaly data base for the initial system.

- 7-12. E.R. Engdahl and C.P. Felix, "Nature of Travel-Time Anomalies at LASA," Journal of Geophysical Research, Vol. 76, No. 11, April 1971.

This study of LASA travel-time anomalies for various seismic phases supports the hypothesis that the relative time anomalies from subarray to subarray are phase-independent and therefore may be considered as functions of the observed inverse-velocity coordinates only.

- 7-13. H. Mack, "Nature of Short-Period P-Wave Signal Variations at LASA," Journal of Geophysical Research, Vol. 74, pp. 3161-3170, June 1969.

This paper discusses the multipath structure of seismic signals at LASA. The fact that the multiple arrivals appear and disappear in distances of the same order as a subarray diameter suggests that these multiples are produced by the structure of the deep crust underneath LASA. The complexity of the structural model which is required to explain the observed multipath phenomena is consistent with that which is required to explain the relative subarray time anomalies of the initial arrivals.

Section 8

EVENT PROCESSING

This section describes the Event Processor (EP) as it was actually implemented for use at SAAC and at NDPC for short period data from a single array. Additional recommended signal processing functions such as long-period and multiple-array processing were not included, but the program architecture was designed to accommodate them.

Following a statement of the EP system objectives immediately below, Section 8.1 describes the EP structure and identifies the basic processing components. Ensuing sections then describe each component in greater detail. All the actual values used at SAAC for the various system parameters are listed in Section 8.7 and those used at NDPC in Section 8.8.

EP determines the parameters of seismic events from the detections reported by the Detection Processor (DP). System requirements for EP were formulated as follows.

The process should satisfy dual system objectives:

- a. The publication of a daily seismic bulletin
- b. The support of seismic research through provision of a tool for process experimentation and data manipulation, and through the formation of a data base of seismic information stored on digital magnetic tape.

EP contains the signal processing and seismic parameter extraction algorithms required to perform the following functions:

- a. Seismic signal phase identification of all significant detections reported by DP, and grouping of detections from the same event

- b. Selection of specific detections for further processing, based on the computer time available, and detection location
- c. Formation of a "best" array beam and estimation of a corresponding U-space location for each selected event
- d. Extraction of short period seismic signal parameters from the "best" beam of each selected event
- e. Estimation of seismic epicenter parameters from the seismic phase, U-space location and signal parameter estimates of the event in process, and from data files generated offline
- f. Rapid reporting of the appropriate arrival time, amplitude and location of large events detected in the Large Event Processor of DP (SAAC only).

In addition, EP provides the following:

- a. The data necessary to demonstrate the surveillance and measurement capabilities of large arrays.
- b. The ability to monitor and improve the process as event processing experience is accumulated
- c. Expansion capability for future additions such as a Long Period Signal Processor and a Multiple Array Event Processor.

8.1 SYSTEM STRUCTURE

The overall EP configuration is shown in Figure 8-1. EP includes an Event Process Controller, which can utilize other signal processor components: a Short Period Signal Processor and a Large Event Processor are the only ones included in the SAAC system; at NDPC, the Short Period Signal Processor is the only signal processor component implemented in EP. The quick reaction capability for large events at NDPC is implemented entirely within DP, as described in Section 5.

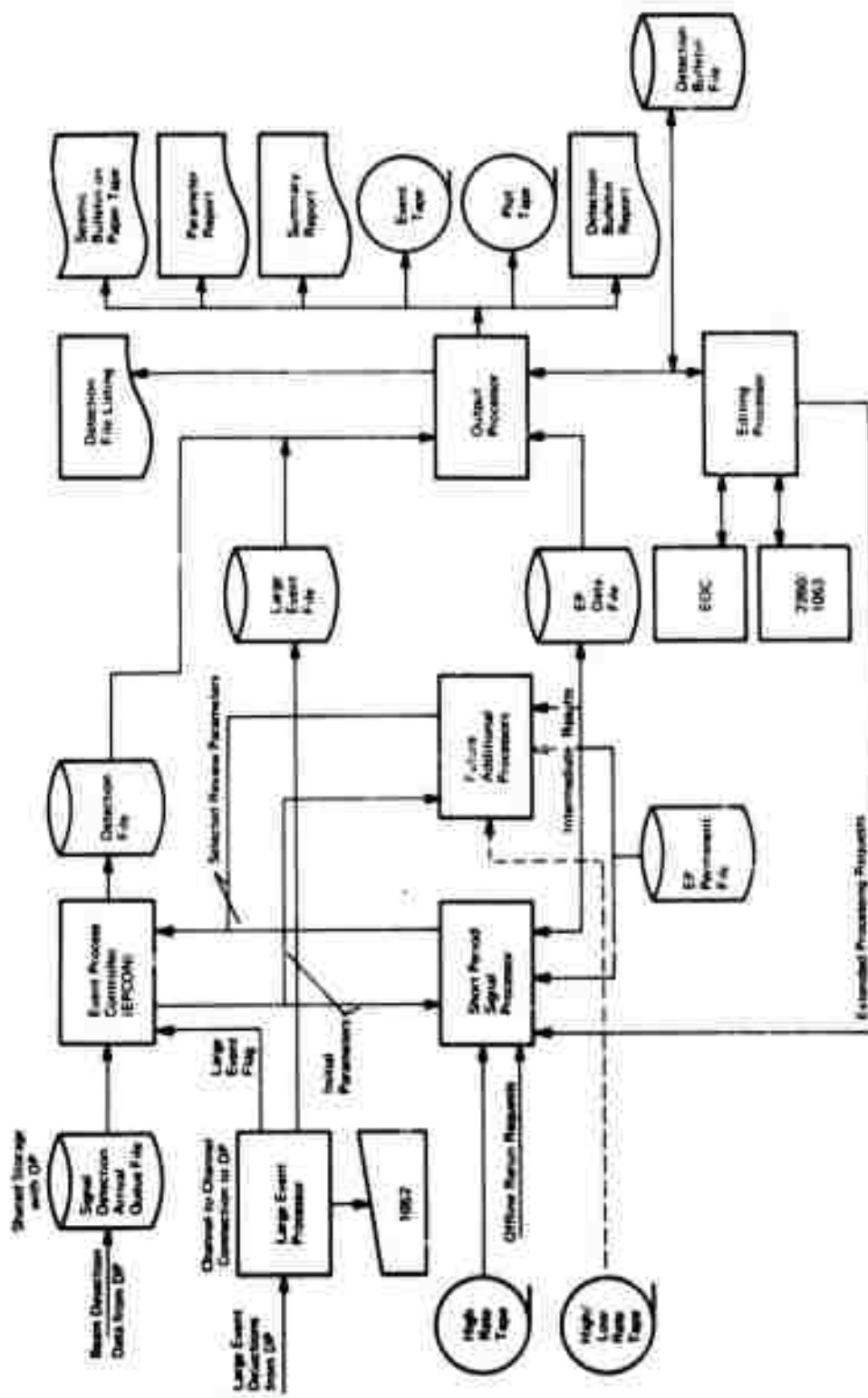


Figure 8-1. EP System Configuration

EP consists of the following components:

- a. Event Process Controller (EPCON)
- b. Short Period Signal Processor (SPSP)
- c. Large Event Processor (SAAC only)
- d. Output Processor
- e. Editing Processor

EPCON processes detections from DP and organizes them into event families in a Detection File. The Short Period Signal Processor obtains more information about each event from the short period data recorded on the Data (high rate) Tape. It creates an EP Data File containing waveforms and intermediate results. The Output Processor uses the Detection File and EP Data File to produce a daily Seismic Bulletin, Event Tapes, Plot Tapes, a Summary Report, a Parameter Report, a Detection report, and a Detection/Bulletin report. The Editing Processor uses the Experimental Operations Console (EOC) and a 2260 Display Unit to allow the operator to edit the results in this file and to request extended processing. All constants, parameters, and tables required by EP are stored in the EP Permanent File.

EP program structure provides maximum overlapping of I/O and CPU operations. EP components are programmed to exploit the efficiencies of the microcoded signal processing algorithms previously described in Section 5.1. In addition, EP allows support programs to run simultaneously in the same computer.

The Event Processor uses the following inputs:

- a. Arrival detection data from DP which appears in the Signal Detection Arrival Queue File, and a common disk storage area shared by DP and EP--This includes the U-space location of the DP beam declared as a detection, the maximum short term average (STA) of that beam when in the detection state,

the detection time of that beam, stop time of the detection group and the long term average (LTA) of that beam at the beginning of the detection group.

- b. Short period seismometer data and status information recorded on ISRSPS SAAC Data or ISRSPS NDPC Data (i.e., high rate) Tapes.
- c. Large Event Detection data received from DP using channel-to-channel communication--This includes the detection time and maximum STA of the seismometers selected for large event detection (SAAC only).
- d. Requests for extended processing as determined by an analyst during execution of the Editing Processor.

Event Processor outputs are described in Section 8.5.

8.2 EVENT PROCESS CONTROLLER (EPCON)

8.2.1 EPCON Functions

EPCON is the main logic and control portion of EP. Its objective is to create the Detection File from the Signal Detection Arrival Queue File using the Short Period component to extract specific short period data. AT SAAC, EPCON also receives input messages from the Large Event Processor. EPCON performs the following functions:

- a. Merging of DP detection groups from both the general and the selected surveillance beam sets into a single stream of detection groups in arrival time order--This includes the identification of pairs of detections, one from each beam set, which are considered to correspond to a single detection, and the selection of one of these detection groups to represent the pair.

- b. Assignment of a seismic phase identification to each detection group, including the identification of the various members of each event family.
- c. Variation of EP thresholds in order to maintain the estimated EP workload at a reasonable level between specified time limits.
- d. Determination for each detection group whether it will be processed by SPSP--This depends upon the signal phase, the signal amplitude, detection signal-to-noise-ratio (as estimated by the ratio: STA/LTA), the detection location in U-space, and the amount of time available in the process. EPCON initializes SPSP for signal detections which have been so indicated.
- e. Updating the Detection File for each detection group.

8.2.2 Process Description

EPCON is perhaps best described by examining the flow of the signal arrivals received from DP through the EP system. EPCON reads signal arrivals from the Signal Detection Arrival Queue on the shared disk pack. These arrivals originate from two distinct beam sets (partitions). Arrivals from the selected surveillance beam set (partition 1) are referred to as s-arrivals, and arrivals from the general surveillance beam set (partition 2) are referred to as g-arrivals. A series of tests is applied to each arrival to determine if it should be processed. The following describes these tests as applied to an arrival designated as p.

EPCON first performs thresholding on p. If the signal-to-noise-ratio (SNR) does not exceed a system parameter (set to 6.3), that arrival is flagged as not to be processed and is not allowed to initiate a matching or chaining operation. Hence, this parameter establishes a minimum EP SNR threshold.

At this point in the NDPC EP system only, a grouping technique has been implemented to reject side lobe detections of an event whenever a main lobe detection can be found in the same beam partition. The start time of each detection group is checked to determine if it is within DELTA (currently 9.0) seconds of the end time of the preceding detection group in that same beam partition. If so, the detection group is added to a list which is accumulated until the DELTA test is no longer satisfied. The list is then searched for the detection group having the largest STA value, and the U-space location of that group is taken as a reference location estimate for the event. All detection groups currently on the list for that beam partition having U-space location beyond a specified distance from the reference location (set to 0.006 secs/km for partition 1, and 0.015 secs/km for partition 2) are flagged as not to be processed, and are excluded from the tests which follow. A new list is then formed for that beam partition beginning with the first detection group which failed to satisfy the DELTA test for the previous list.

EPCON then finds any arrivals which "match" arrival p. An s-arrival and a g-arrival match if their time intervals have a non-empty intersection and satisfy

$$-T_1 \leq ST(s) - ST(g) \leq T_2$$

where $ST(s)$ is the start time of the s-arrival, $ST(g)$ is the start time of the g-arrival, and T_1 and T_2 are system parameters which define the "matching window," set to 150 deciseconds and 10 deciseconds, respectively. If an arrival has one or more matches, then for each pair of matching arrivals, the squared magnitude of the difference of the U-space locations of the two arrivals is compared to a system parameter (set to $0.0004 \text{ sec}^2/\text{km}^2$). If $[\hat{u}(s) - \hat{u}(g)]^2$ is less, matching arrivals are "confirming."

If arrival p is an s-arrival and has one or more matching arrivals, but none of them is confirming, p is assumed to be a side lobe and is not processed any further. If arrival p is a g-arrival and has at least one matching arrival that is also confirming, p is not processed any further, thereby giving preference to the matching s-arrival (this is overridden for large events). In all other cases, including no matches, p remains eligible for the next test.

The next test, "chaining," checks for related later phases and for additional detection groups generated by the coda of the initial phase. If arrival p has already been identified as a related phase of a previous arrival it will not be processed further. Otherwise each arrival which occurs later than arrival p is checked to see if its start time is within a specified time after p (set to 900 deciseconds) and its U-space location is within a specified distance from p (set to 0.006 secs/km for partition 1, and 0.015 secs/km for partition 2). If so it is considered to be related to p.

8.2.3 Priority Assignments

If the arrival p passes the tests, a priority is assigned and it is added to the process list. Certain specially flagged beams are always assigned priority 1. Otherwise, the ratio R of the arrival SNR to the beam SNR threshold (from the Beam/Location Table) determines the priority as follows:

$$S_1 \leq R, \quad \text{priority} = 1$$

$$S_2 \leq R < S_1, \quad \text{priority} = 2$$

$$S_3 \leq R \leq S_2, \text{ priority} = 3$$

$$S_4 \leq R \leq S_3, \text{ priority} = 4$$

$$R \leq S_4, \text{ priority} = 10 \text{ (not selected)}$$

where the four parameters S_n are currently set to 1024, 2, 1 and 1, respectively. Each time an arrival is added to the process list, the total processing time (assuming a fixed time per event-set to 8 minutes) for each of the priorities is computed. The process level is set to the priority which results in a total workload closest to a predefined optimum level (set to 480 minutes), but not exceeding the maximum tolerable workload (set to 960 minutes). Should the load of priority 1 jobs exceed the maximum tolerable workload, the number of excess jobs is determined. Then this number of jobs, regardless of priority level, is deleted from the most active interval of time. The operator is warned before this situation occurs, and he is given the option of that time of modifying the workload control parameters.

8.2.4 Event Family Grouping (NDPC Only)

The Event Process Controller function of assigning a seismic phase identification to each detected group has been expanded at NDPC to make that assignment based not only on the detection location and prior knowledge of the earth's seismicity, but also on the other detection groups currently present in the Detection File.

Up to three phase identifications may be hypothesized for each detection location. The assignment is made for each detection group to be processed, depending on the occurrence of other detection groups that correspond to the predicable related phase arrivals from the same seismic event. The

hypothesis for which the detection file contains the largest number of confirming related phases is accepted. In case of this, or if no confirming phases are found for a given detection group, the choice shall be based on the relative likelihood of occurrence, depending on the detection location and the seismicity history.

Relative time, U-space and relative amplitude limits, derived from observed seismic data, are specified for each related phase that can be predicted for each hypothesis for each location. These limits define a time window to be searched for potential entries: if more than one is found, those closer to the window center are examined first. The first entry that satisfies the relative amplitude test described below and also falls within the (two-dimensional) U-space window is accepted as being the related phase.

If the seismic data dictates the setting of limits so broad that the chance of a false related phase identification is significant, such a phase identification is discounted 50 percent in counting confirmations of the pertinent hypothesis. Once assigned, a phase identification is not re-evaluated unless this latter circumstance applies.

If the amplitude of the original (initial arrival) detection group is less than a parameterized value, the following test is imposed on each of its potential related phases. To be accepted as a related phase, the ratio of each detection group amplitude to the initial arrival amplitude must not exceed a specified ratio for that related phase.

Activity Numbers and Confirmation Counts are included in the EP Detection Report output.

8.3 SHORT-PERIOD SIGNAL PROCESSOR

The Short-Period Signal Processor (SPSP) contains algorithms for generating a "best" unfiltered array beam waveform and extracting detailed waveform and event parameters. In addition to data of direct usefulness for offline analysis and bulletin publication, the SPSP is capable of determining improved subarray delays for detection beamforming; these delays are included as a part of the normal output. Request for execution of SPSP may be generated automatically by EPCON, or manually by an offline rerun request or from the Editing Processor (see Section 8.6). In manually requested executions the process control parameters supplied by EPCON may be changed. The other form of input data for SPSP is the raw instrument data and status obtained from the Data Tapes (see Figure 8-1). All output from SPSP is put on disk in the EP Data File.

As shown in Figure 8-2, SPSP consists of three major sections:

- a. Array Beamsteering
- b. Waveform Parameter Extraction
- c. Event Characterization

Each of these sections is outlined in the following paragraphs. The values of the parameters named in this section may be found in Sections 8.7 and 8.8. There the parameter names have suffixed numbers 1 to 5 for identification with the five major computational programs; these suffixes have been eliminated in the following text.

8.3.1 Array Beamsteering

The objectives of the Array Beamsteering portion of SPSP are to:

- a. Form subarray beams for all unmasked subarrays (except when using padded seismometers).

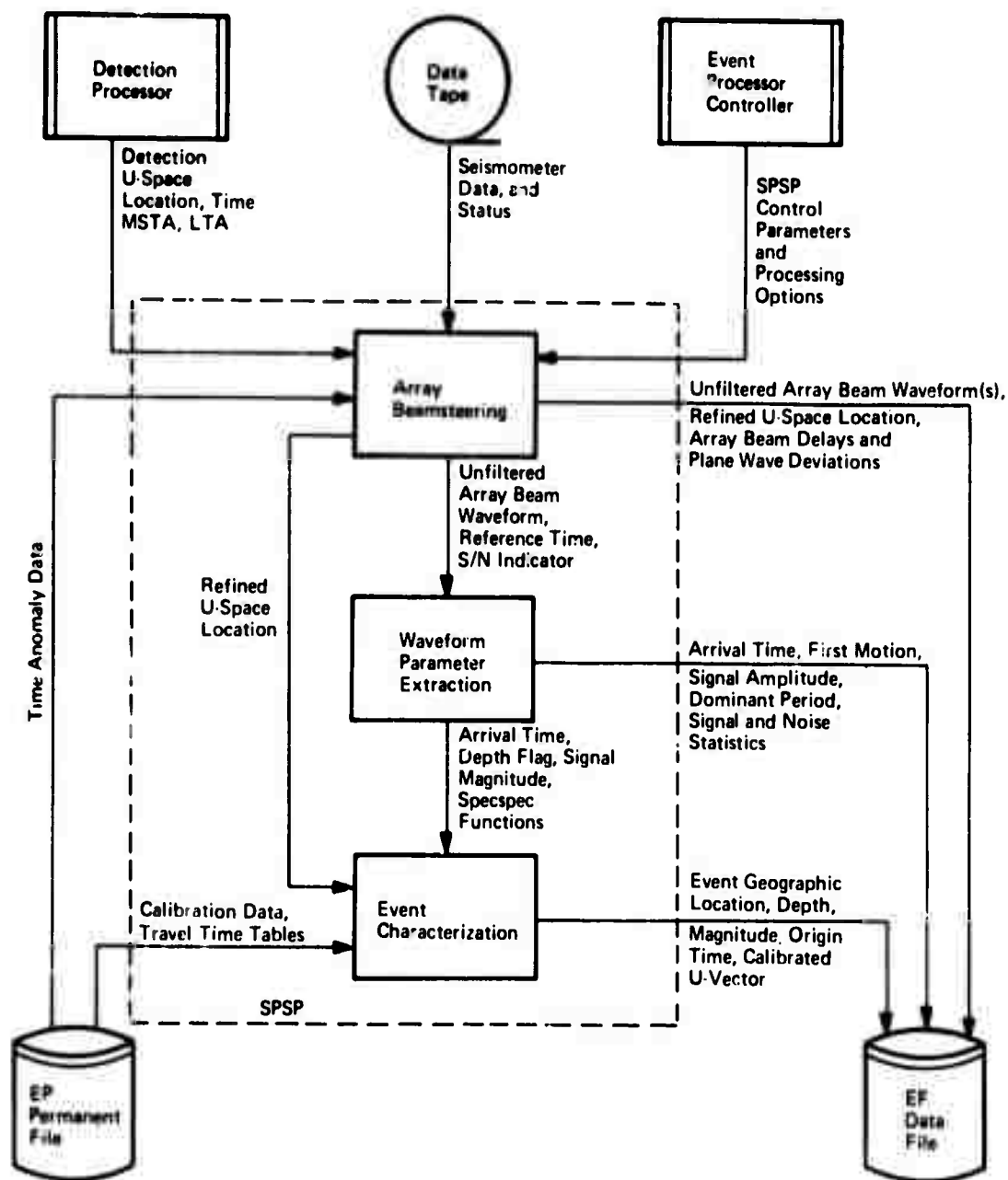


Figure 8-2. Data Flow for the Short-Period Signal Processor

- b. Form an array beam having minimum signal distortion and maximum signal-to-noise ratio.
- c. Generate improved subarray delays and plane wave deviations for the time anomalies data base (see Section 7).
- d. Refine the U-space location provided by the Detection Processor (for determination of the epicenter in Event Characterization).
- e. Refine the arrival time estimate provided by the Detection Processor.

Array Beamsteering is carried out in SPSP by one of the following methods:

- a. Correlation and Sequential Estimation
- b. Beampacking
- c. Default to Detection Processor Parameters

Any one of these three methods of Array Beamsteering may be selected as the standard processing option. The Correlation and Sequential Estimation process is preferred because it is the only process that meets all of the above objectives; specifically, it is the only process which generates improved plane wave deviations. Furthermore, the Correlation and Sequential Estimation process usually generates the best signal waveform and it provides the most accurate U-space location. The output of Array Beamsteering depends on the process employed although SPSP is always initialized with the same data. Figure 8-3 indicates in greater detail the input and output data and the internal control structure of the Array Beamsteering process.

As shown in Figure 8-3, subarray beams are initially steered to the detection U-space location unless (at SAAC only) padded seismometers are used in place of subarray beams. The initial array beam is formed by obtaining the anomalies (Section 7) for the detection location and adding them to the plane wave delays to form a starting set of array beam delays. Unless the

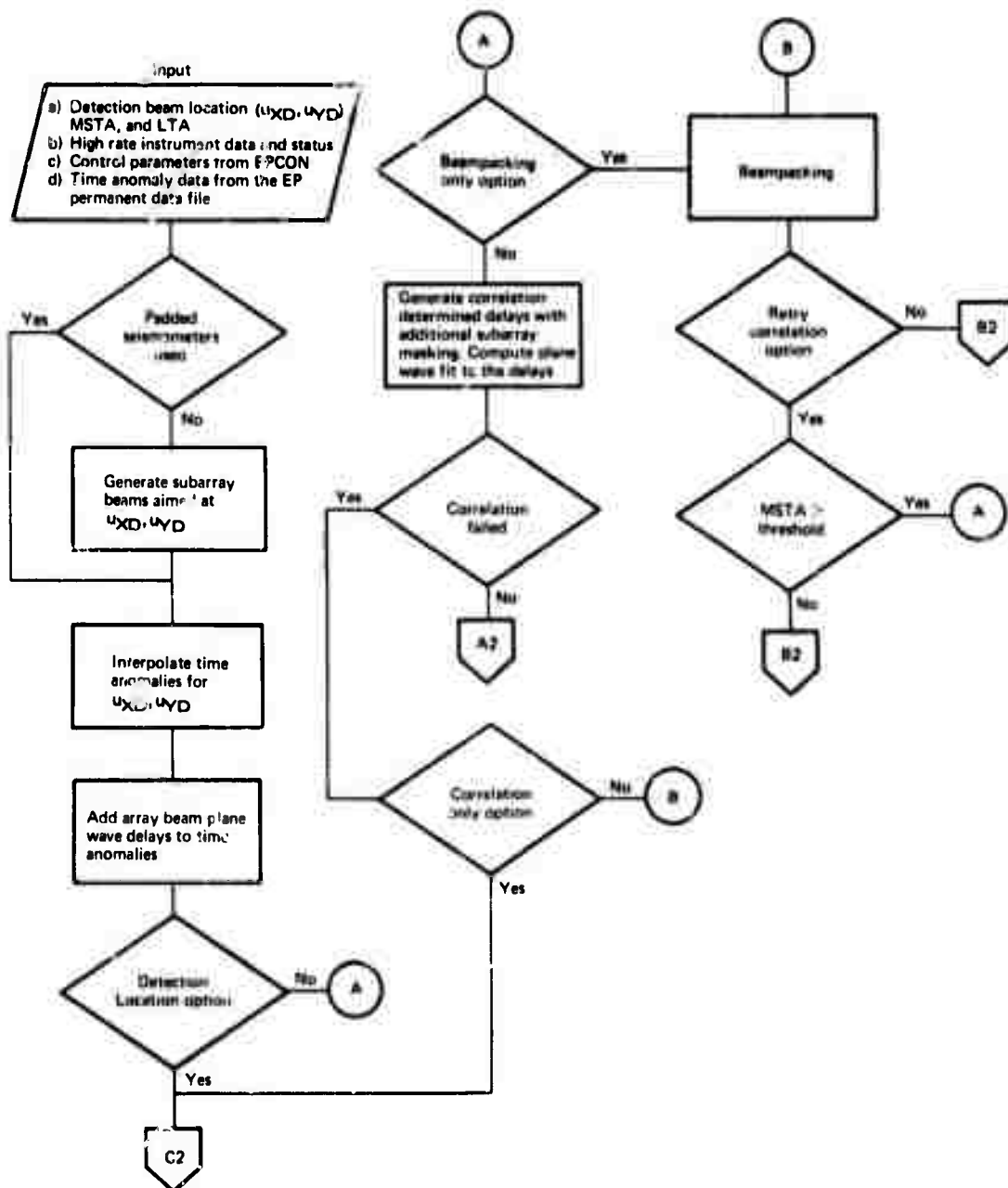


Figure 8-3. Array Beamsteering (Sheet 1 of 2)

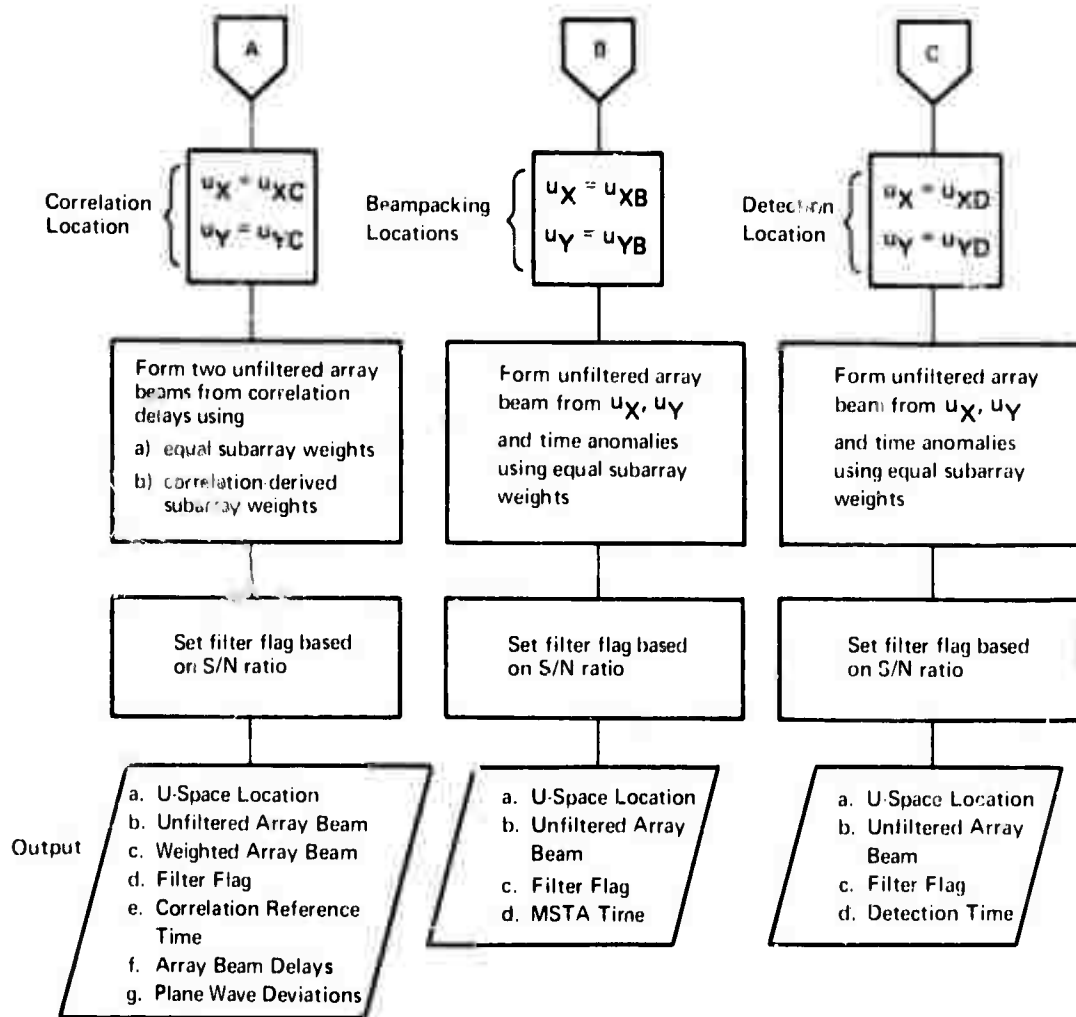


Figure 8-3. Array Beamsteering (Sheet 2 of 2)

detection location option has been selected, the array beam is steered to a refined U-space location using the correlation or the beampacking process. If correlation is selected and successfully executed, then all of the previously described objectives are achieved and a complete output is obtained. If the correlation process fails, then (depending on the control parameters) the beampacking process may be used as a backup procedure.

Figure 8-3 does not show that new subarray beams are formed and Array Beamsteering is repeated whenever the correlation or beampacking process results in a refined U-space location that deviates from the previous subarray beam aiming point by an amount greater than DELTA. Also not shown is the fact that the detection U-space location is used if beampacking should fail.

8.3.1.1 Subarray Beamforming

Subarray beams are used for array beamsteering by either the correlation or the beampacking method; they are also plotted and preserved on event tapes for offline analysis. Subarray beams are formed for a specified U-space location for all unmasked subarrays by applying instrument delays computed from a plane wave model. The initial subarray beam aiming point is the U-space location of the detection beam. If the refined U-space location determined by array beamsteering differs significantly from the subarray beam aiming point, subarray beams are re-aimed to the refined location. In order to extend the dynamic range for large events at SAAC, subarray beams are replaced by the outputs of the padded (attenuated) LASA seismometers, which have 30 dB attenuation compared to the unpadded short period instruments. There are 20 padded instruments in the LASA array, distributed one per subarray with the exception of E3.

8.3.1.2 Subarray Delays for Array Beamforming

Array beamsteering is essentially the process of modifying a set of initial subarray delays in order to improve the array beam. The set of initial subarray delays is obtained by computing plane wave delays and adding interpolated time anomalies for a specified U-space location. The plane wave delays are computed from the specified U-space location and the subarray locations within the array. The time anomaly values are interpolated from a stored data base of selected past events, as described in Section 7.

8.3.1.3 Correlation and Sequential Estimation Process

Figure 8-4 outlines the correlation process for Array Beamsteering. The procedure is one of relative alignment of subarray beams corresponding to peak values of correlation functions computed from the subarray beams and appropriate reference array beams. This is an iterative technique for steering the array beam by adjusting one subarray at a time, until no further improvements are possible within the limits of the specified correlation interval. The procedure uses the relative time location and amplitude of up to three correlation function peaks for each subarray beam. Subarray delays derived from the correlation peak times are first employed for a simultaneous weighted least squares estimate of the inverse velocity vector, where the estimation weights are derived from the correlation amplitudes. Using this inverse velocity vector estimate as a new starting point, the correlation process is repeated and a sequential minimum variance estimate of the inverse velocity vector is then computed. Here, the correct correlation peak is selected for each subarray delay by application of Bayes' decision logic. Those subarray delays having large residual deviations from the plane wavefront are then adjusted to the correlation peak nearest the wavefront, and the correlation and sequential estimation cycle is executed once more to produce the final estimate. The

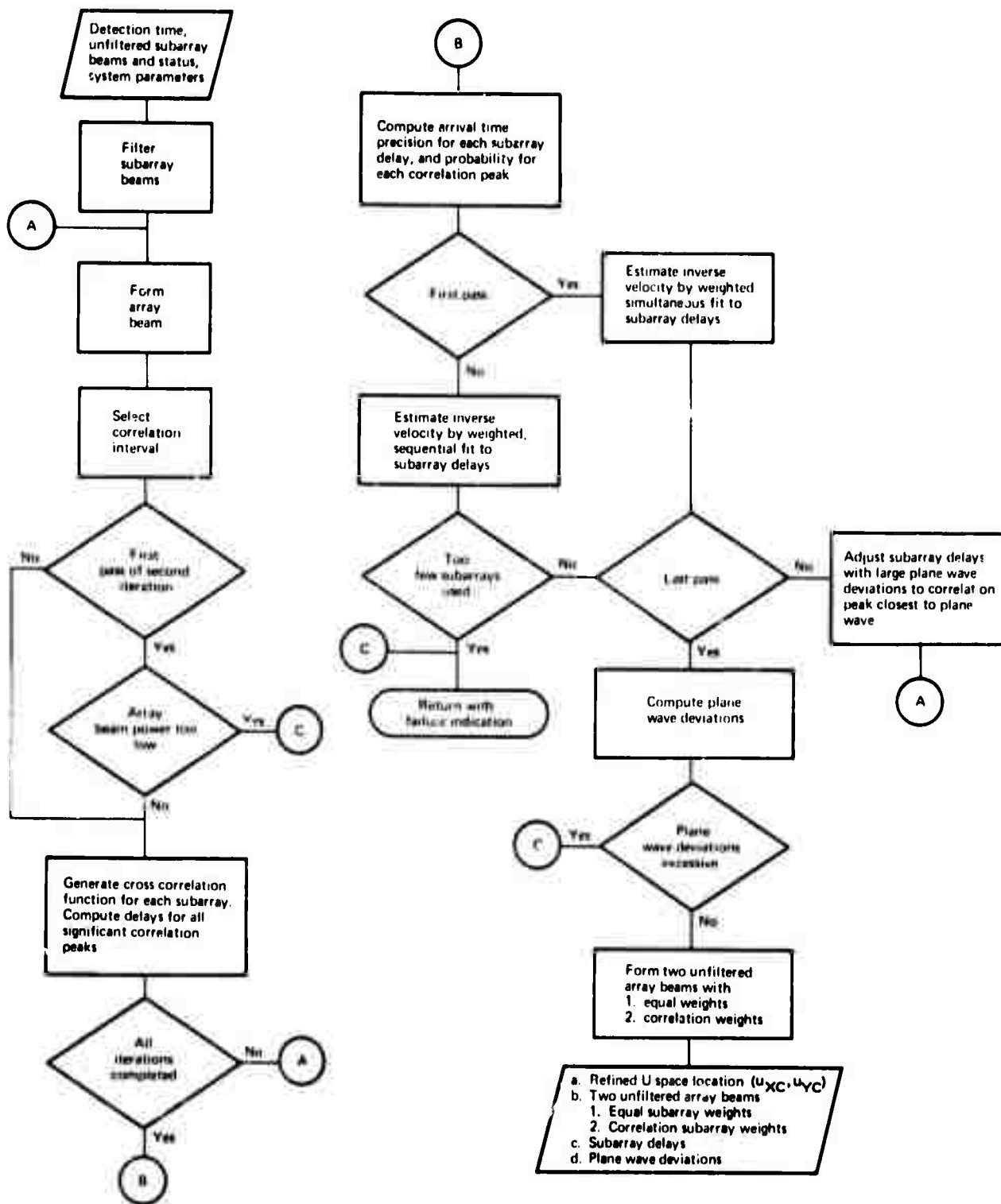


Figure 8-4. Correlation Process for Array Beamsteering

validity of the estimate is tested by comparing a Chi-square value computed from the plane wave deviations against a predetermined confidence level. On the basis of this validity test, the correlation results are either accepted or rejected.

The placement of the correlation interval is achieved as follows: first the instantaneous array beam power envelope is computed over N samples. The sample position of the array beam envelope associated with the maximum derivative over the interval immediately preceding the peak of the array beam power envelope is located. The start time of the correlation interval is given by the sample time of this maximum value less M samples. The correlation interval extends over NA samples. The maximum value of the array beam power envelope in nanometers must exceed the parameter PRTST; otherwise the correlation process is terminated.

Before the correlation function is computed, both the reference array beam and the subarray beam are bias compensated by subtracting out their average values. The reference array beam for the k^{th} subarray is simply a bias-compensated array beam which contains no contribution from the k^{th} subarray. Each of the subarray beams is cross-correlated against its reference array beam with a maximum lead and lag of LD samples. The cross-correlation values are obtained from the correlation formula as in 8-4. The peaks of the correlation function are located and the corresponding peak times are estimated by fitting a quadratic function to the sample correlation values surrounding each correlation peak. If the largest correlation peak of a given subarray does not exceed the parameter RLOWC the corresponding subarray beam is excluded from the array beam because of low correlation. A maximum of NPNAX correlation peaks for a single subarray are candidates for the determination of the corresponding subarray delay. The signal-to-noise ratio of all candidate correlation peaks must exceed 75 percent of the signal-to-noise ratio of the largest correlation peak.

Subarray weights used in estimating the U-space location are proportional to a variable called the subarray precision. The subarray precision is computed for each subarray as the product of the subarray signal-to-noise ratio, the correlation interval time-bandwidth product and the mean-squared angular frequency of the array beam waveform during the correlation interval, as described in Section 6. The subarray signal-to-noise ratio is estimated directly from the maximum correlation peak of that subarray. The selection of the correct subarray delay from multiple correlation peaks is achieved in the sequential estimation process, as described below. This process utilizes an initial probability value which is assigned to each of the correlation peaks. These observation probability values are computed as functions of the subarray signal-to-noise ratio and the relative value of the candidate correlation peak to the maximum subarray correlation peak (see Section 6).

The simultaneous procedure for the U-space estimation is described in Section 6. The subarray delays and subarray locations are used to compute a weighted least squares estimate of a plane wavefront inverse velocity vector. The subarray delay for subarrays with a single significant correlation peak is the time of that correlation peak; for subarrays with multiple correlation peaks, the subarray delay is computed as the weighted average of the times of the candidate peaks using the correlation peak probabilities as weighting factors.

A linear, sequential estimation of the inverse velocity vector is used on the second and third passes of the correlation process and provides the final value of the U-space location. The objective here is to obtain the best possible estimate of the U-space location by selecting the correct correlation peak for each subarray delay. This estimation procedure uses the subarray delays one at a time for the purpose of improving the existing value of the inverse-velocity vector. At each application of a subarray delay, an improved value of the inverse-velocity vector is computed. At each stage, the correlation peak times and probabilities, and the current U-space location mean and variance are used to choose (by means of

a Bayes' decision technique) the correct correlation peak for a selected subarray (see Section 6). The covariance matrix of the inverse-velocity vector and the variance of the subarray delay are computed and used in the estimation process. The a priori information is based on the current inverse velocity vector estimate and the associated error covariance matrix. Only the observed mean and variance of the chosen peak are used for updating (in the minimum variance sense) the estimate and covariance matrix of the inverse velocity vector.

8.3.1.4 Beampacking Process

The beampacking procedure is outlined in Figure 8-5. Each time the beampacking procedure is executed, a set of 19 hexagonally packed array beams is formed. As shown in Figure 8-6, these array beams are arranged in two rings around a specified center beam. Time anomalies are obtained for the center beam only, and used for computing the delays of all 19 beams. The array beam having the maximum short term average (MSTA) over RPRIM samples is found. If the selected array beam is on the outer ring of beams, it is selected as a new center beam and the beampacking process is repeated until an interior array beam is selected. A set of time anomalies are then computed for the U-space location of the selected beam. The time of occurrence of the MSTA for the selected beam is recorded. Significant outputs of the beampacking process include the U-space location, MSTA and MSTA time for the selected beam, and a set of time delays for this beam with the appropriate time anomaly corrections.

8.3.1.5 Final Array Beamforming

An array beam is formed from the unfiltered subarray beam waveforms using all unmasked subarrays and the array beamforming delays generated by the array beamsteering process. If the correlation method was used for array

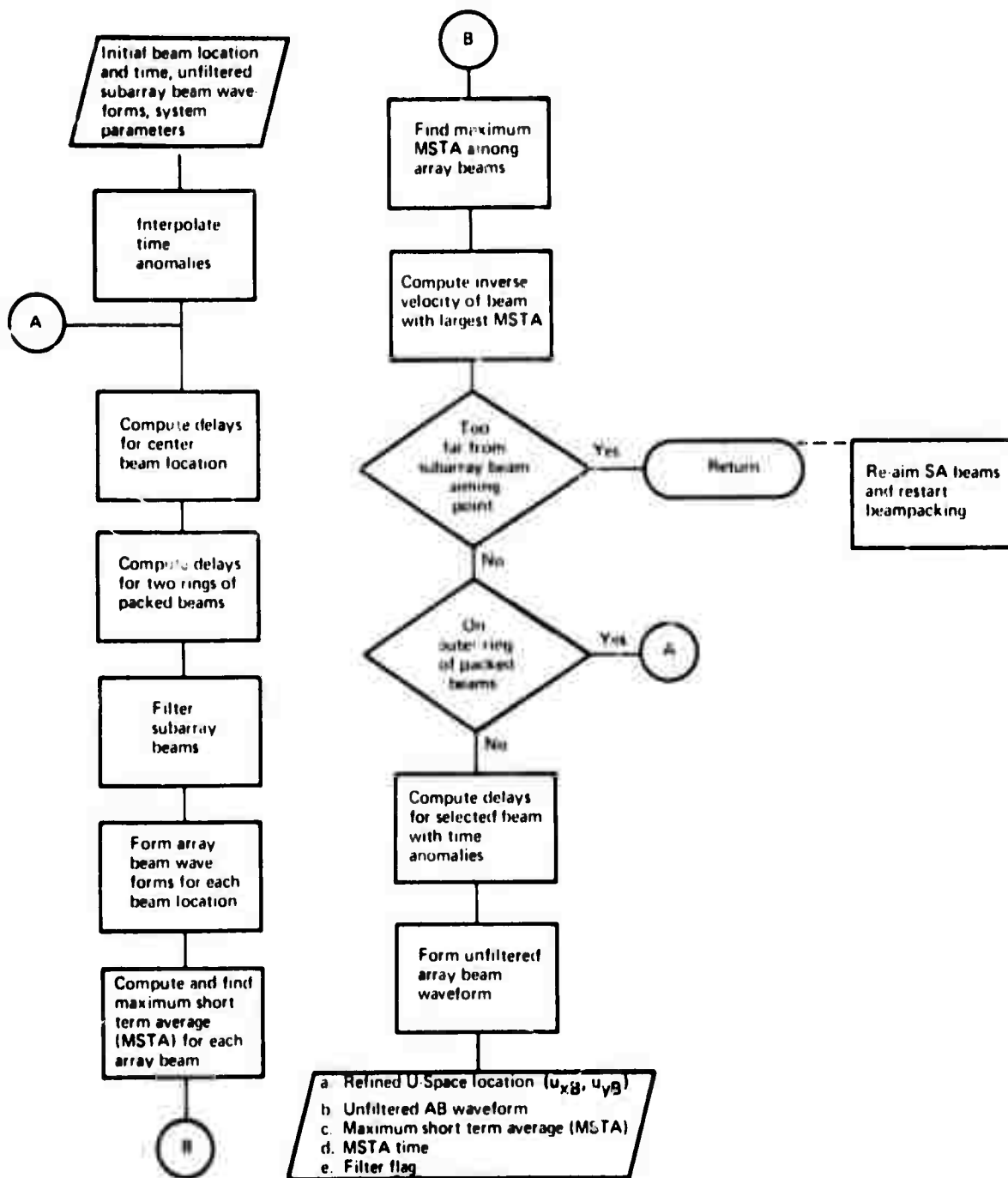


Figure 8-5. Beampacking Process for Array Beamsteering

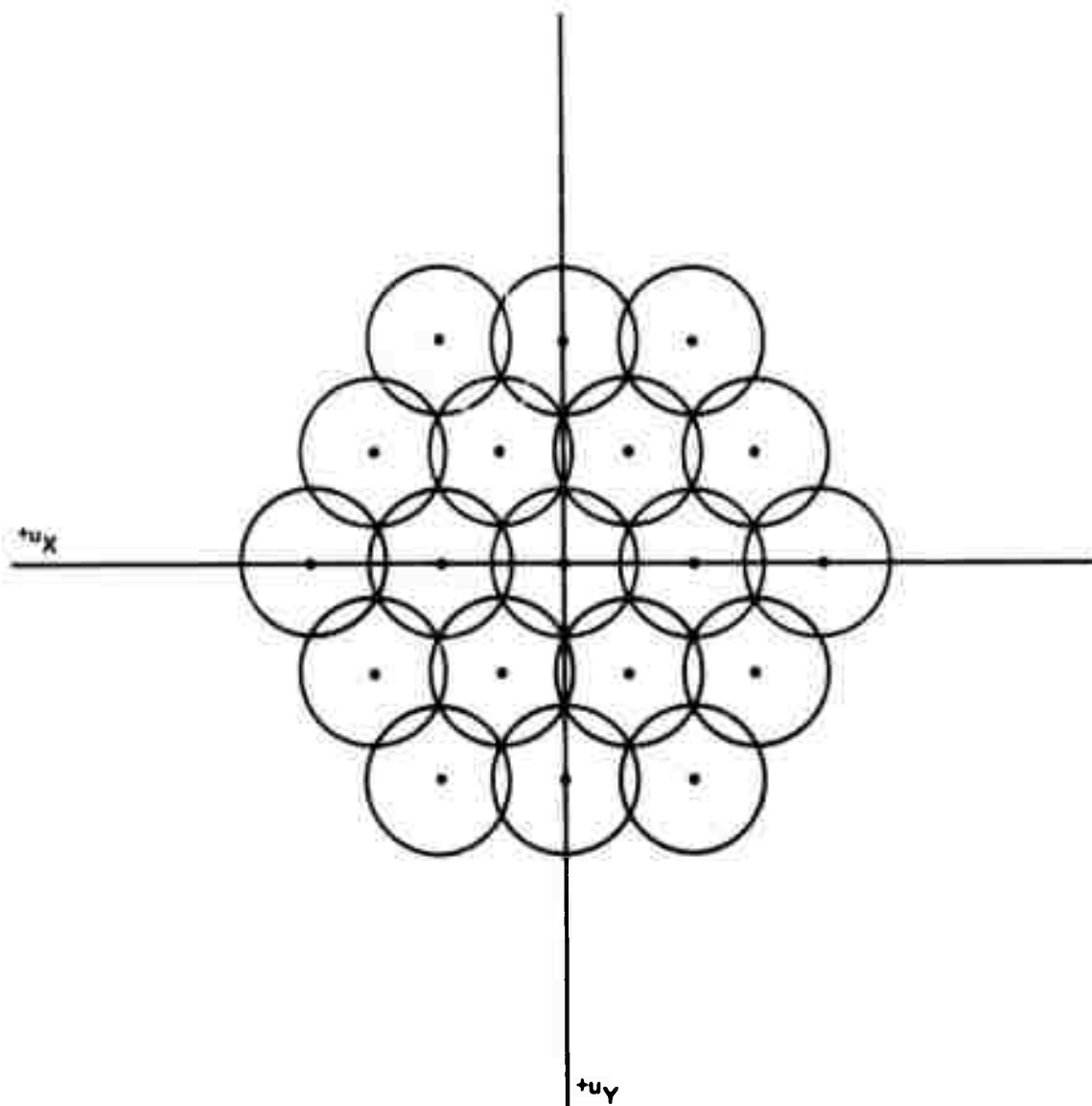


Figure 8-6. Hexagonal Packing Grid

beamsteering, then a weighted array beam is also formed using the same array beamforming delays. The subarray weights are chosen to maximize the array beam signal-to-noise ratio, using estimates of the coherent signal amplitude and the noise power as described in [8-17, Appendix IV].

For each array beam, an estimate of the signal-to-noise ratio is computed and compared with a threshold value. The outcome determines the choice of filter to be used in Waveform Parameter Extraction.

8.3.2 Waveform Parameter Extraction

The Waveform Parameter Extraction portion of SPSP is outlined in Figure 8-7. The objectives of Waveform Parameter Extraction are to:

- a. Filter the unfiltered array beam waveform that was generated in Array Beamsteering
- b. Process this filtered waveform to extract parameters such as arrival time, dominant period, waveform magnitude and amplitude, and array beam signal and noise power estimates.

In addition, multiple signal arrival modes are identified from the envelope waveform, and waveform parameters are extracted for each mode. The first mode is processed to determine the event arrival time and to classify the event as impulsive or emergent. If certain test conditions are satisfied (see Section 8.3.2.5), the first motion direction is computed. Multiple envelope modes indicate the possibility of depth phases being present. If more than one mode is detected for a P phase, then an associated function called the specspec function is computed for both the filtered and unfiltered array beams. This specspec function is used to compute event depth in the Event Characterization portion of SPSP.

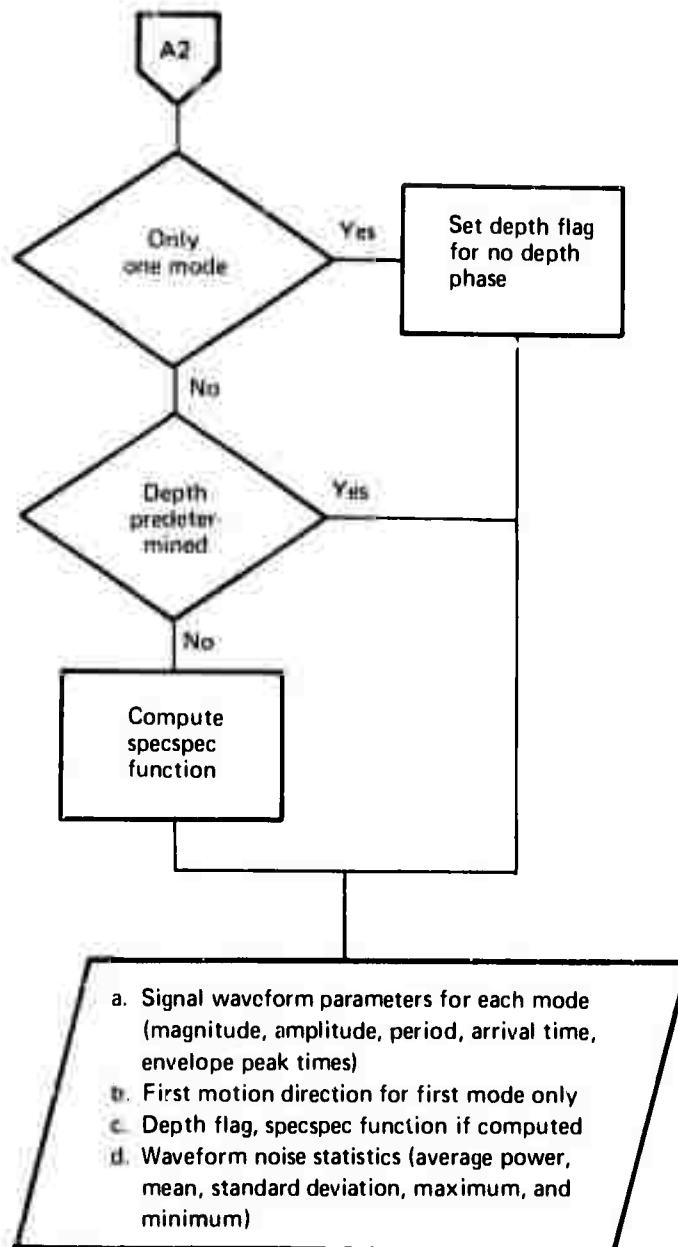


Figure 8-7. Waveform Parameter Extraction (Sheet 2 of 2)

Waveform magnitude and dominant period are determined directly from the waveform, and the amplitude of the seismic event is computed from these two values, as described in Section 8.3.2.6.

8.3.2.1 Instrument Frequency Compensation and Array Beam Filtering

Instrument frequency compensation filtering is done so that the velocity transfer function of the analog channel including the seismometer is made flat from 0.7 to 2.0 Hz. This ensures that the array beam waveform is of sufficient fidelity and has the best possible values for the magnitude and dominant period computations. Frequency compensation of the unfiltered array beam waveform is provided by a fourth order convolution filter as described in [8-11] and whose coefficients are given in Table 8-1. Band-pass frequency filtering is applied to the complete processing interval of NA samples of the frequency-compensated array beam waveform to reduce the noise outside the frequency band of the event. At SAAC either a 0.9-1.4 Hz or a 0.6-2.0 Hz filter is employed depending on the signal-to-noise ratio computed in Array Beamsteering; at NDPC, either a 0.8-2.5 Hz or a 0.75-4.0 Hz filter is used. These are sixth order recursive filters of the Butterworth type as described in [8-4, Section 3.7] and whose coefficients are shown in Table 8-1.

8.3.2.2 Array Beam Signal and Noise Power Envelopes

The array beam signal power envelope is used to determine the waveform magnitude, to select event modes, and to classify the event as impulsive or emergent. The power envelope is computed by averaging the instantaneous waveform power over an interval of NS samples. The computation starts NC samples before detection (or correlation) time and continues to the end of the available array beam data.

Table 8-1. Filter Coefficients-NDPC and SAAC ISRSPS EP Systems

<u>0.9 - 1.4 Hz Butterworth</u>		<u>0.6 - 2.0 Hz Butterworth</u>	
Input	Feedback	Input	Feedback
0.00290	1.00000	0.04188	1.00000
0.00000	-4.08142	0.00000	-3.23828
-0.00870	7.95592	-0.12563	4.90670
0.00000	-9.09282	0.00000	-4.50232
0.00870	6.44500	0.12563	2.66955
0.00000	-2.67754	0.00000	-0.94902
-0.00290	0.53208	-0.04188	0.15977

<u>0.8 - 2.5 Hz Butterworth</u>		<u>0.75 - 4.0 Hz Butterworth</u>	
Input	Feedback	Input	Feedback
0.06696	1.00000	0.31184	1.00000
0.00000	-2.32226	0.00000	-0.32011
-0.20087	2.82102	-0.93552	-0.82768
0.00000	-2.29733	0.00000	0.09831
0.20087	1.38567	0.93552	0.53270
0.00000	-0.51074	0.00000	-0.03876
-0.06696	0.10031	-0.31184	-0.09209

Channel Compensation Filter

Input	Feedback
17166	1.0
2352	0.0
3393	0.0
3290	0.0
1812	0.0

The average noise power over an interval of NL samples is computed starting NB samples before detection time and ending NF samples before detection time. The average noise power is subtracted from the signal power envelope to obtain a better estimate of the signal waveform magnitude. The noise power estimate is also used with the peak value of the signal power envelope to estimate the signal-to-noise power ratio. This S/N value determines the method of computing arrival time as described in Section 8.3.2.5.

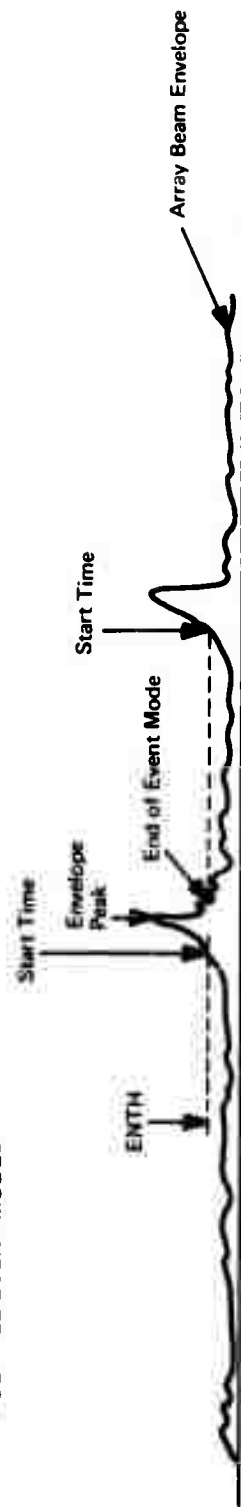
8.3.2.3 Mode Selection and Waveform Classification

The start of an event mode is declared when the power envelope first exceeds the threshold ENTH for ND consecutive samples. The event mode is ended whenever the envelope falls below the threshold ENTH as shown in Figure 8-8. ENTH is computed as the minimum of FR times the signal power envelope peak and ALPHA times the noise power estimate. The times of the first and the largest power envelope peak are determined for each mode. The waveform parameters are extracted from the first four modes as described in Sections 8.3.2.4 and 8.3.2.6.

Multiple envelope modes are an indication that depth phases (such as pP and sP) may be present. The times between the largest peaks of multiple modes may be useful to an analyst for determining depth.

The waveform is classified as impulsive if the number of envelope samples between the start and the first peak of the first mode is less than NG samples; otherwise, the waveform is classified as emergent. The parameter NG was based on the envelope rise times of typical impulsive events.

MULTIPLE EVENT MODES



MULTIPLE PEAKS

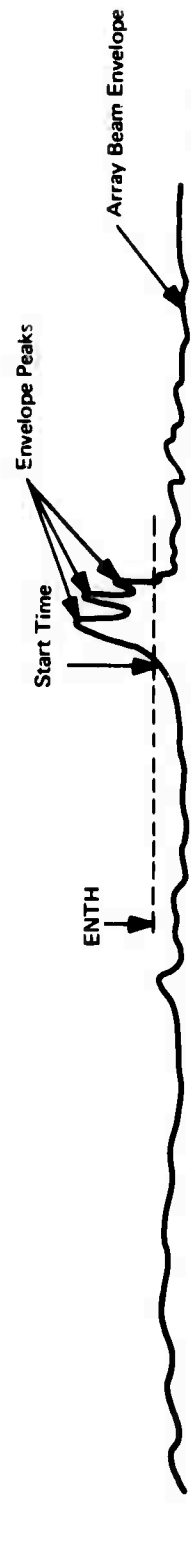


Figure 8-8. Event Mode Determination

8.3.2.4 Waveform Magnitude

The waveform magnitude is computed from the peak value of the signal power envelope. The signal power (RMAG) is estimated by subtracting the average noise power from the peak envelope value; the average noise power is limited to an upper value of 25 percent of the peak envelope value for this purpose. The equation for magnitude uses the average waveform energy and was derived in [8-7] based on the amplitude-dominant period equation by Gutenberg and Richter [8-28]. The waveform magnitude (AMAG) is computed by:

$$AMAG = 0.5 \log_{10} RMAG + B1 + \log_{10} QU + F(I)$$

where

- B1 = factor including the conversion from amplitude and period to average energy of a sine wave, plus a factor 10^6 in Gutenberg's original equation.
- QU = factor for conversion from quantum units to meters
- F(I) = Recursive filter bias factor; I = 1 or 2 depending on the choice of filter.

The coefficients of the frequency compensation filter are scaled so as not to modify the waveform energy.

The waveform magnitude as computed above has not been corrected for distance, phase, or depth; these additional corrections are described in Section 8.3.3.4. A magnitude function made up of values of AMAG over different time points is generated for purposes of determining mode arrival time by model fit as described in Section 8.3.2.5.

8.3.2.5 Arrival Time and First Motion Detection

The event arrival time is determined from the first event mode by one of two methods. The choice is made by comparing the ratio of maximum-signal-plus-noise to average-noise against the parameter THSN. If the ratio exceeds THSN, then the waveform is sufficiently noise-free to use the threshold method; otherwise the arrival time is estimated by the model fit method. The arrival times of all later event modes are determined by model fit.

In the threshold method, the instantaneous signal power waveform is searched over an interval of NAL samples ending with the first peak time to find the first time that a threshold TH is the average noise power scaled by the square of the parameter S. The arrival time is then defined to be the first of the NI samples which exceed the threshold.

A refinement of this threshold arrival time is attempted by correlating the unfiltered array beam waveform with a first motion model function R. The R function consists of two half-cycles of a sine wave with the dominant period of the array beam. The first half-cycle is positive and has amplitude one; the second half-cycle is negative and has amplitude FA. If the maximum absolute value of the correlation function (computed over the interval from NAA samples before to NAB samples after the threshold arrival time) exceeds the parameter FB, this peak correlation time is substituted for the threshold arrival time. Also the first motion of the event is determined to be positive or negative according to the sign of the correlation functions at the (new) arrival time. If the correlation function fails to exceed the value FA, then the threshold arrival time is accepted and no first motion direction is declared.

The model fit method determines arrival time by selecting the minimum point of the mean-squared deviation between the computed magnitude function (AMAG) and the magnitude function of a reference event. The squared

deviations are summed over an NJ sample interval. JSTOP mean-squared deviations are computed, beginning NO samples before the first event mode start time. The event arrival time is declared to be two samples before the beginning of the NJ sample interval corresponding to the minimum mean-squared deviation. The reference magnitude function is chosen from one of two stored functions depending on the selection of array beam filter. The mean values of both the computed and the referenced magnitude functions over each NJ sample interval are removed before the corresponding mean squared deviations are computed.

8.3.2.6 Waveform Dominant Period and Amplitude

The waveform dominant period (T) is determined for each mode by finding the largest Fourier coefficient of the filtered array beam waveform as computed by the Cooley-Tukey fast Fourier transform algorithm [8-11]. These coefficients are computed for a time interval of NH samples centered about a point NTB samples after the correlation reference time (from Array Beamsteering). On later modes the time interval is centered NTB after the mode peak time.

The waveform amplitude (A) is computed from the values of the waveform dominant period and magnitude (AMAG) as follows:

$$A = T \times 10^{AMAG+3}$$

The derivation of this equation is presented in [8-7].

8.3.2.7 Multiple Event Modes and the Specssec Function

The relative arrival time between the first event mode and each of the later event modes is determined. Also, the relative power between the first event mode and the later ones is found by taking the ratio of the respective magnitudes. This information serves to aid the analyst in determining event depth manually.

When depth is computed in Event Characterization, the specssec functions are required. The specssec function is a modified double spectrum function as described in [8-14]. The specssec functions are computed only when:

- a. The depth has not been predetermined
- b. More than one mode has been found in the filtered array beam waveform
- c. The event phase is P or is unknown.

A specssec function is extracted from both the filtered and unfiltered array beam waveform. Computations are made over an interval of NY samples starting NYZ samples before the arrival time.

8.3.3 Event Characterization

Figure 8-9 outlines the tasks performed by Event Characterization. The objectives here are to:

- a. Determine the epicenter (and focus) of the event
- b. Estimate the event origin time
- c. Estimate the event magnitude.

To achieve these objectives, the U-space location is adjusted (calibrated) for the station bias so that it may be used as an input to the travel-time

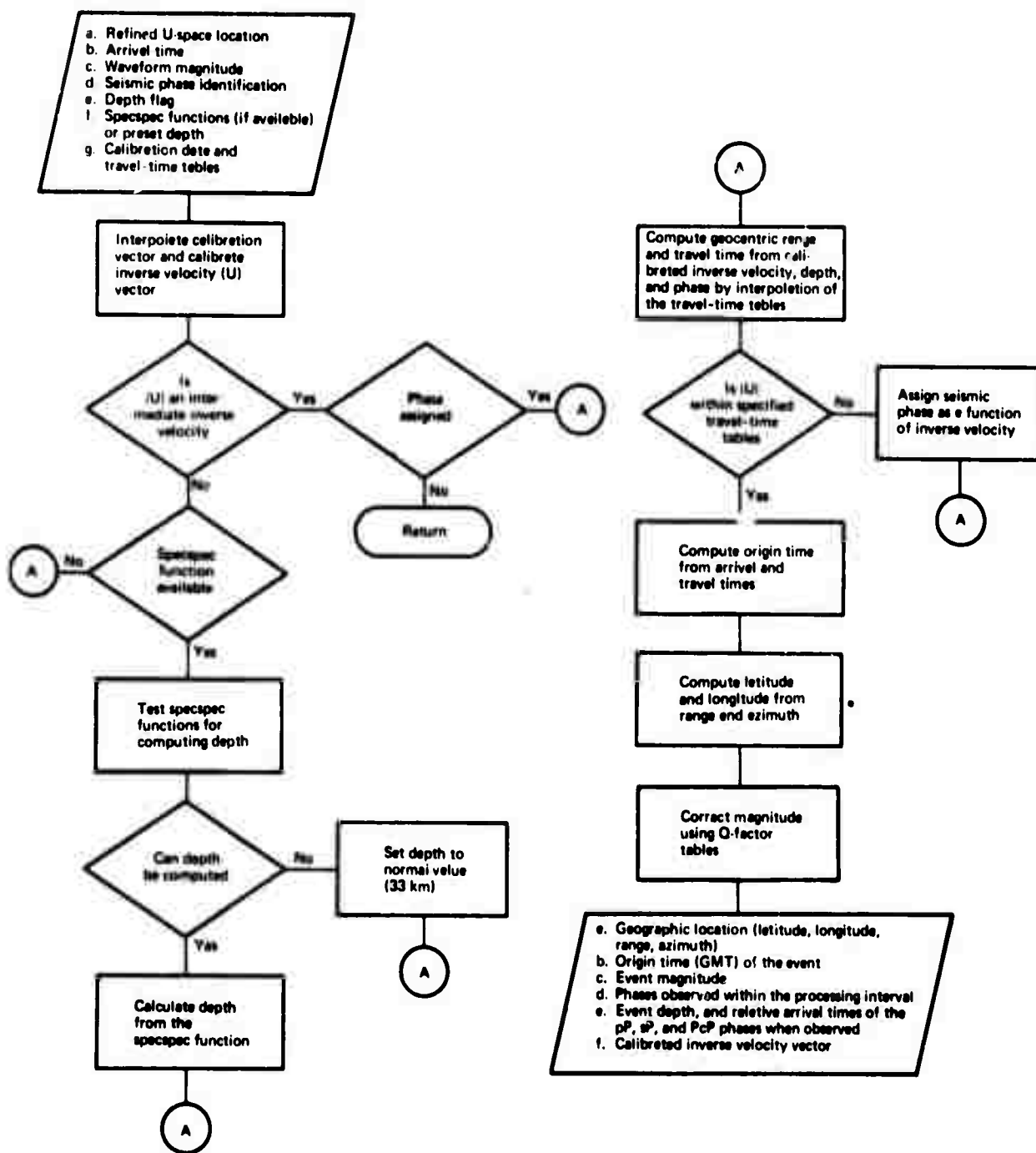


Figure 8-9. Event Characterization

tables which relate inverse velocity, travel time and geocentric range according to a spherical earth model. Under certain conditions described below, the event depth is determined from one of the two specspec functions that were generated in Waveform Parameter Extraction. The travel-time tables for the designated seismic phase are entered with the calibrated inverse velocity and depth to obtain geocentric range and travel time. The travel time is then subtracted from the arrival time (computed in Waveform Parameter Extraction) to obtain the event origin time. The latitude and longitude of the event are computed from the observed azimuth and geocentric range, and from the known geographic location of the seismic array. The waveform magnitude determined in Waveform Parameter Extraction is corrected for distance attenuation (by means of a table-look-up procedure for the appropriate seismic phase) as a function of the event depth and geocentric range.

8.3.3.1 Inverse Velocity Calibration

The inverse velocity (U-space location) may be converted to geocentric range by the use of travel-time tables. These travel-time tables are based on average world-wide observations and therefore do not apply specifically to LASA or NORSAR observations. In order to compute the accurate geographic location of an event, the inverse velocity vector observed at either LASA or NORSAR must be modified by a local bias vector before applying average travel-time tables to obtain geocentric range. This process of modifying the inverse velocity is called calibration, and is implemented in ISRSPS by the access and interpolation process described in Section 7. The depth estimation process also requires calibrated inverse velocity values.

8.3.3.2 Depth Estimation

The estimation of an event depth is attempted if the specs spec functions are available (see Section 8.3.2.7). The procedure (as explained in [8-14]) is to determine the relative delay between the P phase and pP phase by a complex series of tests on the peaks of the specs spec functions. This relative delay is then converted to depth by evaluation of a polynomial. As part of the process of identifying the particular peak of the specs spec function associated with the pP phase, the relative arrival times of the sP and PcP phases may also be determined whenever the peaks of the specs spec functions indicate their presence. If the depth process fails to identify a pP phase or if the event phase is later changed to a non-P phase, the event depth is set to the parameter F9. The depth estimation procedure, as implemented, is limited by the extent of the relative travel time-depth polynomial to the determination of depths between 12 and 250 kilometers.

8.3.3.3 Event Location and Origin Time

The geocentric range of the event is computed by interpolation within the travel-time tables. The travel-time tables are a precomputed set of relative values of calibrated inverse velocity magnitude, geocentric range, and travel time, which have been compiled and stored for various seismic phases and event depths. These tables are entered with known values of phase, depth, and calibrated inverse velocity magnitude; range and travel time are obtained by a four point, divided difference interpolation formula with respect to inverse velocity magnitude, and a linear interpolation of depth. If the event phase has not been specified, the phase is assigned as P, PKPD, or intermediate velocity depending on the inverse velocity magnitude. If the phase is assigned as intermediate velocity, Event Characterization is terminated with no determination of the epicenter parameters.

It may happen that the value of the calibrated inverse velocity magnitude is outside the range of the inverse velocity listed in the table. If it is within the tolerance factor DELTA of the end of the table, the calibrated inverse velocity is changed to coincide with the end of the table for purposes of determining range and travel time. Otherwise, the process attempts to identify the phase as if it was unspecified.

The event origin time is determined by subtracting the estimated travel time from the arrival time previously computed in Waveform Parameter Extraction.

The arrival azimuth is computed directly from the calibrated U-space vector. The latitude and longitude of the event are then computed as described in [8-11] from the range, the known geographic location of the seismic array, and the arrival azimuth.

8.3.3.4 Magnitude Correction

The magnitude found in Waveform Parameter Extraction is adjusted by a correction factor that is a function of event phase, depth, and distance. The correction factors are discussed in [8-20], and are stored on disk in a format similar to the travel-time tables; the same interpolation routine is used in the lookup procedure. The event magnitude (MAG) is estimated by adding the interpolated correction factor (Q) to the waveform magnitude (AMAG) computed by Waveform Parameter Extraction.

8.4 LARGE EVENT PROCESSOR (SAAC ONLY)

The EP Large Event Processor at SAAC rapidly extracts and reports data in response to large event detections passed from DP by channel-to-channel communication. It produces, on the computer operator's typewriter, a

Large Event Report which consists of two messages. The first message contains the following:

- a. The approximate event arrival time, which is the detection time of the seismometer closest to the center of the array
- b. The approximate event amplitude, which is the average of the maximum STAs of the seismometers (in nanometers)

Each LASA subarray except E3 includes a short-period channel with 30 dB attenuation, usually using the seismometer at the subarray center. AT NOR-SAR no attenuated channels are available: large event processing in the NDPC DP uses an unclipped, unfiltered channel from the center seismometer of each subarray.

If a beam detection in the arrival queue can be found which corresponds to the large event, the second message contains the location in latitude and longitude of the most likely seismic phase for that beam. If no beam detection corresponding to the large event can be found, then the second message indicates this condition. The EP Large Event Processor at SAAC also communicates to EPCON that a large event has been associated with a specific detection group, and that detection group is flagged to be processed in SPSP with high priority using attenuated seismometer data rather than subarray beam data.

8.5 OUTPUT PROCESSOR

The Output Processor formats and creates permanent EP outputs from data in the Detection File and EP Data Files. The permanent outputs are created either when all EP Data files become full, or when the analyst (via the Editing Processor) requests the Output Processor to do so. The Output Processor also produces the Detection/Bulletin File for use by the Editing Processor, and a (hard copy) Detection/Bulletin Report for the analyst.

8.5.1 Output Description

EP produces six permanent outputs.

- a. **Parameter Report**—This report contains a listing of all current EP parameters and is produced at least once a day. (See Section 8.7.)
- b. **Summary Report**—This report is produced for each execution of the Short-Period Signal Processor and contains selected intermediate results from that processor. (See Figure 8-10. The brackets indicate output which may either appear or be omitted depending on the course taken by SPSP in processing a particular event.)
- c. **Event Tape**—This tape contains the contents of the EP Data File for each execution of the Short Period Signal Processor and the contents of the Detection File. (See Figure 8-11. All beam traces are 120 seconds in length, beginning 30 seconds before the detection time.)
- d. **Detection Report**—This report lists the contents of the Detection File. (See Figure 8-12.)
- e. **Plot Tape**—This tape contains the data necessary to create subarray and array beam plots for each SPSP execution. (See Section 8.5.3.)
- f. **Seismic Bulletin**—This report is output daily. (See Figure 8-13.)

The Detection/Bulletin File and Report consist of Seismic Bulletin line entries. For every arrival determined by EPCON there is a Detection Line entry, and there is a separate line entry for every signal processed by the Short Period Signal Processor (See Figure 8-14).


```

EVENT DATE: 12/31/70 13651
EVENT NUMBER 9030
DATA TAPE NUMBER 10711 [ ... ]
ISRS/PS EVENT PROCESSING
VERSION 9
12/21/70
XXXXXXXXX
EXPROC
RERUN
ONLINE
JOB MODE
RUN DATE 12/31/70

```

OF PARAMETERS-	VERSION NUMBER	11	PARAMETER SET	14934	BEAM SET	133
	THRESHOLD,ON	10 DB	THRESHOLD,OFF	T 08	Q/Q:	3/3
CONTROLLER INITIALIZATION DATA						
					T 0.4 S	DU 6.0 MS/MM

CRITERIA- S/M 6.3

DETECTION TIME	3/35/53.6	DET UX.UV	-39.9	58.4 MS/KM	LAT.LCN	-1.00	-78.00 DEG	WSTA	308 QU	LTA	370 QU
GROUP START TIME	3/35/53.6	PHASE P		[BEAM NO 268-1]			[DEPTH SET TO XXX.X KM]		0.8P NM		0.0T NM
GROUP STOP TIME	3/36/ 6.0										

REGION CORRECTIONS - Q M Q M LTP114 110-26-701 IC5 NODES WITH R.C. MULTIPLIED BY -1

PROGRAM SPI-1 DATA ACQUISITION AND SUBARRAY BEAMFORMING EXECUTED 1 TIME(S) LAST ENTERED FROM SPO

```

REFERENCE SUBARRAY LAO
BEAM REFERENCE TIME 3/35/10.8
TOTAL SAB SHIFT 0

[PADED SEISMO METER DATA USED]
UX,UY -39.9 58.4 MS/MS
[XXX SAB OVERFLOWS OCCURRED]

[XXX DATA REPLACED]
[XXX READ ERRORS]
[XXX SAMPLES ZEROED]
[XXX SAMPLES REPLACED]
[XXX TIME NOT LOCATED]
[XXX START TIME NOT LOCATED]
[XXX START FILL CANNOT BEGIN]
[XXX NO TAPE/INVALID TAPE FORMAT]
[XXX NO HIGH RATE TAPES ASSIGNED]
[XXX NO PC DATA TYPE NOT SUPPORTED]

[BYPASSED] 1 TIME IS1 LAST ENTERED FROM SPI
[EXECUTED]

PROGRAM SP2-1 MINIMUM VARIANCE ESTIMATION

```

```

PROGRAM SP2-1  MINIMUM VARIANCE ESTIMATION
BYPASSED { EXECUTED } 1 TIME ISI  LAST ENTERED FROM SPI
08-0  0.0-2.5 MZ ORDER 3 FILTER  CORRELATION WINDOW LENGTH 3.2 S  BACKED OFF 1-5 S
CONVERGENCE TOLERANCES-  CHI-SQUARED 4.2-31  MAXIMUM DEV 0.50 S  SIDE LOBE U CHANGE 20 M/J/HR  POWER LEVEL -6.0 DB
PARAMETERS-  F=.25, .25, .25  C=.01, .01, .01  H=.050, 0.50, 0.50  Q1, T0  QUALITY OF CORREL OF POWER
INITIAL CONDITIONS- DATA FROM 3/35/38 TO 3/36/ 8  CORRELATION WINDOW POSITIONED BY MAXIMUM { POWER OF CORREL OF POWER }
WINDOW START TIME 3/35/54.6  UX,UY -36.9  58.4 MS/HR  POWER 0.4 DB
TEST VARIABLES-  CHI-SQUARED 4.27  NUMBER OF SUBRAYS PROCESSED 21  FIRST ITERATION PEAK AVG POWER 2.3 DB

```

FINAL CONDITIONS-		PEAK AVG POWER		NUMBER OF ITERATIONS	
WINDOW START TIME	5/35/53.0	UX,UY	-32.0	50.2 MS/MM	6
		UY SDV	0.83T	UX,UY CROSS CORRELATION	-0.009
		UX SDV	0.99S		

[SUBARRAY BEAMS REALIGNED] [INTERMEDIATE MASKING OF OUTER RINGS]

CORRELATION FAILED - { LACK OF POWER
CHI-SQUARED TEST
TOO MANY SUBARRAYS MASKED }

CORRELATION ABNORMALLY TERMINATED. ERROR CODE IS XX
CORRELATION TERMINATED DUE TO PROGRAM INTERRUPT - ILEXXXXI

SUBARRAY LABEL		NO. OF SETS.	MASKS INIT/FINAL	BEAMPACKING DETECTION										SUBARRAY PN DEV (S)	RC (S)	CC	S/N(CCC)	SA AMP MIN/DB	AB WT
				INITIAL DELAY (S)	CHANGE IN DELAY (S)	INTERPOLATED DELAY (S)	EST. SDV (S)												
L40		14	1 1	0.0	-C.00	-0.00	0.16	0.04	0.0	0.02	1.06	0.51-6.71	1.55						
L41		16	1 1	0.0	-C.84	-0.84	0.15	0.03	-0.08	0.87	3.03	0.61-5.11	1.84						
L42		16	1 1	0.5	-C.79	-0.79	0.18	-0.29	-0.05	0.67	0.41	0.51-6.51	0.59						
L43		16	1 1	-0.1	-C.90	-1.00	0.16	0.03	0.02	0.78	2.79	0.41-7.71	1.28						
L44		14	1 1	-0.7	-C.78	-1.46	0.15	-0.02	0.06	0.85	2.67	0.71-2.71	1.23						
L45		15	1 1	0.8	-C.83	-1.63	0.15	0.01	0.04	0.86	2.86	0.91-1.21	1.10						
L46		16	1 1	0.6	-C.83	-0.03	0.17	-0.02	-0.07	0.75	0.64	0.71-3.31	0.63						
L47		16	1 1	-1.0	-C.79	-0.15	0.15	-0.06	0.02	0.87	3.10	0.71-2.51	1.40						
L48		16	1 1	-1.0	-C.79	-1.79	0.15	0.02	0.15	0.86	2.91	0.91-0.91	1.08						
L49		16	1 1	0.0	-C.82	-0.82	0.17	0.00	-0.04	0.75	0.64	1.31-2.11	0.34						
L50		16	1 1	1.9	-C.96	0.94	0.17	0.11	-0.07	0.77	0.73	0.51-5.61	0.93						
L51		14	1 1	-0.1	-C.90	-1.00	0.15	0.07	0.20	0.93	5.94	1.51-3.21	1.38						
L52		15	1 1	-2.7	-C.84	-3.54	0.16	0.09	0.47	0.78	0.80	0.61-3.81	0.83						
L53		16	1 1	-3.1	-C.90	-4.00	0.15	-0.12	0.44	0.93	6.35	1.41-2.91	1.54						
L54		12	1 1	3.8	-C.85	-2.95	0.17	-0.05	-0.10	0.55	0.63	0.41-7.51	0.34						
L55		15	1 1	2.3	-C.80	-2.00	0.15	0.08	0.21	0.90	4.48	1.21-1.41	1.29						
L56		14	1 1	-2.7	-C.83	-3.73	0.15	0.07	0.29	0.90	4.23	1.41-2.71	1.04						
L57		16	1 1	-1.8	-C.99	-2.79	0.18	-0.01	0.43	0.68	0.44	1.21-1.81	0.24						
L58		15	1 1	6.8	-1.66	-5.74	0.15	0.17	0.48	0.91	4.68	2.51-7.81	0.64						
L59		15	1 1	1.6	-C.73	-0.87	0.16	0.03	0.27	0.90	2.11	1.01-0.21	1.40						
L60		15	1 1	-7.0	-C.80	-7.80	0.15	0.11	0.02	0.98	3.54	1.31-2.51	0.89						
ARRAY BEAM 20.1126-11																			
WEIGHTED ARRAY BEAM NOISE IMPROVEMENT 1.3 DB																			
PROGRAM SP3-1 BEAMPACKING AND ARRAY BEAMPACKING {BYPASSED {EXECUTED 1 TIME(S)} LAST ENTERED FROM SP2																			
BEAM RADIUS 2.0 MS/MH NO OF RINGS 2 OU 20.0 MS/MH MSTA CHECK 2 MH DP-8 0.9-1.4 HZ ORDER 3 FILTER																			
INTEGRATION INTERVAL 1.8 S RATE 3.33 MZ SEARCH INTERVAL 15 S BEGINNING 12 S BEFORE DETECTION TIME																			
BEAMS PACKED 1 TIMES MAXIMUM ALLOWED 25 TIMES																			
NEIGHBORING BEAM ARRANGEMENT																			
INITIAL INTERMEDIATE(1) FINAL																			
6 1																			
5 F 2																			
4 3																			
ARRAY BEAM SHIFT 0																			
UX (MS/MH) -40.0 -40.0 -40.0																			
UY (IPS/MH) 58.0 58.0 58.0																			
MSTA MSTA REL TO FINAL																			
0.71 0.01 0.5(-0.5) 0.71 0.01																			
35/54.2 35/52.1 35/54.2																			
0.51-2.91 0.31-7.41 0.41-4.91 0.41-4.91 0.41-4.91 0.61-1.31 0.31-7.41																			
35/54.2 35/53.9 35/54.2 35/53.9 35/53.9 35/53.9 35/53.9																			

Figure 8-10. Short-Period Summary Report (Sheet 2 of 3)

PROGRAM SP4-1 EVENT PARAMETER EXTRACTION

SIGNAL AVERAGING WINDOW 1.8 S RMS NOISE WINDOW 21 S MODE DETERMINATION PARAMETERS-- .25 TIMES MAX POWER
 USED (WEIGHTED) ARRAY BEAM 31.8 SEISMOMETERS TOTAL SHIFT 0 PROCESS (LATER MODES FIRST MODE ONLY)
 SP4 COULD NOT COMPLETE PROCESSING NO NOISE NO EVENT MODES - JOB TERMINATED
 BP-B 0.6-2.0 HZ ORDER 3 FILTER E.KAZAKH 10/17/67 4 MODE(S) FOUND, 4 MODE(S) PROCESSED
 NOISE- WINDOW LENGTH 17.5 S MEAN -0.0 NM RMS 0.2 NM MAX 0.5 NM MIN -0.5 NM
 DETECTION CORRELATION TIME 3/35/55.4
 BEAMPACKING
 MODE 1 ARRIVAL TIME DETERMINED BY ENVELOPE MODEL FIT-- MEAN 0.000, SDV 0.027
 THRESHOLDING
 MODE THRESHOLD TIME ARRIVAL TIME FIRST PEAK MAX PEAK AMPLITUDE (NM) HERTZ (HZ) LOG A/T
 1 3/35/51.8 3/35/51.2 3/35/53.0 3/35/53.0 2.06 1.82 0.16
 2 3/35/55.4 3/35/55.1 3/35/56.8 3/35/56.8 3.26 1.77 0.43
 3 3/36/ 0.4 3/36/ 0.5 3/36/ 0.5 3/36/ 0.5 1.56 1.07 0.17
 4 3/36/ 3.1 3/36/ 3.7 3/36/ 3.7 3/36/ 3.7 1.64 0.98 0.22
 PHASE INCONSISTENT WITH VELOCITY
 INTERMEDIATE VELOCITY
 PHASE-DEPTH TABLE ERROR
 DEPTH GREATER THAN 250 KM

PROGRAM SP5-1, SP6-1 EVENT CHARACTERIZATION
 SP5 DR SP6 COULD NOT COMPLETE PROCESSING
 AP-P 5.5 S EXPECTED XP-P 7.7 S
 NO DEPTH PRESENT ON BEAM
 DEPTH PREDETERMINED
 NO DEPTH PHASE FOUND
 PRIMARY PHASE IS XXXXXX
 EVENT LOCATION
 UX(MS/KM) UY(MS/KM) LAT(DEG) LON(DEG) RANGE(OEG) AZ(DEG)
 OBSERVED -38.77 58.24 4.03 -82.12 47.3 146.4
 CALIBRATION 0.47 -5.32 -5.89 4.40 7.1 -2.2
 CORRECTED -38.50 52.92 -1.86 -77.72 54.4 144.1
 PHASE VELOCITY 15.3 KM/S TOTAL U 65.3 MS/KM

DEPTH 17.8 KM
 NO DEPTH CALCULATED
 EVENT TIMES
 ARRIVAL TIME 3/35/51.2
 TRAVEL TIME 9/25.0
 ORIGIN TIME 3/26/26

SP5 DR SP6 COULD NOT COMPLETE PROCESSING
 OBSERVED PCP-P [XX.X S]
 NO PCP-P
 MAGNITUDE CORRECTION
 LOG A/T 0.16
 MAG CORR FACT 3.67
 CORRECTED MAG 3.83

LASA SEISMO BULLETIN FOR 31 DEC 1970 (DAY 365/70) FORMAT 5
 1 31 DEC 1970
 2 3 26 26 1.95 77.7M 17 C 3.8 107 ECUADOR
 3 3 35 51.2 LAO P 2.1 1.4 15.3 54.4 144.1

Figure 8-10. Short-Period Summary Report (Sheet 3 of 3)

Record Identifier	Record Length (Bytes)	Record Description	Reason for Absence
CM	3000	Global COMMON	
SV	2926	Short Period Variable File	
SB	8602	Subarray Beam Data (8 records of 150 samples each for 22 channels)	
UR	2402	Unweighted Array Beam (aimed at calculated event location)	
WB	2402	Weighted Array Beam (aimed at calculated event location)	Correlation Failed
SU	2052	Unfiltered Specspectrum Function (1025 values)	No Depth Calculation
SF	2052	Filtered Specspectrum Function (1025 values)	No Depth Calculation
CU	1404	Unfiltered Confidence Function (701 values)	Not used in Depth Calculation
CF	1404	Filtered Confidence Function (701 values)	Not used in Depth Calculation
BU	242	Unedited Bulletin Entry	Premature Termination of SPSP
DF	6602	Detection File Data (1 - 5 records)	
EB	3210 - header 4002 - data	Seismic Bulletin (Edited) (header + 1 - 8 data records)	

Figure 8-11. Event Tape Record Characteristics

Legend:

P	Partition Number
PRIOR	Priority
EPC	EPCON Processing Code
MTC	Arrival Matching Code
SAQRNO	Signal Arrival Queue Record Number
DFRECNO	Detection File Record Number

EPX	ARRIVAL INTERVAL	UC	DETECTION REPORT			HEAM P	PRIOR	EPC	PHASE	MTC	SAQRNO	DFRECNO	PAGE
			UV	MSTA	LTA								
10	286/ 4.13. 3.1 - 4.13.13.3	35.0	15.1	74.9	706	17.0	3	1	3	2	62	1	1
20	286/ 4.13. 4.0 - 4.13.11.2	33.0	17.1	612	740	13.2	10	7	0	2	63	2	2
30	286/ 4.51.28.1 - 4.51.38.9	-10.0	41.1	2645	3052	13.9	2	1	1	2	64	3	3
40	286/ 4.51.33.2 - 4.51.38.6	-13.0	40.0	1698	3650	17.9	10	7	1	2	65	4	4
50	286/ 6.45.24.3 - 6.45.28.5	59.3	-54.1	428	697	9.8	1	1	1	2	66	5	5
60	286/ 6.45.25.8 - 7. 6.49.3	66.0	-62.9	245	574	7.8	10	7	1	2	67	6	6
70	286/ 7. 6.57.7 - 7. 7. 4.3	37.4	19.5	891	1027	13.9	2	1	1	2	68	7	7
80	286/ 7. 6.58.6 - 7. 7. 5.2	26.4	28.6	521	781	10.7	10	7	0	2	69	8	8
90	286/ 8. 2.26.0 - 8. 2.30.2	39.6	77.1	297	617	17.7	10	0	1	0	70	9	9
100	286/ 9. 4.17.1 - 9. 4.21.3	-32.5	45.4	1797	1191	24.3	2	1	1	0	71	10	10

Figure 8-12. Detection Report

IBM SAAC

MIT LINCOLN GROUP 64/ATTN. DR. RICHARD T. LACOSS

COAST AND GEODETIC SURVEY/ATTN. MR. JAMES LANDER

AFTAC/VSC/ATTN. MR. HARTENBERGER

U.S. GEOLOGICAL SURVEY/ATTN. DR. IYER

LASA SEISMO BULLETIN FOR 06 APR 1970 (DAY 09 6/70) FORMAT 5

1 06 APR 1970

2	3	49	34	38.2N	26.9E	16	C	6.1	365	AEGEAN	SEA	
3	4	2	11.7	LAO	P	198.7		1.0		22.6	85.7	35.3
4	4	2	17.2	LAO	E	238.1		1.1		22.6	85.7	35.3
2	4	3	39	50.6N	177.9E	15	C	4.6		6	RAT ISLANDS, ALEUTIANS	
3	4	12	18.6	LAO	P	11.8		1.3		14.4	48.3	304.2
4	4	12	24.3	LAO	E	7.8		1.1		14.4	48.3	304.2
4	4	12	47.7	LAO	E	6.0		1.2		14.4	48.3	304.2

REPORTING INTERVALS FOR 06 APR 1970

START	STOP
0355	0413

RECORDING INTERVALS FOR 06 APR 1970

START	STOP	RETENTION
0355	0420	1 YEAR

(ALL TIMES ARE GMT)

DATA TAPES ARE AVAILABLE FOR THE DESIGNATED
RETENTION PERIOD.

10 DEC 1970

SEISMIC ARRAY ANALYSIS CENTER
4301 CONNECTICUT AVE. N.W.
WASHINGTON, D.C. 20008
TWX 710 822-1963 IBM SAAC

Figure 8-13. Seismic Bulletin

13 OCT 1970

PART 1

DETECTION BULLETIN FILE REPORT

LINE IND	ARRIVAL TIME	SA	PHASE	AMP	PERIOD	VEL	RANGE	AZI	LINE NUM	EPX NUM	REL EPX	EP CODE	EDIT PRINT
0	4 13	3-1	LAO KPRA	2-1	-	26.3	-	246.6	10	10	10	1	0
2	3 50	24	18-85	33C C	5.1	182	FIJI ISLANDS	-	20	10	10	1	
3	4 12	58.8	LAO P	8.1	1.2	24.4	94.7	247.7	30	10	10	1	
4	4 13	4.0	LAO E	6.9	1.8	24.4	94.7	247.7	42	10	10	1	
4	4 13	6.0	LAO E	6.0	1.7	24.4	94.7	247.7	50	10	10	1	
4	4 13	18.4	LAO E	7.7	1.3	24.4	94.7	247.7	60	10	10	1	
0	4 13	4.0	LAO	1.7	-	26.9	-	242.5	70	20	20	7	0
0	4 51	28.1	LAO P	7.6	-	19.7	-	143.9	80	30	30	1	U
2	4 39	26	23-55	33C C	5.6	122	NEAR COAST OF N. CHILE	-	90	30	30	1	
3	4 51	26.0	LAO P	73.2	1.0	19.7	76.8	146.9	100	30	30	1	
0	4 51	33.2	LAO P	4.6	-	19.3	-	143.5	110	40	40	7	0
0	4 45	24.3	LAO P	1.2	-	12.4	-	312.1	120	50	50	1	0
2	6 39	44	61-24	33C C	4.0	2	SOUTHERN ALASKA	-	130	50	50	1	
3	6 45	18.3	LAO P	5.1	1.2	12.0	25.2	318.3	140	50	50	1	
0	6 45	25.8	LAO P	0.7	-	11.0	-	313.6	150	60	60	7	0
0	7 6	57.7	LAO P	2.6	-	23.7	-	242.5	160	70	70	1	0
2	6 53	36	17-95	20 C	4.9	182	FIJI ISLANDS	-	170	70	70	1	
3	7 6	51.4	LAO P	7.2	1.3	24.2	93.6	247.9	180	70	70	1	
4	7 6	59.1	LAO E	3.6	0.6	24.2	93.6	247.9	190	70	70	1	
0	7 6	58.6	LAO	1.4	-	25.7	-	222.7	200	80	80	7	0
0	8 2	26.0	LAO P	0.8	-	9.5	-	202.2	210	90	90	0	U
0	9 4	17.1	LAO P	5.2	-	17.9	-	144.4	220	100	100	1	U
2	8 52	32	21-55	68.7W	120 C	5.1	124	CHILE-BOLIVIA BORDER RES.	230	100	100	1	
3	9 4	13.5	LAO P	30.4	1.0	19.5	75.8	144.2	240	100	100	1	
4	9 4	43.2	LAO E	29.8	1.1	19.5	75.8	144.2	250	100	100	1	
4	9 4	55.7	LAO E	15.9	1.0	19.5	75.8	144.2	260	100	100	1	
			0346	0915					270	99998	99998		*
			0000	0315					280	99999	99999		*
			0315	0346					290	99999	99999		*
			0346	2400					300	99999	99999		*

Detection Processing Interval

Figure 8-14. Detection/Bulletin Report-Partition 1

8.5.2 Processor Execution

The Output Processor is executed either:

- a. Upon operator request
- b. Automatically after the Editing Processor has requested publication of the seismic bulletin
- c. Automatically when the EP Data Files have become full
- d. Automatically when the Detection/Bulletin File has become full.

Output processing (see Figure 8-15) follows one of two sequences, depending on conditions at the time the processor is called. If there is a Detection/Bulletin File (DBF) partition which is to be published, the Output Processor first prints the Parameter Report and also checks some of the parameters against reasonable constraints. If a constraint is violated a warning message is printed. The Output Processor then copies the DBF onto the Event Tape and produces TWX Bulletin output. Publication is either requested by the analyst via the Editing Processor or is automatic if, in trying to generate or update the DBF, the DBF is found to be full. (Once the bulletin has been published, that DBF partition is freed.)

When there is no bulletin publication pending, the Output Processor generates a Summary Report for each processed event (if this has not already been done), writes the appropriate files on the Event tape for these events, generates or updates the Detection/Bulletin File (reruns are not included), produces a current Detection/Bulletin File Report and Detection Report, and creates a Plot Tape entry for each event if a plot request exists.

8.5.3 Plot Output

The request for a plot can be made in the following four ways:

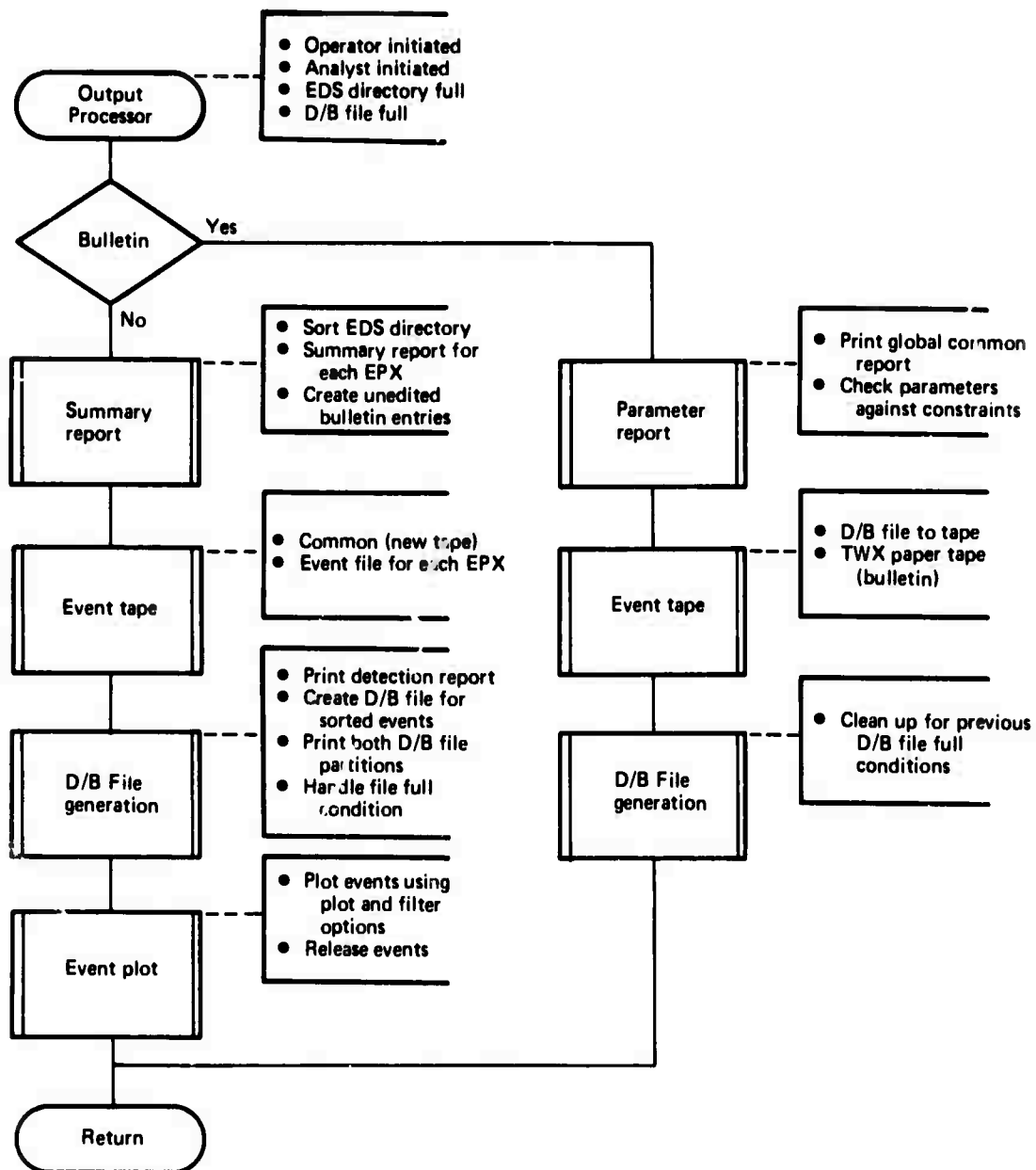


Figure 8-15. Output Processor General Flow

- a. The analyst may specifically request a given plot via the Editing Processor. He may specify the filter and other plot parameters.
- b. When automatic publication occurs, plots are automatically requested for all events in the DBF not already plotted or released.
- c. When the analyst requests Bulletin publication via the Editing Processor, plots are automatically requested for all events in the DBF as above.
- d. If the EP Data Files become full, plots are automatically requested for the earliest five events for which files are available.

The default plot parameters (used for all automatically requested plots) are typically set to provide a bandpass Butterworth sixth order filter (0.6 - 2.0 Hz at SAAC; 0.75 - 4.0 Hz at NDPC), three plot panels, and center segment (40 seconds) plots only. Alternate options are array beams panels only (40 seconds) or full 120 seconds of plotted traces on all panels.

Figure 8-16 shows examples of 40 second panels. The plot shows the unfiltered array beam normalized relative to the amplitude of the noise preceding the event (ABN), the unfiltered array beam normalized to the signal amplitude (AB), the filtered array beam (FAB), the filtered array beam with relative subarray weighting (WAB), and four partial array beams (PAB1-4) formed from subsets of subarrays as indicated. Filtered subarray beam waveforms are plotted on sheets 2 and 3.

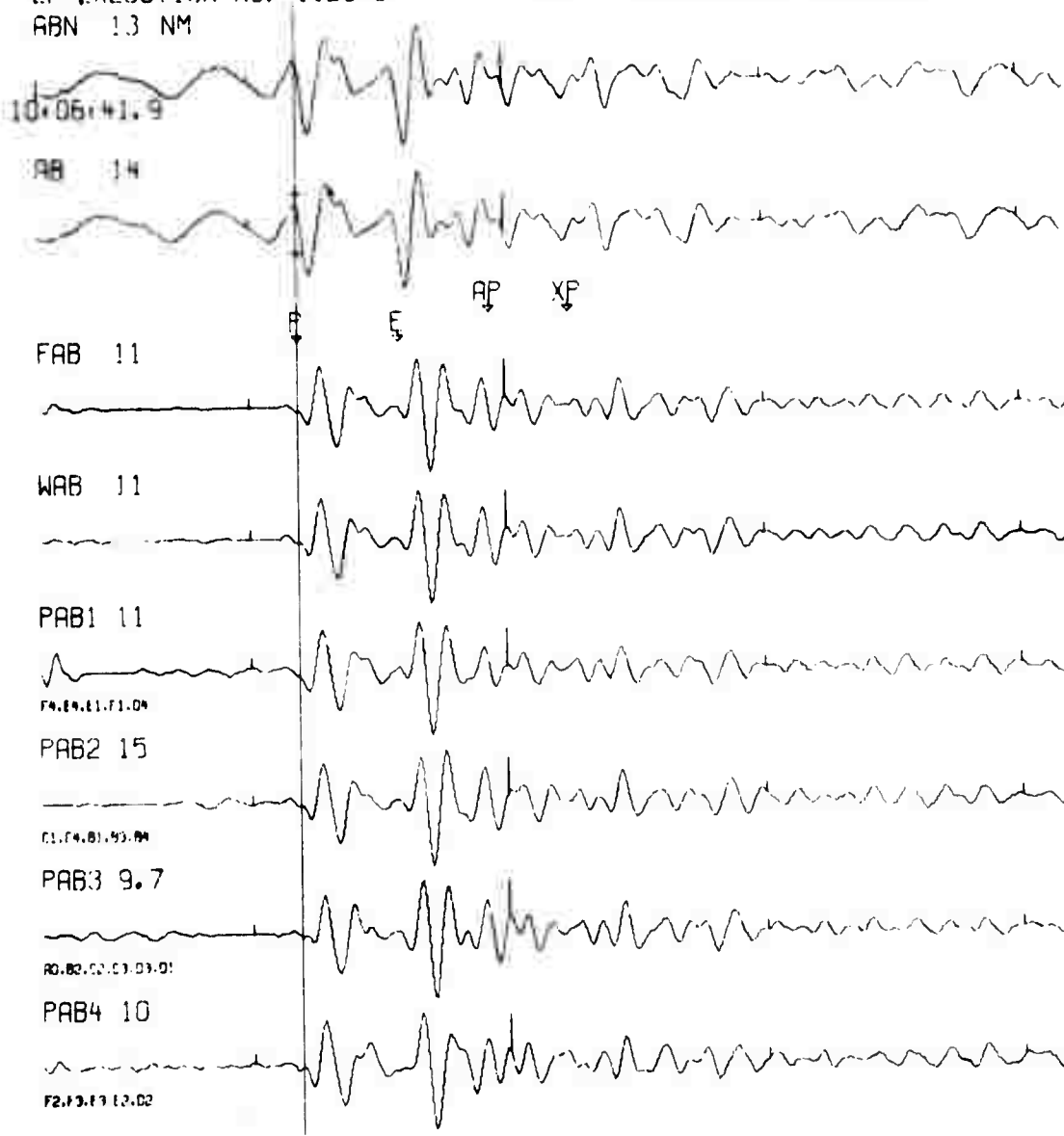
8.6 EDITING PROCESSOR

The Editing Processor provides the analyst with a flexible and efficient means for EP system performance evaluation and system output editing. The Editing Processor allows the analyst to:

LASA SEISMO BULLETIN FOR 26 DEC 1970 (DAY 360/70) FORMAT 5
 1 26 DEC 1970
 2 9 57 37 40.2N 31.1W 25 0 4.3 404 AZORES ISLANDS REGION
 3 10 6 51.9 LAC P 6.4 1.4 15.1 53.0 67.9

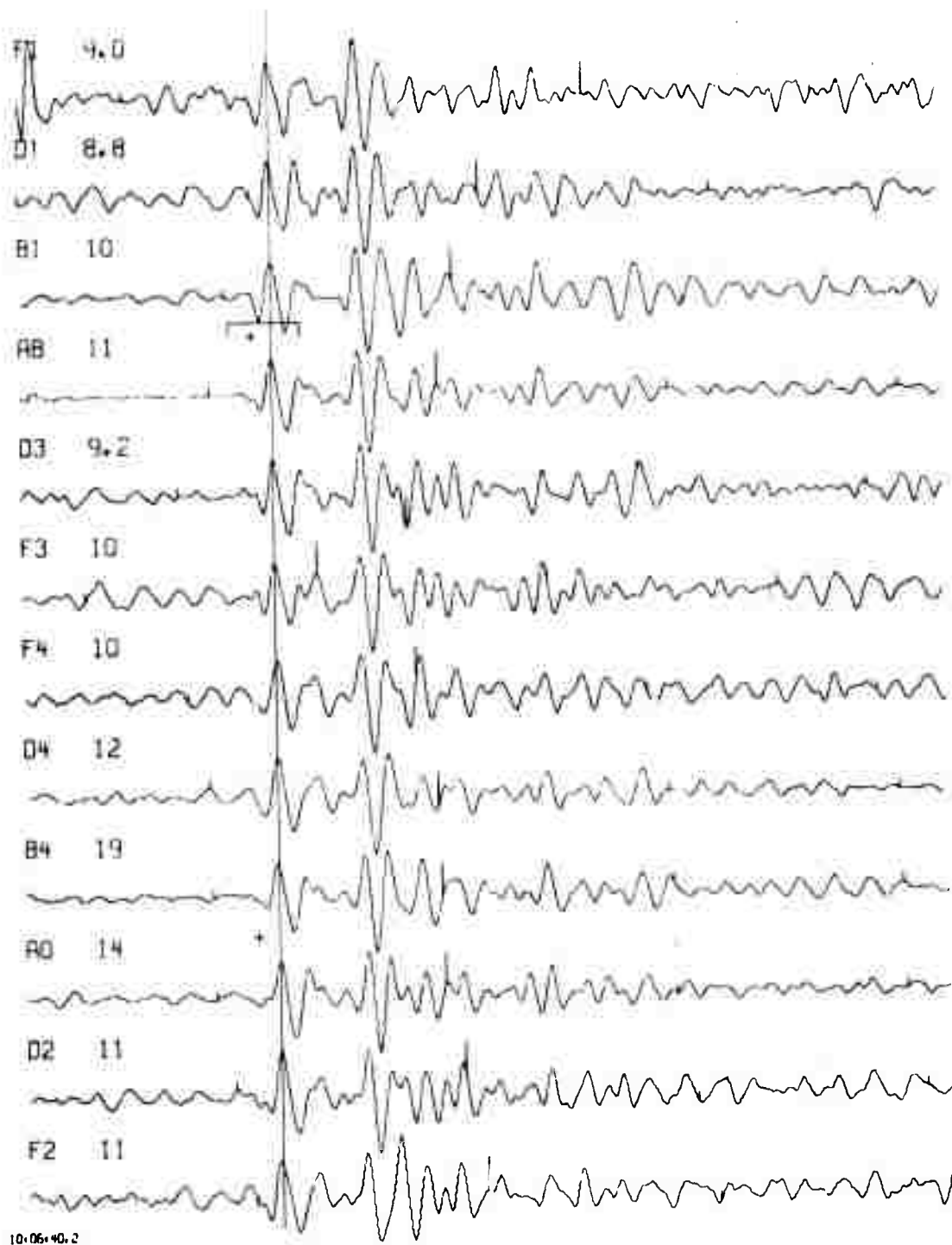
EP EXECUTION NO. 112870
 ABN 13 NM

BP-B 0.5-2.0 HZ ORDER 3 FILTER



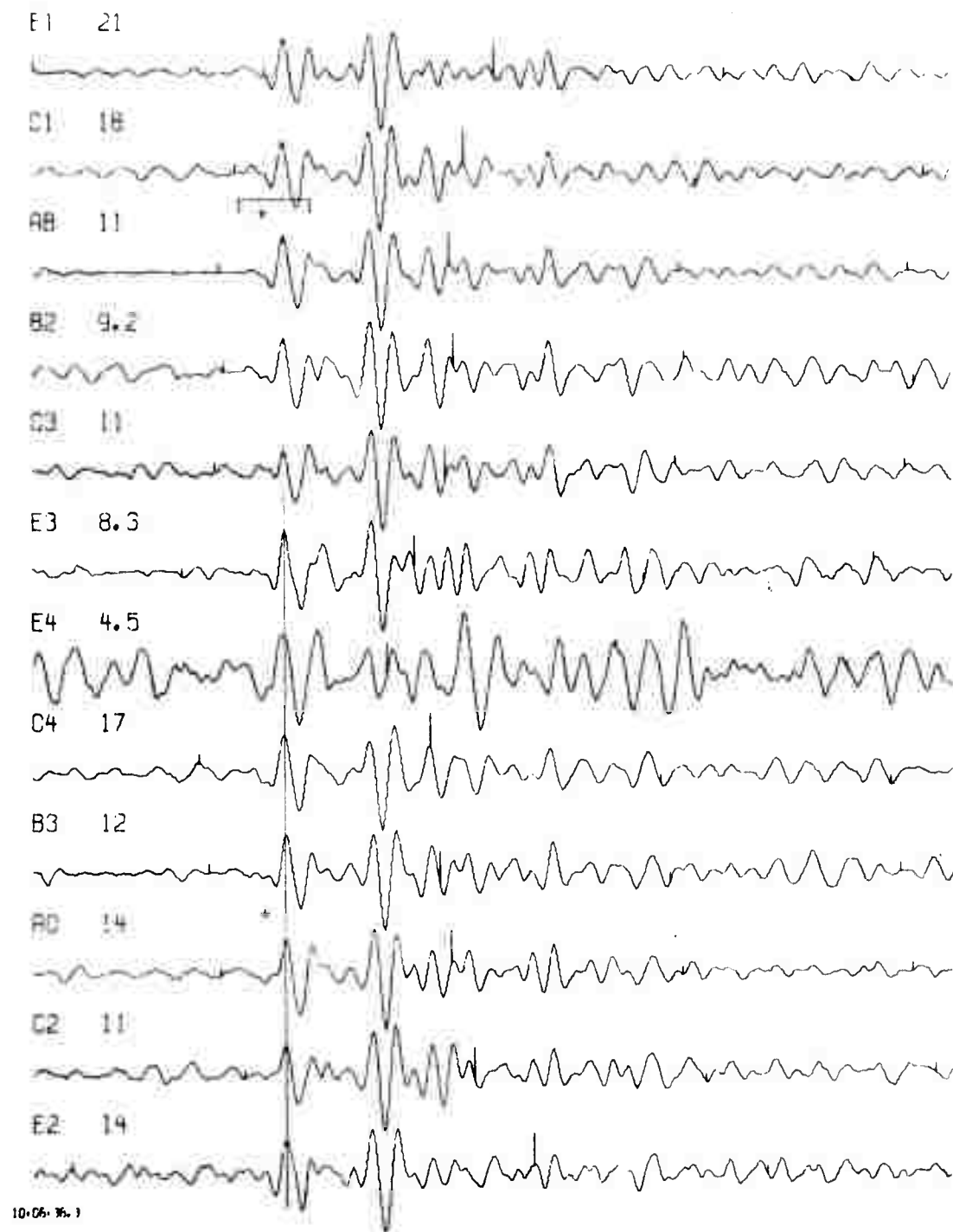
a. Array Beam Panel

Figure 8-16. Partial Event Plot (Sheet 1 of 3)



b. Subarray Beam Panel 1 (Center Segment)

Figure 8-16. Partial Event Plot (Sheet 2 of 3)



c. Subarray Beam Panel 2 (Center Segment)

Figure 8-16. Partial Event Plot (Sheet 3 of 3)

- a. Review and edit the Detection/Bulletin File in preparation for publishing a bulletin
- b. Review event waveforms on the EOC
- c. Initiate extended processing, i.e., re-executing the Short-Period Signal Processor with limited parameter specification ability
- d. Request that the editing bulletin be published, i.e., transmitted to teletype for TWX hard copy and paper tape output.

8.6.1 Detection/Bulletin File Review

Prior to the analyst's request for execution of the Editing Processor, the Output Processor has produced a summary report and an event tape entry for each processed event, has incorporated any new entries into the Detection/Bulletin File (DBF), and has produced a current Detection/Bulletin Report listing all detection entries and bulletin entries in the DBF. Thus the analyst has a list of the events available on the DBF, and a summary report for each event with a bulletin entry. A plot has also been generated for any event for which the files have been released, unless the plot was suppressed by the analyst. Using these aids, the analyst can select those events he wishes to review. In addition to the events currently in the system, the analyst may review any event by reading its files from an event tape. This brings it back into the system. He may also read an entire DBF from an event tape, edit it, and re-publish the bulletin from it.

The Editing Processor is designed to use the following equipment:

- a. 2260 Display Station (consists of the 2260 Display Unit, the Alphameric Keyboard, and the 1053 Printer)
- b. Waveform element of the Experimental Operations Console (EOC)

- c. Strip Chart Recorder (from the EOC Waveform Data Buffer).

All processing is under the control of the analyst. Each processing unit is executed only when the analyst specifically requests that function. Functions may be requested via either the 2260 or the EOC; the 2260 is the primary control element, and the EOC is used only after the analyst requests it via the 2260. Reference [8-20] describes in detail all of the functions available to the analyst.

The Editing Processor can display or edit a single event at a time. The analyst selects the desired event by EP execution number, entered via the 2260. He may display the bulletin entry corresponding to the selected event and edit it. If the disk files for the event are still available, or can be retrieved from an event tape, the EOC may be used to review the event. Several sixth order recursive filters are available for filtering the data which goes into the EOC display buffer.

Event data is available to the analyst for review in several display forms:

- a. Array beams and subarray beams as waveform traces displayed on the waveform element-Data can be displayed in either filtered or unfiltered form.
- b. A stripchart plot of waveform data from the EOC display buffer.
- c. Event variables (e.g., seismic bulletin) as an alphameric display on the 2260.
- d. A 1053 printout of the contents of the 2260 display.
- e. 1053 printouts of the DBF and edited DBF.

8.6.2 EOC Waveform Display Usage

When the EOC function is requested, if all conditions are valid, the EP/EOC program builds the data base necessary for using the EOC. After the data base has been completed, the event variables are automatically displayed on the 2260 and a selected set of filtered beams are automatically displayed on the waveform element of the EOC. Function codes are entered via EOC thumbwheels and switches at SAAC, and by means of a function keyboard at NDPC. The waveform unit can display up to eight traces of data selected by the operator. These traces may be selected as a predefined beam set or may be manually selected as any combination of the following:

- a. Unfiltered and/or filtered subarray beams
- b. Unfiltered and/or filtered array beams
- c. A spikes trace locating the correlation window and the period
- d. Null (zero) traces.

See [8-20] for a more detailed description of the waveform display capabilities.

The event variables display (see [8-20]) is automatically generated on the 2260 screen when the EOC function is requested. The operator, while reviewing the event data, can change certain variable event parameters by measuring the new values. The event parameters which can be changed via the console are:

- a. Subarray delays
- b. Subarray masks
- c. Event arrival time
- d. Event period length (two time measurements are required)

- e. Event amplitude (in nanometers--two amplitude measurements are required)
- f. Correlation window start time
- g. Length of correlation window (two time measurements are required)
- h. Estimated depth of event (in kilometers).

All parameter changes are entered from the EOC. If a parameter measurement uses the array beam trace, the time or value of the sample at the cursor intersection point is used. Any changes the analyst makes in event variables via the EOC are automatically shown on the 2260 event variables display. The analyst may continue to change event variables as long as he is using the EOC to review the event.

8.6.3 Extended Processing

As a result of his event review, decisions may be made on the accuracy, completeness, and quality of the automatic event processing. If he desires, the analyst may initiate extended processing of the event, using the new values for some or all of the event variables which he has modified via the EOC. Extended processing is the reexecution of Correlation, Beampacking and Array Beamforming, Event Parameter Extracting, and Event Characterization. New values can be used for delays, masks, correlation window start time, correlation window length, depth phase, method of determining location, and lead/lag selection. The results of this processing become available for review using the Editing Processor in the manner described above.

If the analyst does not choose to do extended processing, he may edit the bulletin entry for an event using the 2260. He may also choose to request a plot, or to release the data files for an event. If he is satisfied with all the bulletin entries in a DBF partition, the analyst may

choose to publish the bulletin. This automatically produces plots for all events not previously plotted or released.

8.7 SAAC PARAMETER VALUES

The EP Parameter Report, produced by the Output Processor (see Section 8.5) lists the SPSP parameter values in current use. Figure 8-7 is one of these reports for SAAC. The values shown in this illustration are those in use at the end of December 1970.

8.8 NDPC PARAMETER VALUES

Figure 8-18 is the SPSP Parameter Report for NDPC, showing the parameter values in use in August 1971.

ISRSPS EVENT PROCESSING PARAMETER REPORT 12/30/70

COMPON BLOCK	VARIABLE NAME	CURRENT VALUE	DESCRIPTION
STSP10	ITAB	300	NUMBER OF DECISECONDS THAT AN ARRAY BEAM IS TO BE FORMED PRIOR TO TOIDETECTION TIME)
	ITAB	120	MAXIMUM DELAY IN DECISECONDS EXPECTED FROM THE CENTER SUBARRAY TO ANY OTHER SUBARRAY
	ITSAB	12	MAXIMUM DELAY EXPECTED FROM THE CENTER SEISMOMETER OF ANY SUBARRAY TO ANY OTHER SEISMOMETER IN THE SAME SUBARRAY
	R	10.0000	DATA RATE IN SAMPLES PER SECOND
	ITP	900	NUMBER OF DECISECONDS THAT AN ARRAY BEAM IS TO BE FORMED FOLLOWING TO
	BETA	0	POST SHIFT VARIABLE FOR 88F MICROCODE
STSP20	AT2	1.0000	CONSTANT FOR COMPUTING DERIVATIVE OF POWER ENVELOPE
	AT12	2.0000	CONSTANT FOR COMPUTING DERIVATIVE OF POWER ENVELOPE
	AM12	1.0000	CONSTANT FOR COMPUTING DERIVATIVE OF POWER ENVELOPE
	AM12	0.0	CONSTANT FOR COMPUTING DERIVATIVE OF POWER ENVELOPE
	CUMAX2		UNUSED
	CUMPT2	30.0000	CONSTANT USED IN DETECTION TIME UPDATE (KMI
	OVALP2	0.8095	CONSTANT TO DEVALUE PRECISIONS (PASS 1)
		0.8095	(PASS 2)
		0.8095	(PASS 3)
	FVCT2	0.2500	RATIO OF SNR TO THRESHOLD SNR (PASS 1)
		0.2500	(PASS 2)
		0.2500	(PASS 3)
	HPPRB2	0.5000	CONSTANT USED IN CALCULATING PRIOR PROBABILITIES (PASS 1)
		0.5000	(PASS 2)
		0.5000	(PASS 3)
	PDEV2	0.5000	MAXIMUM DELAY DEVIATION FROM WAVEFRONT (SECONDS)
	PRST2	0.5000	THRESHOLD POWER (KMI)
	QUANM2	0.0427	QUANTUM UNIT TO NANOMETER CONVERSION FACTOR
	RHO2	10.0000	THRESHOLD FACTOR USED IN WINDOW POSITIONING
	RLOM2	0.5000	MINIMUM ALLOWABLE CORRELATION COEFFICIENT BEFORE SUBARRAY IS MASKED
	RLOPR2	1000.0000	LARGE PARAMETER USED IN CREATING COVARIANCE MATRIX
	SOLOB2	0.0200	STOE LOBE THRESHOLD (1/KMI)
	SIGLO2	0.7000	LOWER SIGNIFICANCE LIMIT FOR SPLSOE
	SIGUP2	0.9500	UPPER SIGNIFICANCE LIMIT FOR SPLSOE
	DYNA2		UNUSED (WAS STGCN2)
	SNRM2	24.2525	MAXIMUM ALLOWABLE SNR FOR THRESHOLD
	UPC2	0.9800	MAXIMUM ALLOWABLE CORRELATION COEFFICIENT FOR CALCULATING SNR
	VSUBR2	0.0225	VARIANCE ESTIMATE FOR REGION CORRECTIONS
	WNEW2	1000.0000	RATIO OF STA TO LTA
	X2	(SEE BELOW)	X COORDINATE OF SUBARRAY WITH RESPECT TO THE REFERENCE SUBARRAY AD (KMI)
	Y2	(SEE BELOW)	Y COORDINATE OF SUBARRAY WITH RESPECT TO THE REFERENCE SUBARRAY AD (KMI)
	IB1ST2	15	BACKOFF TIME IN SAMPLES FOR FIRST WINDOW POSITIONING METHOD
	IB2ND2	15	BACKOFF TIME IN SAMPLES FOR SECOND WINDOW POSITIONING METHOD
	IDELT2	30	NUMBER OF SAMPLES BEYOND DETECTION TIME CONSIDERED IN WINDOW POSITIONING
	IDTL2	20	NUMBER OF SAMPLES PRIOR TO PEAK AB POWER FOR CALCULATING CORRELATION WINDOW
	IFLTP2	4	FILTER TYPE FLAG BP-B 0-8-2-5 HZ ORDER 3 FILTER
	INTYM2	9	INTEGRATION TIME IN SAMPLES FOR POSITIONING WINDOW
	IRATE2	10	SAMPLING RATE IN SAMPLES PER SECOND
	KBFDR2	2	USED IN DETERMINING PEAK AB POWER (SAMPLES BEFORE)
	KAPTR2	2	USED IN DETERMINING PEAK AB POWER (SAMPLES AFTER)
	L2	5	WINDOW POSITIONING IS BASED ON MAX PEAK WITHIN L2 SAMPLES OF FIRST TIME THRESHOLD IS EXCEEDED
	L2	17	CORRELATION LEAD AND LAG IN SAMPLES (PASS 1)
		1	(PASS 2)
		1	(PASS 3)
	NWOW2	32	CORRELATION WINDOW LENGTH IN SAMPLES

Figure 8-17. SAAC SPSP Parameter Report (Sheet 1 of 5)

NRTBP2	300	NUMBER OF SAMPLES TO BE PROCESSED									
NSUB2	21	NUMBER OF SUBARRAYS									
NUM2	ISEE BELOW)	ORDER IN WHICH SUBARRAYS, AS FOUND ON TAPE, ARE TO APPEAR IN OUTPUT									
RCFIL2	0	FLAG FOR RETRIEVAL OF FILTER TYPE FROM REGION CORRECTION FILE									
NPIN2	7	MINIMUM NUMBER OF SUBARRAYS FOR SUCCESSFUL SPLSC PROCESSING									
NPMX2	3	MAXIMUM NUMBER OF PEAKS LISTED PER SUBARRAY									
NUMV2	ISEE BELOW)	INVERSE OF NUM2									
NIT2	7	NUMBER OF ITERATIONS FOR EACH PASS (PASS 1)									
	4	(PASS 2)									
	225	(PASS 3)									
ITOM2	225	NRTBP2 LESS MINIMUM NUMBER OF SAMPLES REQUIRED FOR ARRAY BEAMFORMING									
DEF2	ISEE BELOW)	TRUE/FALSE DEFINING WHICH SUBARRAYS ARE ON D,E AND F RINGS									
SIGMT2	1.0000	MULTIPLIER FOR SIGMA-0 IN SPLSC TO MAKE IT LESS IMPORTANT									
CHIMP2	0.0	CHI-SQUARED TEST VALUES FOR 1,2,3,4,5,6,7,8,9,10,11,12 DEGREE OF FREEDOM FOR 90 PERCENT CONFIDENCE									
	0.0	0.0	10.8210	13.8160	16.2660	18.4670	20.5150	22.4580	24.3220	26.1250	
DUREG2	27.8770	29.5880	31.2640	32.9090	34.5280	36.1230	37.6970	39.2520	40.7900	42.3120	43.8200
MAXX2	0.000009	SQUARE OF MAXIMUM CHANGE IN U BEFORE NEW REGION CORRECTIONS ARE NEEDED									
TOPSA2	411A01	MAXIMUM NUMBER OF TIMES SP2 SHOULD BE EXECUTED PER EVENT									
NLSOE2	3	DETECTION PROCESSOR REFERENCE SUBARRAY NUMBER (SUBARRAY)									
ITOM2	120	LIMIT ON NUMBER OF TIMES DELTA-U TEST MAY FAIL AFTER SPLSC									
TRUNC2	32.0000	MAXIMUM REFERENCE SUBARRAY DELAY THAT WILL BE TOLERATED IN SP3FR									
		0.5*SOV002, WHERE SOV IS NUMBER OF STANDARD DEVIATIONS PERMITTED IN PEAK'S POSITION FROM PLANE WAVE BEFORE PEAK IS DISCARDED									
SUBARRAY	LB1	LF3	LF4	LA0	LR3	LC4	LB4	LC1	LC2	LB2	LC3
NUM2	2	20	21	1	4	9	5	6	7	3	8
X2	9.975	-66.607	-54.447	0.0	-7.250	-11.592	-1.592	7.226	16.049	4.552	-2.108
Y2	7.079	-79.205	80.571	0.0	-3.268	5.199	8.831	16.772	-2.109	-5.958	-12.772
DEF2	F	T	T	F	F	F	F	F	F	F	F
SUBARRAY	LD3	LD4	LO1	LO2	LF3	LE4	LE1	LF1	LE2	LF2	
NUM2	12	13	1C	11	16	17	14	1R	15	19	
X2	-19.791	-12.267	25.168	16.226	-0.648	-53.052	12.596	78.155	65.808	57.157	
Y2	-15.406	28.175	16.856	-20.605	-59.925	7.715	52.724	76.357	-19.189	-86.340	
DEF2	T	T	T	T	T	T	T	T	T	T	
SUBARRAY	LA0	LB2	LB3	LB4	LC1	LC2	LC3	LC4	LO1	LO2	
NUMV2	4	1	10	5	7	6	9	11	6	14	15
SUBARRAY	LD3	LD4	LE1	LE2	LE3	LE4	LF1	LF2	LF3	LF4	
NUMV2	12	13	18	20	16	17	19	21	2	3	
STP30	0.0020	BEAMPACKING RADIUS IN SECONDS/KILOMETER									
UMAX3	0.0200	MAXIMUM DIFFERENCE PERMITTED BETWEEN INITIAL DETECTION LOCATION AND BEAMPACKING LOCATION									
SNRF3	20.0000	BEFORE BEAMPACKING IS REDONE (S/PM)									
RSUBT3	4.4700	SIGNAL TO NOISE RATIO THRESHOLD FOR USE OF WIDE BAND FILTER IN PARAMETER EXTRACTION									
DATRT3	10	TEST RATIO FOR DETERMINING FILTER TYPE IF CORRELATION WAS NOT SUCCESSFUL									
JSUB3	21	SUBARRAY DATA RATE IN SAMPLES PER SECOND									
NR3	2	NUMBER OF SUBARRAYS									
TSUBI3	12	NUMBER OF RINGS TO FORM PACKED BEAMS									
TSUB23	3	TIME BEFORE DETECTION TO PERFORM BEAMPACKING (SECONDS)									
RSTAS3	3	TIME AFTER DETECTION TO PERFORM BEAMPACKING (SECONDS)									
APRI3	6	SHORT TERM AVERAGE RATE = DATRT3/RTSA3 (HZ)									
STAT03	2	NUMBER OF INTERMEDIATE VALUES USED TO FORM ONE SHORT TERM AVERAGE									
MAXBP3	25	STA THRESHOLD IF STAMAX GREATER THAN STAT03, CORRELATION WILL BE RESTARTED IF BEAMPACKING									
TSUBA3	30	MAXIMUM NUMBER OF TIMES BEAMS MAY BE PACKED PER CALL									
TSUBP3	90	TIME BEFORE DETECTION TO FORM FINAL ARRAY BEAMS (SECONDS)									
IFTP3	1	TIME AFTER DETECTION TO FORM FINAL ARRAY BEAMS (SECONDS)									
		FILTER TYPE INDICATOR BP-B 0.9-1.4 HZ ORDER 3 FILTER									

Figure 8-17. SAAC SPSP Parameter Report (Sheet 2 of 5)

STSP40

NN4 32
NV14 1
NV24 1800
WINL4 32
THABP4 -6.3220
NA4 1200
NB4 300
NB4 200
NS4 18
NC4 170
ND4 3
NE4 90
NF4 4
NG4 50
NH4 0.2500
NIS4 10
NR4 35
NS4 60
NT4 10
RMD4 0.2500
THSM4 50.0000
S4 4.0000
NAL4 50
NT4 3
NJ4 14
ND4 40
JSTOP4 40
NT4 256
NTB4 1
NM4 30
FA4 2.0000
NAB4 10
FRA 10
NY4 0.7500
NY4 1024
F14 100
F24 0.0397
ALPHA4 0.0831
ICOM4 16.0000
17166
2352
3393
3290
1812

UNFILTERED ARRAY BEAM POWER WINDOW LENGTH(SAMPLES)
START SAMPLE TO CALCULATE UNFILTERED BEAM POWER(SAMPLES)
END SAMPLE TO CALCULATE UNFILTERED BEAM POWER(SAMPLES)
WINDOW LENGTH FOR POWER CALCULATION(SAMPLES)
UNFILTERED ARRAY BEAM POWER THRESHOLD (DB)
PROCESSING INTERVAL LENGTH (SAMPLES)
START SAMPLE BEFORE DETECTION(CORRELATION) TIME IN PROCESSING INTERVAL (SAMPLES)
START SAMPLE AFTER OTHER DETECTION TIME IN PROCESSING INTERVAL (SAMPLES)
SIGNAL POWER AVERAGING WINDOW LENGTH (SAMPLES)
SAMPLE NUMBER TO START SIGNAL POWER AVERAGING BEFORE DETECTION(CORRELATION) TIME (SAMPLES)
SAMPLE NUMBER TO EXCEED FROM MAX FOR EVENT MODE TO START (SAMPLES)
SAMPLE NUMBER TO FALL BELOW TRUE PEAK IN EVENT MODE (SAMPLES)
END SAMPLE BEFORE FIRST PEAK IN NOISE POWER AVERAGING (SAMPLES)
WHEN TOTAL EVENT MODE NUMBER EXCEEDS THIS, THE EXCEPTION MODE IS SET
MINIMUM TIME FIRST EVENT MODE IS OUTSIDE DETECTION(CORRELATION) TIME (SAMPLES)
FACTOR USED TO MULTIPLY SUMAX
SAMPLING RATE IN HZ (SAMPLES PER SECOND)
SAMPLE NUMBER FOR EVENT CLASSIFICATION (SAMPLES)
START SAMPLE BEFORE FIRST PEAK IN MAGNITUDE CALCULATION (SAMPLES)
END SAMPLE AFTER FIRST PEAK IN MAGNITUDE CALCULATION (SAMPLES)
S/N RATIO IN GENERATING DIFFERENCE FUNCTION IN MAGNITUDE CALCULATION
S/N RATIO IN CHOOSING ARRIVAL TIME ALGORITHMS
SCALAR MULTIPLIER IN THRESHOLD PICK
START BEFORE FIRST PEAK FOR THRESHOLD PICK (SAMPLES)
THRESHOLD PICK WINDOW LENGTH (SAMPLES)
MODEL FIT WINDOW LENGTH (SAMPLES)
START SAMPLE BEFORE START TIME FOR MODEL FIT WINDOW TO MOVE (SAMPLES)
NUMBER OF TIMES MODEL FIT WINDOW IS MOVED
DOMINANT FREQUENCY WINDOW LENGTH (SAMPLES)
SAMPLE NUMBER AFTER ARRIVAL TIME TO CENTER DOMINANT FREQUENCY WINDOW (SAMPLES)
SAMPLE NUMBER IN TRIANGULAR FUNCTION FOR DOMINANT FREQUENCY CALCULATION (SAMPLES)
CONSTANT IN GENERATING SINE WAVE IN FIRST MOTION DIRECTION (SAMPLES)
START SAMPLE BEFORE ARRIVAL TIME IN FIRST MOTION DIRECTION (SAMPLES)
END SAMPLE AFTER ARRIVAL TIME IN FIRST MOTION DIRECTION (SAMPLES)
CORRELATION FUNCTION THRESHOLD
GENERATION OF SPECSPEC LENGTH (SAMPLES)
START SAMPLE BEFORE ARRIVAL TIME IN SPECSPEC CALCULATION (SAMPLES)
MINIMUM VALUE OF UNCALIBRATED U ALLOWED IN DEPTH ESTIMATION (S/KM)
MAXIMUM VALUE OF UNCALIBRATED U ALLOWED IN DEPTH ESTIMATION (S/KM)
FACTOR USED TO FIND ALTERNATE ENVELOPE THRESHOLD
CONVOLUTION FILTER COEFFICIENTS

RECURSIVE FILTER COEFFICIENTS

-276	276	-92	13264	-20098	18441	-10934	3887	-654
-9	9	-3	8359	-16294	18622	-13199	546	-1090

MODEL FIT COEFFICIENTS

-0.1288	-0.1288	-0.0971	-0.0295	0.0145	0.0214
0.0499	0.0793	0.0892	0.0879	0.0914	0.0959
-0.2108	-0.1445	-0.1442	-0.0728	0.0270	0.0766
0.0868	0.1091	0.1382	0.1569	0.1623	0.1624

COEFFICIENTS FOR AMPLITUDE CORRECTION

TIME BEFORE DETECTION (CORRELATION) TIME TO END NOISE POWER AVERAGING (SAMPLES)
UNUSED

IREC4 92
3
-0.1690
0.0238
0.0238
-0.4306
0.0837
-13.2709
25.2771
-17.4039
6.7306
-1.5565
90

AMF4

COF4

NNM4
NODP4

Figure 8-17. SAAC SPSP Parameter Report (Sheet 3 of 5)

[illegible]

ISRSPS EVENT PROCESSING PARAMETER REPORT			10/21/71
COMMON BLOCK	VARIABLE NAME	CURRENT VALUE	DESCRIPTION
STSPIC	ITA	300	NUMBER OF DECISECONDS THAT AN ARRAY BEAM IS TO BE FORMED PRIOR TO TOIDETECTION TIME)
	ITAB	75	MAXIMUM DELAY IN DECISECONDS EXPECTED FROM THE CENTER SUBARRAY TO ANY OTHER SUBARRAY
	ITSAR	7	MAXIMUM DELAY EXPECTED FROM THE CENTER SPISOMETER OF ANY SUBARRAY TO ANY OTHER SPISOMETER IN THE SAME SUBARRAY
	R	1C.000C	DATA RATE IN SAMPLES PER SECCNC
	ITM	900	NUMBER OF DECISECONDS THAT AN ARRAY BEAM IS TO BE FORMED FOLLOWING TO POST SHIFT VARIABLE FOR ABF MICROCODE
STSPM2D	AM12	1.000C	CONSTANT FOR COMPUTING DERIVATIVE OF POWER ENVELOPE
	AM12	2.000C	CONSTANT FOR COMPUTING DERIVATIVE OF POWER ENVELOPE
	AM12	1.000C	CONSTANT FOR COMPUTING DERIVATIVE OF POWER ENVELOPE
	AM12	0.0	CONSTANT FOR COMPUTING DERIVATIVE OF POWER ENVELOPE
	AM12	0.0	CONSTANT FOR COMPUTING DERIVATIVE OF POWER ENVELOPE
STSPM2D	AM12	3C.0000	CONSTANT USED IN DETECTION TIME UPDATE (K)
	AM12	0.8095	CONSTANT TO DEVALUE PRECISIONS (PASS 1)
	AM12	0.8095	CONSTANT TO DEVALUE PRECISIONS (PASS 2)
	AM12	0.8095	CONSTANT TO DEVALUE PRECISIONS (PASS 3)
	AM12	0.8095	CONSTANT TO DEVALUE PRECISIONS (PASS 4)
STSPM2D	AM12	0.250C	RATIO OF SNR TO THRESHOLD SNR (PASS 1)
	AM12	0.250C	RATIO OF SNR TO THRESHOLD SNR (PASS 2)
	AM12	0.250C	RATIO OF SNR TO THRESHOLD SNR (PASS 3)
	AM12	0.250C	RATIO OF SNR TO THRESHOLD SNR (PASS 4)
	AM12	0.250C	RATIO OF SNR TO THRESHOLD SNR (PASS 5)
STSPM2D	AM12	1.000C	CONSTANT USED IN CALCULATING PRIOR PROBABILITIES (PASS 1)
	AM12	1.000C	CONSTANT USED IN CALCULATING PRIOR PROBABILITIES (PASS 2)
	AM12	1.000C	CONSTANT USED IN CALCULATING PRIOR PROBABILITIES (PASS 3)
	AM12	1.000C	CONSTANT USED IN CALCULATING PRIOR PROBABILITIES (PASS 4)
	AM12	1.000C	CONSTANT USED IN CALCULATING PRIOR PROBABILITIES (PASS 5)
STSPM2D	AM12	0.5000	MAXIMUM DELAY DEVIATION FROM WAVEFRONT (SECONDS)
	AM12	0.5000	THRESHOLD POWER (NM)
	AM12	0.0427	QUANTUM UNIT TO WAVELENGTH CONVERSION FACTOR
	AM12	10.0000	THRESHOLD FACTOR USED IN WINDOW POSITIONING
	AM12	0.5000	MINIMUM ALLOWABLE CORRELATION COEFFICIENT BEFORE SUBARRAY IS MASKED
STSPM2D	AM12	1000.000C	LARGE PARAMETER USED IN CREATING COVARIANCE MATRIX
	AM12	0.010C	SIDE LOBE THRESHOLD (1/NM)
	AM12	0.750C	LOWER SIGNIFICANCE LIMIT FOR SPLSQE
	AM12	0.950C	UPPER SIGNIFICANCE LIMIT FOR SPLSQE
	AM12	0.950C	UPPER SIGNIFICANCE LIMIT FOR SPLSQE
STSPM2D	AM12	24.2525	MAXIMUM ALLOWABLE SNR FOR THRESHOLD
	AM12	0.9000	MAXIMUM ALLOWABLE CORRELATION COEFFICIENT FOR CALCULATING SNR
	AM12	0.040C	VARIANCE ESTIMATE FOR REGRESSION CORRECTIONS
	AM12	1000.000C	RATIO OF STA TO LTA
	AM12	1000.000C	X COORDINATE OF SUBARRAY WITH RESPECT TO THE REFERENCE SUBARRAY (0 IN)
STSPM2D	AM12	15	Y COORDINATE OF SUBARRAY WITH RESPECT TO THE REFERENCE SUBARRAY (0 IN)
	AM12	15	RACKOFF TIME (IN SAMPLES) FOR FIRST WINDOW POSITIONING METHOD
	AM12	30	RACKOFF TIME (IN SAMPLES) FOR SECOND WINDOW POSITIONING METHOD
	AM12	20	NUMBER OF SAMPLES BEYOND DETECTION TIME CONSIDERED IN WINDOW POSITIONING
	AM12	20	NUMBER OF SAMPLES PRIOR TO PEAK OR POWER FOR CALCULATING CORRELATION WINDOW
STSPM2D	AM12	4	FILTER TYPE FLAG BR-R 0.8-2.5 HZ ORDER 3 FILTER
	AM12	10	INTEGRATION TIME IN SAMPLES FOR POSITIONING WINDOW
	AM12	10	SAMPLING RATE IN SAMPLES PER SECCNC
	AM12	2	USED IN DETERMINING PEAK OR POWER (SAMPLES BEFORE)
	AM12	2	USED IN DETERMINING PEAK OR POWER (SAMPLES AFTER)
STSPM2D	AM12	5	WINDOW POSITIONING IS BASED ON MAX PEAK WITHIN L2
	AM12	17	CORRELATION LEAD AND LAG IN SAMPLES (PASS 1)
	AM12	7	CORRELATION LEAD AND LAG IN SAMPLES (PASS 2)
	AM12	7	CORRELATION LEAD AND LAG IN SAMPLES (PASS 3)
	AM12	32	CORRELATION WINDOW LENGTH IN SAMPLES (PASS 4)

Figure 8-18. NDPC SPSP Parameter Report (Sheet 1 of 5)

NTBP2 300 NUMBER OF SAMPLES TO BE PROCESSED
 NSUB2 22 NUMBER OF SUBARRAYS
 [SEE BELOW] ORDER IN WHICH SUBARRAYS, AS FOUND ON TAPE, ARE TO APPEAR IN OUTPUT
 NMU2 0 FLAG FOR RETRIEVAL OF FILTER TYPE FROM REGION CORRECTION FILE
 RCFIL2 7 PRIMUM NUMBER OF SUBARRAYS FOR SUCCESSFUL SPLSQC PROCESSING
 NPMX2 3 MAXIMUM NUMBER OF PARS LISTED PER SUBARRAY
 NPMAX2 3
 NUMNV2 [SEE BELOW] INVERSE OF NUM2
 NIY2 7 NUMBER OF ITERATIONS FOR EACH PASS IPASS 11
 4 (PASS 2)
 4 (PASS 3)
 ITOMX2 225 NTBP2 LESS MINIMUM NUMBER OF SAMPLES REQUIRED FOR ARRAY BEAMFORMING
 [SEE BELOW] TRUE/FALSE DEFINING WHICH SUBARRAYS ARE ON O.E. AND F. RINGS
 SIGM2 2.0000 MULTIPLIER FOR SIGMA-O IN SPLSQ TO MAKE IT LESS IMPORTANT
 CHIMP2 0.0 CM1-SQUARED TEST VALUES FOR 1.2...22 DEGREE OF FREEDOM FOR 9C PERCENT CONFIDENCE
 29.5880 0.0 10.8280 13.8160 16.2660 18.4670 20.5150 22.4580 24.3220 26.1250
 31.2640 32.9090 34.5280 36.1230 37.6970 39.2520 40.7900 42.3120 43.8200
 SQUARE OF MAXIMUM CHANGE IN U BEFORE NEW REGION CORRECTIONS ARE NEEDED
 DMUEG2 27.8770 MAXIMUM NUMBER OF TYPES SP2 SHOULD BE EXECUTED PER EVENT
 MAXF2 6 MAXIMUM NUMBER OF TYPES SP2 SHOULD BE EXECUTED PER EVENT
 TMSA2 11C1A1 DETECTION PROCESSOR REFERENCE SUBARRAY NUMBER (SUBARRAY)
 MLOE2 3 LIMIT ON NUMBER OF TIMES DELTA-U TEST MAY FAIL AFTER SPLSQE
 ITOR2 75 MAXIMUM REFERENCE SUBARRAY DELAY THAT WILL BE TOLERATED IN SPASFR
 TRUNC2 32.0000 0.54500002, WHERE SOV IS NUMBER OF STANDARD DEVIATIONS PERMITTED IN PEAK'S POSITION FROM
 PLANE HAVE REFERENCE PEAK IS DISCARDED
 SUBARRAY 01A 01B 020 03A 04B 05B 06B 07B 08B 09C 10C 11C 12C 13C 14C 15C 16C 17C 18C 19C 20C 21C 22C 23C 24C 25C 26C 27C 28C 29C 30C 31C 32C 33C 34C 35C 36C 37C 38C 39C 40C 41C 42C 43C 44C 45C 46C 47C 48C 49C 50C 51C 52C 53C 54C 55C 56C 57C 58C 59C 60C 61C 62C 63C 64C 65C 66C 67C 68C 69C 70C 71C 72C 73C 74C 75C 76C 77C 78C 79C 80C 81C 82C 83C 84C 85C 86C 87C 88C 89C 90C 91C 92C 93C 94C 95C 96C 97C 98C 99C 100C 101C 102C 103C 104C 105C 106C 107C 108C 109C 110C 111C 112C 113C 114C 115C 116C 117C 118C 119C 120C 121C 122C 123C 124C 125C 126C 127C 128C 129C 130C 131C 132C 133C 134C 135C 136C 137C 138C 139C 140C 141C 142C 143C 144C 145C 146C 147C 148C 149C 150C 151C 152C 153C 154C 155C 156C 157C 158C 159C 160C 161C 162C 163C 164C 165C 166C 167C 168C 169C 170C 171C 172C 173C 174C 175C 176C 177C 178C 179C 180C 181C 182C 183C 184C 185C 186C 187C 188C 189C 190C 191C 192C 193C 194C 195C 196C 197C 198C 199C 200C 201C 202C 203C 204C 205C 206C 207C 208C 209C 210C 211C 212C 213C 214C 215C 216C 217C 218C 219C 220C 221C 222C 223C 224C 225C 226C 227C 228C 229C 230C 231C 232C 233C 234C 235C 236C 237C 238C 239C 240C 241C 242C 243C 244C 245C 246C 247C 248C 249C 250C 251C 252C 253C 254C 255C 256C 257C 258C 259C 260C 261C 262C 263C 264C 265C 266C 267C 268C 269C 270C 271C 272C 273C 274C 275C 276C 277C 278C 279C 280C 281C 282C 283C 284C 285C 286C 287C 288C 289C 290C 291C 292C 293C 294C 295C 296C 297C 298C 299C 300C 301C 302C 303C 304C 305C 306C 307C 308C 309C 310C 311C 312C 313C 314C 315C 316C 317C 318C 319C 320C 321C 322C 323C 324C 325C 326C 327C 328C 329C 330C 331C 332C 333C 334C 335C 336C 337C 338C 339C 340C 341C 342C 343C 344C 345C 346C 347C 348C 349C 350C 351C 352C 353C 354C 355C 356C 357C 358C 359C 360C 361C 362C 363C 364C 365C 366C 367C 368C 369C 370C 371C 372C 373C 374C 375C 376C 377C 378C 379C 380C 381C 382C 383C 384C 385C 386C 387C 388C 389C 390C 391C 392C 393C 394C 395C 396C 397C 398C 399C 400C 401C 402C 403C 404C 405C 406C 407C 408C 409C 410C 411C 412C 413C 414C 415C 416C 417C 418C 419C 420C 421C 422C 423C 424C 425C 426C 427C 428C 429C 430C 431C 432C 433C 434C 435C 436C 437C 438C 439C 440C 441C 442C 443C 444C 445C 446C 447C 448C 449C 450C 451C 452C 453C 454C 455C 456C 457C 458C 459C 460C 461C 462C 463C 464C 465C 466C 467C 468C 469C 470C 471C 472C 473C 474C 475C 476C 477C 478C 479C 480C 481C 482C 483C 484C 485C 486C 487C 488C 489C 490C 491C 492C 493C 494C 495C 496C 497C 498C 499C 500C 501C 502C 503C 504C 505C 506C 507C 508C 509C 510C 511C 512C 513C 514C 515C 516C 517C 518C 519C 520C 521C 522C 523C 524C 525C 526C 527C 528C 529C 530C 531C 532C 533C 534C 535C 536C 537C 538C 539C 540C 541C 542C 543C 544C 545C 546C 547C 548C 549C 550C 551C 552C 553C 554C 555C 556C 557C 558C 559C 560C 561C 562C 563C 564C 565C 566C 567C 568C 569C 570C 571C 572C 573C 574C 575C 576C 577C 578C 579C 580C 581C 582C 583C 584C 585C 586C 587C 588C 589C 590C 591C 592C 593C 594C 595C 596C 597C 598C 599C 600C 601C 602C 603C 604C 605C 606C 607C 608C 609C 610C 611C 612C 613C 614C 615C 616C 617C 618C 619C 620C 621C 622C 623C 624C 625C 626C 627C 628C 629C 630C 631C 632C 633C 634C 635C 636C 637C 638C 639C 640C 641C 642C 643C 644C 645C 646C 647C 648C 649C 650C 651C 652C 653C 654C 655C 656C 657C 658C 659C 660C 661C 662C 663C 664C 665C 666C 667C 668C 669C 670C 671C 672C 673C 674C 675C 676C 677C 678C 679C 680C 681C 682C 683C 684C 685C 686C 687C 688C 689C 690C 691C 692C 693C 694C 695C 696C 697C 698C 699C 700C 701C 702C 703C 704C 705C 706C 707C 708C 709C 710C 711C 712C 713C 714C 715C 716C 717C 718C 719C 720C 721C 722C 723C 724C 725C 726C 727C 728C 729C 730C 731C 732C 733C 734C 735C 736C 737C 738C 739C 740C 741C 742C 743C 744C 745C 746C 747C 748C 749C 750C 751C 752C 753C 754C 755C 756C 757C 758C 759C 760C 761C 762C 763C 764C 765C 766C 767C 768C 769C 770C 771C 772C 773C 774C 775C 776C 777C 778C 779C 780C 781C 782C 783C 784C 785C 786C 787C 788C 789C 790C 791C 792C 793C 794C 795C 796C 797C 798C 799C 800C 801C 802C 803C 804C 805C 806C 807C 808C 809C 810C 811C 812C 813C 814C 815C 816C 817C 818C 819C 820C 821C 822C 823C 824C 825C 826C 827C 828C 829C 830C 831C 832C 833C 834C 835C 836C 837C 838C 839C 840C 841C 842C 843C 844C 845C 846C 847C 848C 849C 850C 851C 852C 853C 854C 855C 856C 857C 858C 859C 860C 861C 862C 863C 864C 865C 866C 867C 868C 869C 870C 871C 872C 873C 874C 875C 876C 877C 878C 879C 880C 881C 882C 883C 884C 885C 886C 887C 888C 889C 890C 891C 892C 893C 894C 895C 896C 897C 898C 899C 900C 901C 902C 903C 904C 905C 906C 907C 908C 909C 910C 911C 912C 913C 914C 915C 916C 917C 918C 919C 920C 921C 922C 923C 924C 925C 926C 927C 928C 929C 930C 931C 932C 933C 934C 935C 936C 937C 938C 939C 940C 941C 942C 943C 944C 945C 946C 947C 948C 949C 950C 951C 952C 953C 954C 955C 956C 957C 958C 959C 960C 961C 962C 963C 964C 965C 966C 967C 968C 969C 970C 971C 972C 973C 974C 975C 976C 977C 978C 979C 980C 981C 982C 983C 984C 985C 986C 987C 988C 989C 990C 991C 992C 993C 994C 995C 996C 997C 998C 999C 1000C 1001C 1002C 1003C 1004C 1005C 1006C 1007C 1008C 1009C 1010C 1011C 1012C 1013C 1014C 1015C 1016C 1017C 1018C 1019C 1020C 1021C 1022C 1023C 1024C 1025C 1026C 1027C 1028C 1029C 1030C 1031C 1032C 1033C 1034C 1035C 1036C 1037C 1038C 1039C 1040C 1041C 1042C 1043C 1044C 1045C 1046C 1047C 1048C 1049C 1050C 1051C 1052C 1053C 1054C 1055C 1056C 1057C 1058C 1059C 1060C 1061C 1062C 1063C 1064C 1065C 1066C 1067C 1068C 1069C 1070C 1071C 1072C 1073C 1074C 1075C 1076C 1077C 1078C 1079C 1080C 1081C 1082C 1083C 1084C 1085C 1086C 1087C 1088C 1089C 1090C 1091C 1092C 1093C 1094C 1095C 1096C 1097C 1098C 1099C 1100C 1101C 1102C 1103C 1104C 1105C 1106C 1107C 1108C 1109C 1110C 1111C 1112C 1113C 1114C 1115C 1116C 1117C 1118C 1119C 1120C 1121C 1122C 1123C 1124C 1125C 1126C 1127C 1128C 1129C 1130C 1131C 1132C 1133C 1134C 1135C 1136C 1137C 1138C 1139C 1140C 1141C 1142C 1143C 1144C 1145C 1146C 1147C 1148C 1149C 1150C 1151C 1152C 1153C 1154C 1155C 1156C 1157C 1158C 1159C 1160C 1161C 1162C 1163C 1164C 1165C 1166C 1167C 1168C 1169C 1170C 1171C 1172C 1173C 1174C 1175C 1176C 1177C 1178C 1179C 1180C 1181C 1182C 1183C 1184C 1185C 1186C 1187C 1188C 1189C 1190C 1191C 1192C 1193C 1194C 1195C 1196C 1197C 1198C 1199C 1200C 1201C 1202C 1203C 1204C 1205C 1206C 1207C 1208C 1209C 1210C 1211C 1212C 1213C 1214C 1215C 1216C 1217C 1218C 1219C 1220C 1221C 1222C 1223C 1224C 1225C 1226C 1227C 1228C 1229C 1230C 1231C 1232C 1233C 1234C 1235C 1236C 1237C 1238C 1239C 1240C 1241C 1242C 1243C 1244C 1245C 1246C 1247C 1248C 1249C 1250C 1251C 1252C 1253C 1254C 1255C 1256C 1257C 1258C 1259C 1260C 1261C 1262C 1263C 1264C 1265C 1266C 1267C 1268C 1269C 1270C 1271C 1272C 1273C 1274C 1275C 1276C 1277C 1278C 1279C 1280C 1281C 1282C 1283C 1284C 1285C 1286C 1287C 1288C 1289C 1290C 1291C 1292C 1293C 1294C 1295C 1296C 1297C 1298C 1299C 1300C 1301C 1302C 1303C 1304C 1305C 1306C 1307C 1308C 1309C 1310C 1311C 1312C 1313C 1314C 1315C 1316C 1317C 1318C 1319C 1320C 1321C 1322C 1323C 1324C 1325C 1326C 1327C 1328C 1329C 1330C 1331C 1332C 1333C 1334C 1335C 1336C 1337C 1338C 1339C 1340C 1341C 1342C 1343C 1344C 1345C 1346C 1347C 1348C 1349C 1350C 1351C 1352C 1353C 1354C 1355C 1356C 1357C 1358C 1359C 1360C 1361C 1362C 1363C 1364C 1365C 1366C 1367C 1368C 1369C 1370C 1371C 1372C 1373C 1374C 1375C 1376C 1377C 1378C 1379C 1380C 1381C 1382C 1383C 1384C 1385C 1386C 1387C 1388C 1389C 1390C 1391C 1392C 1393C 1394C 1395C 1396C 1397C 1398C 1399C 1400C 1401C 1402C 1403C 1404C 1405C 1406C 1407C 1408C 1409C 1410C 1411C 1412C 1413C 1414C 1415C 1416C 1417C 1418C 1419C 1420C 1421C 1422C 1423C 1424C 1425C 1426C 1427C 1428C 1429C 1430C 1431C 1432C 1433C 1434C 1435C 1436C 1437C 1438C 1439C 1440C 1441C 1442C 1443C 1444C 1445C 1446C 1447C 1448C 1449C 1450C 1451C 1452C 1453C 1454C 1455C 1456C 1457C 1458C 1459C 1460C 1461C 1462C 1463C 1464C 1465C 1466C 1467C 1468C 1469C 1470C 1471C 1472C 1473C 1474C 1475C 1476C 1477C 1478C 1479C 1480C 1481C 1482C 1483C 1484C 1485C 1486C 1487C 1488C 1489C 1490C 1491C 1492C 1493C 1494C 1495C 1496C 1497C 1498C 1499C 1500C 1501C 1502C 1503C 1504C 1505C 1506C 1507C 1508C 1509C 1510C 1511C 1512C 1513C 1514C 1515C 1516C 1517C 1518C 1519C 1520C 1521C 1522C 1523C 1524C 1525C 1526C 1527C 1528C 1529C 1530C 1531C 1532C 1533C 1534C 1535C 1536C 1537C 1538C 1539C 1540C 1541C 1542C 1543C 1544C 1545C 1546C 1547C 1548C 1549C 1550C 1551C 1552C 1553C 1554C 1555C 1556C 1557C 1558C 1559C 1560C 1561C 1562C 1563C 1564C 1565C 1566C 1567C 1568C 1569C 1570C 1571C 1572C 1573C 1574C 1575C 1576C 1577C 1578C 1579C 1580C 1581C 1582C 1583C 1584C 1585C 1586C 1587C 1588C 1589C 1590C 1591C 1592C 1593C 1594C 1595C 1596C 1597C 1598C 1599C 1600C 1601C 1602C 1603C 1604C 1605C 1606C 1607C 1608C 1609C 1610C 1611C 1612C 1613C 1614C 1615C 1616C 1617C 1618C 1619C 1620C 1621C 1622C 1623C 1624C 1625C 1626C 1627C 1628C 1629C 1630C 1631C 1632C 1633C 1634C 1635C 1636C 1637C 1638C 1639C 1640C 1641C 1642C 1643C 1644C 1645C 1646C 1647C 1648C 1649C 1650C 1651C 1652C 1653C 1654C 1655C 1656C 1657C 1658C 1659C 1660C 1661C 1662C 1663C 1664C 1665C 1666C 1667C 1668C 1669C 1670C 1671C 1672C 1673C 1674C 1675C 1676C 1677C 1678C 1679C 1680C 1681C 1682C 1683C 1684C 1685C 1686C 1687C 1688C 1689C 1690C 1691C 1692C 1693C 1694C 1695C 1696C 1697C 1698C 1699C 1700C 1701C 1702C 1703C 1704C 1705C 1706C 1707C 1708C 1709C 1710C 1711C 1712C 1713C 1714C 1715C 1716C 1717C 1718C 1719C 1720C 1721C 1722C 1723C 1724C 1725C 1726C 1727C 1728C 1729C 1730C 1731C 1732C 1733C 1734C 1735C 1736C 1737C 1738C 1739C 1740C 1741C 1742C 1743C 1744C 1745C 1746C 1747C 1748C 1749C 1750C 1751C 1752C 1753C 1754C 1755C 1756C 1757C 1758C 1759C 1760C 1761C 1762C 1763C 1764C 1765C 1766C 1767C 1768C 1769C 1770C 1771C 1772C 1773C 1774C 1775C 1776C 1777C 1778C 1779C 1780C 1781C 1782C 1783C 1784C 1785C 1786C 1787C 1788C 1789C 1790C 1791C 1792C 1793C 1794C 1795C 1796C 1797C 1798C 1799C 1800C 1801C 1802C 1803C 1804C 1805C 1806C 1807C 1808C 1809C 1810C 1811C 1812C 1813C 1814C 1815C 1816C 1817C 1818C 1819C 1820C 1821C 1822C 1823C 1824C 1825C 1826C 1827C 1828C 1829C 1830C 1831C 1832C 1833C 1834C 1835C 1836C 1837C 1838C 1839C 1840C 1841C 1842C 1843C 1844C 1845C 1846C 1847C 1848C 1849C 1850C 1851C 1852C 1853C 1854C 1855C 1856C 1857C 1858C 1859C 1860C 1861C 1862C 1863C 1864C 1865C 1866C 1867C 1868C 1869C 1870C 1871C 1872C 1873C 1874C 1875C 1876C 1877C 1878C 1879C 1880C 1881C 1882C 1883C 1884C 1885C 1886C 1887C 1888C 1889C 1890C 1891C 1892C 1893C 1894C 1895C 1896C 1897C 1898C 1899C 1900C 1901C 1902C 1903C 1904C 1905C 1906C 1907C 1908C 1909C 1910C 1911C 1912C 1913C 1914C 1915C 1916C 1917C 1918C 1919C 1920C 1921C 1922C 1923C 1924C 1925C 1926C 1927C 1928C 1929C 1930C 1931C 1932C 1933C 1934C 1935C 1936C 1937C 1938C 1939C 1940C 1941C 1942C 1943C 1944C 1945C 1946C 1947C 1948C 1949C 1950C 1951C 1952C 1953C 1954C 1955C 1956C 1957C 1958C 1959C 1960C 1961C 1962C 1963C 1964C 1965C 1966C 1967C 1968C 1969C 1970C 1971C 1972C 1973C 1974C 1975C 1976C 1977C 1978C 1979C 1980C 1981C 1982C 1983C 1984C 1985C 1986C 1987C 1988C 1989C 1990C 1991C 1992C 1993C 1994C 1995C 1996C 1997C 1998C 1999C 2000C 2001C 2002C 2003C 2004C 2005C 2006C 2007C 2008C 2009C 2010C 2011C 2012C 2013C 2014C 2015C 2016C 2017C 2018C 2019C 2020C 2021C 2022C 2023C 2024C 2025C 2026C 2027C 2028C 2029C 2030C 2031C 2032C 2033C 2034C 2035C 2036C 2037C 2038C 2039C 2040C 2041C 2042C 2043C 2044C 2045C 2046C 2047C 2048C 2049C 2050C 2051C 2052C 2053C 2054C 2055C 2056C 2057C 2058C 2059C 2060C 2061C 2062C 2063C 2064C 2065C 2066C 2067C 2068C 2069C 2070C 2071C 2072C 2073C 2074C 2075C 2076C 2077C 2078C 2079C 2080C 2081C 2082C 2083C 2084C 2085C 2086C 2087C 2088C 2089C 2090C 2091C 2092C 2093C 2094C 2095C 2096C 2097C 2098C 2099C 2100C 2101C 2102C 2103C 2104C 2105C 2106C 2107C 2108C 2109C 2110C 2111C 2112C 2113C 2114C 2115C 2116C 2117C 2118C 2119C 2120C 2121C 2122C 2123C 2124C 2125C

Variable	Value	Variable	Value	Variable	Value	Variable	Value	Variable	Value
UNFILTERED ARRAY BEAM POWER WINDOW LENGTH ISAMPLES	32	START SAMPLE BEFORE DETECTION TIME IN PROCESSING INTERVAL ISAMPLES	1000	END SAMPLE AFTER DETECTION TIME IN PROCESSING INTERVAL ISAMPLES	1000	SIGNAL POWER AVERAGING WINDOW LENGTH ISAMPLES	20	SAMPLE NUMBER TO START SIGNAL POWER AVERAGING BEFORE DETECTION ISAMPLES	170
WINDOW LENGTH FOR POWER CALCULATION ISAMPLES	32	UNFILTERED ARRAY BEAM POWER THRESHOLD (DB)	-6.320	PROCESSING INTERVAL LENGTH ISAMPLES	1200	START SAMPLE BEFORE DETECTION TIME IN PROCESSING INTERVAL ISAMPLES	300	SAMPLE NUMBER TO START SIGNAL POWER AVERAGING AFTER DETECTION ISAMPLES	200
UNFILTERED ARRAY BEAM POWER THRESHOLD (DB)	-6.320	START SAMPLE AFTER DETECTION TIME IN PROCESSING INTERVAL ISAMPLES	200	SAMPLE NUMBER TO START SIGNAL POWER AVERAGING AFTER DETECTION ISAMPLES	170	SAMPLE NUMBER TO EXCEED PROSUMAX FOR EVENT MODE TO START ISAMPLES	3	SAMPLE NUMBER TO FALL BELOW TRUE PEAK IN EVENT MODE ISAMPLES	2
START SAMPLE BEFORE DETECTION TIME IN PROCESSING INTERVAL ISAMPLES	1000	END SAMPLE AFTER DETECTION TIME IN PROCESSING INTERVAL ISAMPLES	1000	SAMPLE NUMBER TO EXCEED PROSUMAX FOR EVENT MODE TO START ISAMPLES	3	END SAMPLE BEFORE FIRST PEAK IN NOISE POWER AVERAGING ISAMPLES	90	WHEN TOTAL EVENT MODE NUMBER EXCEEDS THIS, THE EXCEPTION MODE IS SET	4
SIGNAL POWER AVERAGING WINDOW LENGTH ISAMPLES	20	SAMPLE NUMBER TO START SIGNAL POWER AVERAGING BEFORE DETECTION ISAMPLES	170	SAMPLE NUMBER TO FALL BELOW TRUE PEAK IN EVENT MODE ISAMPLES	2	MINIMUM TIME FIRST EVENT MODE IS OUTSIDE DETECTION CORRELATION TIME ISAMPLES	120	FACTOR USED TO MULTIPLY SUMAX	0.2500
SAMPLE NUMBER TO START SIGNAL POWER AVERAGING BEFORE DETECTION ISAMPLES	170	SAMPLE NUMBER TO FALL BELOW TRUE PEAK IN EVENT MODE ISAMPLES	2	WHEN TOTAL EVENT MODE NUMBER EXCEEDS THIS, THE EXCEPTION MODE IS SET	4	SAMPLING RATE IN HZ ISAMPLES PER SECOND	10	SAMPLE NUMBER FOR EVENT CLASSIFICATION ISAMPLES	35
SAMPLE NUMBER TO EXCEED PROSUMAX FOR EVENT MODE TO START ISAMPLES	3	SAMPLE NUMBER TO FALL BELOW TRUE PEAK IN EVENT MODE ISAMPLES	2	WHEN TOTAL EVENT MODE NUMBER EXCEEDS THIS, THE EXCEPTION MODE IS SET	4	START SAMPLE BEFORE FIRST PEAK IN MAGNITUDE CALCULATION ISAMPLES	40	END SAMPLE AFTER FIRST PEAK IN MAGNITUDE CALCULATION ISAMPLES	10
SAMPLE NUMBER TO FALL BELOW TRUE PEAK IN EVENT MODE ISAMPLES	2	WHEN TOTAL EVENT MODE NUMBER EXCEEDS THIS, THE EXCEPTION MODE IS SET	4	MINIMUM TIME FIRST EVENT MODE IS OUTSIDE DETECTION CORRELATION TIME ISAMPLES	120	S/N RATIO IN GENERATING DIFFERENCE FUNCTION IN MAGNITUDE CALCULATION	0.2500	S/N RATIO IN GENERATING DIFFERENCE FUNCTION IN MAGNITUDE CALCULATION	0.2500
FACTOR USED TO MULTIPLY SUMAX	0.2500	SAMPLING RATE IN HZ ISAMPLES PER SECOND	10	SAMPLE NUMBER FOR EVENT CLASSIFICATION ISAMPLES	35	SCALAR MULTIPLIER IN THRESHOLD PICK ALGORITHMS	50.0000	START BEFORE FIRST PEAK FOR THRESHOLD PICK ISAMPLES	4.0000
SAMPLE NUMBER FOR EVENT CLASSIFICATION ISAMPLES	35	END SAMPLE AFTER FIRST PEAK IN MAGNITUDE CALCULATION ISAMPLES	10	S/N RATIO IN GENERATING DIFFERENCE FUNCTION IN MAGNITUDE CALCULATION	0.2500	THRESHOLD PICK WINDOW LENGTH ISAMPLES	100	MODEL FIT WINDOW LENGTH ISAMPLES	14
END SAMPLE AFTER FIRST PEAK IN MAGNITUDE CALCULATION ISAMPLES	10	S/N RATIO IN GENERATING DIFFERENCE FUNCTION IN MAGNITUDE CALCULATION	0.2500	THRESHOLD PICK WINDOW LENGTH ISAMPLES	100	START SAMPLE BEFORE START TIME FOR MODEL FIT WINDOW TO MOVE ISAMPLES	40	NUMBER OF TIMES MODEL FIT WINDOW IS MOVED	40
S/N RATIO IN GENERATING DIFFERENCE FUNCTION IN MAGNITUDE CALCULATION	0.2500	THRESHOLD PICK WINDOW LENGTH ISAMPLES	100	START SAMPLE BEFORE START TIME FOR MODEL FIT WINDOW TO MOVE ISAMPLES	40	DOMINANT FREQUENCY WINDOW LENGTH ISAMPLES	254	SAMPLE NUMBER AFTER ARRIVAL TIME TO CENTER DOMINANT FREQUENCY WINDOW ISAMPLES	1
THRESHOLD PICK WINDOW LENGTH ISAMPLES	100	START SAMPLE BEFORE START TIME FOR MODEL FIT WINDOW TO MOVE ISAMPLES	40	DOMINANT FREQUENCY WINDOW LENGTH ISAMPLES	254	SAMPLE NUMBER IN TRIANGULAR FUNCTION FOR DOMINANT FREQUENCY ISAMPLES	30	CONSTANT IN GENERATING SINE WAVE IN FIRST MOTION DIRECTION ISAMPLES	2.0000
START SAMPLE BEFORE START TIME FOR MODEL FIT WINDOW TO MOVE ISAMPLES	40	DOMINANT FREQUENCY WINDOW LENGTH ISAMPLES	254	SAMPLE NUMBER IN TRIANGULAR FUNCTION FOR DOMINANT FREQUENCY ISAMPLES	30	START SAMPLE BEFORE ARRIVAL TIME IN FIRST MOTION DIRECTION ISAMPLES	10	END SAMPLE AFTER ARRIVAL TIME IN FIRST MOTION DIRECTION ISAMPLES	10
DOMINANT FREQUENCY WINDOW LENGTH ISAMPLES	254	SAMPLE NUMBER AFTER ARRIVAL TIME TO CENTER DOMINANT FREQUENCY WINDOW ISAMPLES	1	CONSTANT IN GENERATING SINE WAVE IN FIRST MOTION DIRECTION ISAMPLES	2.0000	CORRELATION FUNCTION THRESHOLD	0.9000	GENERATION OF SPECIFIC LENGTH ISAMPLES	1024
SAMPLE NUMBER AFTER ARRIVAL TIME TO CENTER DOMINANT FREQUENCY WINDOW ISAMPLES	1	CONSTANT IN GENERATING SINE WAVE IN FIRST MOTION DIRECTION ISAMPLES	2.0000	CORRELATION FUNCTION THRESHOLD	0.9000	START SAMPLE BEFORE ARRIVAL TIME IN SPECIFIC CALCULATION ISAMPLES	100	MINIMUM VALUE OF UNCALIBRATED U ALLOWED IN DEPTH ESTIMATION IS/KM	0.0397
CONSTANT IN GENERATING SINE WAVE IN FIRST MOTION DIRECTION ISAMPLES	2.0000	CORRELATION FUNCTION THRESHOLD	0.9000	START SAMPLE BEFORE ARRIVAL TIME IN SPECIFIC CALCULATION ISAMPLES	100	MAXIMUM VALUE OF UNCALIBRATED U ALLOWED IN DEPTH ESTIMATION IS/KM	0.0397	FACTOR USED TO FIND ALTERNATE ENVELOPE THRESHOLD	16.0000
CORRELATION FUNCTION THRESHOLD	0.9000	START SAMPLE BEFORE ARRIVAL TIME IN SPECIFIC CALCULATION ISAMPLES	100	MAXIMUM VALUE OF UNCALIBRATED U ALLOWED IN DEPTH ESTIMATION IS/KM	0.0397	CONVOLUTION FILTER COEFFICIENTS	17166		2352
START SAMPLE BEFORE ARRIVAL TIME IN SPECIFIC CALCULATION ISAMPLES	100	MAXIMUM VALUE OF UNCALIBRATED U ALLOWED IN DEPTH ESTIMATION IS/KM	0.0397	CONVOLUTION FILTER COEFFICIENTS	17166		3353		3290
MAXIMUM VALUE OF UNCALIBRATED U ALLOWED IN DEPTH ESTIMATION IS/KM	0.0397	CONVOLUTION FILTER COEFFICIENTS	17166		3353		1812		1812
FACTOR USED TO FIND ALTERNATE ENVELOPE THRESHOLD	16.0000		2352		3353		1812		1812
CONVOLUTION FILTER COEFFICIENTS	17166		3353		1812		1812		1812
	2352		3353		1812		1812		1812
	3353		1812		1812		1812		1812
	1812		1812		1812		1812		1812
RECURSIVE FILTER COEFFICIENTS	-1425	7425	-2475	5245	13561	-1611	-8728	635	1509
MODEL FIT COEFFICIENTS	-927	927	-309	19024	-23110	14820	-11351	4184	-822
COEFFICIENTS FOR AMPLITUDE CORRECTION	-0.1690	0.0238	-0.4306	0.0837	-13.2709	25.2771	-17.4036	6.7906	-1.5565
	0.0238	-0.4306	0.0837	-13.2709	25.2771	-17.4036	6.7906	-1.5565	50
	-0.1690	0.0238	-0.4306	0.0837	-13.2709	25.2771	-17.4036	6.7906	50
	0.0238	-0.4306	0.0837	-13.2					

Figure 8-18. NDPC SPS Parameter Report (Sheet 3 of 5)

FBIASA		RECURSIVE FILTER BIAS FACTORS									
0.0631											
C.1927											
0.0											
0.0085											
0.0175											
0.0395											
0.0990											
60.8237											
10.8327											
0.120C											
86											
10											
9											
9999											
1025											
40											
0.500C											
13.000C											
-2.200C											
3											
20											
75.000C											
1.2500											
20.000C											
35.0000											
1.2500											
0.4000											
129.0123901367											
9.038324501C											
1.379672053C											
-0.5838659632											
-0.0022258565											
0.2504300475											
0.041865364											
54.8919982910											
-C.3607624593											
0.002447910C											
-0.0079901293											
-0.0064114705											
0.0019911788											
0.0007519462											
118.2171936335											
53.3142029844											
-4.141222717											
-1.3489198685											
0.9035588841											
0.2729436755											
-0.1780322858											
POLYNOMIAL ARRAY											
0.066277682P											
0.814911484P											
0.0533333272											
0.0											
100.000C											
85											
F135											
F145											
F155											
F165											
F175											
GALATS											
GALOMS											
R5											
M55											
N75											
N95											
N95											
N15											
N25											
F35											
F45											
F55											
N35											
N45											
F65											
F75											
F85											
F95											
F105											
F115											
A5											
129.0123901367											
9.038324501C											
1.379672053C											
-0.5838659632											
-0.0022258565											
0.2504300475											
0.041865364											
54.8919982910											
-C.3607624593											
0.002447910C											
-0.0079901293											
-0.0064114705											
0.0019911788											
0.0007519462											
118.2171936335											
53.3142029844											
-4.141222717											
-1.3489198685											
0.9035588841											
0.2729436755											
-0.1780322858											
POLYNOMIAL ARRAY											
0.066277682P											
0.814911484P											
0.0533333272											
0.0											
100.000C											
85											
F135											
F145											
F155											
F165											
F175											
GALATS											
GALOMS											
R5											
M55											
N75											
N95											
N95											
N15											
N25											
F35											
F45											
F55											
N35											
N45											
F65											
F75											
F85											
F95											
F105											
F115											
A5											
129.0123901367											
9.038324501C											
1.379672053C											
-0.5838659632											
-0.0022258565											
0.2504300475											
0.041865364											
54.8919982910											
-C.3607624593											
0.002447910C											
-0.0079901293											
-0.0064114705											
0.0019911788											
0.0007519462											
118.2171936335											
53.3142029844											
-4.141222717											
-1.3489198685											
0.9035588841											
0.2729436755											
-0.1780322858											
POLYNOMIAL ARRAY											
0.066277682P											
0.814911484P											
0.0533333272											
0.0											
100.000C											
85											
F135											
F145											
F155											
F165											
F175											
GALATS											
GALOMS											
R5											
M55											
N75											
N95											
N95											
N15											
N25											
F35											
F45											
F55											
N35											
N45											
F65											
F75											
F85											
F95											
F105											
F115											
A5											
129.0123901367											
9.038324501C											
1.379672053C											
-0.5838659632											
-0.0022258565											
0.2504300475											
0.041865364											
54.8919982910											
-C.3607624593											
0.002447910C											
-0.0079901293											
-0.0064114705											
0.0019911788											
0.0007519462											
118.2171936335											
53.3142029844											
-4.141222717											
-1.3489198685											
0.9035588841											
0.2729436755											
-0.1780322858											
POLYNOMIAL ARRAY											
0.066277682P											
0.814911484P											
0.0533333272											
0.0											
100.000C											
85											
F135											
F145											
F155											
F165											
F175											
GALATS											
GALOMS											
R5											
M55											
N75											
N95											
N95											
N15											
N25											
F35											
F45											
F55											
N35											
N45											
F65											
F75											
F85											
F95											
F105											
F115											
A5											
129.0123901367											
9.038324501C											
1.379672053C											
-0.5838659632											
-0.0022258565											
0.2504300475											
0.041865364											
54.8919982910											
-C.3607624593											
0.002447910C											
-0.0079901293											
-0.0064114705											
0.0019911788											
0.0007519462											
118.2171936335											
53.3142029844											
-4.141222717											
-1.3489198685											
0.9035588841											
0.2729436755											
-0.1780322858											
POLYNOMIAL ARRAY											
0.066277682P											
0.814911484P											
0.0533333272											
0.0											
100.000C											
85											
F135											
F145											
F155											
F165											
F175											
GALATS											
GALOMS											
R5											
M55											
N75											
N95											
N95											
N15											
N25											
F35											
F45											
F55											
N35											
N45											
F65											
F75											
F85											
F95											
F105											
F115											
A5											
129.0123901367											
9.038324501C											
1.379672053C											
-0.5838659632											
-0.0022258565											
0.2504300475											
0.041865364											
54.8919982910											
-C.3607624593											
0.002447910C											
-0.0079901293											
-0.0064114705											
0.0019911788											
0.0007519462											
118.2171936335											
53.3142029844											
-4.141222717											
-1.3489198685											
0.9035588841											
0.2729436755											
-0.1780322858											
POLYNOMIAL ARRAY											
0.066277682P											
0.814911484P											
0.0533333272											
0.0											
100.000C											
85											
F135											
F145											
F155											
F165											
F175											
GALATS											
GALOMS											
R5											
M55											
N75											
N95											
N95											
N15											
N25											
F35											
F45											
F55											
N35											
N45											
F65											
F75											
F85											
F95											
F105											
F115											
A5											
129.0123901367											
9.038324501C											
1.379672053C											
-0.5838659632											
-0.0022258565											
0.2504300475											
0.041865364											
54.8919982910											
-C.3607624593											
0.002447910C											
-0.0079901293											
-0.0064114705											
0.0019911788											
0.0007519462											
118.2171936335											
53.3142029844											
-4.141222717											
-1.3489198685											
0.9035588841											
0.2729436755											
-0.1780322858											
POLYNOMIAL ARRAY											
0.066277682P											
0.814911484P											
0.0533333272											
0.0											
100.000C											
85											
F135											
F145											
F155											
F165											
F175											
GALATS											
GALOMS											
R5											
M55											
N75											
N95											
N95											
N15											
N25											
F35											
F45											
F55											
N35											
N45											
F65											
F75											
F85											
F95											
F105											
F115											
A5											
129.0123901367											
9.038324501C											
1.379672053C											
-0.5838659632											
-0.0022258565											
0.2504300475											
0.041865364											
54.8919982910											
-C.3607624593											
0.002447910C											
-0.0079901293											
-0.0064114705											
0.0019911788											
0.0007519462											
118.2171936335											
53.3142029844											
-4.141222717											
-1.3489198685											
0.9035588841											
0.2729436755											
-0.1780322858											
POLYNOMIAL ARRAY											
0.066277682P											
0.814911484P											
0.0533333272											
0.0											
100.000C											
85											
F135											
F145											
F155											
F165											
F175											
GALATS											
GALOMS											
R5											
M55											
N75											
N95											
N95											
N15											
N25											
F35											
F45											
F55											
N35											
N45											

```

STSPSR
IVER          14
IGEN          072271
MODSP1        1
MODSP2        1
MODSP3        1
MODSP4        1
MODSP5        1
MODSP6        1
ISSEF BELOW1  1
ISSEF BELOW1  1
SALABS        01A 01B 02B 03B 04B 05B 06B 07B 01C 02C 03C 04C 05C 06C 07C 08C 09C 10C 11C 12C 13C 14C
SALARS        1 2 3 4 5 6 7 8 9 10 11 12 13 14 15 16 17 18 19 20 21 22
SADROS        01A 01B 02B 03B 04B 05B 06B 07B 01C 02C 03C 04C 05C 06C 07C 08C 09C 10C 11C 12C 13C 14C
OUTPUT ORD.   01A 01B 02B 03B 04B 05B 06B 07B 01C 02C 03C 04C 05C 06C 07C 08C 09C 10C 11C 12C 13C 14C

SUBARRAY LABELS IN ORDER OF APPEARANCE ON TAPE (23RD AND 24TH LABELS ARE FOR ARRAY BEAMS)
SUBARRAY LABELS IN ORDER OF APPEARANCE ON TAPE (23RD AND 24TH LABELS ARE FOR ARRAY BEAMS)
TIME BEFORE ARRIVAL TIME UP TO WHICH ARRAY BEAM IS TO BE SCALED FOR NOISE (SECONDS)
SECONDS BEFORE ARRIVAL TIME AT WHICH TO STOP SCALING ALL OTHER BEAMS
TIME BEFORE ARRIVAL TIME TO PLOT BEAMS (SHORT FORM)
TIME AFTER ARRIVAL TIME TO PLOT BEAMS (SHORT FORM)
TIME AFTER ARRIVAL TIME TO PLOT BEAMS (LONG FORM)

SUBARRAYS THAT ARE USED TO FORM EACH PARTIAL ARRAY BEAM
ORDERING OF BEAMS ON SUBARRAY BEAM PANELS
DEFAULT PLOT CRITERION = 0, ARRAY BEAM PANEL ONLY (SHORT FORM)
= 1, ARRAY BEAM PANEL AND TWO SUBARRAY BEAM PANELS (SHORT FORM)
= 2, ARRAY BEAM PANEL AND TWO SUBARRAY BEAM PANELS (LONG FORM)
NUMBER OF SUBARRAYS PER ARRAY
SUBARRAY DATA SAMPLING RATE (SAMPLES/SECOND)
PLOT OFFSET FILTER TYPE INDICATOR 80M INS-IRGCBH--IKC-IRJATSGEHO-YC-6A

PARTIAL ARRAY SUBARRAY 02A 03A 03C 04C 05C --
BEAM 1          PBSRP 3 4 11 12 13 0
PARTIAL ARRAY SUBARRAY 04A 05A 06C 07C 08C 09C
BEAM 2          PBSRP 5 6 14 15 16 17
PARTIAL ARRAY SUBARRAY 01A 06A 10C 11C 12C --
BEAM 3          PBSRP 1 7 18 19 20 0
PARTIAL ARRAY SUBARRAY 01A 07A 01C 02C 13C 14C
BEAM 4          PBSRP 2 9 9 10 21 22
SUBARRAY BEAM 01C 02C 01B 05A 08C 09C AB 12C 06B 01A 03A C5C
PANEL 1          SRPBLP 9 10 2 6 16 17 23 20 7 1 4 13
SUBARRAY BEAM 03C 04C 02A 11C 10C AB 13C 14C 07A C7A 06C 07C
PANEL 2          SRPBLP 11 12 4 19 14 23 21 22 8 5 14 15

```

Figure 8-18 NDPC SPSP Parameter Report (Sheet 5 of 5)

8.9 ANNOTATED BIBLIOGRAPHY

The references listed in this section are classified in three categories. Subsection 8.9.1 consists of relevant IBM quarterly and final reports, subsection 8.9.2 lists pertinent IBM special technical reports, and subsection 8.9.3 contains an external reference on magnitude determination.

8.9.1 IBM Quarterly and Final Reports

- 8-1. "Large Aperture Seismic Array Signal Processing Study,"
IBM Final Report, Contract SD-296, 15 July 1965.

This report documents LASA beamforming, digital beam prefiltering and output filtering, array geometry, and experimental steering delay determination. Appendix A discusses computer programs used to design and evaluate beam patterns. Appendix C describes methods for calculating best-fitting wavefronts by least-squares techniques. Appendix D discusses the deviation of quadratic steering delay corrections, and Appendix F documents digital filtering techniques.

- 8-2. "LASA Signal Processing, Simulation, and Communications Study," IBM First Quarterly Technical Report. Contract AF 19(628)-5948, 1 May 1966.

Appendix A discusses surveillance coverage (requirements for conventional beamforming). Appendix C discusses scaling specifications, seismometer sensitivity tolerances, and sampling rate. Appendix D describes a time delay determination technique.

- 8-3. "LASA Signal Processing, Simulation, and Communications Study," IBM Second Quarterly Technical Report, Contract AF 19(629)-5948, September 1966.

In Appendix A, developments in beam analysis are reported, including U-space mapping and surveillance beam requirement estimating. Appendix B discusses scaling requirements for the LASA beamformer. Appendix C extends the description of the functional system and certain operating parameters contained in reference [8-2]. Appendix E discusses data analysis programs, including a number that are important in event processing. Appendix F contains comments and recommendations concerning utilization of the LASA system.

- 8-4. "LASA Signal Processing, Simulation, and Communications Study," IBM Final Report, Contract AF 19(628)-5948, ESD-TR-66-635, March 1967.

Section 1 discusses array geometry and event location capability, signal processing, and data analysis programs. Section 2 is devoted exclusively to the subject of signal processing, including event processing and event monitoring. Section 3 discusses beam requirements, event location capability, steering delays, time delay probability distributions, digital filtering, data analysis, and event beam selection. Section 4 continues the documentation of data analysis programs, a number of which are directly involved in event processing.

- 8-5. "LASA Experimental Signal Processing System," IBM First Quarterly Technical Report, Contract AF 19(628)-C-67-0198, ESD-TR-458, February 1967.

Appendix A is a preliminary discussion of the Experimental System data flow and associated hardware configuration; Event Processor peripheral devices (displays and printers) are discussed. Appendix C includes some discussion of software requirements. Appendix D provides a preliminary report on microcode development.

- 8-6. "LASA Experimental Signal Processing System," IBM Second Quarterly Technical Report, Contract F 19(628)-67-C-0198, ESD-TR-67-602, May 1967.

This report primarily addresses the development of the composite detection system, but there is some discussion of the experimental Event Processor monitor. Appendix A describes the initial Event Processor machine configuration. Array monitoring and seismic data compression are discussed in Appendices B and C, respectively. The experimental waveform display and its function in event processing are discussed in Appendix E. Appendix F is a generalized summary of seismic array data collection and processing requirements.

- 8-7. "LASA Experimental Signal Processing System," IBM Third Quarterly Technical Report, Contract F 19(628)-67-C-0198, ESD-TR-68-149, August 1967.

Appendix I documents the then current and planned equipment configurations for the Detection and Event Processors. Appendix II discusses the technique of automatic time delay generation and the estimated event location accuracy of large arrays. Appendix III discusses the library organization of phase delays, a key requirement for event processing, and procedures developed for calculating improved steering delays. Appendix IV documents two studies which support event processing: an energy "density" method of calculating event magnitude, and the least-squares orthogonal polynomial fitting of travel-time data.

- 8-8. "LASA Experimental Signal Processing System," IBM Fourth Quarterly Technical Report, Contract F 19(628)-67-C-0198, ESD-TR-68-309, November 1967.

Appendix I discusses detailed changes in the SAAC computer configuration, including some Event Processor modifications. Appendix II presents results of the initial and the interim systems studies, in which the Event Processor was specifically addressed.

- 8-9. "LASA Experimental Signal Processing System," IBM Contract F 19(628)-67-C-0198, ESD-TR-68-450, February 1968.

Appendix III discusses a synthetic test signal library, used in testing and evaluating the experimental system. Appendix IV describes the Interim

Integrated Signal Processing System Operations Console, which was equipped to permit seismic data process supervision, as well as operator participation in array calibration and event process editing. Appendix V comments on planned configuration changes which will provide identical Detection and Event Processor configurations. Additional microcoding developments are discussed in Appendix VI. Appendix IX reports some special processing studies among which is one on earthquake frequency-magnitude relationships, and another on event classification. Appendix X presents the functional characteristics of support programming requirements in the areas of two-dimensional polynomial fitting, matrix inversion, and an event sort and print capability.

8-10. "LASA Experimental Signal Processing System," IBM Sixth Quarterly Technical Report, Contract F 19(628)-67-C-0198, ESD-TR-68-451, May 1968.

In Section II, work on the identification of the structure of an initial event processing capability (phase zero) is briefly described.

8-11. "LASA Experimental Signal Processing System," IBM Final Technical Report, Contract F 19(628)-67-C-0198, ESD-TR-69-60, Volume I, March 1969.

The initial integrated detection and event processing (Phase Zero) system capability, is outlined and reviewed in Appendix VI. The constituent parts of this processor are detailed in Appendix VII, while Appendix VIII reviews the location calibration procedure, which is one of the principal components of the implemented event processing structure. The use of fidelity optimum processing to separate an event of interest from an interfering event is reviewed in Appendix X.

8-12. "Integrated Seismic Research Signal Processing System," IBM First Quarterly Technical Report, Contract F 19(628)-69-C-0400, ESD-TR-69-299, November 1968.

Appendix I describes the Long Period Signal Processing Subsystem which was implemented for the Event Processor; this system, however, was implemented in the later revisions of the system. Appendix II describes methods

of detecting post-P arrivals (correlation and spectrum) to obtain depth estimates. Appendix V describes the ISRSPS equipment configuration.

- 8-13. "Integrated Seismic Research Signal Processing System,"
IBM Second Quarterly Technical Report, Contract F 19(628)-
68-C-0400, ESD-TR-69-357, February 1969.

Appendix IV describes the processing of a group of seven events, using Oyer Astrodata short period data. Appendix VIII discusses the feasibility of extending the linear range of the LASA system through instrument rescaling.

- 8-14. "Integrated Seismic Research Signal Processing System,"
IBM Third Quarterly Technical Report, Contract F 19(628)-
68-C-0400. ESD-TR-70-25, May 1969.

Appendix describes in detail the capabilities and system structure of the ISRSPS Event Processor. Appendix II includes a discussion of system processing results in April 1969. Appendix III describes work on depth estimation done since the work reported in [8-12, Appendix II]. Appendix IV discusses a LASA modification study, including the effect of such modification on location estimation potential. Appendix V summarizes the processing parameters used in the SAAC Phase Zero Event Processor. Appendix VI includes a discussion of Multiple-Array event location.

- 8-15. "Integrated Seismic Research Signal Processing System,"
IBM Fourth Quarterly Technical Report, Contract F 19(628)-
68-C-0400, ESD-TR-70-265, August 1969.

Appendix I describes the Extended Phase Zero Event Processing. Appendix II describes processing results for May through July 1969. Appendix III describes the implementation of improved region correction techniques.

Appendix V, dealing with Experimental Operations Console applications, includes a discussion of event process supervision and post edit functions.

- 8-16. "Integrated Seismic Research Signal Processing System,"
IBM Fifth Quarterly Technical Report, Contract F 19(628)-
68-C-0400, ESD-TR-70-306, November 1969.

Appendix II summarizes the results of the Long Period Event Processor (LPEP) operations during the current work period. Appendix III discusses processing results for August through October 1969. Appendix V describes the channel-recursive Bayes processing technique for post-detection estimation of source location. Appendix VII discusses the ISRSPS event processing programming monitor structure. Appendix VIII describes the objectives for a seismic research console, which is characterized as a logical extension of the SAAC event processing capability, among other functions. Further microcode development is reported in Appendix X. Appendix XI describes comprehensively the time intervals used by each Event Processor function that analyzes waveform data.

- 8-17. "Integrated Seismic Research Signal Processing System,"
IBM Sixth Quarterly Technical Report, Contract F 19(628)-
68-C-0400, ESD-TR-71-388, February 1970.

Appendix I describes processing results for November 1969 through January 1970, and also for the seven month period of July through December 1969. Appendix II describes the distribution of earthquakes over certain seismic areas. Appendix IV presents a technique for weighted beamforming to maximize the signal-to-noise ratio. Appendix V describes a heuristic nonlinear method of discriminating between seismic events of explosive origin and natural earthquakes.

- 8-18. "Integrated Seismic Research Signal Processing System,"
IBM Seventh Quarterly Technical Report, Contract F 19(628)-
68-C-0400, ESD-TR-72-128, May 1970.

Appendix I discusses processing results for February through April 1970. Appendix III describes advanced event processing logic for initially associating multiple arrivals with a single event. Appendix V describes the use of arrivals from multiple arrays and multiple phases at a given array to improve event location estimation accuracy.

- 8-19. "Integrated Seismic Research Signal Processing System,"
IBM Eighth Quarterly Technical Report. Contract F 19(628)-
68-C-0400, ESD-TR-71-393, August 1970.

Appendix I describes processing results for May through July 1970. Appendix II describes the technique developed for ISRSPS for representation of travel time anomalies. Appendix III presents the preliminary results of an analysis of signals received by the Interim NORSAR system; applications are primarily to detection processing, but the final subsection discusses aspects pertaining to event processing. Appendix V describes the experience gained from editing events on the SAAC Experimental Operations Console.

- 8-20. "Integrated Seismic Research Signal Processing System,"
IBM Ninth Quarterly Technical Report, Contract F 19(628)-
68-C-0400, ESD-TR-72-122, November 1970.

Appendix I describes processing results for August through October 1970. Included are a discussion of magnitude depth-distance factors (Q factors) for later phases, and a quantitative seismicity study of the earth. Appendix II describes the ISRSPS Event Processor Experimental Operations Console/2260 event analysis and bulletin editing capability. Appendix III presents the development and analysis of a LASA subarray time-anomaly and

location calibration data file based on the nonuniform triangular grid data storage and access method. Appendix IV summarizes the entire operation of the Interim NORSAR system. Appendix V documents the Interim NORSAR signal and noise analysis, including discussion of event selection and analysis procedure.

- 8-21. "Integrated Seismic Research Signal Processing System,"
IBM Tenth Quarterly Technical Report, Contract F 19(628)-
68-C-0400, ESD-TR-72-123, February 1971.

Appendix II summarizes LASA processing results for November and December 1970; this appendix also presents a compendium of travel-time, slowness, period, and magnitude depth-distance factors for about 14 months of LASA data processing. Appendix III describes the final SAAC ISRSPS Configuration, and Appendix IV summarizes the SAAC ISRSPS system and acceptance tests.

- 8-22. "Integrated Seismic Research Signal Processing System,"
IBM Eleventh Quarterly Technical Report, Contract F 19(628)-
68-C-0400, ESD-TR-72-133, May 1971.

Appendix VI describes the Event Processor as it was actually implemented for use at SAAC and at NDPC. Appendix VII describes the ISRSPS application to scaled events. In order to evaluate the performance of ISRSPS signal processing algorithms and techniques as a function of event size, the offline versions of the ISRSPS processors at SAAC were applied to an extensive data set of various amplitude seismic signals having known epicentral and waveform parameters.

- 8-23. "Integrated Seismic Research Signal Processing System,"
IBM Final Technical Report, Contract F 19(628)-68-C-0400,
ESD-TR-72-139, August 1971.

Appendix I describes an evaluation of the implemented NORSAR short period signal processing system. Appendix II describes an NDPC equipment utilization study. Appendix IV gives a summary analysis of data gathered during routine operation of the SAAC system through 1970. Sections are included on system performance in locating events and on regional estimation of magnitude biases.

8.9.2 IBM Special Technical Reports

- 8-24. "LASA Experimental Signal Processing System Programming Manual: Volume I, Program Descriptions; Volume II. Programming Subsystem Testing," Contract F 19(628)-67-C-0198, July 1968.

These documents describe the experimental system, which did not specifically include an Event Processor, but which did provide data that permitted testing of EP functions on an experimental basis.

- 8-25. "Evaluation of LASA Beam Precision Test Results," Contract F 19(628)-67-C-0198, ESD-TR-69-187, June 1968.

This document reviews an experiment designed to evaluate the LASA beam precision as portrayed by the observed scatter in epicenter surface image estimates. The report describes the tests performed, the results obtained, and the conclusions reached.

- 8-26. "Parametric Study of Seismic Array Gain Test Results," Contract F 19(628)-67-C-0198, ESD-TR-68-425, June 1968.

This document reviews an experiment designed to estimate the improvement in the seismic signal-to-noise power ratio achieved by LASA, as compared with that observed in the case of a single instrument. The report describes the tests performed, the results obtained, and the conclusions reached.

- 8-27. "Kinetic Energy Estimates of Seismic Magnitude Test Results," Contract F 19(628)-67-C-0198, ESD-TR-68-424, June 1968.

This document reviews an experiment to evaluate the consistency of automatic magnitude estimates based on the calculation of kinetic energy in the seismic "P" wave as derived from LASA short-period data. The report describes the tests performed, the results obtained, and the conclusion reached.

8.9.3 Miscellaneous Reference

- 8-28. B. Gutenberg and C.F. Richter, Magnitude and Energy of Earthquakes, *Annali di Geofisica*, Volume IX, No. 1, pp. 1-14, 1956.

This paper documents the classical method of magnitude determination which was implemented in the Event Processor magnitude calculation algorithm.

Section 9
IBM REPORT BIBLIOGRAPHY

All IBM technical reports of the Large Aperture Seismic Array Signal Processing Study, Experimental Signal Processing System, Integrated Seismic Research Signal Processing System, and NORSAR Systems Evaluation are listed in Section 9.1. Subsection 9.2 lists all special technical reports, and subsection 9.3 lists reference documentation for the Integrated Seismic Research Signal Processing System.

9.1 IBM QUARTERLY AND FINAL REPORTS

- 9-1. "Large Aperture Seismic Array Signal Processing Study,"
IBM Final Report, Contract SD-296, 15 July 1965.
- 9-2. "LASA Signal Processing, Simulation, and Communications
Study," IBM First Quarterly Technical Report, Contract
AF 19 (628)-5948, 1 May 1966.
- 9-3. "LASA Signal Processing, Simulation, and Communications
Study," IBM Second Quarterly Technical Report, Contract
AF (629)-5948, September 1966.
- 9-4. "LASA Signal Processing, Simulation, and Communications
Study," IBM Final Report, Contract AF 19 (628)-5948,
ESD-TR-66-635, March 1967.
- 9-5. "LASA Experimental Signal Processing System," IBM First
Quarterly Technical Report, Contract W19628-67-C-0198,
ESD-TR-67-458, February 1967.

- 9-6. "LASA Experimental Signal Processing System," IBM Second Quarterly Technical Report, Contract F19628-67-C-0198, ESD-TR-67-602, May 1967.
- 9-7. "LASA Experimental Signal Processing System," IBM Third Quarterly Technical Report, Contract F19628-67-C-0198, ESD-TR-68-149, August 1967.
- 9-8. "LASA Experimental Signal Processing System," IBM Fourth Quarterly Technical Report, Contract F19628-67-C-0198, ESD-TR-68-309, November 1967.
- 9-9. "LASA Experimental Signal Processing System," IBM Fifth Quarterly Technical Report, Contract F19628-67-C-0198, ESD-TR-68-450, February 1968.
- 9-10. "LASA Experimental Signal Processing System," IBM Sixth Quarterly Technical Report, Contract F19628-67-C-0198, ESD-TR-68-451, May 1968.
- 9-11. "LASA Experimental Signal Processing System," IBM Final Technical Report, Contract F19628-67-C-0198, ESD-TR-69-60, Volume I, March 1969. Volume II is a classified section.
- 9-12. "Integrated Seismic Research Signal Processing System," IBM First Quarterly Technical Report, Contract F19628-68-C-0400, ESD-TR-69-299, November 1968.
- 9-13. "Integrated Seismic Research Signal Processing System," IBM Second Quarterly Technical Report, Contract F19628-68-C-0400, ESD-TR-69-357, February 1969.

- 9-14. "Integrated Seismic Research Signal Processing System,"
IBM Third Quarterly Technical Report, Contract F19628-
68-C-0400, ESD-TR-70-25, May 1969.
- 9-15. "Integrated Seismic Research Signal Processing System,"
IBM Fourth Quarterly Technical Report, Contract F19628-
68-C-0400, ESD-TR-70-265, August 1969.
- 9-16. "Integrated Seismic Research Signal Processing System,"
IBM Fifth Quarterly Technical Report, Contract F19628-
68-C-0400, ESD-TR-70-306, November 1969.
- 9-17. "Integrated Seismic Research Signal Processing System,"
IBM Sixth Quarterly Technical Report, Contract F19628-
68-C-0400, ESD-TR-71-388, February 1970.
- 9-18. "Integrated Seismic Research Signal Processing System,"
IBM Seventh Quarterly Technical Report, Contract
F19628-68- -0400, ESD-TR-72-128, May 1970.
- 9-19. "Integrated Seismic Research Signal Processing System,"
IBM Eighth Quarterly Technical Report, Contract F19628-
68-C-0400, ESD-TR-71-393, August 1970.
- 9-20. "Integrated Seismic Research Signal Processing System,"
IBM Ninth Quarterly Technical Report, Contract F19628-
68-C-0400, ESD-TR-72-122, November 1970.
- 9-21. "Integrated Seismic Research Signal Processing System,"
IBM Tenth Quarterly Technical Report, Contract F19628-
68-C-0400, ESD-TR-72-123, February 1971.

9-22. "Integrated Seismic Research Signal Processing System,"
IBM Eleventh Quarterly Technical Report, Contract
F19628-68-C-0400, ESD-TR-72-133, May 1971.

9-23. "Integrated Seismic Research Signal Processing System,"
IBM Final Technical Report, Contract F19628-68-C-0400,
ESD-TR-72-139, August 1971.

9-24. "NORSAR Systems Evaluation," IBM Interim Technical
Report, Contract F19628-68-C-0400, ESD-TR-72-145
January 1972.

9-25. "NORSAR Systems Evaluation," IBM Final Technical
Report, Contract F19628-68-C-0400, July 1972. To
be published.

9.2 IBM SPECIAL TECHNICAL REPORTS

9-26. "Beam Patterns," Contract SD-296, November 1965.

9-27. "Experimental Signal Processing System Interface
Equipment Specifications," Contract F19628-67-
0198, July 1967.

9-28. "Experimental Signal Processing System Array Monitor
and Control Specification," Contract F19628-67-C-
0198, July 1967.

9-29. "Experimental Signal Processing System - Montana Facility
Requirements," Contract F19628-67-C-0198, July 1967.

- 9-30. "LASA Experimental Signal Processing System General Specification," Contract F19628-67-C-0198, July 1967.
- 9-31. "LASA Experimental Signal Processing System Acceptance Test Plan," Contract F19628-67-C-0198, July 1967.
- 9-32. "Experimental Signal Processing System Evaluation Plan," Contract F19628-67-C-0198, ESD-TR-68-427, February 1968.
- 9-33. "LASA Algorithm Hardware Documentation," Contract F19628-67-C-0198, March 1968.
- 9-34. "LASA Experimental Signal Processing System Programming Specification," Contract F19628-67-C-0198, May 1968.
- 9-35. "Evaluation of LASA Beam Precision Test Plan," Contract F19628-67-C-0198, ESD-TR-218, May 1968.
- 9-36. "Parametric Study of Seismic Array Gain Test Plan," Contract F19628-67-C-0198, ESD-TR-219, May 1968.
- 9-37. "Kinetic Energy Estimates of Seismic Magnitude Test Plan," Contract F19628-67-C-0198, ESD-TR-68-220, May 1968.
- 9-38. "ESPS Operating Manual," Contract F19628-67-C-0198, June 1968.
- 9-39. "Evaluation of LASA Beam Precision Test Results," Contract F19628-67-C-0198, ESD-TR-69-187, June 1968.
- 9-40. "Parametric Study of Seismic Array Gain Test Results," Contract F19628-67-C-0198, ESD-TR-68-425, June 1968.

- 9-41. "Kinetic Energy Estimates of Seismic Manitude Test Results,"
Contract F19628-67-C-0198, ESD-TR-68-424, June 1968.
- 9-42. "Interim Integrated Signal Processing System (IISPS) Norway
Data Center Facility Requirements," Contract F19628-67-C-
0198, June 1968.
- 9-43. "LASA Experimental Signal Processing System Programming
Manual - Volume I, Program Descriptions," Contract
F19628-67-C-0198, July 1968.
- 9-44. "LASA Experimental Signal Processing System Programming
Manual - Volume II, Programming Subsystem Testing,"
Contract F19628-67-C-0198, July 1968.
- 9-45. "Signal Processing Studies for Large Array Research,"
Contract F19628-67-C-0198, March 1970.
- 9-46. "Computer Network Feasibility Considerations for SAAC,"
Contract F19628-68-C-0400, June 1970.
- 9-47. "Evaluation of the Transatlantic Data Link of the Integrated
Seismic Research Signal Processing System," Contract
F19628-68-C-0400, September 1970.
- 9-48. "NORSAR Long-Period Processing," Contract F19628-68-C-
0400, April 1971.
- 9-49. "SAAC Final Bulletin," Volume I, April 1969 - December
1969; Volume II, January 1970, - December 1970, Contract
F19628-68-C-0400, June 1971.

9-50. "Seismic Data Base Study," Contract F19628-68-C-0400,
1 October 1971.

9-51. "ISRSPS/ARPA Network Study," Contract F19628-68-C-0400,
1 November 1971.

9.3 ISRSPS REFERENCE (REF) DOCUMENTATION, ANNOTATED

Technical documentation of the Integrated Seismic Research Signal Processing System (ISRSPS) is contained in the set of documents that is listed and annotated below. Each document is assigned a REF number that is used to identify it in all cross-referencing within this set of documents. Separate documents, distinguished by an alphabetic suffix, were created when substantial differences existed between subsystems for the LASA Data Center (LDC), the Norwegian Data Processing Center (NDPC), and the Seismic Array Analysis Center (SAAC). When a single document is used to describe subsystems for several locations, specified chapters may apply to only one subsystem.

Each REF has a separate binder, except that REFs 110 and 111 are in a series of binders labeled Program Reference Manual.

9-52. REF 101, ISRSPS General System Specification.

REF 101 establishes performance and design requirements for both equipment and programs in the ISRSPS. These requirements are expressed in functional terms.

9-53. REF 102, ISRSPS General Equipment Specification.

REF 102 identifies all items of ISRSPS equipment and specifies equipment interfaces with already existing or GFE items. Standard IBM commercial

equipment items are identified by model and feature numbers. Performance and design requirements are established for all other items of ISRSPS equipment except the Interface Equipment (SPS) (REF 103), the prototype Integrated Array Electronics (SLEM) (REF 18), and the Experimental Operations Console (EOC) (REF 8 and REF 107N). Diagrams of all equipment configurations, including test configurations, are included.

9-54. REF 103, ISRSPS Interface Equipment Design Specification.

REF 103 establishes the detailed performance and design requirements for the design, development, test and qualification of the Interface Equipment (SPS), excluding microcoded functions.

9-55. REF 104N, ISRSPS Interface Equipment Processing Specification (NDPC).

9-56. REF 104S, ISRSPS Interface Equipment Processing Specification (SAAC).

REF 104 establishes the detailed performance and design requirements for the SPS microprograms. The organization and design of the programs are described. Implementation details are provided in a separately bound appendix.

9-57. REF 105, ISRSPS Interface Equipment Test Specification.

REF 105 establishes detailed qualification requirements, criteria, methods and responsibilities for testing the SPS, excluding microcoded functions.

9-58. REF 106, ISRSPS Interface Equipment Operations and Maintenance Manual.

REF 106 contains information for the use, guidance and training of personnel operating and maintaining the SPS. The manual contains a detailed technical description of the equipment, with timing and logic diagrams.

9-59. REF 107N, ISRSPS Experimental Operations Console Specification (NDPC).

REF 107N establishes detailed performance and design requirements for the design, development, test, and qualification of the NORSAR Experimental Operations Console.

9-60. REF 108N, ISRSPS Experimental Operations Console Test Specification (NDPC).

REF 108N establishes detailed qualification requirements, criteria, methods, and responsibilities for testing the NORSAR Experimental Operations Console.

9-61. REF 109N, ISRSPS Experimental Operations Console Operations and Maintenance Manual (NDPC).

REF 109N contains information for the use, guidance, and training of personnel maintaining the NORSAR Experimental Operations Console.

9-62. REF 110L, ISRSPS Program Specification (LDC).

9-63. REF 110N, ISRSPS Program Specification (NDPC).

9-64. REF 110S, ISRSPS Program Specification (SAAC).

REF 110 establishes the performance and design requirements for the ISRSPS System/360 programs. This document translates the functionally

expressed specifications of REF 101 into distinct computer program tasks. The organization of the programs is described and also the overall data flow in the system. All program interfaces are fully detailed.

9-65. REF 111L, ISRSPS Program Manual (LDC).

9-66. REF 111N, ISRSPS Program Manual (NDPC).

9-67. REF 111S, ISRSPS Program Manual (SAAC).

REF 111 contains detailed technical descriptions of the ISRSPS System/360 programs, including program functions, structures, operating environment, data organization and implementation. Flowcharts and narrative descriptions are included.

9-68. REF 112, ISRSPS System Test Specification.

REF 112 establishes the tests to be performed for ISRSPS to verify that equipment and programs function together to fulfill the requirements of REF 101.

9-69. REF 113N, ISRSPS System Operating Manual (NDPC).

9-70. REF 113S, ISRSPS System Operating Manual (SAAC).

REF 113 contains information for the use and guidance of the personnel operating ISRSPS. It contains a summarized functional analysis, comprehensive operator instructions, and a physical description of the equipment and its interconnections.

9-71. REF 114N, ISRSPS NORSAR Integretion Plan.

REF 114N establishes the plan for integretion of the several elements of the Norwegian Seismic Arrey into an operational system. The plan includes a set of test procedures which demonstrates the performance of the SLEM.

The following volumes also describe a portion of ISRSPS. The documents were generated as part of the Interim Integrated Signal Processing System (IISPS).

9-72. REF 4, IISPS System Opereting Manuel - LASAPS.

REF 4 was updated to reflect certain chenges to the LASA Dete Center opereting procedures needed for ISRSPS operation.

9-73. REF 8, IISPS Experimental Console Specifiction.

9-74. REF 9, IISPS Experimental Console Test Specification.

9-75. REF 10, IISPS Experimental Console Maintenance Manuel.

REF's 8, 9 and 10 pertain only to the Experimental Operations Console for SAAC.

9-76. REF 18, ISRSPS Integrated Array Electronics Specification.

9-77. REF 19, ISRSPS Integrated Array Electronics Test Specification.

9-78. REF 20, ISRSPS Integreted Arrey Electronics Meintenance Manual.

REFs 18, 19 and 20 pertain to the four prototype SLEMs; reference should be made to Philco-Ford Company documentation for specification of SLEMs installed in NORSAR.